Towards mitigation and adaptation to climate change : Contribution to Building Design

Anaïs Machard

LA ROCHELLE UNIVERSITÉ

ÉCOLE DOCTORALE EUCLIDE

Laboratoire des Sciences de l'Ingénieur pour l'Environnement

UMR – 7356 CNRS

Towards mitigation and adaptation to climate change: Contribution to Building Design

Anaïs MACHARD

Thèse soutenue le 21 juillet 2021
pour l'obtention du grade de Docteur de La Rochelle Université

Discipline : Génie Civil

Thèse dirigée par Christian INARD

JURY :		
Christian INARD	Professeur, Université de la Rochelle	Directeur de thèse
Dionysia KOLOKOTSA	Professeur, Technical University of Crete	Rapportrice
Christophe MENEZO	Professeur, Université Savoie Mont Blanc	Président du jury
Mathilde PASCAL	Docteur HDR, Santé Publique France	Examinatrice
Charles PELE	Docteur, Ingénieur CSTB	Examinateur
Mattheos SANTAMOURIS	Professeur, University of New South Wales	Rapporteur
Etienne WURTZ	Directeur de recherche, CEA/LITEN	Examinateur
INVITES :		
Sylvain GASTE	Maitre de conference ENSA Nantes, Architecte, Altersmith	Invité
Jacques RIBERON	Docteur, Chercheur CSTB	Invité

Remerciements

Tout d'abord, je voudrais remercier Christian Inard, mon directeur de thèse, pour la confiance qu'il m'a accordé durant toutes ces années, pour sa disponibilité, sa présence et son investissement dans ma thèse. Je le remercie également pour m'avoir donné l'opportunité d'apprendre à mener mes recherches de façon autonome et pour la liberté qu'il m'a octroyé, pour m'avoir aidé à consolider mes acquis, n'avoir jamais jugé mes failles et pour m'avoir épaulé dans la continuité du développement de mon esprit critique. Merci également pour ton humanité et toutes nos discussions, qui me manqueront.

Je remercie également mes co-encadrants de thèse Jean-Marie Alessandrini, Jacques Ribéron et Charles Pelé, pour avoir proposé ce beau sujet de thèse, pour avoir amorcé ces travaux de recherche d'adaptation du bâtiment au changement climatique au sein du CSTB, pour vos commentaires précieux et votre point de vue terre à terre et concret lors de nos échanges. Je suis très heureuse d'avoir pu mener à bien ces travaux de thèse multi-pluridisciplinaire mêlant climatologie, microclimat urbain, bâtiment et santé.

Je remercie mon jury de thèse, tout d'abord Sylvain Gaste, architecte de l'agence ALTERSMITH, pour nous avoir gracieusement offert son bâtiment en guise de cas d'étude. Ce bâtiment, par sa configuration intéressante, innovante et peu commune, nous a révélé plus d'une surprise, et a surtout confirmé qu'avec un bel effort de conception en amont, la diminution drastique des besoins énergétiques est tout à fait possible. Merci pour cette parenthèse de rêve. J'aimerais remercier Matheos Santamouris et Denia Kolokotsa pour avoir rapporté et commenté ma thèse, pour vos travaux de recherche innovants, qui ont fait partie de nombreuses de mes lectures et m'ont grandement inspirée. Merci également à Christophe Menezo, Etienne Wurtz et à Mathilde Pascal pour avoir preside ou participé à mon jury, pour vos questions pertinentes et pour m'avoir suggéré de nouvelles perspectives.

J'aimerais évidemment remercier la Rochelle Université, le laboratoire LaSIE et son personnel administratif, ainsi que l'école doctorale EUCLIDE et l'association Adocs pour leur accueil. J'ai fortement apprécié l'univers bienveillant dans lequel j'ai évolué durant ces années de thèse ainsi que le soutien et les opportunités apportées par les différentes personnes investies à l'université.

J'aimerais beaucoup remercier Jean-Philippe Ndobo-Epoy et Artemis Agelaridou-Twohig, qui m'ont insufflé l'envie de faire une thèse après un an et demi à avoir travaillé avec eux lorsque j'étais chez Saint-Gobain. Vous m'avez transmis ce goût pour la recherche, attisé ma curiosité, orienté mes yeux vers des portes que je ne voyais pas. Merci de m'avoir suggéré cette belle aventure. Je ne la regrette pas.

Voici maintenant une ode à mes collègues, impossible de vous classer par ordre de préférence, alors je vous citerai par ordre d'arrivée dans ma vie. Premièrement Fanny, ma jumelle de thèse, ma duponne, mon rayon de soleil, merci d'avoir choisi nos bureaux pour

qu'on vive notre aventure ensemble. Oh comme je t'en suis reconnaissante ! Ensemble on a créé notre bureau des plantes, notre petit nid d'amour féministe, on a décortiqué EnergyPlus dans tous les sens, couru chez Djolly pour notre pause goûter, fait des détours par le distributeur à 17h, galéré avec les yélos et les glaçons pour les mojitos, véloté sur l'île de ré par vents et marées. Sans toi ces années de vie n'auraient sans aucun doute pas eu le même sens.

J'aimerais ensuite remercier Simon qui tenait tant à son paragraphe, avec qui on s'est découvert un samedi soir chez Hortense, s'en est suivi un abonnement à vie au service après-vente Python, entre 2 apéros ou 2 teams de confinement. Oh Simon, roi des plots Seaborn, mes figures ont bien moins de couleur et d'audace depuis que tu es parti chez Tipee. Mention spéciale pour ces heures de discussions microclimat avec Manu et notre rêve de partir à Bali du fin fond de notre salon.

Merci à Manu pour m'avoir ouvert la porte à tes travaux et ton savoir sur le microclimat, pour m'avoir initié à mon baptême de rappel, pour ta patience avec moi sur une voie d'escalade, pour m'avoir guidé sur les murs de Crozon, pour nos discussions indicateurs et optimisation. Merci à Jérôme pour ta bonne humeur légendaire et tes blagues, et pour m'avoir poussé à publier mes travaux en insistant sur la nouveauté (relative) de mes recherches. Merci à Max pour nous avoir aidé avec ce code, ce qui, personne ne l'a sans doute compris à part moi, a grandement consolidé mes travaux. Merci aussi pour m'avoir initié au surf et m'avoir ouvert de nouveaux horizons à la fois fun, beaux et sereins.

Merci à Marika, mon italienne que j'ai kidnappée dans mon bureau car j'avais envie de rire. Merci pour avoir gardé notre arbre en vie, pour notre amitié, merci pour toutes ces discussions confort thermique, merci d'avoir été ma grande sœur de recherche, avec qui j'ai pu me retrouver dans notre passion commune pour la lecture, l'analyse et l'écriture. Merci aussi à Kévin pour ces diners du dimanche soir, nos débats, et pour ces randonnées. Merci à vous deux d'être des exemples pour moi !

Merci à Manon, reine du maithai, qui a été ma compagne de fin de thèse. Merci pour nos seuls petits instants de vie de ces marchés du samedi matin. Merci d'être une super star who-got-it-all-together et d'être donc une belle source d'inspiration et de motivation. Merci à Feryal d'avoir été ma copine de bureau et d'avoir été un support durant cette dernière année difficile. Merci à mon amie Elise pour m'avoir épaulée, écoutée, accompagnée durant ces années. Nos séances de grimpe et discussions en tout genre restent gravées dans ma mémoire. Merci à Amélie pour ta fraicheur de la jeunesse, ta vivacité d'esprit, ta franchise et pour m'avoir forcé à sortir de chez moi plus d'un vendredi soir. Tu as contribué à ma santé mentale pendant ma these ! Merci à Henri, Marie, Aline, Thibault, Pierre et Antoine pour m'avoir ouvert votre maison et pour ces moments partagés.

Merci à Roiel, pour m'avoir poussé à toujours donner le meilleur de moi-même et ne pas revoir mes ambitions à la baisse. Merci pour ton soutien, la patience dont tu as fait preuve et pour ton intérêt à mes recherches. Merci d'avoir été mon premier fan, pour m'avoir encouragé à creuser, discuter, communiquer et défendre mes idées, et à être toujours plus créative.

Merci à toutes les autres personnes qui m'ont aidé durant ma thèse et mes rencontres professionnelles, Jean-Louis Dufresne pour m'avoir parlé de la plateforme Eurocordex,

Antoine, pour m'avoir aidé avec mon code pour télécharger les données de climat lors de mes débuts en Python, Laurent pour avoir été un soutien considérable à l'utilisation de DesignBuilder, et plein d'autres personnes qui m'ont aidé ponctuellement. Merci à tous les membres du LaSIE, les doctorants et professeurs, entre autres merci à Patrick, à Marc, Claudine, Cyrille, Jean-Luc, Ghislain, Julien, Antoine(s), Pierre, Loulou, Guigui, Suelen et Caroline. Merci à la dream team patins à roulettes. Merci à mes rencontres professionnelles, Agnese, Mamak, Abhishek Gaur et Samy pour nos discussions climat futur. Merci à Jeanne Goffart pour ses conseils avisés sur l'analyse de sensibilité, et à l'ensemble de la communauté IBPSA.

Enfin, merci à mes amis parisiens et toutes les personnes chères à mon coeur, merci à ma Matou et à mes soeurs pour m'avoir supportée pendant ces difficiles années. Merci à mes parents qui par leur amour et conviction que je peux entreprendre et mener à bien tous mes rêves me donnent la force de croire en moi et d'avancer tous les jours.

Il parait qu'une thèse c'est comme un marathon, et je suis bien d'accord. Plus précisément, je l'avais comparé avant de commencer à une paroi d'escalade. Alors que le marathon se court en ligne droite, la grimpe est composée d'une multitude de tâtonnements, de découverte, d'appréhension, parfois de retours en arrière, et de certains élans souvent poussés par son partenaire. Le partenaire qui lui est là pour nous motiver, nous donner une vision parfois différente de la voie, et s'assurer qu'on ira jusqu'au bout. Parfois, on voit des compagnons dans des cordées parallèle, et c'est un peu comme les doctorants avec qui on a commencé. Peu importe à quel moment on arrive à la fin, et même si on y arrivera finalement, car ce qui compte c'est la découverte, l'aventure, et les rencontres en chemin. Pour ma part, c'est quand j'étais presque en haut que ça a été le plus dur, quand il était déjà bien trop tard pour faire demi-tour, mais que j'étais si essoufflée d'avoir déjà tant donné. Je n'oublierai pas les belles personnes qui ont été présentes dans ma vie et qui ont pris soin de moi pendant ces moments difficiles, qui m'ont insufflé une énergie régénératrice, ont écouté mes plaintes et m'ont aidé à guérir mes maux, elles se reconnaitront. Merci à toutes les personnes qui ont fait partie de ma vie de près ou de loin. Enfin merci à la nature, et tout particulièrement au ciel et l'océan de la Rochelle pour cette magnifique palette rose-violet-orangé dont j'ai pu profiter quasiment tous les soirs lors de mon daily commute.

On dit qu'il faut être passionné pour faire de la recherche, oh comme je suis heureuse d'avoir frayé mon chemin pour me créer un travail qui chaque jour asservit mon insatiable curiosité !

Résumé

Compte tenu de l'augmentation de la fréquence des canicules, il est nécessaire de s'assurer que les bâtiments conçus et construits aujourd'hui seront adaptés aux futures températures plus élevées.

Le périmètre de cette thèse consiste à proposer une méthodologie de contribution à la conception des bâtiments considérant à la fois les enjeux d'atténuation (réduction des besoins énergétiques) et d'adaptation (confort thermique estival, réduction du risque sanitaire en période de canicule) au changement climatique. La méthodologie a pour vocation d'être adaptable à différents types de bâtiments et de climats.

Dans ce but, nous avons développé des fichiers météorologiques dont le biais a été corrigé contenant des séquences typiques, ainsi que des vagues de chaleur futures. Par la suite, des méthodes d'analyse de sensibilité et d'optimisation couplées à des simulations thermiques dynamiques du bâtiment ont permis d'évaluer le potentiel de différentes techniques et solutions de rafraîchissement passif utilisées pour diminuer la surchauffe l'été en climats futurs.

Les résultats de ces travaux de recherche mettent en évidence que les stratégies évaluées (zones tampons, inertie, propriétés optiques des parois extérieures, ratio de vitrage, solutions de rafraichissement par ventilation ou puits provençal) sont efficaces pour maintenir un confort thermique estival lors des étés futurs types à Paris et à La Rochelle. Cependant, à Carpentras, pour un été futur type, et pour ces trois villes en périodes de canicules futures récurrentes, les limites de ces solutions sont mises en exergue.

En effet, les résultats de l'étude montrent que les occupants sont exposés à la chaleur lors de plusieurs jours consécutifs au-dessus de seuils à la fois diurnes et nocturnes ce qui résulte en un risque sanitaire pour les personnes vulnérables. Ces séquences ne sont pas détectées en utilisant des fichiers futurs types uniquement, ce qui démontre la pertinence de ces travaux.

La combinaison d'enveloppes de bâtiments optimisées, de stratégies de rafraîchissement et d'adaptation des occupants se révèle être nécessaire afin d'atténuer le risque sanitaire récurrent auguré pour le milieu du siècle en France.

Abstract

Due to climate change projecting increased heatwaves occurrence, ensuring that buildings designed and built today will be adapted to future warmer temperatures is essential. The scope of this Ph.D. is to propose a methodological contribution to the design of buildings that both mitigate (minimize yearly energy needs) and adapt (minimize summer indoor overheating, limit health-heat-related risk) to climate change.

The methodology can be applied to any building case study in any climate. For this purpose, bias-adjusted weather files containing both present, future typical conditions and future heatwave periods were developed. The potential of different passive cooling mitigation and adaptation strategies to reduce summer indoor overheating is evaluated using these weather files through dynamic thermal simulations, sensitivity analysis, and optimization methods.

The results of this research work highlight that for the building case study, the evaluated strategies (buffer spaces, thermal mass, roof optical properties, glazing ratio, ventilative cooling) have a strong capacity to enable summer thermal comfort in future typical summers in Paris and La Rochelle. However, in Carpentras, and under recurring heatwaves in all three cities, the limits of these mitigation and adaptation measures are recognized.

In fact, future heatwaves consistently lead to consecutive days of indoor overheating exposure during both daytime and nighttime for building occupants, leading to a health-heat-related risk especially for the most vulnerable. These sequences are not detected when using only future typical years, which stresses the relevance of this work.

Only the combination of optimized building envelopes, ventilative cooling strategies and adaptive opportunities from building occupants (solar control, increased indoor air velocities) have the potential to offset the projected recurring health-heat-related risk, particularly elevated in the South of France.

Glossary

Mitigation to climate change ***(Atténuation au changement climatique)***

Reducing the flow of heat-trapping greenhouse gases into the atmosphere by reducing the sources of these gases. In the building sector, climate change mitigation is achieved by reducing the building energy needs or increasing the energy efficiency of HVAC systems. In this Ph.D. we only focus on the reduction of the building energy needs *(sobriété énergétique).*

Adaptation to climate change ***(Adaptation au changement climatique)***

Changes in practices to moderate potential damages (current or projected) associated with climate change. In this Ph.D. we focus on the adaptation of buildings to warming temperatures due to climate change, the potential damage being the health-heat-related risk for building occupants due to indoor overheating.

Building resilience to overheating ***(Résilience du bâtiment à la surchauffe)***

Anticipation of future overheating risks to better prepare and adapt buildings to protect from extreme heat.

Heatwave ***(Vague de chaleur)***

Consecutive days of abnormally warm temperatures.

IBM Heatwave ***(Canicule)***

Consecutive days of abnormally warm temperatures during daytime and nighttime with potential heat-related health impact.

French Thermal Regulation ***(RT-2012/RE-2020)***

National regulation with maximum objective criteria such as energy needs or summer thermal comfort.

Building design ***(Conception du bâtiment)***

Building design from the sketch phase until the execution phase.

Bioclimatic design *(Conception Bioclimatique)*

Building design that accounts for and takes advantage of the outdoor climate to enhance the building indoor environment. Bioclimatic design connects the human inside the building to the outdoor climate. A bioclimatic design aiming to reduce heating needs could be to implement large windows facing South. A bioclimatic design aiming to reduce summer thermal discomfort could be to use passive cooling strategies such as natural ventilation, i.e designing the building to enhance air movement.

HVAC sizing *(Dimensionnement des systèmes)*

Calculating the system size needed to meet the heating or cooling needs under most climatic conditions. It is a balance between the system cost and its ability to deliver energy in extreme climatic conditions.

Contribution to the building design *(Accompagnement à la conception)*

Contribution to the building design to incorporate mitigation and adaptation to climate change strategies from the design stage of the building.

Contracting private firm or public organizations *(Maitrise d'ouvrage, MOA)*

Firm who specifies the building project needs, constraints, budget and planning.

Project management consortium *(Groupement de Maitrise d'œuvre, MOE)*

Group of actors (architect, consulting firm, urbanists, economists) in charge of the building design. Our contribution to the building design will be within the project management consortium, more specifically it could be used by the consulting firm *(Bureau d'études).*

Nomenclature

Acronyms

AR4	IPCC 4th Assessment Report
AR5	IPCC 5th Assessment Report
BC	Bias Correction
CDF	Cumulative Distribution Function
CNRM	Centre National de Recherches Météorologiques
EAHX	Earth-to-air heat exchanger
EPW	EnergyPlus Weather file
EURO-CORDEX	European Coordinated Regional Climate Downscaling Experiment
FC	Free-cooling through ventilation system
GCM	Global Climate Model
HADGEM	Hadley Center Global Environment Model
HHRR	Health-heat-related risk
HW	Heatwave event
IBM	Meteorological bio-indicator
IEA	International Energy Agency
IPCC	International Governmental Panel on Climate Change
IPSL	Institut Pierre Simon Laplace
MBC	Multivariate Bias Correction Method
MPI-M	Max Planck Institut for Meteorology
NETCDF	Network Common Data Form
NSGA-II	Fast Non-Dominated Sorting Genetic Algorithm
NV	Natural Ventilation
PNACC	Plan National d'Adaptation au Changement Climatique
RCA4	Rossby Centre Regional Atmospheric Climate Model
RCM	Regional Climate Model
RCP	Representative Concentration Pathway
RF	Radiative Forcing
RE-2020	Réglementation environnementale 2020
RT-2012	Réglementation thermique 20212
SA	Sensitivity Analysis
SET	Standard Effective Temperature
SRES	Special Report on Emissions Scenarios
SSP	Shared Socio-Economic Pathway
TAR	IPCC 3rd Assessment Report
TEB	Town Energy Balance
TMY	Typical meteorological year
UHI	Urban Heat Island
UWG	Urban Weather Generator

Latin characters

Character	Description	Unit
Upper letters		
A	Surface area	m²
A_s	Amplitude of temperature at soil surface	°C
AP	Atmospheric pressure	Pa
C	Human body heat exchanged by convection	W
CC	Cloud cover	tenths
Cp	Specific heat	J/(kg.K)
D_{pipe}	Tube diameter	m
DH	Degree-hours	°C.h
DHR	Diffuse horizontal solar radiation	Wh/m²
DNR	Direct normal solar radiation	Wh/m²
$DN'R$	Direct horizontal solar radiation	Wh/m²
E_{sud}	Human body heat exchanged by sudation	W
E_{res}	Human body heat exchanged by respiration	W
E_{diff}	Human body heat exchanged by perspiration	W
EE	Elementary effect	W
F	View factor between the building surface and surrounding environment	-
FS	Finkelstein-Schafer statistic	-
GHR	Global horizontal solar radiation	Wh/m²
H	Heat generated by the human body	W
HN	Heating needs	kWh/(m².year)
I	Irradiation	
$Iext_0$	Extra-terrestrial spectral distribution of the solar radiation outside the atmosphere	Wh/m²
$Iext$	Extra-terrestrial spectral distribution of the solar radiation outside the atmosphere attenuated by air mass, molecular and particular scatter	Wh/m²
IBM_x	Three-days moving daily maximal temperature	°C
IBM_n	Three-days moving daily minimal temperature	°C
$J(i)$	Rank in the series of the daily averages i for each year	-
L	EAHX tube length	m
$L(i)$	Rank in the series of the daily averages i for the 30 years	-
LWR	Horizontal infrared radiation intensity	Wh/m²
N	Number	-
N_d	Number of days	-
N_{dy}	Number of days per year	-
OF	Objective function for sensitivity analysis	-
P	Pressure losses	Pa
P_w	Wind pressure	Pa
PL	Linear pressure losses	Pa
$Pvar$	Partial variance	-
Q	Heat transfer from the skin to the exterior surface of clothing	W
$Qvol_{pipe}$	Air change	ACH
Qv_{pipe}	Volumetric flow rate	m³/h
R	Human body heat exchanged by radiation	W
R_f	Surface roughness multiplier	-
Re	Reynolds number	-

RH	Relative Humidity	%
S	Attenuated radiation	Wh/m²
S_n	IBM threshold for daily minimal temperature	°C
S_x	IBM threshold for daily maximal temperature	°C
S_{1i}	Sobol first order index	-
S_{Ti}	Sobol total order index	-
S_{pipe}	Pipe cross-section	m²
SCp	Surface pressure coefficient	-
Sl	Sunlit surface area	m²
SR	Side ratio	-
T	Dry-bulb temperature	°C
T_s	Soil surface temperature	°C
TD	Thermal delay	hours
TK	Dry-bulb temperature	K
U_t	Heat transfer coefficient	W/(m².K)
V	Variance	-
VL	Living space volume	m³
VK_{air}	Air kinematic viscosity	m²/s
VP	Vapor pressure	hPa
VP_s	Saturated vapor pressure	hPa
WS	Wind speed	m/s
WV	Water vapor of the atmosphere	g/kg
Lower letters		
a	Thermal diffusivity	m/s
b	Thermal effusiveness	$(J/K/m).s^{-1/2}$
cp	Climate parameter of first order	-
d	Day	-
f	Evaporation fraction at the soil surface	-
fr	Friction coefficient	-
h	Sun elevation	°
h_c	Convection coefficient	W/(m².K)
h_r	Radiation coefficient	W/(m².K)
i	Input parameter for sensitivity analysis	-
j	Input parameter for sensitivity analysis	-
k	Thermal conductivity	W/(m.K)
m	Optical air mass	-
$\dot{m}$	Airmass flow rate	kg/s
mo	Month	-
p	Number of levels in Morris method	-
q	Correction factor for the distance between the Earth and the sun	-
r	Reflectivity coefficient	-
t	Time-step	
t_0	Phase constant	days
th	Thickness	m
tr	Number of Morris trajectories	-
x	Water content	kg/kg
x_{0h}	Present hourly value of climate variable	-
x_{0m}	Present monthly mean value of climate variable	-
x_h	Future hourly value of climate variable	-
y	Point in the earth-to-air heat exchanger tube	m
yr	Year	

z	Height	m
zg	Depth	m
z_{t}	Zenith angle	radians
Δx_{m}	Monthly average climate change	-

Greek characters

Character	Description	Unit
Upper letters		
Φ	Distribution function over 30 years	-
Σ	Tilt angle	°
Lower letters		
α_{d}	Absorption coefficient for particular scatter	-
α_{m}	Monthly average daily range climate change	-
α_{r}	Absorption coefficient for molecular scatter	-
α_{SW}	Solar absorptivity	-
β	Turbidity coefficient	-
δ	Layer thickness	m
ε	Emissivity	-
θ	Surface angle	radians
λ	Wavelength	nm
μ^*	Absolute mean of elementary effects	-
v_{pipe}	Air velocity inside EAHX pipe	m/s
x	Soil absorption coefficient	-
ρ	Density	kg/m^3
σ	Stefan-Boltzmann constant	-
σ	Variance of elementary effects	-
φ	Radiation flux	W/m^2
ψ	Distribution function over 1 year	-
$w\alpha$	Wind angle	°

Indices

Character	Description	Unit
n	Wavelength	
dp	Dew-point	
dbt	Dry-bulb	
da	Daily average of climate variable	
d	Day	
max	Maximum	
min	Minimum	
ext	Exterior	
int	Interior	
rad	Radiation	
$cond$	Conduction	
$conv$	Convection	
nat	Natural	
met	Meteorological station	
q	Index of incident angle at 30° increments	

Table of contents

Introduction

Today, it is widely accepted that climate change is a global phenomenon. Scientific evidence shows that the world is already more than one degree warmer than before the industrialization area (Figure 1), and that the past five years 2015-2020 were the warmest recorded. Not only the average temperature is rising, but extreme temperatures are also witnessed more and more frequently, and heatwaves are becoming more frequent. In recent decades, worldwide policies have put emphasis to reduce greenhouse gases (GES) emissions and mitigate climate change. Indeed, to overcome this challenge, Europe has undertaken the European Green Deal, which goal is for Europe to be carbon neutral by 2050.

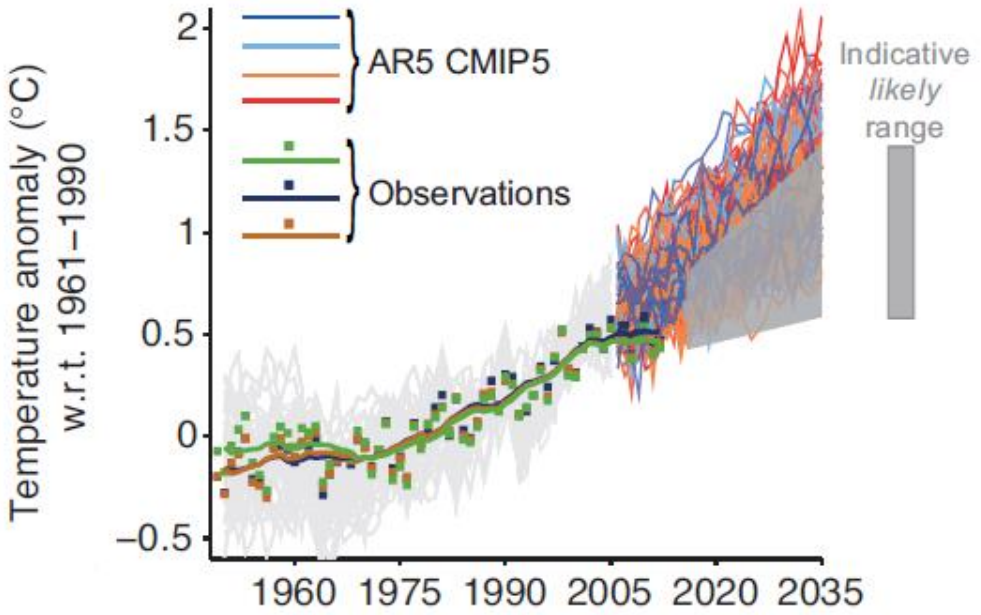

Figure 1 - Temperature anomaly vs. observations (Sutton et al., 2011)

In France, buildings account for the largest energy consumption amongst the other sectors (about 40 %). In response to the need to mitigate climate change, emphasis has been placed on reducing energy consumption in the building sector, which objectives are set by the buildings Thermal Regulation (RT). With heating needs reduction as a primary driver, buildings have been constrained to be more energy-efficient and airtight. The main measures to reduce heating needs are thermal insulation or bioclimatic design with large window glazing on the South façade. These produced two contrasting outcomes: While new buildings now achieve very low heating needs during the winter period, some of them have started to experience overheating during the summer period.

Unfortunately, there is strong evidence at the global scale that some climate change effects are already irreversible, and that the sixth mass extinction, also referred to as the Holocene extinction, has been precipitated because of human activity (Shivanna, 2020). There

is no point of return, and humans as society need to adapt to this ever-changing climate. Even with the most optimistic socio-economic pathway for the 21st century, the earth's temperature will not stop rising before the mid-21st century. Not only average temperatures are rising, but so is the frequency of extreme events occurrence, such as heatwaves (Figure 2). Similar to the poles warming faster than equatorial continents, extremes of temperatures are rising more quickly than averages. More warm events, more severe, and more frequent, are expected. According to the Intergovernmental Panel on Climate Change (IPCC), towards the end of the century, the number of heatwaves will only increase in terms of frequency, duration, and intensity, which lead to the statement that heatwaves are today one of the most threatening events of the XXIth century for society (Folland et al., 2001).

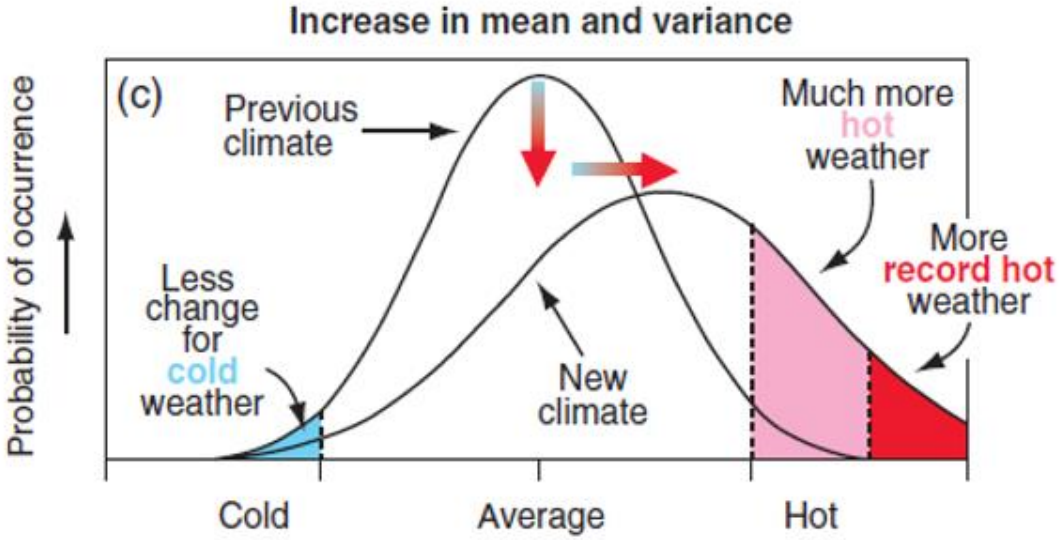

Figure 2 - Increase of temperature in mean and variance (Folland et al., 2001)

France adopted a climate change adaptation strategy at the national level in 2006, followed by the National Adaptation Plan to Climate Change (PNACC) in 2011-2015, updated in 2018-2022 (Ministère de la Transition écologique et Solidaire, 2011). A section of this plan is targeted to the urban built fabric, with four main themes: integrate adaptation in urbanism documents, promote nature and biodiversity in cities, mitigate the effects of heatwaves enhanced by urban heat island effects, and act on building indoor thermal summer comfort/discomfort in a context of overheating due to increasingly warmer temperatures. In response to this last theme, the Building Thermal Regulation RE-2020 has reinforced the summer comfort criterion, which now accounts both for duration and intensity of summer thermal discomfort above a specific threshold. Additionally, each newly-built building must pass an overheating assessment to the climate of the 2003 heatwave, which is a much more stringent criterion than before. At the city level, many cities have put together adaptation to climate change and resilience to extreme event plans, such as the city of Paris (Mairie de Paris, 2017). Research work in France has been done on the city's vulnerability and resilience to future heatwaves (Hallegatte et al., 2013), but the adaptation and resilience of buildings to climate change have not been studied at the national level.

In the last three decades, we can observe that heatwaves have already become more intense (Figure 3). The 2003 heatwave was exceptional in terms of high temperatures and sanitary impact, with 15,000 excessive deaths in France. Numerous research reports

demonstrate the relationship between extreme high temperatures and human mortality (Koppe et al., 2004; Corso et al., 2017). Heatwaves represent a particular high risk to the most vulnerable members of society, such as the elderly and children.

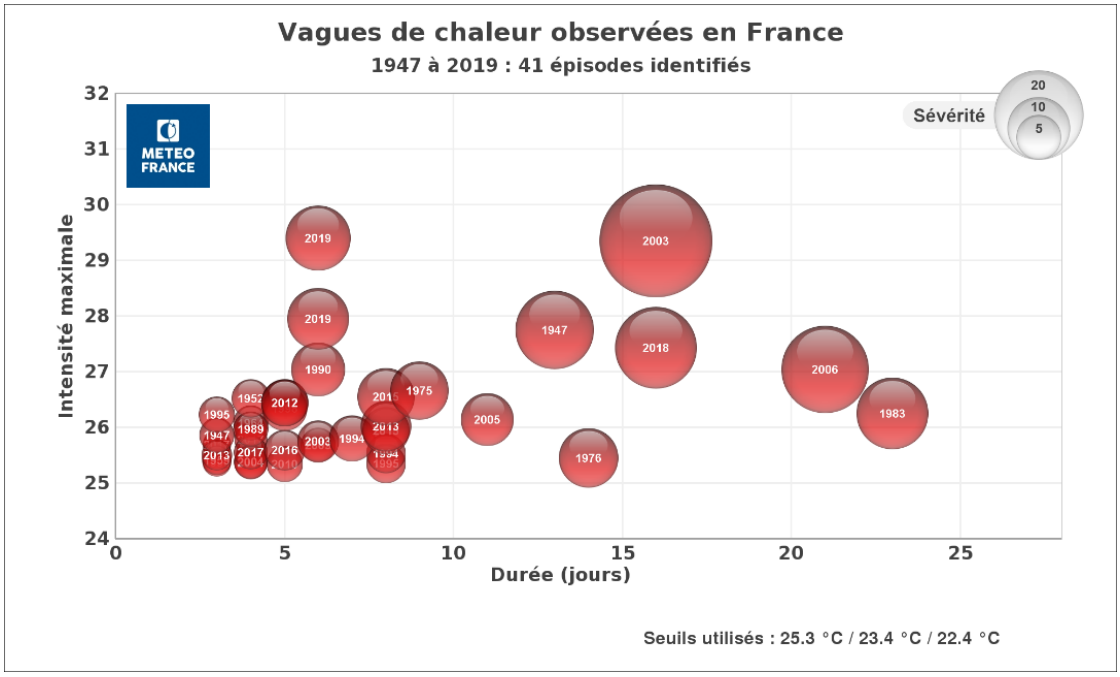

Figure 3 – Heatwaves observed in France between 1947 and 2019 (©MeteoFrance)

Heat-related risk factors can be related on one hand to the urban and built environment, on the other hand to the building occupants' capacity to withstand heat based on a number of factors (age, health, heat acclimatization, behavioral mobility, etc.)(Alessandrini et al., 2019). The people most at risk are the elderly, people with physical disability or mobility issues, people with pre-existing conditions and illnesses, and children. Hot indoor temperatures can cause or worsen cardiovascular and respiratory disorders.

In 2003, it was demonstrated that the vast majority of deaths occurred in overheated top-floor dwellings with no roof insulation and were linked to elderly people which were either unable to create airflow by window openings, or did not feel the heat sensation (Vandentorren et al., 2006; Ribéron et al., 2006). Furthermore, the most vulnerable people also include the poorest, as they often live in the worst thermal buildings (Santamouris & Kolokotsa, 2015).

As the French population's age is predicted to increase towards the end of the century, overheating in buildings is a problem that needs to be addressed seriously. According to (INSEE, 2021), in 2070 twice more people than today will be aged more than 75 years old. Up to the present, the built fabric in France is simply not adapted to extreme heat. With the projected increase of heatwaves and the aging population, the heat-related health risk could consequently become quite significant, as is demonstrated for many cities around the world (Lee et al., 2020). Furthermore, heatwave effects are exacerbated by the urban heat island effect, especially increasing night-time temperatures in French cities. During heatwaves, if people cannot rest from heat during the night, they are even more at risk (Laaidi et al., 2012). Due to

the fact that in France, 75% of the population lives in cities, and that deaths usually occur in buildings during heatwaves, there is a critical need to design heat-safe buildings.

In response to heatwaves, population resilience is defined by its capacity to cope, respond and resist to the perturbation. According to the IPCC, coping is very different than adapting: While coping is similar to survival, and is a response to imminent stress that requires a quick response reproducing previous experiences, adapting is a reorientation and anticipates a future change; it is constrained by assumptions about the future more than pre-conceptions. When adapting, decisions are focused on anticipating the change and on providing solutions for future conditions (Lavell et al., 2012; Miller et al., 2020). During heatwaves, individuals buy fans, air-conditioning units or seek refuge in air-conditioned buildings, while it is common that governments propose shelters such as libraries with air-conditioning, or parks being opened all night in the cities: these are coping mechanisms. In response to this, after the 2003 heatwave in France, the Heat Wealth Warning System was created to anticipate future heatwaves and prepare the population (Laaidi et al., 2013), this is a good example of an adaptation strategy. Heatwaves were only recently recognized as an extreme event and therefore slowly receive the attention they deserve. Many other countries have recently developed their own heatwave national plans (McGregor, 2015). The relative mortality risk was compared in eighteen French cities between 2000 and 2019, and even though more deaths were related to cold than to heat, it appeared that at very high temperatures, heat represented a higher risk of mortality than extreme cold temperatures (Figure 4).

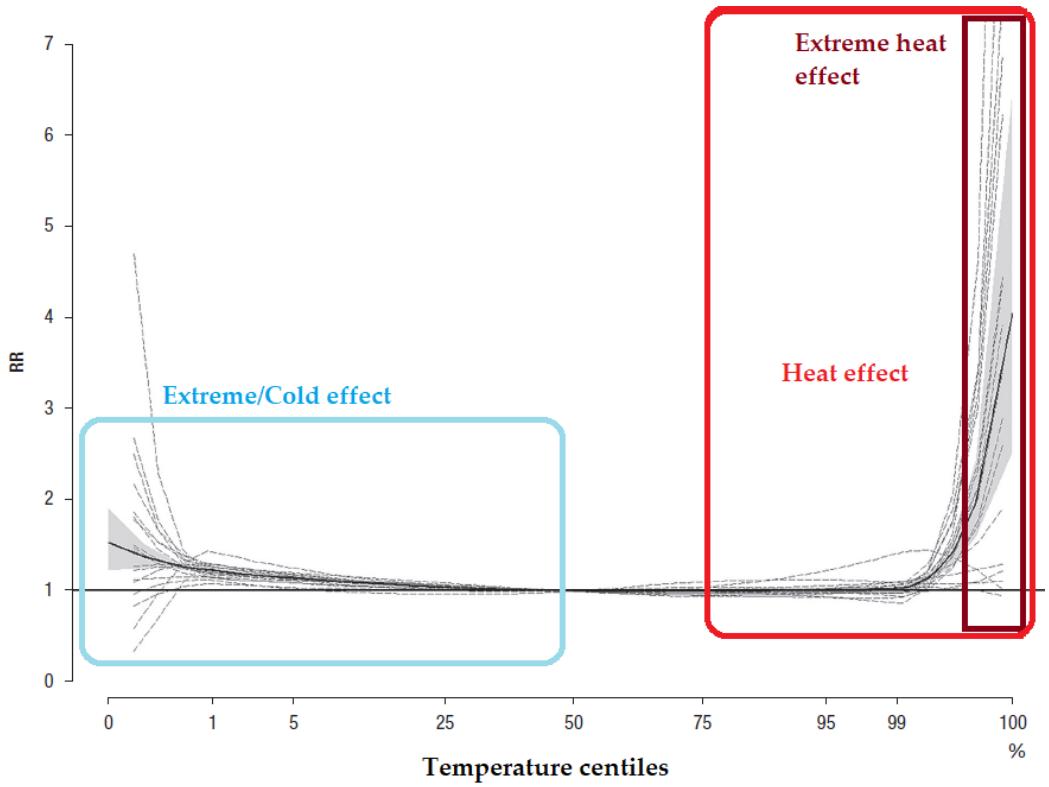

Figure 4 – Influence of temperature on relative risk of cumulative deaths during 21 days following heat exposure percentile, compared to expected mortality for a median temperature – Meta analysis of eighteen French cities during the period 2000-2010 – Adapted from (Corso et al., 2017; Pascal et al., 2018)

Because air-conditioning is an easy option to cope with extreme heat, its use in future years may largely increase if our buildings keep overheating. The downside is double, as this option is both energy consuming and contributes to the warming of street air temperatures. A study calculated that the air temperature in Paris would increase in average by +2 °C with twice the current amount of power (projection of 10 GW sensible heat released) used for air-conditioning at the city scale (De Munck et al., 2013). Unfortunately, the use of AC is becoming predominant in many countries for a number of reasons (increasing comfort requirements, global and local warming, growth in local income, price of equipment and electricity, social equity) while it does the opposite to mitigating climate change. This rapid and dangerous increase in the last thirty years has led the International Energy Agency (IEA) to declare in 2018: "The world is facing a looming cold crunch". Even further, the IEA predicts that by 2050, the global energy demand from air conditioners is expected to triple (International Energy Agency, 2018). In China, air-conditioning in households was about 1% in 1990 and is almost at 100% in 2010 (Santamouris, 2016). In Europe, electricity consumption related to air-conditioning was about 1,900 GWh in 1990 and was predicted to be around 44,430 GWh in 2020 (Santamouris et al., 2007). In Europe, today air-conditioning has penetrated less than 10 % of households. However, the questions we must ask ourselves is how will climate change impact this?

Many ancient and innovative alternative cooling strategies and systems exist. Well-known ancient bioclimatic strategies were used to keep indoor environments cool in hot climates. Today, cutting-edge research is developing new innovative materials and systems to maintain current standard comfort levels. Some techniques are already available and ready to be implemented on buildings, while others are still under development. Due to the climate change urgency, research is evolving fast on these topics and new very efficient materials and systems might be ready for the market within the upcoming decade.

In this Ph.D. thesis, we aim to provide a contribution to the design of resilient buildings to indoor overheating under future summers, at the crossroad of mitigation and adaptation measures. This work is complex and dual: it is needed to both mitigate and adapt to climate change, it is needed to design buildings suited for both the winter and summer period, and it is needed to design buildings that fit both the present and future climate. The choice of future weather files is equally complex, due to the number of different tools, scenarios, and models available. While future typical weather files are easily available, practitioners find it difficult to find future weather files containing intense heatwave periods to assess the limits of their building design. Additionally, even though some passive cooling strategies are very ancient, they are not necessarily widespread and implementing them in the building design might not always be obvious for building practitioners, especially considering it might not be necessary to implement these under typical summer conditions. For this purpose, this work aims to be a methodological contribution to guide building practitioners on how to adapt their building designs to future climate conditions, and understand if a building design change is needed between present and future climate.

This thesis aims to create a change in paradigm: We do not only wish to analyze how our building design will impact the climate, but also how the future climate should impact our building design. The building design must be made using measures at the convergence of both mitigation and adaptation to climate change. While mitigation measures reduce the CO_2

emissions at the global scale, adaptation measures are local, adapted to a case study: They aim to reduce the impact of climate change, in our case of interest the heat-health related risk inside buildings (Figure 5).

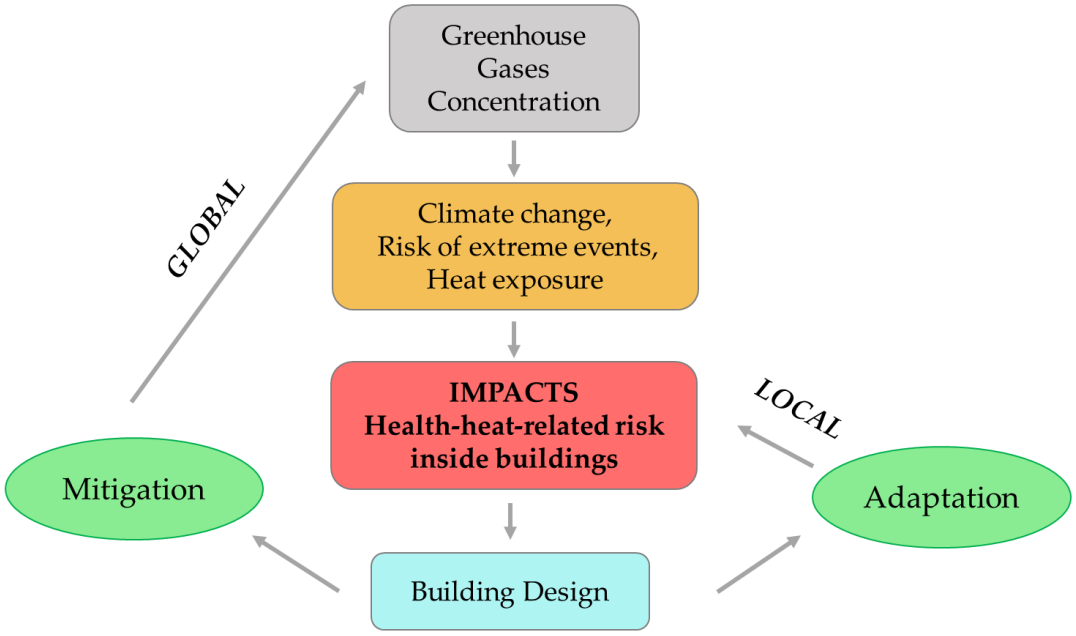

Figure 5 – Relationship between building design and climate change through mitigation and adaptation measures

Adaptation is therefore the new challenge and a crucial matter, since in France we are used to designing buildings mostly to prevent cold in winter, the summer discomfort criterion becomes second or an afterthought during the design process. Today, heat-health-related risk is real, and designing buildings to prevent excessive heat might be at least as relevant as designing buildings to prevent from cold. The proposed methodology should be able to be utilized by building practitioners and architects to provide design guidelines for building resilient indoor environments to heat under a variety of future climate conditions. The provided design methodology will help to assess the limits of the buildings built today, from the design stage. Such an effort to anticipate future heatwave threats would ensure that buildings will be resilient to indoor overheating. If used appropriately, buildings will be able to provide a comfortable indoor environment in future summers and protect occupants from heat stress during future heatwaves.

In France, practical implications for the implementation of this methodology will be difficult for a number of reasons: Currently, the built fabric is adapted to the present climate and current regulations do not anticipate future climate. National socio-professional oppositions might occur if additional measures are implemented in future building regulations, and as the exact occurrence of future heatwaves cannot be predicted, adaptation measures implemented today might only be paid back in years or decades when the future severe heatwave will occur. Until this time, building practitioners might not understand the urgent need to adapt buildings today to the future climate (Salagnac, 2015).

This body of work is limited to new buildings, and to the residential sector. For this purpose, we use as case study an apartment in a new residential collective building that is RT-2012 compliant. We will use this case study to test the proposed methodology in three French cities with three distinct climates: The oceanic climate of Paris, La Rochelle, in a maritime climate, and Carpentras, located in the South of France were temperature heat records were registered. We wish to study the building conditions under future "typical" summer conditions as well as under future heatwaves, to assess the limits of the proposed building design and the building resilience to different indoor overheating magnitudes. The proposed methodology will account for the uncertainty related to future climate projections (i.e warmer temperatures and heatwaves frequency, occurrence, and intensity) at the design stage, to assess the potential heat-health related risk for different climate sequences. For the specific case study, sensitivity analysis and optimization algorithms will be used to find the best optimum solutions that converge to mitigating climate change (minimum energy needs) and adapt to climate change (minimum summer discomfort), beyond a variety of proposed passive strategies and systems. These methods are well-known and have been used by building practitioners for the last thirty years, however, they have not been applied to future climate in the French context. This thesis wishes to provide general tendencies for building design, for the specific building case-study in the studied cities. However, the methodology is to be used for any climate and any building type.

This Ph.D. thesis consists of five distinct chapters. In the first chapter, we analyze the state of the art on three different topics: relationship between humans and extreme heat, studies on passive strategies and systems that can be used for summer bioclimatic design, and future climate data that can be used for building thermal simulations. In the second chapter, we present the proposed research methodology for this thesis. We introduce our design contribution and provide an overview of the methodology. After which, we present how we assemble future weather files for building simulations, explain how we navigate through the different spatial scales: from the climate at the regional scale to the urban microclimate scale, to the building scale, and finally to the building's occupants. We then introduce the building case study and the EnergyPlus model, and the different passive strategies and systems that will be modelled and analyzed. Finally, we outline the sensitivity analysis and optimization methods that will be used. In the third chapter, we present the future climate data reassembled in this work, and the justification of the climate sequences used for the building thermal simulations. In the fourth and five chapters, we model the building case study with the climate data introduced in the third chapter, using the sensitivity analysis and optimization methods to identify design guidelines for multi-objective criteria. Finally, we analyze the health-heat-related risk in optimized building designs during future climate.

Throughout the chapters, we will drive our research with the aim to address the following research questions:

- *Which type of future climate data is available to assemble future weather files for building simulations? (Chapter 1)*
- *Is it possible to assemble future weather files that contain future heatwaves? (Chapter 1)*
- *How to account for future climate uncertainties and how to consider the risk related to this uncertainty in the building design process? (Chapter 2, Chapter 3)*

- *Which passive cooling systems and strategies exist for bioclimatic summer design adapted to the French climate? Which ones are in concurrence with the winter design? What are the local climate limitations of each of these technologies? (Chapter 1 and Chapter 3)*
- *How can we design resilient buildings to climate change at the cross-road of adaptation and mitigation measures? (Chapter 2)*
- *Which climate sequences to select for the building thermal simulations? (Chapter 3)*
- *How will the future climate influence the building design? To which intensity? What are the differences with the climate of today? (Chapter 2 to Chapter 5)*
- *What are the limits of the buildings built today to future climate? (Chapter 4)*
- *What are the most important building design parameters on the indoor building conditions? Do they vary from one city to another with different climate and climate projections? Which combinations of strategies and systems perform best in which cities? (Chapter 4 and Chapter 5)*
- *Which design criteria can we use to assess warm discomfort and heat-health-related risk during heatwaves? (Chapter 4 and Chapter 5)*
- *Is it possible to design resilient and safe buildings under future typical and heatwaves conditions without air-conditioning? (Chapter 5)*

Chapter 1
State of the art

In this chapter, we investigate the state of the art on three complementary aspects on this Ph.D. research: human vulnerability to heat, building resilience to heat and future climate projections of extreme heat. In the first section, we analyze the human response to heat, and the different thermal comfort models that can be used to assess indoor summer thermal comfort or discomfort, and indoor overheating. In a second section, we review the different passive cooling strategies that can be used to increase the building resilience to extreme heat. As passive techniques are based on local climatic potentials, the limitations of each solution are assessed. Finally, in the last section, we investigate if future heatwaves can be used and selected from climate models for assessing the building resilience to these future heatwaves. This chapter aims to answer the following research questions:

Which models and tools are available to assess summer thermal comfort, discomfort, and health-related heat risk for the building occupants under heatwaves?

Which passive cooling systems and strategies exist for bioclimatic summer design adapted to French climate? Which ones are in concurrence with the winter design? What are the local climate limitations of each of these technologies?

Which type of future climate data are available to assemble future weather files for building simulations? Is it possible to assemble future weather files that contain future heatwaves?

Summary

1.1 Humans vulnerability to heat

1.1.1 The complex relationship between extreme heat and human mortality

Many studies correlate heat-related deaths to the exterior temperature, especially during heatwaves. Because heat-related deaths depend both on the occupant's and the local built environment fabric's vulnerability, it is hard to decorrelate the two. Epidemiologists in many countries have identified different thresholds at which deaths occur, ranging from the 60th percentile in tropical areas to the 80-95th percentile in temperature regions (Armstrong et al., 2011; Gasparrini et al., 2015). Statistics also confirmed that much more deaths take place in cities than in the countryside (Armstrong et al., 2011; Besancenot, 2002). In France, mortality was correlated to day and night outdoor temperature thresholds (Pascal et al., 2013). (Laaidi et al., 2012) highlighted that elevated nighttime temperatures in cities during heatwaves have a strong influence on mortality, which was also confirmed by (Pyrgou & Santamouris, 2020).

While most research has focused on correlating excessive deaths to exterior temperatures, research is lacking to link health-heat effects to indoor temperatures. Correlating the number of deaths during heatwaves to interior temperatures is needed to estimate the exposure risk of building occupants. Indoor thresholds for heat-related morbidity are a complex function of both people and building fabric vulnerability, which is strongly dependent on location and climate. This was attempted recently in two modelling studies by (Liu et al., 2017) who used probabilistic hot summer years over current and future periods to calculate "risk to human life from overheating" in different buildings in the city of Sheffield. They used the local UK percentile defined on outdoor temperatures (93rd percentile of the summertime 2-day mean external temperature) from (Armstrong et al., 2011) and considered the same criterion for indoor temperatures. (Taylor et al., 2018) quantified mortality reductions in buildings due to efficient adaptations of buildings to heat such as upgrades in energy efficiency and windows shutters. They simulated 19,200 different buildings and calculated for each building the "temperature anomaly" (difference between the maximum temperature inside the building and the average maximum indoor temperature of all the simulated buildings), which allowed them to then calculate the temperature exposure of the residents in each dwelling type, as the sum between the maximal outdoor temperature and the building temperature anomaly. Finally, they used the mortality risk calculated by (Armstrong et al., 2011) in the West Midlands to calculate the excess mortality for different populations' age groups. Using future weather climate files, they could calculate the exposure temperatures in each dwelling and associated predicted mortalities. (Taylor et al., 2018). (Hajat et al., 2014) also calculated the predicted mortality increase due to climate change in the UK and concluded that heat-related deaths were expected to rise by about 257% by the 2050s. During previous heatwaves, and especially in 2003 in France, many deaths happened in top floor apartments, that were poorly insulated and where natural ventilation through windows was not effective (Ribéron et al., 2006), however the indoor thermal environment of these apartments is not known.

Empirical studies correlating heat stress and excessive morbidity with internal temperatures in buildings are lacking, and also practical indicators to calculate health-heat-related risk indoor from modelling studies. Furthermore, as indoor thresholds will be different depending on the population vulnerability and acclimation to heat, the investigation is complex. (Nicol et al., 2020) gathered questionnaires from people in buildings in many countries worldwide and reported different acceptable indoor temperatures thresholds depending on the countries, up to 30-35 °C in countries where occupants are acclimatized to heat. Between thermal discomfort and death, there is a wide range of thermal conditions that people experience, that present a gap in literature. The most vulnerable, under extreme heat, experience illnesses such as heat stroke and heat exhaustion, and indoor thresholds at which these occur are even less reported in the literature.

In the next section, we introduce the mechanisms of the human body that allow to adapt to heat, the most famous models that establish the basis of human thermal comfort, and different building thermal indexes to quantify thermal discomfort or indoor overheating.

1.1.2 Indoor overheating in building and thermal indexes

1.1.2.1 Background on human response to heat

According to (Hanna & Tait, 2015), acclimatization and thermoregulation determine human heat tolerance and vulnerability to heat stress, and heat response can vary greatly among individuals depending on their sensitivity.

Thermoregulation and adaptation

Humans have the ability to regulate their body temperature via physiological or behavioral thermoregulation. The range of physiological thermoregulation is very narrow given that heatstroke occurs when the body temperature reaches 40°C. Children and the elderly are more sensitive to heat, as thermoregulation is fully mature for an individual who is between 20 and 60 years old. Thermoregulation is also reduced for obese and ill people (Hanna & Tait, 2015). Behavioral thermoregulation, also called behavioral adaption, is based on perception and occurs when individuals take appropriate action to reduce their body temperature. Behavioral adaptations to heat include clothing adjustment, moving from one place to another, hydration by drinking, wetting oneself by taking a shower or being under sprayed water, and others (Hansen et al., 2011). Within buildings, behavioral adaptations can be the use of window shades, windows opening during the day to create comfort ventilation, night ventilation to cool the building envelope, the use of fans to create airflow, etc. Behavioral adaptation is also limited for people with disabilities or people that cannot move. It is known that vulnerable individuals have fewer protective factors than others, such as the elderly that can have a reduced capacity to perceive heat (Roelofsen, 2017). Because of this, they will not adapt to reduce their core body temperature, and they might also forget to drink, which will worsen heat effects. Indeed, dehydration increases the risk of heat stress since sweating is the main way the body can evacuate heat (Hansen et al., 2011).

Acclimatization

Acclimatization is when a person becomes physiologically accommodated to a new climatic environment, and therefore their heat tolerance improves. In places where temperatures are rising due to climate change and hot events are new, people are non-acclimated to heat and therefore vulnerable. People used to experience outdoor heat but relying on air-conditioning to cool themselves are also more vulnerable to hot temperatures than people used to experience heat. Health is individual to each people but the social and physical resources they are able to access are very important and has an impact on it. Exogenous factors within people's environment can be the society, institutions and community, in their capacity to help the individuals to cope with the event, or the building, in its capacity to protects the occupants.

1.1.2.2 From human thermal comfort to heat stress

Human thermal comfort is a wide area of research, that keeps evolving, as predicting human thermal response to different environmental conditions has been the interest of the research community for over a century now.

Fanger comfort model

The famous Fanger steady-state heat balance model is based on the human physiological response to its surrounding environment (Fanger, 1972). It assumes that the human body reaches thermal equilibrium, given by Equation (1) with each term outlined below.

$$H - E_{sud} - E_{diff} - E_{res} = Q = R + C \quad (1)$$

H represents the heat generated by the human body, it is expressed in W/m² and is the difference between M the metabolic rate and W the work. The metabolic rate is also expressed in met, 1 met corresponds to 58.2 W/m² of the body surface, while the body surface is calculated with the Dubois equation, it is of 1.8 m² for a standard individual. Standard activities are: 0.7-0.8 met sleeping, 1 met seating, 1.2 met light activity, and so on. Empirical studies have shown that the metabolic rate depends on human age, gender, weight, and height.

- The heat generated by the body H is evacuated outside of the body by the skin, by perspiration (E_{diff}) and sudation (E_{sud}) and by the sensible and latent respiratory exchanges (E_{res})
- This heat is equal to the heat transfer from the skin to the exterior surface of the clothing Q
- This heat is equal to what is absorbed by the environment, by convection (C) and by radiation (R)

Fanger comfort model assumes that the degree of discomfort depends on the thermal load, which is defined as the difference between the heat produced by the body and the one lost to the environment. It assumes that when the thermal load is null, thermal neutrality is reached. The thermal sensation recorded from around 1200 individuals in climatic chambers allowed to derive equations to evaluate the difference from thermal neutrality and to derive

the famous comfort index predicted mean vote (PMV). It is assumed that thermal comfort is a physiological response related to the interactions of six parameters: air temperature, mean radiation temperature, relative humidity, air velocity, metabolic rate and clothing insulation. Using these six parameters, it is possible to calculate the PMV and associated percentage of dissatisfied people (PPD). This comfort model is implemented in the standard ISO 7730 (ISO, 2005). However, empirical studies in free-running buildings have demonstrated significant differences between monitored data and PMV predictions (Brager and de Dear, 1998; Humphreys, 1976), which was partially explained by the fact that Fanger comfort model does not fully account for occupants adaptions.

Adaptive comfort models

In contrast to Fanger empirical studies in climatic chambers, the adaptive comfort models use data from free-running buildings. Since the buildings are not conditioned, people sensation to heat is different than in climatic chambers, and they will tend to adapt. Adaptation is done both via personal and environmental adjustments: Personal adjustments include removing clothing, changing activity levels, moving to a different location, taking showers; while environmental adjustments include for instance the use of solar shading or curtains, turning on fans, opening/closing windows, or reducing internal heat gains. The difference with the steady-state model of Fanger is that it defines a range of acceptable indoor temperatures within which occupants can find thermal comfort via dynamic thermal adjustments, given they have sufficient adaptive opportunities. From analyzing more than ten thousand field-studies data, it was found that the range of comfort temperatures was much larger than the one predicted by Fanger, and a linear correlation between indoor and outdoor air temperature was found.

The adaptive comfort models have been implemented in the ASHRAE Standard 55 and in the European Standard EN 15251, and they are today widely-used for overheating assessments in free-running buildings. The acceptable indoor temperatures from ASHRAE Standard 55 and European Standard EN 15251 are presented in Figure 6. The upper temperatures between the two standards differ mostly because they are from different databases (ASHRAE is worldwide while EN 15251 is from European measurements), and because EN 15251 can be applied to mixed-mode buildings while ASHRAE 55 cannot. In EN 15251, three categories differ in comfort levels expectations: Category I is a high level of expectation, recommended for spaces occupied by vulnerable people. Category II is a normal level of expectation, for new or renovated buildings, and Category III is an "acceptable" level of expectation for existing buildings. We can observe that the acceptable indoor operative temperature goes above 32 °C with the use of ceiling fan, in category III of the norm EN 15251.

In France, the adaptive comfort model EN 15251 has been recently included in the most recent thermal regulation RE-2020. The upper acceptable indoor temperature during daytime is the one given by the EN 15251 Category I, which can be increased by the presence of increased air velocity or a diminution of relative humidity. The adaptive comfort is applicable when the running mean temperature T_{rm} is above 16 °C. During nighttime, it is assumed that no adaptations occur and it is set to a fixed threshold such as a cooling set-point, which is of 26 °C in residential dwellings. The summer thermal discomfort is counted in degree-hours above this threshold.

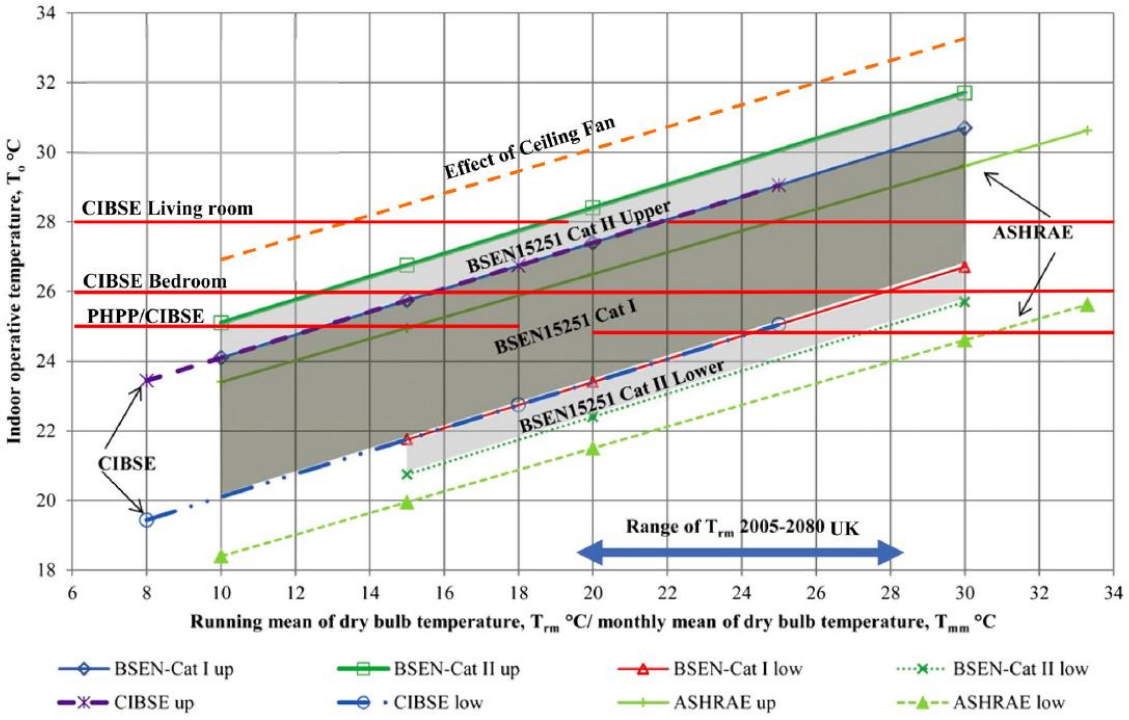

Figure 6 - Adaptive thermal comfort and indoor overheating criteria from (Lomas & Porritt, 2017)

Physiological comfort models

Different thermophysiological models have been developed, from simple to more complex models with different levels of characterization, and they have been reviewed recently by (Katić et al., 2016). Single segment and multi-segments approaches exist, here we detail only the famous single segment model developed by (Gagge et al., 1972), as a more detailed model is not needed in the scope of the Ph.D. thesis. Gagge model represents the human body in two nodes: the body (or "core") and skin temperatures (Gagge et al., 1986).

The comfort model is also based on the heat balance equation but the difference with Fanger model is that it is transient and not steady-state. Indeed, the metabolism is regulated by the body actions (sweating, perspiration) that evolve over time. Two heat balance equations are used to calculate the evolution of the body and skin temperatures, which are composed of the same variables as in Fanger's comfort model, plus a variable accounting for the transient conditions, the heat storage inside the body.

From the Gagge comfort model, the Standard Effective Temperature (SET) could be calculated, it is defined as the operative temperature of a hypothetical reference isothermal environment at 50 % relative humidity in which a human subject, wearing standardized clothing for a specific activity, would have the same skin wetness and heat exchange at the skin surface that he would have in the actual environment. From the dry-bulb and radiant temperatures in the environment, relative humidity and air velocity, the core and skin temperatures can be calculated, resulting in the equivalent SET (Gagge et al., 1986). Thermal sensations and physiological states have been attributed to different categories of SET, which ranges from thermal comfort to heat stroke (Table 1). Other heat stress indexes exist, such as

the wet-bulb globe temperature (WBGT), predicted heat strain (PHS) or Heat Index. However, the scale of the SET allows to describe a wide variety of indoor environments and interpret various thermal sensations from neutral to heat stress (cold thermal discomfort is not presented here), allowing to assess thermal comfort, discomfort, heat stress or heat strain with the same thermal index.

Table 1 - Quantitative thermal sensation scale of the SET index (Nishi & Gagge, 1977)

SET (°C)	Thermal Sensation	Physiological state
> 37.5	Very hot, very uncomfortable	Failure of thermoregulation
34.5 – 37.5	Hot, very unacceptable	Profuse sweating
30.0 - 34.5	Warm, uncomfortable, unacceptable	Sweating
25.6 - 30	Slightly warm, slightly unacceptable	Slight sweating, vasodilation
22.2 – 25.6	Comfortable and acceptable	Neutrality

1.1.2.3 Criteria for quantifying indoor overheating in buildings

The transition from thermal comfort to thermal discomfort is not straightforward and depends highly on the occupant's vulnerability. The term "indoor overheating" is somewhat different as it refers to the building itself rather than to the building occupants, and leads to question the building's vulnerability. While indoor overheating is strongly linked to thermal comfort since it is usually quantified from thresholds derived from comfort models, it does not distinguish thermal discomfort, heat stress and heat strain, but rather generally designates a building that has failed to maintain acceptable thermal conditions. Because it is highly dependent on the building's characteristics and on the local climate, a definition for indoor overheating has not reached consensus over the research community (Lomas & Porritt, 2017).

In order to quantify indoor overheating in buildings, it is necessary to define:

- The variable used to assess indoor overheating (is it a comfort vote, a fixed temperature, an adaptive temperature, a mean daily temperature?)
- The threshold of this variable from which indoor overheating occurs (usually, comfort models are used to define this threshold and it depends on the occupant's vulnerability);
- A metric to quantify the indoor overheating.

Usually, researchers use comfort metrics to relate indoor overheating with human thermal comfort or discomfort. While some authors use the PMV indexes to attribute thermal comfort, more and more authors are calculating threshold temperatures based on the adaptive comfort models and quantifying temperatures above. Regarding the metric used, many studies attribute indoor overheating to a sum of degree hours above a certain threshold, calculated from thermal comfort models or as a static indoor operative temperature. However, this aggregated measure above a certain threshold does not allow to distinguish if the temperature is highly above the threshold for a short period of time, or slightly above the threshold for a prolonged period of time. This allows to quantify the building indoor overheating in a simple aggregated metric, however it does not allow to relate this indoor overheating with the thermal risk put on the building occupants, as it is not known if occupants are subject to consecutive days of heat exposure. Analyzing the building occupant's

vulnerability to indoor overheating, and especially the health-heat-related risk during heatwaves requires more detailed indexes, lacking today in the literature.

While in France historically punctual hot temperatures did not require detailed overheating assessment, the dangerous projected heatwaves occurrence reinforces the need to assess the health risk of building occupants, especially of the most vulnerable. Developing indicators to assess indoor overheating during heatwaves is relatively new. Recently, (Gondian et al., 2019) used two indicators to assess the building thermal performance: A resistance indicator, which quantifies the "intensity" of a high indoor temperature, and a resilience indicator, which quantifies the duration of the indoor temperature above a certain threshold. The two indicators bring two different information on the building response during a heatwave, which can after then allow interpretation on human potential heat stress. (Laouadi et al., 2020) developed a methodology to evaluate overheating in buildings, based on the detection of indoor overheating events with daytime and nighttime thresholds specific for vulnerable people during heatwave periods. Their work allows to assess the building occupant's vulnerability to extreme heat during a prolonged period of consecutive days, and therefore to derive the potential health-heat-related risk.

Within buildings, human's vulnerability to heat is a function of both human heat tolerance and building fabric vulnerability. Human heat tolerance depends on their physiological thermoregulation, possibilities for adaptation to heat, and heat acclimatization. However, during heatwaves the people more at risk are the most vulnerable: non-acclimatized to heat, with limited adaptation opportunities, and/or with reduced thermoregulation abilities (Vellei et al., 2017; Itani et al., 2020). Most heatwave deaths occur in buildings and are driven both by the indoor conditions, the environment around the building, and the adaptive opportunities of building occupants. In order to decrease the heat time exposure to buildings occupants, the built fabric must be adapted to heat. Analyzing the building response under future heatwaves conditions will allow to increase the building resilience to future heat events, via the combination of various strategies (building envelope and architecture modifications, implementing low energy or passive cooling systems, educating people on how to adapt to heat inside buildings via the use of shades, natural ventilation, etc.).

The next section introduces the state of the art of the different passive cooling strategies and systems that can be used to increase the building resilience to indoor overheating, thus decreasing the exposure to indoor heat for building occupants. In contrast to traditional air-conditioning that ensures maintaining safe conditions independent on the outdoor weather and in most extreme climatic conditions (given that the building is powered with electricity), most passive cooling solutions, as they function using the local climate advantages are limited in their potential. This state of the art aims to investigate each of these possible alternative solutions to energy consuming air-conditioning, balancing the risk between mitigation (reduced heating and cooling energy needs) and adaptation (reduced heat-related health impacts) to climate change.

1.2 Passive cooling strategies to increase building resilience to indoor overheating

Historically, buildings have been designed to respond to a certain known and predetermined set of climatic conditions. However, the climate is today changing and will continue to change, which induces both the need to plan and adapt to warming temperatures and the need to prepare for uncertain and changing climatic conditions. With climate change and the increased heatwaves occurrence and risk, a change of paradigm is necessary as the cooling requirements might be higher than the heating requirements in future French climate. Therefore, this review is inspired by bioclimatic architecture in warm climates, targeted to the summer period.

In this section, we introduce several design propositions, strategies and systems that act on one hand as adaptation measures to increase the building resilience to heat, and on the other hand as mitigation measures as they do not consume or very little energy. These strategies include bioclimatic architecture, the prevention of solar heat gains, or passive cooling solutions. Some of these strategies do not impact the winter design as they apply only to the summer period, some benefit both for winter and summer design, while some others are in concurrence with the winter period. These are evaluated in details.

We start by introducing the role that bioclimatic architecture has to play in the building design. In recent years, the term of bioclimatic architecture in France has been used to design buildings for the winter, therefore buildings that are passively heated. In this review we analyze bioclimatic architecture from a summer point of view. In a second part, we introduce new developments in glazing and opaque materials to reduce solar heat gains on the building fabric. Research and developments are strong in this sector and new innovative materials are under development in different fields. Finally, we present various "almost" passive cooling technologies and systems to cool the air. These include traditional techniques like natural ventilation and ground cooling, and the most recent promising developments in evaporative cooling and radiative cooling.

1.2.1 Bioclimatic architecture

Initially, architecture's goal was to protect man from the outdoor environment. In early settlements, the so-called vernacular architecture was employed, determining the building practices via cultural traditions, local climate, and available raw materials. While these traditional architectures were well established, the industrial revolution totally changed the way buildings were designed and constructed. Buildings became much more isolated to the outdoor environment, with systems supplied by intensive "infinite" energy, forgetting basic principles of bioclimatic architecture. In parallel, comfort requirements increased and the building role is today not only to protect from the outdoors, but also to guarantee comfortable, healthy and pleasant indoor environments.

With climate change concerns in recent decades, the concept of sustainability became popular which led to a resurgence of bioclimatic architecture. The Greek roots of the word bioclimatic are « bio » (life) and climatic (climate), and bioclimatic architecture's goal is to link the human to the exterior climate. For this purpose, bioclimatic architecture takes advantage of the local conditions, using the surrounding microclimate to enhance life inside the building via different strategies such as natural lighting, visual, sensorial and thermal comfort, etc. A well-designed bioclimatic building must be able to ensure comfortable indoor conditions all year, along the seasons, with minimum energy needs. Hence, depending on the climate, the building must meet both winter and summer requirements, which are often opposed and increase the design complexity in temperate climates. A more in-depth concept, linking the buildings to the surrounding environment even further is biomimetic architecture, which takes inspiration of designs that exist in nature to better connect buildings to their natural environment. One recent example of this type of architecture is the commercial building Eastgate center in Zimbabwe from the famous architect Mike Pearce, which relies on natural ventilation to provide passive cooling with a design inspired from the termite animals' natural habitat (Figure 7). This building is one innovative demonstration of how simple principles of bioclimatic architecture can drastically reduce or replace the need of cooling in modern buildings (Cabeza & Chàfer, 2020). Other architects have included bioclimatic practices in their building design, such as Alvar Aalto. Many architectural features influence the indoor thermal conditions, they are: the building's layout or morphology (i.e compactness), its orientation considering the sun path and the winds direction, the size and location of windows, their shading condition, etc. These features have been extensively studies, and summarized in (Olgay, 1963) and (Givoni, 1998).

Figure 7 - Eastgate center (left) and ventilation principles based on termite mound (right) (Okeke et al., 2019)

Several strategies exist in bioclimatic architecture to maintain cool indoor environments during the summer period, they consist in dampening outdoor climatic variations, reducing the solar heat gains on the buildings, storing the heat in the building structure, or evacuating the heat. In order to dampen the outdoor climatic variations, and reduce both heating and cooling loads, the building morphology has a key impact. Recently in France, "compact" buildings (small wall to floor surface area) have been recognized as energy efficient since they limit the heat losses during winter. However, is this strategy still efficient for a bioclimatic architecture functional during the summer period? Buffer spaces, such as traditional verandas, patios, porches, atriums or open spaces, allow to isolate the indoor space from the exterior through a non-conditioned volume. Both in winter and summer, outside conditions are dampened through these buffer spaces before they reach the building. Buffer spaces were mostly used in ancient buildings, but in recent building practices, due to space constraints in city, they are often not considered, even though they can be very efficient to dampen the outdoor air temperature. Buffer spaces, or "semi-attached" spaces, if linked to the interior rooms by windows or doors, can efficiently be operated: partitions must be closed in winter and during the summer day hours, while open during summer nights (Givoni, 1998).

Another key strategy to limit the heat loads is the building and windows orientation, though in an urban context it is not always possible to choose. The presence of surrounding buildings can be beneficial (i.e by creating shadows) or non-beneficial (i.e increased solar heat gains due to high albedo or reduced wind speeds, etc.). The orientation does not only influence the solar heat gains received on the building, but also the wind potential for natural ventilation and therefore these two points must be considered together (Givoni, 1998). In France, in summer, the solar irradiance is maximum on the East façade (morning sun) and on the West façade (afternoon sun). A small amount of direct beam radiation reaches the North façade on early morning and early evenings, while it reaches the south façade around mid-day. In winter, the solar radiation is at its maximum on the South façade. If possible, when designing a building, these must be considered, in parallel to the wind directions and windows openings. Strong irradiance on West windows in summer have been correlated to high values of outdoor temperatures, therefore, care should be taken with this window orientation (M. Santamouris et al., 2007). Beyond the windows orientation, the windows size is subject to debate, as while they contribute to decrease the heating needs in winter if orientated south, they can contribute to increase cooling needs or summer thermal discomfort if no appropriate solar control is used.

Storing the heat in the building thermal mass is another well-known strategy. Indeed, in hot and dry climates, it is common to design buildings with high thermal mass, allowing to both dampen and time shift outdoor temperatures variations. In France, traditional houses were made of massive stone with low glazing ratio, allowing to keep the interior of the house cool even on hot days. In the last decades in France, the building envelope has been given a lot of attention, especially in regards to insulation. Indeed, it has a key role in being the protective barrier from the environment. If designed well, it can lead to a reduction in both heating and cooling needs, as emphasized by (Fosas et al., 2018). The building envelope must be thought of at the early stage of the building design, in parallel with the building morphology. This is detailed more in section 1.2.3. To reduce the heating loads, additional strategies such as covering walls with plants, or adding a layer of whitewash paint on walls and roofs is an ancient technique of Mediterranean cities, this is detailed in section 1.2.2.

Finally, the last strategy is to evacuate the heat. In bioclimatic architecture this can be achieved via natural ventilation. The windows placement has a great impact on the natural ventilation potential, as according to (Givoni, 1994), cross flow ventilation will induce at least two to three times higher average and maximal air flow rates than single-sided design. Cross-flow ventilation can be created with windows on adjacent or opposed facades (Olgay, 1963). Furthermore, Givoni also observed that when the airflow changes direction inside a room, the design is better: A study in Israël demonstrated that when windows are on opposite facades, the air flow will go straight inside the room, therefore the corners of the room will only be little affected by the air flow. However, when the air flow is forced at 45 °C with windows on adjacent facades, the air moves around the room and along the walls before exiting by the adjacent window. In this configuration, it is better when the wind faces the window with a 90 °C angle. However, in case of cross ventilation, the windows on opposite facades must be of the same size, or the "exit" windows of the air must be larger, but not the opposite effect. The window height is also important, as windows placed above the occupant's height will only provide little effect of comfort ventilation. Finally, the windows size is also important, as larger windows will induce larger airflows, but induces higher solar heat gains if not protected appropriately. Many designs to enhance natural ventilation exist, such as wind towers, solar chimneys, atriums, or double skin facades. In order to enhance stack pressure, the "entering" openings must be placed down a façade, while the "exiting" openings should be placed towards the façade top, that the air moves up while enhancing cross ventilation. Atriums are good design to enhance stack pressure. Many design guidelines for windows to enhance natural ventilation have been given in (Allard, 1998; O'Donovan, 2018). The windows size, their orientation according to winds, their height to account for stack effects, and if the design is single-sided or cross flow greatly affect the building natural ventilation potential. Therefore, these need to be well-thought in the early design stages. Natural ventilation is introduced more in depth in section 1.2.4.1. In the next sections, each principle for summer design is illustrated more in detail via different strategies. We examine the limits of these passive solutions in regards to the climatic variations, and in contrast with the winter design.

1.2.2 **Preventing solar heat gains**

The solar spectrum is first introduced here, to understand how to design glazed or opaque materials targeted to block specific wave-lengths of the electromagnetic spectrum, depending on the climate. The incoming sun radiation is from 0.25 to 2.5 μm, it includes ultraviolet (0.25 – 0.38 μm), visible light (0.38 – 0.78 μm) and near infrared wavelengths (0.78 - 2.5 μm). On the opposite, the outgoing radiation from the earth is in the infrared (2.5 – 70 μm). Part of the incoming and outgoing energy is absorbed by the atmosphere, which is shown in Figure 8. Therefore, most of the incoming radiation from the sun is in the visible (48%) and near-infrared (46%), while most of the outgoing radiation reaching the dark atmosphere occurs in the atmospheric windows, around 8-13 μm (Santamouris et al., 2007).

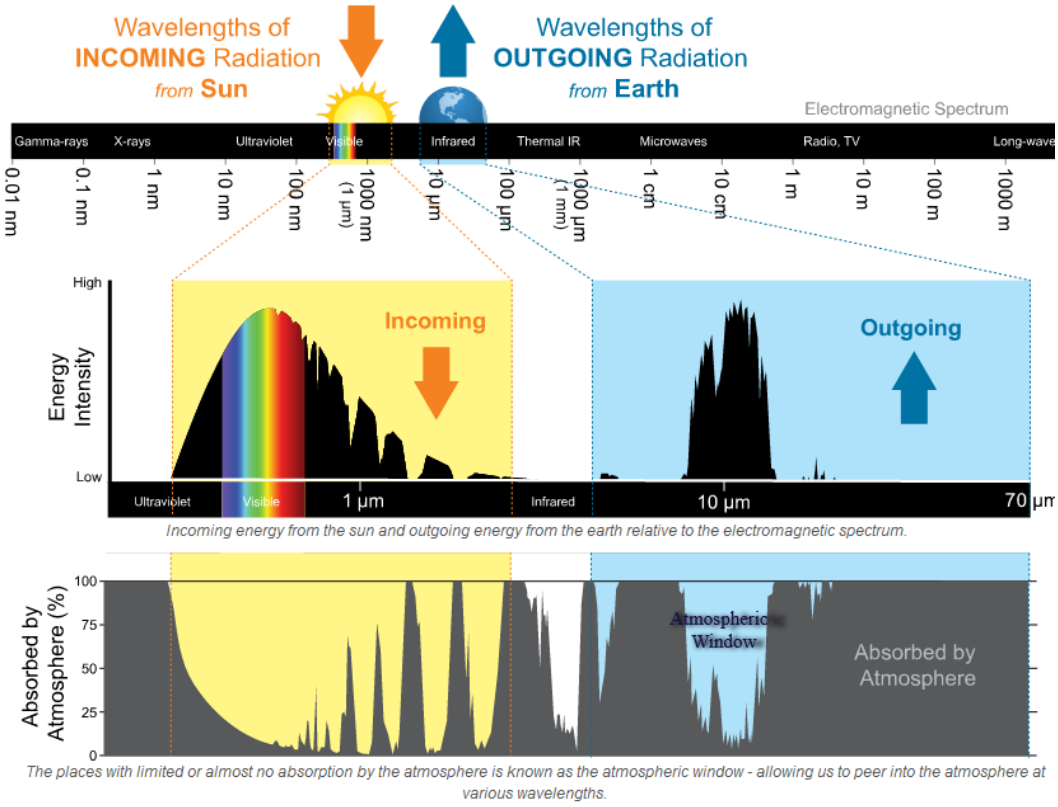

Figure 8 – Incoming and outgoing radiation (National Weather Service, 2020)

1.2.2.1 Glazed surfaces: windows and shading

Glazing properties

While in the summer new highly-insulated and airtight buildings with large windows tend to overheat, they are recommended to benefit from passive solar heat gains during the winter. In France, a subtle balance has to be found between the two, while daylighting and visual comfort also need to be considered as it is a key aspect for building users. According to (McLeod et al., 2013) who conducted a recent study about the tendency of PassivHaus to overheat in the future British climate, the glazing percentage and shading control are two of the most important design parameters to optimize to mitigate overheating risks. While the PassivHaus standard was initially designed for the temperate climate of Germany with mostly heating needs, this study reinforces the need to adapt the building design to future warmer summers. According to (Long & Ye, 2014), the "perfect window" has opposite properties depending on winter and summer requirements. In winter, it is ideal if all solar and long-wave radiation enters the building, while the long-wave radiation emitted from the interior equipment remains inside. During summer, the requirements are opposite, as it is desired that all radiation is blocked or transferred towards the outdoor, allowing only rays of the visible spectrum to enter the building (Figure 9).

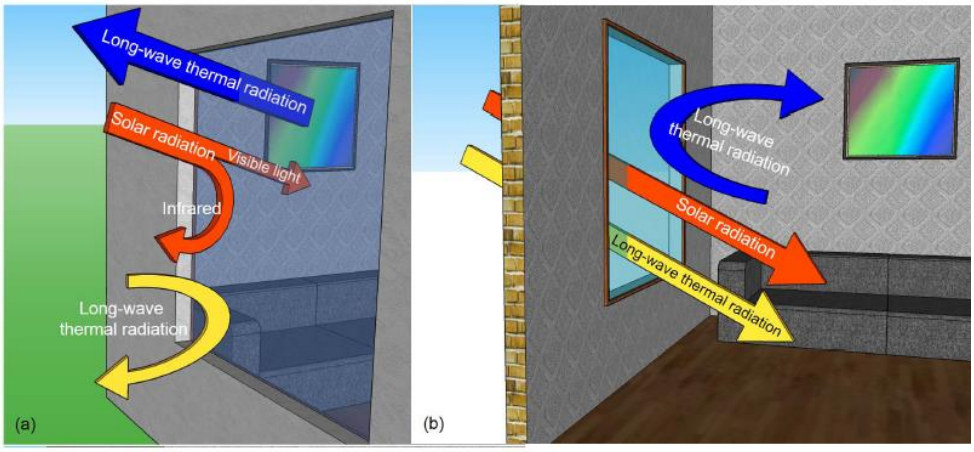

Figure 9 the "perfect window" depending on summer (a) and winter (b), from (Long & Ye, 2014).

These properties can almost be achieved with low emissivity glazing. For winter design, for a double plane window, the low emissivity coating should be placed on the exterior of the interior glass. However, the summer design it is the opposite and the coating must be placed on the interior of the exterior glass. This is illustrated in Figure 10.

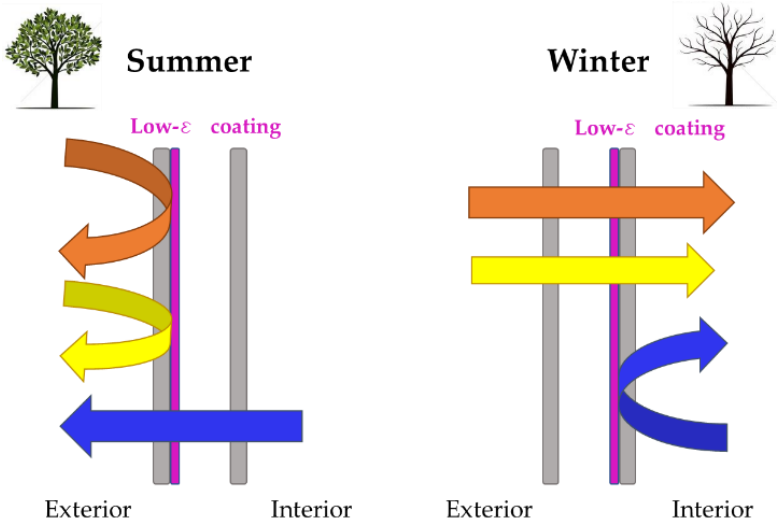

Figure 10 – Ideal low emissivity coating placement depending on season requirements

These properties can also be achieved with advanced glazing: passive smart glazing technologies (thermochromic and photochromic windows) and active smart glazing technologies (electrochromic and gasochromic windows) allow to dynamically control the windows characteristics. The most developed ones are thermochromic and electrochromic glazing, they are presented here. Thermochromic windows regulate the solar transmittance of the glass, according to its temperature, they have the advantage to be passive, require only a single layer of coating and are easy to manufacture. Building simulations showed that they can decrease the cooling energy consumption by 81.7 % compared to single glazing and 70.5 % compared to low-e glazing (Aburas et al., 2019). Thermochromic windows should be made from materials that adapt their solar absorption according to the temperature, because some high absorption materials have shown to actually increase the solar heat gains by thermal

radiation and convection when the temperature is elevated (Long & Ye, 2014). These windows have the advantage to increase the daylight illuminance inside the building in comparison to classic shading. However, as the window thermal properties are controlled directly by the sun and not by the users, their acceptability can be very low. In the winter period, they can behave poorly, limiting wanted solar heating gains. Finally, their cost (around 370 €/m²) is also a drawback to their penetration in residential buildings (Long & Ye, 2014). The alternative well-developed and advanced glazing technology is the electrochromic window (EC), which actively controls the amount of solar radiation passing through the glass using a low voltage electric current. This time, the building occupant has full control over the window properties. A potential difference (DC voltage between 0 and 5 V) is applied between two electrodes which provokes a change in the coating optical properties (transmissivity, reflectivity and absorptivity). (Tavares et al., 2014) conducted building simulations comparing single, double and EC glazing in Portugal and could observe that EC was most advantageous to reduce energy consumption compared to single glazing when located on the West (up to 35 % decrease) or East façade (up to 25 % decrease). On the south façade, EC glazing did not prove to be more advantageous than double glazing, as it contributed to an increase in heating consumption in the winter. Electrochromic glazing exists on the French market, such as the SageGlass manufactured by Saint Gobain. However, it is mostly implemented in office buildings due to its elevated cost. For these reasons, the implementation of advanced glazing is limited in residential buildings, in which solar shading is generally used to protect from solar gains. A complete review on advanced glazing technologies has been done in the Chapter "solar control" (Santamouris et al., 2007).

Window integrated shadings

Buildings with large glazed areas need to use proper solar shading during the summer to reduce potential indoor overheating. Different types of shadings exist, from external permanent shading such as overhangs and sidefins, to roller shutters, venetian blinds, curtains, etc. A fine balance is to be found between blocking the sun rays and allowing daylighting and view to the outside from within a house. External shutters are very effective to block solar heat gains, while they can also be used during winter nights. In the south of France, it is a traditional practice to keep the external shutters closed all days to prevent the house to overheat. Alternatively, light-colored external shutters allow daylight to enter the indoor space, or aesthetic designs such as the traditional moucharabieh stop the sun while allowing light to penetrate the building resulting in aesthetically pleasing light patterns. The *Institut du monde arabe* cultural building in Paris showcases moucharabieh on its entire façade. It is possible to control their opening percentage according to the different building uses (Figure 11). (Alawadhi, 2018) measured an illuminance level of 200 lux and a reduction in heat flow through the window up to 52 % for different solar screens inspired from the moucharabieh design in Kuwait. Traditional Italian louvered shutters have also inspired the most recent *jalousies*, which are windows with adjustable strips to regulate both incoming radiation and airflow. These have been used in humid areas of the United States to aerate the house while preventing rain. Today, in France the most recent are integrated into the window structure, allowing to ventilate the building naturally without security concerns.

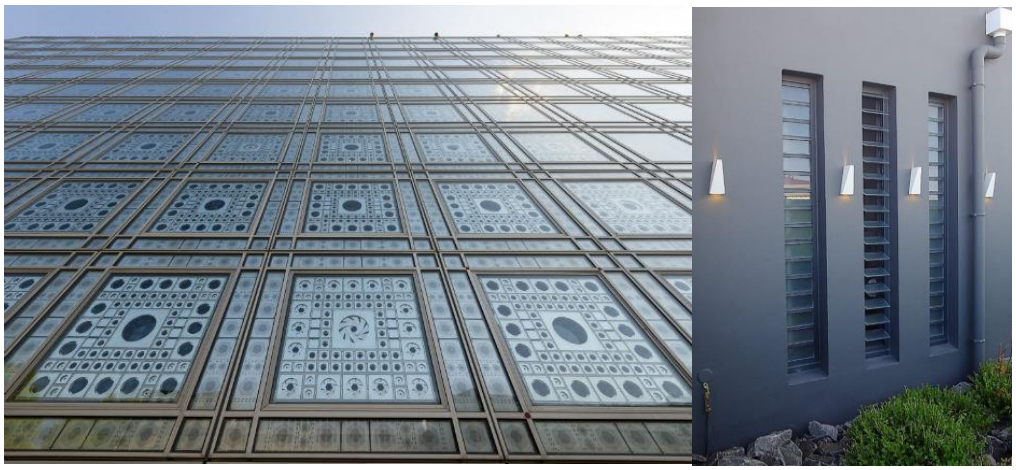

Figure 11 - Window integrated shadings –left: moucharabieh (Institut du monde arabe – Rambaud, 2018) and right: *jalousies* (Savima, 2020)

Mechanical shading devices (interior & exterior)

Internal shading devices, such as venetian blinds or curtains, are also helpful to block the light, however once the sun hits the shading device, the solar heat gains have already entered the building envelope. For this reason, external shading devices are much more effective to reduce incoming solar heat gains (Figure 12). As these are mechanically controlled by the user, they are an effective strategy to reduce solar heat gains without decreasing the winter solar gains (given that they are used appropriately).

Figure 12 - Interior (left) vs. Exterior (right) shading devices

Fixed shading devices (Overhangs and sidefins)

According to (Givoni, 1994), in the Northern hemisphere, the most appropriate shading on the South façade is a horizontal overhang to provide shading during midsummer while allowing solar gains in the winter. On the opposite side, in the North facade, shading must be provided from vertical sidefins, to protect the windows from the summer morning and night sun hours (Figure 13). Givoni argues that windows located on East & West facades must be protected from both overhang and sidefins, while horizontal overhangs are more beneficial than vertical sidefins only. Even though these shadings are very efficient to protect windows, they are usually dictated by architectural and aesthetic concerns. A more flexible alternative (or addition) is the exterior mechanical shading devices.

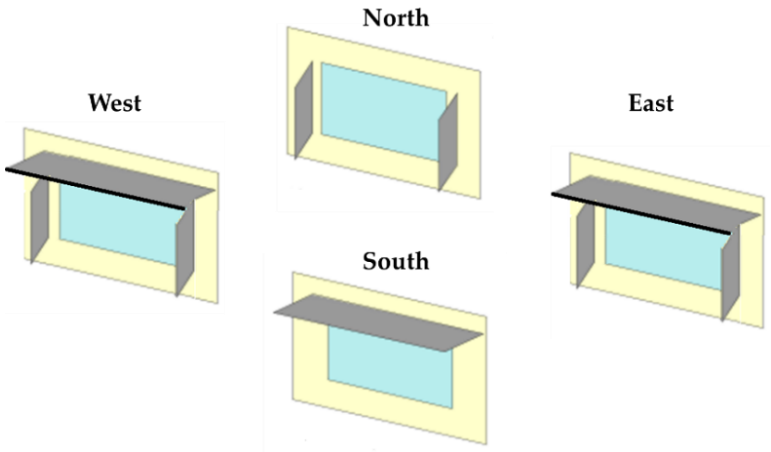

Figure 13 - Overhang and sidefins depending on the façade orientation in the Northern hemisphere, according to (Givoni, 1994)

1.2.2.2 Opaque surfaces

While glazed surfaces are a direct entry point for the sun rays, opaque surfaces also receive a large amount of solar radiation and must be treated accordingly. The roof is the building component that is most exposed to solar radiation, and its outermost surface can reach quite elevated temperatures under the sun, resulting in indoor overheating especially for poorly insulated buildings. During the 2003 heatwave, Parisian apartments under non-insulated zinc roofs of dark color overheated greatly (Vandentorren et al., 2006; Ribéron et al., 2006). Different passive roof designs exist to protect the roof, we present here cool roofs, and more generally cool selective materials that can also be located on walls, and green roofs (Figure 14). Roof ponds are also a passive strategy, they are investigated in the section 1.2.4.4. There exist also open roof ponds, which usually cool down the roof structure by water evaporation during the day. An extensive review of roof ponds was made by (Sharifi & Yamagata, 2015).

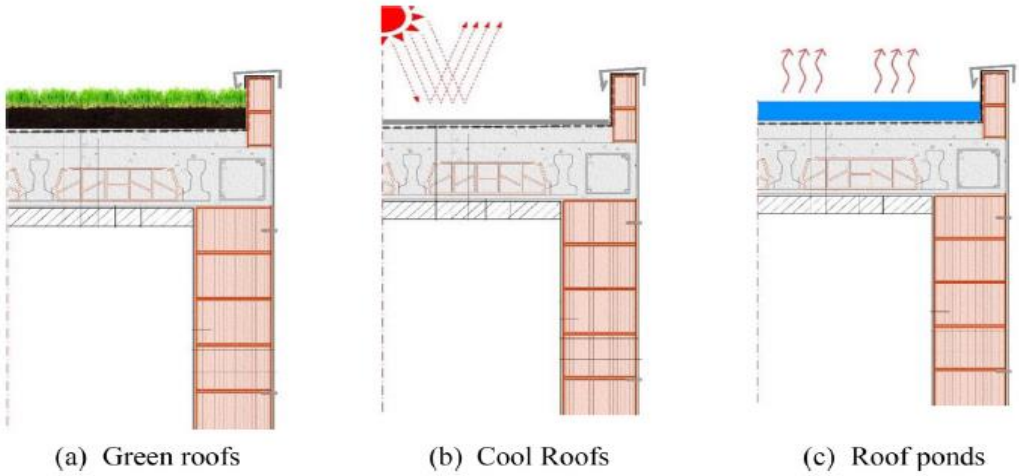

Figure 14 - Passive roof technologies from (Cabeza & Chàfer, 2020)

Cool selective materials

According to (Givoni, 1994), above an exterior temperature of 32 °C, not only insulation is necessary to reduce the heat transfer from outdoor to indoor, but also some kind of reflective coating that should regulate the amount of sun absorbed, and the amount of longwave radiation emitted towards the sky. The most ancient and traditional technique was the use of whitewash paint, which has been used to a large extent in the South of France and other Mediterranean cities, especially in Greece and Southern Spain. This paint is a cool selective material, with a high albedo that reflects the sun, consequently reducing the incoming solar heat gains on the building roof and facades. The albedo value is calculated as an integral over the solar spectrum which means that to achieve the highest value, the reflexivity coefficient has to be elevated in the UV, in the visible and in the near-infrared wavelengths. Cool roofs have proven to considerably reduce the cooling loads in regions with warm summers. In Iraklion, Crete, a 27 % energy saving was achieved using cool paint with a reflectivity coefficient $r = 0.89$ (Kolokotsa et al., 2012). In Catania, Italy, on the hottest day of the year, the roof temperature was decreased from 60 °C down to 30 °C and the cooling peak load reduced by 44 % with a paint of $r = 0.85$ (Costanzo et al., 2013). Because of architectural constraints, it is not always possible to use white as a color for the building's exterior coatings. To solve this constraint, materials with an elevated albedo only in the near-infrared (780 - 2500 nm) have been developed, allowing the materials to keep their color. These paints are today available on the market and can be a very cost-efficient solution in a refurbishment context. The most recent developments are fluorescent paints, which maintain the visual properties, reflect the sun in the near-infrared wavelength and in addition reemit the sun by fluorescence. The albedo value of 0.2 for a roof painted in dark red could be improved to 0.41 with selective dark red paint, and up to 0.64 for fluorescent paint (Berdahl et al., 2016; Levinson et al., 2007).

Selective cool materials have proven to be very efficient to reduce air-conditioning consumption or summer overheating, especially for buildings with no or low insulation on the roof. In free-running buildings, the interior roof surface temperature can be greatly reduced, indirectly reducing the air and operative temperature. However, the effectiveness of cool roofs decreases with the increasing roof R-value (Lapisa, 2016). Furthermore, as in collective buildings, the selective cool paint applied on the roof mostly impacts the top dwelling, cool paints are usually also applied to walls, which is also a strategy to counterbalance the urban heat island effect (Gros et al., 2014). However, a downward effect can occur with inter-reflections in between walls in an urban canyon: A wall without selective cool paint facing one could then absorb the reflected solar radiation (Doya et al., 2012). This effect can be avoided with the use of retroreflective materials (Rossi et al., 2015). In his Ph.D. thesis, Kyriakodis found that inter-reflections in between walls could actually benefit moderate climates, as they resulted in heating needs reduction during the winter.

In temperate climates, such as in France, a selective cool material is desired only during the summer period, given that in the winter the solar gains reduce the building heating needs. To counterbalance this effect, it is possible to use the selective coating on an inclined portion of the roof that will receive the sun only during the summer (so called "hybrid cool roof") (Bozonnet et al., 2019). Another promising adaptation of selective cool materials is thermochromic materials, whose properties change with the temperature. Thermochromic materials based on dyes have received a lot of attention in recent years but have aging issues

in outdoor applications. Other new innovative thermochromic materials, are currently under development: Instead of dyes they use molecular rearrangement or nanoscale optical effects to change their properties, they are quantum dots, plasmonic, photonic crystals, conjugated polymers, Schiff bases, and liquid crystals (Garshasbi & Santamouris, 2019). These materials are cutting-edge research but have not been tested yet at the building scale, at the moment they are still at an elevated cost. (Fabiani et al., 2019) have experimentally tested and modelled thermochromic materials based on leuco-dyes for the city of Princeton in the United States (climate zone ASHRAE 4A, such as Paris). They concluded that compared to a dark roof and cool roof, the thermochromic roof would offset almost as much cooling needs in the summer, while not increasing the heating needs in winter for an optimized transition temperature of 25 °C. These results suggest promising applications for thermochromic materials, given that their aging issues are resolved and cost lowered.

Further than reflecting the solar radiation, the cooling of a material can be achieved via its outgoing longwave radiation. It is based on its potential to dissipate heat towards the cool atmosphere. Terrestrial structures emit in the atmospheric window (8-13 μm) while absorbing in the shortwave and longwave radiation outside of that window. The window is almost transparent to infrared radiation, given that the atmosphere is dry. Using this cooling potential has been researched for more than a century, and cooling structures have been built with a very high emissivity to radiate in a continuous broadband. The recent development of nanotechnologies allowed the manipulation of the spectral and angular selective properties of materials to emit energy only at specific wavelengths. This reduced band makes the emitted energy within the atmospheric window much higher than classic structures, resulting in a net balance between the radiation emitted and the one absorbed, even under strong solar radiation (Lu et al., 2016). Therefore, sub-ambient temperatures can be achieved, lower than those attainable by a blackbody. This daytime radiative cooling potential is very promising, as the cooling demand is most prominent during the day. Different types of materials are currently under investigation (multilayer thin films, polymer foils, pigmented paint films, silicon-based coatings on metal surfaces, photonic crystals) for which comprehensive reviews have been made by (Santamouris and Feng, 2018; Vall and Castell, 2017). Experimentations usually include using these materials not only as a coating for buildings, but as a radiative cooling device that can provide cooling to the building via the means of air or water (Raman et al., 2014). These various prototypes will be introduced in section 1.2.4.4 on radiative cooling.

Green roofs & walls

The use of plants is a strategy that can provide shading (trees exterior to the buildings), limit heat penetration through roofs and walls, and provide some local cooling via evapotranspiration of the plants given that water is supplied. Different types of green roofs exist, they are extensive, intensive, or semi-intensive, differentiated by the type of plants section of the green roof, the plant layer height and weight, and the level of maintenance they require. Over the last decades in Europe and in North America, the green roof has been a subject intensively researched and their design is now implemented in standards (Raji et al., 2015), which has resulted in a large supply of manufacturers. (Feng et al., 2010) found that 58.4 % of the heat gained by an extensive green roof is released via evapotranspiration, while (Lazzarin et al., 2005) found that 60 % of the incoming heat gains were either absorbed or reflected by the green roof. When the green roof was wet, they found that the heat flux through

the roof was outgoing due to the evapotranspiration of plants, confirming the cooling potential of this strategy. Regarding energy consumption, (Ascione et al., 2013) modelled a building with a green roof in Spain and in Italy, and concluded that it could contribute to reducing the annual primary energy demand by 8-11 %. (Niachou et al., 2001) found out that the monthly cooling load of a nursery building in the Mediterranean could be reduced between 6-33 %, and the top floor by 12-76 % compared to an insulated roof. (Jaffal et al., 2012) found that green roofs could reduce the cooling demand by 52 % in Athens and by 96 % in La Rochelle. While roof temperatures are usually around 60 °C in summer, many studies have reported a temperature of around 30 °C for green roofs, which leads to an indoor temperature reduction of around 2 °C in unconditioned buildings (Jaffal et al., 2012). Regarding green walls, (Djedjig et al., 2013) have developed a model for green walls in TRNSYS, and modelled a building with two green walls in Athens, concluding that for this case study, the cooling load was reduced by 33-37 % with the use of the green facades. Besides decreasing energy consumption, green roofs have many benefits such as storm water management, biodiversity increase, heat island mitigation, and sometimes social activities such as community garden roofs. Finally, green roofs are much more efficient when wet, which could be an issue during heatwaves as water is becoming a scarce resource (Zinzi & Agnoli, 2012). In the winter, plants generally lose their leaves so this strategy is not in concurrence with the winter design.

1.2.3 Dampening the heat with thermal mass

Thermal mass is a very ancient practice in construction, which uses the building structural materials natural heat sink to store the incoming outdoor heat gains, smoothen the thermal fluctuations between the outdoor climate and the indoor environment, and release the heat later towards the indoors. Traditional building materials are sensible heat storage materials, whereas phase change materials (PCMs) are latent heat storage materials, which allow increasing further the building's thermal mass. With sensible materials, heat is released or stored by modifying the structural thermal mass material's temperature, whereas for latent materials the heat is released or stored during the material's phase change.

1.2.3.1 Sensible heat storage materials

Traditional building materials with high sensible heat storage properties are concrete, brick, adobe, rammed earth, or water. The building's thermal mass and related heat storage capacity depend on its materials properties. The three properties related to thermal mass are the material density ϱ (kg/m^3), the specific heat C_P (J/(kg.K)), and the thermal conductivity λ (W/(m.K)). The specific heat C_P is related to the mass while once multiplied by the material density, it is related to a volume. For instance, water has the highest volumetric heat capacity, almost double that of concrete, which explains why it has been used in building applications such as roof ponds to dampen the incoming heat gains. Two secondary parameters, calculated from the three introduced here, allow to characterize the thermal mass, they are the thermal effusiveness b Equation (2) and the thermal diffusivity a Equation (3). The effusiveness represents the material capacity to store and restore energy towards the indoor environment. The diffusivity is the rate at which the heat spreads through the material, it is linked to the surrounding temperature variations. The heat exchange between the building materials and

the outdoor environment depends on the radiative and convection coefficients, and on the optical properties of the building material.

$$b = \sqrt{\lambda . \rho . Cp} \tag{2}$$

$$a = \frac{\lambda}{\rho . Cp} \tag{3}$$

The comparison between a building with low and high thermal mass is illustrated in Figure 15.

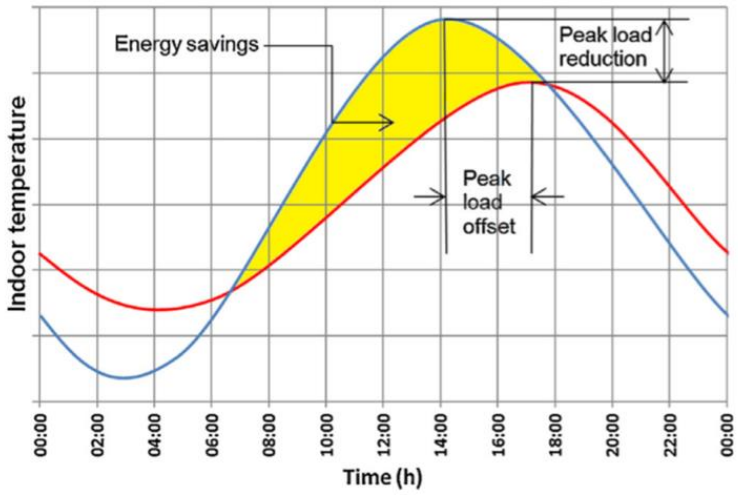

Figure 15 - Potential peak load shifting due to thermal mass (Akeiber et al., 2016)

From Figure 15, it can be observed that the building thermal mass highly influences the indoor temperature variations. For buildings with high thermal mass (red in Figure 15), two phenomena occur: the temperature peak is both dampened (lower amplitude) and time shifted (peak takes place later during the day). Thermal mass is often coupled to nocturnal natural ventilation, as the cooler nighttime air is stored in the building structure and released during the day. While daytime indoor temperatures are reduced, the downside effect is that nighttime temperatures are more elevated, which can be unwanted especially during heatwave periods. In conditioned buildings, the indoor air will take longer to reach a temperature set-point (for heating or cooling) in a high thermal mass building. For winter design, exterior insulation is preferred (to interior) to allow the thermal mass to exchange energy with the warm indoors and not the cold outdoors. (Gondian, 2019) compared the impact of the building occupants' control of windows opening and solar shading on the indoor temperature for two buildings with high and low thermal mass through a sensitivity analysis. She could conclude that the building with high thermal mass was more robust to occupants' actions than the building with low thermal mass: the high thermal mass building allowed to reduce both the maximum temperatures intensity and duration of indoor overheating for any occupants' actions.

1.2.3.2 Latent heat storage materials: PCMs

Some recent advances to increase buildings' thermal mass are the development of PCMs within the last two decades. These innovative materials are capable of storing and releasing higher amounts of energy per volume. Latent heat storage can be achieved through different

phase changes, such as: solid-solid, solid-gas, liquid-gas, and solid-liquid. For building applications, the solid-liquid phase change is preferred for its practicality, since it presents high energy density and no volume expansion (Zeinelabdein et al., 2018).

PCMs absorb and store heat during the daytime during their solid-state, cooling the air passing through the PCM storage unit. At a nearly constant and specific temperature, named the phase change temperature, the PCM starts melting and releases heat while it becomes liquid. During the nighttime, the cool ambient air takes away the heat from the liquid PCM which will solidify once the constant temperature is reached again. For this reason, PCMs perform best when coupled to nocturnal ventilation, given that the outdoor night temperature is lower than the PCM temperature melting point (Safari et al., 2017). In that sense, with climate change and the increase of heatwaves, PCMs might not be effective as the outdoor night temperature could be too elevated for the PCM to recharge. PCMs behave better in climates with a large diurnal temperature variation, and their application is limited in hot and humid regions because their ability to absorb latent heat is very limited (Safari et al., 2017; Waqas & Ud Din, 2013).

PCMs products can be found in several forms such as powder, granule, or rubber, contained in tubes, spheres, or panels, which allow a wide range of integration into the building envelope (Zeinelabdein et al., 2018). PCMs can be incorporated into the building as active or passive systems, and different techniques have been investigated to integrate PCMs within the building envelope (in walls, roofs, slabs, fenestration, insulation…), such as direct incorporation, immersion, vacuum impregnation, macro encapsulation, shape stabilization, and etc (Cabeza & Chàfer, 2020). (Safari et al., 2017) conducted a review of building simulations incorporating PCMs into the building envelope to reduce summer thermal discomfort. They could observe that the largest number of studies were conducted with the software EnergyPlus and reported from 9% to 87% in cooling reduction depending on the PCMs installation and on the climate.

Despite their theoretical potential to reduce summer thermal discomfort, PCMs have a number of drawbacks that require further research and testing which in turn limit their development. One of the main problems is in the phase change of the PCM, as in many experiments PCMs do not solidify completely at the desired time, which complicates their operational mode (Waqas & Ud Din, 2013). Since they have low thermal conductivity, this can also slow the charging process of the PCM during nighttime, and heat transfer enhancement techniques might be needed. Furthermore, according to (Waqas & Ud Din, 2013) some studies calculated that between 6.5 and 30 kg/m^2 of PCM floor plan were required to achieve thermal comfort, which is a major concern for their large-scale implementation. Many laboratory experiments and numerical studies have investigated the potential of PCMs, however, no large-scale testing of PCMs in a building has been tested. The initial cost of PCMs at the moment is elevated, and most studies do not include economic analysis into consideration. Full-scale testing of PCMs is therefore necessary before commercialization becomes possible.

1.2.4 **Passive cooling systems**

Passive cooling systems transfer the heat from the building towards a heat sink. There exist four different types of heat sinks: air, water, ground, and the dark atmosphere. Respectively, the passive, or "almost" passive systems used to dissipate heat and therefore cool the air are natural ventilation (air), evaporative cooling (water), ground cooling (ground) and radiative cooling (atmosphere). Givoni has written a very thorough and comprehensive book about the basics of passive cooling systems (Givoni, 1994). Twenty-three years later, Santamouris edited a book about advances in passive cooling (Santamouris et al., 2007). Since these books were written, many new developments in passive cooling systems have occurred. In this section, we describe the basics of passive cooling systems, a brief overview of recent technologies in each of the fields, and explanations on the limitations of the penetration of the different investigated systems. As these solutions only apply to the summer period, they are not in concurrence with the winter design.

1.2.4.1 Natural ventilation

Renewing air in buildings is necessary to ensure air quality, which is important for both the occupant's health and to avoid elevated indoor relative humidity leading to potential mold growth. For this purpose, a minimal mechanical air flow is imposed in new buildings. In ancient buildings, as they were not airtight, renewal of air would naturally occur through cracks in the building structure. However, new building regulations impose very air-tight buildings to reduce the heat losses during the winter. In the summer, natural ventilation for cooling can be achieved either by mechanical fans indoor or by natural ventilation through windows opening, with higher airflow rates than for air renewal. According to (Chen et al., 2017), the yearly number of hours with a natural ventilation potential is about 3451 h in Paris and 3909 h in Nice. However, with climate change, this number might diminish and be even more reduced during the heatwave periods.

Comfort ventilation

Comfort ventilation is the use of ventilation to create an airflow rate that feels comfortable for the building's occupants. For this purpose, high airflow rates are needed and sometimes mechanical ventilation such as ceiling fans or free cooling can be used to increase the airspeed. While occupants feel warm during the day and open the windows for comfort ventilation, this results in warming the building fabric if exterior temperatures are more elevated than indoors. It is, therefore, preferable to use comfort ventilation (during the day) in light-structured buildings with low thermal mass, in which the heat does not accumulate. According to (Givoni, 1992), comfort ventilation can be used up to 28-32 °C, above these temperatures it would not be satisfying. Usually, comfort ventilation is used in climates where the temperature daily variations are small, and that nocturnal ventilation cannot be achieved.

Nocturnal ventilation

Nocturnal ventilation is the coupled effect of lowering the indoor temperature of the building while cooling down the building structure (via massive elements such as walls, roof, floor slabs) by convection during the night. Nocturnal ventilation coupled with thermal mass

is much more efficient, as the cooled building structure allows to dampen the interior temperature during daytime when higher temperature and solar heat gains occur. In summer, nighttime outdoor temperatures are usually lower than indoors, therefore opening the windows will provide a heat sink through the air for the building's indoor heat to dissipate. In France, nocturnal ventilation has regained popularity in the last decades with overheating problems in new energy-efficient buildings. Many studies have demonstrated its potential and efficiency to reduce summer discomfort hours. The efficiency of nocturnal ventilation mostly depends on three main factors: building thermal mass, the operation strategy for windows opening, and the local climatic conditions. Indeed, high daily fluctuations of exterior dry-bulb air temperature will result in a higher potential for night cooling (a minimum of 12 °C is recommended by Givoni). However, night cooling potential is reduced in cities where the urban heat island effect is present, and where wind speeds might be lowered. As it is not possible to influence the local climatic conditions (besides mitigating the urban heat island effect), the windows operation strategy will be presented in this section.

In the Annex 62 project, for which many buildings with natural ventilation strategies were monitored, the control of windows opening for night ventilation usually depended on a temperature set-point inside the building. The range of internal temperatures was between 15 °C and 23 °C and the lower limits of incoming external air temperature were between 10 °C and 18 °C. However, one of the takeaways of the extensive studies was that the outside air could be exploited with lower external air control limits (except for cold climates) during typical and nighttime operation while using thermal mass was also key. The night ventilation was also limited by the presence of rain and high wind speeds (from 10 or 14 m/s). Relative humidity could also be a limiting factor in certain climates, and when the outdoor relative humidity would exceed 70 %, the windows could not be opened (O'Donovan, 2018). In his Ph.D. thesis, (Lapisa, 2016) found that for a commercial building case study, the optimal control temperature for window openings was between 19 °C and 26 °C inside in Poitiers and Marseille. The windows opening was also controlled by a schedule. They were opened only between 8 pm and 6 am. The seasonal aspect of window opening also had its importance, as in Poitiers windows were opened from June to August, while in Marseille where the climate is warmer, from mid-May until mid-October. The minimal indoor temperature for night ventilation was set to 19 °C, as a lower set-point temperature would meet the one for the heating system. In Jakarta, where no heating is ever needed, the indoor temperature for windows opening was lowered to 16 °C. Finally, he pointed out that when windows remained open all night to meet the interior set-point, it meant that the nocturnal ventilation was not enough to cool the building. With warmer temperatures induced by climate change, nocturnal ventilation might not be sufficient to dissipate the indoor heat. Furthermore, nocturnal ventilation is limited by noise and security concerns, especially in dense urban cities, and can also be affected by the presence of mosquitos.

1.2.4.2 Ground cooling

The earth is a heat sink and therefore represents a natural cooling source for buildings in summer. Using the earth is not new as many centuries ago, underground air tunnels were used for cooling and heating buildings in Iran (Bordoloi et al., 2018). Indeed, from a certain depth (2.5 - 3 m), the ground temperature is undisturbed and remains constant throughout the year. For each location, the undisturbed earth temperature is dependent on the yearly mean

outdoor dry-bulb temperature. According to (Santamouris et al., 2007), earth-to-air heat exchangers (EAHX) have a very strong cooling potential in Europe, where the climate is moderate throughout the year. Modern EAHX systems consist of a network of pipes buried underground, with intake air entering from one side and the exhaust air being transferred towards the indoor building space through the ventilation system (Figure 16). Along the pipes, the air is cooled down by conduction towards the ground. EAHX have only received attention in the last decades, and a few monitoring projects exist around the world. An EAHX system implemented in a school building in Italy, where summer air temperatures were up to 38 °C during the day and between 20-25 °C during the night, allowed to cool down the temperature to 22-25 °C (Chiesa et al., 2014). Many factors can influence the efficiency of EAHX systems, while the first is related to the soil characteristics. Furthermore, the geometrics of the system (pipes depth, length, and diameter) will influence the airflow rate and thus the heat transfer throughout the system. EAHX systems have been implemented in many building simulation tools (EnergyPlus, TRNSYS, COMFIE), and more detailed Computational Fluid Dynamics (CFD) programs. (Thiers & Peuportier, 2008) implemented a EAHX model in the simulation tool COMFIE, and modelled a PassivHaus with the EAHX analyzing the heating need under a present typical winter and the summer discomfort under the 2003 heatwave in the North of France. While comparing the PassivHaus with the EAHX to a standard French building with only mechanical ventilation, they could conclude that while the heating load could be reduced by 12 for the PassivHaus, the summer degree-days of discomfort was divided by two. However, for the summer period, it is unclear to which extend the PassivHaus design or the EAHX cooled air contributed to reducing the summer discomfort. Nowadays, most of the research is focused around validating models with full-scale monitoring campaigns, identifying the most important factors for each case-study system, building, and location, and the EAHX potential for different regions over the world.

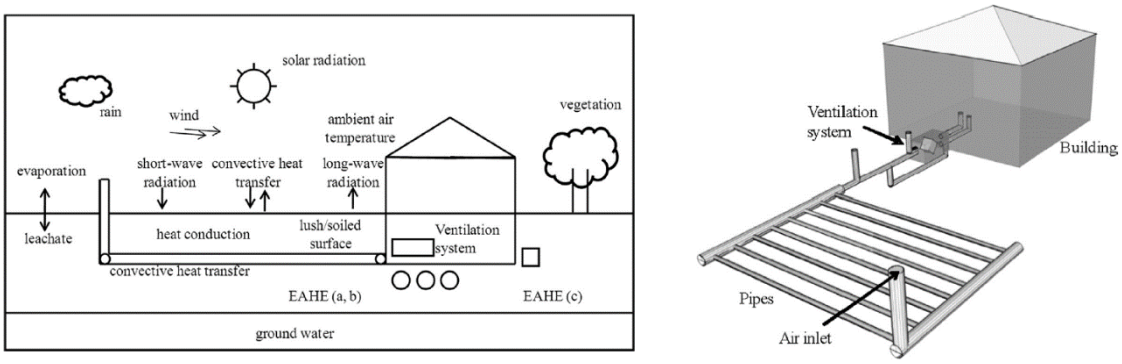

Figure 16 - EAHX System, left: (M. Santamouris et al., 2007), right: (Peretti et al., 2013)

According to (Santamouris et al., 2007), design characteristics are lacking in the literature, since each earth tubes are designed to meet specifically the local climate, building needs and construction possibilities on site. Regarding the cooling potential, (Chiesa, 2017) has calculated with a simple method that using a EAHX system in Paris would offset the total building cooling demand for a 22 °C set point temperature under the present typical summer. Earth-to-air heat exchanger therefore, presents a good potential to lower indoor air temperatures during summer, while it also reduces the winter heating needs. Earth-to-air heat exchangers have not penetrated in France, which could be due to several reasons: design is dependent on the local climate and local ground characteristics, installation and maintenance

costs can be elevated. Also, it requires land use which can be problematic in cities. A promising and innovative EAHX was recently patented in France with the potential to be buried under the building, therefore increasing the cooling potential by increased buried depth, reducing construction costs and using no extra land space (Taurines, 2019).

1.2.4.3 Evaporative cooling

Evaporative cooling takes place during the state change of liquid-vapor to water vapor. The process absorbs heat which results in a decrease in dry-bulb temperature. This cooling technique has been used for many centuries, especially in hot arid regions, i.e. people used to place water in clay pots, or to wet the floor during warm days. The change of temperature is called adiabatic because the total energy content of the air is kept constant, without the addition or removal of heat to the system. Evaporative cooling can be direct or indirect, direct (DEC) is when water is directly added to the air, which results in cooled and humidified air, whereas indirect evaporative cooling (IEC) occurs when the cooled humidified air cools down another independent intake air via a heat exchanger, which water vapor content remains constant (Figure 17). Obviously, DEC requires a simpler system, however its application is limited to very dry and warm locations.

Direct evaporative cooling (DEC)

The simple direct evaporative cooler is composed of a fan that blows air through a wet pad, which is then redirected inside the building. This type of cooler reduces the dry-bulb temperature to 60-80% of the wet-bulb temperature, which is the lowest temperature that the dry-bulb can reach. For this process, high airflow rates are needed, around 15-30 ACH, which also increases the upper comfort limit (Givoni, 1994). One example of a large-scale implementation of direct evaporative cooling is the famous downdraft passive evaporative cooling towers designed by Cunningham and Thompson, which performed very well in Tucson, Arizona (very dry climate) since they allowed to cool down the outdoor dry-bulb temperature of 40 °C to 24.6 °C indoors. This type of tower was also installed in Seville (Salmeron et al., 2012). However, the implementation of this type of system in a more humid climate is limited, due to the humidity levels increasing indoors. (Leroux et al., 2019) tested an experimental low-cost innovative system on a house based on the ingenious combination of direct evaporative cooling, water storage in the ground and radiant floor cooling. While still at the prototype stage, the direct evaporative cooling wall is placed outside of a house, and the indoor air is cooled from the cool water circulating in the radiant floor. However, they recorded a water consumption of around 42 l/day for a single home.

Indirect evaporative cooling (IEC)

Indirect evaporative cooling has more potential to be implemented in modern buildings, as it can cool the air while maintaining comfortable indoor humidity levels. IEC chillers are currently installed in many large buildings in Northern China, in the Middle East, and in North America. For instance, an IEC chiller installed in the Xinhian Traditional Medicine Hospital (13,000 m²) allowed to cool an outdoor dry-bulb temperature of 30 °C to 15-17 °C. The cooling air temperature was delivered by fan coil units around 19-20 °C, which was almost equivalent to the local inlet wet-bulb temperature (Xie & Jiang, 2015). Another IEC system was

monitored in a small office building, in a climate with outdoor temperatures up to 42 °C: The supply air temperature into the building was between 20 and 24 °C. (Yang et al., 2019). IEC has gained a lot of popularity in recent decades, and the traditional IEC systems have been improved to dew point evaporative coolers, in which the dry-bulb temperature can be lowered below the wet-bulb temperature, almost equal to the dew-point temperature (Duan et al., 2012). A dew-point evaporative cooler was modelled and validated in EnergyPlus by (Badiei et al., 2020). Nowadays, many researchers are modelling and testing different system structures, different heat exchanger materials and design, analyzing the optimal water evaporation and heat transfer, and giving attention to the distribution, consumption and treatment of water to achieve this dew-point temperature (De Antonellis et al., 2020; Al Horr et al., 2020; Kashyap et al., 2020; Boukhanouf et al., 2017; Xuan et al., 2012). For even more efficient cooling, other developments include multi-stage IEC, vapor compression systems, and enhanced evaporative cooling (using air pre-dried by desiccants) (Yang et al., 2019), see Figure 17. Knowledge gaps in evaporative cooling are mostly related to their applicability in different types of climates, and to the variety of different IEC systems that exist. While IEC chillers are manufactured and commercialized in North America and Asia, their use and large-scale implementation in Europe is limited (Duan et al., 2012). In France, some prototypes of evaporative IEC systems are currently being developed at the pre-industrialization stage. However, beyond being limited with the exterior outdoor dew-point temperature, evaporative cooling requires water, which might be an issue especially during heatwave periods. Some research is focused on designed IEC systems with minimum water consumption (Moshari et al., 2016).

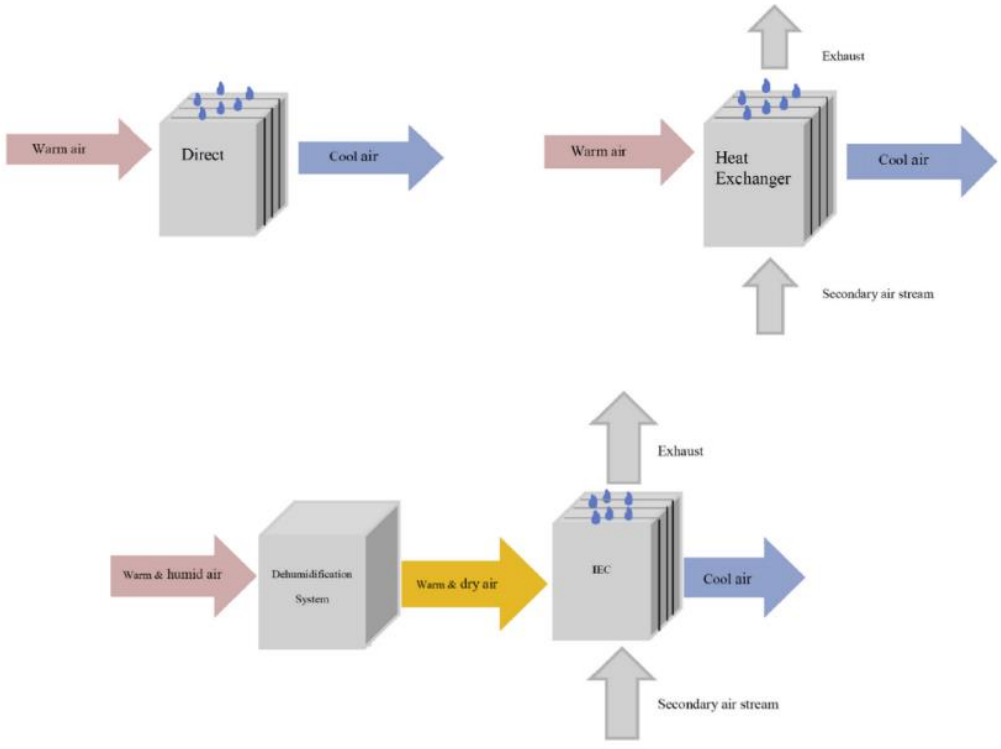

Figure 17 - DEC, IEC and IEC with pre-dried air from (Yang et al., 2019)

1.2.4.4 Radiative cooling

Two types of systems are used to circulate cooling energy from radiative cooling: air-based systems and water-based systems. Because of the higher heat capacity of water compared to air, water-based systems have better efficiency than air-based systems, and are therefore more popular, they are presented in this section.

Nocturnal radiative cooling

Water-based systems use water to both achieve cooling and act as a cold storage device. The first scientific investigations of radiative cooling systems were closed roof ponds such as the Skytherm system invented by Harold Hay, implemented on buildings on the West coast of the United States in the early 1970s. Large plastic bags (depth of 10-30 cm) filled with water were placed on the roof, which would cool down during the night via radiation towards the sky and by convection towards the air. The bags were in direct thermal contact with a structural steel plate on the roof, radiating cooled energy towards the building ceiling. During the day, automated moveable insulation panels would protect the pond of solar gains. The system showed good performance to cool down (the indoor temperature would remain inferior to 27 °C in Phoenix climate zone 2B), but the moveable panels were not mechanically reliable, and it was concluded that the design must be improved. More recently, guidance for better designs was proposed in (Santamouris et al., 2007). Since then, many researchers have studied water radiative cooling systems and over the years the design has changed: Nowadays, most of them consist of a thermal radiator (usually a flat plate collector), an insulated water tank, a heat exchanger, and a water pump. The thermal radiator cools the water during the night, which is stored in the tank and circulated in the building when there is a cooling demand. Numerous experiments have proven the viability of this technology, but its implementation on the market is still very low (TRL around 2-3). (Lu et al., 2016) wrote a complete review of the various different types of systems and their major drawbacks. They emphasize technical problems such as formulating the right material properties, manufacturing issues, and an elevated cost of the overall system for building applications. To reduce these costs, hybrid systems are under development, and one example of them is the RCE (Radiative Collector and Emitter) system proposed by (Vall et al., 2020). The RCE combines radiative cooling and solar collection for heating and hot water needs, and was validated against a laboratory experiment and implemented in TRNSYS. They argue that coupling both functions within one system might accelerate the manufacturing process of radiative cooling systems, and lower the cost. Once optimized, the RCE system could provide a cooling output up to 100 W/m² almost constant under ambient night temperatures between 20 °C and 30 °C, which is consistent with the results for other nocturnal radiative cooling systems. It is important to emphasize that radiative cooling efficiency is directly linked to ideal climatic conditions (no clouds, low relative humidity), and that its application is limited in other climates. The ideal properties of a radiative cooler are given in Figure 18.

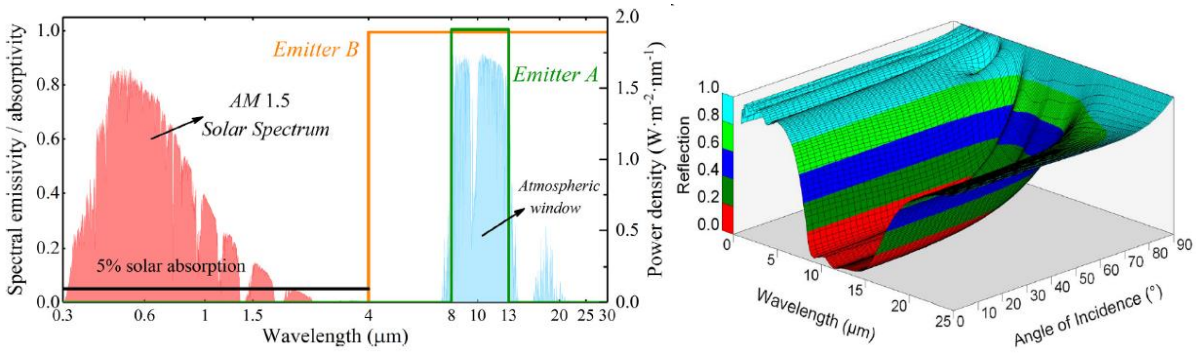

Figure 18 - Ideal properties of a radiative cooler

Daytime radiative cooling, water-based

Due to the potential of daytime radiative cooling materials to provide cooling energy during the day, these materials have been integrated into a water-based system to circulate cooling to the building. (Raman et al., 2014) developed a prototype named Skycool, a water-based system in which it integrated their material that reflects 97 % of the solar radiation, and has an emissivity of 0.84 in the atmospheric window. They measured the water temperature in the radiant panels about 3-5 °C below the air ambient temperature during the summer in Las Vegas under strong solar radiation, equivalent to a heat rejection rate between 40 and 70 W/m² (Goldstein et al., 2017). Their innovative daytime cooling radiator is ground breaking in the field and opens the path for further developments. In their first experiment, the system allowed to replace 21 % of the electricity for air-conditioning in the hot and dry climate of Las Vegas. In France, their system could potentially offset all the future cooling needs of a building, given that the sky is clear and with low humidity. The application of these panels would be buildings with a large roof area, therefore individual homes, low collective buildings or commercial buildings. (Wang et al., 2018) created a model of this photonic radiative cooling system in EnergyPlus, using the code provided by (Raman et al., 2014) to calculate the net heat transfer with the sky water. They compared the daytime radiative cooler with a variable air volume (VAV) and other night radiant cooling systems in different cities in the United States, and concluded that the new daytime system would reduce the cooling electricity of around by half in comparison with the VAV (Wang et al., 2018). Many research is undertaken on the modelling of these materials, which has been reviewed by (Santamouris & Feng, 2018). Modelling photonic materials is part of the future developments of EnergyPlus, as it requires a complex discretization in different wave-lengths of the material properties. However, the efficiency of daytime radiative cooling is strongly dependent on ideal climatic conditions: dry and sunny. More research is needed to overcome this challenge, as reported by (Ulpiani et al., 2021).

1.2.5 **Concluding remarks on passive cooling strategies and systems**

In this section, diverse passive strategies effective to reduce, dampen, time shift or exhaust heat have been reviewed. While some strategies are not dependent on the local climate and easy to implement (i.e using solar shutters), some others have their efficiency relying heavily on the local climate conditions (i.e all cooling systems to exhaust heat via a medium). Furthermore, while some strategies are not in concurrence with passive winter design (i.e cooling strategies), some others behave oppositely in winter and summer (i.e cool selective materials that are not thermochromics, or windows surface and orientation). This emphasizes that designing passive buildings maintaining comfortable indoor conditions along all seasons in temperate climate is a rather complex procedure. While all techniques are based on ancient knowledge, recent technological developments allow the prototyping and manufacturing of promising systems based on sophisticated materials. However, the cost of these systems is often stopping their penetration on the residential market.

Passive cooling strategies represent a huge potential alternative to air-conditioning, given that these measures are implemented at the early stage of the building design. However, the potential and the limits of these different strategies and systems has not been analyzed in future French climate yet, and especially during future heatwave periods. In this Ph.D. thesis, we will analyze the potential of these different solution to both mitigate and adapt to climate change, in future winters and summers. Some combinations of strategies might be efficient during heatwave periods, while some others might not, and this is what we aim to investigate. The heat-health related risk indoor once the different solutions reach the limits of their efficiency is to be analyzed and represents a crucial matter for the design of future resilient buildings under climate change. A summary of the different passive cooling solutions, their limitations in regards to local climate related potential and winter concurrence is presented in Table 2.

Table 2 – Summary of some passive cooling strategies to increase building resilience to extreme outdoor heat and climatic limitations

	Passive cooling strategy	Winter Concurrence	Advantages	Disadvantages	Limits based on local climatic conditions	RE-2020
Bioclimatic architecture	Use of buffer spaces	No	Dampens outdoor climate variations, extra space	Space usage, might require a specific architectural design	None	Yes
Preventing solar heat gains through glazed surfaces	Low-emissivity coating	Yes	Reduces solar heat gains while allowing daylight	Must be designed either for winter or summer (coating placed on the inside or outside of glass), expensive	None	Yes
	Thermochromic glazing	Yes		Cannot be controlled by the user, expensive	None	No
	Electrochromic glazing	No		Control can be complex, expensive	None	No
	Fixed window integrated shading	Yes	Allows reduced daylight in aesthetic patterns; can be cost-efficient	Design can be complex Reduces winter solar heat gains	None	Yes
	Movable window integrated shading	No		Control can be complex	None	No
	Interior shading device	No	Cost-efficient	Compromise between daylighting and intimacy	None	Yes
	Exterior shading device	Yes	Allows daylight; cost-efficient	Need to be integrated from early architectural design	None	Yes
Preventing solar heat gains through opaque surfaces	Cool selective paints applied on roofs	Yes	Cost-efficient, UHI mitigation	Effectiveness decreases with insulation; reduces winter solar heat gains; mostly impacts top-dwelling in collective buildings	Performs well under hot and sunny conditions	Yes
	Cool selective paints applied on walls			Not as efficient as when applied on roofs; can create inter-reflexions in urban context		Yes
	Thermochromic selective paints	No	Not in concurrence with winter design, UHI mitigation	Effectiveness decreases with insulation value; problems, still at the prototype stage		No
	Hybrid cool roof			Effectiveness decreases with insulation value; ageing problems		No
	Green roofs	No	Cools down the roof by evapotranspiration; storm water management; biodiversity increase;	Requires water to be most efficient, which can be scarce when most needed; maintenance costs	Performs well under hot and sunny conditions if	Yes

			communal gardening; urban heat island mitigation		supplied with water (depends on the species)	
	Green walls	No	Cools down the wall by evapotranspiration; biodiversity increase; urban heat island mitigation	Requires water to be most efficient, which can be scarce when most needed (heatwaves); complex maintenance; installation costs		Yes
Dampening and time shifting outdoor temperatures	High thermal mass	No	Dampens and time shift outdoor temperatures; lower daytime indoor temperatures	Indoor nighttime temperatures warmer than with lower thermal mass	Requires diurnal temperature range > 10°C; less efficient on warm nights (> 25°C)	Yes
	PCMS	No	Same as above, more effective than traditional thermal mass	Currently expensive, problems in phase change		No
Cooling the air inside the building	Daytime comfort ventilation	No	Provides immediate cooler thermal sensation by increased air velocity	If building with high thermal mass, might store heat in the building structure with windows open	Can only be used up to 28-32 °C outdoor air temperatures	Yes
	Nocturnal ventilation (NV)	No	Simple, free of costs, no additional system needed	Constrained by noise, air pollution, security especially in urban context, and presence of mosquitos, requires high thermal mass and cross-ventilation windows configuration to perform best	Requires diurnal temperature range > 10°C; less efficient on warm nights (> 25°C) especially in urban context; limited by wind, rain and relative humidity	Yes
	Earth-to-air heat exchanger (EAHX)	No	Can be used as well in winter to reduce heating needs	Installation cost increase with depth; needs land space; design requires knowledge	Limited in potential by the yearly mean outdoor dry-bulb temperature	Yes
	Direct Evaporative cooling (DEC)	No	Simple design, high efficiency	Legionella concerns in France with storage of warm water, requires water to function, increase humidity levels indoors	Limited in potential by the outdoor wet-bulb and/or dew-point temperature, requires water to function	No
	Indirect Evaporative cooling (IEC)	No	Indoor air temperatures equivalent to the outdoor wet-bulb/dew-point temperatures	Requires water to function, complex design		Yes
	Nighttime radiative cooling	No	Same panels can be used as for solar thermal	Needs roof space; still at the prototype stage	Requires dry and non-cloudy conditions	No
	Daytime radiative cooling	No	Lower temperatures than air under direct sunlight			No

1.3 Future climate data including heatwaves for building simulations

In this section, we analyze the possibility to integrate future heatwaves in weather files for building simulations. In order to assess the health related to heat risk inside buildings during future climate and more specifically during future heatwave periods, it is necessary to have access to such data. Furthermore, the behavior of the above presented passive cooling strategies and techniques need to be assessed under future periods of extreme heat.

Nowadays, building practitioners are using historical years during the building design process, not considering future climate variations due to climate change. The new French building regulation, the RE-2020 that will be in place starting January 1st 2021, uses a recent typical year, assembled using the most recent observations from years 2000 to 2018. However, the lifetime of a building in France is between 50 and 100 years, and as the climate is changing, building built for the climate of the beginning of the century might not be adapted to the climate of the middle or end of the century. As temperatures are quickly rising and heatwaves are expected to increase both in frequency, duration, and intensity, it is much needed to evaluate the indoor overheating and heat stress related risk. This evaluation must be done at the building design stage, that effective mitigation and adaptation measures, systems and strategies can be planned and implemented to ensure buildings are designed today to be resilient to warmer temperatures induced by future climate.

For this purpose, it is crucial to analyze future climate variations. In fact, in the research community, using future weather files as inputs for building energy simulations has been of interest for the past two decades. However, while the so-called "typical years" have been a standard practice for many years, the use of typical conditions to assess building resilience to future climate might not be appropriate. Indeed, as French new buildings have already to overheat during current summers and especially during heatwaves, it is necessary to assess the building resilience under future typical years, but as well under future heatwaves. Such a practice has been anticipated by the new RE-2020, which imposes an overheating assessment under the climate of the disastrous heatwave of 2003. A similar requirement was implemented in England by the CIBSE, which provides design summer years for overheating assessment, constituted from past heatwaves. However, in the building community the return period of a heatwave such as 2003 is today unknown. Would worse heatwaves take place? How intense? And for how long? And how to consider the "heatwaves risk" in the building design process? These questions have not been asked before, and they must be answered at the design stage of buildings, or recurring overheating periods might occur. If not planned well, short-responses such as energy consuming adaptations will occur, while planned and long-term adaptations at the building design stage would ensure resilient and more robust buildings, that also mitigate climate.

Therefore, using appropriate future climate data to assess the resilience of buildings to overheating becomes a key challenge. As future climate data are nowadays not standardized in national regulations, there is a lack of common agreement on which methods, which tools and which future climate data to use. Which climate model, which socio-economic scenario to

choose? Furthermore, the uncertainties in climate projections are often not understood or not known by building practitioners, which adds complexity in the decision-making process on which future climate data to use.

In order to fill this gap, we analyze the literature on future climate data to be used for building simulations with the following research questions:

Which kind of future climate data and which tools can be used to reassemble future weather files for building simulations?

Can we assemble future weather files including heatwaves to analyze buildings resilience to indoor overheating and assess heat stress risk?

What are the uncertainties in future climate projections?

A journal article was written to summarize this state of the art (Machard et al., 2020a).

1.3.1 **Background on climate projections**

The IPCC, created in 1988, is in charge of studying, analyzing, evaluating and disseminating scientific and socio-economic information on climate change. IPCC experts are not producing new science, but instead combining knowledge from the different research institutions around the world (195 countries). In 2000, the "Special Report on Emissions Scenarios" (SRES) was produced, from about forty different possible future socio-economic scenarios. The different assumptions laid on several hypotheses about society evolution (fossil or renewable energy, local or global economy…) The impact of each scenario was evaluated in terms of carbon emissions. Following this, the famous scenarios under the name A1F1, A1B, A1T, A2, B2 and B1 (from the most pessimistic to the most optimistic) were selected and used in the 3rd IPCC report (TAR) in 2001 (Folland et al., 2001). For the 4th IPCC report in 2007 (AR4), the SRES were actualized accounting for mitigation policies, and quantifying this time not only in carbon but greenhouse gases (IPCC, 2007). Since 2009, the term "projections" has been replaced by "representative concentration pathways" (RCPs), which were defined according to a new methodology created by economists and scientists who worked in parallel and not sequentially this time (O'Neill et al., 2014). The RCPs account for the socio-economic changes from the beginning of the XXIth century, and mitigation and adaptation policies (the RCP 8.5 being less pessimistic than the previous A1F1 scenario). The sequencing from RCPs scenarios to future climate data is introduced in Figure 19.

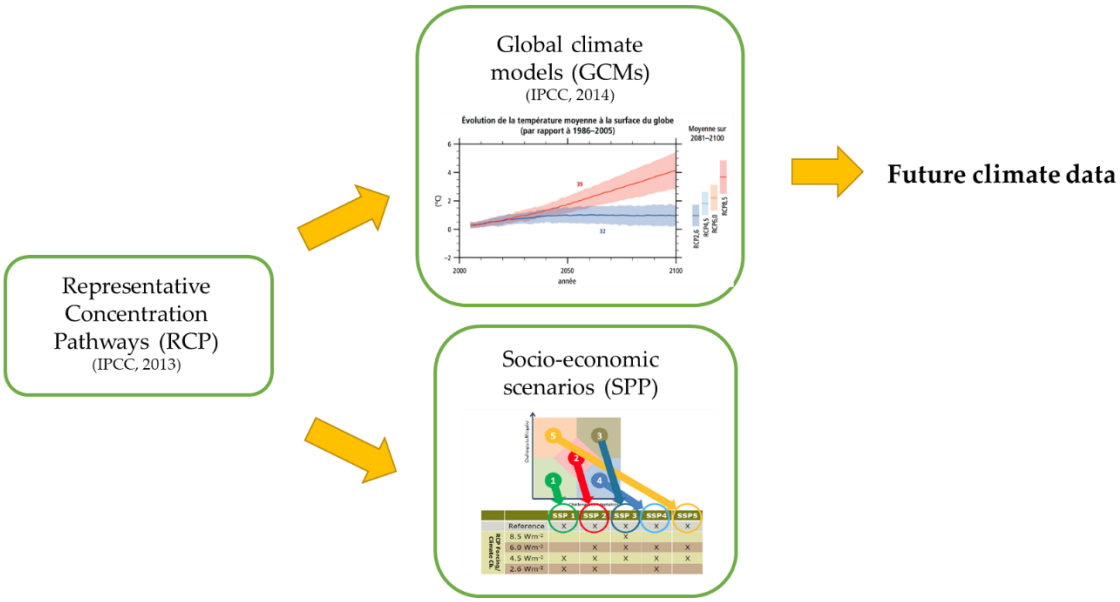

Figure 19 - From IPCC RCP to future climate data

The RCPs account for ozone and aerosols (Moss et al., 2010), and their value is representative of radiative forcing:

"*Radiative forcing is a measure of the influence a factor has in altering the balance of incoming and outgoing energy in the Earth-atmosphere system and is an index of the importance of the factor as a potential climate change mechanism. Positive forcing tends to warm the surface while negative forcing tends to cool it. Radiative forcing values are for changes relative to a pre-industrial background at 1750, are expressed in Watts per square meter (W m–2) and, unless otherwise noted, refer to a global and annual average value.* » (Solomon, et al., 2007)

Radiative forcing is described by Equation (4). The radiative energy affecting the earth climate is coming from the sun. The planet and atmosphere absorb and reflect a part of this energy, whereas another part is reemitted towards space. The term "radiative" is used because different factors are modifying the solar radiation equilibrium. This equilibrium, between absorbed and emitted energy, controls the temperature at the earth surface. The term "forcing" refers to the fact that the equilibrium is being modified. The different factors influencing radiative forcing are presented in Figure 20. In 2005, the principal factors influencing the radiative forcing are the greenhouse gases (positive *RF*), albedo and aerosols (negative *RF*). In 2005, the value of radiative forcing was about 1.6 W/m² (confidence interval from 0.6-2.4 W/m²). In 2011, its value was of 2.8 W/m².

$$Radiative\ forcing\ (RF)\ \left(\frac{W}{m^2}\right) = Absorbed\ radiative\ energy\ \left(\frac{W}{m^2}\right) - Emitted\ radiative\ energy\ \left(\frac{W}{m^2}\right) \quad (4)$$

If RF > 0, the system warms up
If RF < 0, the system cools down

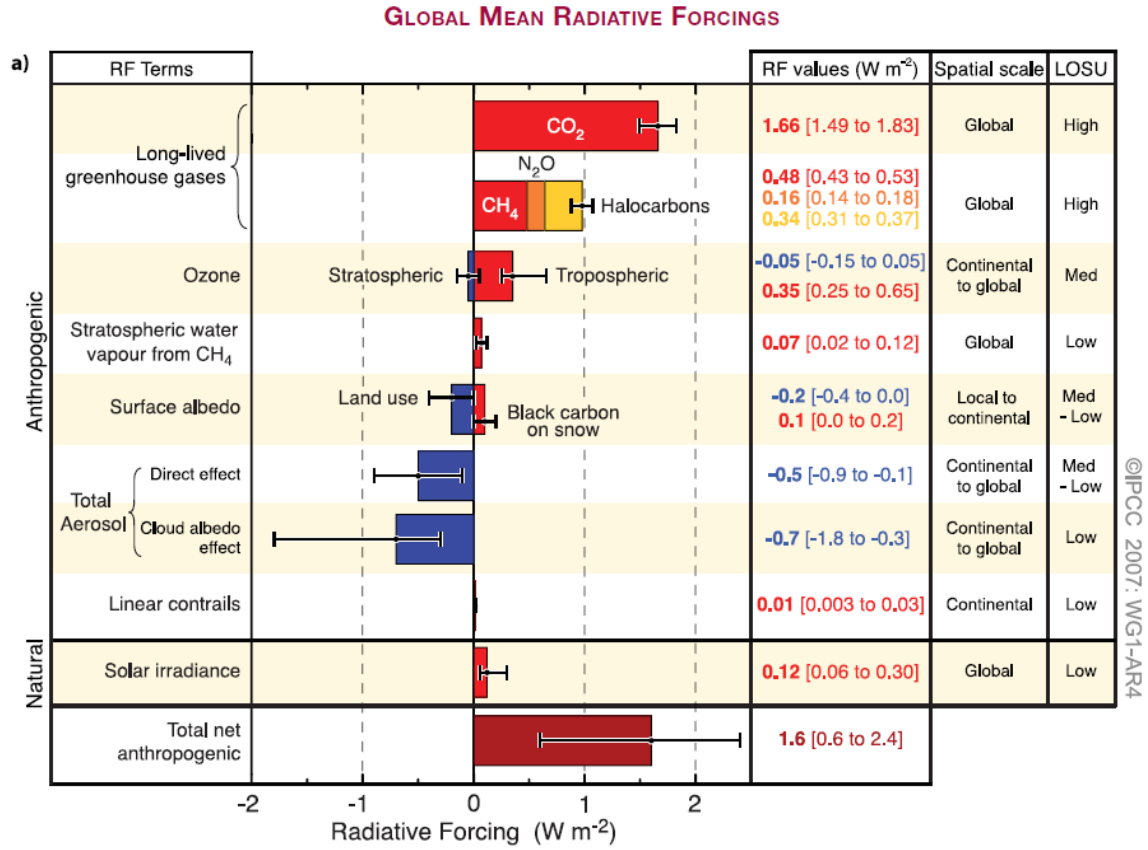

Figure 20 - Global mean radiative forcings (*RF*) and their 90% confidence intervals in 2005 for various agents and mechanisms. (Solomon et al., 2007)

The RCPs represent the possible evolutions of radiative forcing from 2006 to 2030. The RCPs value 2.6, 4.5, 6, and 8.5 are representative of radiative forcing projections towards 2100 (Meinshausen et al., 2011). RCPs were used in the 5th IPCC report (Assessment Report 5, AR5 (IPCC, 2014)). The different socio-economic profiles are named Shared Socio-Economic Pathways (SSPs), presented in a matrix that position their contribution to mitigation and adaptation to climate change, different than the SRES who only indicated CO_2 emissions (O'Neill et al., 2014; Figure 21).

The SSP1 corresponds to policies that mitigate and adapt to climate change. On the contrary, the SSP3 scenario represents a world highly competitive amongst countries, not preoccupied with climate change. The SSP4 describes a world with high inequalities, with mitigation but no adaptation whereas the SSP5 represents the opposite: a fast development of developing countries adapted to climate change, but without mitigation. The SSP2 is the intermediate scenario.

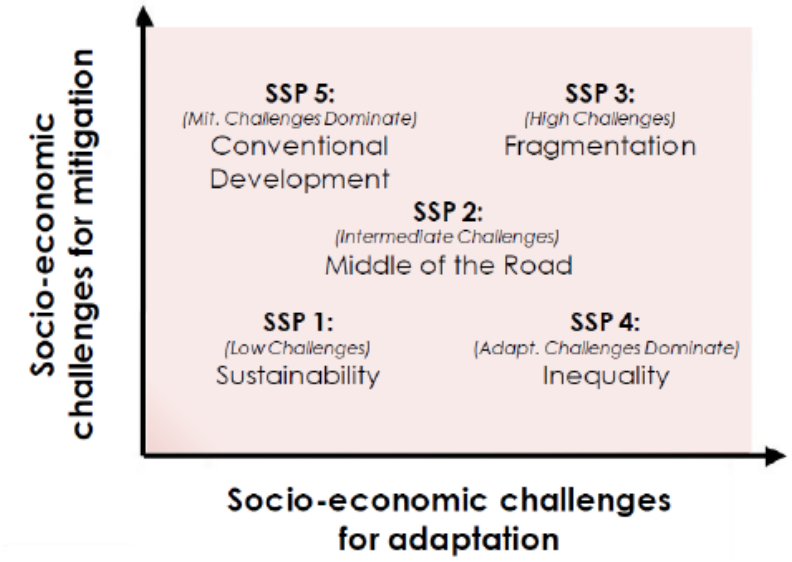

Figure 21 - Shared socio-economic pathways, between socio-economic challenges of mitigation & adaptation to climate change (Ministère de l'Ecologie, 2013)

In Figure 22, the relationship between RCPs and SSPs is highlighted (van Vuuren et al., 2014). We can observe that only the SSP1 would limit radiative forcing to 4.5 W/m². On the opposite, the SSP 3 is the only scenario corresponding to the highest radiative forcing 8.5 W/m², which is the current climate trajectory.

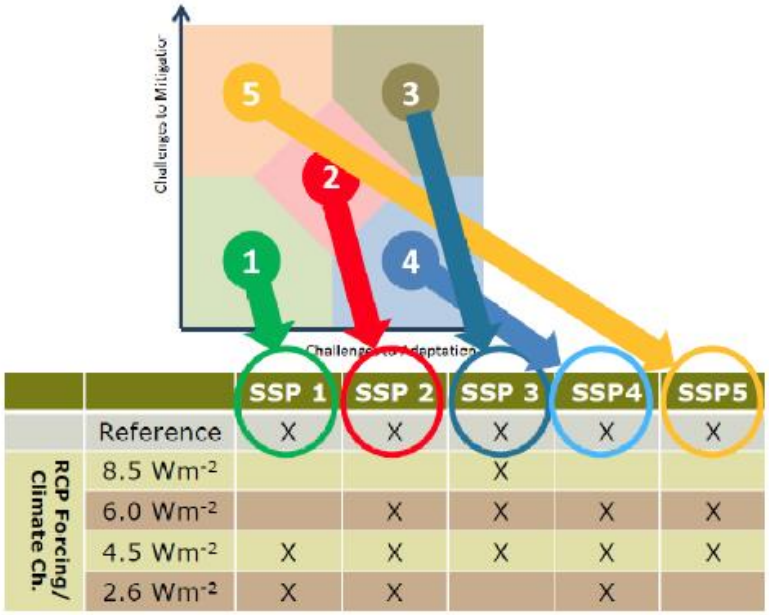

Figure 22 – Relationship between RCP and SSP (Ministère de l'Ecologie, 2013)

A summary of the evolution of IPCC scenarios is presented in Table 3.

Table 3 – Summary and evolution of IPCC scenarios from TAR, AR4 and AR5

Year	**2001**	**2007**	**2013**	**Scenario trajectory**
IPCC report number	3	4	5	
IPCC report name	TAR	AR4	AR5	
Emissions accounted for	CO_2 emissions	GES emissions	Radiative forcing	
Number of climate models	6	23	50, including 2 French models: CNRM-CM5 et IPSL-CM5	
Scenario/Concentration Pathway, see Table 4	SRES A1F1			Increase
	SRES A2		RCP 8.5	Increase
	SRES A1B		RCP 6	Stabilization before 2100
	SRES B1		RCP 4.5	Stabilization before 2100
			RCP 2.6	Peak and decrease before 2100

1.3.2 **Global climate models**

The most sophisticated tools available today to represent climate simulations are coupled atmosphere–ocean general circulation models, or global climate models. GCMs are developed by climatologists in many research centers worldwide, and the climate outputs are assessed by the Intergovernmental Panel on Climate Change at a worldwide level, identifying agreements in the scientific community on topics related to climate change. These general circulation models, or global models, are driven by large-scale climatic forcing, such as the input of solar radiation, the concentration of greenhouse gases (outputs of the Representative Concentration Pathways, RCP), the distribution of oceans and continents, the presence of large continental surfaces such as mountains, etc. These models are spatially divided into a grid in which interactions between each cell of the grid are represented by physical equations. GCMs cover the entire globe, and their spatial resolution is quite coarse: At the time of the IPCC First Assessment Report (FAR), in 1990, their resolution was about 500 km, it has been about 100 km since the IPCC Fourth Assessment Report (AR4) in 2007. The representation of the relief, coastal, and ground occupation is sparse and, therefore, the resolution of these models is too high to be used for building thermal simulations. The full methodology on the production of climate change predictions was summarized by (Giorgi, 2005).

Despite the precision of global climate models, uncertainties remain regarding future climate. According to the work of the authors Hawkins and Sutton, uncertainties can be sorted into three main categories (Hawkins and Sutton, 2011; Hawkins and Sutton, 2009):

- **The internal climate variability**: these are natural fluctuations of climate from one year to another, or what is commonly called meteorology. For instance, from one

year to the next, the weather can be abnormally cold even though the tendency over ten years is a warming temperature.

- **The climate model**: climate projections can vary greatly from one model to another because the assumptions in the climate models can vary, or some climate aspects may be better represented in one model than another, such as their representation of different climate feedbacks (sea ice albedo, water vapor, and cloud–climate; (Giorgi, 2019))

- **The socio-economic scenario**: this is the uncertainty related to societal development, adaptation, and mitigation policies for climate change.

(Hawkins & Sutton, 2009) compared temperature climate outputs from different models over the historical period 1955–2000 with observations, and showed that the observations laid within the model uncertainty range, which suggests that model outputs are reliable over the historical period (Figure 23). In Figure 23, the uncertainties are represented in three different colors. First, it is noticeable that with time, the overall uncertainty in temperature predictions increases. At the end of the century, depending on uncertainties, the global mean temperature is expected to increase from +1.2 °C to +4 °C. Second, we can notice that depending on the time-period, uncertainties from the three categories vary differently: at the beginning of the century, the uncertainty related to the internal climate variability is predominant in comparison to the other uncertainties, but is less significant with time. In the middle of the century, the uncertainty related to the climate model is the most significant; whereas, towards the end of the century, the uncertainty related to the socio-economic RCP scenario is the most important one, even though the uncertainty related to the climate model is still quite significant. In their articles, the authors also mention that the period around 2050 is when temperatures are best predicted in comparison with other periods of the century.

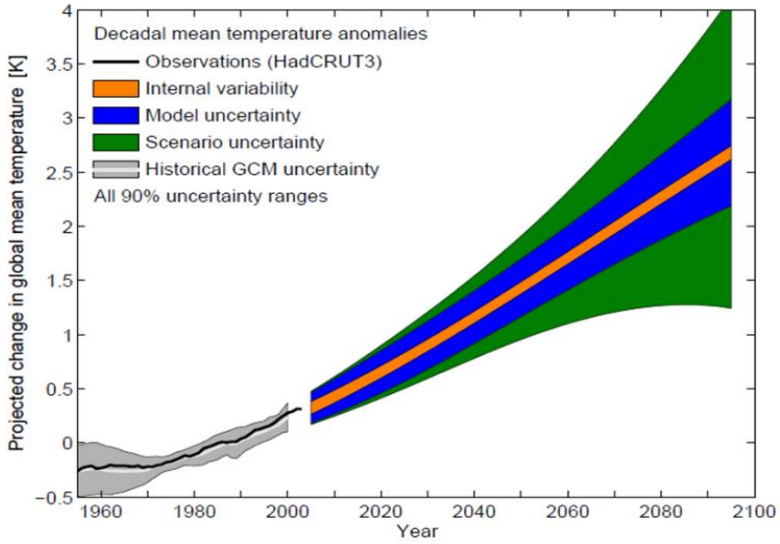

Figure 23 - Uncertainty in average temperature decanal projections during the 21st century from global climate models (GCMs), part of the Coupled Model Intercomparison Project Phase 5 (CMIP3) project: uncertainty related to the climate internal variability (orange), model uncertainty (blue), and scenario uncertainty (green). Projections are calculated compared to the period 1971–2000. Historical uncertainty (grey), models average historical (white), observations (black) (Hawkins & Sutton, 2011)

1.3.3 **Climate data downscaling**

Since the resolution of global climate models is too coarse (monthly averages, 100 km resolution), the climate community has undertaken data "downscaling" in order to realize local impact studies. Downscaled climate data, representing the surrounding climate are required for building thermal simulations. According to (Ouzeau et al., 2014), two distinct downscaling methods exist: statistical downscaling and dynamical downscaling An exhaustive and comprehensive review comparing the two methods was made by (Herrera et al., 2017).

1.3.3.1 Statistical downscaling

The morphing method

Beyond several statistical downscaling methods, the most widely used for building simulations is the morphing method, developed by Belcher et al. in the United Kingdom (Belcher et al., 2005). This method was used by the CIBSE in 2008, who produced future morphed typical weather test reference years (TRY) and design summer years (DSY), two types of weather files ready to be used for building simulations. The principle is that from an existing weather file under present day climate (for instance, a typical weather file), a morphing equation is applied to each variable $x_{0\mathrm{h}}$. Three types of possible equations «shift» Equation (5), «stretch» Equation (6), or "shift and stretch" Equation (7) are used to calculate each future climate variable x_{h}. The climate change aspect, issued from one or several GCMs, is integrated through Δx_{m} and α_{m}, which are respectively the monthly average and monthly average daily range of the climate variable. In the equation shift and stretch, $x_{0\mathrm{m}}$is the monthly mean value of the climate variable.

Morphing equation "shift":

$$x_{\mathrm{h}} = x_{0\mathrm{h}} + \Delta x_{\mathrm{m}} \quad (5)$$

Morphing equation "stretch":

$$x_{\mathrm{h}} = \alpha_{\mathrm{m}}.x_{0\mathrm{h}} \quad (6)$$

Morphing equation "shift and stretch":

$$x_{\mathrm{h}} = x_{0\mathrm{h}} + \Delta x_{\mathrm{m}} + \alpha_{\mathrm{m}}.(x_{0\mathrm{h}} - x_{0\mathrm{m}}) \quad (7)$$

The equation shift is used for variables who evolve with an absolute change in average, such as the atmospheric pressure. The stretch equation is used to represent a coefficient change in the average or in the variance, such as the wind speed. It is also used if the climate variable needs to be set to zero (for instance the solar radiation during the night). Finally, the equation shift and stretch combination is used to represent both a change in average and standard deviation. For example, it is used for the dry-bulb temperature to represent a change in average, minimal and maximal temperatures. The morphing equations for most climate variables are described in (Belcher et al., 2005).

The morphing method was implemented in the Climate Change World Weather Generator (CCWWeatherGen), an online free Excel tool created by the Sustainable Energy Research Group from the University of Southampton. The tool allows to convert a reference weather climate file to a future climate change weather file, both in Energy Plus Weather (EPW) format. This format was specifically chosen to make the data easily available for building simulations. The methodology of the CCWWeatherGen is described in (Jentsch et al., 2013). The tool is based on data generated by the GCM HadCM3, following the A2 socio-economic scenario (generation before RCPs), and allows users to recreate future weather files on three future periods: 2011–2040, 2041–2070, and 2071–2100. The details of the morphing equations for each variable used by the generator are described in the technical reference manual for the CCWWeatherGen (Jentsch, 2012). Some of these equations have been revised in (Jentsch et al., 2013). This tool is one of the mostly used in building simulations with future climate data, probably due to its open accessibility, ease of use and extensive documentation. It is recognized worldwide and has been used in most research articles analyzing building conditions with future climate data, such as in (Berardi & Jafarpur, 2020; Invidiata & Ghisi, 2016; Triana et al., 2018; Ciancio et al., 2019). Even though this tool is very practical to generate future weather files, it has a number of drawbacks. In our case, the two main drawbacks are that first it uses only one global climate model so it is not possible to consider the model uncertainties, and second as climate change is included in monthly averages, future extreme events (such as heatwaves) are not represented.

The morphing method has also been implemented in the Weather File Module of the WeatherShift commercial tool, developed by Arup and Argos Analytics. They used future climate data from 14 GCMs used for the IPCC Fifth Assessment Report (AR5), on three future periods: 2026–2045, 2056–2075, and 2081–2100 from the reference period 1976–2005 under the scenarios RCP 4.5 and 8.5. The morphing method is applied to eight climate variables from typical weather files: the mean, maximum, and minimum daily temperatures, the relative humidity, the daily total solar irradiance, the wind speed, the atmospheric pressure, and the precipitations. Cumulative distribution functions (CDF) are created via interpolation between the monthly means from each climate model (Troup & Fannon, 2016). One advantage of this tool is that it allows to consider the climate model uncertainty, as the user can select the percentile value of the CDF when selecting a future weather file. (Moazami et al., 2017) compared future climate predictions from the CCWWeatherGen and WeatherShift and concluded that WeatherShift presents a major drawback by modifying only a few climate variables beyond those having an important impact on buildings, such as the global solar radiation. However, WeatherShift allows for comparing outputs from different climate models and, therefore, assessing climate model uncertainties, which the CCWWeatherGen cannot (Troup et al., 2019). Since it also uses the morphing method, the limitation related to representing future extreme events is the same as for the CCWWeatherGen.

Stochastic weather generators

Other types of models exist, such as Weather Generators that recreate future stochastic weather files. For instance, the software Meteonorm proposes ready-to-use future climate weather files, under three IPCC future scenarios (B1, A1B, and A2 from AR4) for several ten-year future periods from 2010 until 2100. It is based on a stochastic method, which consists of

applying statistics to a set of climate data observations. The future generated climate data are an "average" of data issued from the 18 climate models used during the AR4. However, only three climate variables are modified during the generation of future weather files: the temperature, the solar radiation, and the precipitations and the documentation is very scarce (Meteonorm, 2017). Similar to the morphing method, climate change projections for Meteonorm are integrated in a monthly average and applied to the present data. In England, a stochastic weather generator (WG) was developed along with the UK Climate Projections 2009 (UKCP09). This generator produces future probabilistic years and future extreme years at an exceptional grid of 2 km (Jones et al., 2010). Future years can be generated for thirty-year periods every ten years, from 2010 until 2100, under three future emission scenarios (high, medium, low). Data were calibrated against observations for eleven RCM projections, allowing to reproduce future probabilistic projections through a vast number of future weather files and to consider climate model uncertainties. These projections are used today in the UK for studying indoor conditions in buildings under climate change, and they are able to reproduce future extreme temperatures (Kershaw et al., 2011). However, such climate data are not available for France.

Investigation on the projections of future heatwaves in statistical downscaling

In statistical downscaling, climate change projections are embedded through monthly averages, which induces that daily variations and temperature extreme events (e.g., heatwaves) are not well represented. Jentsch et al. compared statistically downscaled data with the morphing method from the GCM HadCM3 and dynamically downscaled data from the Regional Climate model (RCM) HadRM3, which was generated from the same GCM. They concluded that, despite a good correlation in the average variations, the morphed data could not accurately represent climate extremes such as heatwaves or cold spells (Jentsch et al., 2013). (Moazami et al., 2019) conducted a review of papers that used future climate data for building simulations. According to them, out of 34% of the authors who used extreme conditions, half of the papers are from the United Kingdom, where future extreme weather files are available at a national level from the stochastic Weather Generator. In France, such Weather Generator is not available and if future data containing extremes were available at the national level in France, they would probably be highly used in climate change impact studies for building simulations. However, at the present moment such a weather generator is not available, and the future weather years generated by Meteonorm do not contain future extreme temperatures either. Therefore, to analyze future heatwaves, other methods need to be investigated.

Uncertainties and limitations of statistical downscaling

In statistical downscaling, new uncertainties are added during the process (in addition to the uncertainties laying in the forcing GCMs) (Jentsch et al., 2013):

- **The spatial scale:** GCMs data are from a 100 km grid; whereas, the spatial scale of the observed weather data used to reconstitute the future EPW is much smaller. The projections are captured as an average of this spatial scale.
- **The time scale:** Uncertainties related to the time factor also need to be considered, since climate change variations are integrated through monthly averages.

- **The morphing equations**: The authors of the morphing method mention uncertainties in the equations themselves, since climate variables vary independently from each other.
- **The model and scenario:** Other uncertainties are the uncertainties related to the climate model and to the scenario chosen. While the WeatherShift tool allows to select through CDF a percentage (%) of future predictions beyond the climate models, and to choose between two future socio-economic scenarios, the CCWWeatherGen only predicts future climate data based on one climate model (HadCM3) and one future socio-economic scenario (A2, equivalent to RCP 8.5). Therefore, to this latter, neither uncertainties related to the scenario nor to the climate model can be assessed. Meteonorm database is from several climate models but does not inform users on how uncertainties in climate models are accounted for.

The CCWWeatherGen has been widely used in recent building simulation studies, however, none of the studies mention the impact of the uncertainties on the results. Some authors, to consider model uncertainties, directly applied the morphing technique to multiple GCMs or the GCM developed in their country and used the downscaled data for building thermal simulations (Wang et al., 2012; Zhai and Helman, 2019; Ren et al., 2011). However, systematically considering model uncertainties for building simulations is not yet a practice in the building research community, even though its necessity is explicitly expressed by the climate community (Giorgi, 2019).

Concluding remarks on statistical downscaling

Despite the uncertainties related to statistical downscaling and the limitations of the various tools, statistically downscaled future weather files are the ones most largely used by the building research community, as they are the easiest to manipulate and to use. Many authors use the future weather files provided by Meteonorm or by the CCWeatherGen, without mentioning climate uncertainties. Indeed, such climate data can be used for a quick climate change impact assessment. In the context of this Ph.D. thesis, we consider that these data cannot be used to analyze health related heat impact under climate change, since future heatwaves cannot be modelled. Table 4 summarizes the different tools available to statistically downscale data from global climate models.

Table 4 - Summary and description of the tools for future climate data statistically downscaled

	Tool	Availability	Number of climate models	RCP Scenario	Projections of future heatwaves
Morphing method	CCWWeatherGen	Open source	1	8.5	Not possible
	WeatherShift	License needed	14	4.5, 8.5	Not possible
Stochastic method	Meteonorm	License needed	18	4.5, 8.5	Not possible
	Weather Generator	Not available for France	Many	4.5, 8.5	Possible

1.3.3.2 Dynamical Downscaling

Regional climate models

Regional climate models (RCMs) are climate models issued from global climate models with a smaller spatial resolution (10 to 50 km), they are "dynamically downscaled" by the climate research community. Since only a specific part of the world is represented in a RCM (usually a continent or a portion of a continent), the grid has a higher spatial resolution, allowing better representation of local climate effects. The regional climate models use meteorological boundary conditions (temperature, water vapor and cloud variables, wind speed, etc.) from global climate models. Each RCM is downscaled from one GCM, but the same RCM can be downscaled from other GCMs as well, resulting in various GCM_RCM combinations. RCMs allow simulations of climate phenomena that happens on a smaller scale, such as the state of the atmosphere (precipitations, storms, etc.), the physical representation of the complex land topography and coastline, the surface vegetation distribution, the inland bodies of water, the land occupation including urban settlements, etc. Oceanic characteristics are not modelled (they are boundary conditions); the RCMs only model the atmosphere and the vegetation. RCMs also have a refined time resolution, down to one hour. Regional climate modelling originated in the late 1980s and the European community has been very active in RCM development. RCMs allow the representation of extreme events, both spatially and temporally, which is why they are considered necessary for local adaptation studies.

(Giorgi, 2019) compared the total precipitation above the 95th percentile over the Alpine region in Europe modelled with a GCM and a RCM to observations (Figure 24). He could conclude that RCMs allow to represent with a greater accuracy both the spatial and temporal complexity of the observed extreme precipitations. Furthermore, RCMs have proven to well represent spatially other extreme events, such as heatwaves (Lhotka et al., 2017; Vautard et al., 2013; Fischer and Schär, 2010).

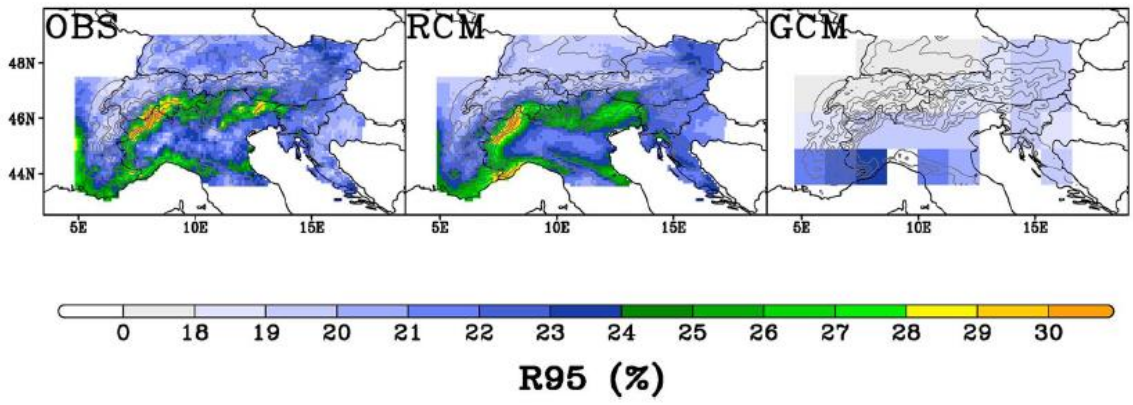

Figure 24 - Fraction of total precipitation above the 95th percentile (R95) over the Alpine region. Units are in percent of total precipitation and the simulation period is 1975–2004. OBS = observations, RCM = regional climate model, GCM = global climate model;

Several projects initiated by the World Climate Research Program (WCRP) allowed to improve the accuracy of regional climate models. As inconsistencies were noticed along with regional climate models, these projects allow to establish a common simulation protocol among climate laboratories. The model's resolution was improved to ~ 25 km through the

PRUDENCE & ENSEMBLES projects. Today, an unprecedented resolution of ~12 km is available for the models that are part of the European Coordinated Regional Downscaling Experiment (EURO-CORDEX; Jacob et al., 2014), and the project is the main reference framework for regional downscaling research (Kotlarski et al., 2014). Its main goals are to evaluate and improve the different RCMs via a better understanding of regional and local climate phenomena and uncertainties and to foster communication and knowledge exchange among the climate community. The project also aims to generate and maintain a consistent database of downscaled multi-year projections over regions worldwide that can be used for adaptation studies in various sectors, such as agriculture, fire risk, air quality, or heat stress (Giorgi, 2019). A large amount of RCM data is available on the CORDEX project platform (WRCP, 2019). The platform is updated regularly, and new climate data are uploaded often. CORDEX domains are available for all parts of the globe (Figure 25). EURO-CORDEX projections are available for Europe, on a grid resolution of 12.5 km; CORDEX projections are available at a 25 km grid resolution in the Middle East and in North Africa and about 50 km in the rest of the world. Data are available at the multi-year format on different time scales: monthly, daily, every six, three or each hour, during the historical period from 1976 to 2005 and for the future period, from 2006 to 2100. Depending on the model, data are available for the RCP 4.5 and or RCP 8.5 scenarios. At the three-hour time step, all necessary climate data to reconstruct a weather file for building simulations are available for many models. At larger time steps, more climatic variables are available. The detail of the available climate data is described in (EUROCORDEX, 2019b).

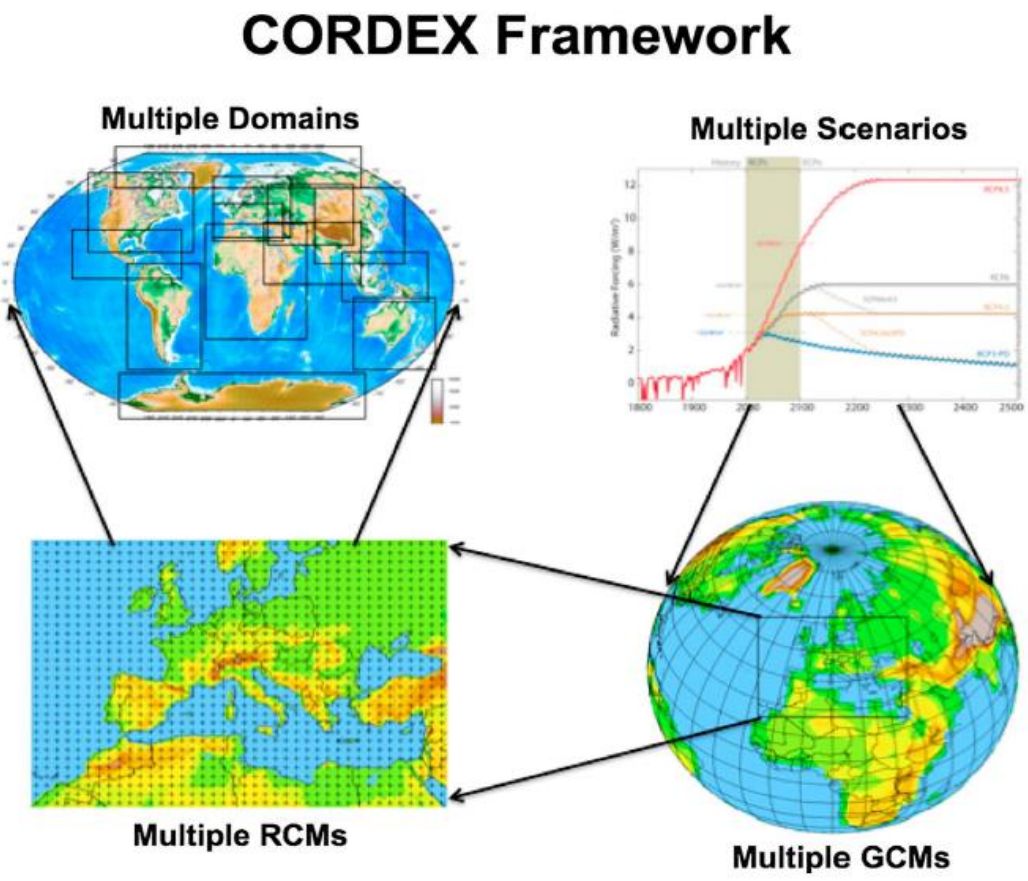

Figure 25 - Representation of the Coordinated Regional Downscaling Experiment (CORDEX) Framework (Giorgi, 2019)

As of the beginning date of this thesis, future climate data from the CORDEX platform were available at the 3-hour time-step for four climate models. In order to be used for building simulations, these data need to be interpolated down to the hourly time-step. Some data are today available at the hourly time-step, for the model (MPI-REMO). Furthermore, for some climate variables, data are not instantaneous but they are three-hour averages, which increases the complexity of the process. The advantage of the CORDEX project is that it provides many climate data from different climate models and different socio-economic scenarios for all regions in the world, allowing impact studies considering models and scenario uncertainties. Furthermore, as future climate data are available in a multi-year format from 2005 until 2100, extremes of the distribution on different timescales can be investigated. EURO-CORDEX multi-year projections are also available on the French DRIAS platform (Ministère de la Transition Ecologique et Solidaire), dedicated to adaptation studies. However, data on this platform are daily averages, which do not fit the time-step required for dynamic building simulations. According to (Moazami et al., 2019), who conducted a review on scientific papers assessing the impact of climate change on building performances, only 10% of the articles reviewed used dynamical downscaling. This might be because regional climate data have only very recently become easily accessible.

Investigation on the projections of future heatwaves in dynamical downscaling

To the author's knowledge, Nik is the only author who developed a methodology in 2016 to reconstitute future weather files containing temperature extremes, using data from regional climate models. He created the so-called "future extreme years" (cold and warm), selected from a centile of the dry-bulb temperature (Nik, 2016). (Ramon et al. 2018) suggested the use of future multi-year datasets to assess the resilience in extreme weather conditions, and recreated several typical and extreme year methods for comparison with regional climate data. Many authors have characterized the occurrence, frequency, and duration of future heatwaves in the climate research community; however, little of this research has been used by the building research community. In France, the National Center for Meteorological Research (CNRM) and Pierre Simon Laplace Institute (IPSL) laboratories are conducting research on future climate data and are particularly active in future climate data research. (Lemonsu et al., 2015; Lemonsu et al., 2014) characterized and identified future heatwaves from different Representative Concentration Pathway (RCP) scenarios and climate models under both historical and future scenarios, and used these future heatwaves to assess different mitigation and adaptation scenarios at the urban level, but not at the building scale. More recently, (Ouzeau et al., 2016) developed a method to detect future heatwaves from a climatological point of view from a EURO-CORDEX dataset. Therefore, these future climate data present good potential to be used to reproduce weather files for building simulations including future heatwaves.

Uncertainties in dynamical downscaling (RCMs)

According to (Giorgi, 2019), in the last generations of GCMs the range of temperature difference between the models remains fairly high, from 1.5 °C to 4.5 °C which is in accordance with Hawkins et Sutton. Model uncertainty increases when downscaling from global scale to regional scale, and the regional temperatures from various models can vary from 3 ° C up to 10 ° C, with the highest differences found in northern high latitude regions. In an older article,

Giorgi assessed the uncertainty from GCM and RCM separately of temperature and precipitations in Europe, both in summer and winter (Figure 26). Regarding summer temperatures, he showed that the highest uncertainties were the one related to the scenario and the GCM, followed by the uncertainty related to the RCM. Only a small part of the uncertainty was related to the internal climate variability. By summing the uncertainty related to RCM and GCM, it appears that the model uncertainty becomes higher than the uncertainty due to the scenario. In order to assess the impact of these uncertainties on the results, it is necessary to conduct simulations with climate predictions from various climate models and socio-economic scenarios. According to (Giorgi, 2019), for impact assessment studies, it is necessary to use well-designed scenario-GCM_RCM matrices to fully assess the uncertainties associated with regional and local climate change information (Giorgi, 2019). Since numerous climate data are available on the CORDEX platform, it is possible to assess the climate data uncertainty by using multiple future climate files for building simulations. In the literature, most authors are using one climate model to assess future temperatures, sometimes with two socio-economic scenarios under different future periods. This can be explained by the fact that up until very recent years, future climate data from regional climate models were hard to find. To the author knowledge, to date only few researchers have considered regional climate model uncertainties by comparing the temperature outputs from several climate models and their impact on building thermal simulations (Moazami et al., 2019b; Nik et al., 2012; Ren et al., 2011).

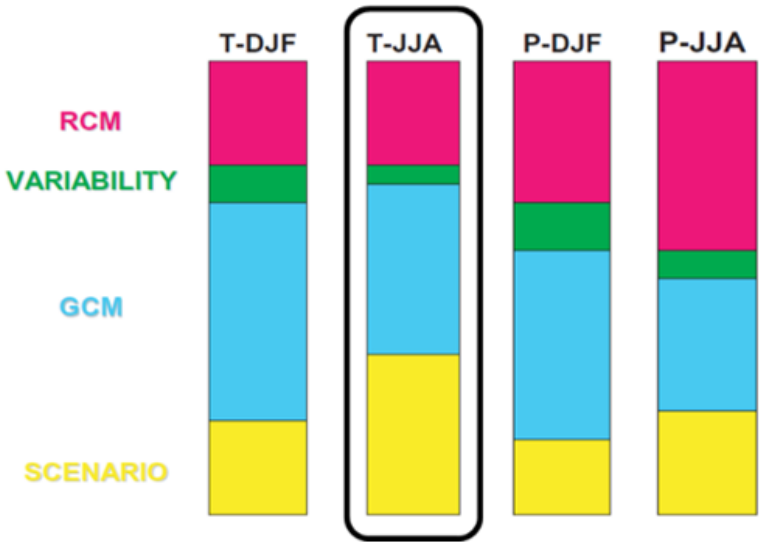

Figure 26 - Relative contribution to the uncertainty in the simulation of climate change over Europe originating from various sources: RCMs (8 models), internal variability of GCMs, GCMs (4 models), scenarios (2 used). T is the temperature and P is the precipitation. DJF is winter and JJA is summer. The highlighted column is the summer temperature (Giorgi, 2006)

Concluding remarks on dynamical downscaling

Regional climate models provide multi-year future datasets for a wide range of models and scenarios. These datasets include extremes of the distribution for the several weather variables, allowing to detect heatwaves. Furthermore, these future climate data can be used to consider uncertainties by using multiple climate models and scenarios. Table 5 summarizes the databases that can be used to gather future downscaled climate data for French cities.

Table 5 – Summary and description of the databases for future climate data dynamically downscaled

Database	Availability	Number of climate models	RCP Scenario	Projections of future heatwaves	Lowest time-step of the data
CORDEX	Open source	Many	4.5, 8.5	Yes	3-hourly or hourly depending on the model
DRIAS	Open source	Many	4.5, 8.5	Yes	Daily

1.3.4 **Bias in climate data**

Raw output data from regional climate models are not bias adjusted and, therefore, need to be post processed to correct the bias between models and observations. Especially for local adaptation studies, bias-correction is needed. The bias is the difference between calculated projections from the climate models and measured observations. In articles from authors using data from regional climate models for building thermal simulations, most of the time, the question of the bias correction is not addressed, and it is difficult to know if it was considered or not. In other fields of research, climate outputs are systematically bias-corrected, however, in the building research community bias-adjustment of climate data for impact assessment is not an automatic practice yet. It is of importance that when using future climate data, one should be aware if the data were bias-adjusted or not since non-bias-adjusted climate outputs can vary a lot compared to bias-adjusted ones. A few authors bias-adjust future climate data for building simulations (Arima et al., 2016). Different techniques exist to correct the model bias, commonly called "bias-adjustment" methods. These methods usually compare the raw-data outputs from climate models with measurements during the reference period and calculate a correction factor. This correction factor is then applied to both historical (historical-bias-adjusted) and future data (future-bias-adjusted) from climate models. Bias-adjusted values of different climate variables are not expected to match exactly with the observations, as they do not represent day-to-day evolution of the weather. However, bias-adjustment methods allow correcting all the climate variables distribution functions; and they do not only correct the average values, but also the extremes of the distribution curve. Many bias-adjustment methods exist in the climate community, for instance the distribution-based scaling method used by the Swedish Meteorological Hydrological Institute (SMHI)(Yang et al., 2010), the quantile mapping method used by the Norwegian Meteorological Institute (METNO), the cumulative distribution function method (used by IPSL), or the multivariate quantile mapping method (Cannon, 2018). The main assumption is that the correction factor does not change with the changing climate and, therefore, the bias will be the same in the future. However, it is not known if the model bias will change in the future or not, adding a supplementary uncertainty.

1.3.5 **Concluding remarks on future climate data**

This section has described the two different downscaling methods that exist, the tools available to reproduce future weather data, and the main advantages and disadvantages of each method (summarized in Table 6). It compared the possibility to include heatwaves in future climate data and assessed the different uncertainties related to future climate data.

Table 6 - Advantages and disadvantages of downscaling methods

	Statistical (Morphing, Stochastic)	**Dynamical (Regional Climate Models)**
Available tools	CCWeatherGen WeatherShift Meteonorm	No available tool, but databases: CORDEX, DRIAS
Advantages	Simple method Low computational power Energy Plus Weather (EPW) files (future typical years) ready to use for building simulations	Physically consistent datasets across different weather variables Extreme events (such as heatwaves) are well represented
Disadvantages	Climate change is only represented through monthly averages, future extreme events are not represented Lack of physical consistency between weather variables Models and scenarios used depend on the tool, which makes it difficult to assess uncertainties Analogies to present-day climate, assumptions that future weather patterns will be similar to present-day observations It is not known if climate data from the GCMs have been bias-adjusted	High storage capacity needed All data needed to reconstruct a weather file not available at the hourly format yet on the CORDEX platform (3 h time-step data available) Formatting and interpolations are required to reconstruct an EPW file (time-consuming and requires some knowledge) Most data on the CORDEX platform are not bias-adjusted

Most authors using future climate data to assess the impact of climate change on building thermal simulations are using future typical weather years. In fact, this underestimates climate change effects, since temperature extremes are increasing faster than temperature means (Lewis & King, 2017), which has been proven recently with multiple heatwave occurrences (Russo et al., 2014). Despite the lack of future weather files containing temperatures extremes, some authors have been using recorded hot years or heatwave observed data to assess the resilience of the building to hot external temperatures (Alessandrini et al., 2019; Synnefa, et al., 2018; Pyrgou, et al., 2017). In the UK, (Liu et al., 2016; Liu et al., 2019) used the UKCP09 British weather generator to generate future probabilistic hot summer years and, more recently, future hot event probabilistic years (Jentsch et al., 2015) developed near-extreme summer reference years (SRY) for the United Kingdom, adapting the UK design summer reference years (DSY) by adding the solar radiation and cloud cover in the selection process to better represent typical outdoor conditions for buildings overheating (high temperature, high solar radiation, and low cloud cover) (Du et al., 2012). On a risk point of

view, it is crucial to evaluate indoor building conditions under future hot temperatures during heatwave events. Assessing the resilience of buildings to future climate with future weather files containing warm years, extreme hot years, or heatwaves, is a very recent practice. (Nik, 2016) has reconstituted future extreme years, which is interesting to use for conditioned buildings, to assess building peak loads and consumption during extreme years. However, extreme years do not necessarily capture heatwaves. For non-conditioned buildings, our interest is to assess buildings resilience to future heatwaves. To our knowledge, reconstituting weather files containing future heatwaves to assess the resilience of buildings during a hot event has only been done by (Liu et al., 2019), however they used stochastic data which are not available in France. For this Ph.D. thesis, we propose to reassemble future weather files containing future heatwaves detected from regional climate models.

In the climate community, it is advised to do impact assessments with several climate models, if not all, to quantify uncertainties. However, in the building community, many articles display results for one climate model and assess the effects of climate change in absolute future temperatures. Most authors do not mention model biases and only a few consider uncertainties by comparing several climate models and socio-economic scenarios (Nik et al., 2012). Figure 27 summarizes the different methods and tools used to reconstruct future weather files from multi-years climate projections, and the uncertainties propagation along the modelling chain.

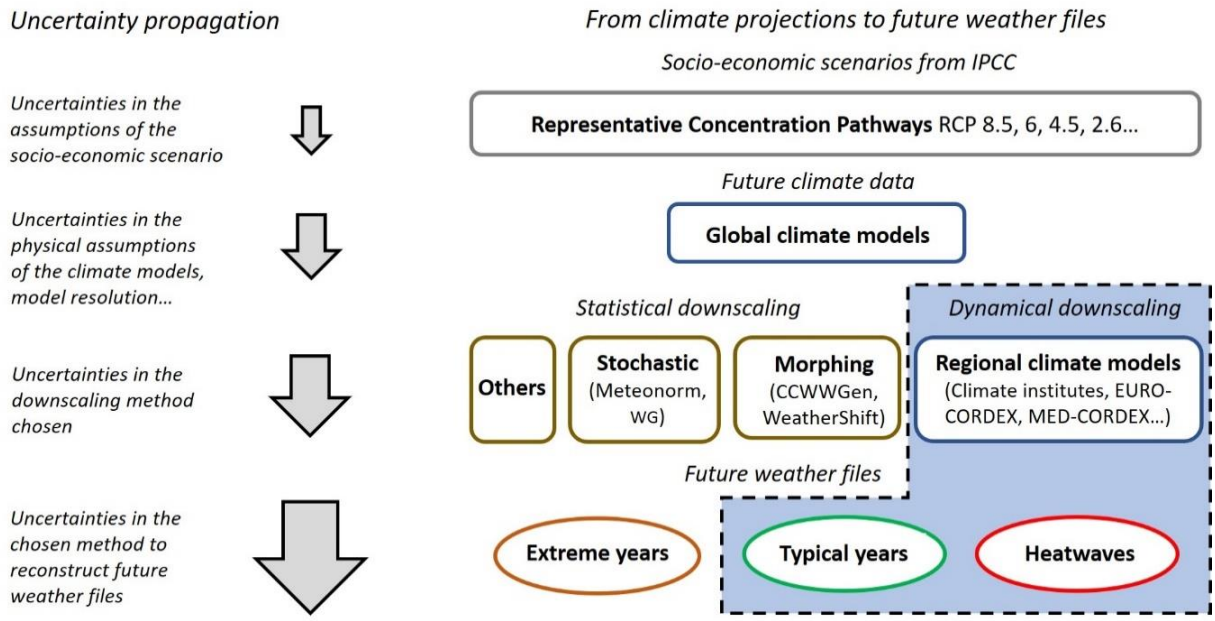

Figure 27 - Uncertainty propagation along the modelling chain from multi-years climate projections to future weather files., method proposed highlighted

1.4 Conclusive remarks on the state of the art

In this chapter, we reviewed the state of the art on three aspects: human, building and climate. We reviewed the models and tools available to assess the summer thermal comfort, discomfort or health-heat-related risk inside buildings. From the state of the art, many comfort models and heat stress indexes exist. Since we are interested in an easy-to-calculate indicator to assess the different stages from thermal comfort, discomfort to health risk, the use of the standard effective temperature seems to be a good compromise. However, the state of the art revealed that metrics are lacking to assess the potential health risk related to indoor overheating during consecutive days of heat exposure. In the second part, we reviewed several passive cooling strategies, techniques and systems that can be used to increase the building resilience to extreme heat. Many solutions exist to mitigate and adapt the building to warming temperatures induced by climate change, however they are either in concurrence with the winter design, either depending on the local climatic conditions and therefore limited in potential. In order to assess the building ability to maintain comfortable and safe indoor environments under periods of extreme heat, these different techniques will be evaluated through thermal building simulations. The building case-study, amongst with the modelling software and choices made to model these solutions are presented in the next chapter. Finally, the state of the art revealed that future heatwaves projections are available from regional climate models. In Chapter 2, the collection, selection and assembly of these future heatwaves into ready-to-use weather files for building simulations will be presented.

Chapter 2
Research methodology

In this chapter, we present our research methodology developed for the purpose of this Ph.D. We introduce first our methodological approach, which goal is to provide a contribution to building design resilient to heat, that both mitigate and adapt to climate change. Beyond traditional assessment of energy needs and summer thermal discomfort in France, a new performance objective is introduced, to analyze the building indoor thermal conditions, and associated potential health-heat-related risk under recurring future heatwave periods. Our contribution into the building design process is outlined in the second section.

In the third section, we present the method developed to reassemble two types of weather files: present and future typical years, and future extreme years containing heatwaves, based on regional downscaled bias-corrected climate data. In the fourth section, we introduce the building used as a case study, and explain our modelling choices. The fifth section presents the sensitivity analysis and optimization methods and tools used to evaluate the most impactful building design parameters on the performance objectives.

This chapter aims to answer the following research questions:

Where would our design contribution fit during the building design process?

Which future climate data to use, from which climate model, under which socio-economic scenario? How to consider climate uncertainties?

Which methods and tools can be used to propose building designs that both mitigate and adapt climate change?

Summary

2.1 Methodological approach

One of the research questions is if it is possible to design comfortable, robust, resilient and safe buildings under future climate. From these questions, underlie multiple questions: *How do we define future climate, and to which climate conditions must the building be comfortable, or present a minimal heat-related health risk? How do we assess the impact of the future climate on the building indoor overheating? How do we define comfortable, uncomfortable, health-heat-related risk?* The ultimate goal is to propose a methodology that allows to assess if the building indoor conditions can both mitigate and adapt to the future climate. Figure 28 showcases the methodological approach undertaken in this Ph.D. thesis.

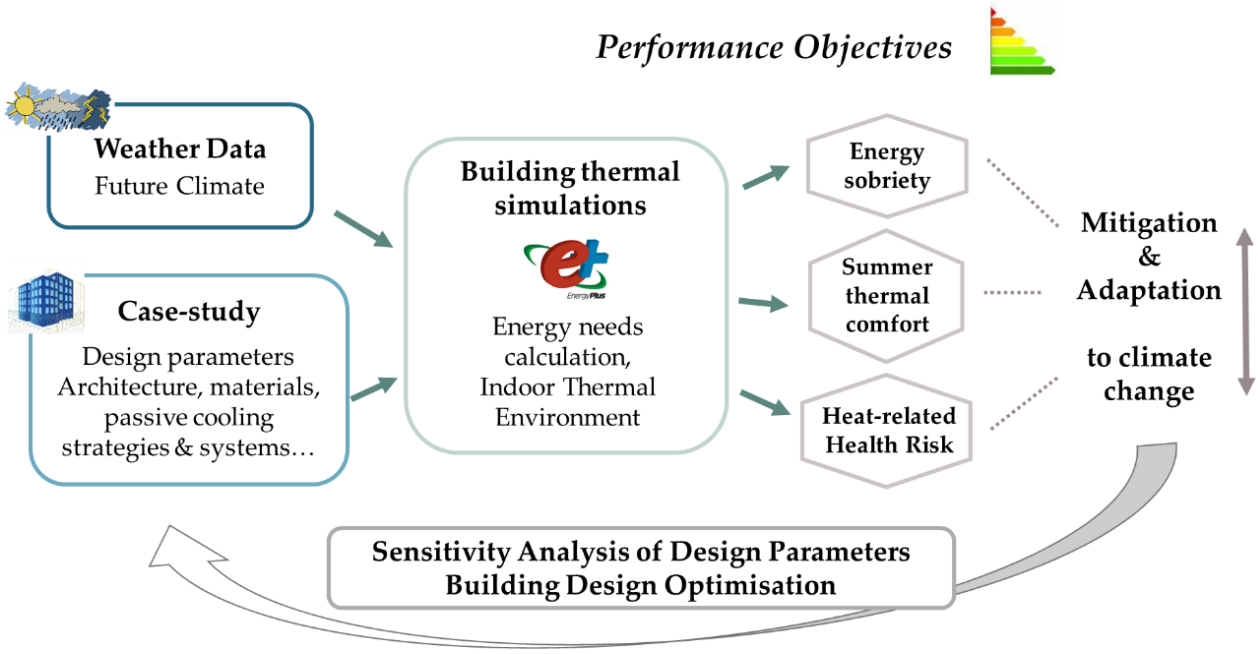

Figure 28 – Thesis methodology overview

In this chapter, we present the different methods and tools used and the different steps. The first step is to select a set of future climatic conditions that will be the boundary conditions to our building simulations. From Chapter 1, we have identified that it is possible to access future multi-years data sets from several climate models under different socio-economic scenarios. In section 2.3, we will explain the methodology used to reassemble two types of future weather files, future typical years and future heatwaves. This section will aim to answer the questions:

Which future climate data, which type of weather file should we use?
From which climate model? Under which socio-economic scenario?
How to consider climate uncertainties?

The second step is to define a case-study building, and to model it with a simulation tool. The building was given by an architect and has an initial architecture and material properties. We chose to model the building with EnergyPlus, it is presented in section 2.4. Along the EnergyPlus simulations, through the sensitivity analysis and building optimization, presented

in section 2.5, we will modify the building initial configuration to understand which fits best for which climate and a given set of performance objectives. Alternative or additional passive strategies and systems will be added, and their modelling is introduced in section 2.4 as well. In Chapter 3, we will analyze the future climate data reassembled, and present the climate sequences that will be used for the building thermal simulations.

The EnergyPlus building simulations, as well as the results of the sensitivity analysis to understand the dynamics and behavior of the strategies and systems under different climatic conditions, will be outlined in Chapter 4. Finally, in Chapter 5 we will present the results from the building optimization to propose design guidelines for specific case-studies, as well as the analysis of the optimized solutions. In that last chapter, the optimized solutions will be assessed and compared using the different performance objectives.

In the second part of Chapter 4 and the first part of Chapter 5, we will aim to answer this question:

How will the future climate influence the building design?

In the second part of Chapter 5,, we will aim to answer this question:

How will the building design influence indoor overheating under future climate?

The difficulty of the work is to find the balance between mitigation to future typical climate (energy sobriety, summer thermal comfort), and adaptation to future heatwaves (reduced heat stress). With this Ph.D., we aim to propose a methodology that allows to assess if the building indoor conditions can both mitigate and adapt to the future climate. The performance objectives should help to:

- Ensure that the proposed building design **mitigates the future climate.** For this purpose, building energy needs will be quantified: Can we propose a comfortable building during both future typical winters and summers with low energy needs?

- Ensure that the proposed building design **is adapted to future climate**. This will require to assess if the building is comfortable under typical future climate summer conditions, and if the building will be safe under future heatwaves, which is an increased risk in the future.

Figure 29, adapted from (Folland et al., 2001) and (Alessandrini et al., 2019), illustrates the present and future air temperature distribution over multi-years. Compared to the contemporary climate (previous), for the future new objectives need to be investigated. We can observe on the graph the evolution of the temperatures that constitute the "mitigation" part: The average, or typical temperatures will be warmer, and more spread out. Also, in that sense mitigation refers to present and future typical conditions, while adaptation refers to future warmer conditions, typical or extremes. Indeed, on the right part of the graph we can observe that the region of "much more hot weather" and "more record hot weather" signifies that there is a need for adaptation to future hot temperatures, as these will be much more recurrent than in contemporary climate. Finally, the "more record hot weather" part of the graph is new, these temperatures were not observed in contemporary climate. It represents

the resilience part: will our building design provide safe indoor thermal conditions for the occupants under future extreme hot record temperatures? Definitions for these three concepts are given below.

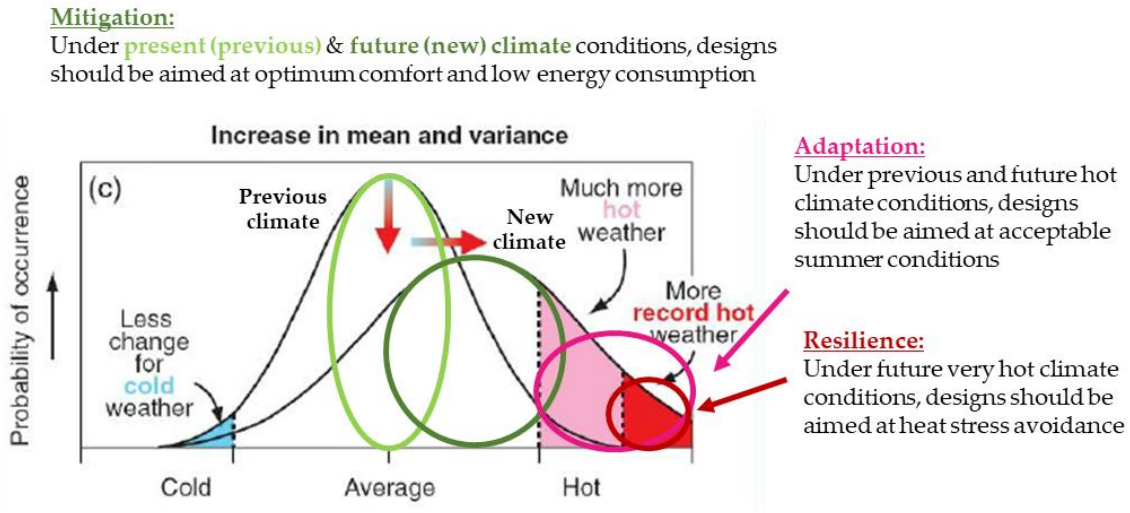

Figure 29 - Mitigation, adaptation and resilience to future climate changed induced temperatures, adapted from (Folland et al., 2001) and (Alessandrini et al., 2019)

Mitigation

One of the research questions is to find out if it is possible to provide a building design, for a specific case-study (building and city) that will not be overheating in future climate, so as not to use air-conditioning? While buildings are today designed as "bioclimatic", they are mostly designed to minimize heating needs in the winter. However, in the future, warmer temperatures will occur more often while cold temperatures will occur less often: As can be seen in Figure 29, there is a shift in mean temperatures towards the right: In France, a shift between passive winter design and passive summer design might occur. This shift would lead to a change in paradigm, as maybe more emphasis should be then put on passive summer design. *Would the cooling needs then be higher than heating needs?* Some passive summer design strategies are in opposition with passive winter design strategies. *For instance, cool paints are a good solution to reduce solar heat gains, but do they increase the heating needs in the winter? Which will be the most important in French climate? We know that high thermal inertia coupled to exterior insulation functions well in the winter, but does this design apply well to the summer as well? We currently design buildings with large glazed windows in the South façade, how does this design influences summer overheating, especially during the future?* These are all questions that we aim to answer within this research. Mitigating climate change can lead to opposite objectives in the building design, which brings the question: *Can we design buildings that behave thermally well in both winter and summer in contemporary and future French climate? Can we provide such a bioclimatic design with reduced both heating and cooling needs?* This objective performance will be quantified as yearly energy needs, which will be assessed in Chapter 5.

Adaptation

From Figure 29, we can observe that the temperature does not only change in warmer means, but also in a larger distribution: there will be much hotter weather, and as well much more extreme hot weather. What is known as typical warm weather today, will be different

than typical warm weather tomorrow. For instance, typical summer temperatures in Paris might be around 25 °C nowadays, and extreme temperatures around 35 °C, while tomorrow 35 °C might become typical, and 45 °C extreme. We must adapt the building design, to be comfortable to future typical summer temperatures. Therefore, part of this work will be to define what will be typical future summer temperatures. In France, the thermal regulation includes a criterion for summer comfort, that is that summer indoor temperatures must remain under certain thresholds. The summer comfort criterion, introduced in 2005 and recently reinforced in 2021 (RE-2020), now requires a more complete overheating assessment during the past 2003 heatwave which was known for its health-related to heat adverse effects. In this Ph.D., we will provide an analysis of future warm temperatures, and future heatwaves occurrence to provide guidelines to minimize heat stress risk during the building design, these are presented in Chapter 3. The indicators related to this performance objective are those related to summer thermal comfort and health-heat-related risk. Different indicators will be tested and used in Chapter 4 and Chapter 5.

Resilience

Beyond adaptation, is the concept of resilience. It is an emerging concept within the field of building design, and it has so far, no precise definition (Miller et al., 2020), but it is closely linked to the ability of the building to withstand extreme events. While adaptation is linked to adapt the building to typical future conditions, a resilient building would be a building adapted to future extreme conditions, for our specific case future intense and extreme heatwaves. Nowadays, at the building scale, little work has been done so far to analyze building resilience to future indoor overheating under future intense heatwaves. In this Ph.D., we focus on adaptation to climate change, i.e. contribution to building design to recurring conditions. However, the methodology proposed here allows to reassemble future weather files containing future extreme heatwaves, then can be used for further work.

2.2 Contribution to the building design process

In this section, we present where our proposed building design research methodology could be used in practice. We believe our methodology could be used by an engineering consulting firm (*bureau d'études,* BE in French). This actor would conduct the building simulations and give insights on the building design to both mitigate and adapt to climate change. To understand more in detail at which step of the building design, we first introduce the different building design phases. The building design is based on a number of factors (project constraints and objectives from the different partners, budget, local climate, culture, urban context around the building, life cycle analysis, etc). Our methodology aims to give insights on which building designs would be best on an energy and indoor thermal conditions perspective. This section aims to answer the following question: *Where would our design contribution fit during the building design process?*

Specifications (*Cahier des charges*)

Prior to the building design and construction, the first step is initiated by the *Maitrise d'ouvrage, MOA* (contracting private firm or public organization) which specifies the building needs, the project constraints, the budget, and the planning. Different actors are involved, depending on the project specificities. This phase results in an *appel d'offres* (call for tenders).

Design sketch (*Esquisse, phase concours*)

Different *Groupement de Maitrise d'œuvre, MOE* (project management consortiums) answer the call for tenders with a building design sketch ("esquisse" in French). *Groupement de Maitrise d'œuvre* are usually constituted by an architect, specialized engineering teams, economists, urbanists, paysagists. They must answer the project specifications and propose a feasibility study and different sketches for the building considering the building site and budget constraints. At this stage, they propose several solutions regarding the building function, volumes, orientation, bioclimatic features, with a cost estimation for each proposed solution. At the outcome of this phase, the contracting firm chooses the project management consortium (*MOE*) which will be in charge of the project implementation. The *MOE* will be in charge of the project during the remaining design phases. In between each design step, the *MOE* interacts with the *MOA* which provides feedback and ask for re-adjustments of the design.

Basic Preliminary Design (*Avant-Projet Sommaire*)

During this phase, the selected *MOE* must define and describe more precisely the different proposed options answering the specifications, in terms of plans, volume, interior circulations, and exterior aesthetic aspect. It must also include preliminary technical notes on the building structure, fluids, thermal (such as an approximation of the building energy needs) and acoustics, and an energy provision study (*Faisabilité Approvisionnement Energie*). Finally, it must provide a planning of execution, and a preliminary estimation of costs. Following this step, the *MOE* and *MOA* discuss to classify the different proposed solutions and selects the final proposed designed based on the different project objectives and costs.

Detailed Preliminary Design (*Avant-Projet Détaillé*)

During this phase, the *MOE* refines the selected design. The building dimensions, surfaces, technical solutions such as HVAC systems, materials choice become definitive. The costs are

estimated by trade (*Lot*). The different technical provisions are more detailed and must comply with the Thermal Regulation (RT). For new buildings larger than 1000 m², a thermal study must be done to detail the building energy needs. The documents constituted during this phase, wrote by the *MOE* and validated by the *MOA*, are used to apply for the building permit (*Dossier de demande de permis de construire*).

Project

Once the building permit is obtained, the project phase can begin. The final design of solutions is established (such as the sizing of HVAC systems), and their position within the building. The final thermal study is realized (with the RT compliant tool or with a STD software) with detailed thermal zones: the Bbio, Cep are calculated such as the summer thermal comfort study and carbon emissions in the new RE-2020. The exploitation costs are also calculated. At the end of the project phase, the tender documents (*Dossier de consultation des entreprises, DCE*) are made public, to recruit the material suppliers and building contractors. After the project phase, the construction steps begin. A complementary mission of the *MOE* can be to help the *MOA* to select the contractors, who adjust the execution plans with the final materials and technologies. The *MOE* synthetases the documents from the different trades and ensure that they are well coordinated. Finally, the construction can begin.

Our design contribution

We believe our design contribution will be used by an engineering consultant firm (*Bureau d'études, BE*), part of the *MOE*. At each step of the building design, the architect is in contact with the *BE* which provides him feedback on the design and technical studies. Our contribution along the design phases is illustrated in Figure 30.

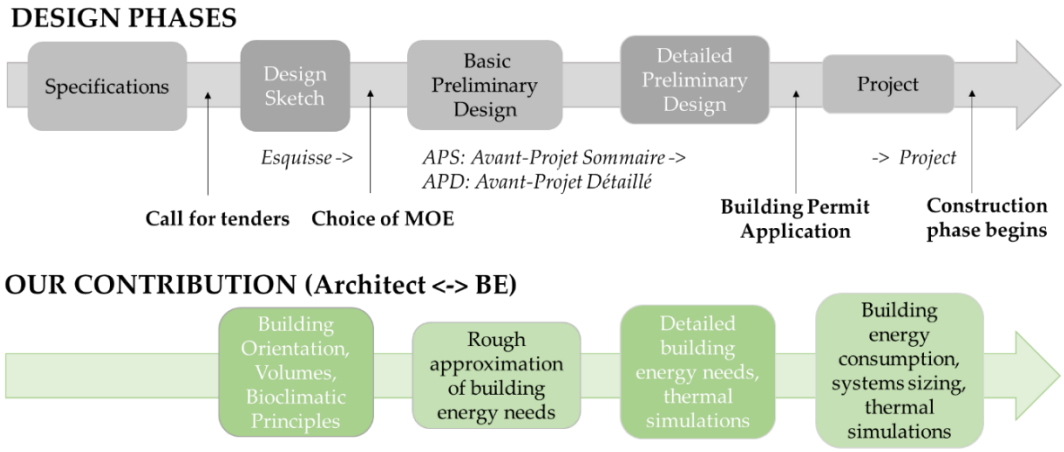

Figure 30 - Our design contribution within the building design process

During the sketch phase, our contribution can already be used through principles of bioclimatic design for summer, and especially for future summers. During the basic and detailed preliminary design phases, thermal building simulations are made to ensure the building is RT compliant. At these stages, the results of the building optimization (in terms of energy needs and consumption, summer comfort and future climate uncertainties) can be used to assist in the building design to find a balance between low heating consumption during winter and passive cooling strategies and systems to adapt the building design to future summers. Finally, at term, the future weather files and associated performance objectives could be implemented in national regulations.

2.3 Future climate data selection, collection and assembly

In this section, we aim to answer the following questions:

Which weather file to use to respond to the different performance objectives?

How can we consider the climate uncertainties in future weather files?

The most complicated question remains how to consider the uncertainty linked to future climate, which lies beyond the climate socio-economic scenarios, and the climate models. In the context of this Ph.D. thesis, we will limit the scope of our research to the following points:

- **Time period: Analysis of the mid-century (2040-2069)** because climate uncertainties are too uncertain towards the end of the century, and it is too far in the future to account for the development of new innovative passive cooling systems. Furthermore, as a building lifetime is around 50 and 100 years, we thought it would be best to design a building for the mid-century, which will be the middle of the use of a building built today. This way, the summer design will not be either under or over thought.

- **Socio-economic scenario: Analysis of the RCP 8.5 only**, because we are investigating health risk, we assess the worst-case scenario. Furthermore, there is evidence that this socio-economic scenario will become the new "normal" in the new IPCC report in 2021. Reducing the scope of this study to only one scenario will reduce the number of future weather files to investigate.

We will analyze the climate over the mid-century in three case-study cities: Roissy (and Paris considering the urban heat island (UHI)), La Rochelle and Carpentras. Paris is the French capital and is characterized by a continental/oceanic climate. La Rochelle is a city located in the middle of the West Atlantic coast of France and is characterized by an oceanic climate. Carpentras is a city located in the South of France, where record temperatures have been registered, it is characterized as Mediterranean climate. Summer temperatures are very warm during the day, but become colder during the night due to its proximity to the *Mont Ventoux* (French mountain of about 1,900 m high).

In order to account for future climate uncertainties, we will analyze climate data from different climate models, as we have understood in Chapter 1 that the uncertainty related to climate models is the highest in comparison with the others (socio-economic scenario and natural climate variability) for the mid-century period. To analyze the building robustness to a variety of climate conditions, we will investigate both contemporary and future typical summers, as well as heatwaves. The use of the future heatwaves weather files will allow us to analyze not only the potential of the building design to maintain comfortable indoor conditions under future summers but also to assess the building resilience to indoor overheating, quantifying the potential heat stress under future heatwaves. The future weather files are defined based on exterior climate conditions, in order to eliminate the dependence to the building design.

2.3.1 **Future weather files assembly – Methodology**

In this section, we describe the methodology we used to assemble future weather files from the CORDEX climate multi-year projections. Two types of future weather files were assembled: future typical years (TMY) and future heatwave events (HW). Figure 31 displays a summary on the methodology to assemble the future weather files. We first downloaded the files containing the climate data (NETCDF4 format) and extracted the climate data from these files. Then we present the future weather variables available and of our interest for building simulations. We used data from four climate models available at the time of the analysis, that we compared with other climate models (Step 1 and 2, section 2.3.1.1). We then interpolated the data available at a three-hourly time step to hourly time-step (Step 3, section 2.3.1.2). The hourly climate data were then bias-adjusted (Step 4) using hourly weather data observations (Step 1bis), this is explained in section 2.3.1.3. Then, the direct and diffuse solar radiation were calculated from the bias-adjusted global solar radiation (Step 5), detailed in section 2.3.1.4 Finally, we followed the norm EN-15927-4 to reassemble typical years over the historical and future periods (Step 6), and two different methods to detect heatwaves (Step 7), these are respectively explained in section 2.3.1.5 and 2.3.1.6. Part of this work was published in a journal article (Machard et al., 2020a) and the methodology was shared amongst the ongoing Annex 80 project "Resilient cooling for buildings" within the Weather Data Task Force group to reproduce future extreme weather files for many cities worldwide to analyze the resilience of different cooling technologies under future climate and future heatwaves.

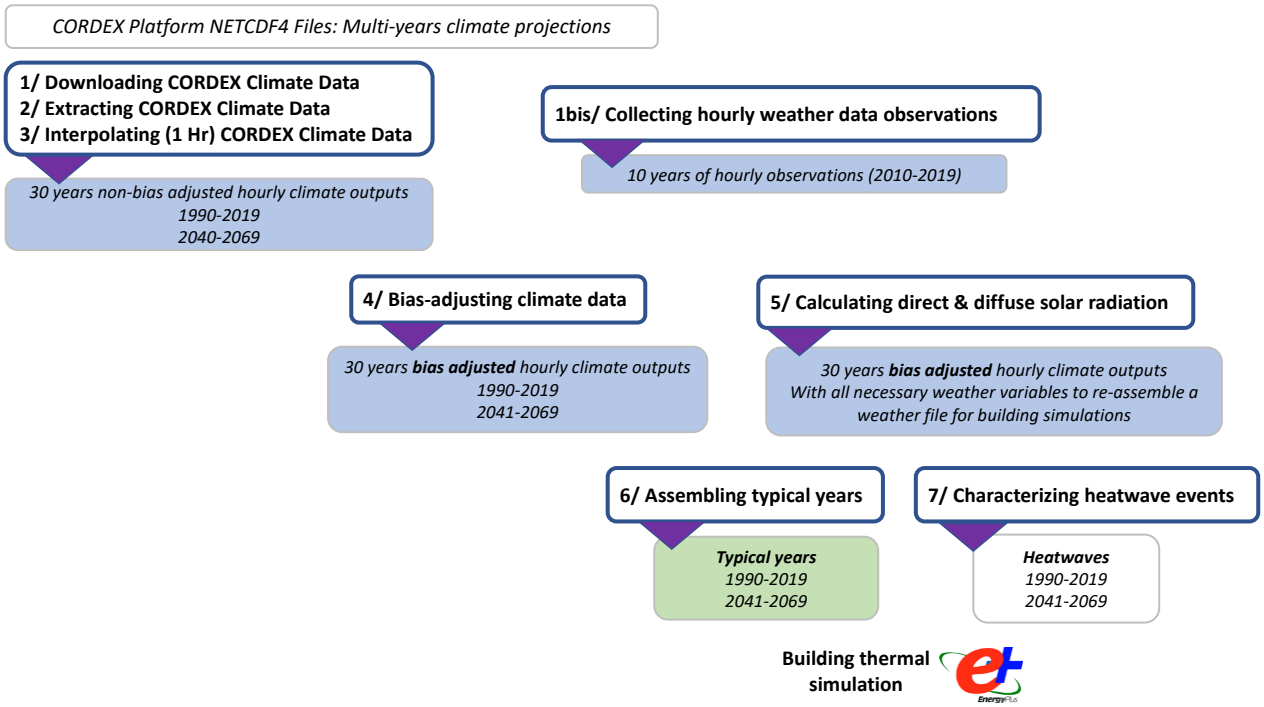

Figure 31 - Methodology for assembling future weather files from CORDEX Climate Data

2.3.1.1 Data extraction from the CORDEX platform

The CORDEX climate models' outputs can be accessed from different "node" points, through the Earth System Grid Federation (ESGF). We used the one from the IPSL laboratory: ESGFNODE.IPSL.UPMC.FR (ESGF, 2019). The data are available under the Network Common Data Form (NetCDF4) format, largely used by the climate community. Each file contains all the grid of one CORDEX domain for one year and for one climate variable (Example for the dry-bulb temperature on the European CORDEX domain shown in Figure 32 using the Python *cartopy* module).

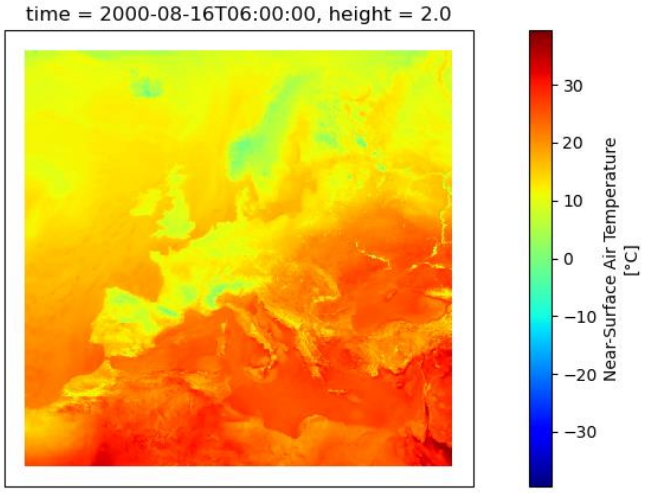

Figure 32 - Representation of the temperature over the Europe CORDEX Domain the 16th of August 2000 at 6 am

We downloaded climate data for the Europe domain on a 0.11° grid in rotative coordinates, equivalent to 12.5 km. The architecture of the NetCDF4 files is explained in the CORDEX Archive Design document (EUROCORDEX, 2019a). NETCDF4 files are 3-dimensional files, of latitude, longitude and time. NETCDF4 files are commonly used by the climate community but are not by the building simulations community and understanding this data storage type and how to access the data was not simple. On the Europe domain, there is a data point every 12.5 km containing the data for one weather variable over one year. For instance, the NETCDF4 file in Europe for the dry-bulb temperature contains all temperatures in many cities every 12 km for one year. For one climate model, we downloaded NETCDF4 files from multiple years for multiple weather variables. Then, we had to extract the data for our specific case-study cities. We programmed a Python code which finds the closest data point (lat, lon) on the grid for a given set of latitude and longitude (Figure 33). The code uses the Python modules *xarray* and *netcdf* to open the file, calculate the distance between the grid point of interest and all of the domain grid points, and return the grid point with the shortest distance. Once this grid point is found, the third dimension (time) can be accessed to get the data every three hours for that year. This step had to be repeated for all years of interest, and for each weather variable of our interest (dry-bulb temperature, specific humidity, global horizontal radiation, cloud cover, atmospheric pressure, and wind speed). The tasks were automatized in a Python code but this step was time consuming since the NETCDF4 files containing the data are large (Around 1 ko for one year for one weather variable over the Europe grid). As a later step was to bias-adjust the data, we needed to extract the CORDEX data from the closest grid point than from observations. We identified observations for the different weather variables of interest over multi-years period from the following weather

stations: Roissy-charles-de-gaulle (49.02, 2.53), La Rochelle-aerodrome (46.17, -1.19), and Carpentras (44.08, 5.06). Figure 33 showcases the NETCDF4 file structure. A NETCDF4 extractor can also be used to extract the data, but it is a commercial tool and it is more time-consuming than the Python code. However, for people with no programming knowledge, this is an alternative.

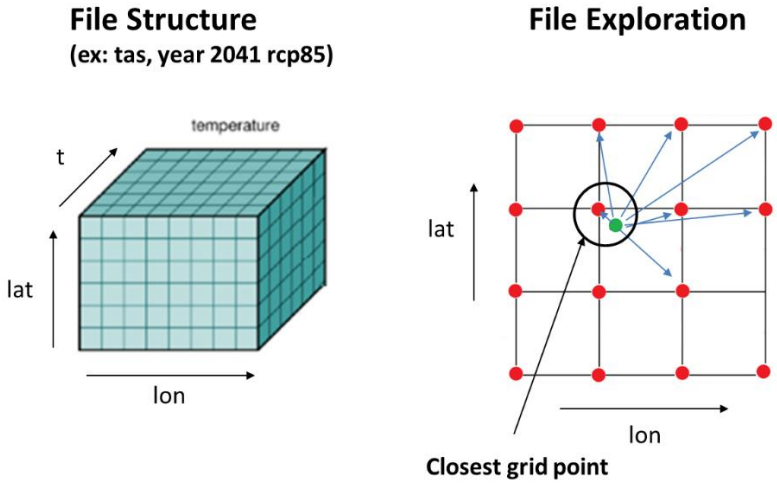

Figure 33 – NETCDF4 file structure and file exploration to select the closest grid point to desired city coordinates

Climate Data Variables Overview

The time this work was completed was in March 2018. At this time, five climate models were available on the CORDEX platform, with six weather variables (dry-bulb temperature, specific humidity, global horizontal radiation, cloud cover, atmospheric pressure, and wind speed) at the time-step every three hour. One limitation for our study is that no climate data exist for future wind direction. However, these are only used to calculate wind pressure coefficients for natural ventilation in building simulations. We used wind direction from current observations, the remaining limitation is not being able to estimate the bests building orientations, but these are usually already rough approximations as wind patterns are greatly modified within an urban context. Additional CORDEX data of interest for building simulations are today available, such as longwave incoming radiation and precipitations. We did not include them in the weather files as they were not available at the time we downloaded the data. The longwave radiation is recalculated by EnergyPlus Weather Convertor from cloud cover data. The precipitations were not necessary for our study, but they might be needed for some passive cooling systems (i.e green roofs or roof ponds). Nowadays (end of 2020), these climate data are available on the CORDEX platform for many models and these will be included in the weather files in future work.

Climate Models Selection

In late 2019, eleven models were available with three-hourly data on the EUR domain, with more weather variables. Model names have been abbreviated in this thesis. In 2020, more models have been uploaded, one (MPI-REMO) including hourly data instead of three-hourly data which simplifies the process. For a more complete analysis and a holistic assessment, as many climate models as possible should be used, as advised by climatologists. However, due

to time constraints and computational resources, in this thesis we use only four out of the five climate models that were available at the time of the analysis (CNRM-RCA, MPI-RCA, IPSL-RCA and HadGEM-RCA). MPI refers to the Max Planck Institut for Meteorology, HADGEM to the Hadley Center Global Environment Model, and RCA to the Rossby Centre Regional Atmospheric Climate Model.

In order to have an overview of the climate models chosen in comparison to the eleven climate models, we compared the monthly summer mean dry-bulb temperatures over multi-years historical (1976-2005) and future periods (2040-2069, RCP 4.5 and 8.5 scenarios) from the eleven climate models (Figure 35). These are monthly mean temperatures, meaning that the extreme of the distribution on the plot still represent extreme monthly mean, extreme hourly temperatures are not shown here. We represent the monthly summer (from June to September) mean temperatures as violin plots. The summer period, for this Ph.D. thesis, is considered from the 1st of June until the 30th of September, as (Ouzeau et al., 2016) observed that in the future the summer period in France will be extended. One violin plot is represented for each climate model and for each time period (historical 1976-2005), mid-term RCP 4.5 and mid-term RCP 8.5. Violin plots are a combination of boxplots and kernel density plots: the large black bar in the middle of each violin plot represents the interquartile range, with the median temperature as the white dot (The thin grey line that extends amongst the thick black rectangle represents the rest of distribution with the minima and maxima. On each side of the thin grey line the data are represented as a kernel density distribution, which represents the probability of occurrence that the temperature will take a specific value. Figure 34 shows a representation of a violinplot compared to a boxplot and a kernel density distribution.

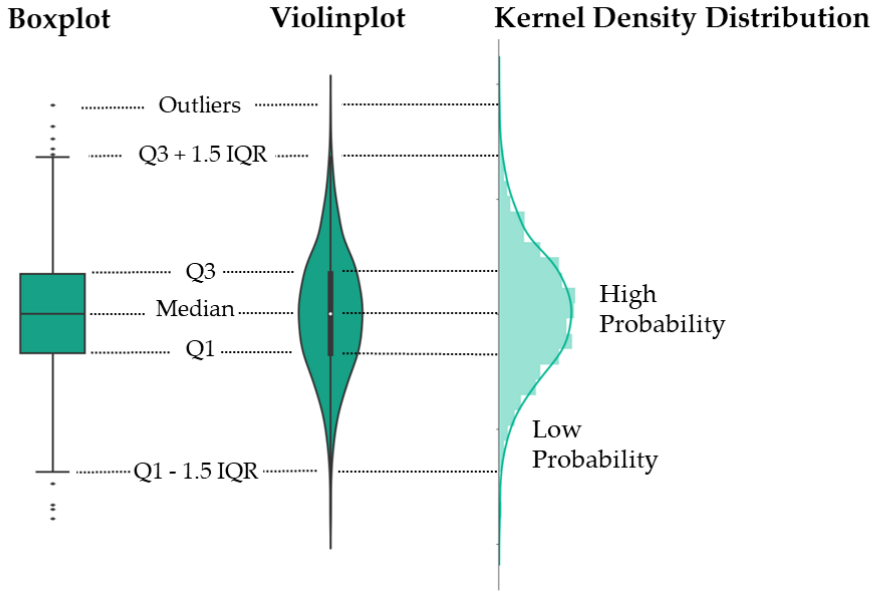

Figure 34 - Violin plot (middle) representation compared with boxplot (left) and kernel density distribution (right)

From Figure 35 we can observe that we have selected the model with the lower temperature predictions, having the lowest mean temperature increase and lowest summer temperature mean in comparison with all other models (CNRM_RCA). We selected a model that seems within the middle of the range of the other models (MPI_RCA), a model with middle-high predictions (IPSL_RCA) and one model with high predictions (HadGEM_RCA),

but not the model with the warmest predictions of summer temperatures. The model IPSL_RCA has a high increase in mean value (+ 3.3 °C in mean summer temperature) but in absolute value, it is "only" the 5th warmest model with the summer mean temperatures over the future period 2040-2069 with the scenario RCP 8.5. HadGEM_RCA is the 4th warmest model for the period considered. While comparing GCMs and RCMs, we can observe that RCMs can force the summer temperatures, as both MPI_RegCM and HadGEM_RegCM showcase the warmest predictions. Also, RCMs can lead to very different predictions when coupled to the same GCM, see the output differences of MPI and HadGEM using RCA and RegCM: up to 3.5 °C difference in the mean temperature related to the RCM only.

On the opposite, GCMs can also force the outputs since if we compare CNRM and HadGEM with the same RCM (RCA or ALADIN), the outputs are very different (up to + 3.5 °C difference in average). Finally, the 4 models we selected use the same RCM, the model RCA. If we compare the difference in summer temperatures predictions from the same climate model with the two different RCP scenarios, the temperatures vary of around 1 °C. In contrast, comparing the temperatures predictions for the same RCP scenario of different models lead to much more contrasted outputs: A difference up to 7 °C for different GCM and RCM. This contrast in uncertainty confirms our choice (based on the literature) that for the future mid-century period under study (2040-2069), the uncertainty related to the climate model is higher than the uncertainty related to the RCP scenario. This reinforces our decision to study only the uncertainty related to the climate model as to limit the scope of this study. However, for a full uncertainty analysis and a holistic assessment, all models should be used under the two different RCP scenarios.

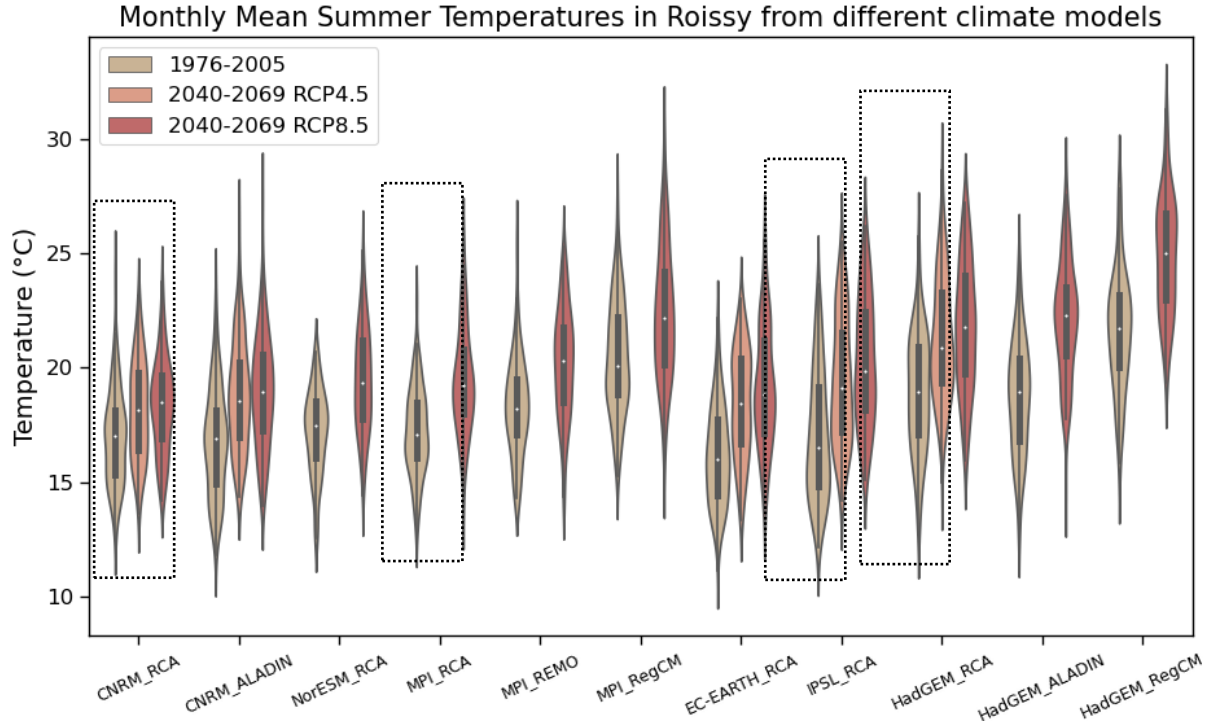

Figure 35 - Monthly mean summer (June to September) dry-bulb temperatures for 11 CORDEX Climate models

2.3.1.2 Climate data interpolation

The data of each climate variable were first interpolated to the 1-hour time-step, a standard for weather files for building simulations. With the software EnergyPlus, different times-steps than one hour are possible, however with the graphical interface DesignBuilder, only 1-hour time-step weather files can be used. While using EnergyPlus, if a smaller time-step than 1 hour is chosen, the internal EnergyPlus weather convertor interpolates linearly the weather variables to the smaller time-step. The dry-bulb temperature, initially in Kelvin was converted to Celsius, the cloud cover, initially in percentage was converted into tenths and the specific humidity, initially in kg/kg was multiplied by thousands to convert to g/kg. We used polynomial regressions for the dry-bulb temperature and the global solar radiation and linear regressions for the other weather variables. Six weather variables available every three hours were used, but some others needed to be recalculated. Table 7 displays the data available from the NetCDF4 file and the data needed to reconstruct a weather file in the EPW format, typical for building simulations. We calculated the relative humidity using the dry-bulb temperature, the specific humidity and the atmospheric pressure (Equations (8) to (10)). Most data were given as instantaneous at a given time, while the global solar radiation and the cloud cover were averaged over three hours. The fact that data for global horizontal radiation were given as average of 3 hours caused problems, as it happened that there would be a data point when the sun is actually down or no data point when the sun is already up. Therefore, the data needed a lot of formatting and check-ups to ensure that they matched reality, and this task was strenuous. From the 3-hourly data, the global solar radiation was first set to 0 before sunrise and after sunset and was then interpolated to hourly data.

Table 7 - Climate variable conversions from NetCDF4 files to EPW weather files

Climate variable from EURO-CORDEX every 3 hours	**Data point type**	**Interpolation method to the hourly time-step**	**Climate variable needed for the EPW file (Department of Energy, 2017)**	**Equations used to calculate the missing climate variable**
Dry-bulb temperature (K)	Data point*	Polynomial order (n-1) with n the number of points per day	Dry-bulb Temperature (°C)	
Specific Humidity (kg/kg)	Data point *	Linear	Relative Humidity (%)	Equations (8) to (10)
Atmospheric Pressure (Pa)	Data point*	Linear	Atmospheric Pressure (Pa)	
Cloud cover (tenths)	Average**	Linear	Direct Normal Radiation (Wh/m²) Horizontal Infrared Radiation Intensity	Equations (11) to (21), (26) and (27)
Global Horizontal Radiation (W/m²)	Average**	Polynomial order (n-1) with n the number of points per day	Diffuse Horizontal Radiation (Wh/m²)	Equations (24) and (25)
Wind Speed (m/s)	Data point*	Linear	Wind Speed (m/s)	

* Data point: Data available at 00 am, 03 am, 06 am, 09 am, 12 pm, 3 pm,6 pm, 9 pm every day

**Average: The data are averages from 0-3 am at the point 01.30 am, from 3-6 am at the point 04.30 am, etc and at points 07.30 am, 10.30 am, 1.30 pm, 4.30 pm, 7.30 pm, and 10.30 pm every day

In Equation (8), T the dry-bulb temperature (°C) was used to calculate VP_s, the saturated vapor pressure (hPa). In Equation (9), the water vapor pressure VP is calculated from AP, the atmospheric pressure (Pa), x the water content (kg/kg), and e = 0.62198. Both expressions are taken from the standard NF EN ISO 15927-1 (ISO, 2004). From (ASHRAE, 2001), the specific humidity is almost equal to the water content so the water content was assumed equal to the specific humidity. Knowing the water vapor pressure VP (hPa) and the saturated vapor pressure VP_s (hPa), the relative humidity RH (%) could be calculated Equation (10).

$$T > 0 : VP_s = 6.105 . e^{\frac{17.269.T}{237.3+T}} \quad (8)$$

$$VP = \frac{x . \frac{AP}{100}}{e + x} \quad (9)$$

$$RH = \frac{VP}{VP_s} \quad (10)$$

Figure 36 illustrates an example of interpolating the climate data to 3-hourly to hourly. As all weather data were not available at the same time (some data at 0am, 3am… and others at 1.30 am, 4.30 am…) we first interpolated the data to every 30 min and then kept only hourly data. As mentioned, the global solar radiation was first set to 0 when the sun height was inferior to 0 and the interpolation was forced to pass by the 0 at sunrise and sunset times. The Python *pvlib* module was used to calculate the sun height. Equations regarding the direct and diffuse solar radiation are outlined later in the text, as this step was conducted after the bias-adjustment of the global horizontal radiation. Figure 36 showcases the interpolation of data from 3-hourly to hourly for the dry-bulb temperature (polynomial interpolation), the wind speed (linear interpolation) and the global horizontal radiation (polynomial interpolation). For the global horizontal radiation, we can observe that the interpolation allows to recreate the daily "peak", while forcing the interpolation to pass by the data point 0 at 3 am and at 8 pm (data are in UTC) ensures that there is not solar radiation data when the sun is down.

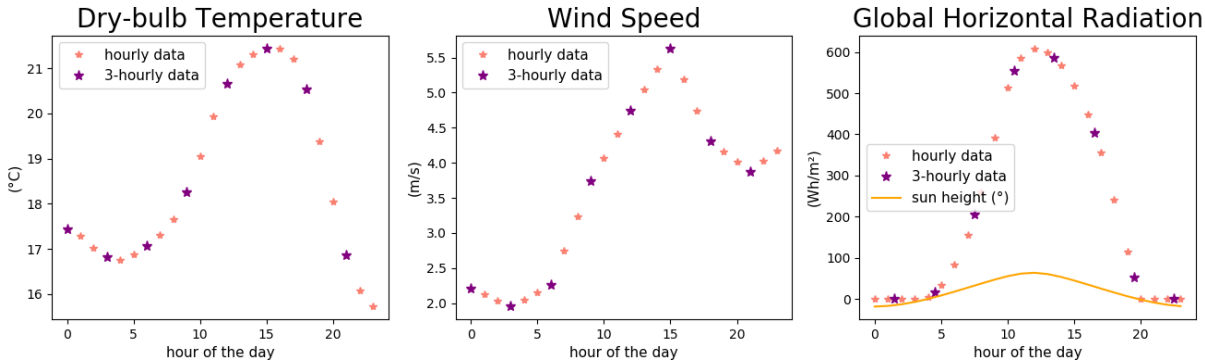

Figure 36 – Example of interpolation from 3hourly data to hourly data for the 1st of July 2041 in Roissy

2.3.1.3 Climate data bias-adjustment

We bias-adjusted the long-term multi years climate data (dry-bulb temperature, relative humidity, atmospheric pressure and wind speed) using the Multivariate Bias Correction (MBCn) method implemented by (Cannon, 2018). The method ensures that projected changes in climate are preserved and that the bias-corrected data are physically consistent. The method has two main advantages in the context of our study: First, it conserves the interdependence between the variables, by transferring all aspects of a multivariate distribution from observations to the multivariate distribution of climate model outputs. This was an important point as not all bias-adjustment methods preserve the correlation in between weather variables, which is necessary for building thermal simulations. Second, the method preserves well the extremes of the distribution, in comparison to other bias-adjustment methods, which is also a crucial point for this study since we are interested in heatwaves data. The MBCn method has been validated, compared to a univariate quantile mapping algorithm (neglecting the relationship between the variables) and to two other MBC algorithms and showed a better performance in all cases, especially for maxima of the distribution (Cannon, 2018). The global solar radiation and cloud cover were bias-adjusted using the quantile delta mapping (QDM) method (Cannon et al., 2015), as it showed better performance for the Northern hemisphere and because observational data were available only on shorter time periods. We used hourly observations and climate outputs from the models over the same multi-years calibration period to conduct the bias-adjustment. Observations were collected for the following calibration periods:

- **From the station Roissy-Charles-de-Gaulle:** Years 2000 to 2019 for the dry-bulb temperature, atmospheric pressure, relative humidity, wind speed, 2013 to 2019 for cloud cover, and 2015 to 2019 for global horizontal radiation from the station Roissy-Charles-de-Gaulle and from the station Orly-athis-mons to fill gaps in the observations.
- **From the station Carpentras**: Years 2000-2019 for the dry-bulb temperature, atmospheric pressure, relative humidity and wind speed, 2012-2019 for global horizontal radiation and 2011-2016 for cloud cover data from the station Montelimar-Ancone.
- **From the station La Rochelle-aerodrome:** Years 2004 to 2019 for the dry-bulb temperature, atmospheric pressure, relative humidity and wind speed, and 2014 to 2019 for the cloud cover and global horizontal radiation.

The observational data need to be continuous for the bias-adjustment procedure and short gaps in data (i.e. some hours) can be filled by interpolations. Ensuring that collected observational data had no gaps and that observations were accurately reported was a time-consuming step. The method was first applied to the present period climate model data (Grey curve “Climate Model” in Figure 37) using the observations as calibration (Red curve “Observations” in Figure 37) to produce the present period bias-corrected climate model data Blue curve “BC Climate Model in Figure 37) during the calibration period.

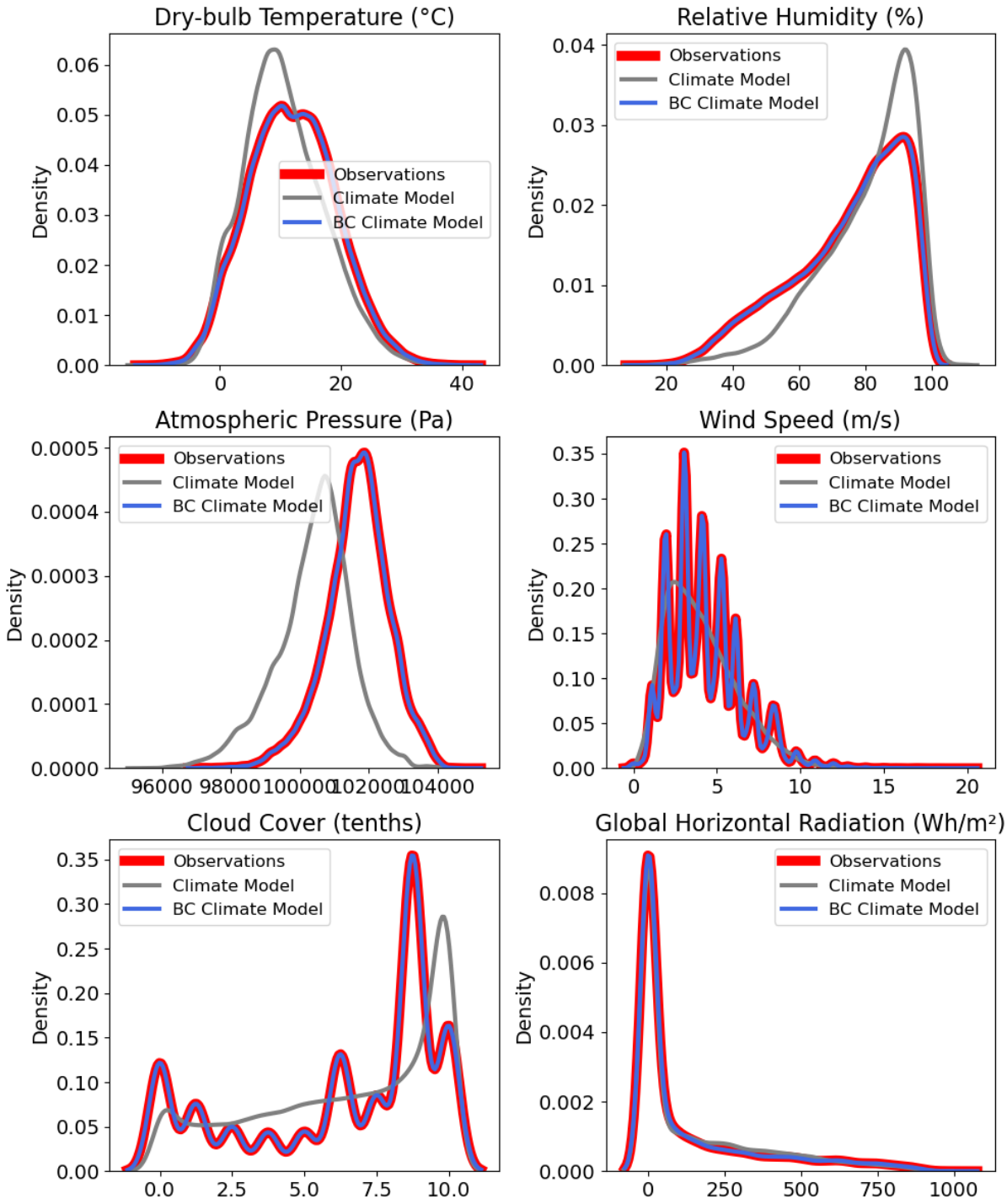

Figure 37 – Multi-years Bias correction (BC) of the 6 weather variables during the calibration period using observations (Illustration with data from the climate model IPSL-RCA4 for Roissy)

Bias correction is applied via a transfer function that links cumulative distribution functions of the modelled and observed data during the calibration period (Figure 37). It calculates a correction factor between before and after bias-correction climate model data, that is then applied to the climate model projections over the full present period (1990-2019, blue curve BC Present in Figure 37) and to the future period (2049-2060, dark blue curve BC Future in Figure 38).

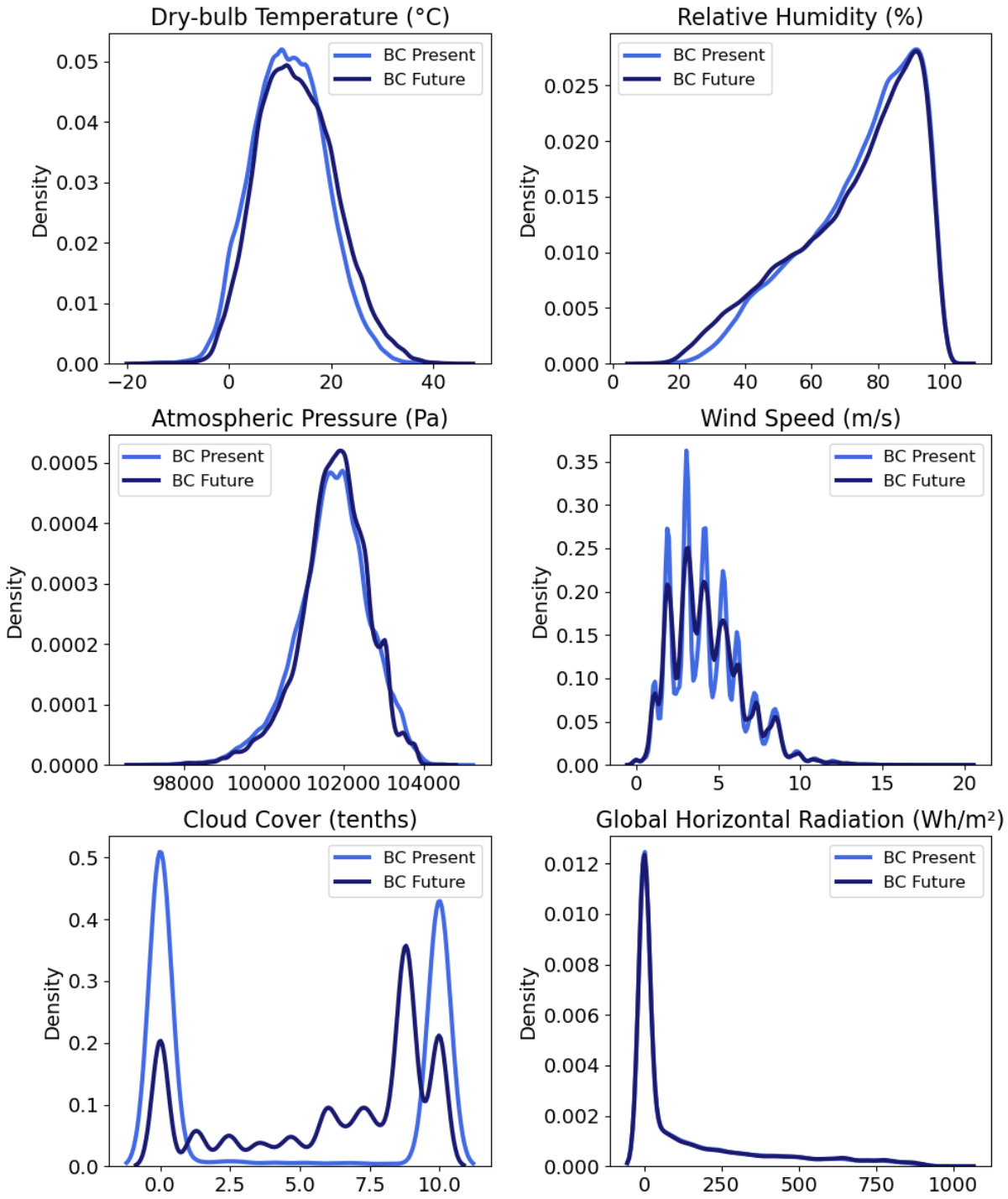

Figure 38 - Bias corrected (BC) data during the present (1990-2019) and future periods (2040-2069 RCP8.5), illustration with data from the climate model IPSL-RCA4 in Roissy

The method preserves projected changes in climate quantiles. The latitude and longitude from the climate outputs were chosen to be the exact same as the ones from the observation station: Roissy (49.02, 2.53), Carpentras (44.08, 5.06), La Rochelle (46.17, -1.19). This method was used for the outputs from the four climate models, for each of the three cities. We used the open source R package developed by (Cannon, 2018)[1] to complete this step of the methodology.

[1] The R-package can be downloaded at https://CRAN.R-project.org/package=MBC.

Figure 37 and Figure 38 illustrate the bias correction method for the city of Roissy with the climate outputs from the model IPSL-RCA4, we can make multiple observations:

- **Dry-bulb temperature** data are warmer after bias-correction (comparison curves Present & BC Present in Figure 37), implying that the climate model IPSL-RCA4 was underestimating the temperature during the calibration period. Dry-bulb temperatures will be warmer in the future (Figure 38);
- **Relative humidity** data are dryer after bias-correction (Figure 37), and will also be drier in the future (Figure 38). This is due to the increase in dry-bulb temperature but might also be due to a decrease in water content/precipitations. The same is observed in La Rochelle and Carpentras (not shown here);
- **Atmospheric Pressure** is slightly higher after bias-correction, and does not seem to change with climate change (The same is observed in La Rochelle and Carpentras);
- The **wind speed** has higher variations after bias-correction procedure, which is probably due to the fact that the data from the climate model are 3-hours averages whereas the observations are more precise. The wind speed does not change much in the future (The same is observed in La Rochelle and Carpentras);
- **Cloud cover** data are more spread out after bias correction, and cloud cover will increase in the future in Roissy. The opposite is observed in Carpentras, where cloud cover will highly decrease (not shown here), and in La Rochelle, where it will slightly decrease (not shown here);
- **Global horizontal radiation** data are quite similar before and after bias correction, and do not seem to vary in future climate for the three case-study cities.

2.3.1.4 Direct and diffuse solar radiation calculation

Once global horizontal radiation data were bias-adjusted, we could calculate the direct normal radiation and the diffuse horizontal radiation. Many methods exist to do so, with no scientific consensus. According to this recent article (Gueymard & Ruiz-Arias, 2016) comparing 140 models in various cities around the world, amongst the models reporting the best predictions for direct normal solar radiation calculated from global horizontal radiation are the Perez (DIRINDEX) model (Perez et al., 2002) which provides hourly predictions and the Engerer method which provides minute predictions (Engerer, 2015). The Perez model is one of the most used models for the application of building thermal simulations. These models use a clearness index calculated from extra-terrestrial radiation and air mass, and account for the amount of water in the atmosphere. As we had data for cloud cover, we decided to use it to calculate better estimations for direct normal solar radiation. We used the method proposed by Nik outlined in his master thesis (Nik, 2010) to recalculate direct normal solar radiation using global horizontal radiation and cloud cover data from climate models. The method is based on the work of (Taesler & Andersson, 1984), the methodology used is described in the following steps:

We first discretized the extra-terrestrial spectral distribution of the solar radiation outside the atmosphere $I_0(\lambda)$ into 78 data points at 78 wavelengths from 115 nanometers (nm) to 5000 nm, so that each data point is an average of the spectral radiation between two consecutives wavelengths. Then for each data point, we included the effects of the attenuation by the air mass and the turbidity, so $I_0(\lambda)$ became $I(\lambda)$ (Equation (11)).

$$I(\lambda) = I_0(\lambda).\,\mathrm{e}^{-(\alpha_\mathrm{r} + \alpha_\mathrm{d}).m} \tag{11}$$

We then calculated, for each wave length, α_r the coefficient of absorption for molecular scatter Equation (12) and α_d the coefficient of absorption for particular scatter Equation (13), and m the optical air mass Equation (14) from Young (Young, 1994). In Equation (13), the turbidity coefficients β were taken from (Taesler & Andersson, 1984). In Equation (14), z_t the zenith angle in radians was calculated from Equation (15) with h the sun height in degrees. The sun height was calculated using the Python *pvlib* module.

$$\alpha_\mathrm{r} = 0.00816.\lambda^{-4} \tag{12}$$

$$\alpha_\mathrm{d} = \beta.\lambda^{-1.3} \tag{13}$$

$$m(z_\mathrm{t}) = \frac{1.002432.\cos^2(z_\mathrm{t}) + 0.148386.\cos(z_\mathrm{t}) + 0.0096467}{\cos^3(z_\mathrm{t}) + 0.149864.\cos^2(z_\mathrm{t}) + 0.0102963.\cos(z_\mathrm{t}) + 0.000303978} \tag{14}$$

$$z_\mathrm{t} = (h - 90).\frac{\pi}{180} \tag{15}$$

For each hour, we calculated the sum S of the attenuated radiation between two consecutive wavelengths with Equation (16).

$$S = \sum_{\mathrm{n}=1}^{78} \left(\frac{i(\lambda)_\mathrm{n} + i(\lambda)_{\mathrm{n}+1}}{2} \right).\mathrm{e}^{-(\alpha_\mathrm{r} + \alpha_\mathrm{d}).m}.(\lambda_{\mathrm{n}+1} - \lambda) \tag{16}$$

We added the effects of the cloud cover (CC) (Equation (17)).

$$S_1 = S.1000.(1 - CC/10) \tag{17}$$

We adjusted with the correction factor q, accounting for the variation during the year of the distance between the Earth and the sun (Equations (18) and (19)) with N_dy the number of days per year and $w_\mathrm{n} = \frac{2\pi}{366}$

$$S_2 = q.\,S_1 \tag{18}$$

$$\begin{aligned} q = \frac{1}{1353}.\big(&1353 + 45.326.\cos(w_\mathrm{n}).N_\mathrm{dy} + 0.88018.\cos(2w_\mathrm{n}).N_\mathrm{dy} \\ &- 0.00461.\cos(3w_\mathrm{n}).N_\mathrm{dy} + 1.8037.\sin(w_\mathrm{n}).N_\mathrm{dy} \\ &+ 0.097462.\sin(2w_\mathrm{n}).N_\mathrm{dy} + 0.18412.\sin(3w_\mathrm{n}).N_\mathrm{dy}\big) \end{aligned} \tag{19}$$

We calculated WV, the water vapor present in the atmosphere (Equation (20)) from m ((Equation (14)) and VP ((Equation (9)) that we subtracted from S_2 in Equation (21) to finally calculate the direct normal radiation DNR.

$$WV = 70 + 2.8.m.VP \tag{20}$$

$$DNR = S_2 - WV \quad (21)$$

Finally, we calculated the diffuse horizontal radiation DHR from the global horizontal radiation GHR and direct horizontal radiation $DN'R$ from Equation (22) to (25).

When the sky is clear:

$$DHR = GHR.\acute{\eta} \quad (22)$$

With

$$\acute{\eta} = \frac{1}{1 + 8.\sin(h)^{0.7}} \quad (23)$$

When the sky is not clear:

$$DN'R = DNR.\sin(h) \quad (24)$$

$$DHR = GHR - DN'R \quad (25)$$

Additionally, the horizontal infrared radiation intensity (LWR) is calculated by the EnergyPlus Weather Convertor (Equation (26)). The formula for the sky emissivity ε_{sky} is given in Equation (27), calculated from the cloud cover CC in tenths and the dew-point temperature T_{dp}, calculated from the EnergyPlus Weather Convertor. TK is the dry-bulb temperature in Kelvin and σ is the Stefan-Boltzmann constant (5.6697.10^{-8} W/(m².K^4))

$$LWR = \varepsilon_{\text{sky}}.\sigma.TK^4 \quad (26)$$

$$\varepsilon_{\text{sky}} = \left(0.787 + 0.764.\ln\left(\frac{T_{\text{dp}}}{273}\right)\right).(1 + 0.0244.CC - 0.0035.CC^2 + 0.00028.CC^3) \quad (27)$$

Figure 39 illustrates the split of global radiation into direct normal and diffuse horizontal, considering the cloud cover. The limitation in the calculation of the direct normal and diffuse horizontal radiation is that the initial data from cloud cover and global horizontal radiation are averages of 3 hours data point, the calculation would be more precise with hourly datasets.

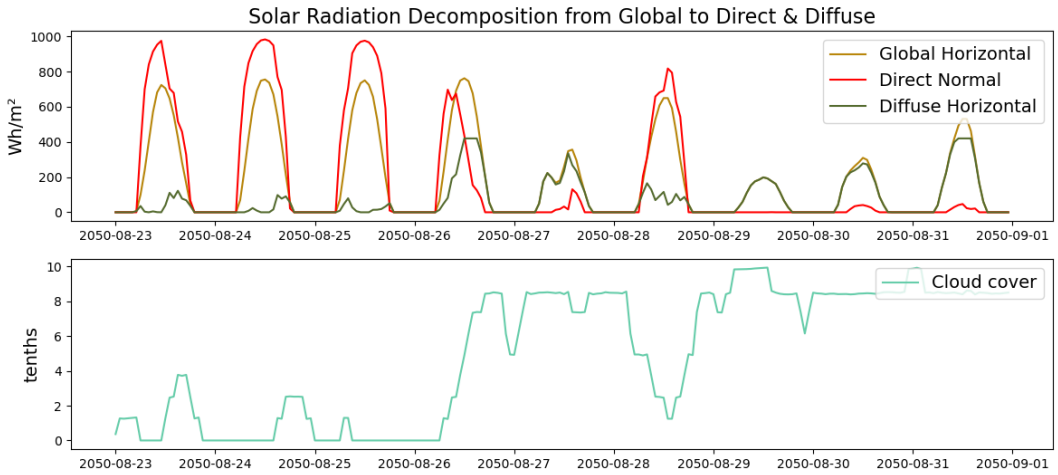

Figure 39 – Illustration of the split of global horizontal radiation into direct normal radiation & diffuse horizontal radiation on a summer week in Roissy, for the model CNRM-RCA4

From here, all the weather variables that we consider necessary for our building thermal simulations are available. We have the necessary data (dry-bulb temperature, relative humidity, atmospheric pressure, wind speed, cloud cover, direct normal radiation, diffuse horizontal radiation) for the three case-study cities (Roissy, La Rochelle, Carpentras) over multi-years during the present period (1990-2019) and the future period (2040-2069) following the socio-economic scenario RCP 8.5 for four climate models (CNRM-RCA, MPI-RCA, IPSL-RCA and HadGEM-RCA). The models are abbreviated respectively to CNRM, MPI, IPSL and HadGEM for the rest of the manuscript. In the next two sections we will detail the methods we used to assemble typical years and heatwaves weather files.

2.3.1.5 Typical years assembly

For building thermal and energy simulations, typical years are commonly used. A typical year is composed of 12 months issued from different years over a period of time (between 10 and 30 years). The selected months are the statistically most "typical" over the period, selected amongst different weather variables. The selection process is explained in this section. Each country has its own method to reproduce typical years, and the EPW format typical year format differs from the International Weather for Energy Calculation (IWEC) format or from the Typical Meteorological Year (TMY) format (Herrera et al., 2017). The main difference among the methods is the weight given to each weather variable in the selection process. We used the methodology of the standard NF EN ISO 15927-4 (ISO, 2006) as it was used in France to reconstitute the typical year used for the French Thermal Regulation RT-2012. This method considers four climate parameters to select the most statistically common months among the years: The dry-bulb temperature, the humidity, the global horizontal radiation of equivalent first order and the wind speed of second order. Regarding the humidity, it is possible to use the relative humidity, the specific humidity, the vapor pressure or the dew point temperature. We decided to use the specific humidity. Trial and error revealed that using for instance the relative humidity instead of the specific humidity resulted in different years selected, but with slight differences between them. We also questioned the use of these four weather variables to select the typical years. For instance, Nik defined future typical years using only the dry-bulb temperature, since it is the most impacted parameter by climate change (Nik, 2016). However, we considered that for building thermal simulations

these four weather variables can all be important, even though their weighting remains questionable as it is strongly correlated to the building design.

We created a Python code to automate the process to select the typical months. For selecting each month mo, the method is as follows: For each climate parameter cp of first order, we sorted a series of daily averages (da) in ascending order over the 30 years period, which allowed to calculate the distribution function Φ (Equation (28)) over 30 years. Φ has 900 data points (N_d = 900) for months of 30 days. $L(da)$ is the rank in the series of the daily averages for the 30 years.

$$\Phi(cp, mo, da) = \frac{L(da)}{N_d + 1} \tag{28}$$

Secondly, we sorted a series of daily averages also in ascending order for each year to calculate the distribution function ψ (Equation (29)) for each year yr. $J(da)$ is the rank in the series of the daily averages for each year. ψ has 30 data points (N_d =30) for a month of 30 days.

$$\psi(cp, yr, mo, da) = \frac{J(da)}{N_d + 1} \tag{29}$$

The representation of the distribution functions Φ and ψ and the dry-bulb temperature classified in ascending order in January over the period 1990-2019 is presented in Table 8 and Figure 40.

The final step allowed to select the most typical months. We classified the FS in ascending order and for each month of each year for each climate parameter of first order, we attributed a rank. Then we summed the ranks of the three climate variables of first order (temperature, humidity, solar radiation) and classified them by ascending order. For each month, the three lowest sums equivalent to three years are considered the three most typical years. The last climate variable, the wind speed, allowed to determine which of these three pre-selected years is the most representative year.

We then compared the two distribution functions Φ and ψ for each year and for each month and calculated for each day $\psi - \Phi$ and then summed these absolute values for the considered month (Equation (30)), it is the Finkelstein-Schafer statistic (FS). We repeated this calculation for each month of each year and for each climate parameter of order 1.

$$FS(cp, yr, mo) = \sum_{da=1}^{n} |\psi(cp, yr, mo, da) - \Phi(cp, mo, da)| \tag{30}$$

The final step allowed to select the most typical months. We classified the FS in ascending order and for each month of each year for each climate parameter of first order, we attributed a rank. Then we summed the ranks of the three climate variables of first order (temperature, humidity, solar radiation) and classified them by ascending order. For each month, the three lowest sums equivalent to three years are considered the three most typical years. The last climate variable, the wind speed, allowed to determine which of these three pre-selected years is the most representative year.

Table 8 - Distribution functions Φ and ψ for one climate variable sorted in ascending order. Example for the dry-bulb temperature (cp) over the period 1990-2019 in the month of January (mo), climate data from CNRM-RCA in Roissy

$L(da)$	$\Phi(cp, mo, da)$	Serie of daily averages of the climate variable classified in ascending order (year 1990 to 2019)	$\psi(cp, yr, mo, da)$	Serie of daily averages of the climate variable classified in ascending order (yr = 2018)
1	0.0010	-8.10	0.03	-0.93
2	0.0021	-7.83	0.06	-0.28
3	0.0032	-6.88	0.09	-0.10

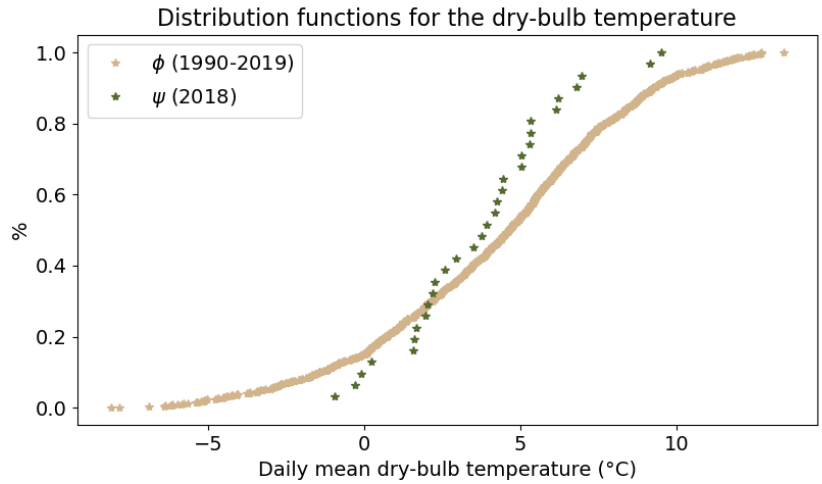

Figure 40 - Distribution functions Φ and ψ for one climate variable sorted in ascending order. Example for the dry-bulb temperature (cp) over the period 1990-2019 in the month of January (mo).

We sorted in ascending order the difference between the monthly average wind speed of each year with the monthly average wind speed of the 30 years. Finally, for each month, within the three pre-selected years, we selected the year with the lowest wind speed difference as being the typical year for this month. We repeated this process for each month, allowing to detect the twelve most typical months among the 30 years of data. We interpolated linearly for each climate variable of each month the eight last hours of the previous month and the next first eight hours of the following month.

2.3.1.6 Heatwaves detection and characterization

There is no consensus around the world over the definition of a heatwave. Numerous authors are studying the occurrence and intensity of future heatwaves and are using different indicators to identify them. Some authors detect heatwaves based on their impact on the population, some others consider only the meteorological aspect, which is usually characterized as an extreme event on the temperature distribution over a reference period. In the United States, Robinson defined a heatwave based on daily minima and maxima temperature thresholds, calculated for each state based on the body's reaction to temperature and humidity (Robinson, 2001). In Switzerland, Fischer and Schär detected a heatwave when the daily maximal temperature is above the 90th percentile of the temperature distribution over a reference period for at least five days. They characterize heatwaves by their amplitude (maximal temperature of the hottest yearly heatwave event), duration and frequency (number

of heatwaves per year) (Fischer & Schär, 2010). In Australia, Nairn and Fawcett developed excess heat factor indices to detect heatwaves, based on three-days moving average of the daily mean temperature above the 95th percentile of the temperature distribution and on the previous 30 days daily mean temperature average to consider the population adaptation to the heatwave (Nairn & Fawcett, 2013; Nairn & Fawcett, 2014). Perkins and Alexander defined two criteria, based on fifteen days moving average around the daily minimal and maximal temperatures (Perkins & Alexander, 2013). Liu has used percentiles correlated with mortality data after heatwaves in the UK (Liu et al., 2019). Depending on the goal (building design, building resilience, population protection), heatwaves detection can be based on daily temperature maxima, minima or averages. We used two distinct French definitions to detect heatwaves: One that is a definition from a climatic point of view (i.e) based on percentile thresholds of temperature anomalies on a multi-year dataset distribution, and one that is a definition from epidemiologists, for which thresholds were determined by mortality data. The two definitions are introduced in this section.

Method from French climatologists ("vague de chaleur" in French)

In France, a new method to detect heatwaves was recently adapted to a EURO-CORDEX dataset (Ouzeau et al., 2016). They used the basis of the operational method of heatwaves detection in France since 2006 that they updated to be suitable to any time series and to any spatial scale. The method is based on three percentile thresholds *Spic*, *Sdeb* and *Sint* which were originally absolute thresholds and have been redefined as percentiles of the daily mean temperature distribution over several years in an effort to make the method accessible to any dataset. *Spic* represents the threshold beyond which a heatwave event is detected (99.5 percentile of the temperature distribution over the multiyear historical period). *Sdeb* defines the beginning and the end of the heatwave (97.5 percentile) and *Sint* is the interruption threshold, used to merge two consecutive heatwave events without a significant drop in temperature (95 percentile). This method was validated with the SAFRAN indicator, previously used to detect French heatwaves in (Ouzeau et al., 2014). The method allows to characterize the heatwaves in term of maximal temperature, duration and global severity (the sum of positive differences between each daily mean temperature and the threshold *Sdeb*, divided by the difference between the *Spic* and *Sdeb* thresholds, quantified as °C.days (Soubeyroux et al., 2016). A graphical representation of the heatwave detection is presented in Figure 41.

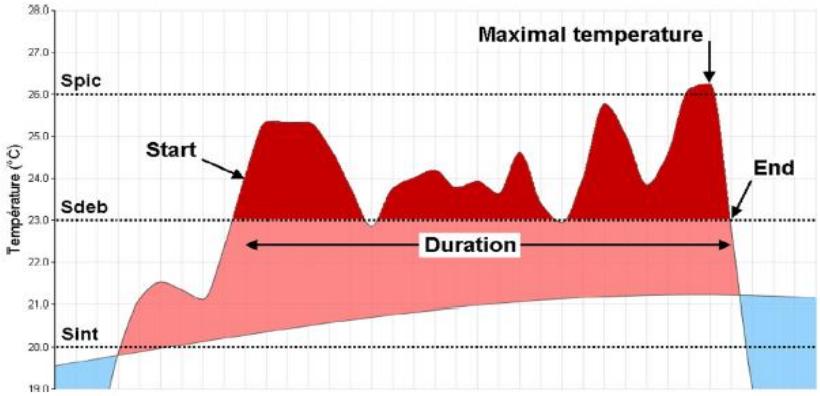

Figure 41 - Heatwave detection adapted from (Ouzeau et al., 2016). The *Spic* threshold is used for heatwave detection, the *Sdeb* threshold defines the heatwave duration, the *Sint* threshold ends the heatwave. Global severity: read area of the plot in degree-days.

Method from French epidemiologists ("canicule" in French)

In France, the 2003 heatwave was exceptional in terms of record temperatures and sanitary impact. About 15,000 excessive mortalities are estimated, 400% on the 12th of August more than on a "usual" 12th of August in Paris, and 50% more in many French cities (Laaidi et al., 2013). After this event, the Heatwave National Plan (Plan National Canicule) was established in order to anticipate heatwaves and define prevention measures. In this context, the Sanitary Watch Institute (INVS) established meteorological bio-indicators (IBM) to identify heatwaves. The term bio indicates that the indicator is linked to high mortality. IBM is the couple (IBM_x, IBM_n) where IBM_x is the three-days moving daily maximal temperature and IBM_n is the three-days moving daily minimal temperature. A heatwave is defined when the IBM couple (IBM_x and IBM_n) is above the thresholds during at least three consecutive days d (Laaidi, et al., 2013). S_x and S_n are the thresholds for maximum and minimum temperatures respectively. The definition for these "sanitary heatwaves" is illustrated in Equation (31).

$$IBM_x = \frac{T_{max_d} + T_{max_{d-1}} + T_{max_{d-2}}}{3} > S_x$$

$$IBM_n = \frac{T_{min_d} + T_{min_{d-1}} + T_{min_{d-2}}}{3} > S_n$$

Heatwave If: (31)

$$(IBM_{x,}\, IBM_n) > (S_x, S_n)$$
$$\boldsymbol{AND}\ \ (IBM_{x-1,}\, IBM_{n-1}) > (S_x, S_n)$$
$$\boldsymbol{AND}\ (IBM_{x-2,}\, IBM_{n-2}) > (S_x, S_n)$$

The thresholds *Sx* and *Sn* are different for each French department, they were built based on mortalities data in 14 pilot cities in France during historical heatwaves especially in 1976, 1983 and 2003. The thresholds for the remaining departments were calculated from the 99.5th percentile of the temperature distribution during the historical period 1973-2003, found to be the most representative of the excess deaths due to heat. It can be noticed that this percentile is the same as for the *Spic* indicator. The full description of how the thresholds were defined is in (Laaidi et al., 2013). The heatwave event has been added to the vigilance map (Figure 42) maintained by MeteoFrance (http://vigilance.meteofrance.com). Figure 42 displays the applicable thresholds for each French department in 2017. The thresholds are different for each city, as they account for the population's adaptation to heat and local building practices. They are adjusted over the years, considering the population adaptation to heatwave events. How to define the temperature warning thresholds remain an open question in the epidemiologists research (Pascal et al., 2013).

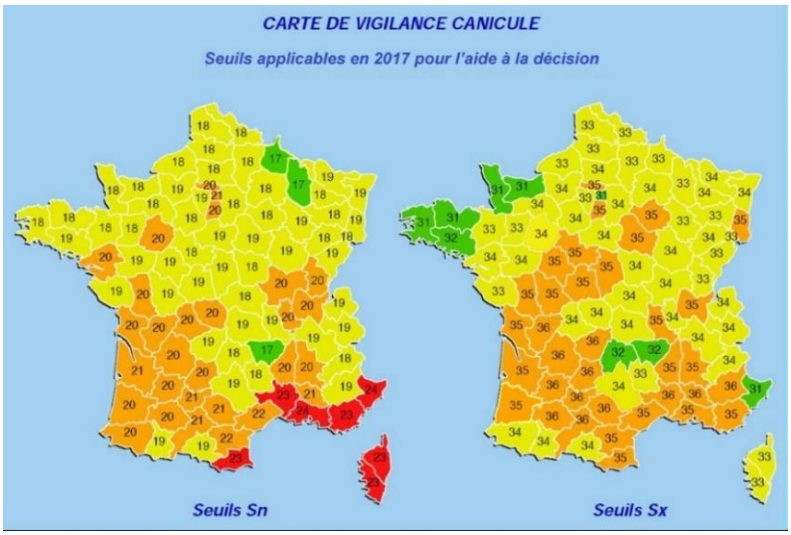

Figure 42 - Vigilance map with *Sn* and *Sx* thresholds for IBM calculation in 2017 – MeteoFrance

Once typical years and heatwave data were assembled, we converted the data from .csv format to .epw, the weather file format for building thermal simulations. For this purpose we created .cst and .def files and used the EnergyPlus Auxilliary Program WeatherConvertor (EnergyPlus, 2015).

2.3.2 **Including urban effects**

In Section 2.3.1 we presented how to assemble two types of future weather files: typical years and heatwaves from regional climate model data. The RCMs have a spatial resolution of 12.5 km, however they do not model an urban canopy, while it is known that Urban Heat Island (UHI) effect in cities can greatly amplify temperatures. During heatwaves, the UHI effect is even more exacerbated. In 2003, the UHI had an adverse effect, especially during nighttime temperatures: the link between morbidity and elevated night temperatures was clearly identified for the city of Paris (Pascal et al., 2006; Laaidi, et al., 2012). For this reason, to analyze the resilience of buildings to overheating in an urban context, it is crucial to consider this UHI effect as boundary condition for building simulations. We decided to account for the UHI effect by modifying the future weather files to future urban weather files, using a simple model.

Urban Weather Generator (UWG)

Many models exist to represent an urban context, and different approaches are possible (Bozonnet et al., 2015). We decided to use a simple model to reproduce the local microclimate: the Urban Weather Generator (UWG), developed by Bueno at the Massachusetts Institute of Technology (MIT) (Bueno et al., 2013; Bueno et al., 2014). It is a numerical simulation program (Python code) using rural observational data and urban characteristics as inputs to reproduce the urban local microclimate (modification of the dry-bulb temperature). It is based on the Town Energy Balance (TEB) scheme (Masson, 2000; Hamdi & Masson, 2008). TEB is usually used by climatologists and coupled to a high-resolution atmospheric model to represent the urban temperatures in different parts of a town. This procedure requires complex input data,

and knowledge about climatology. For instance, TEB was used by (Lemonsu et al., 2015) to simulate historical and future heatwaves (from regional climate models) in Paris over a 100 km grid with a resolution of 1 km. They coupled TEB to the heatwaves output from the high-resolution atmospheric model, this way the temperature in Paris was dynamically calculated for each grid point, including the urban effect. They could observe that during the daytime, the UHI effect was quite spread out around the city but not too intense, while during nighttime it was most significant and much more intense in a smaller circus (5 km around the city center). More recently, the same authors used a statistical-dynamical downscaling method to couple 12 CORDEX regional climate models with high-resolution urban climate simulations using a mesoscale atmospheric model in which is integrated TEB, replicating precisely the UHI effect during nighttime (Le Roy et al., 2021). These climate data including the UHI would be highly beneficial as input data for building simulations, however these are not available to a larger community yet.

For the purpose of urban and building design, the UWG model was created, to incorporate the urban effect as a boundary condition to use for building simulations (UWG morphs a "rural" EPW file into an urban EPW file, ready to use for building simulations). UWG is based on TEB, but is not coupled to a climate model, instead it is coupled to the atmospheric boundary layer, which uses the climate data as an input (or a boundary condition). It is a simplified one-node model (there is only one temperature grid point for a modelled neighborhood), which gives a first order estimation of the UHI phenomenon. This approach is not as precise as coupling with the atmospheric model, but the simulation time is reduced, and the required level of details is more consistent with a neighborhood scale study. Therefore, it can be used both by urban planners and building designers without a background in climatology. From the modified urban temperature, it is possible to calculate both the outdoor microclimate thermal comfort and discomfort, and to use the urban microclimate as input data for building thermal simulations instead of "rural" weather data (usually airport stations). The main limitation of the model is that since the climate model is a boundary condition and not dynamic, it does not account for horizontal advection in the urban canopy layer, which could result in an overestimation of the air temperature inside the canyon. However, UWG was validated in the cities of Toulouse in France and Basel in Switzerland and shows accurate results with a precision of around 1 °C (Bueno 2012). In the context of this Ph.D., we have used the UWG model to replicate the urban microclimate for the city of Paris, using the climate data from the city of Roissy from the Regional Climate Models as "rural" weather data. UWG is divided into four sub-models (Figure 43), the vertical diffusion model (VDM) and urban boundary layer model (UBML) were validated against high-resolution atmospheric models (Bueno et al., 2014).

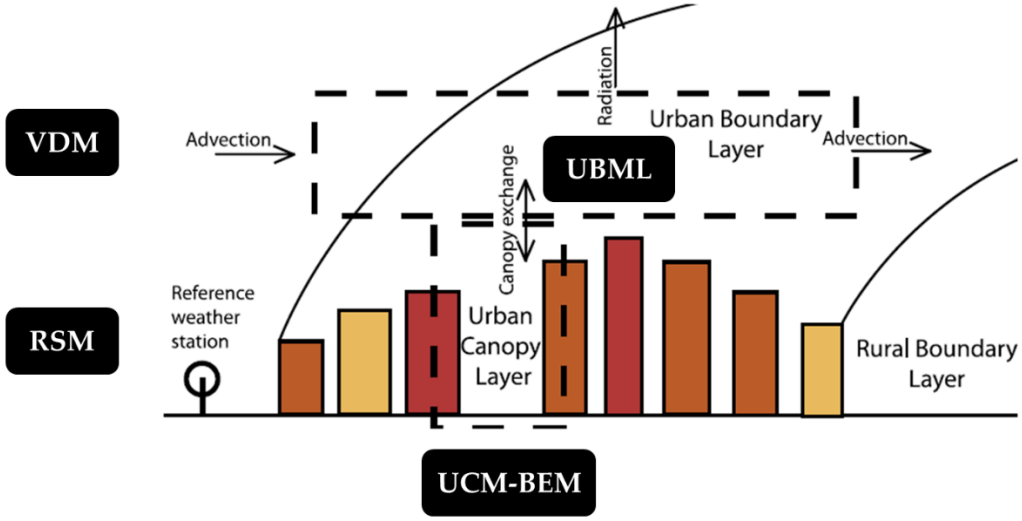

Figure 43 - Representation of the 4 sub-models of UWG and their interactions (Bueno et al., 2014)

- **The rural station model (RSM)** uses observational data at the rural reference site and calculates the sensible heat fluxes at the rural site based on an energy balance at the soil surface;
- **The vertical diffusion model (VDM)** uses the air temperatures and wind velocities at the rural reference site and the sensible heat fluxes from the RSM to discretize the rural atmospheric layer in a vertical grid and provide profiles of air temperature, pressure and density in the rural boundary layer;
- **The urban boundary layer model (UBLM)** designs the Urban Boundary Layer (UBL) above the city, it uses the profiles provided by the VDM model and the sensible heat fluxes from the RSM and Urban Canyon Layer (UCL). It transforms the temperature at the reference height from the VDM into the air temperature in the UBL, above the UCL by determining the surface and advection heat coefficients. The UBLM assumes that the UBL is not affected by changes in the urban surface, which limits the use of the model to compare different urban scenarios;
- **The urban canyon model (UCM)** is a representative street canyon model and computes the canopy and building energy heat fluxes to calculate the urban canopy air temperature and humidity. It is bounded by the UCL, the road and the building surfaces. Coupled to the UCM is the building energy model (BEM) which calculates all heat fluxes inside the building, simplified as one zone. The BEM was validated with EnergyPlus (Bueno et al., 2012). All buildings are represented with the same geometrics, defined by their floor space relative to total urban ground area and the building height. The UCM is based on the TEB scheme which was validated for different building case-studies in Paris (Pigeon et al., 2014).

Neighborhood case-study

In order to parametrize the urban canyon model, information on the urban neighborhood is needed as input data. In the context of this Ph.D., we represented the eco-neighborhood Clichy-Batignolles in the 17th district of Paris as case-study, which is still under completion (Figure 44). On 50 hectares, it is expected to host 3,400 apartments, 30,000 m² of shops, 140,000 m² of office buildings and many public facilities in an environment made

particularly attractive by the presence of the 10-hectares Martin Luther King Park. Seeking the eco-district label, the project is intended to be a model for sustainable urban development in terms of mixed functions and social diversity, energy efficiency, reduction in greenhouse gas emissions and biodiversity. The neighborhood design includes some adaptations to heat, planning ahead for potential future heatwaves. The adaptation measures include the presence of the park, watering of the earth's soil, solar shutters on buildings and adiabatic cooling in the office buildings. However, only the presence of the park as an adaptation measure can be represented with UWG, as latent fluxes are not implemented yet within the model. We modelled all buildings as residential. The neighborhood case-study is represented in Figure 44. In a first approach, we modelled a part of the eco-neighborhood with a historical building in Sketchup, to impose a ratio of new/old buildings (work of the intern Eleonora Lacedra). The Sketchup model was used to gather information about building geometrics and green area. In a second approach, we gathered the information for the entire eco-neighborhood (buildings footprint and height) using the software Quantum Geographic Information System (QGIS), which was a more efficient option timewise. Some buildings' heights were missing in the database and these were filled from Google Maps observations. Buildings typologies were modelled as new constructions from the TABULA project database, they are equipped with heaters but no air-conditioning. The anthropogenic heat is assumed to be about 4 W/m², which is lower than the standard value of 8 W/m² measured in Toulouse commonly used in the literature, and that corresponds to a residential district in Singapore (Pigeon et al., 2008), as the eco-neighborhood has a limited presence of cars.

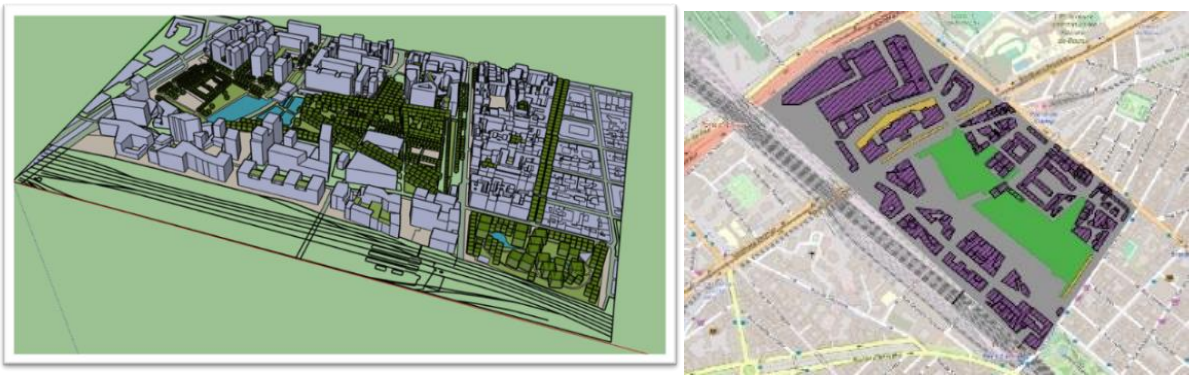

Figure 44 - Eco-neighborhood Clichy-Batignolles representation with Sketchup (left) & QGIS (right)

The simulation input parameters for the neighborhood case-study are given in Table 9. According to (Bueno 2012), the input parameters influencing the most the output urban microclimate air temperature are morphological parameters of the building and the reference height at which the vertical profile of potential temperature is assumed uniform.

Table 9 - UWG Input Parameters for the case-study neighborhood Clichy-Batignolles

	Input parameter	Value	Unit
Morphological parameters	Horizontal building density	33	%
	Average building height	24.06	m
	Vertical to horizontal urban area ratio	1.11	-
	Characteristic length	650	m
Urban characteristics	Wall and roof albedo	0.7	-
	Road albedo	0.2	-
	Vegetation coverage	0.16	-
	Tree coverage	0.15	-
	Anthropogenic heat from traffic	4	W/m^2
Building parameters	R-value wall	4.8	$m^2 \cdot K/W$
	R-value roof	5.2	$m^2 \cdot K/W$
	U-factor window	1.6	$W/m^2 \cdot K$
	Glazing ratio	0.20	-
	Windows SHGC	0.57	-
	Internal heat gains	5	W/m^2
	Infiltration air flow rate	0.17	ACH
	Ventilation air flow rate (per building floor)	0.6	ACH
	Heating system efficiency	0.94	-
	Cooling system efficiency	None	-
Simulation parameters	Day urban layer boundary height	700*	m
	Nighttime urban layer boundary height	80*	m
	Reference height at which the vertical profile of potential temperature is assumed uniform	150*	m
	Urban breeze scaling coefficient	1.2*	-

*These values are default values from UWG. (Bueno 2012) varied the nighttime height between 30 and 100 m and the daytime height between 800 and 2000 m and concluded that these parameters only influence the output temperature by 0.1 K. The default values for reference height and urban breeze scaling coefficient were used.

Model verification for the 2003 heatwave in Paris

We first verified the UWG model's ability to replicate the urban heat island effect during the 2003 heatwave: Figure 45 left shows the daily average temperature profile from the 7th of August until the 14th of August. We compared observations from the weather station Roissy-Charles-De-Gaulle as input to UWG (light red curve in Figure 45-left), and compared the outputs (dark red curve in Figure 45-left) with observations from the weather station downtown Paris, Paris-Montsouris (dotted black curve in Figure 45-left) located in an urban park. The pink area represents the time at which there is an urban heat island effect, while the blue area represents the time at which there is an urban cooling effect, during the day. The model calculates night temperatures around 1-1.5 °C superior on average to the observations for the reference neighborhood. As the observations were recorded in a park, this difference is expected because local microclimate temperatures around mineral surfaces were actually more elevated. Furthermore, the average temperature from 4 am to 6 am between the 10th and 13th of August from the modelled temperature with UWG is about 27.5 °C, while it was recorded to be about 28 °C downtown Paris in boulevard Sebastopol. It is about 23.5 °C in Roissy before UWG and 25.5 °C at the station Paris-Montsouris. According to Bueno, UWG has an accuracy of +/- 1 °C. For our case-study we consider UWG as capable to replicate the UHI effects. On the right of Figure 45, we show a heatwave of similar amplitude than 2003

modelled by the model MPI during the contemporary period, the light-red curve is the direct output of the climate model while the dark red curve is the output of UWG. The model UWG was used only for the city of Roissy, it could have been used as well for the cities of Carpentras and La Rochelle but in a first approach we investigated only Paris. This model is a simple tool that can easily be used to incorporate UHI effects within weather files as input for building simulations.

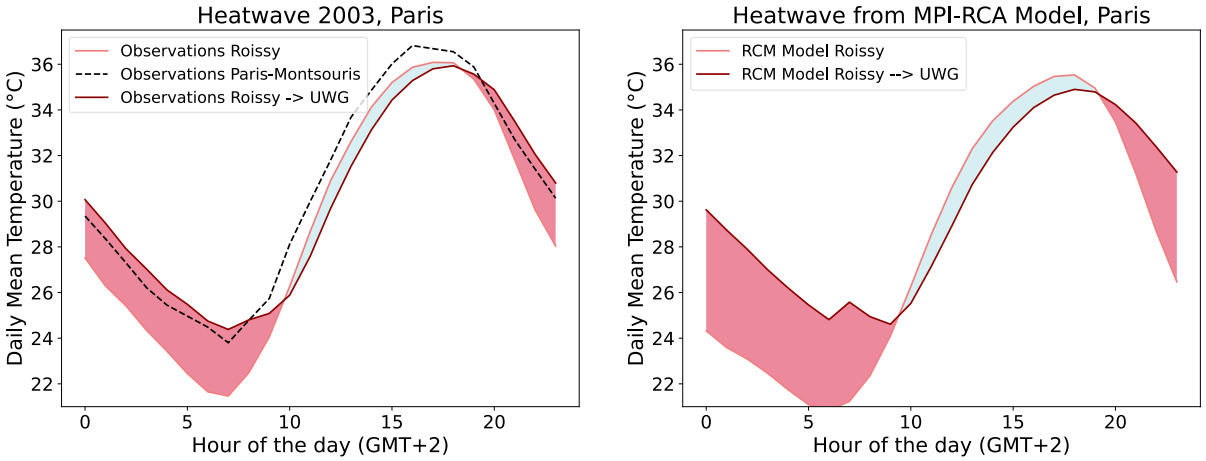

Figure 45 - Daily average dry-bulb temperature profile during the 2003 heatwave in Paris: Comparison between observations in Roissy, observations in Paris and modelled temperatures for Paris using UWG

2.3.3 Spatial framework correlating regional climate exposure to indoor overheating

How to correlate the different spatial scales of the exposure from the regional climate to the building indoor overheating perceived by the occupants? For the purpose of our study, we propose a spatial framework, using different tools, to assess the building indoor conditions and its impact on the occupants (Figure 46). The first spatial scale is the regional climate, climate data used from models run by climatologists, it could be for instance a future reassembled typical summer, or a future heatwave.

The second spatial scale is the local microclimate scale: Most of the time, the microclimate is not considered in building thermal simulations, even though there is evidence that the urban heat island effect changes the climate conditions around an urban building. This is usually not modelled as boundary conditions in building simulations because of the complexity to model the urban microclimate in a time-efficient manner to be coupled with the building simulation. In the context of this Ph.D., we modelled the local microclimate as a dry-bulb temperature and relative humidity modification with the software Urban Weather Generator (UWG), for the case-study city of Paris. These urban weather files were created but not used in the rest of this Ph.D., due to lack of time to represent the urban context (such as surrounding buildings creating shadows) around the building within the EnergyPlus simulations, as suggested by (Salvati et al., 2020). However, these future urban weather files represent potential for future research. At the urban microclimate scale, the exposure is now

at the scale of the urban fabric surrounding the building case study. If the urban fabric is adapted to heat, it will positively influence the local microclimate and therefore the building exposure. On the latter, if it is not adapted to heat it might negatively influence the building exposure by enhancing the exposure to heat. The heat exposure at the urban microclimate scale was studied in a conference article (Machard et al., 2020b), but this is not in the scope of this Ph.D.

Finally, the last spatial scale is at the building level: From the outdoor temperature, indoor temperature is calculated by the building thermal simulation model (EnergyPlus), to which the occupants are directly exposed. The building case-study used in this thesis is introduced in section 2.4. By analyzing the summer thermal discomfort, the building case study vulnerability can be assessed, and then improved using optimization methods.

The passive cooling strategies that we modelled to improve the building resilience to heat with the software EnergyPlus are described in section 2.4 as well. The built environment (at both the urban and building scale), if designed appropriately, can play the role of a protective factor for the occupant, but if not adapted to climate change it might actually increase people exposure to elevated temperatures (both in the outdoor local microclimate and inside the building).

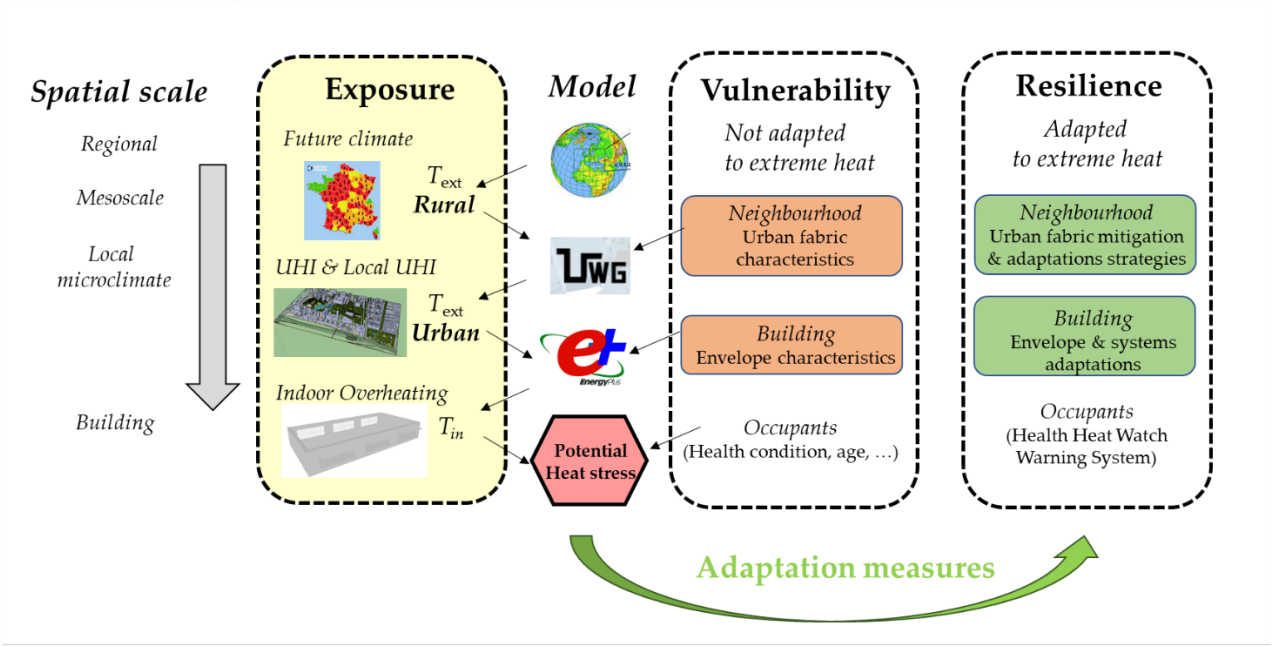

Figure 46 - Different scales and tools of the resilience framework from outdoor climate to indoor overheating (Machard et al., 2020b)

2.4 Case-study building and EnergyPlus model

2.4.1 Presentation of the building case-study

The building case-study is an eight-stories residential collective building located in an urban context. It was originally a sketch made by an architect in the first design stage of a project (Figure 47). We decided to use this attractive case-study because of its interesting design: The building has large glazed windows oriented North and South, with buffer spaces between each conditioned apartment and the glazed exterior facades. The desire of the architect was to design a building with a nice visual comfort through the large glazed facades, to make the space modular by the occupants, using the buffer spaces along the seasons and with a minimal environmental impact.

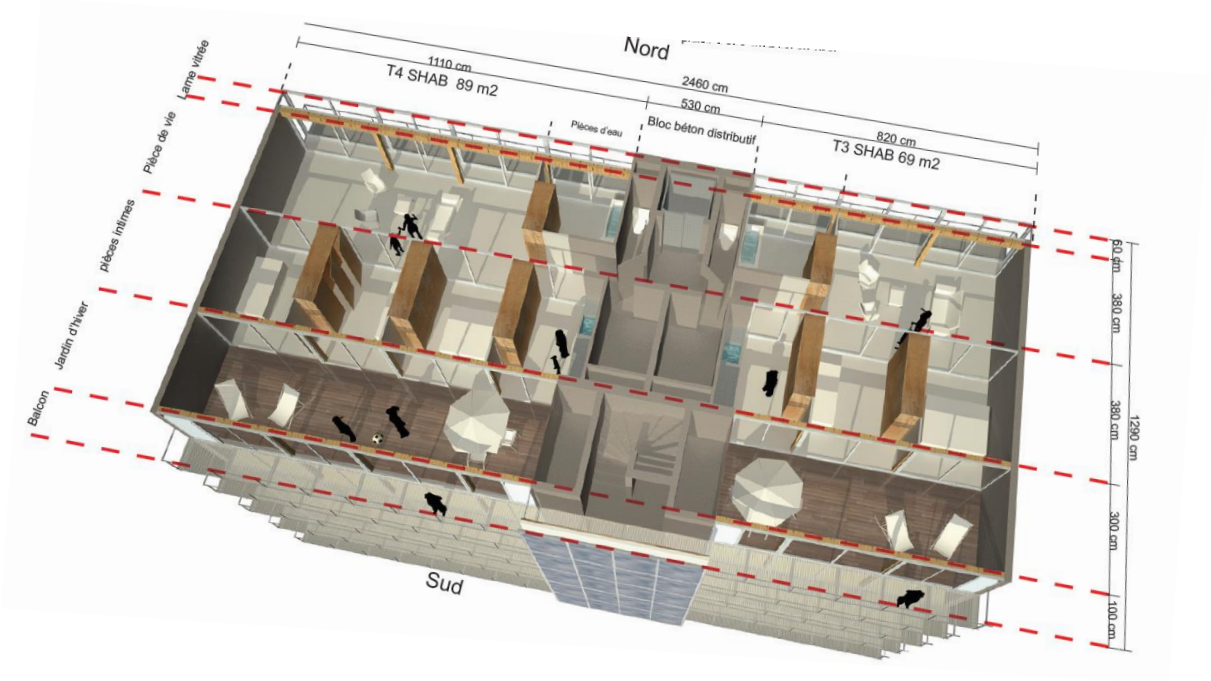

Figure 47 - Top view from the building case-study

From this building, we focus on the apartment located on the top floor on the Westside. The apartment has a living space with a surface area of 120 m² with an additional 50 m² veranda oriented South, with a glazed cavity zone of 0.6 m width located on the North façade (Figure 48 and Figure 49). The initial design of the apartment is fully glazed on the North and South façade to allow a generous amount of daylight in the house. The architectural choice to glaze the North façade is backed up by a trombe wall, exterior to the veranda on the South façade which gathers warm air during the winter, transferred to the North glazed closed cavity. For the purpose of this study, this initial architectural choice (glazed North façade) is conserved but the trombe wall is not modelled as the winter period is not the purpose of the study. The goal is to analyze if such a design is suited for future summers.

Figure 48 – Vertical view from the apartment case-study

Thermal zoning

We divided the apartment into three distinct thermal zones: the glazed cavity (unconditioned), the living space (conditioned) and the veranda (unconditioned). These three zones are shown in Figure 49. The west side of the apartment is in contact with the outdoors, whereas the East side is considered to be adjacent to an apartment and is therefore modelled as adiabatic. The ceiling is in contact with the exterior and the floor is modelled as adiabatic, to simulate it in contact with the under dwelling.

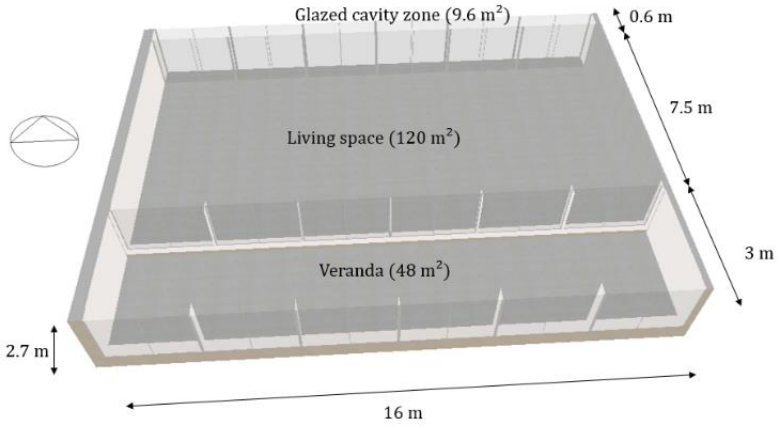

Figure 49 - Representation of the apartment case-study in DesignBuilder

Bioclimatic features

The apartment has some initial architectural features favoring bioclimatic summer design. The living space is located in between the veranda (*jardin d'hiver*) and the glazed cavity (*lame d'air*), and these two rooms act as buffer spaces between the living space (*cellule logement chauffé*) and the exterior environment. The configuration of the windows favors cross-ventilation, to enhance summer natural ventilation. All the flats have exterior balconies which act as overhangs for the flats under them, allowing to reduce solar heat gains in the summer

on the South façade (0.5 m on the North façade and 1 m on the South façade). Rendering of the cross-ventilation disposition and overhangs are shown in Figure 50.

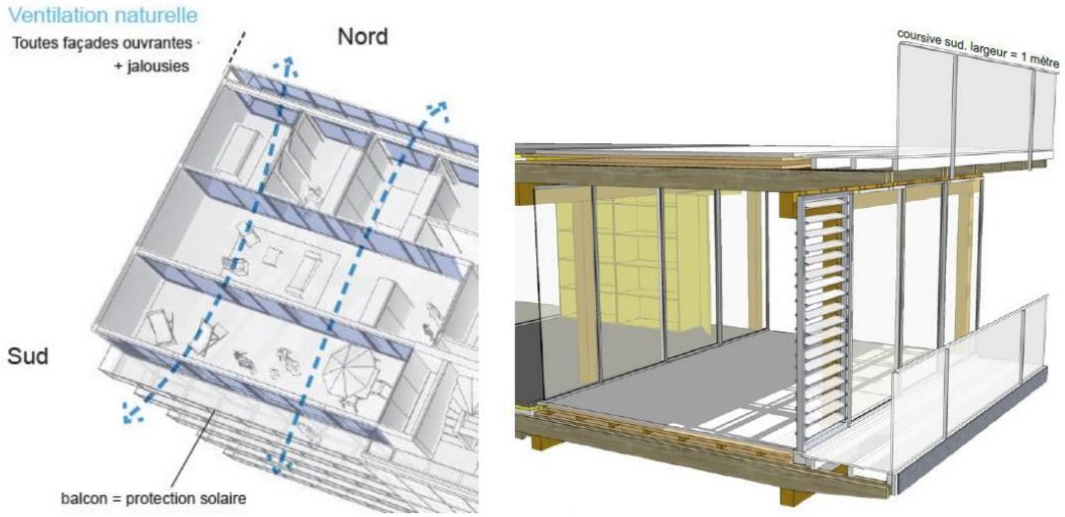

Figure 50 – Rendering of natural cross ventilation (left) and of balconies acting as overhangs (right)

Building construction and material properties

The building constructions and materials are presented in Table 10. The building is RT-2012 compliant and has double glazing windows and efficient U-value in exterior walls and roof. The building opaque material properties are given in Table 11. The window glass properties are given in Table 12, they were taken from the building thermal regulation RT-2021.

Table 10 - Description of the building case-study constructions

	Construction layers from interior to exterior	**U-value [W/m².K]**
Exterior wall	18 cm concrete + 14 cm polystyrene insulation	0.23
Interior wall	18 cm concrete	Adiabatic
Floor (intermediate) of the living space	18 cm concrete + 3 cm polyurethane insulation	Adiabatic
Ceiling of the living space	18 cm concrete + 15 cm polyurethane insulation	0.16
Floor (intermediate) of the veranda and of the glazed cavity	5 cm concrete screed	Adiabatic

Table 11 - Description of the building material properties

	Thermal conductivity λ (W/(m.K))	**Specific Heat Cp (J/(kg.K))**	**Density r (kg/m^3)**
Concrete	2.00	930	2300
Concrete screed	1.05	930	1700
Polystyrene	0.032	1470	25
Polyurethane	0.025	1500	30

Table 12 - Description of the building window properties

Location	Glass type	Ug (W/m²/K)	Uw (W/m²/K)	Sg (-)	Sw (-)
Cavity / Ext North	Single 4 mm	1.1	1.30	0.60	0.34
Cavity / Living	Double 2 x 4 mm (Filled with Argon 16 mm)	1.1	1.23	0.60	0.34
Living / Veranda	Double 2 x 4 mm (Filled with Argon 16 mm)	1.1	1.40	0.60	0.33
Veranda / Ext South	Double 2 x 4 mm (Filled with Argon 16 mm)	5.7	5.50	0.79	0.67

On the exterior windows of the glazed cavity on the North façade, shutters are assumed to be used during the night (10 pm to 7 am) from the 1st of November until the 1st of May. They add a thermal resistance DR = 0.25 m².K/W and help reduce the heating needs because of the large glazed surface.

We modelled some thermal bridges on the building, they are given in Table 13. In EnergyPlus the thermal bridges are modelled as a no mass layer.

Table 13 – Linear thermal bridges

	Thermal bridge (W/(m.K))
Roof/Wall	0.38
Wall/Intermediate floor	0.18
Wall/Wall (exterior corners)	0.08
Wall/Floor veranda	0.05
Window framing	0.02

According to the RT-2012, in collective buildings the infiltration rate must be of 1 m³/h/m² at 4 Pa. For the building case-study, because of the efficient window frames we consider this infiltration rate to be about 0.8 m³/h/m² at 4 Pa, which corresponds to 2.77 ACH (120 m² and height of 2.7 m). In EnergyPlus there are two ways to model this, that depends on the model used for natural ventilation via windows openings if there is a window opening scenario:

- If the simplified ventilation model is used, it is possible to use the simplified infiltration model where the infiltration rate is input and can be modulated with wind and temperature-dependent coefficients. This option can be used in combination with the simplified ventilation model;

- If the Airflow Network (explained later in section 2.4.2.3) is used for natural ventilation through windows, the Airflow Network will be used to model infiltrations around each building surface. In DesignBuilder it is possible to select between five types of "cracks" ranked from very bad to excellent, we choose the second-best type of crack. Note that modelling cracks and natural ventilation through the windows considerably extend the simulation time and it is advised not to model cracks if simulating only during the summer period to reduce the computational time.

As through the sensitivity analysis and optimization we will compare the different ventilative cooling strategies, and that the natural ventilation strategy is modelled with the Airflow Network, we decided not to model infiltrations to remain consistent amongst the different solutions. While it does not affect greatly the results for the summer periods, this modelling choice result in a heating needs reduction in all simulations.

Internal Gains

The case-study apartment accommodates five people with the assumption that four persons are at work during the day, but one person stays in the apartment all day. The average metabolic heat produced by the individuals is assumed to be equal to 81 W. According to the occupancy schedule proposed by the French Thermal Regulation, we multiplied the heat gain produced by all five individuals by 0.7 at night (10 pm-7 am), by 1 in the mornings and the evenings (7 am-9 am and 7 pm-10 pm) when the flat is fully occupied, and by 0.2 during the weekday (9 am-7 pm) when only one person is in the apartment. During the week-end we assume all occupants are present in the apartment. The occupants' vesture is about 1 clo in the winter and 0.5 clo during the summer, it varies with a fixed schedule between the winter and summer periods.

Regarding internal gains related to specific equipment, due to the European Union's Ecodesign Directive (Directive 2009/125/EC), all household equipment must be of grade A+++ in 2035, the lowest energy consuming grade. The French electricity transmission system operator RTE has recently produced a report including projections towards 2035 for the specific equipment electricity consumption in residential households, including this upgrade in efficiency (RTE, 2017). The RTE projections were made for an "average" household, we assume it is about 90 m² as in the RT-2012. Specific equipment consumption relates to all electricity consumption in a dwelling (cooking, washing and advertisement) excluding lighting and HVAC systems. Comparing the RT-2012 and the RTE-2016 reference scenarios, the yearly specific electric consumption is about 2367 kWh/year and 2280 kWh/year respectively. In contrast, the predicted electricity consumption of the RTE scenario number 3 for 2035 (3rd highest electricity consumption trajectory out of 4) is about 1210 kWh/year, therefore a decrease of 53 %. We use the same schedule as in the present, but with a maximum value of 3.0 W/m² instead of 5.8 W/m².

The same methodology can be applied to the electricity consumption related to lighting. The reference values of the RT-2012 are of 360 kWh/year, of the RTE-2016 of 300 kWh/year, when the projected value of the RTE-2035 is about 110, which is equivalent to 132 kWh/year in reference to RT-2012, corresponding to a decrease of 36.7 %. We use the same schedule as in the present, but with a maximum value of 0.5 W/m² instead of 1.4 W/m². The sum of these three types of internal gains is illustrated in Figure 51 for both the present and future periods.

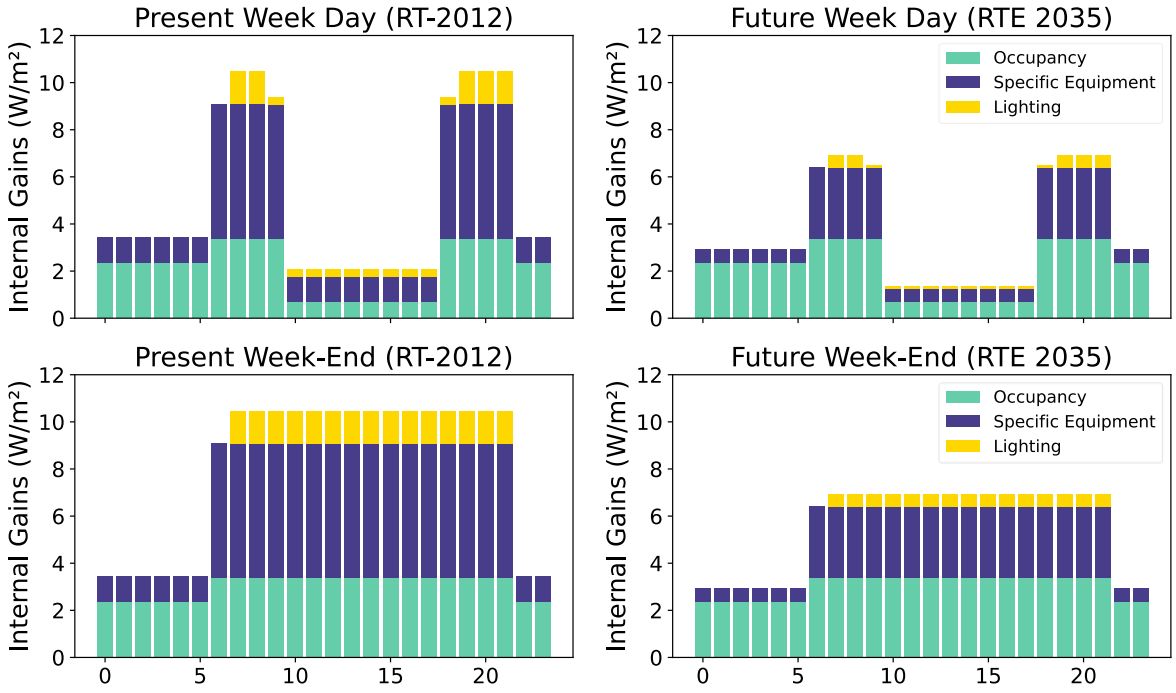

Figure 51 – Internal gains as a sum of occupancy, specific equipment and lighting in a household in France for a week day: 2012 vs. 2035

Mechanical ventilation and heating scenarios

According to the RT-2012, the heating set-point temperature must be 19 °C and reduced during the day at 16 °C when the building is unoccupied. As one person is always present in the apartment, the heating set-point temperature is constant. We set the set-point at 20 °C air temperature in order to reach an operative temperature between 19 °C and 20 °C. Only the living space is heated.

Regarding the hygienic ventilation, we consider a minimal ventilation airflow rate of 105 m^3/h following the French legislation (arrêté 1982). The maximum airflow rate is about 210 m^3/h which corresponds to 0.65 ACH for the living space, it is used at maximum capacity during three hours per day, between 8 am and 10 am and between 7 pm and 8 pm.

Occupant behavior

It is well-known that occupant behavior can have a huge impact on the building's indoor thermal comfort as well as energy consumption. (Gondian et al., 2019) investigated the impact of the occupant's behavior (blinds usage, windows opening, specific electric usage and mechanical night ventilation usage) and demonstrated that these could impact the indoor operative temperature during a heatwave of about 3 °C. (Yao, 2020). modelled different scenarios for shades control and showed that depending on the shades control used it can influence up to 50 % of the cooling rate on an hourly basis. (Wang et al., 2020) monitored people opening windows and could notice that people are more inclined to open windows when it is hot, to create some airflow, which could be counterproductive in some climate as it most likely increases the indoor temperature during the day.

However, as it is not in the scope of the thesis, the occupant behavior is not modelled as dynamic. We assume that specific electric usage follows a fixed schedule, as defined in section 2.4.1. We assumed that the windows opening and shades control are automatized and therefore can be optimized.

2.4.2 **Modelling choices with EnergyPlus**

The building was modeled with the software EnergyPlus. EnergyPlus is a well-reputed, open-source and internationally used building simulation software, developed in the United States by the Department of Energy (DOE). It is based on two older programs, namely BLAST and DOE-2 and is programmed in FORTRAN, the code was developed from the International Energy Agency (IEA) BESTEST. It has no user-interface, but different possibilities are to use OpenStudio, 3D Google Sketchup, or the commercial interface DesignBuilder. In the context of this Ph.D., we used DesignBuilder as a graphical interface. DesignBuilder allows to run RT-2012 compliance simulations, LEED certifications, lighting and airflow calculations and embodies a parametric and optimization platform. EnergyPlus allows modelling a wide range of systems, even though their implementation can be complex.

2.4.2.1 Heat balance

The heat balance on external surfaces in EnergyPlus is solved by Equation (32).

$$\varphi_{longwave\_rad\_ext} + \varphi_{shortwave\_rad\_ext} + \varphi_{conv\_ext} - \varphi_{cond} = 0 \quad (32)$$

$\varphi_{longwave\_rad\_ext}$ is the net longwave (thermal) radiation flux exchange with the air and surroundings, $\varphi_{shortwave\_rad\_ext}$ is the absorbed shortwave radiation from sunlight (direct, diffuse and reflected) heat flux, φ_{conv_ext} is the convective flux exchange with the outside air, and φ_{cond} is the conduction heat flux through the surface.

The heat balance on opaque internal surfaces in EnergyPlus is solved by Equation (33).

$$\varphi_{longwave\_rad\_int} + \varphi_{shortwave\_rad\_int} + \varphi_{conv\_int} + \varphi_{cond} = 0 \quad (33)$$

$\varphi_{longwave\_rad\_int}$ is the longwave radiation from internal sources (such as specific equipment) and the exchange flux with other surfaces in the zone, $\varphi_{shortwave\_rad\_int}$ is the shortwave transmitted solar radiation absorbed by the surface and shortwave radiation flux to surface from lights, φ_{conv_ext} is the convective heat exchange with the zone air, and φ_{cond} is the conduction flux through the building surface from the exterior.

The heat balance on external and interior building surfaces in EnergyPlus is illustrated in Figure 52.

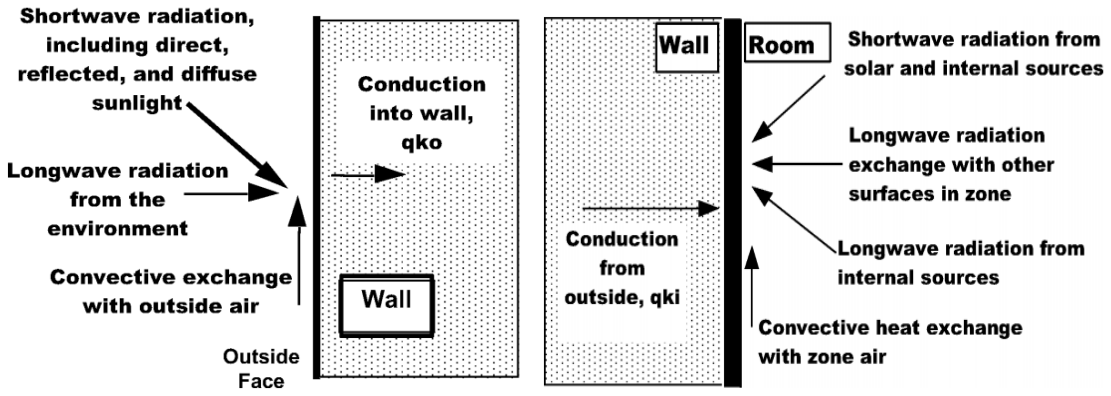

Figure 52 - Heat balance on external building surface (left) and on internal building surface (right), taken from EnergyPlus documentation

Radiance distribution from the sky

The shortwave radiance distribution of the sky ($\varphi_{shortwave\_rad}$) is modelled as anisotropic. It is detailed in the Engineering Reference in Chapter 5, Sky Radiance Model. The diffuse sky irradiance on a surface is the product of the diffuse solar irradiance from the sky on the ground (horizontal diffuse solar irradiance from the input weather file) and a multiplier accounting for the building surface orientation and shading effects from overhangs, but not for the reflection of the diffuse radiation from the shadowing surfaces. The sky radiance distribution model is empirical, based on radiance measurements of real skies (Perez et al., 1990). The sky longwave radiation distribution ($\varphi_{longwave\_rad}$) is isotropic, and in the presence of overhangs, it is multiplied by an isotropic shading factor. The obstructions and ground are assumed to have an emissivity of 0.9.

Conduction algorithm

We chose as heat balance algorithm the conduction transfer function (CFT) for the three thermal zones (this is the default algorithm in EnergyPlus). This algorithm calculates only heat transfers but not humidity. It is detailed in the Engineering Reference in Chapter 3, Conduction Through the Walls. It is based on the famous State-Space method developed by (Seem, 1987). This method, in comparison to other transfer function methods is that it allows getting CFTs for smaller time-steps without being unstable even for massive walls.

Convection algorithm

The convection flux is calculated using the heat transfer coefficient (Equations (34) and (35)). There are many different methods to calculate the convection coefficient h_{c_ext} and h_{c_int}. The different methods are presented in the Engineering Reference in Chapter 3, Outside Surface Heat Balance, Outdoor / Exterior Convection and in the section Inside Heat Balance, Interior Convection.

$$\varphi_{conv\_ext} = h_{c\_ext}.A.(T_{surface\_ext} - T_{air\_ext}) \quad (34)$$

$$\varphi_{conv\_int} = h_{c\_int}.A.(T_{surface\_int} - T_{air\_int}) \quad (35)$$

Exterior

There are many methods in EnergyPlus to calculate the exterior heat transfer coefficient. The method can be set at zone level (i.e. the same method will be used for all exterior surfaces of the zone), or at surface level (i.e. several methods can be used for different surfaces). We chose to set the method at zone level and use the default method proposed by EnergyPlus, the DOE-2 which is a combination of the MoWiTT and BLAST detailed convection models. The exterior heat transfer coefficient h_{c_ext} (Equation (36)) depends on h_{nat}, the natural convection component, R_f, the surface roughness multiplier, a and b that are constants, and $h_{c,glass}$ the convection coefficient for very smooth surfaces such as glass (Equation (37)). The constants g and s are MoWiTT coefficient given in the documentation. The coefficient h_n is calculated with a detailed natural convection model that correlates the h_{c_ext} to the surface orientation and the difference between the surface and air temperatures (ΔT), see Equation (38).

$$h_{c\_ext} = h_{nat} + R_f.(h_{c,glass} - h_{nat}) \tag{36}$$

$$h_{c,glass} = \sqrt{h_{nat}^2 + [g.WS_z^s]^2} \tag{37}$$

When ΔT = 0 or for a vertical surface:

$$h_{nat} = 1.31.\ |\Delta T|^{\frac{1}{3}}$$

For ΔT < 0 and an upward facing surface, or: ΔT > 0 and a downward facing surface with Σ the surface tilt angle:

$$h_{nat} = \frac{9.482.|\Delta T|^{\frac{1}{3}}}{7.283 - |cos\Sigma|} \tag{38}$$

For ΔT > 0 and an upward facing surface, or: ΔT < 0 and a downward facing surface:

$$h_{nat} = \frac{1.810.|\Delta T|^{\frac{1}{3}}}{1.382 + |cos\Sigma|}$$

Interior

The different methods are based on correlations for natural, mixed or forced convection. We choose to use the interior natural convection model algorithm TARP (Thermal Analysis Research Program)(Walton, 1983) which uses ASHRAE coefficients for the living space and the veranda. It is the default convection model in EnergyPlus. The equations are the same as for h_{nat}. We use the TrombeWall algorithm for the glazed cavity.

Interior solar distribution algorithm

In EnergyPlus, there are five choices for interior solar distribution ($\varphi_{shortwave\_rad\_int}$). These are detailed in the Engineering Reference in Chapter 5, Shading Module, Solar Distribution. We use the "Full Interior And Exterior" distribution, which is a detailed solar distribution on interior surfaces but does not consider shadowing around exterior surfaces, since no urban context is modelled around our building. The Full Interior and Exterior distribution algorithm calculate the amount of transmitted beam solar radiation that falls on each surface of the zone (floor, walls, interior windows), considering the sun orientation and

beams projection inside the zone, while accounting for window shading devices. It also calculates how much beam radiation falling on an interior window is absorbed, transmitted to an adjacent zone, or rejected back into the zone. EnergyPlus calculates the short-wave radiation distribution in each thermal zone. It is the sum of the beam and diffuse solar radiation and short-wave radiation from indoor electric lights. The interior solar distribution for our apartment case-study is introduced in Figure 53. Exterior windows are drawn in blue and interior windows are drawn in grey. The beam radiation entering an exterior window either falls on the ground or on interior surfaces and is considered as "beam to diffuse" (drawn in blue), either falls on the interior window and is then considered as "beam to beam". If it falls on the interior window, it is either absorbed, transmitted, or rejected back into the zone. The beam solar radiation transmitted through an interior window becomes diffuse in the habitable zone and is uniformly redistributed. Therefore, as the habitable zone only has "interior windows", short-wave radiation is only transmitted as diffuse. The diffuse radiation entering an exterior window either falls on the floor, on the wall, or on an interior window. Depending on the case, it is either distributed uniformly or with view factors. All diffuse radiation from the outdoors and short-wave radiation from interior lights in the habitable zone are either absorbed by walls, floor or interior windows (drawn in purple), either transmitted out towards the adjacent zones through the interior windows (drawn in brown).

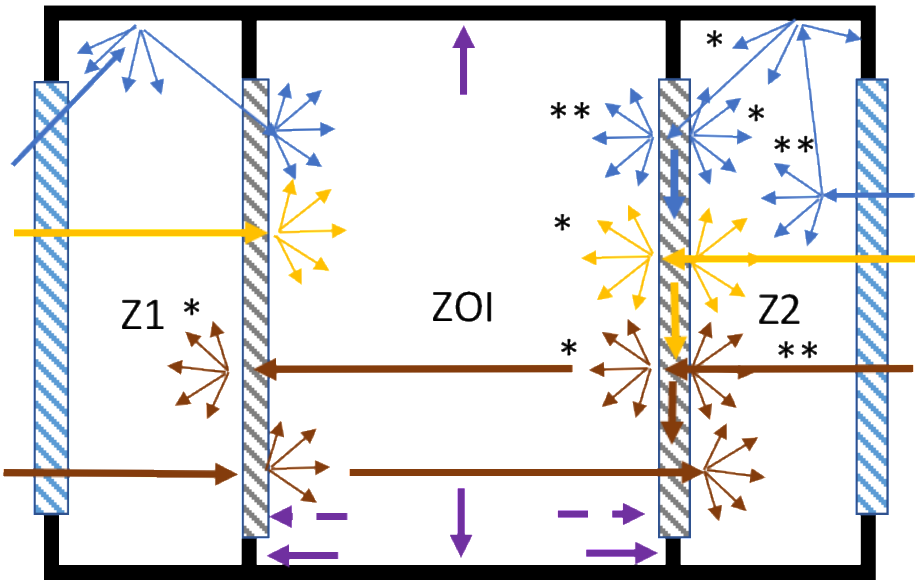

Figure 53 - Representation of the interior solar distribution in the apartment case-study created by Fanny Devys-Peyre - * the radiation is distributed uniformly, ** the radiation is distributed by view factors. Z1 refers to the glazed cavity, ZOI stands for zone of interest (the living space) and Z2 is represents the veranda

2.4.2.2 Daylighting calculation

In EnergyPlus there are two daylighting calculation methods: Split-Flux (default) and DElight. Both are detailed in the Engineering Reference, Chapter 7. We used the Split-Flux method, derived from the method in DOE-2.1E (Winkelmann & Selkowitz, 1984) because it accounts for the dynamic use of windows shading during the daylight calculation at each time-step (The DElight method doesn't). The Delight method does not account for the presence of overhangs so we use the Split-Flux. The Split-Flux method is quickly summarized as follows: First, daylight factors are calculated, they are ratios of interior illuminance to exterior

illuminance, calculated from a coordinate reference point in the zone input by the user. EnergyPlus then calculates the contribution of the windows to this ratio, and the contribution from the light reflected by interior surfaces, accounting for the window sizes and orientation, the glazing transmittance, shading devices, and overhangs. Shades on windows are assumed to be almost perfect diffusers, and their luminance is independent of the angle of emission of light, on their position, and on the angle of incidence of the sun falling on the shade. The daylight factors are calculated for hourly sun positions on sun-paths for representative days. At each time-step, the illuminance at the reference point in the zone is calculated, interpolating the daylight factors using the time step sun position and sky condition. From this illuminance, the lighting energy needed from interior lights to reach the illuminance set-point is calculated, and a zone lighting electric reduction factor is quantified to reduce internal gains from interior lights that are not used at the current time-step.

2.4.2.3 Passive cooling strategies and systems

From the state of the art, a variety of passive cooling strategies and systems can be explored to adapt the building design to future summer climate. However, for different reasons explained in Table 14, all techniques and strategies could not be tested in the context of this study, due to the building design and software limitations. As one of the objectives of the study is to conduct optimization of the different input parameters of the building, the building must be modelled in a time-efficient manner. For this reason, we excluded systems that required to use the Conduction Finite Difference Solution Algorithm which is a Finite-Element method (FEM), such as green roofs and PCMs. Also, considering the design of the building (two buffer spaces around the conditioned space), we considered that the use of smart glazing technologies was not strategic as their full potential could not be considered. Finally, we did not model innovative radiative cooling systems nor indirect evaporative cooling, as these are already semi-active technologies and are more complex to model. Therefore, the final investigated strategies and systems are the following: shades on windows, natural nocturnal (by windows opening) and mechanical ventilation (free cooling), thermal inertia, cool paints, and earth-to-air heat exchanger. As architectural features, we will also question the initial building design and the use of buffer spaces, overhangs, and large glazed facades.

Table 14 - Model used for each strategy/system identified in the State of the Art, Chapter 1

	Strategy/System	Tested on the building case-study?	EnergyPlus algorithm
Bioclimatic architecture	Use of buffer spaces	Yes	
	Glazing percentage	Yes	
	Use of overhangs	Yes	
Preventing solar heat gains	Smart glazing technologies	No	As the living space is in between two buffer spaces, the solar heat gains do not fall directly on the exterior windows. Therefore, on this design it is not possible to fully test the potential of smart glazing technologies
	Shading (blinds) on windows	Yes	
	Cool selective materials	Yes	
	Green roofs and walls	No	FEM algorithm
	Roof ponds	No	No simple system implemented in E+
Dampening the heat	Thermal mass	Yes	
	PCMs	No	FEM algorithm
Ventilative cooling strategies	Natural ventilation	Yes	Airflow Network
	Free cooling	Yes	Simple Ventilation Algorithm + EMS language for control (models for free cooling + AC are implemented)
	Earth-to-air heat exchanger	Yes	Simplified model
Other passive cooling systems	Radiative cooling	No	Requires complex modelling of wave-lengths that are not discretized in EnergyPlus
	Indirect evaporative cooling	No	Indirect Research Special model

Overhangs and window shades

In EnergyPlus it is possible to model fixed horizontal overhangs, sidefins, or both on the same façade. Regarding exterior or interior blinds, many options exist. It is not possible to add shading devices to interior windows, so in our case shading devices can only be applied to the South exterior windows of the veranda or to the North exterior windows of the glazed cavity. We modelled exterior white shutters. Blinds are either fully on or off, but it is not possible to model them half opened. One option is to vertically divide the windows and add shades on some and not on others. This is the option we used: For instance, we decomposed each glazed façade into six windows, modelling either blinds on zero windows, three windows, or six windows. Different types of control are possible, such as blinds are on if there is air-conditioning inside, or if the indoor air temperature is above a defined set-point temperature, or depending on a fixed schedule, or depending on the amount of exterior solar radiation falling on the exterior window. We used this latter control option. The properties of the

modelled shutters are the standard ones defined by the RT-2012. Furthermore, exterior shutters are modelled on the exterior windows of the North façade during the night in the winter and mid-season (from the 1st of November until the 30th of April.)

Cool selective paints

In EnergyPlus it is not recommended to model a thin layer of paint, but it is preferred to change directly the optical properties of the outer material of the building exterior surface construction. The absorptivity is a coefficient between 0 and 1 that determines the fraction of incident radiation absorbed by a body. In EnergyPlus, it is discretized through three portions of wavelengths:

- The absorptivity in the visible wavelength (0.4 – 0.76 μm), $\alpha_{visible}$
- The absorptivity in the solar wavelength (0.3 – 2.5 μm), α_{SW}
- The absorptivity in the long wavelength (2.5 – 50 μm), α_{lgw} (or ε)

A low absorptivity in the solar wavelength means that the body absorbs only a small portion of the heat, which is the opposite of high reflectivity in the solar wavelength, also called albedo.

According to Kirchhoff law, the absorptivity in the long wavelength is equal to the emissivity ε.

The property $\alpha_{visible}$ is used for daylighting calculations, while the properties α_{SW} and ε have an impact on the external heat balance ($\varphi_{shortwave\_rad\_ext}$ and $\varphi_{longwave\_rad\_ext}$). In EnergyPlus, on each spectrum (visible, shortwave or longwave) only one average value can be entered, it is not discretized further. Therefore, it is not possible to model innovative cool selective materials who for instance have a high emittance only in the atmospheric window. The coefficient $\alpha_{shortwave}$ has a direct impact on the solar gains ($\varphi_{shortwave\_rad\_ext}$) on any exterior surface which are calculated with Equation (39).

$$\varphi_{shortwave\_rad\_ext} = \alpha_{shortwave} \cdot \left(I_{beam} \cdot \cos\theta \cdot \frac{Sl}{A} + I_{diffuse} \cdot F_{ssky} + I_{reflected(ground)} \cdot F_{sground} \right) \quad (39)$$

I is the irradiation, θ the surface angle, A the surface area, Sl the sunlit surface area, F_{ssky} the angle factor between the surface and the sky, F_{sgrd} the angle factor between the surface and the ground. The coefficient $\alpha_{longwave}$ (ε) has a direct impact on the net longwave radiative heat flux $\varphi_{longwave\_rad\_ext}$, which is the sum of radiation exchanges between the building surface (surf), sky and ground (grd), applying the Stefan-Boltzmann law (Equation (40)).

$$\varphi_{longwave\_rad\_ext} = \varepsilon . \sigma . F_{grd} . \left(T_{grd}^4 - T_{surf}^4\right) + \varepsilon . \sigma . F_{sky} . \left(T_{sky}^4 - T_{surf}^4\right) + \varepsilon . \sigma . F_{air} . \left(T_{air}^4 - T_{surf}^4\right) \quad (40)$$

With σ = 5.67.10−8 W/(m².K^4) the Stefan-Boltzmann constant, T the temperatures, and F the view factors of the building surface to the ground surface temperature, to the sky temperature and to the environment temperature which is assumed as the air temperature. The heat transfer coefficients are linearized which give Equation (41):

$$\varphi_{longwave\_rad\_ext} = h_{r,grd}.\left(T_{grd} - T_{surf}\right) + h_{r,sky}.\left(T_{sky} - T_{surf}\right) + h_{r,air}.\left(T_{air} - T_{surf}\right) \quad (41)$$

With T_{sky} used in EnergyPlus is given by Equation (42):

$$T_{sky} = \left(\frac{I_{longwave}}{\sigma}\right)^{0.25} - TK \quad (42)$$

The equations for the view factors and h_r are given in the Engineering Reference in Chapter 3, Outside Surface Heat Balance, External Longwave Radiation, while the one for $I_{longwave}$, calculated from the sky emissivity (calculated from the dew point temperature and cloud cover) and air temperature is given in Chapter 5.1 Climate Calculations.

Natural ventilation

In EnergyPlus there are three options to model natural ventilation. The simplified algorithm is named "Design Flow Rate" and allows to define a maximum airflow that can be modulated according to a schedule and/or interior and exterior temperature conditions. There exists an intermediate algorithm, "Wind and Stack Open Area", that is not implemented in DesignBuilder. The third algorithm is more complex, it is the Airflow Network model that has a nodal approach, calculating air flows considering stack pressure and wind-driven air exchanges (Gu, 2007). We decided to use this one. It consists of four sequential steps outlined in Figure 54. In this section, we introduce the calculation for step 1 for our building case-study. The full equations can be found in the Engineering Reference Chapter 13, Airflow Network Model.

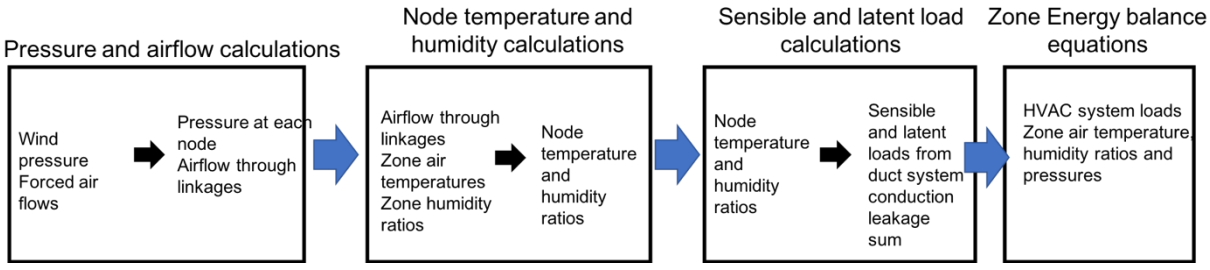

Figure 54 - Sequential steps and calculations of the Airflow Network

The Airflow Network model calculates multizone airflows driven by outdoor wind. The network consists of a set of nodes connected by airflow components through linkages, the network for our case-study apartment is represented in Figure 55.

Wind Pressure calculation

In EnergyPlus, the wind pressure is determined by Equation (43):

$$P_w = C_{p\_air}.\rho_{air}.\frac{WS_{ref}^2}{2} \quad (43)$$

WS_{ref} is the local wind speed at the height z of the pressure node considered in front of the building façade (Equation (44)), whereas WS_{met} is the wind speed at the meteorological station at the height z_{met} of 10 m. ρ_{air} is the air density and is about 1.2 kg/m^3.

$$WS_{ref} = WS_{met} \cdot \left(\frac{\delta_{met}}{z_{met}}\right)^{c_{met}} \cdot \left(\frac{z}{\delta}\right)^{c} \quad (44)$$

The wind speed at the station is corrected with the factors c and δ which are terrain-dependent coefficients, δ is the boundary layer thickness for the given terrain type. The values of these coefficients are shown in Table 15.

Table 15 - Coefficients for correcting the local wind speed according to the terrain (ASHRAE, 2001)

Terrain description	**δ, layer thickness**	**c, exponent**
Flat, open country	270	0.14
Rough, wooded country	370	0.22
Towns and cities	460	0.33
Ocean	210	0.10
Urban, industrial forest	370	0.22

Our building case-study is located in a city terrain, so the value 460 is used for δ and 0.33 for c whereas 270 and 0.14 were used for δ_{met} and c_{met}. Some calculated values of the wind speed at different pressure nodes heights compared to the wind speed in the open land are shown in Table 16. In our study, as we model the top-floor, we can see from Table 16 that the local wind speed is actually higher than at the meteorological station. However, we have not modelled the urban neighborhood around the building, which we know could greatly modify (increase or decrease) the local wind speed. The coefficient SC_p is the pressure coefficient on the façade of the building, it depends on the angle of the wind when it hits the building wall, and on the height and the density of the buildings around.

Table 16 - Local wind speeds at different pressure node heights compared to the wind speed from the meteorological station

WS_{met} (m/s) (z_{met} = 10 m)	**WS_{ref}(m/s) at bottom floor (z = 1.5 m)**	**WS_{ref}(m/s) at top floor (z = 26.5 m)**
1	0.24	1.32
3	0.72	3.97
5	1.20	6.61

In EnergyPlus, it is possible to use standards coefficients issued from AIVC tables, however these coefficients are only valid for square buildings. In the literature, a lot of measurements were made to measure the wind pressure coefficients of rectangular buildings. Two empirical formula could be calculated for rectangular buildings by Swami and Chandra, one for "low-rise buildings" and one for 'high-rise buildings". A building is considered high-rise if its height is superior to three times its length. As the building case-study has a height of 30 m and a length of 94 m, it is considered as a low-rise building. The empirical formula for low-rise buildings of the normalized surface pressure coefficient is given by Equation (45): (Swami & Chandra, 1988)

$$SC_{p,q} = 0.6.\ln\left[1.248 - 0.703.\sin\left(\frac{w\alpha}{2}\right) - 1.175.sin^2(w\alpha) + 0.131.sin^3(2.w\alpha.\mathrm{G}) + 0.769.\cos\left(\frac{w\alpha}{2}\right) + 0.07.G^2.sin^2\left(\frac{w\alpha}{2}\right) + 0.717.cos^2\left(\frac{w\alpha}{2}\right)\right] \quad (45)$$

With: $w\alpha$ the wind angle [°] and SR is the side ratio (Equation (46)), a coefficient considering the geometry of the building, q is the index of incident angle at 30° increments.

$$G = \ln(SR)$$
$$SR = \frac{width\ of\ the\ considered\ wall}{width\ of\ the\ adjacent\ wall} \quad (46)$$

Depending on the façade, the considered wall width is either 11.86 m (East and West walls), or 94 m (North and South walls). The number 0.6 is the SC_p value at zero incidence. For Energyplus to calculate the wind pressure coefficients, the following values need to be input:

- The building type: low-rise;
- The longest width to shortest width ratio: 0.126;
- The azimuth angle of long axis: It is the angle between the North (0°) and the longest width of the building, which gives the orientation of the building. For the building case-study it is 90°.

The wind pressure coefficients of the four façades of the building calculated by EnergyPlus using Equation (43) for the city of Roissy are displayed in Table 17.

Table 17 - Wind Pressure Coefficients SC_p for the building case-study in Roissy

Wind angle on the façade [°]	North	East	South	West
0	0.60	-0.28	-0.09	-0.28
30	0.49	0.20	-0.24	-0.41
60	0.10	0.45	-0.32	-0.04
90	-0.28	0.60	-0.28	-0.11
120	-0.32	0.46	0.10	-0.04
150	-0.24	0.20	0.49	-0.41
180	-0.09	-0.28	0.60	-0.28
210	-0.24	-0.41	0.49	0.20
240	-0.32	-0.04	0.10	0.45
270	-0.28	-0.11	-0.28	0.60
300	0.10	-0.04	-0.32	0.46
330	0.49	-0.41	-0.24	0.20

Windows modelling

The windows on each façade are discretized as six windows of 2 x 2.5 m (height x width). Windows are modelled as detailed opening (they are considered "close to vertical") through which airflow can be bi-directional, depending on stack effects and wind conditions. The equations used for the detailed opening linkage component were extracted from the COMIS Fundamentals manual 1990 (Allard et al., 1990). For each window, different coefficients need to be defined. The opening factor, which defined if the window is opened or closed. The discharge coefficient, that we set to 0.65.

Airflow Network

The Airflow Network for our apartment case-study is represented in Figure 55. We assumed that out of the six windows on each façade, it is always only possible to open three of them, such as if they were sliding doors. Each opened window is represented in yellow as an airflow component (three per façade). There are six exterior nodes (in red): Three on the North facade, facing each opening on the exterior windows of the glazed cavity, and three on the South facade, facing each opening on the exterior windows of the veranda. Inside each thermal zone, there is an interior node. Through each window there is the possibility for a bi-directional airflow. From each interior node, the sum of ingoing and outgoing airflows equals zero. EnergyPlus has the following assumptions are made: airflows are unaffected by the presence of shading devices, and the calculation of conductive heat transfer and solar gain through a window assumes that the window is always closed.

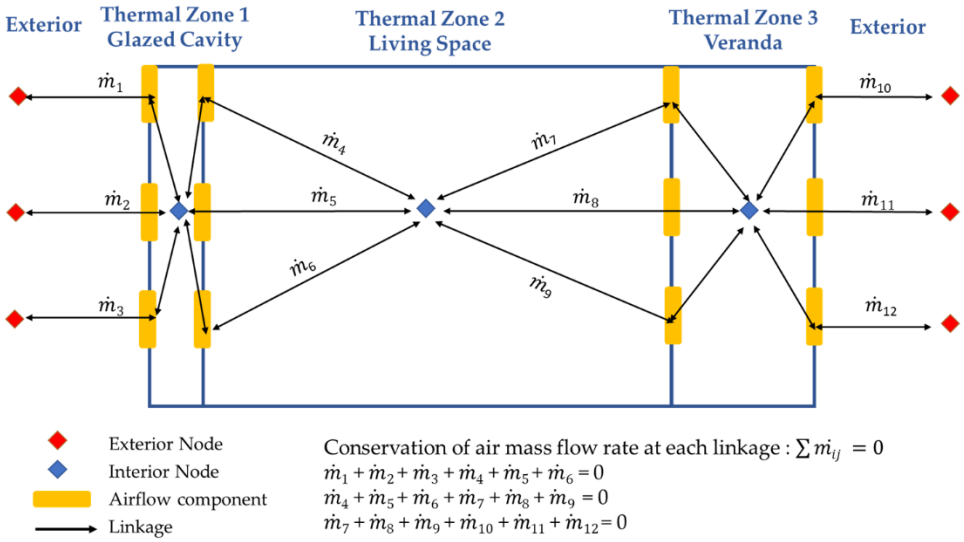

Figure 55 - Airflow network representation for the apartment case-study

Control for windows opening

In EnergyPlus, windows opening can be controlled by different conditions: a scheduled availability, an inside air temperature set-point, an exterior temperature set-point, an indoor comfort limit, a minimum difference between indoor and exterior air temperature, etc. We decided to control windows opening based on an interior temperature minimum set-point and on a schedule. Therefore, windows are opened if the three following conditions are met:

- $T_{air\_zone} > T_{air\_outdoor}$
- $T_{air\_zone} > T_{setpoint}$
- Schedule allows it (summer period)

Free cooling using mechanical ventilation

In EnergyPlus, there is not a simple system to model free-cooling via the use of mechanical ventilation. There exists a system, but it is an air-conditioning system that allows switching to free-cooling when there is a potential. We decided to use the simple ventilation algorithm in EnergyPlus (Engineering Reference, Chapter 7 Ventilation Design Flow Rate). We used the EnergyPlus Energy Management System (EMS) that allows to custom controls

(EnergyPlus, 2017) created a small EnergyPlus Runtime Language (ERL) routine to modulate the airflow.

Control for the free-cooling operation

Our programmed routine calculates X (Equation (47)), a number between 0 and 1, which is multiplied by the design airflow rate to calculate the airflow at each time step, depending on the interior air temperature (Equation (48)). It follows a linear rule; the airflow is reduced when T_{air_zone} gets closer to $T_{setpoint}$.

The law we created is the following (Figure 56):

$$\begin{gathered} if\ T_{air\_zone} < T_{setpoint}, X = 0 \\ if\ T_{air\_zone} > T_{setpoint} + \Delta FC, X = 1 \\ if\ T_{setpoint} + \Delta FC > T_{air\_zone} > T_{setpoint}, X = \frac{T_{air\_zone} - T_{setpoint}}{\Delta FC} \end{gathered} \quad (47)$$

$$Airflow = Airflow_{design}.X \quad (48)$$

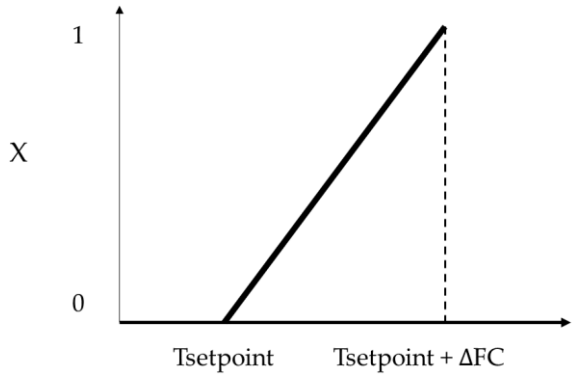

Figure 56 - Control of the airflow for the free-cooling system

For instance, with a ΔFC= 4 °C and $T_{setpoint}$ = 24 °C, when the air temperature inside the living space is equal to 29 °C, X = 1 and the airflow will be at full capacity, whereas if the air temperature inside the zone is of 25 °C, it will be divided by four.

Earth-to-air heat exchanger model

The EnergyPlus Auxiliary program CalcSoilSurfTemp (EnergyPlus, 2015) allows to calculate the yearly average soil temperature at the ground surface T_s, the yearly variation in amplitude of the temperature at the ground surface A_s, and the phase constant t_0. The user can choose between different soil conditions (heavy or light, damp or dry) and different ground surface conditions (covered or bare, wet or dry), and the program allocates values for the ground thermal diffusivity a_{ground}, the ground thermal conductivity λ_{ground}, the evaporation fraction at the soil surface f, and the soil absorption coefficient x. The soil surface temperature T_s is calculated with a heat balance of convective, latent, short-wave and longwave solar radiation heat exchanges at the soil surface. We select soil conditions as "heavy & damp" and ground surface as "moist & covered", assuming covered is for urban areas. The corresponding

coefficients are given in Table 18. Wet soil lead to higher ground temperatures than dry soil, however the heat transfer with the ground is increased which usually results in lower outlet air temperatures than dry soils.

Table 18 - Soil properties selected for all case-study cities

Heavy & damp		**Moist & covered**	
a_{ground} **(m²/days)**	λ_{ground}**(W/m.°K)**	***f* (-)**	**x** ***(-)***
0.055728	1.3	0.315	0.8

The calculated values output of the CalcSoilSurfTemp program for T_s, A_s and t_0 are given in Table 19. These were calculated using present and future typical years weather files reassembled following the methodology described in 2.3.1.

Table 19 - Calculated values for soil surface temperature T_s, amplitude of the temperature at the ground surface A_s, and phase constant t_0

	T_s		A_s		t_0	
	Present	*Future*	*Present*	*Future*	*Present*	*Future*
La Rochelle	13.3	14.6	13.1	9.3	6	1
Paris	11.5	13.2	7	7.9	8	7
Carpentras	15.1	16.5	9.5	15.1	32	51

The ground temperature at depth zg is calculated daily with Equation (49):

$$T_{zg,d} = T_s - A_s . e^{-zg.\sqrt{\frac{\pi}{365.a_{ground}}}} . \cos\left\{\frac{2\pi}{365}\left[d - t_0 - \frac{zg}{2}.\sqrt{\frac{365}{\pi . a_{ground}}}\right]\right\} \quad (49)$$

The heat transfer between the ground and the air inside the tube is given by Equation (50), which allows to determine the air temperature at any point y of the tube ($Ta(y)$), with U_t the heat transfer coefficient (including heat transfer by convection at the tube inlet and heat transfer by conduction towards the ground), Cp_{air} the air specific capacity, and $\dot{m}_{EAHX}$ the air flow rate inside the tube. The heat transfer depends on both the temperature difference between the air and the ground, and of the airflow rate.

$$U_t dy\left[T_a(y) - T_{zg,d}\right] = -\dot{m}_{EAHX} . Cp_{air}[dT_a(y)] \quad (50)$$

By solving Equation (50), we get Equation (51) to (55) (Lee & Strand, 2006):

$$U_t y = -\dot{m}_{EAHX} . C_a . ln\left|T_a(y) - T_{zg,d}\right| + C \quad (51)$$

The air temperature entering the earth tube is equal to the outdoor air temperature $T_{air\_outdoor}$ (Equation (52)):

$$T_a(0) = T_{air\_outdoor} \quad (52)$$

The constant C is determined by Equation (53) when y = 0

$$C = \dot{m}_{EAHX} . Cp_{air} . ln\left|T_a(y) - T_{zg,d}\right| \quad (53)$$

Finally, the calculation of $T_{air}(L)$ at the outlet of the earth-to-air heat exchanger with L the tube length in m is given by Equation (54) (Lee & Strand, 2006):

$$\begin{aligned} &If\ T_{air\_outdoor} > T_{zg,t}: \\ &T_{air}(L) = T_{zg,t} + e^{B} \\ &If\ T_{air\_outdoor} = T_{zg,t}: \\ &T_{air}(L) = T_{zg,t} \\ &If\ T_{air\_outdoor} < T_{zg,t}: \\ &T_{air}(L) = T_{zg,t} - e^{B} \end{aligned} \tag{54}$$

With B given by Equation (55):

$$B = \frac{\dot{m}_{EAHX}.Cp_{air}.ln\left|T_{air} - T_{zg,t}\right| - U_t.L}{\dot{m}_{EAHX}.Cp_{air}} \tag{55}$$

The EAHX model in EnergyPlus is a simplified model. The main limitations of the model are the following:

- The ground temperature calculation does not consider the heat exchange between the air in the EAHX and the ground. The ground temperature $T_{zg,d}$ is a simplified sine function which depends only on the depth zg and the day d, it is given by Equation (49).
- It is not possible to model parallel tubes, only one tube is modelled
- The fan energy consumption does not include pressure losses

Control for the earth-to-air heat exchanger operation

The earth-to-air heat exchanger is in operation if the following conditions are met:

- $T_{air\_zone} > T_{setpoint}$
- Schedule allows it (summer period)

2.5 Sensitivity analysis and optimization methods

In this section we present the sensitivity analysis methods and the optimization algorithm used to optimize the building designs. From Figure 28, these methods are used to iterate through the building design until finding the optimized solutions corresponding to the performance objectives. As the optimization is a time-consuming process, it is better to conduct it with a reduced set of design variables. For this purpose, the sensitivity analysis is used prior to the optimization to reduce the number of design variables to optimize. Indeed, the objective of the sensitivity analysis is to identify which design variables have the most impact on a given output. The sensitivity analysis is first conducted during the summer period only, to understand the building design variables that have an impact on the summer thermal discomfort during the future climate (performance objective adapting to climate change). The analysis is also conducted during the present climate to understand if the building responds similarly to outdoor climatic conditions in present and future climate. For this purpose, many building thermal simulations are conducted with the case study building to understand the magnitude of change in the output according to variation in design parameters. Once the most impactful design variables are determined, these are optimized using the optimization algorithm. The results of the sensitivity analysis will be presented in Chapter 4 and the ones of the optimization in Chapter 5. In this section, we describe the methods and tools used.

2.5.1 Sensitivity analysis methods

Sensitivity analysis (SA) methods allow to identify and rank the input parameters that have an impact on an output objective function. Many sensitivity analysis methods exist, and have been used for building thermal simulation applications for many years now, these have been reviewed by (Pang et al., 2020; Lavell et al., 2012; Iooss and Lemaître, 2015; Wei, 2013).

Prior to conducting a sensitivity analysis, it is necessary to define the following:

- The sensitivity analysis method used;
- The design variables included in the sensitivity analysis, and their variation range;
- The objective function.

The two methods we used, Morris (Morris, 1991) and Sobol (Sobol, 2001), are introduced here. The design variables investigated will be presented in the Chapters where the methods are applied.

Figure 57 illustrates the sequencing between the building thermal simulations and the sensitivity analysis algorithm. We used the Python library *SALib* to perform the sensitivity analysis developed by (Herman & Usher, 2018). First, the reference case-study building introduced in section 2.4.1 was created using Design Builder and EnergyPlus. Python is used with the *SALib* library to generate the design matrix (an example of the Morris design matrix is introduced in Table 20: each line of the design matrix corresponds to one building design (set of building design variables variating) and one building thermal simulation. Using the design matrix, the initial reference building model is modified and one input file is created per

line of the design matrix. Then all input files are simulated with EnergyPlus, to accelerate the process the simulations were run in parallel on different processors. The results of the EnergyPlus simulations (in output files format *.eso*) are post-processed to calculate the objective functions for the sensitivity analysis. One objective function is calculated for each building thermal simulation, this function has to be a scalar, so it can be a sum or max energy consumption, or a sum of hours or degree-hours of temperatures above a defined threshold for instance. Finally, the sensitivity analysis is conducted from Python, using the objective functions to calculate the SA indicators. The process is similar for any SA method implemented in *SALib*.

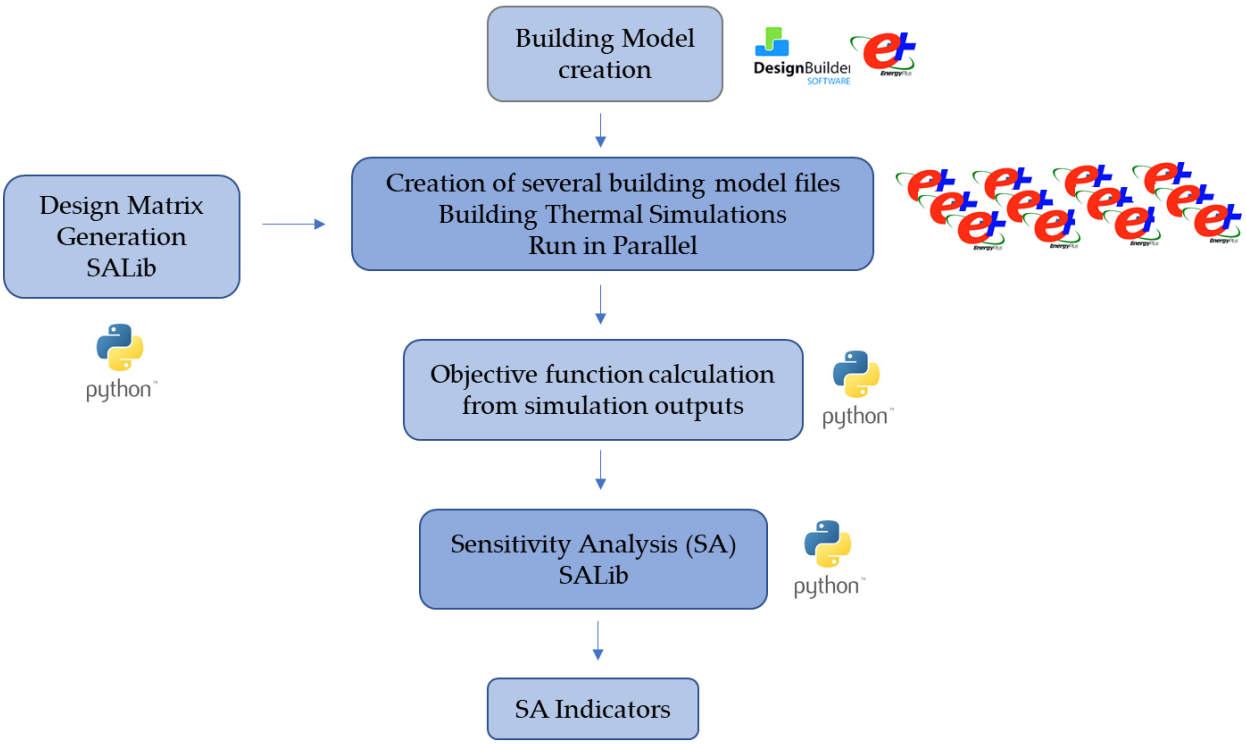

Figure 57 - Sequencing between Building Thermal Simulations and Sensitivity Analysis

2.5.1.1 Morris method

The Morris method is the most engineering-used screening method based on the "one factor at a time" (OAT) design (Morris, 1991; Saltelli et al., 2004). The Morris method allows to quickly identify the input parameters *j* that have an impact on an output variable *OF* that is the objective function. The Morris method follows the Morris design matrix that is illustrated in Table 20.

The variation range of the input variables *j* is discretized in a number of levels *p*. In the design matrix, one parameter is changed at a time, first, parameter *j*2 is changed, then it is parameter *j*0, and so on. The order in which parameters change is aleatory, and the value they take (here A, B) is aleatory selected according to the number of levels within their variation range. For instance, for a number of levels p, and in between the two extreme values 0 and 1, for $p = 4$ the parameter can take values 0, 0.5, 0.75 and 1. The disadvantage of this method is that it does not allow to fully cover the factorial sampling, and might emphasize the extremes as it takes values on the edge of the design matrix.

Table 20 is an example of a design matrix for one trajectory tr. This process is repeated for the number of trajectories; a sufficient number of trajectories is needed to fully explore the space. It requires tr (j +1) simulations. The Morris method is usually used for a large number of input parameters j, and authors often use it to reduce the number of input parameters prior to conducting more computationally expensive SA.

Table 20 – Morris design matrix and elementary effect

Input variable j_0, j_1, j_2, j_3, j_4					**Change in input**	**Output**	**Change in output**	**Elementary Effect**
j_{0_A}	j_{1_A}	j_{2_A}	j_{3_A}	j_{4_A}	Random initialization	OF_0		
j_{0_A}	j_{1_A}	j_{2_B}	j_{3_A}	j_{4_A}	Δj_2	OF_1	$OF_1 - OF_0$	EE_{j2}
j_{0_B}	j_{1_A}	j_{2_B}	j_{3_A}	j_{4_A}	Δj_0	OF_2	$OF_2 - OF_1$	EE_{j0}
j_{0_B}	j_{1_A}	j_{2_B}	j_{3_A}	j_{4_B}	Δj_4	OF_3	$OF_3 - OF_2$	EE_{j4}
j_{0_B}	j_{1_A}	j_{2_B}	j_{3_B}	j_{4_B}	Δj_3	OF_4	$OF_4 - OF_3$	EE_{j3}
j_{0_B}	j_{1_B}	j_{2_B}	j_{3_B}	j_{4_B}	Δj_1	OF_5	$OF_5 - OF_4$	EE_{j1}

The Morris method allows to quickly calculate, for each input parameter j and in between two simulations, the elementary effects EE (Equation (56)). Δ_j is the change in input j, and corresponds to ΔF, the change in output OF. The absolute mean μ* (Equation (57)) and the variance σ (Equation (58)) of the elementary effects are then calculated for each input parameter j, and for each trajectory tri, they are the sensitivity indexes used to rank the design variables.

$$EE_j^i = \frac{\Delta OF}{\Delta_j} \tag{56}$$

$$\mu_j^* = \frac{1}{tr} \cdot \sum_{tri=1}^{tr} \left| EE_j^i \right| \tag{57}$$

$$\sigma_j = \sqrt{\frac{1}{tr-1} \cdot \sum_{tri=1}^{tr} (EE_j^i - \mu_j^*)^2} \tag{58}$$

The method allows to classify the input parameters in three categories:

- Design variables that have a small impact on the objective function (small $\mu^*$and small σ);
- Design variables that an impact on the objective function and with linear effects (high μ^* and small σ);
- Design variables that an impact on objective function and with non-linear effects *or* interactions with other parameters (high μ^* and high σ). The method does not allow to distinguish between these two.

2.5.1.2 Sobol method

Sobol is a sensitivity analysis global method, based on the variance decomposition. It is usually used for a problem for which the design variables behave non-linearly or non-monotonously, or if their behavior is not known. We used this method because the results provided by Morris resulted in variables with high μ^* and high σ. With the variance decomposition, it is possible to quantify more precisely the influence of the different design variables on the model output. For this purpose, it requires a large number of simulations and is therefore much more computationally expensive than the Morris method, especially for the calculation of higher-order effects. The Sobol sensitivity indexes represent the variance of one design variable or of the interactions of several design variables.

The total variance of a model can be decomposed as a sum of all the variances from the different input variables and the variance of their interactions, it is the ANOVA decomposition of total model variance (Equation (59)). V_i relates to the variance of the variable i (Equation (60), V_{ij} denotes the variance of the interaction between variable i and variable j (Equation (61), while $V_{12\dots k}$ is the variance of interaction between all input variables. By diving Equation (59) by the total variance, we get Equation (62) which is the sum of all Sobol indexes, equal to 1. It is the sum of first order indexes S_i, second order indexes S_{ij} and higher order effects.

$$V(Y) = \sum_i V_i + \sum_i \sum_{j>i} V_{ij} + \cdots + V_{12\dots k} = 1 \tag{59}$$

$$V_i = V\big(E(Y|X_i)\big) \tag{60}$$

$$V_{ij} = V\left(E\big(Y|X_i, X_j\big)\right) - V_i - V_j \tag{61}$$

$$\sum_i S_i + \sum_i \sum_{j>i} S_{ij} + \cdots + S_{12\dots k} = 1 \tag{62}$$

For each input variable, each first order effect S_i is calculated following Equation (63). It represents the influence of the input parameter i only on the model output. Each S_i is the variance of that input parameter divided by the total variance, it is thus the partial variance normalized between 0 and 1. The expected value of Y ($E_{X_{\sim \mathrm{i}}}(Y\,|X_i)$ is calculated over all possible values of $X_{\sim \mathrm{i}}$, the matrix of all input parameters but i, while the value of i is fixed. This means that S_i is calculated using a sample matrix where the values of X_i are unchanged and all variables are varied within their range. The outer variance V_{X_i} is calculated over all possible values of X_i. If the sum of the first orders S_i only is equal or close to 1, it means that there are no interactions, that the model is linear or additive. If the sum of first orders is inferior to one, it means higher order effects are present in the model (right term of Equation (63).

$$S_i = \frac{V_i}{V(Y)} = \frac{V_{X_i}(E_{X_{\sim \mathrm{i}}}(Y\,|X_i))}{V(Y)} = 1 - \frac{E_{X_{\sim i}}(V_{X_{\mathrm{i}}}(Y\,|X_i))}{V(Y)} \tag{63}$$

The other popular Sobol indexes are the total orders S_{Ti} (Equation (64)). They are a measure of all (first and higher order) effects involving each input parameter X_i. Each total order S_{Ti} is calculated by analyzing the expected value of the variance when all input parameters are fixed except X_i that varies within its variation range. If interactions exist between input parameters, the sum of total orders will be superior to 1, as higher-order interaction effects are accounted for within all total orders, so several times. If the sum of total orders is close to 1, this means that few interactions occur and that the model is linear or additive.

$$S_{Ti} = \frac{E_{X_{\sim i}}(V_{X_i}(Y|X_{\sim i}))}{V(Y)} = 1 - \frac{V_{X_{\sim i}}(E_{X_i}(Y|X_{\sim i}))}{V(Y)} = S_i + S_{ij} + \cdots + S_{ij\ldots k} \quad (64)$$

Finally, second order Sobol indexes S_{ij} can be calculated (Equation (65)). They represent the variance in the model output caused by the interaction of the parameter pair (X_i, X_j). To calculate S_{ij}, input parameters X_i and X_j are kept constant while other variables are changed.

$$S_{ij} = \frac{V_{X_{ij}}\left(E_{X_{\sim ij}}(Y|X_i,X_j)\right)}{V(Y)} - S_i - S_j \quad (65)$$

The indexes S_i, S_{Ti} and S_{ij} are calculated, such as for Morris indexes, by the Python library *SALib*.

Other variances-based methods exist and have been used for building thermal simulations, part of the *SALib* library, they are FAST and RDB-FAST. These methods have lower computational cost than Sobol, but they allow to calculate only first and total orders.

2.5.2 **Optimization algorithm: NSGA-II**

Optimization algorithms have been used for several decades now to assist decision-making during the design stage of a building. The aim of the optimization is to propose design solutions with optimized design variables to answer a specific problem, defined with objective functions that are often opposed. Building optimization has been ongoing for the past two decades, however optimizing buildings to future climate is an on-going area of research and much recent work is currently under development on this topic. Authors explore a variety of objectives: reducing energy loads or consumption, minimizing lighting consumption, maximizing daylighting, reducing summer thermal discomfort, reducing building construction or energy system costs, reducing the carbon emissions, or most related to climate change, reducing future climate uncertainty (Moazami et al. 2019; Forde et al. 2020; Lapisa 2018; Kim and Clayton 2020; Nguyen et al. 2021; Bamdad et al. 2021). In the context of this Ph.D., the optimization problem has two opposite objectives: to minimize the heating needs and to minimize the indoor summer overheating, in the context of climate change. As the problem is multi-objective, it will provide a set of optimal solutions and abstain from giving a single solution. During the building design stage, many criteria need to be accounted for (for instance costs, environmental impact, visual and acoustic comfort, etc). If these other criteria are not objectives of the optimization problem, they can be used to narrow-down the best solutions to answer the given problem while post-processing the optimized solutions.

We used one of the most used multicriteria genetic algorithms for building design, the NSGA-II algorithm (Deb et al., 2002). It is an evolutionary algorithm, based on the Darwin evolution theory. The steps are represented in Figure 58. Each individual building is represented such as a chromosome with a set of genes which are the design variables. A population of individuals (each individual represents a building design) is randomly initialized, with random genes within their variation range. Some individuals of the initial population are selected (through the tournament phase) to reproduce and have children, based on a probability of crossovers and mutations. Then the best children are selected, amongst with the best parents, to be part of the next generation. The process is repeated times the number of generations. The selection is made according to each individual performance (in terms of objective functions, minimizing heating needs and summer indoor overheating). Along several generations of populations, the best individuals remain (based on natural evolution), these are the ones present on the Pareto front.

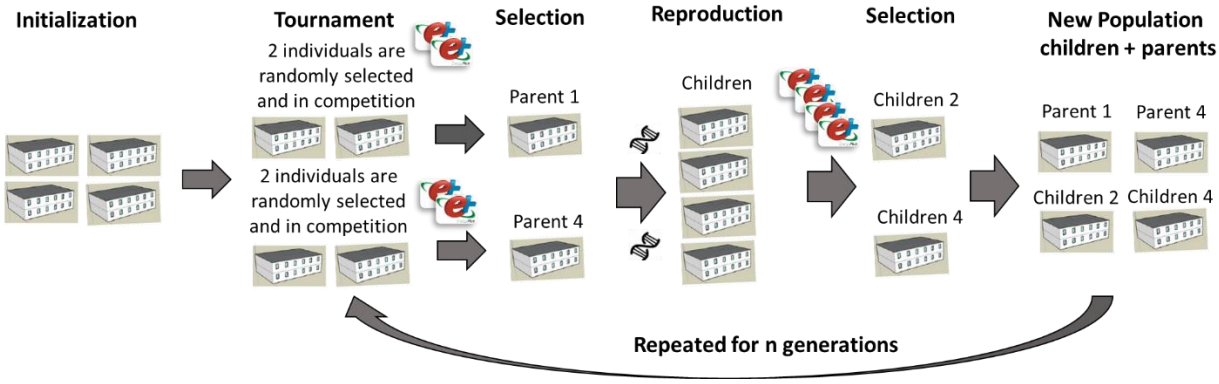

Figure 58 - Steps of the evolutionary algorithm

Four parameters to configure the algorithm need to be defined, they are: the number of generations, the number of individuals within the population, the crossover and mutation coefficients. In Figure 59, the reproduction is illustrated more in detail. The probability that two parents will produce children is based on the crossover probability, which is usually high. In the example, genes are aleatory mixed between parent 1 and parent 2 to create children 1, and then children 2 reflects children 1. After the children are produced, and before they are evaluated, it is possible that their genes mutate. This means that one randomly selected gene takes a random value within its possible variation range, it contributes to diversify the population. This probability is based on the mutation coefficient input by the user.

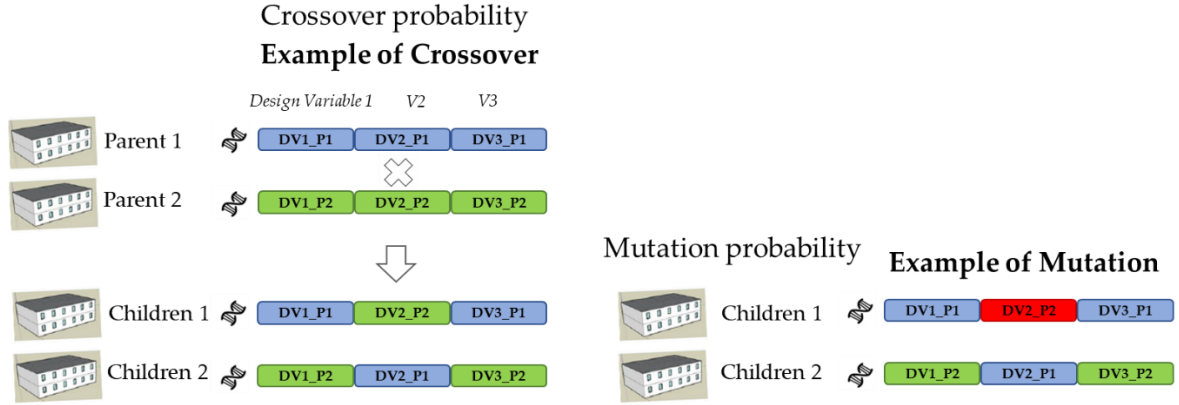

Figure 59 - Illustration of crossover and mutations during the reproduction

The algorithm NSGA-II selection process is made through two consecutive steps:

- Non-dominated sorting;
- Crowding distance sorting.

The comparison between two individuals is made with the concept of domination. Individual A (coordinates x_1, y_1) dominates individual B (coordinates x_2,y_2) based on Equation (66) with one objective function on the x axis and the other on the y axis (Figure 60).

$$A\ dominates\ B\ when: (x_1 \leq x_2\ and\ y_1 \leq y_2)\ and\ (x_1 < x_2\ or\ y_1 < y_2) \quad (66)$$

By comparing all individuals to each other individual within the population based on Equation (66), the Pareto front can be created. As the Pareto front size might exceeds the population size that remains constant, the solutions on the Pareto front are compared using the crowing distance sorting. It consists to select the solutions with the highest crowding distance, i.e the ones which have the largest centroid surface area delimitating it from the solutions around them, this is illustrated in Figure 60. The success of the NSGA-II is mainly due to the crowding distance sorting which ensures diversity amongst the non-dominated solutions. In between each generation the Pareto front is updated, and towards the end the solutions are only becoming slightly better because they have converged. The last Pareto front contains the final non-dominated solutions, which are the optimized solutions.

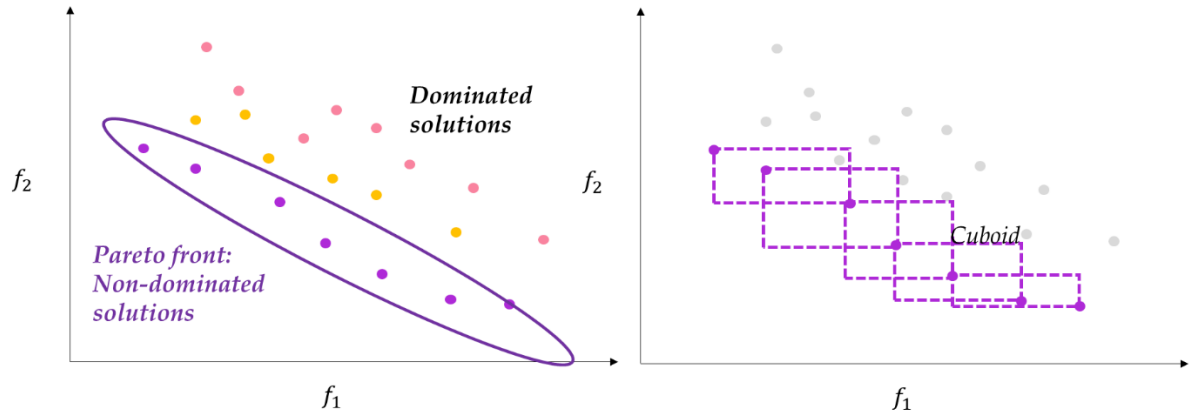

Figure 60 – Illustration of the selection process – left non-dominated sorting, right – crowding distance

2.6 Conclusive remarks on the methodological contribution

In this chapter we described the research methodology used in this Ph.D. The methodology proposed here aims to be used as a contribution during the design stage of the building to ensure that goals of mitigation and adaptation to climate change are respected. Indeed, some passive strategies must be integrated early in the building design (i.e envelope, morphology, windows size and orientation, etc). One of the goals is also to propose a methodology that can be used by building practitioners to assess the potential health-heat-related risk in buildings in the mid-century in France.

For this purpose, we proposed a method to develop new future weather files including heatwaves for building thermal simulations, which has never been done before. Having access to multiyear climate data allowed us to detect heatwaves, which are not included in the "typical years" commonly used for building thermal simulations. This task was tedious, compiling a large amount of data from regional climate models into easy and practical weather files to use. Furthermore, the bias-adjustment of the climate data was also a time-consuming and strenuous task, but it consolidates the climate data and is not commonly done especially not incorporated into weather files ready to use for building simulations. It allows assessment of future building indoor conditions in absolute values. We also reassembled present and typical years for comparison. Reassembling the future heatwaves weather files is based on two methods to detect heatwaves in the multiyear datasets. The first one was created by climatologists, based on outdoor temperature extremes, which allow to detect temperature anomalies over a multiyear dataset. The second method was developed by epidemiologists, based on morbidity thresholds correlated to exterior daytime and nighttime temperatures, to specify the heatwaves with a potential health-heat-related risk. Finally, the urban heat island effect was included for the city of Paris, because climate models do not model the urban canopy.

This work aims to bridge the gap between the climate and building communities and transfer the knowledge and models built by the climate community to be used as input for building simulations. Using many climate models allows to quantify climate uncertainties, whereas other methods/tools commonly used such as the CCWWeatherGen or Meteonorm do not consider or hide these climate uncertainties. Since climate models lead to higher uncertainty than the socio-economic RCP scenario in the mid-century, we compiled weather files from four different climate models. A total holistic assessment would include as many as possible climate models and several RCP scenarios, however the purpose in this Ph.D. is to test the proposed methodology. Having access to future heatwaves as input for building simulations provides a strong potential to analyze the building response to indoor overheating under a variety of different types of exterior climate exposure. This methodology was published in (Machard et al., 2020a). The Python code for downloading the CORDEX data and assembling future weather files as typical years or heatwave files is open-source, and intends to give the tools to the building simulations community to analyze the adaptation and resilience of buildings to future climate, which is more than necessary and becoming urgent

considering the climate projections. The analysis of the different weather files reassembled is presented in the next Chapter 3.

In this chapter the building case study and related modelling assumptions were presented, we will use this building to test the proposed methodology. It has an advantageous bioclimatic design that benefits both winter and summer. We presented the different passive cooling strategies and systems that will be tried out to improve the building design resilience to heat, with their modelling assumptions and limitations. We also outlined the mathematical methods (sensitivity analysis and optimization algorithm) that we will use to propose building design guidelines under future climate. The sensitivity analysis will allow to determine which design variables are the most impactful on indoor overheating during future summer periods, while the optimization algorithm will allow to propose a balanced building design between the winter and summer periods.

Chapter 3
Selection of climate sequences

In this chapter, we analyze the climate data and associated weather files assembled from the previous section. We first analyze the multi-years temperatures distribution, to understand the evolution between present and future (mid-century) climate. Then, we present an overview of the variation of each weather variable between the present and future typical years. We also investigate the increase in nighttime temperatures when the urban heat island is included into the weather files. During this analysis we include the uncertainty related to the climate models since we investigate the climate variations for the four climate models used in this Ph.D. We then analyze the heatwaves evolution between present and future periods for each climate model, in the three cities investigated. We quantify the occurrence of a heath-heat-related risk heatwave such as the 2003 heatwave in the future. Finally, we justify our choice of which heatwave, and which typical year to use to conduct the building thermal simulations in the next two chapters.

This chapter aims to answer the following research questions:

What is the evolution of each of the weather variables, and the climate "potentials" per city related to each cooling passive system?

How to assess future climate uncertainties and how to consider the risk related to this uncertainty in the building design process?

How frequent a heatwave such as in 2003 might occur in the future?

Which future heatwave(s) should we use to analyze the indoor heat stress and the building resilience to overheating and its ability to protect the occupants ?

Summary

3.1 Future climate data analysis

In this section, we present the contemporary and future climate data assembled in section 2.3. All climate data presented in this section are bias-adjusted. We first present the data for the multi-year datasets, as it is not common to have access to such large datasets of data. Then, we will present the climate data of the typical years for the different weather variables, and finally, the temperatures during the defined heatwave periods.

3.1.1 Summer temperatures multi-years distribution

Figure 61 showcases violin plots of hourly summer (June, July, August and September) dry-bulb temperatures over the contemporary (1990-2019, the 2010s in green) and future mid-century (2040-2069, the 2050s) periods for the three case-study cities La Rochelle, Roissy and Carpentras. All future climate data used in this Ph.D. are from the socio-economic scenario RCP 8.5. Roissy refers to the data without the inclusion of urban effects whereas Paris includes the urban heat island effect.

We can observe that the temperature distribution is much more spread out in Carpentras (due to the high daily maxima and the large diurnal temperature range), then in Roissy, then in La Rochelle (due to its oceanic climate). In the future, temperatures up to 50 °C are expected in Carpentras, and up to 45 °C in La Rochelle and Roissy, however these are outliers and represent a minimal part of the distribution (i.e rare heatwaves). The large dotted lines represent the median, while the small dotted lines represent the interquartile range. We can observe a temperature increase of between + 1.5 and + 4°C depending on the model and on the city in both median, and 75 % of the maxima and minima temperatures distribution.

In Figure 62, we observe the end of the tail of the temperature distribution over the present and future 30 years periods. These are particularly important for the sizing of active cooling systems. For instance, following the European norm EN 15927-2, indications for sizing cooling systems are to define a degree-day selected from the 95 % or 98 % or 99 % of the temperature distribution over the 30 years hourly temperatures (ISO, 2009). The ASHRAE has different indications and provides degree-days that are regularly updated on[2] calculated either as the norm EN 15927-2 over the 30 years hourly temperatures but at the 98 %, 99 % or 99.6 % percentile, or over the 30 years hourly temperatures during the warmest month of the years, at the 90 %, 95 % or 98 % percentile (Thevenart & Humphries, 2005). Coinciding dew-point or wet-bulb temperatures can also be included in the selection depending on the active system used. Figure 62 gives an indication of the increase of temperature for these potential future degree-days for the four climate models in the three case-study cities. We can observe in Roissy an increase of between + 1 °C and + 3 °C depending on the climate model at 95 % of the temperature distribution. In La Rochelle, the increase is between + 1.5 °C and + 3 °C while in Carpentras it is between + 1.5 °C and + 3.5 °C. In all three cities, the temperature increase is higher as we observe higher percentiles of the distribution, with an increase up to + 4°C in each city at the 99 % percentile for the climate model IPSL (the warmest of all models at the end of the distribution tail except for the maxima).

[2] http://ashrae-meteo.info

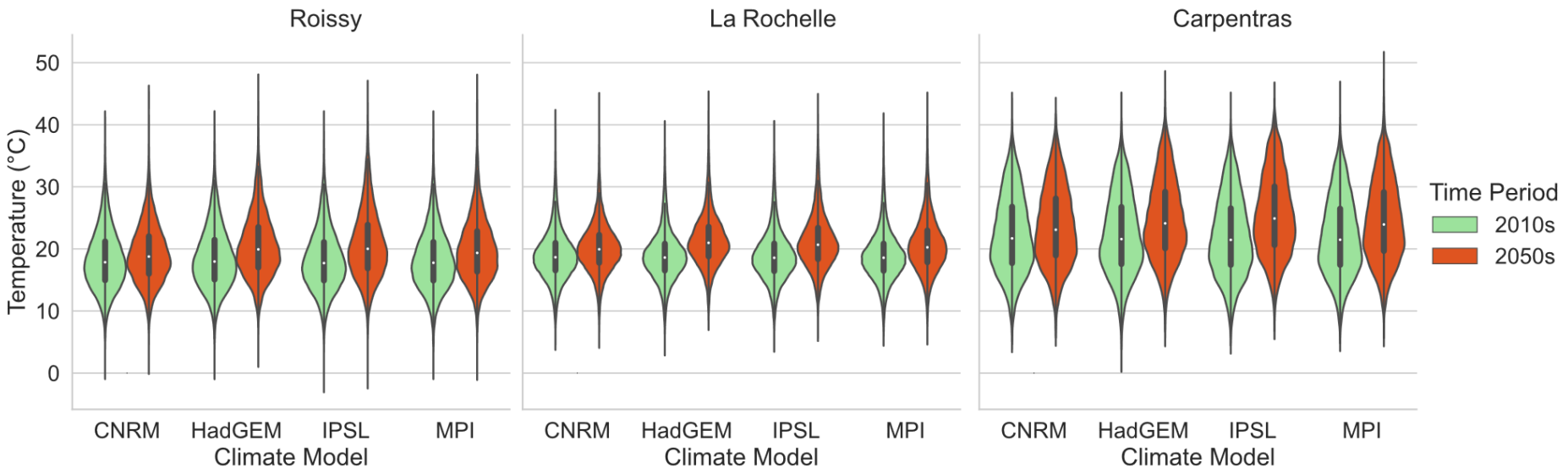

Figure 61 - Hourly summer (June to September) temperatures over 30 years for the present & future periods

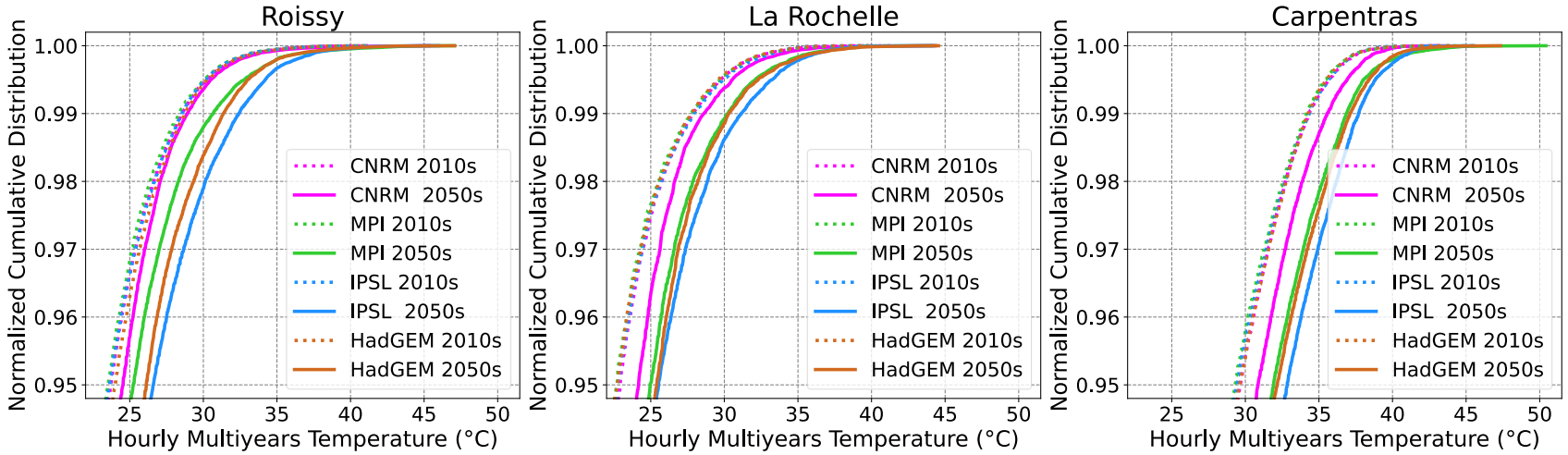

Figure 62 - End of the temperature distribution tail for the four climate models in each case-study city, present and future. The Figures are normed from 0 to 1

3.1.2 **Typical years**

Dry-bulb Temperature

Figure 63 shows the normed cumulative distribution of summer (from the 1st of June until the 30th of September) temperatures during the present and typical years in Roissy, La Rochelle and Carpentras for the four climate models. The temperature uncertainty related to the four climate models is in shaded green during the present period and in shaded red during the future period. We observe that the temperature range between the four climate models varies between 1 and 2 °C. in Roissy. We observe the largest increase for the climate model IPSL in Roissy and in Carpentras, as is has the lowest temperatures during the present period and the highest temperatures during most of the future period, while the order of the other three climate models is more consistent. This could already be observed from Figure 35, that the IPSL compared to the other models has a higher increase in median and overall distribution between the present and future mid-century period following the RCP 8.5. However, as the typical years were assembled weighing equally the dry-bulb temperature, humidity, and solar radiation, these other weather variables had a significant role as well in the typical months' selection. At 0.9 of the normed cumulative frequency, or during 10 % of the warmest summer hours, the temperature in Roissy in the present is between 23.5 °C and 25.8 °C while in the future it will be between 25.3 °C and 28.3 °C, so an increase of around +2 °C to +3 °C in 50 years during the "typical" summer. At 0.5 of the normed cumulative frequency, the increase in Roissy is about + 1.6 °C to + 2.3 °C depending on the climate model. In La Rochelle, the future temperatures are around + 2°C to + 3 °C. In Carpentras the increase is even higher depending on the model, up to + 4 °C.

For the four typical years of the climate Roissy, we used the model UWG to reassemble future typical weather files including UHI effects, that we named "Paris". Figure 64 shows a heatmap of the increase in temperatures in Roissy between the RCM future typical year of Roissy (T_{ref} in Figure 64 from model IPSL, presented in Figure 63) and the outputs of the UWG model which includes UHI effects, similar to the climate of Paris (T_{urb} in Figure 64). When there is a warming effect, it is shaded in red on the plot while when a cooling effect occurs it is shaded in blue. The warming effect is up to 8 °C in early September, but peaks of 5 °C occur often during the spring, summer and autumn seasons. We can notice on the heatmap that the difference is always positive during the evening and night (between 7 pm and 7 am), with some cooling effect during some days. The UHI effects modelled with UWG are similar for the four climate models.

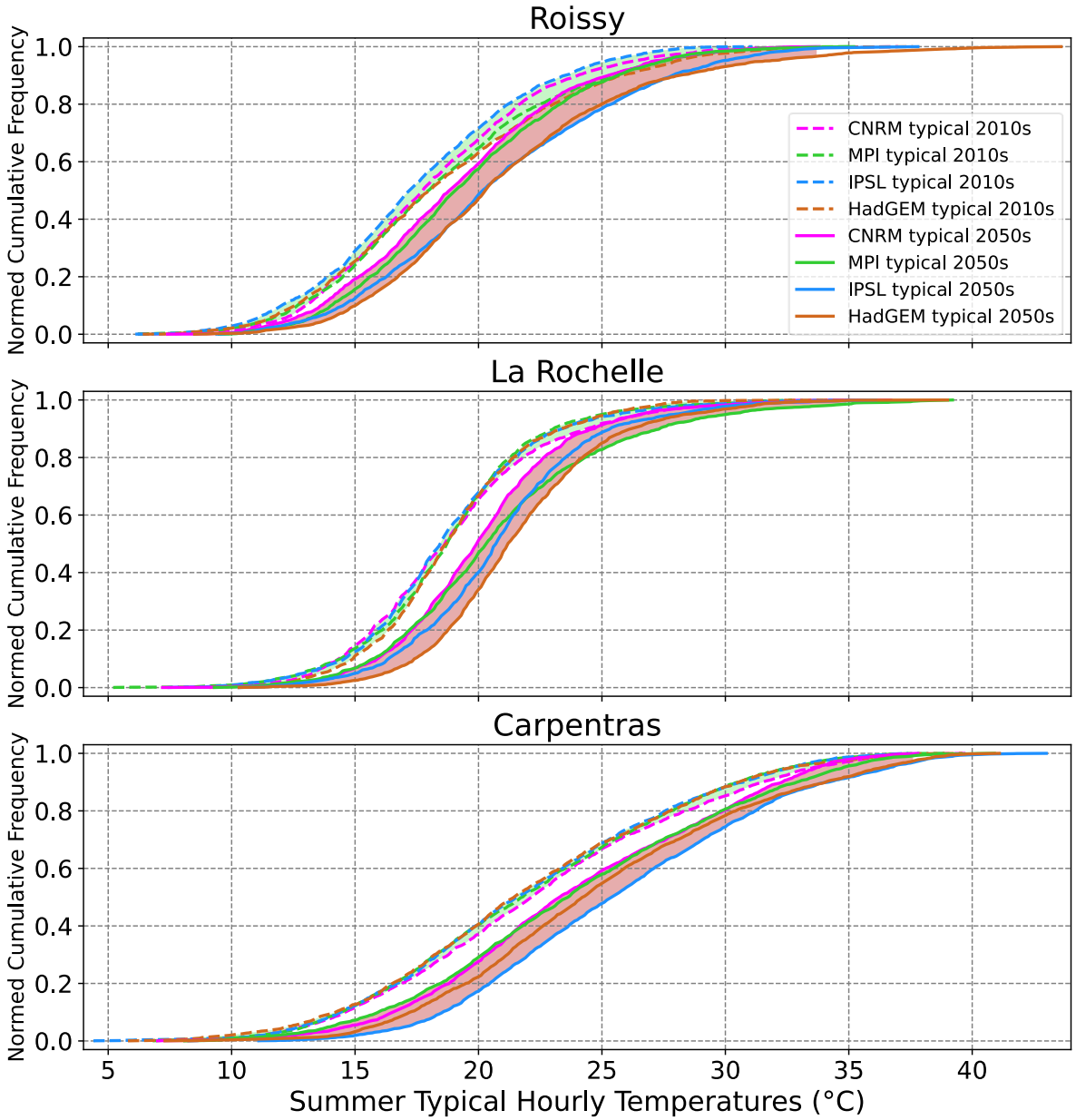

Figure 63 –Normed cumulative distribution of typical summer temperatures in Roissy, La Rochelle and Carpentras

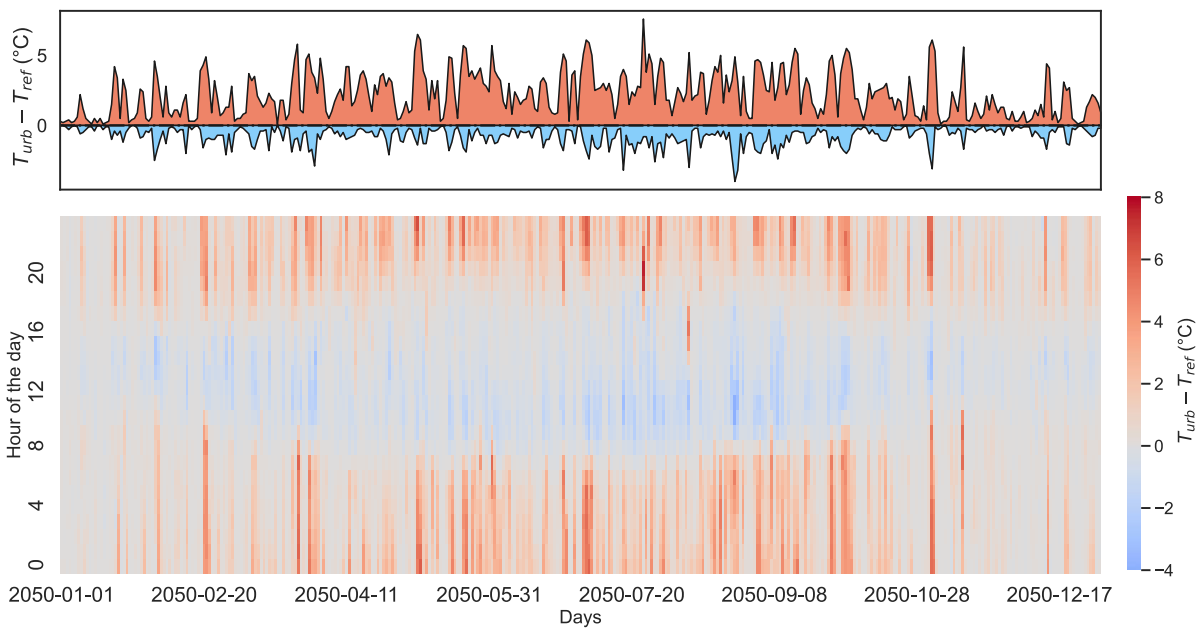

Figure 64 - Heatmap of the increase in temperature between urban (Paris modelled with UWG) and rural (Roissy) climate

In order to illustrate, the potential associated risk to warm night temperatures, Figure 65 represents the calculated daily IBM_{min} during present and future typical summers for the model ISPL. During the present climate in Roissy, the IBM_{min} never reaches 18 °C, which is the *Sn* threshold.

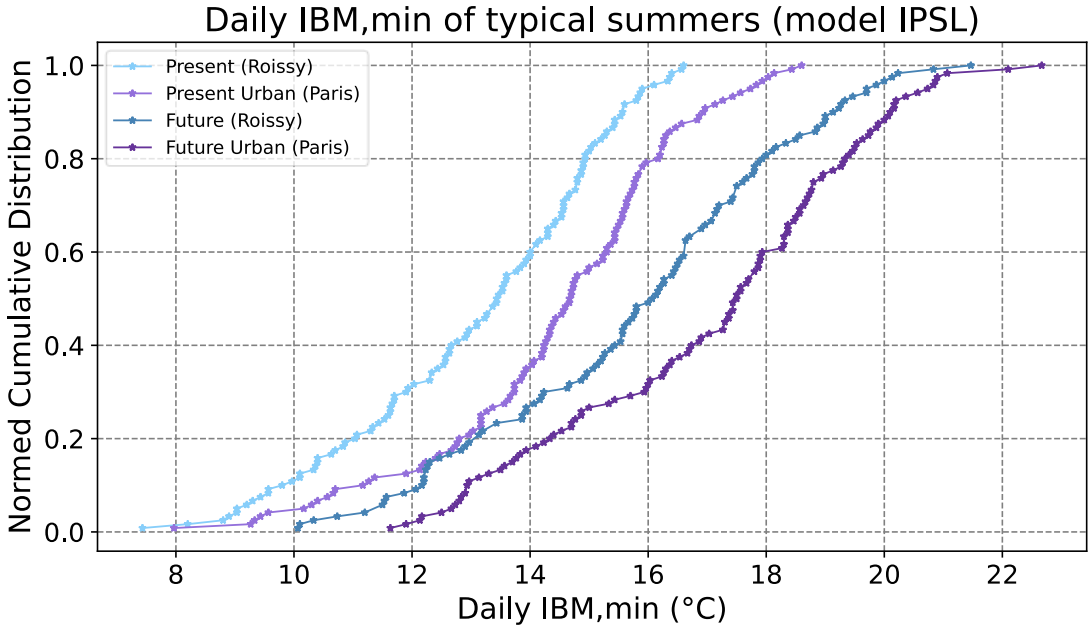

Figure 65 - Daily IBM_{min} of typical summers (model IPSL) in Roissy and Paris, Present & Future

In the future in Roissy, the IBM_{min} reach 18 °C during 20 % of the night summers. This does not necessarily mean that there will be a heatwave, as according to the definition given in section 2.3.1.6, both IBM_{min} & IBM_{max} need to be above the thresholds for three consecutive days minimum. However, Figure 65 is an illustration of this potential risk. In Paris, which here is modelled using UWG using the climate data in Roissy as input, the night thresholds are higher, about 21 °C, to account for the urban heat island effect. The threshold is never reached

in the present and is reached only for three data points in the future. When comparing the present file without UHI effects (light blue curve) and the future file including UHI effects (dark purple curve), the difference in night IBMs is of 4 °C for 50 % of the nights and up to + 6 °C, which showcases the importance to include both effects. Figure 65 is made with the third warmest model out of the four climate models in night temperatures in Roissy, so the uncertainty related to both the climate model and the socio-economic scenario must be fully assessed for a more detailed study. According to Figure 35, IPSL represents the sixth out of eleven climate models' warmest monthly summer temperatures in absolute values, so it is almost "average". During future heatwaves periods, incorporating the urban heat island effect into weather files will result in even higher temperatures. This work was conducted in (Machard, et al., 2020b) but it is not in the scope of this Ph.D.

Figure 66 shows the monthly average maximum, mean and minimum dry-bulb temperatures in the four case-study cities for the entire year. The dotted lines represent the lowest temperature (lowest temperature each month between the four climate models) for both the present and future periods while the full lines represent the highest temperature of all climate models each month. It is clear that for each city, there is an increase in both maxima and minima. In Carpentras, the increase is even more pronounced. Regarding passive cooling system potentials, an increase in mean outdoor air temperatures leads to a decrease in potential for EAHX systems, while an increase in minimum temperatures leads to a decrease in potential for nocturnal natural ventilation.

Dry-bulb Temperature - Mean Daily Range (Potential for Natural Ventilation)

In Figure 67 are shown the monthly mean daily temperature range, i.e potential for night ventilation. As we observed from Figure 66, there is an increase in both maxima and minima, and therefore the effect on the daily range is questionable. In Roissy, even if temperatures are higher, the daily range will be higher in future summer months, which is good for natural ventilation potential. However, from Figure 66, mean maxima go from 22-24 °C to 24-26 °C, so the potential might be limited. In Paris, the increase in mean daily range temperature is less pronounced than in Roissy since night temperatures are warmer. In La Rochelle no significant change can be witnessed, however the potential is lower than in Roissy since the average daily temperature range is around 8 °C in summer. In Carpentras, we observe a slight decrease in the mean daily range temperature in early summer which might be due to an increase even more pronounced in daytime temperatures than nighttime temperatures.

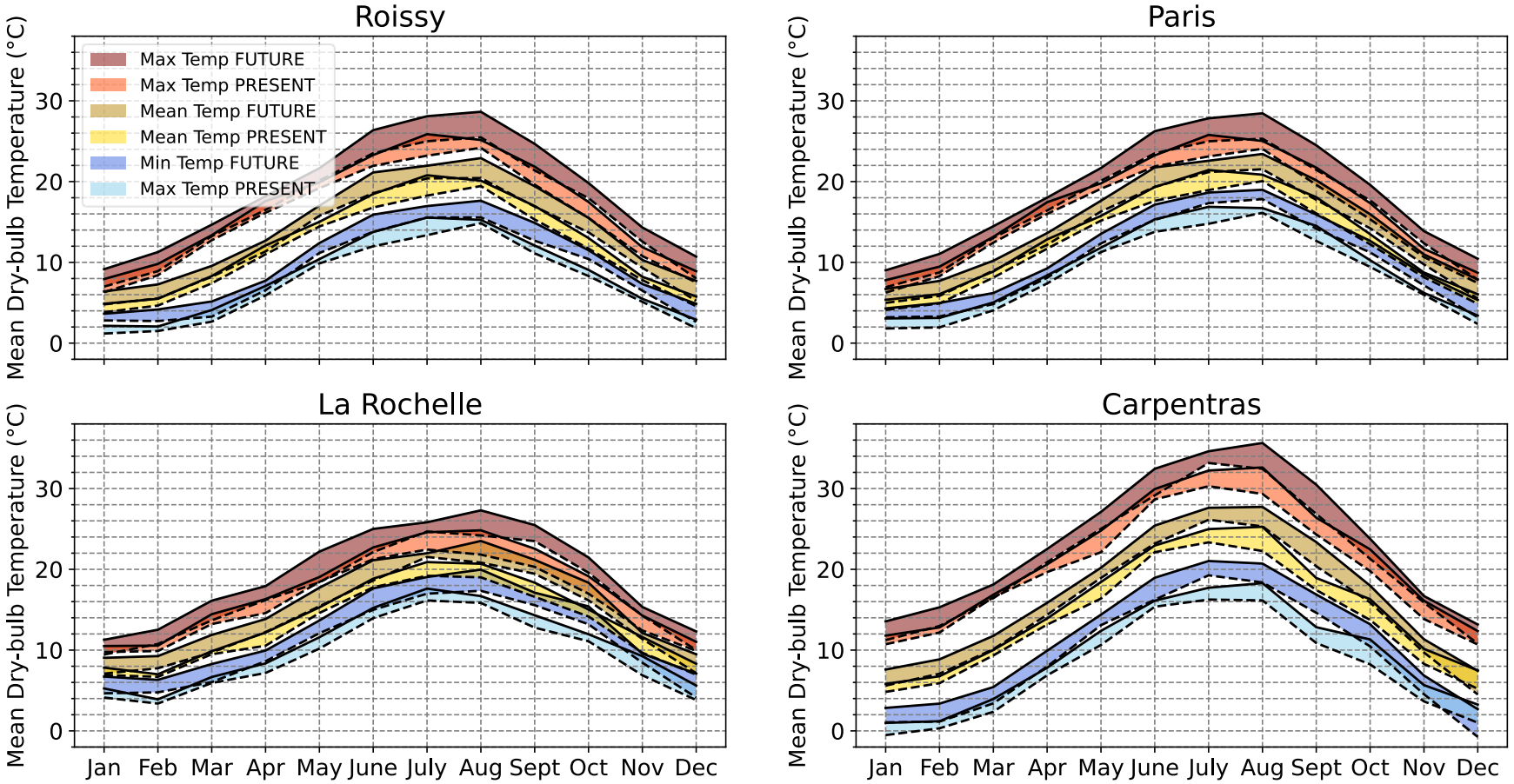

Figure 66 - Monthly max (in red), mean (in yellow) & min (in blue) dry-bulb temperatures in Roissy, Paris, La Rochelle and Carpentras for the 4 climate models - Present & Future. Dotted lines represent the lower monthly temperature of the four models while full lines represent the maximal monthly temperature of the four models

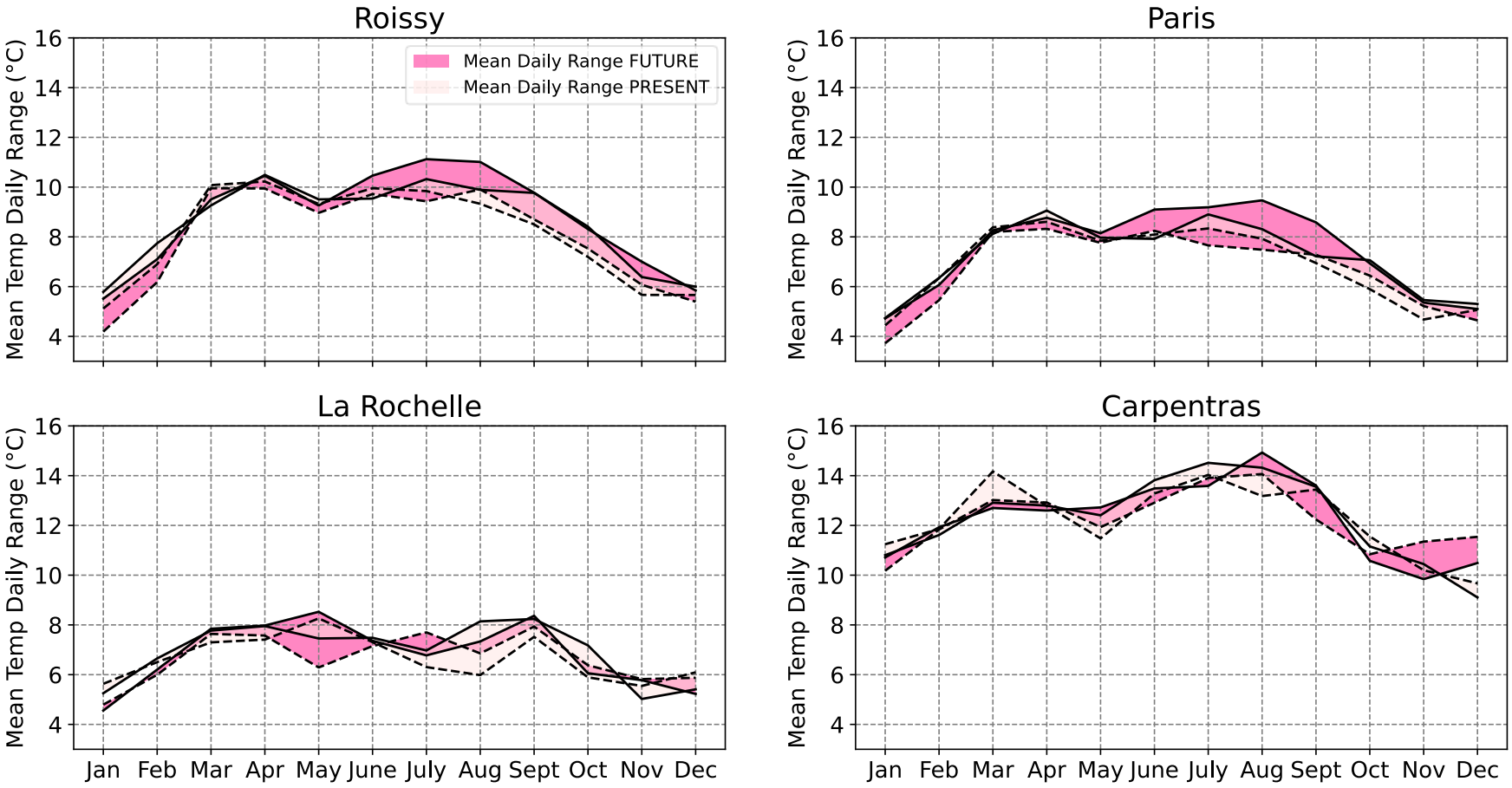

Figure 67 - Monthly mean daily range dry-bulb temperatures in Roissy, Paris, La Rochelle and Carpentras for the 4 climate models - Present & Future. Dotted lines represent the lower monthly temperature of the four models while full lines represent the maximal monthly temperature of the four models

Global Solar Radiation

From Figure 68 we observe the monthly mean global horizontal solar radiation in the three case-study cities. In Roissy, it seems that the radiation will be increasing in the future during the summer months, while the opposite is noticed for La Rochelle. In Carpentras, the uncertainty is higher than the variation.

Cloud cover (Potential Radiative Cooling)

Figure 69 illustrates the monthly mean cloud cover in the present and future typical years. In Roissy and in Carpentras, it seems there will be a slight decrease during summer months while in La Rochelle it is the opposite, an increase in cloud cover is expected. For all cities, the range from the different climate models, therefore the climate uncertainty, is quite spread so it is hard to conclude. Carpentras, in comparison to the other two cities, has a lower cloud cover during summer months, less than 3/10 on average, which demonstrates strong potential for radiative cooling, added to the fact that the relative humidity in summer is low as well.

Relative humidity

In Figure 70 we observe the monthly mean relative humidity in the three cities. In the three cities, it seems that there will be a decrease in relative humidity during the summer months. In the winter months, in Roissy it seems there will be a slight increase in RH. We do not know if the summer decrease in relative humidity is due to higher temperatures, or lower amount of precipitations, and future precipitations projections must be investigated to know. From the literature, it is known that precipitations will be lower in the South of France during summer and as well in the Paris basin (Habets et al., 2013).

Wet-bulb & Dew-point temperatures (Potential Indirect Evaporative Cooling)

Figure 71 shows the wet-bulb and dew-point monthly mean temperatures in the four cities, which are related to the potential for evaporative cooling. We can observe an increase of around + 2 °C in all cities, and the increase is consistent along with the climate models. For advanced innovative indirect evaporative systems (that can reach the dew point temperature) that most likely will develop in the future, the strongest potential is in the city of Paris as the monthly mean dew-point temperature will be under 15 °C in that city.

Wind Speed and Wind Direction

Figure 72 shows the monthly mean wind speed in the present and future in all three cities. The projections are quite spread amongst the four climate models, so it is not possible to conclude on future variation trends. La Rochelle has the strongest wind speeds, followed by Roissy and then Carpentras. Figure 73 displays the wind roses for Roissy, La Rochelle and Carpentras. As future wind direction projections are not available, we used wind direction data from the present typical years for both the present and future typical years.

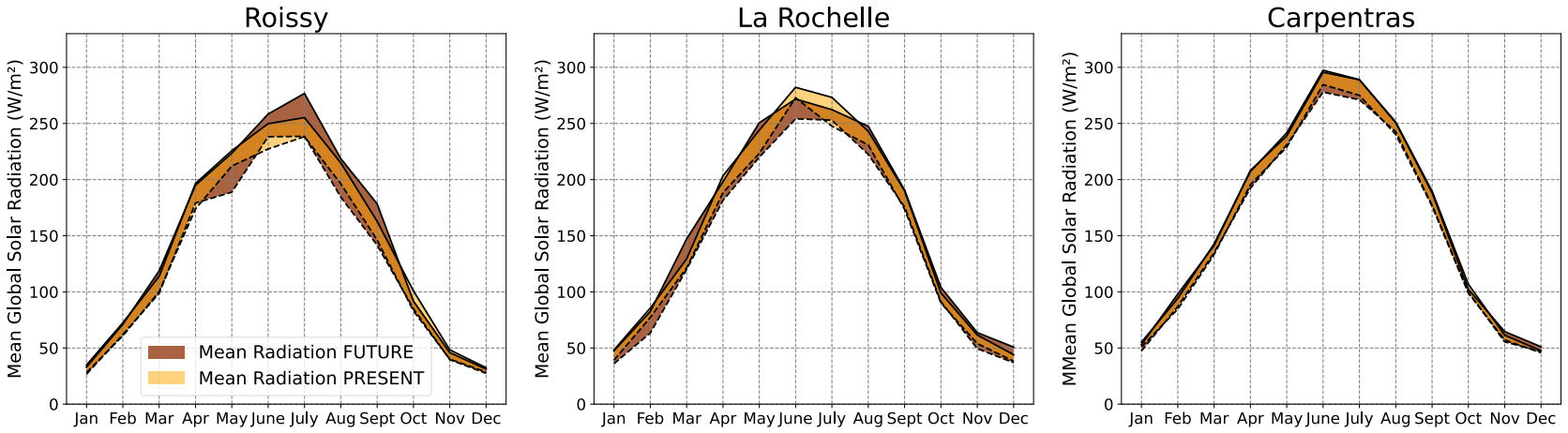

Figure 68 - Monthly mean global solar radiation in Roissy, La Rochelle and Carpentras - Present & Future. Dotted lines represent the lower monthly temperature of the four models while full lines represent the maximal monthly temperature of the four models

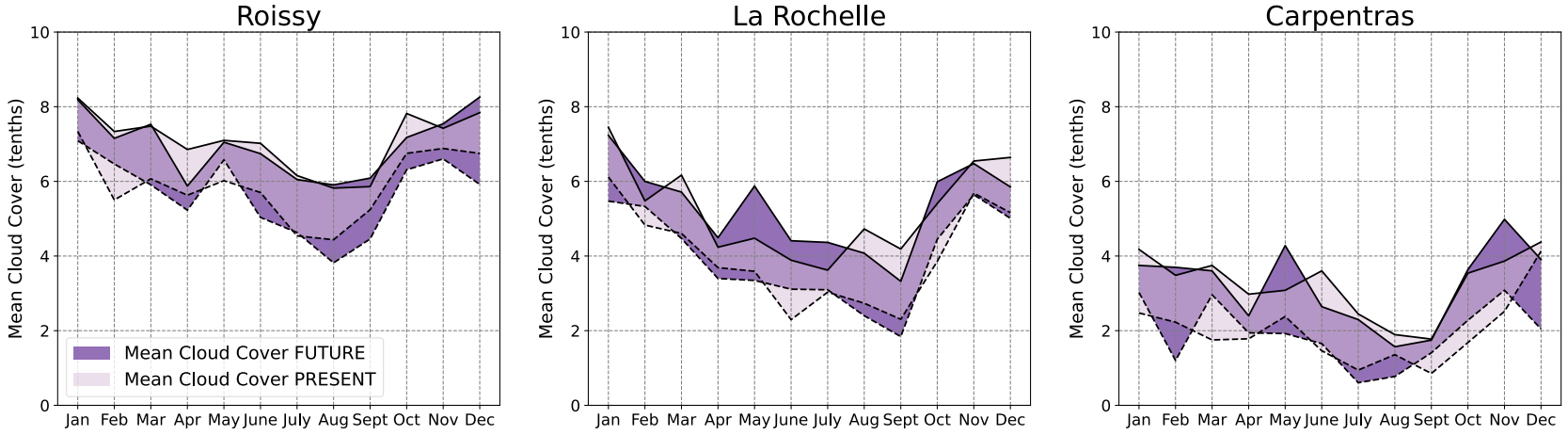

Figure 69 - Monthly mean cloud cover in Roissy, La Rochelle & Carpentras - Present & Future. Dotted lines represent the lower monthly temperature of the four models while full lines represent the maximal monthly temperature of the four models

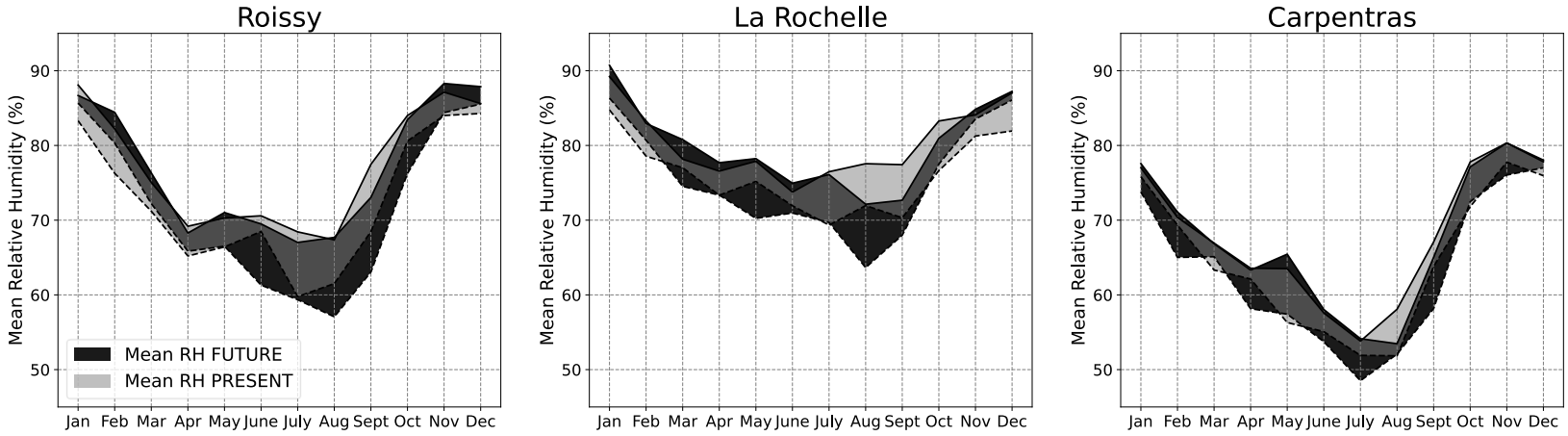

Figure 70 - Monthly mean relative humidity in Roissy, La Rochelle & Carpentras - Present & Future. Dotted lines represent the lower monthly temperature of the four models while full lines represent the maximal monthly temperature of the four models

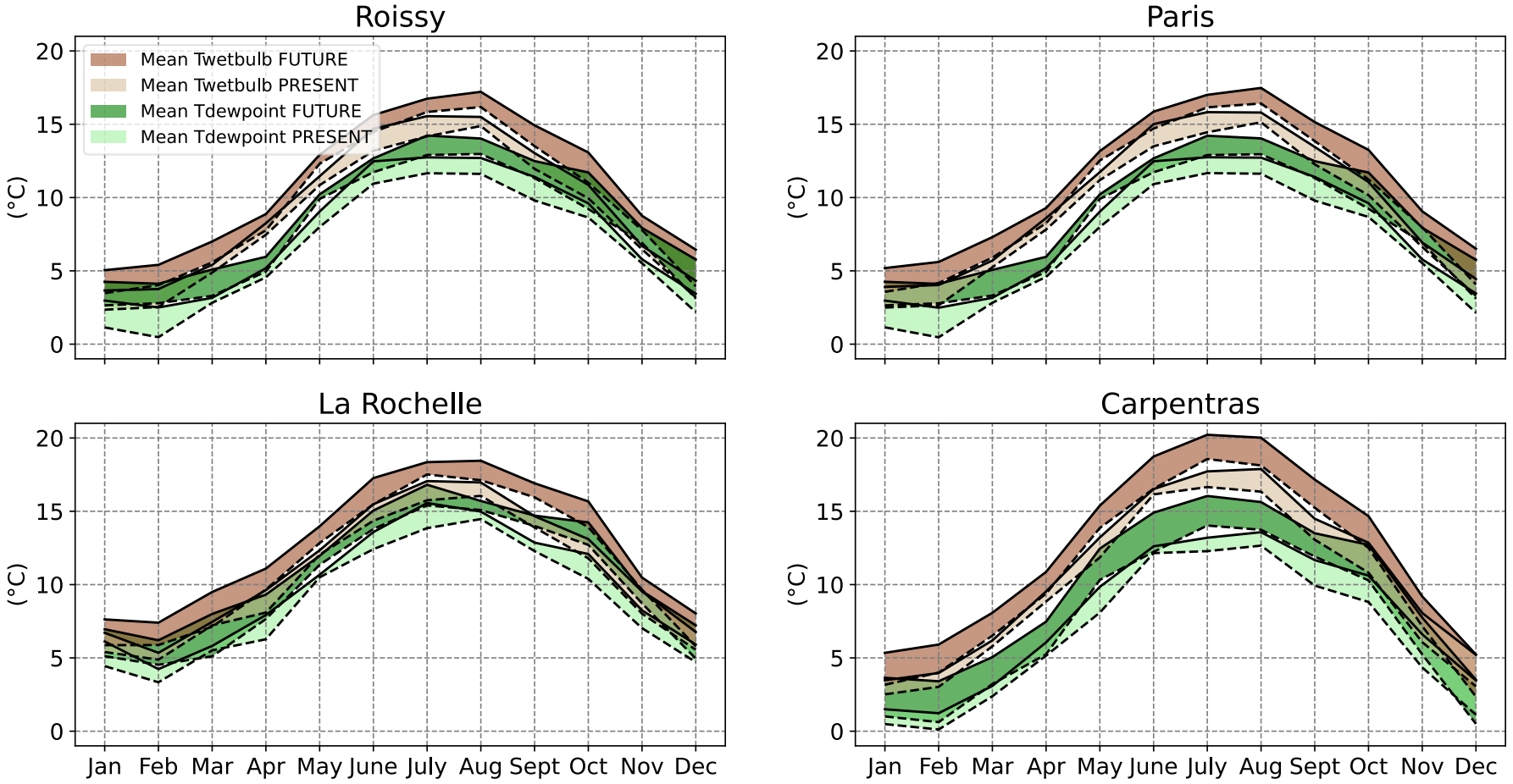

Figure 71 - Monthly mean wet-bulb & dew-point temperatures in Roissy, Paris, La Rochelle & Carpentras for the 4 climate models - Present & Future. Dotted lines represent the lower monthly temperature of the four models while full lines represent the maximal monthly temperature of the four models

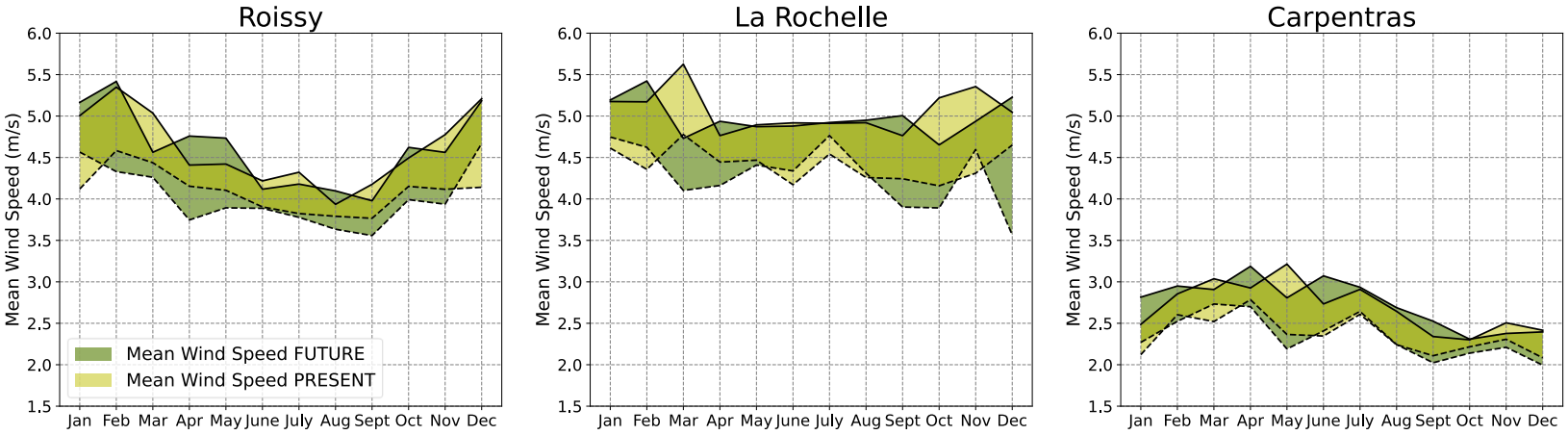

Figure 72 - Monthly mean wind speeds in Roissy, Paris, La Rochelle & Carpentras - Present & Future. Dotted lines represent the lower monthly temperature of the four models while full lines represent the maximal monthly temperature of the four models

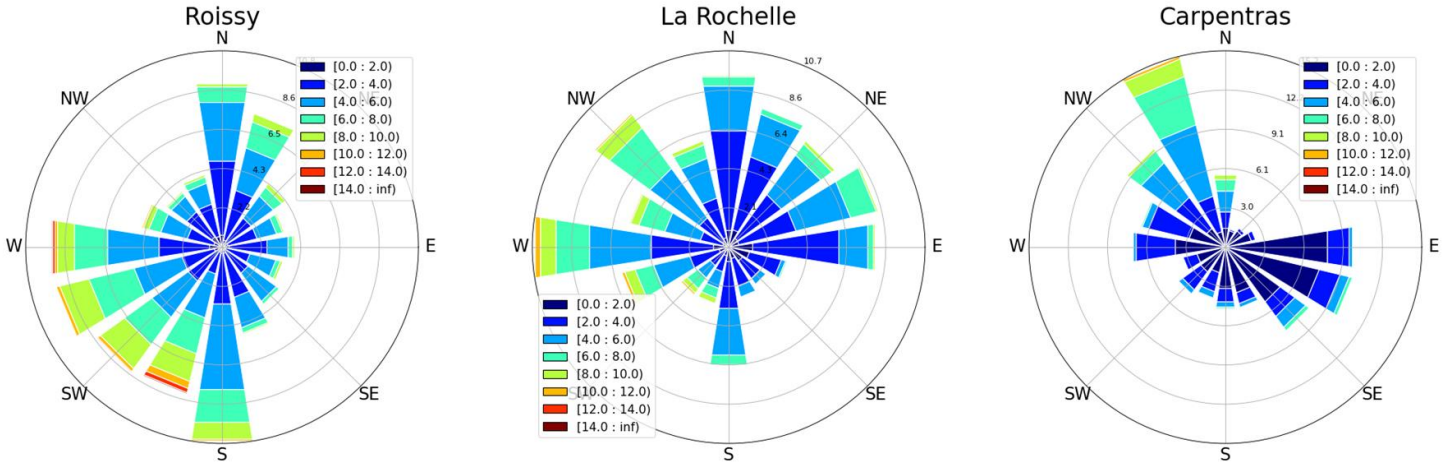

Figure 73 - Wind roses in Roissy, La Rochelle and Carpentras

3.1.3 **Heatwaves**

In order to detect heatwaves from the multi-year datasets, we used both methods defined by climatologists and epidemiologists (explained in section 2.3.1.6) in iterative steps:

1. We first identified heatwaves over the multi-years datasets using the method defined by (Ouzeau et al., 2016);
2. From these identified heatwaves, we narrowed them down to those for which the IBMs were above the thresholds defined by epidemiologists in each city (Laaidi, et al., 2013).

The identified heatwaves during both the contemporary (1990-2019) and mid-century period (2040-2069), RCP 8.5 by each climate model and in each case-study city are shown from Figure 74 to Figure 76 in colors. The 2003 heatwave is also shown as an indication in red, since it is well known for its severity. Bubbles are heatwaves identified at step (1), while bubbles with dots inside are heatwaves narrowed down at step (2), named "IBM heatwaves". The size of each bubble is characterized by its severity (°C.days above the *Sdeb* threshold). The thresholds for heatwave detection in each city are specified in Table 21, for both methods. Heatwaves that are part of the future typical year, for each model in each climate, are displayed in grey.

Table 21 – Temperature warning thresholds for heatwaves detection in Roissy, La Rochelle and Carpentras

	Climatologists (1) **Heatwave – *Vague de chaleur***			**Epidemiologists (2)** **IBM Heatwave - *Canicule***	
	Sint* (95 %)	***Sdeb* (97.5 %)***	***Spic* (99.5 %)***	S_n	S_x
Paris				21	31
Roissy	21.6 – 22.1	23.2 – 23.6	26.0 – 26.5	18	34
La Rochelle	21.8 – 21.9	23.3 – 23.5	25.6 – 26.2	20	35
Carpentras	26.3 – 26.5	27.6 – 27.8	29.0 – 30.3	21	36

* *Sint*, *Sdeb* and *Spic* thresholds are relative thresholds calculated for each climate model during the historical period 1990-2019 (the range written is the range between the lowest and highest model) while *Sn* and *Sx* thresholds are absolute thresholds defined by French epidemiologists.

In comparison to contemporary heatwaves, future heatwaves are more frequent, longer, with higher intensity and higher severity. For each model, the bubble sizes of the contemporary heatwaves, which represent the severity of the heatwaves, are very small in comparison to the future heatwaves. We can observe that the IBM heatwaves are usually the most intense and severe heatwaves. What is also noticeable is that the different climate models display very different types of heatwaves: Some heatwaves have high maxima but on a short period (Big pink bubble above the 2003 heatwave from the model CNRM), some heatwaves are very severe but with similar or lower mean maxima than in 2003 (green bubbles on the right part of the graph for the model MPI), and heatwaves with higher maxima than in 2003 for a longer period, around 20 days (models IPSL, MPI and HadGEM). All these different types of heatwaves will provoke different building responses and very different types of building indoor overheating.

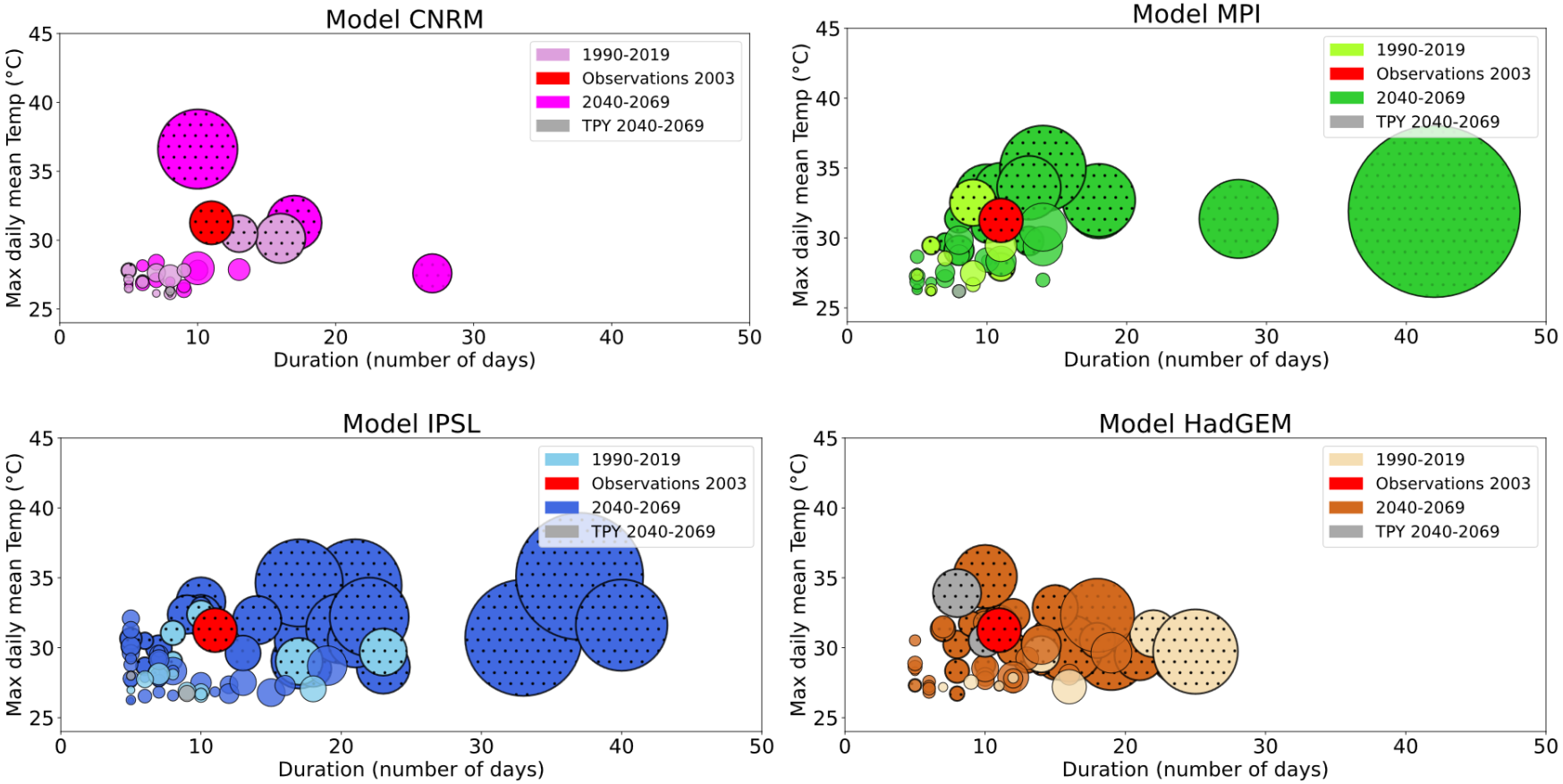

Figure 74 - Heatwaves in Roissy: Present (Model), 2003 (Observations) and Future (Model). A bubble represents a heatwave, a bubble with dots inside represents a heatwave with health-heat-related risk (IBM heatwave), and heatwaves in colored in grey represented heatwaves included in reassembled future typical years. The bubble size is the heatwave severity (°C.days above *Sdeb* threshold).

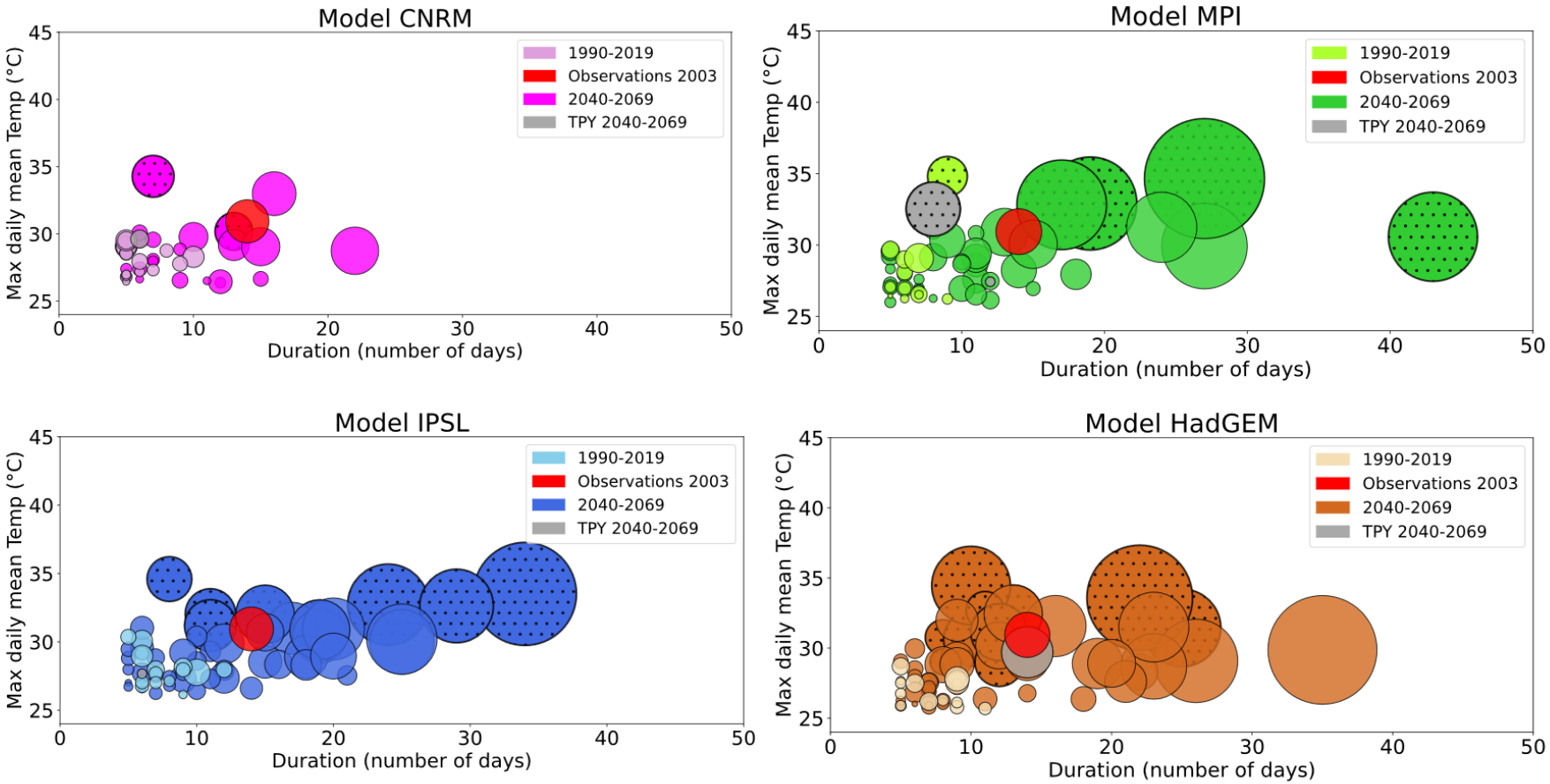

Figure 75 - Heatwaves in La Rochelle: Present (Model), 2003 (Observations) and Future (Model). A bubble represents a heatwave, a bubble with dots inside represents a heatwave with health-heat-related risk (IBM heatwave), and heatwaves in colored in grey represented heatwaves included in reassembled future typical years. The bubble size is the heatwave severity (°C.days above *Sdeb* threshold).

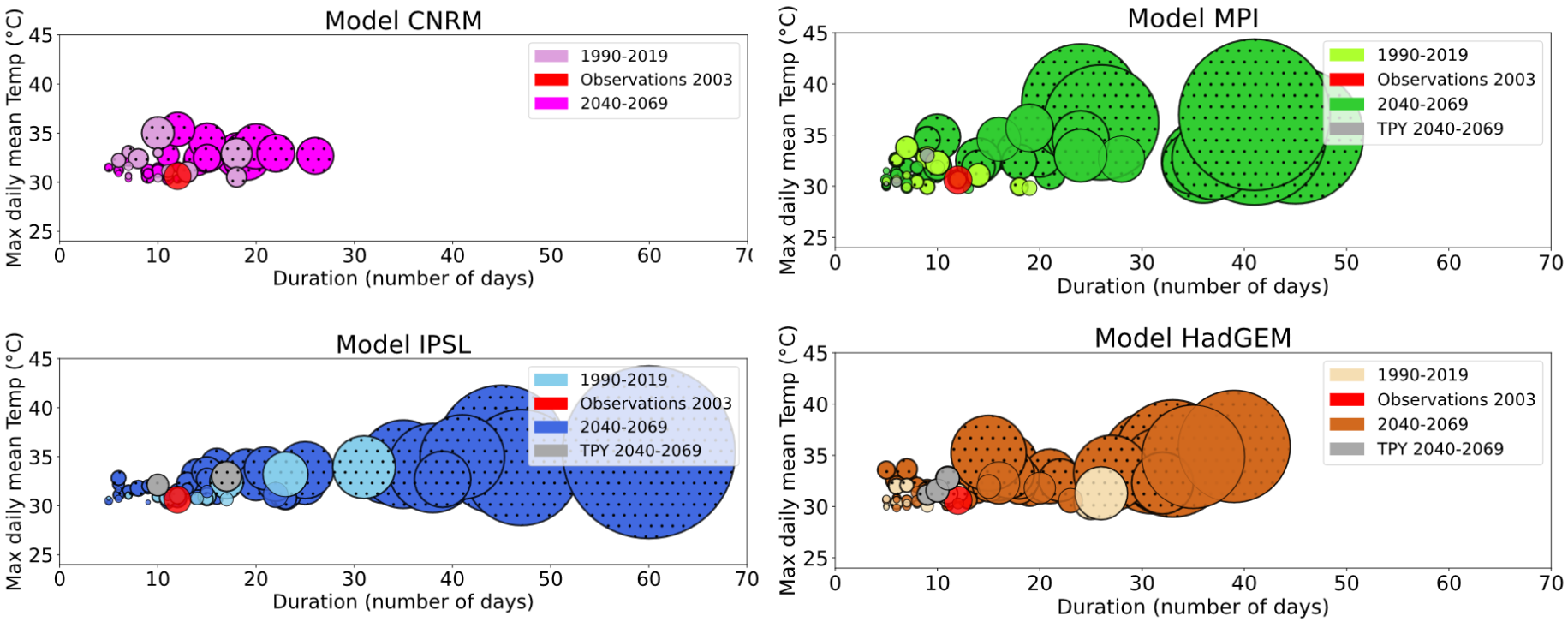

Figure 76 - Heatwaves in Carpentras: Present (Model), 2003 (Observations) and Future (Model). A bubble represents a heatwave, a bubble with dots inside represents a heatwave with health-heat-related risk (IBM heatwave), and heatwaves in colored in grey represented heatwaves included in reassembled future typical years. The bubble size is the heatwave severity (°C.days above *Sdeb* threshold).

A short period of extreme temperatures in comparison to a prolonged period of warm temperatures will surely have a different effect on the exposure for the occupants, and directly on their heat stress, or heat-health related risk. This is a crucial question that emerges from this research:

Which future heatwave(s) should we use to analyze the indoor heat stress and the building resilience to overheating and its ability to protect the occupants ?

Ideally, the impact of different types of heatwaves on indoor overheating should be investigated. However for the number of simulations to be manageable in this Ph.D., we selected one future heatwave per city. For comparison purposes, we analyzed the 2003 heatwave. It is considered as our reference, as we know it had a disastrous health impact on the population, especially in big French cities. We calculated the IBM_{max} and IBM_{min} during early August 2003 for each of the three cities (Figure 77). We can notice that only in Roissy the 2003 heatwave had the IBMs above the thresholds, not in La Rochelle nor in Carpentras. This can be explained by the fact that in La Rochelle, the daily maxima reached above the *Sx* threshold (35 °C) during only one day, while in Carpentras the daily maxima were very high but the daily minima remained just under the *Sn* threshold (21 °C).

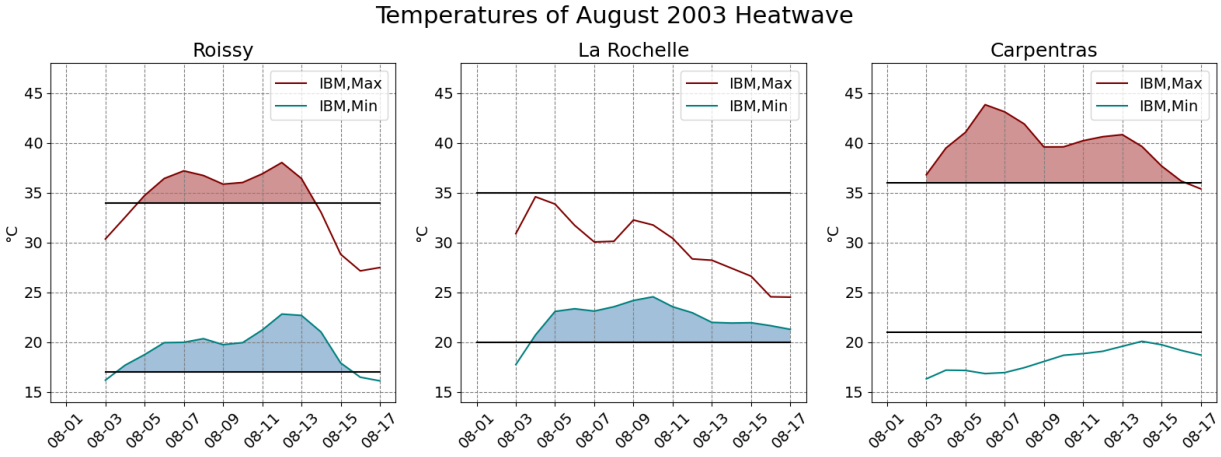

Figure 77 - Characterization of 2003 heatwave observations with IBMs

In Table 22, we display statistics about the future heatwaves. The heatwaves for which both IBM_{max} and IBM_{min} are above the thresholds (heatwaves named "canicules" in France), are named IBM heatwaves in this report. In Roissy around half of the future heatwaves will have the IBMs above the thresholds (18-54 % depending on the climate model), in La Rochelle only a few heatwaves will have heat-health related risk (8-18 % of future heatwaves are above IBM thresholds) while in Carpentras, almost all future heatwaves will present sanitary risks (83-90 %). In Carpentras, future heatwaves will be much more dangerous in comparison to in Roissy and in La Rochelle: longer, up to 2 months, and with daily mean maximal temperatures around 35 °C for some heatwaves. Some other heatwaves are above IBMs thresholds while having lower maximum daily mean temperatures than in 2003, which can be explained by higher night temperatures than in 2003 but lower daytime temperatures.

Table 22 - Future heatwaves statistics from 2040 to 2069 in Roissy, La Rochelle and Carpentras (scenario RCP 8.5) for the four climate models, HW stands for Heatwave, IBM HW stands for Heatwave with Health-heat-related risk (canicule in French)

		Number of HWs	Number of IBM HWs	Number of IBM HWs with T_{max} > 2003	% of HWs that are IBM HWs	% of HWs with T_{max} > 2003	% of IBM HWs with T_{max} > 2003
Roissy	**CNRM**	17	3	2	18	12	67
	MPI	34	13	9	38	26	69
	IPSL	54	24	11	44	20	46
	HadGEM	46	25	8	54	17	32
La Rochelle	**CNRM**	24	2	1	8	4	50
	MPI	42	5	4	12	10	80
	IPSL	47	8	8	17	17	100
	HadGEM	55	10	7	18	13	70
Carpentras	**CNRM**	29	26	23	90	79	88
	MPI	50	42	37	84	74	88
	IPSL	50	44	42	88	84	95
	HadGEM	53	44	42	83	79	95

*T_{max} refers to maximum mean daily temperature during a heatwave

As our reference for a IBM HW with disastrous sanitary impact is the 2003 heatwave, we wondered:

How frequently a heatwave such as in 2003 might occur in the future?

From Table 22, we can answer this question quantitatively, with a large uncertainty related to the four climate models. Considering the way we characterized the heatwaves, (duration, intensity per max daily mean temperature during the heatwave and severity per °C.days above the *Sdeb* thresholds), we could quantify the occurrence of heatwaves either by duration, intensity, or severity. We chose to classify the heatwaves by intensity, where some heatwaves with high severity have a low intensity and reach above the IBM thresholds for only a very short period. This choice is arbitrary and choosing another selection would surely induce different results, such as using a different method for heatwaves selection. The quantification is made in Table 22, column "Number of IBM HWs with max > 2003", it is between 2 and 11 in Roissy, 1 and 8 in La Rochelle, and between 23 and 42 in Carpentras. As we analyzed heatwaves over a 30 years period between 2040 and 2069, this means that in Roissy, a heatwave as least as intense as the 2003 heatwave will be recurring every 3 years (for three climate models) or every 15 years (CNRM model), in La Rochelle every 4, 8 or 30 years, and in Carpentras almost every year, or more than once a year for three climate models. It is important to remind that the data presented in this section have several limitations: First, only four climate models were used, and using more climate models would lead to a more holistic assessment of climate projections. However, from Figure 35, we have chosen four models with quite spread differences in summer dry-bulb temperatures, and not even the models leading to the highest temperatures. It is normal that the CNRM model consistently showcases much

lower heatwave projections in comparison to the three other climate models as it is the one with the lowest dry-bulb temperatures projections in comparison with the eleven climate models (Figure 35). Second, the method used to detect the heatwaves is only based on the dry-bulb temperature, not accounting for relative humidity, solar radiation, or cloud cover. For building thermal simulations, we know that the building response will be very different if the direct normal radiation would be high or low, or that the heat stress on the occupant will be different depending on the humidity or the wind. However, it is very complex to integrate all weather variables into the analysis, and epidemiologists have always correlated indoor deaths to exterior temperatures, sometimes including humidity, Furthermore, accounting for the different weather variables should be done in a different way for each building design, as some buildings are much more dependent on humidity (i.e humidity dependent building materials), some others on solar radiation (i.e large glazing area), and some others on wind speed (i.e with strong potential for natural ventilation.) Finally, we could have characterized the heatwaves following only the methods defined by epidemiologists (IBMs), but the thresholds for this method were defined at a given point in time: The population vulnerability and the built fabric vulnerability are therefore considered as constant, and we know that these might evolve in the future. People might adapt to heat by buying fans and/or small AC units (especially in the South of France), while the building fabric will surely evolve. In that sense, the same thresholds might lead to more deaths, which might lead to an elevation of these thresholds. These thresholds are currently being regularly updated, but how they will evolve in the future is unknown, and it is a constant research question for epidemiologists (Pascal et al., 2021).

We can also observe from Figure 74 to Figure 76 that most future typical years contain a heatwave. In Roissy, the future heatwaves contained in the future typical year have a much lower intensity than the 2003 heatwave (up to 26 °C versus 31 °C maximum daily mean temperature of the heatwave), except for the model HadGEM which contains an IBM heatwave more intense than 2003, but a little shorter. However, from Table 22 we could observe that for three out of the four climate models, the 2003 heatwave will be recurring every 3 years, meaning that it will be a "typical" heatwave in the future. Since the typical years are assembled with equivalent weight being given to the dry-bulb temperature, humidity and solar radiation, future "typical" heatwaves will not necessarily be included in future typical years. Beyond this, assembling typical months is based on the difference in daily mean temperatures over a month, having a heatwave in a typical month means that the other days of the selected month are colder than the 30 years distribution temperatures of that month. In La Rochelle, an IBM heatwave is included in the future typical year for the model MPI, while in Carpentras the future typical years of the model IPSL and HadGEM contain IBM heatwaves. This is in accordance with the higher temperatures at the end of the distribution tail of the typical summer temperatures shown in Figure 63.

In order to answer the question about which future heatwave to use in the building simulations, we can go back our objective performances defined in Figure 28. The first performance objective is energy sobriety under future typical climate conditions. For this, we analyze the energy needs in both winter and future periods, therefore we think that using future typical years is practical to quantify them. The second objective is that the building is comfortable in future typical summer conditions. The third objective is to ensure that the building lead to reduced heath-heat-related risk under future recurring conditions. Since future "typical" heatwaves are not necessarily included in future typical years, we think that

it is necessary to analyze if the building is adapted to both future typical summer conditions (that might or might not include future heatwaves given the method used) and to future typical heatwaves. The future typical year is necessary because it accounts for equals weight to other weather variables (relative humidity, solar radiation) during the entire period, whereas the future heatwaves are only a portion of the summer, during which the weather might not be representative of the other 20 years. We defined as future "typical heatwave" a heatwave recurring every five years, which is an arbitrary choice. Finally, to analyze the building resilience to indoor overheating under very extreme events, we must select the heatwaves with the higher intensities, severities or duration, this is not in the scope of this Ph.D. These are summarized in Table 23.

Table 23 - Different weather files to use for different performance objectives

Performance objective	Exterior conditions	Weather file to use
Energy sobriety (Mitigation)	Future typical climate conditions (winter and summer)	Future typical year
Reduced summer thermal discomfort, reduced heat-related health risk (Adaptation)	Future typical summer climate conditions	Future typical year IBM heatwave occurring every 5 years
Limited heat-related health risk (Resilience)	Future extreme climate summer conditions	IBM Heatwave occurring every 20 years

In order to quantify the return time period of future heatwaves, we observe the future IBM heatwaves occurrence over the period 2040-2069 in Figure 78. These are classified by intensity (maximum daily mean temperature during a heatwave) on the x-axis. Note that the y-axis is different depending on the city, for better readability. As a reference, in 2003, the maximum daily mean temperature was about 31.2 °C in Roissy, 30.9 °C in La Rochelle and 30.8 °C in Carpentras.

We assume that a "typical heatwave" is a IBM heatwave recurring every 5 years is equivalent to a heatwave with intensity or higher intensity occurring six times in 30 years. In Roissy, this is equivalent to a heatwave with an intensity of around 33 °C, in La Rochelle of around 31.5 °C and in Carpentras of around 34.5 °C (Figure 78). Note that these recurring heatwaves are all IBM heatwaves, which mean potential heat-health related risk.

Ensuring that the building will ensure comfortable summer conditions under these future typical heatwaves with passive cooling solutions presents therefore a challenge. For a resilience analysis, exploring the worst-case scenario, heatwaves less frequent, and of higher intensity and/or severity can be used (located towards the right in Figure 78). Finally, we did not present future heatwaves with UHI effects included for Paris, but similarly to the typical years, the UWG model can be used. The night temperatures will be more elevated under future heatwaves in Paris which will present an additional challenge.

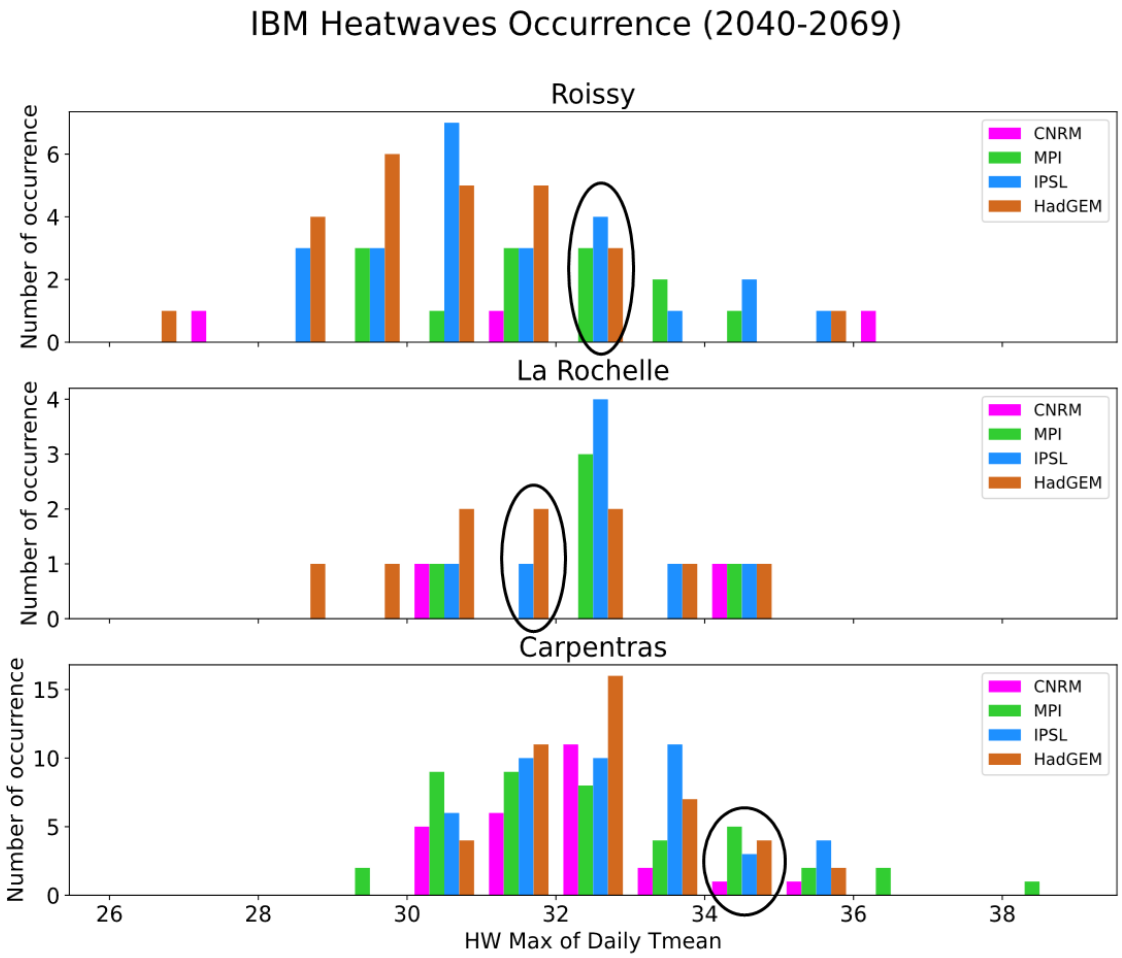

Figure 78 - IBM Heatwaves occurrence (classified by intensity, x-axis) in each case-study city for the four climate models over the future period 2040-2069 RCP 8.5

3.2 Selection of climate sequences for building thermal simulations

3.2.1 Selection of typical years

For each case-study city, four future typical years corresponding to the four climate models were re-assembled. For the sensitivity analysis and optimization algorithms, only one future typical year by case-study city will be used for the analysis in the first step. Then, the sensitivity of the results to the climate models will be assessed.

In Roissy, the typical year from the model IPSL-RCA4 is selected. The typical year from the model HadGEM-RCA4 contains a very intense heatwave so it is discarded, and the typical year MPI-RCA4 displays similar temperatures than the model CNRM-RCA4 which showcases the lowest temperature projections (Figure 63).

In La Rochelle, the typical year from the model IPSL-RCA4 is selected. The typical years from both models MPI-RCA4 and HadGEM-RCA4 contain intense heatwaves so they are discarded.

In Carpentras, the typical year from the model HadGEM-RCA4 is selected. The typical year from the model IPSL-RCA4 contains an intense heatwave so it is discarded. The model HadGEM-RCA4 is chosen as it is the second warmest model, such as in the other cities. It does contain an intense heatwave as well.

For uniformity, the same models are respectively used for building thermal simulations with the typical years under the present climate. As the climate data were bias-adjusted, during the present climate the weather files are very similar amongst them.

3.2.2 Selection of future typical heatwaves

For each case-study city, from the many heatwaves detected, we analyze the building adaptation to one future "typical" heatwave. We defined the typical heatwave as being an IBM heatwave (with potential sanitary impact) recurring every 5 years. "Typical" heatwaves were selected according to the following procedure:

- Heatwaves detection based on outdoor mean daily temperatures above thresholds defined by climatologists;
- From the detected heatwaves, detection of which ones have a potential sanitary impact, based on outdoor daytime and nighttime temperatures thresholds defined by epidemiologists, these are the IBM Heatwaves (Figure 74 to Figure 76);
- From the list of IBM Heatwaves, classification by occurrence during the future 30 years, based on each heatwave intensity (maximum daily mean temperature during the heatwave) (Figure 78)

- Selection of IBM heatwaves with recurring intensity every 5 years (heatwaves with intensity or higher intensity that will occur six times in 30 years) (Figure 78)
    - Roissy: intensity around 32.5 °C
    - La Rochelle: intensity around 31.5 °C
    - Carpentras: intensity around 34.5 °C
- Selection of IBM heatwaves with sunny days (low cloud cover and high direct normal solar radiation).

In Roissy, the selected typical heatwave is from the model HadGEM-RCA4, from the 12th until the 28th of June 2052, with an intensity of 32.3 °C and a severity of 26.2 °C.days. In comparison, the August 2003 heatwave has an intensity of 31.2 °C and a severity of 18.2 °C.days.

In La Rochelle, the selected typical heatwave is from the model IPSL-RCA4, from the 18th of June until the 4th of July 2058, with an intensity of 31.2 °C and a severity of 19.0 °C.days. In comparison, the August 2003 heatwave has an intensity of 30.9 °C and a severity of 16.4 °C.days.

In Carpentras, the selected typical heatwave is from the model HadGEM-RCA4, from the 27th of July until the 12th of August 2051, with an intensity of 34.3 °C.days and a severity of 27.6 °C.days. In comparison, the August 2003 heatwave has an intensity of 30.6 °C and a severity of 7.1 °C.days.

The IBMs calculated from the three future typical heatwaves is shown in Figure 79, which can be compared to Figure 77 for 2003.

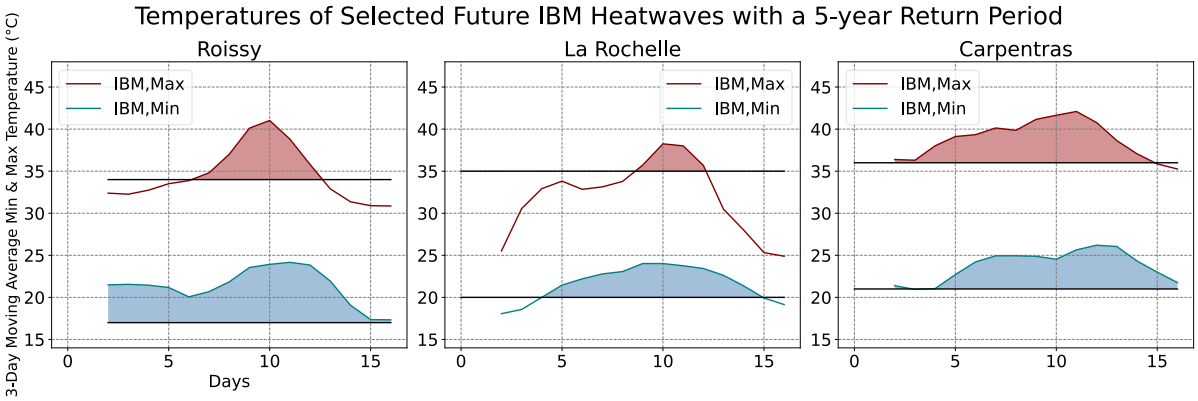

Figure 79 – IBMs during three future typical heatwaves

We can notice that all three selected future typical IBM heatwaves have higher IBM than in 2003. In Roissy, both the maximum IBM_{max} is higher (above 40 °C versus 38 °C in 2003) and maximum IBM_{min} (up to 24 °C for consecutive days), the daytime exposure is shorter though. In La Rochelle, IBM_{max} are above the daily threshold which was not the case in 2003. In Carpentras, IBM_{min} are above the daily threshold which was not the case in 2003. These three heatwaves last around two weeks, which is short in comparison with other identified heatwaves, this is because intense heatwaves are usually shorter than other severe heatwaves with similar severity but lower intensity.

3.3 Concluding remarks on future climate data as input for building simulations

In this chapter, we analyzed the future climate data reassembled in the previous chapter. The analysis of the increase in the hot extreme multiyear temperature distribution demonstrated that, as expected, extreme hot temperatures will be much more frequent. We then investigated the different variations in other weather variables give indications on the potential of different passive cooling technologies (natural ventilation, ground cooling, radiative cooling, evaporative cooling). Considering the climate uncertainty related to the climate models, it is complex to integrate these in building thermal simulations without conductive multiple iterations.

The analysis of heatwaves in typical years demonstrated that heatwaves might or might not be included in future typical years, which is dependent on the method used to reassemble future typical years. We selected future typical years in Roissy and in La Rochelle with no heatwaves on purpose, while in Carpentras we selected a future typical year containing a heatwave, as heatwaves will occur every year in Carpentras in the mid-century. Since we calculated that heatwaves of the same or higher intensity than the 2003 heatwave will occur very frequently during the mid-century, using future heatwaves files containing heatwaves for indoor overheating assessment will be necessary. Indeed, using future typical years weather files might not be enough. We selected future "typical heatwaves" to be used for the indoor overheating assessment in the next Chapters. Heatwaves with similar or higher intensities than the selected heatwaves were calculated to occur every five years during the period 2040-2069, they are all potentially induce a health-heat-related risk based on the epidemiologist's definition. We accounted for climate model uncertainty in their selection as the future typical heatwaves were chosen based on three climate models (MPI, IPSL and HadGEM).

These future typical heatwaves weather files can be used during the design stage of the building to analyze the building response to a variety of future climate conditions and make sure the building maintains comfortable and/or safe indoor conditions, and is therefore adapted to climate change. More extreme heatwave weather files can be used for resilience assessments, as currently undertaken in the project Annex 80 *Resilient cooling of buildings* which is developing future heatwaves weather files following the methodology proposed in this Ph.D. for many cities worldwide. These future heatwaves weather files, ready to be used for building thermal simulations offer great potential quantify the health-heat-related risk and therefore be used for adaptation and resilience assessments.

In the next two chapters, the weather files developed in Chapter 2 and selected here will be used for building thermal simulations during the sensitivity analysis and optimization. Both future typical years and future typical heatwave weather files will be used for the analysis.

Chapter 4

Sensitivity analysis – Adaptation of building design to future summers

In this chapter, we analyze the sensitive parameters that have an impact on indoor overheating during the future climate. Different design configurations are tested, following the passive cooling strategies and systems described in section 2.4.2.3. In the first section, the input parameters and their variation range are presented. In the second section, the results of the Sensitivity Analysis (SA) with the Morris method during future typical summers in the different cities are presented. In the last section, more in-depth analysis with the Sobol method is presented for the configuration with natural ventilation during the warmest days of different climate sequences. High-order interactions are presented, temporal analysis and the analysis of the operative temperature variance above a summer thermal comfort threshold.

Summary

4.1 Variation of building design variables

The objective of the sensitivity analysis (SA) is to evaluate the summer overheating in the living space during future climate sequences. For this purpose, the SA is conducted during the extended summer period (1st June to 30th of September). The design input parameters for the SA were selected as the ones that might impact the indoor overheating. Many researchers have evaluated the sensitivity of indoor building conditions to different design variables, and these were categorized by (Pang et al., 2020). Regarding summer overheating or cooling energy needs, the sensitivity to the following parameters was evaluated in different research works:

- **Building geometry/architecture**: height, surface, orientation, glazing ratio (Garcia Sanchez et al., 2014);
- **Building envelope** (thermal capacity, conductivity, density of building materials)
- **Control strategies for solar protection and ventilation** (Breesch & Janssens, 2010; Gondian et al., 2019; Heiselberg et al., 2009);
- **Occupant behavior**: internal gains, metabolic rate (Gondian et al., 2019; de Wilde & Tian, 2009);
- **Weather variables or weather files** (Goffart et al., 2017; de Wilde & Tian, 2009; Moazami, Carlucci et al., 2019; Tian & De Wilde, 2011).

For our study, we investigated parameters concerning the building envelope, the building geometry and control strategies for solar protection and ventilation. The occupant behavior is not studied and internal gains, metabolic rate, etc. are kept constant as defined in section 2.4. Finally, the weather files were not integrated into the SA for several reasons. First, the variation of the operative temperature above the indoor overheating threshold varies amongst the weather files (for instance, with the model CNRM which has the lowest temperature projections, an operative temperature above a certain threshold might never be reached, or only during short periods). If the cooling needs or peak load were evaluated, it would be easier to include the weather files into the SA. Second, as we aim to run a temporal sensitivity analysis, it will be easier to compare the results in contrast to a fixed climate sequence. We decided to investigate the influence of the weather variables on the SA outputs in independent SA.

For each parameter we defined a range of variations delimited by low and high values. The choice was made to select an extended range, exploring different values that each parameter could take. With the Morris method, a number of levels need to be defined, i.e the number of different values that can be given to an input variable between a range of variation. For our study, we chose a number of levels of 4, which is the minimum value advised according to (Petersen at al., 2019). For instance, if a parameter varies between 0 and 3 with 4 as the number of levels, the parameter can take the value of 0, 1, 2 or 3. The specificity of the Morris design matrix, in contrast to the Saltelli design matrix (used for the Sobol method), is that each parameter will take the extreme values within its variation range.

4.1.1 Bioclimatic architecture

We vary two parameters related to the building architecture: the glazing percentage, and the overhang located on the South façade of the veranda.

Glazing percentage

We vary the glazing percentage of the windows surrounding the living space. The high glazing ratio is conserved on the exterior windows of the glazed cavity and of the veranda, to maintain the initial design proposed by the architect that favors natural daylighting and cross-ventilation for summer thermal comfort. As the living space is initially conditioned within the "exterior wall" (on the West façade), when windows of the living space are reduced (initial design with 95 % of windows), they are replaced with the construction "exterior wall" (see Table 10). A minimum glazing percentage of 15 % is chosen in order to ensure minimal daylight into the apartment. The RT-2012 standard imposes a minimal glazing ratio of a sixth of the conditioned space floor area (1/6 of 120 m²). For the apartment case-study, the minimum recommended surface is then of 20 m². The North and South façade represent a total of 86.4 m², so the minimum glazing % should be of 23 %. However, in order to consider an extended range of possible values, we decided to extend this minimal glazing percentage and to consider a design with less glazing than recommended by the French regulation.

Overhang on the veranda (South façade)

The overhang could be classified within solar control, but as it is a feature of the initial design, we assume that it is an early architectural choice. In the initial design, an overhang is located on the South façade as they are supposed to be the balcony from the above floor. After a summer discomfort study, a maximal value of 1 m was determined enough to reduce the thermal discomfort. Our case-study apartment is located on the top floor but we analyze the presence of the overhang for solar control anyways. This value will vary between 0 (no presence of overhang) and 1.

4.1.2 Building envelope materials to protect from and dampen heat

We vary two kinds of parameters related to the building envelope: the optical properties of the exterior coatings and the thermal mass of the building envelope.

Optical properties of exterior coatings

Regarding the optical properties, two surfaces are varied independently from one another: the roof of the apartment (surface of the living space, glazed cavity and veranda) and the exterior wall (located on the West façade, and on the exterior walls of the living space on which there are no windows). In the SA, the parameter varied is the solar absorptance α_{SW} coefficient. For a specific value of solar absorptance, the value for the emissivity in the long wave-length ε is calculated according to Equation (67). This choice was made to simulate

the "best" exterior coating with a low solar absorptance and a high thermal emissivity and the "worst" with a high solar absorptance and a low thermal emissivity.

$$\varepsilon = 1 - \alpha_{SW} \quad (67)$$

Thermal mass

The initial design of the building has high thermal mass, with concrete of density ρ of 2300 kg/m^3. This thermal mass is in four constructions of the building envelope: Exterior and interior wall, floor and ceiling of the living space. Instead of the concrete, alternative materials with different thermal mass were considered for the simulations with the Morris method: concrete with a density of 2300 kg/m^3, brick with a density of 1750 kg/m^3, earth clay with a density of 1200 kg/m^3 and wood panels with a density of 650 kg/m^3. The thermal conductivity λ, specific heat capacity C_p and the thickness th were changed accordingly. Since the Saltelli design matrix accounts for an infinite possibility of variation within the defined range, a correlation was created between ρ and λ, C_p, and th. These other parameters were changed as for each construction that the U-value remains constant. The correlations are given in Equations (68), (69) and (70). The effect can be seen in the thermal diffusivity a, or on $\rho.C_p$ that impacts the heat conduction calculation (presented in section 2.4.2.1).

$$C_p = -0.4907.\rho + 1995.2 \quad (68)$$

$$\lambda = 0.0437\,.\,e^{0.0016.\rho} \quad (69)$$

$$th = 0000096.\rho - 0.0497 \quad (70)$$

An easy way to understand the thermal mass effect on the indoor temperature is the thermal delay TD (Equation (71)). We calculated it with a simple formula to have an order of magnitude for the two extreme materials on the design matrix, and for each construction (Table 24).

$$TD = \frac{th^2}{a} \quad (71)$$

Table 24 - Thermal delay values of apartment walls

	Thermal delay TD (h)	
	Minimum (ρ = 650 kg/m^3)	Maximum (ρ = 2300 kg/m^3)
Ceiling	11.7	20.6
Exterior wall	6.7	15.6
Floor	0.9	9.8
Interior wall	0.5	9.3

4.1.3 **Solar control strategies**

As the living space is fully glazed in the initial design, we add different strategies for solar control on the glazed facades (North and South). The façade is decomposed in six vertical adjacent windows. With the design matrix, either 0, 2, 4 or 6 shades are used. Therefore, a shade on a window is either fully used (down at 100 %) or not used at all. An alternative would have been to discretize the windows horizontally as in (Gondian, 2019). The maximum of shades used (6 on the North and South façade) does not allow daylight anymore and it is not realistic, however this extended range is explored through the SA. The set-point on the North façade varies between 0 and 200 W/m² and on the South façade between 0 and 600 W/m² which are between the minimal and maximum values that the facades receive in the summer (Figure 80). The South façade incoming solar radiation is the strongest in September, while on the North façade it is stronger close to the summer solstice.

Figure 80 - Incoming solar radiation on the exterior windows (Roissy)

The different design variables and their range of variation is summarized in Table 25.

Table 25 – Range of variation of design variables for the Morris SA

N°	Category	Parameter	Abbreviation	Location	Min	Max	Unit
1	**Building envelope**	**Optical properties of exterior coating***	A&E Extwall	Exterior wall	0.05	0.95	-
2			A&E Roof	Roof	0.05	0.95	-
3		**Thermal mass** (material density ρ)**	TM Ceiling	Ceiling of the living space	650	2300	kg/m^3
4			TM Floor	Floor of the living space	650	2300	kg/m^3
5			TM ExtWall	Exterior wall	650	2300	kg/m^3
6			TM IntWall	Interior wall	650	2300	kg/m^3
7	**Bioclimatic architecture**	**Overhang length**	Overhang L	Veranda (South)	0	1	m
8		**Glazing %**	Glazing %	Windows of the living space	15	95	%
9	**Solar control strategy**	**Number of Shades**	Nb Shades Cavity	Glazed cavity (North)	0	6	-
10			Nb Shades Veranda	Veranda (South)	0	6	-
11		**Shades Control Set-Point: Solar Radiation incident on window**	SP Shades Cavity	Glazed cavity (North)	0	200	W/m^2
12			SP Shades Veranda	Veranda (South)	0	600	W/m^2

*The solar absorptivity is changed in the design matrix and the longwave emissivity is correlated according to Equation (67)

** The material density is changed in the design matrix and the thermal conductivity, the heat capacity and the thickness are correlated according to Equations (68), (69) and (70)

4.1.4 **Ventilative cooling strategies**

In addition to the above-introduced strategies, three types of "passive cooling" strategies via air are investigated, we name them ventilative cooling strategies. For each configuration, the exterior windows of the glazed cavity and of the veranda are assumed as always opened during the entire simulation period to prevent overheating in these buffer zones.

4.1.4.1 Natural ventilation through window openings (NV)

The first passive cooling system is natural ventilation through windows opening, which is modelled with the Airflow Network. The first design variable controls the amount of airflow entering the living space by varying the number of windows that can be opened (0, 1, 2 or 3). We assume that windows are glass doors and that only one out of two windows can be opened (therefore maximum 3 out of 6 windows). An alternative to varying the number of windows opened is to vary the opening coefficient of each window. In these simulations, each window is opened at 100 %, and this parameter does not vary. The second design variable controls the temperature of the incoming air, and it is defined by the set-point operative temperature, the minimal indoor temperature conditioning windows opening. Windows opening is thus defined by two conditions: that the operative temperature of the living space is above the set-point operative temperature, and that the outdoor air temperature is inferior to the air

temperature of the living space (this condition is automatized in EnergyPlus when using the Airflow Network). The minimal set-point temperature is chosen to be 15°C, low on purpose, to maximize the nocturnal ventilation. The control for windows opening is described in 2.4.2.3. The assumption is made that people can always open windows and are not restrained by noise, pollution or security concerns. Windows that are always open and the ones that open based on conditions are illustrated in Figure 81.

Table 26 – Range of variation of natural ventilation (NV) design variables for Morris SA

N°	Category	Parameter	Abbreviation	Location	Min	Max	Unit
13	**Strategies for ventilation control**	**Number of windows opened**	Nb Wopen Living	Windows of the living space	0	3	-
14		**Windows opening Control Set-Point: Operative Temperature**	SP Wopen Living	Windows of the living space	15	24	°C

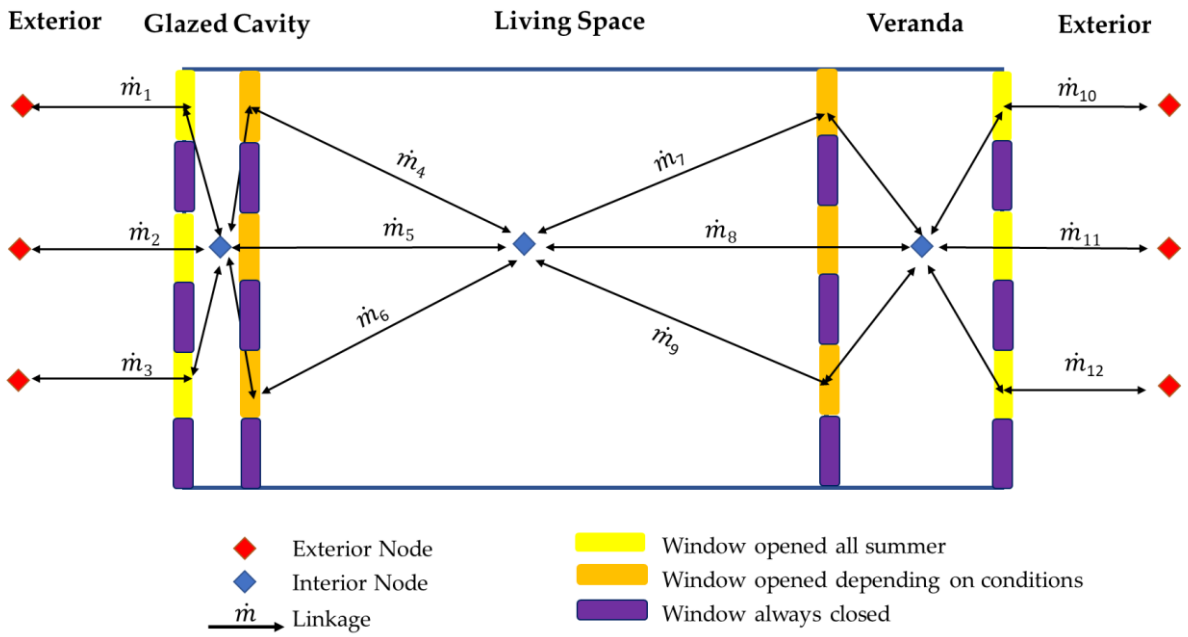

Figure 81 - Openable windows for natural ventilation (Airflow Network)

For the configuration with the larger windows, their height and width are 2.6 m. For the configuration with the smaller windows, their height and width are 1 m. The airflow entering through the windows, therefore, varies according to their size along with the design matrix.

4.1.4.2 Ventilation via mechanical free cooling (FC)

Alternatively, to natural ventilation, simulations are run with the windows of the living closed and air from the exterior is drawn towards the living space by mechanical ventilation. The maximum airflow rate is set to 0.27 m^3/s (equivalent to 3 ACH), which is much lower than

the airflow rates observed by windows opening. However, as the air passes through the ventilation ducts, its airflow rate is limited. As explained in section 2.4.2.3, the delta FC modulates the airflow rate linearly according to the temperature difference between the air temperature and the set-point temperature. As the delta FC varies, the set-point temperature is set to 20°C, with a maximum temperature of 28 °C., this way the ventilation is not at its maximum when the temperature set-point is reached. The delta FC is varied between 0.5 and 8 °C (Table 27).

As the free-cooling is modelled as simple ventilation to be able to control it through the EnergyPlus EMS, it is not possible to model the exterior windows opening of the glazed cavity and of the veranda using the Airflow Network. For these two zones not to overheat, a constant airflow of 0.79 m^3/s in the glazed cavity and of 0.44 m^3/s in the veranda is provided. These values were found using mean values of airflow rates when simulating the exterior windows of the cavity and of the veranda opened and the windows of the living space closed with the Airflow Network.

Table 27 – Range of variation of mechanical free-cooling (FC) design variable for Morris SA

N°	Category	Parameter	Abbreviation	Min	Max	Unit
15	**Strategies for free-cooling control**	**Delta T°**	Delta FC	0.5	8	°C

4.1.4.3 Earth-to-air heat exchanger (EAHX)

The third passive cooling system is an earth-to-air heat exchanger system (EAHX). Similar to the simulations with the free-cooling system, for all simulations with the EAHX, a constant airflow of 0.79 m^3/s in the glazed cavity and of 0.44 m^3/s in the veranda is provided for these two zones not to overheat, simulating windows opening. Design characteristics for EAHX are lacking in the literature, since each earth tube is designed to meet specifically the local climate, building needs and construction possibilities on site. However, researchers have analyzed the influence of different design variables and have distinguished the main design variables impacting the outlet air temperature of the EAHX, which are the pipes depth, diameter and the airflow rate inside the pipes. The climate (type of sol, dry-bulb air temperature) influences most the outlet air temperature (Lee & Strand, 2006), but these are not design variables. According to (Givoni, 1994), covering the ground from the sun during the day is an alternative to lowering the ground temperature.

Pipes depth

Since ground temperatures are lower at higher depths, these are optimal, but they are associated with higher costs. Different depths have been reported in the literature: (Agrawal et al., 2019) conducted a review of the latest research and application of EAHX for different buildings types, they reported tubes depth from 1.5 to 4 m depending on the studies. Depths from 3 to 5 m were reported by (Santamouris et al., 2007). In Raleigh, USA which is humid subtropical, in late August, ground temperatures of 21 °C and 16 °C were reported for depths between 2 m and 6 m for air temperature maxima around 30°C and minima around 20 °C in summer (Mirianhosseinabadi et al., 2014). (Chiesa, 2018) calculated ground temperature at different depths for the city of Turin and three different soil types (wet clay, limestone and

sand composed). For the warmer month (August), the ground temperature was about 26-28 °C at 0 m depth, 22-25 °C at 1 m, 15-20 °C at 2 m, etc while they stabilized around 12 °C (close to the yearly ground temperature) from 5 m depth.

Pipes diameter, airflow rate, and pressure losses

The airflow rate and the pipe diameter have been identified as two important parameters. These two parameters are correlated since the air velocity inside the pipe is equivalent to the airflow rate divided by the pipe section. Diameters of between 0.10 and 0.50 m were reported by (Agrawal et al., 2019), between 0.20 and 0.35 m in the DB Netz AG and Lamparter buildings respectively, while (Santamouris et al., 2007) recommend a pipe diameter of around 0.25 m, that same value also used by (Mirianhosseinabadi et al., 2014) and (Chiesa et al., 2014). (Salomon et al., 2003) recommend a diameter of between 0.15 and 0.25.

Airflow rate and pipe diameter need to be sized together. The pressure losses must be calculated: A large diameter and a low airflow rate will lead to small pressure losses, of around 12 Pa according to (Santamouris et al., 2007). For an efficient heat transfer, a low airflow rate is preferred as the air spends more time in contact with the ground. However, with a low airflow even though the output tube air temperature will be lower, it will not cool down the space as much as a higher airflow rate. The relationship between the airflow rate and inside air temperature is not linear and this parameter needs to be optimized. Installing several tubes in parallel allow to increase the airflow rate while not decreasing the efficiency, but it is not possible to model this with EnergyPlus. (Lee & Strand, 2006) conducted a parametric analysis and concluded that the pipe diameter had influence but less than the airflow rate. This result was previously found by (Mihalakakou et al. 1989). Therefore, we decided to fix the pipe diameter and study the influence of the airflow rate. We calculated the pressure losses for different airflow rates and pipe diameters in Appendix A. From these calculations, we decided to set the pipe diameter to 0.25 m and to vary the airflow rate to a maximal value of 3 ACH to be consistent with the simulations from the free-cooling system. In the worst-case scenario of the design matrix regarding pressure losses (high airflow and low pipes length), linear pressure losses will be of 1.15 Pa/m and air velocity inside the tube of 5 m/s.

Pipes length

For a longer tube, the surface for heat transfer is higher. Therefore, the air will spend more time in the EAHX for a given speed and its temperature will be reduced accordingly. Similar to the depth, a long pipe is always preferable, but these two factors are dependent on the terrain characteristics and of associated costs. (Chiesa et al., 2014) monitored an EAHX made of 32 tubes of 70 m length each for a school building. They recorded that 70 % of the air to earth heat exchange occurred in the first third of the pipe (23 m), with the inlet temperature dropping from 25 °C to 21 °C at 23 m for an outlet temperature of 19 °C. This suggests that a tube of around 25 m length might be a better cost-effective solution. On the contrary, (Salomon et al., 2003) recommend a length between 25 m and 40 m arguing that 25 m is the minimal length for efficient heat transfer while beyond 40 m the efficiency does not increase. (Agrawal et al., 2019) reported lengths between 12 m and 120 m for various buildings. The pipe length needs to be sized in accordance with the airflow rate, as higher airflow rates will require higher length for the same amount of heat transfer to occur.

Control parameters

The control parameters also have an influence on the outlet temperature. With the model implemented in EnergyPlus it is possible to control the minimum set-point temperature of the living space for using the outlet air of the EAHX to cool the zone. A parametric study showed that a small DELTA is always beneficial, so we kept it to 0 °C. The selected design variables for the EAHX and their range of variation are given in Table 28. The control was given in section 2.4.2.3.

Table 28 – Range of variation of earth-to-air heat exchanger (EAHX) design variables for Morris SA

N°	Category	Parameter	Abbreviation	Min	Max	Unit
16	**Strategy for EAHX control**	**Airflow Rate**	Airflow Rate	0.054	0.270	m^3/s
17		**Set-point temperature**	SP EAHX	20	24	°C
18	**EAHX characteristics**	**Pipe Length**	Pipe L	25	40	m
19		**Pipe Depth**	Pipe D	1	3.5	m

4.2 Sensitivity analysis for the entire summer period

Considering the large number of parameters, the SA is first conducted with the Morris method for a quick screening of the impactful parameters on the summer thermal discomfort. Three independent SA are runs for the three different passive cooling systems:

- Natural Ventilation (NV) with parameters 1 to 12 and 13 to 14 (Table 25 and Table 26)
- Free cooling (FC) with parameters 1 to 12 and 15 (Table 25 and Table 27)
- Earth-to-air heat exchanger (EAHX) with parameters 1 to 12 and 16 to 19 (Table 25 and Table 28)

4.2.1 Convergence of the elementary effects mean values

First, it is necessary to assess the number of trajectories *tr* needed to obtain convergence. (Sarrazin et al., 2016) differentiate the number of model evaluations to obtain screening convergence (clusters of non-influential and of influential parameters), ranking convergence (parameters are ordered), and indices convergence (sensitivity indices values are calculated with a low error (Figure 82). Regarding the Morris method in particular, there is no scientific consensus on the ideal setting parameters (number of levels and of trajectories) to reach convergence. A recent article from (Petersen et al., 2019) compared the sensitivity of the Morris indicators (μ* and σ) to different number of levels and trajectories. They compared different articles using the Morris method and observed that while a default value of number of levels equal to 4 is often used (if specified in the study), the number of trajectories is less often discussed or investigated, with some authors using a low number of trajectories as recommended by the Morris method (i.e 10) and some authors a large number (i.e > 100), which is also concluded by (Petersen et al., 2019).

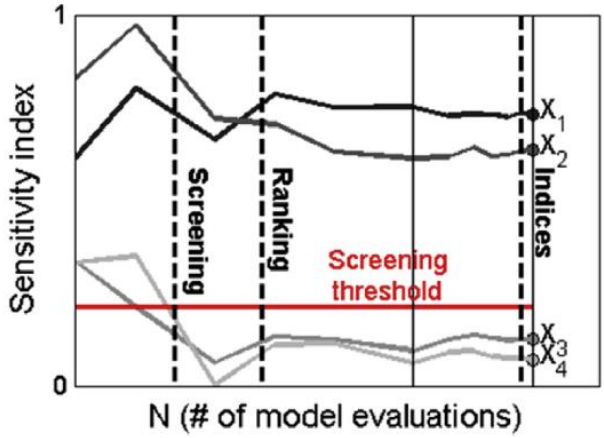

Figure 82 - Screening, ranking and indices convergence according to (Sarrazin et al., 2016)

For our case-study, we analyzed the convergence by setting the number of trajectories *tr* to 500, corresponding to 6500 model runs according to Equation (72) for 12 parameters. The convergence is first evaluated for a simulation without any passive cooling systems, parameters 1 to 12 (Figure 83 and Figure 84).

$$N_{simulations\_Morris} = tr.(N_{param} + 1) \quad (72)$$

We ran the Morris design matrix for 500 trajectories and then calculated sensitivity indexes successively from 5, 10, 50, 100, 200, 300, 400 and 500 trajectories as advised by (Menberg et al., 2016). The convergence of μ* for each design parameter is shown in Figure 83 and the convergence of the bootstrapped confidence interval μ*_conf (confidence interval level of 0.95) is shown in Figure 84. For this case the weather file used is the future typical summer in Roissy with the model IPSL.

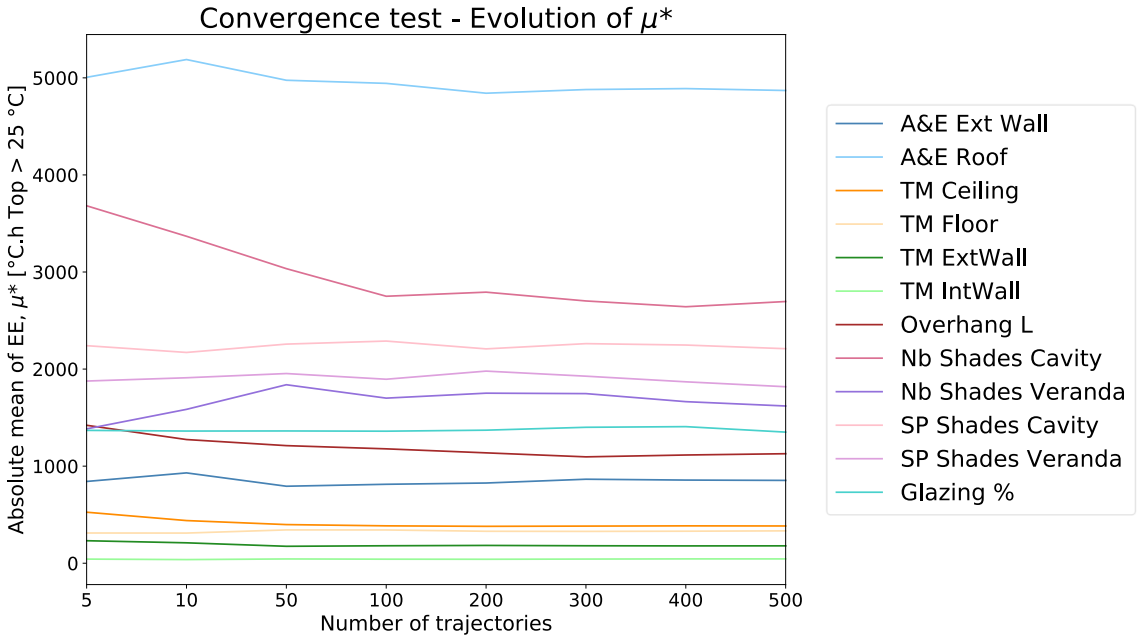

Figure 83 - Convergence of the absolute mean of μ*

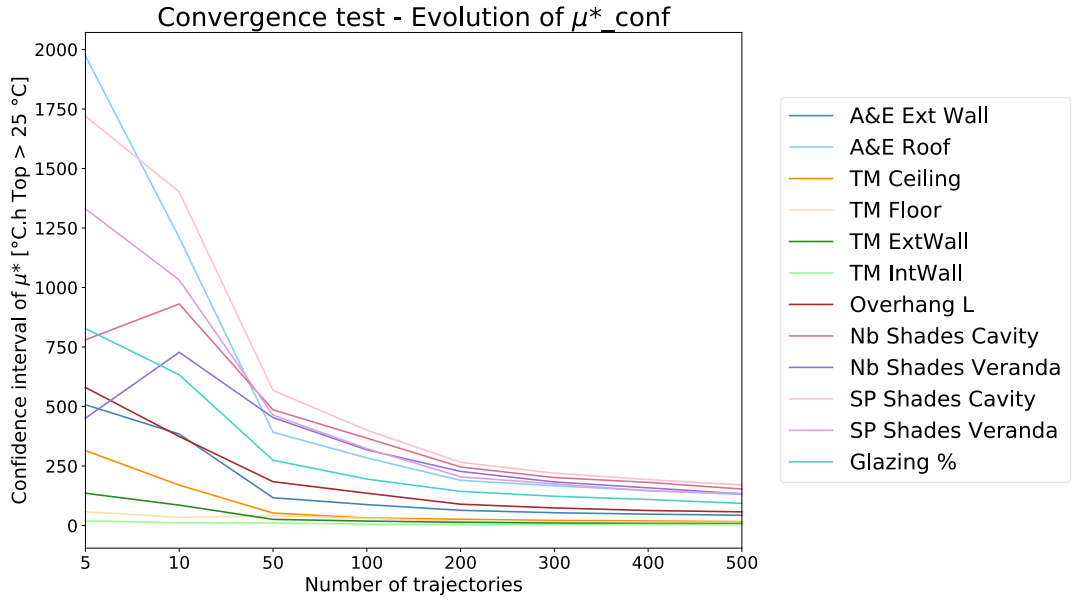

Figure 84 – Convergence of the confidence interval of μ*

From Figure 83 and Figure 84, we can observe that from 50 trajectories, clusters of parameters are well defined. The ranking convergence is obtained from 10 trajectories, while clusters are identified even from 5 trajectories. From 50 trajectories, the confidence interval decreases highly, and indexes are more stabilized. For the 500 trajectories, the indices convergence is better but the additional simulation time (5 hours when parallelized on 15 processors for *tr* = 500 versus 45 min for *tr* = 50) is not worth the extra calculation for the purpose of our study. As the aim of the Morris method is to identify clusters of parameters in a timely efficient manner, we consider that *tr* = 50 is enough to obtain convergence in the context of our study.

4.2.2 **Design case with natural ventilation**

In Figure 85, we present the results for the future typical summer in Roissy (model IPSL). The Figure 85-left presents results with parameters 1 to 14, with the most significant parameter on the summer thermal discomfort being the number of windows opened, by far in comparison to the other parameters. The objective criterion for these two simulations is the sum of degree-hours above a fixed threshold of 25 °C. In Figure 85-right the same results are presented but without parameter 13, and all windows are fully opened. We can observe that the magnitude of thermal discomfort is reduced by a factor 8. In Figure 85-right, as the natural ventilation potential can be fully exploited, the dynamics of the indoor environment are different. A high value of μ* is an indication of a high influence of the input parameter on the output. The error bars represent the μ* confidence intervals.
We can distinguish three different clusters of parameters:

- **Parameters with high μ*:** the set-point operative temperature conditioning windows opening, the glazing percentage, ceiling and floor thermal mass and the optical properties of the roof coating;
- **Parameters with medium μ*:** the four parameters related to shading, the overhang length and the exterior wall thermal mass;
- **Parameters with low μ*:** the interior wall thermal mass and the optical properties of the exterior wall.

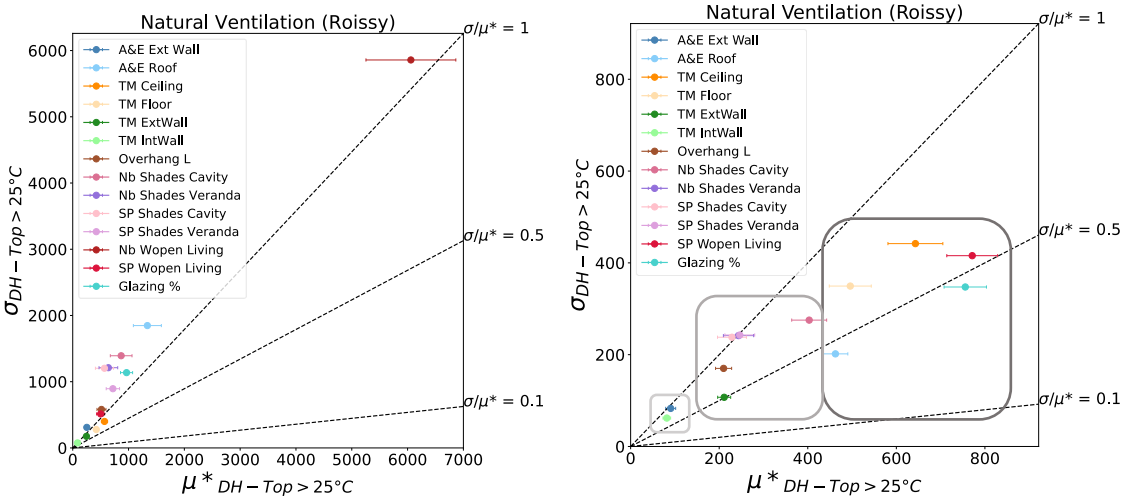

Figure 85 - Morris results for simulations with natural ventilation in Roissy future climate (model IPSL)

According to the classification proposed by (Garcia Sanchez et al., 2014), a value of $\sigma/\mu* < 0.1$ indicates that the input parameter j has a linear effect, whereas a value of $\sigma/\mu* > 0.5$ indicates that the input parameter is either nonlinear, either has interactions with other input parameters Most parameters have a value of $\sigma/\mu* > 0.5$ or close to 0.5.

4.2.2.1 Indicator for summer thermal comfort as SA objective function

The indicator that is the SA objective function can be of great importance. In the context of building energy simulations, researchers analyze different outputs such as the building energy consumption, energy peak power, life cycle analysis, or summer thermal comfort. For this latter, researchers analyzing summer thermal discomfort usually count the number of hours above a certain threshold, or the degree hours above a certain threshold. In this chapter we quantify the summer thermal discomfort at each time step t if the indoor operative temperature is above the threshold, as the temperature difference between the operative temperature and the threshold temperature (Equation (73)). Then, we sum these °C.h (DH) of summer thermal discomfort (Equation (74)).

$$std(t) = (T_{operative,t} - T_{threshold,t})_{T_{operative,t} > T_{threshold,t}} \quad (73)$$

$$DH = \sum_{t=0}^{n\Delta t} std(t).\Delta t \quad (74)$$

The choice of the temperature threshold is debatable. (Gondian, 2019) used a fixed threshold of 28 °C, equivalent to the calculated comfort temperature from the standard EN15251 during their period under study. (Breesch & Janssens, 2010) used the number of weighted temperature excess hours, based on the PMV model. Some authors do not mention the threshold chosen. After trial and error, we believe that the threshold must be chosen in accordance of the case-study. Indeed, if a threshold is chosen too high, the actual period of operative temperatures above that threshold might be limited. For this purpose, we display the operative temperature variation for all the simulations conducted for Figure 85 right in Figure 86. In grey is displayed, at each hour of the summer period, the operative temperature from each of the 700 simulations. In blue is the median operative temperature amongst all simulations at each hour. As the building is naturally ventilated, it is possible to use the comfort standard EN 15251 and we can observe a maximum value of around 31 °C, for which the standard is still applicable when there is air movement. During the day, windows might be closed if the interior temperature is inferior to the outdoor temperature, so using the standard would only be applicable if fans are employed inside the apartment. However, in Figure 86 we observe that the median operative temperature never reaches above this limit, meaning that many simulation results would not be included in the calculation of the summer thermal discomfort if the chosen threshold was the EN 15251 category I or II limit. A fixed threshold of 25 °C seems to be a good compromise.

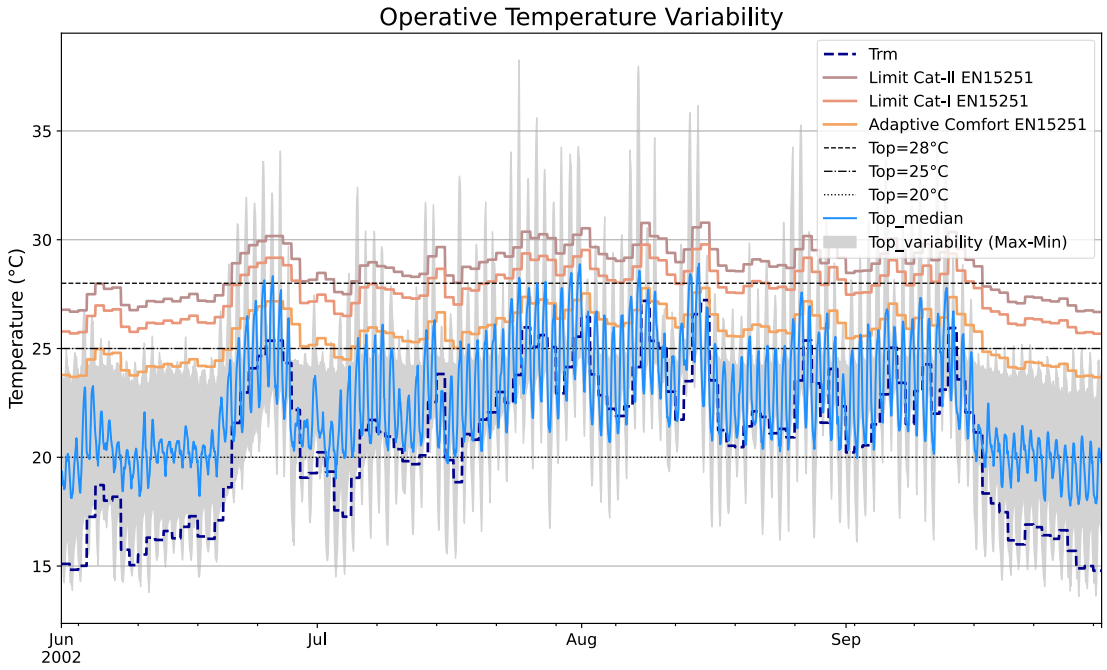

Figure 86 - Operative temperature from the 700 Morris model runs during the summer period – Future typical climate of Roissy, model IPSL

We analyze a warm sequence during the future typical summer more in depth, at the end of July (Figure 87). During this warm period, we can observe that for 9 consecutive days, at least 95 % of the operative temperatures reach above the 25 °C fixed threshold during the day. A lower threshold, i.e. 20 °C, allows encompassing the night temperatures as well. We can also observe a large variation in operative temperature: On the 24th of July around noon, the operative temperature variation is of around 14 °C. On that same day, 50 % of the operative temperatures have a variation of 2.5 °C, and 90 % of the operative temperatures have a variation of 7°C, indicating that the highest variation is found in the extremes. This could be expected because large variations are chosen in the input parameters range, i.e for the glazing percentage or the optical properties of the exterior coatings. Overall, the operative temperature variation follows the exterior temperature variations (i.e the 24th July midday or the 28th July morning).

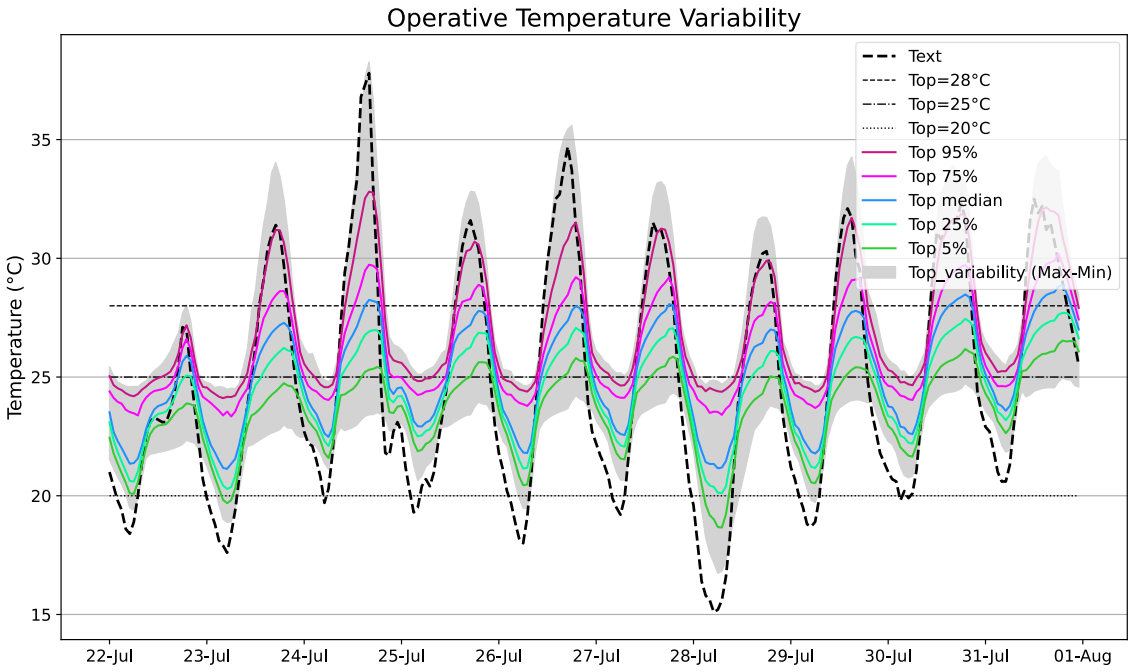

Figure 87 - Operative temperature from the 700 Morris model runs during a warm sequence of the summer period – Future typical climate of Roissy, model IPSL

In Figure 88, we present the results for two other fixed thresholds: 20 °C and 28 °C. We can observe that the results are different in parameters ranking: With a threshold of 20 °C, the set-point temperature controlling the windows opening for natural ventilation is the main parameter to reduce summer thermal discomfort hours above 20 °C, while for a threshold of 28 °C this parameter has less impact and the thermal mass and glazing percentage have more importance. However, the parameters clusters are similar for the thresholds at 28 °C and at 25 °C. Note that for these simulations the number of windows opened is the maximum (three out of six on the North and South facades). For the rest of the analysis, we present the results for the intermediate threshold of 25 °C.

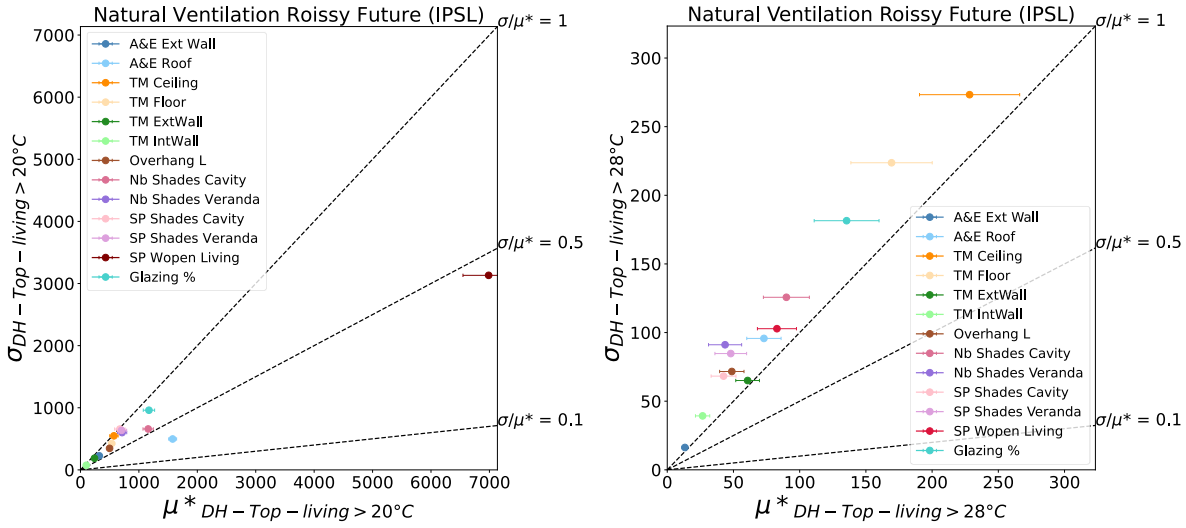

Figure 88 - Morris results for two different thresholds for summer thermal discomfort in Roissy future typical summer

4.2.2.2 Sensitivity to the climate model

The analysis was run independently for the four climate models for the future typical year in Roissy. The model with the lowest summer temperatures (CNRM) and the one with the highest (HadGEM) are shown in Figure 89. While the magnitude of discomfort is different, the different parameters clusters remain similar. However, the ranking is different. For the

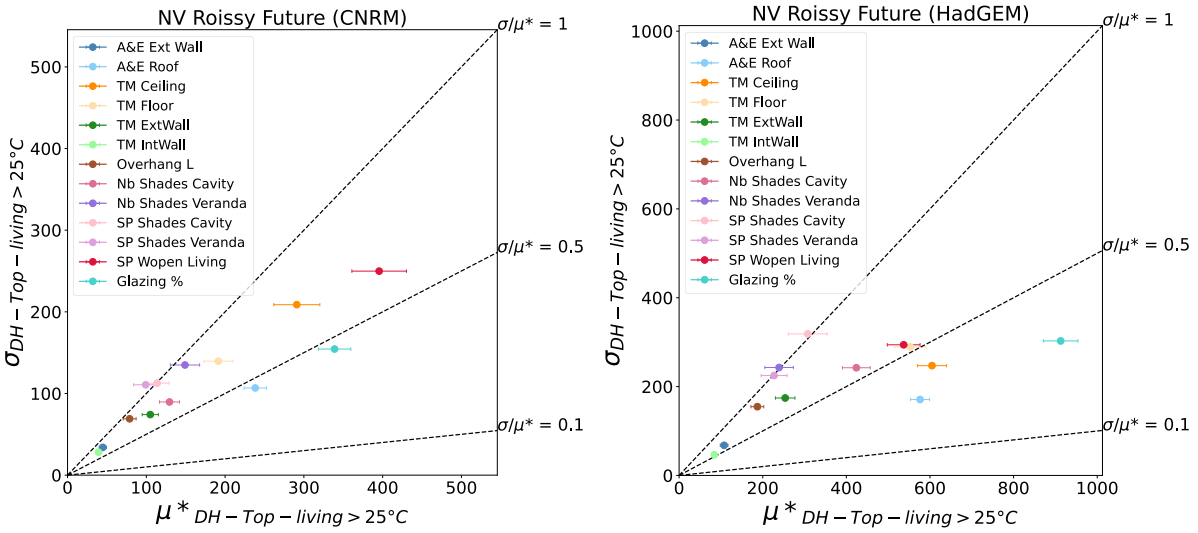

Figure 89 – Sensitivity of results to climate model – Natural ventilation in Roissy future typical summer

model leading to the lowest summer thermal discomfort in Roissy during future typical summer (CNRM, Figure 89-left), the set-point temperature for windows opening is most important, while it is in 3rd position for the higher model. This can be explained by the fact that at moments when night temperatures are above 24 °C (which occurs for the model HadGEM that contains an intense heatwave), then this parameter becomes insignificant. Glazing percentage, ceiling and floor thermal mass, and properties of the roof coating are still in the same order for the two models and are in the cluster with high μ*. The glazing percentage has a strong impact since it controls both the amount of solar radiation entering the living space, and the natural ventilation airflow entering through the windows. The ceiling and floor thermal mass have a strong impact since the apartment is naturally ventilated, their thermal mass has higher impact than the one of the walls, which can be explained by their larger surface area. Indeed, all solar radiation entering the living space is treated as diffuse and split uniformly amongst the surfaces (see section 2.4.2.1), so a larger quantity of radiation is redistributed towards the ceiling and floor than on the walls. The longwave radiation is also redistributed in a uniform manner. As the roof has a large area, the exterior coating of the roof receives a large amount of solar radiation during the day, and it is an impactful parameter on the summer thermal discomfort. In the medium sensitivity cluster are found the parameters related to reducing the incoming solar radiation into the living space. The parameter number of shades of the cavity fits within the cluster with medium μ*, while for the two other models for the warmer models (IPSL and HadGEM) this parameter gets closer to the cluster with high μ*. This can be explained by the fact that when the living space overheats too much, the incoming radiation from the cavity needs to be reduced. Indeed, the amount of solar radiation entering the living space is higher from the cavity than from the veranda, due to a lower floor area. In the veranda, most solar radiation falls and is absorbed by the veranda floor, while in

the glazed cavity a larger amount is transmitted through the windows towards the living space. Furthermore, as all radiation entering the living space is treated as diffuse, no direct radiation enters the living space from the veranda. Finally, two parameters are in the lower cluster: the thermal mass of the interior wall and the optical properties of the exterior wall. This can be explained because the interior wall is not exposed towards the outdoors and has a surface six times smaller than the ceiling and the floor. The exterior wall coating, exposed West, receives less solar radiation per area than the roof, and has a surface area six times smaller than the roof.

In Figure 90, the Morris analysis is conducted for the same run as in Figure 85-right but we analyze the impact of the design variables on the indoor environment of the glazed cavity and of the veranda. For comparison, results are presented for the same climate sequence and for the same summer thermal discomfort threshold. In the glazed cavity, the parameters with the most impact are the ones related to the shading of the cavity, the ceiling thermal mass, the glazing percentage and the optical properties of the exterior wall. This latter parameter can be explained by the fact that in absolute surface area, the difference of the incoming solar gains received by the roof and by the wall is lower than in the living space. The glazing percentage of the living space has an impact as the cavity receives solar gains from the veranda passing through the living space. Also, when the glazing is reduced it is replaced with the exterior wall, therefore the solar radiation falling on this wall is absorbed (instead of being transmitted) and contribute to heat the glazed cavity. The thermal mass of the ceiling coupled to the natural ventilation are probably enough to dampen the incoming solar gains from the roof as the exterior properties of the roof coating do not impact the indoor environment of the glazed cavity nor the veranda. The difference with the living space is that the windows are constantly opened during the summer period when the zone temperature is inferior to the exterior temperature, so natural ventilation potential can fully be used even when temperatures are cold. In the veranda, as expected the most impactful parameters on the indoor discomfort are the parameters related to shading the south façade and the overhang, the glazing percentage and the ceiling thermal mass as in the glazed cavity.

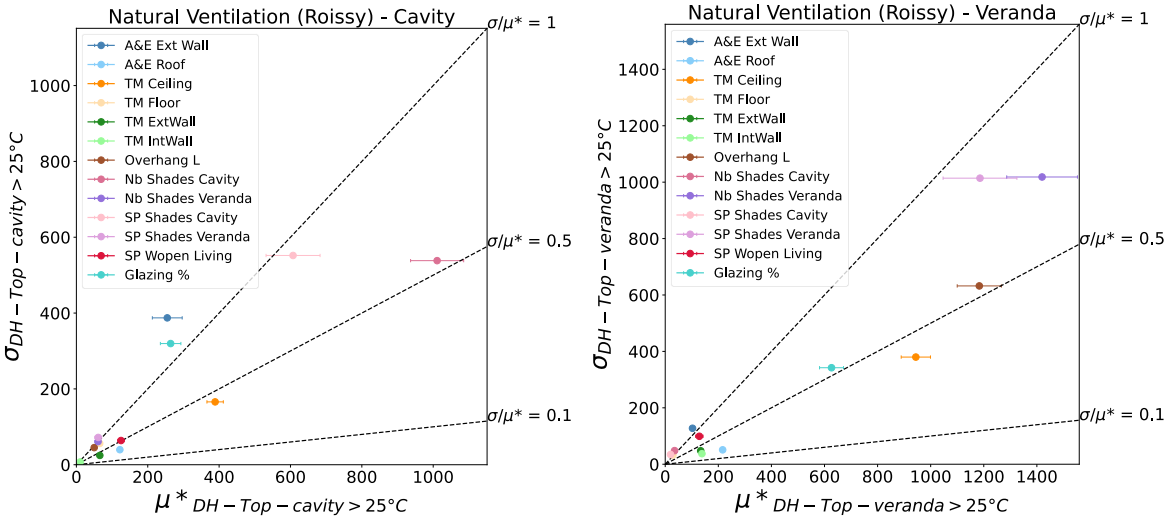

Figure 90 – Morris results for simulations with natural ventilation – Impact on the glazed cavity and veranda indoor environments in Roissy future typical summer

4.2.2.3 Sensitivity to the case study city

In Figure 91, results with natural ventilation are presented for the city of La Rochelle and Carpentras. In La Rochelle the model IPSL is selected as it does not contain a future heatwave, it is the third warmest model. In Carpentras, the second warmest model is selected. We can distinguish the same clusters as in Roissy. In La Rochelle, where the summer thermal discomfort value (sum of degree hours above the threshold) is lower, the distinction between the first and second cluster of parameters is well defined, and we can assume that parameters of the first cluster contribute largely to reduce summer thermal discomfort. In Carpentras, the discomfort level is five times higher than in La Rochelle, and the most impactful parameter is the roof coating absorptivity/emissivity. It seems that the natural ventilation potential is reduced as the set-point for windows opening has less importance, and the shading of the glazed cavity becomes a more impactful parameter, as was already noticed for the warmest model in Roissy.

The sensitivity of the results for these cities to the different climate models is presented in Appendix B. In La Rochelle, the roof coating properties become more impactful than the set-point temperature for windows opening for the warmer models, as noticed also in Roissy and Carpentras. In Roissy this parameter has a higher importance, which might be due to the fact that the summer nights are cooler than in La Rochelle. In Carpentras, for all models the properties of the exterior coating followed by the glazing percentage are the most impactful parameter. As the city of Roissy showcases an indoor summer thermal discomfort level in between those of La Rochelle and Carpentras, next results are presented for these two latter cities.

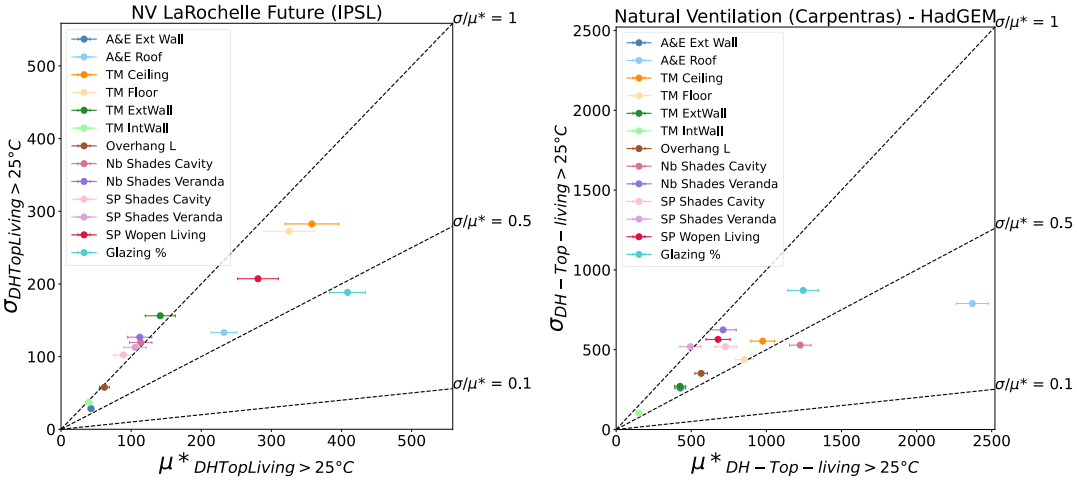

Figure 91 - Morris results for simulations with natural ventilation in La Rochelle and Carpentras future typical summers

4.2.3 Design case with mechanical free-cooling

Results for parameters 1 to 12 and 15 are introduced in Figure 92 for La Rochelle and Carpentras during the future typical summer sequences. As in the previous results, the glazing percentage has the most impact in La Rochelle and the roof optical properties in Carpentras.

The Delta FC (parameter n°15) is the third most important parameter in La Rochelle but in Carpentras it appears in the lower ranking than all parameters related to shading. In Appendix B, results are presented for the present climate, for which we can observe that the thermal mass has a higher impact in La Rochelle and Roissy than in the future, but not in Carpentras. During the present climate the combination of ventilation and thermal mass is the main player in the cooler climates. In Carpentras, the thermal mass has less effect probably because as the airflow rates through mechanical ventilation are much lower than through window opening, the free-cooling system, combined with the thermal mass is probably enough to reduce indoor summer thermal discomfort.

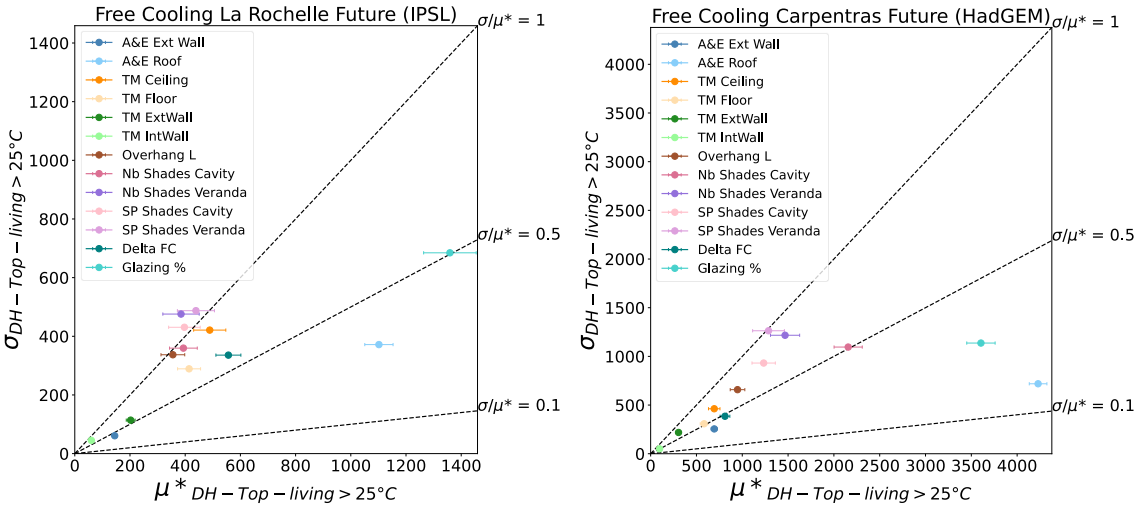

Figure 92 - Morris results for the free-cooling in La Rochelle and Carpentras future typical summers

4.2.4 **Design case with earth-to-air heat exchanger**

Morris results are presented in Figure 93 for input parameters 1 to 12 and 16 to 19. Similar to the simulations with natural ventilation, the airflow rate is the parameter that has the most impact to reduce summer thermal discomfort. The parameters glazing percentage and roof optical properties have a strong impact as previously witnessed. However, the constructions thermal mass has very little impact on the summer thermal discomfort in comparison to the other parameters. This can be explained by the fact that the EAHX provides cool air to the living space both during night and daytime, contrary to the natural ventilation and free cooling solutions, that provide cool air mostly during nighttime. The length of the pipe has a low impact on the summer thermal discomfort in comparison to the airflow rate. However, the depth has a higher significance given its variation range. The set-point temperature has very little influence. The results during the present period and in Roissy are in Appendix B, they are similar to the results presented in Figure 93.

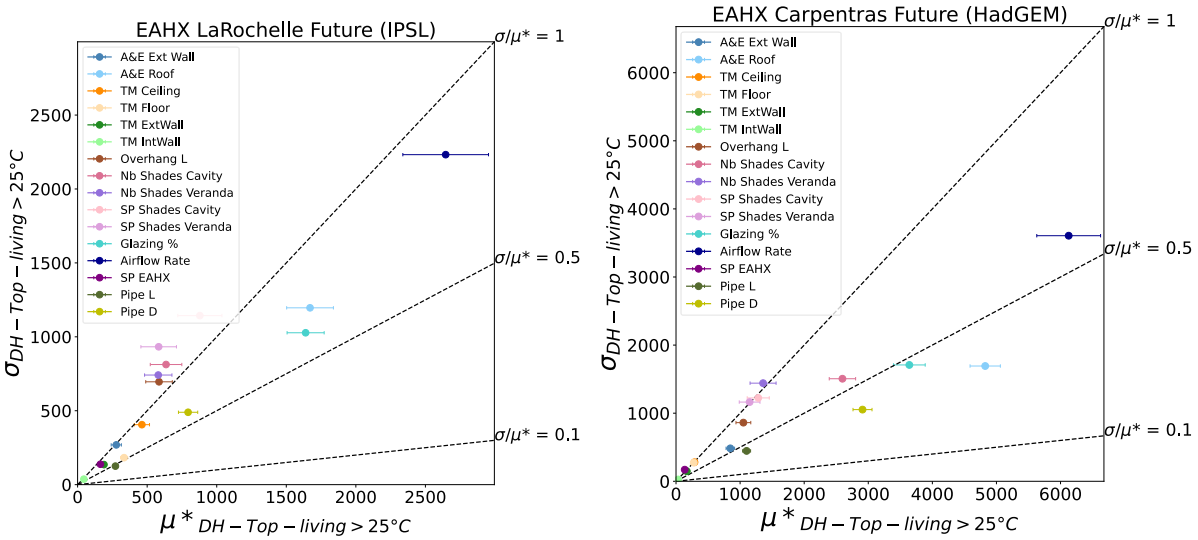

Figure 93 - Morris results for EAHX in La Rochelle and Carpentras future typical summers

4.2.5 **Comparison of the three ventilative cooling strategies**

The three ventilative cooling strategies (natural ventilation, mechanical free-cooling, and air earth tube) have been evaluated separately. For the simulations with natural ventilation and earth tube, the parameters controlling the airflow rate were found to be the most impactful. For the simulation with the free-cooling, it was the third impactful parameter in La Rochelle and had less impact in Carpentras. These results can be explained mainly by the variation in airflow rate in the three simulations. In the simulations with natural ventilation, airflow rates are much more elevated than for the free-cooling and EAHX due to the large window surface area. Even for the lowest window size, windows still have a large surface area. Therefore in Figure 85-left, when we vary the number of windows opened from 0 to 3, is the most impactful in comparison to the other parameters by far. The airflows for the simulations with the free-cooling vary between 0.6 ACH and 3 ACH with the Delta FC variation. However, during the warmest periods of the summer, airflows tend to be closer to 3 ACH even with the lowest Delta FC, because night temperatures are more elevated. The set-point temperature is 20 °C and the highest delta 8 °C. During the warmest nights, for instance if the operative temperature is about 28 °C, the delta will have no more influence because the airflow will be at its maximum. This is why it only has a low impact during the future typical climate in Carpentras, as night temperatures will be mostly warm. For the simulations with the earth-to-air heat exchanger, the airflow varies amongst the simulations between 0.6 and 3 ACH, so even during warm periods some simulations display low airflow. This parameter induces higher variations than the Delta FC for the free-cooling. But in comparison to the natural ventilation these airflow rates are lower, so it leads to lower variations.

In Figure 94 we compare the operative temperature variation during the warmest week of the future typical climate in Roissy. At each time-step is highlighted the median operative temperature for each passive cooling solution. We can observe that during daytime the EAHX solution leads to lowest operative temperatures (median) but for the maximal it is the free-cooling. During the nighttime, simulations with natural ventilation (median and lowest) lead to the lowest temperatures. Simulations with natural ventilation during nighttime also

showcase the highest temperatures, this is because in the worst design no windows are opened, whereas with free-cooling and EAHX there is always a minimum airflow. This is why we observe a much larger difference between operative temperature maxima and median than between median and minimum for the natural ventilation simulations. Simulations with the free-cooling lead to the highest operative temperatures during the day, because night ventilation reduces to a greater extend the air temperatures during the night and therefore the operative temperature during the day, with the thermal mass effect. During the nighttime, the median and lowest temperatures of the earth tube and free cooling are closer, this is because during the night the EAHX temperature outputs are closer to the air temperature. The ideal scenario would therefore be to use the EAHX during the day and open windows during the night, as the airflows are much higher they are more efficient to reduce the indoor operative temperatures. However, at the moment it is not possible to model the earth tube in combination with the Airflow Network with EnergyPlus.

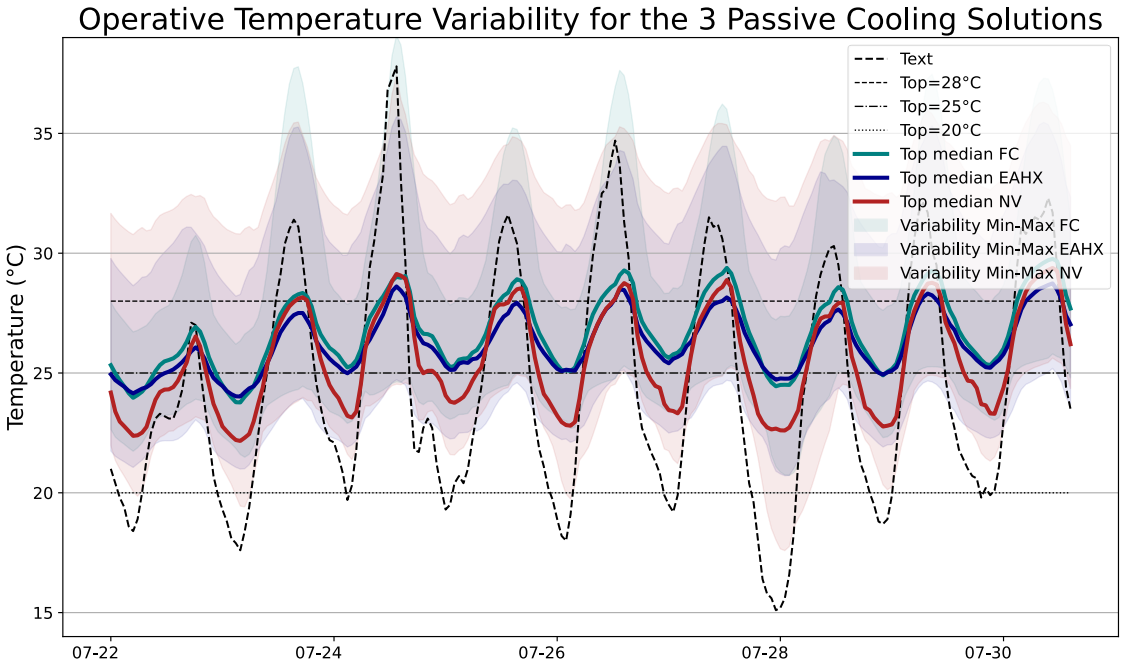

Figure 94 - Operative temperature for the three passive cooling solutions

4.3 Detailed analysis during the warmest summer days

The results from the Morris simulations provided insights on the most impactful parameters for different case-study passive cooling systems in a variety of cities and climates. To analyze more in depth the influence of the different design variables on the indoor operative temperature of the living space, we use the Sobol method. From the Morris computed standard deviations σ, we could conclude that the behavior of most parameters is not linear, or that parameters have interactions with each other. However, the Morris sensitivity indexes do not allow to distinguish if a high value is associated with non-linearity or parameter interactions. For this purpose, we use the Sobol method, which allows computing variance-based indexes for j-1 orders (with j the number of parameters): The first order is linked to the influence of a single input parameter on the model outcome, the second order is related to the influence of a combination of two input parameters on the model outcome, and so on. As the calculation of high orders is computationally intensive, only the calculation of second orders is implemented in the Python *SaLIB* library. The total orders are also calculated, and most authors analyze only the first and total orders since the difference between the two provides indications on the higher order effects. Because the computational cost is elevated, we reduced the simulation period to the warmest 12 days of each weather file.

We conduct the analysis for the present, future typical and future heatwave in Roissy to understand the evolution of the input parameters amongst the warmer climate sequences. The climate of the future heatwave in Carpentras is also analyzed to compare with the climate of Roissy. The two future heatwaves were selected as IBM heatwaves with a 5-years return period within the years 2040-2069, according to Figure 78. The heatwaves were selected with high solar radiation. It was difficult to find heatwaves with very low wind speeds, which might be due to the complexity to calculate accurate projections for wind in climate models. However, the wind speed is usually strongly influenced by the microclimate surrounding the building (which was not modelled in these simulations), so the wind speed calculation would surely be different. Both selected heatwaves have low relative humidity, which does not impact the behavior of the building envelope since the hydrothermal effects are not modelled. The relative humidity will impact the comfort of the occupants but for this analysis we only investigate the indoor operative temperature.

For the simulations with the natural ventilation, the Morris results showed that the most impactful parameters, consistent amongst the cities, are the number of windows opened, the glazing percentage, the ceiling and floor thermal mass, and the optical properties of the roof coating. We select these design variables for the analysis with Sobol. Regarding the number of windows opened, as the number of windows cannot be discretized, we vary the opening coefficient of each openable window, with the opening coefficient of all windows (of the living space) changed simultaneously. For the analysis with Sobol we assume that there is no overhang on the south façade and that no shading is used on the North and South facades. This assumption is made to analyze the worst case-scenario with high solar gains and not to be influenced by the presence of shading to analyze the results. The design variables for the analysis with the Sobol method are presented in Table 29.

Table 29 – Range of variation of design variable for the SA with the Sobol method

N°	Category	Parameter	Abbreviation	Location	Min	Max	Unit
2	**Building envelope**	**Optical properties of exterior coating***	A&E Roof	Roof	0.05	0.95	-
3		**Thermal mass** (material density ρ)**	TM Ceiling	Ceiling of the living space	650	2300	kg/m³
4			TM Floor	Floor of the living space	650	2300	kg/m³
8	**Bioclimatic architecture**	**Glazing %**	Glazing %	Windows of the living space	15	95	%
13	**Ventilation control strategy**	**Percentage of windows opening**	% Wopen	Windows of the living s - pace	10	100	%
14		**Windows opening Control Set-Point: Operative Temperature**	SP Wopen	Windows of the living space	15	24	°C

4.3.1 Convergence of the variance-based sensitivity indexes

First, we analyze the convergence of the variance-based sensitivity indexes (S1: Figure 95, ST: Figure 96, and S2: Figure 97). As for the Morris method, there is no practical guidance about the number of samples $N_{samples}$ needed to reach convergence. This is case-study specific and is conditioned by the complexity of the model itself, and by the behaviour of the different design variables. At a first glance, simulations were run from 50 to 3000 samples. The number of simulations needed is given by Equations (75) and (76). Since we conduct the analysis for 6 design variables j, the number of samples is multiplied by 8 for the calculation of the first orders only and by 14 for the calculation with the second orders (see section 2.5.1.2). The convergence test is made for the twelve warmest days during the future typical summer in Roissy with the climate model IPSL, for a discomfort threshold from an operative temperature of 25 °C. Running the 3000 samples resulted in 42,000 individual EnergyPlus simulations, which were run in parallel on 15 processors and took around 10 hours to compute.

$$N_{simulations\_Sobol\_S1S2} = N_{samples}.(2.j + 2) \quad (75)$$

$$N_{simulations\_Sobol\_S1} = N_{samples}.(j + 2) \quad (76)$$

The full lines represent the values of the indices, while the color spreads represent the confidence interval at 95 % for each design variable. We can observe that the parameters ranking convergence is observed from $N_{samples}$ = 100 (Figure 95). At 3000 samples, the indices values seem to have stabilized. For a more detailed convergence study, the indices convergence could be calculated using the quantitative indicators suggested by (Sarrazin et al., 2016). In Figure 97 we analyze the convergence of the second order indices. The indexes values decrease while convergence increase. It seems that even with 3000 samples the second orders are still unstable, and their uncertainty is high.

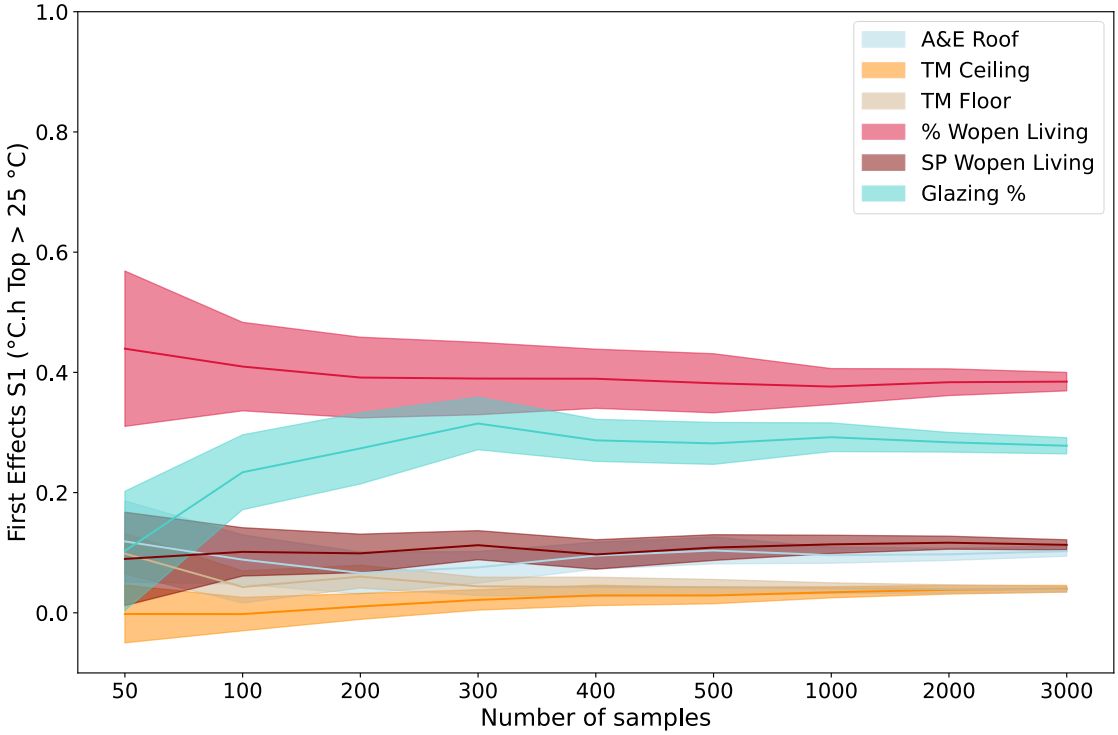

Figure 95 – S1 Sobol index convergence

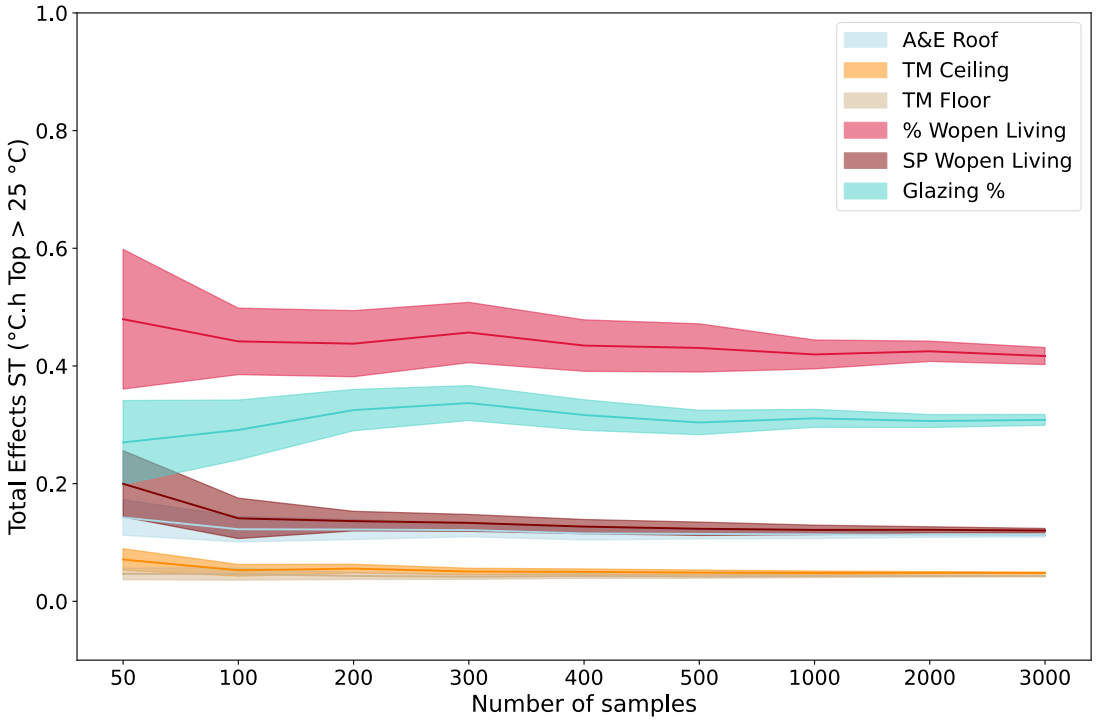

Figure 96 – ST Sobol index convergence

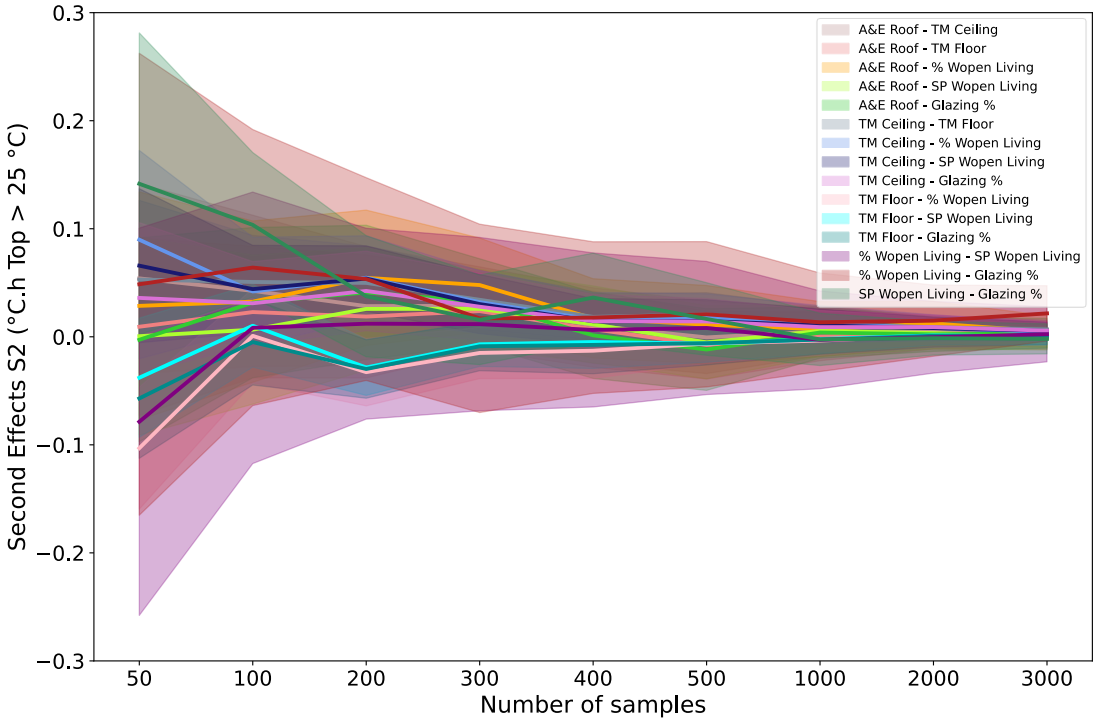

Figure 97 – S2 Sobol index convergence

4.3.2 Sobol indexes for different summer thermal comfort thresholds and high-order parameter interaction effects

We calculated the first, total and second Sobol indexes for four fixed summer thermal discomfort thresholds, they are 20 °C, 25 °C, 28 °C, and 31 °C, as we analyzed from Figure 88 that different thresholds lead to different conclusions. The results, for the warmest days of the future typical summer in Roissy with the model IPSL, are presented for the 3000 samples computed to have the lowest uncertainty of the second orders. We analyze the second indexes to understand the difference in between the first and total indexes that are stabilized.

At first, we analyze the results for a threshold at 20 °C (Figure 98 top). The three most important parameters are the percentage of windows opened, the set-point for windows opening and the glazing percentage. For these parameters there is a difference of around 0.05 between the Sobol total and first indexes. We find that there are interactions between the glazing percentage and the percentage of windows opened, which can be explained because they both control the amount of airflow that can enter by the windows. There are also interactions between the percentage of windows opened and the set-point temperature for windows opening, which control the amount of airflow and the time at which the windows are opened. For the lowest threshold of 20 °C, the parameters related to natural ventilation are the most important ones. In comparison with the Morris results (Figure 88 left) the set-point temperature for windows opening was the most important parameter by far, which can be explained by the fact that it is the only design variable in that simulation controlling when natural ventilation is available. The fact that only the warmest days of the summer are

simulated with Sobol can explain the difference with the results found with the Morris method.

Regarding the results for the threshold at 25 °C (Figure 98 bottom) similar conclusions can be drawn than for the threshold at 20 °C except that the set-point temperature allowing natural ventilation has less impact. This can be explained by the fact that this parameter varies between 15 °C and 24 °C and therefore above 25 °C windows can be opened all the time. In contrast, the glazing percentage has a stronger impact on the summer thermal discomfort hours above 25 °C, it is unclear if it is related to the natural ventilation potential or to the amount of solar radiation impacting summer thermal discomfort In the three cities, for simulations with the free-cooling system (Figure 92), for which the ventilation potential does not depend on the windows surface, the glazing percentage was also found to be one of the most impactful parameters on the indoor summer thermal discomfort hours, indicating that the window percentage might influence to a greater extent the summer thermal discomfort hours by solar gains than by natural ventilation. However, for the simulation with free-cooling the natural ventilation airflow is much lower than with natural ventilation.

For the results with the threshold at 28 °C (Figure 99 top): In the continuity of the two previous thresholds, the parameters related to natural ventilation have less impact on the summer thermal discomfort hours above 28 °C and this time the ceiling and floor thermal mass have a higher importance. The same was observed in the Morris results (Figure 88 right). The second orders give indications on the relationship between the thermal mass and the natural ventilation, between the thermal mass and the glazing percentage and between the glazing percentage and the natural ventilation. These results were expected since the thermal mass stores the cooling potential from the cool air during the night and release it during the day, while it also dampens the solar heat gains incoming during the day. The first, second and total orders related to the thermal mass are emphasized for this high threshold because the operative temperatures reach above 28 °C at times when the windows are closed since the operative temperature is inferior to the exterior temperature.

We then analyzed the results for a higher threshold at 31 °C (Figure 99 bottom), which is a rough limit for health-related risks. However, we can observe that the results do not converge since the sum of total orders is far from 1. We conducted a convergence analysis for this higher threshold which confirmed this conclusion.

With the Sobol method, if interactions are present in the model, the sum of the first orders is inferior to 1. For instance, for the summer thermal discomfort threshold at 25 °C, the sum of the first orders is equal to 0.96 while the sum of the total orders is equal to 1.05. The sum of total orders superior to 1 can be explained by the fact that the higher-orders are counted multiple times. Indeed, there is a second order of about 0.02, so the sum of first and second orders is of 0.98 and if second orders are counted twice (once as a second order of the percentage of windows opened and once as second order of glazing percentage), it sums up to 1 and not to 1.05. It is not clear if third orders interactions exist or if this difference is due to the index convergence.

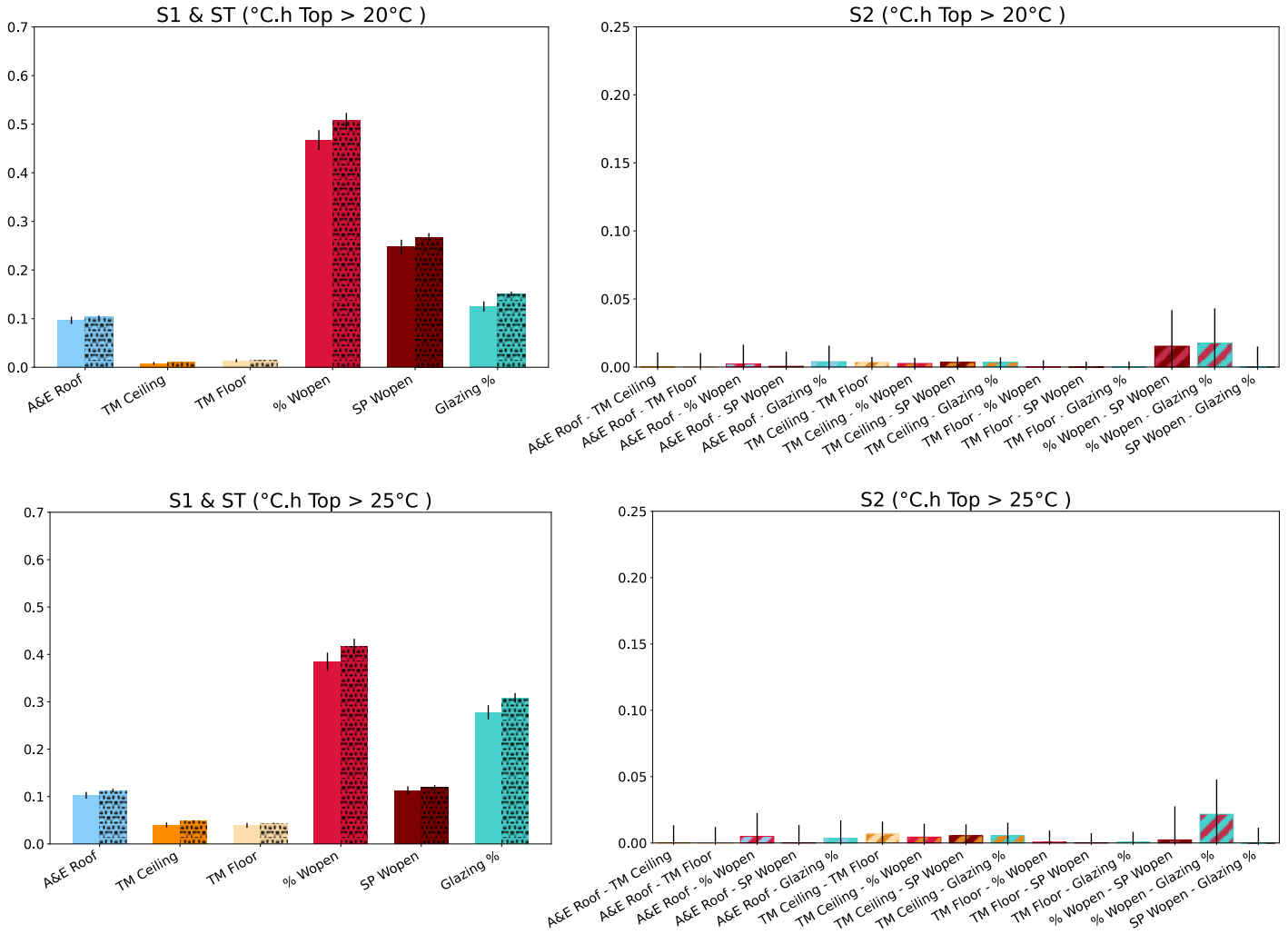

Figure 98 - Sobol indexes S1, ST (ST ≥ S1), and S2 for two thermal discomfort thresholds: 20 °C (top) and 25 °C (bottom) – 3000 samples for the climate of Roissy future typical during the 12 warmest days

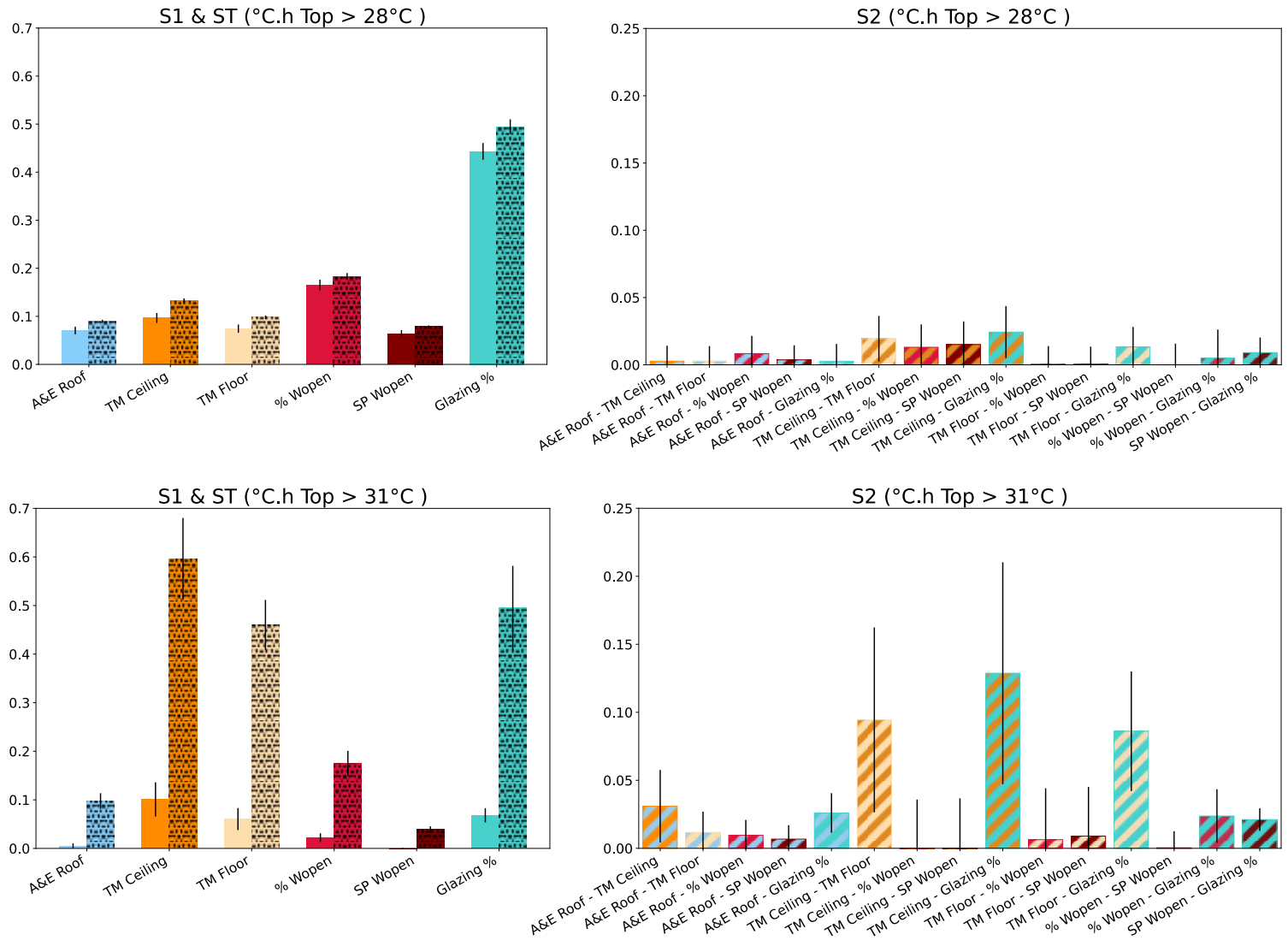

Figure 99 - Sobol indexes S1, ST (ST ≥ S1), and S2 for two thermal discomfort thresholds: 28 °C (top) and 31 °C (bottom) – 3000 samples for the

4.3.3 **Temporal analysis**

In this section, we present a temporal analysis using the variance based indexes. As the analysis is time-consuming, simulations are conducted on the eight warmest days for each climate sequence. The temporal analysis is presented for the present typical (Figure 100), future typical (Figure 101) and future heatwave (Figure 102) warm sequences in Roissy to study the evolution of the influence of design variables on the indoor summer thermal discomfort with changing outdoor temperatures. We also analyze the design variables' influence for the city of Carpentras under the future heatwave (Figure 103), which is the warmer climate sequence. For each warm sequence, we analyze from top to bottom: The ST Sobol total order sensitivity index, the operative temperature variation and the partial variance. The ST indexes are computed for a threshold of Top = 20 °C to encompass most cases, as during the present climate only a few simulations display results above 25 °C or 28 °C. For each design variable, the partial variance is calculated, it is the product of the Sobol index multiplied by the variance of the operative temperature above the 20 °C threshold (Equation (77)). The Sobol indexes are normalized from 0 to 1, but the analysis of the partial variance gives additional information of which input parameter impacts the summer thermal discomfort when there actually is a large variation in output. For the future typical climate sequence we used the results from the 3000 samples, but for the other climate sequences we ran the analysis for 500 samples, which is an acceptable compromise between simulation time (2 hours when parallized on 15 processors) and the convergence criterion. For the future typical climate sequence, due to a larger number of samples, we could analyze the second orders as well (Figure 101).

$$Pvar = V \times ST_j \tag{77}$$

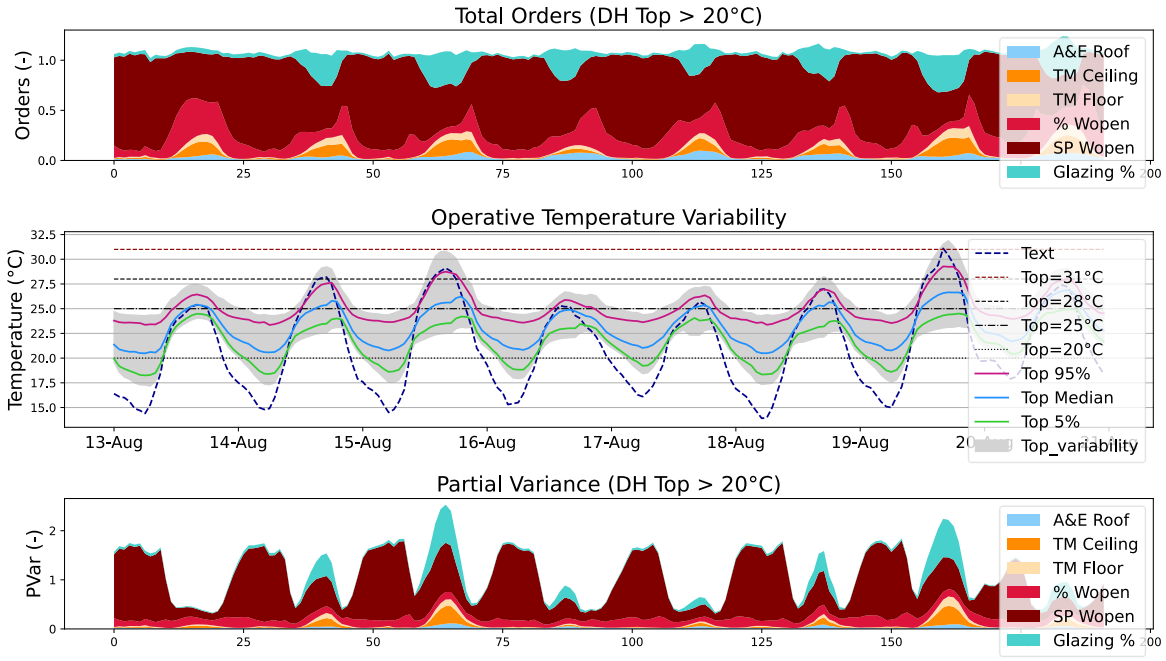

Figure 100 - Temporal analysis during the typical present climate in Roissy – 8 warmest days of the summer. Top: ST Sobol Index, Middle: Operative temperature, Bottom: Partial variance of each design variable

In Figure 100, we can observe that the set-point temperature for natural ventilation is the most important parameter on the summer thermal discomfort above 20 °C during the present summer in Roissy, which was already observed from the Morris method. Indeed, as the operative temperatures are between 17 °C and 25 °C, this design variable varying between 15 °C and 24 °C conditions in most cases the natural ventilation potential. The percentage of windows opened is also an impactful parameter to a lower extent, which could mean that the natural ventilation potential is enough to cool the building, as opening windows is more impactful than the quantity of airflow entering the living space. During the day hours, glazing percentage, ceiling and floor thermal mass and optical properties of the roof coating also have an importance, as they all impact the daily solar heat gains. During the day, the total orders are slightly superior to one, reflecting the presence of higher order interactions. As this occurs especially during the warmest hours, and as the natural ventilation parameters have the most impact, interactions are probably between the thermal mass and ventilation parameters.

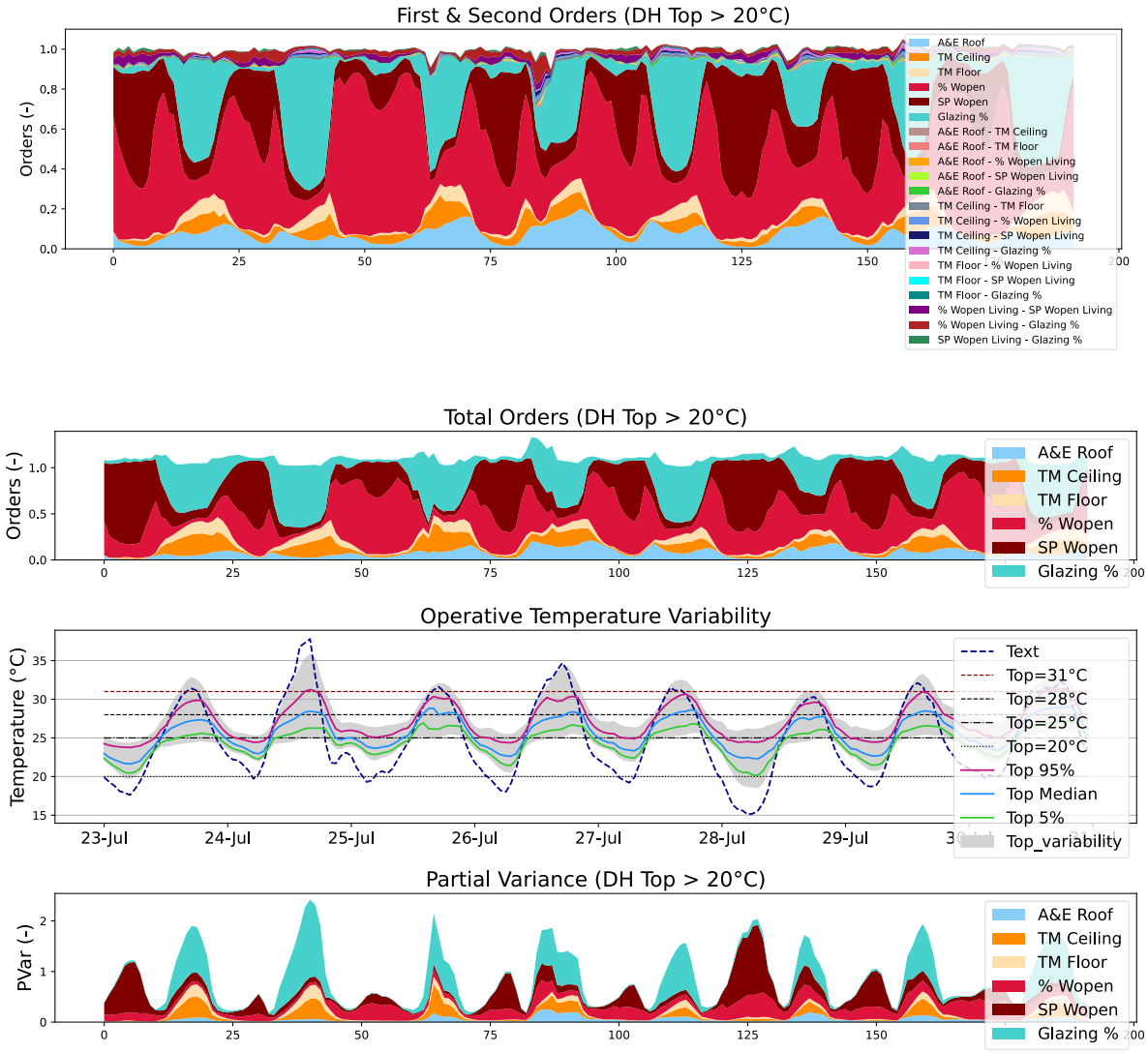

Figure 101 - Temporal analysis during the typical future climate in Roissy – 8 warmest days of the summer. Top: S1 and S2 Sobol Indexes, ST Sobol index, Middle: Operative temperature, Bottom: Partial variance of each design variable

In Figure 101 we can observe the difference between the stacked first and second orders and the total orders. Again, it is not clear if second orders have totally converged (since the sum of first and second orders is still inferior to 1 at times) or if higher order interactions exist. In Figure 101 and Figure 102, the set-point operative temperature condition the windows opening has less impact as the exterior temperature gets warmer, because operative temperatures inside the living space are warmer as well: During the future heatwave in Roissy (Figure 102), operative temperatures are most of the time superior to 25 °C, even for the best designs, so this parameter has no influence anymore. The glazing percentage has an impact during the daytime, as it influences the amount of solar heat gains entering the space, since no shading is used. As the climate sequences get warmer, the percentage of windows opening is more important which might be due to the fact that as the space overheats more, more natural ventilation is needed. We can observe that in Figure 101 and Figure 102, this time the sum of total orders is superior to 1 during the night. During the future typical climate, the percentage of windows opened has interactions with the set-point temperature, and with the percentage of glazing (stacked second orders Figure 101 and second orders from Figure 98). Indeed, we observe that the glazing percentage has influence during the night as well during the future typical sequence and to a greater extent during the future heatwave sequence. During the heatwave the set-point temperature for natural ventilation has no influence anymore so the interactions are probably related to windows opening percentage and percentage of windows, since this last parameter conditions the surface area of the incoming air.

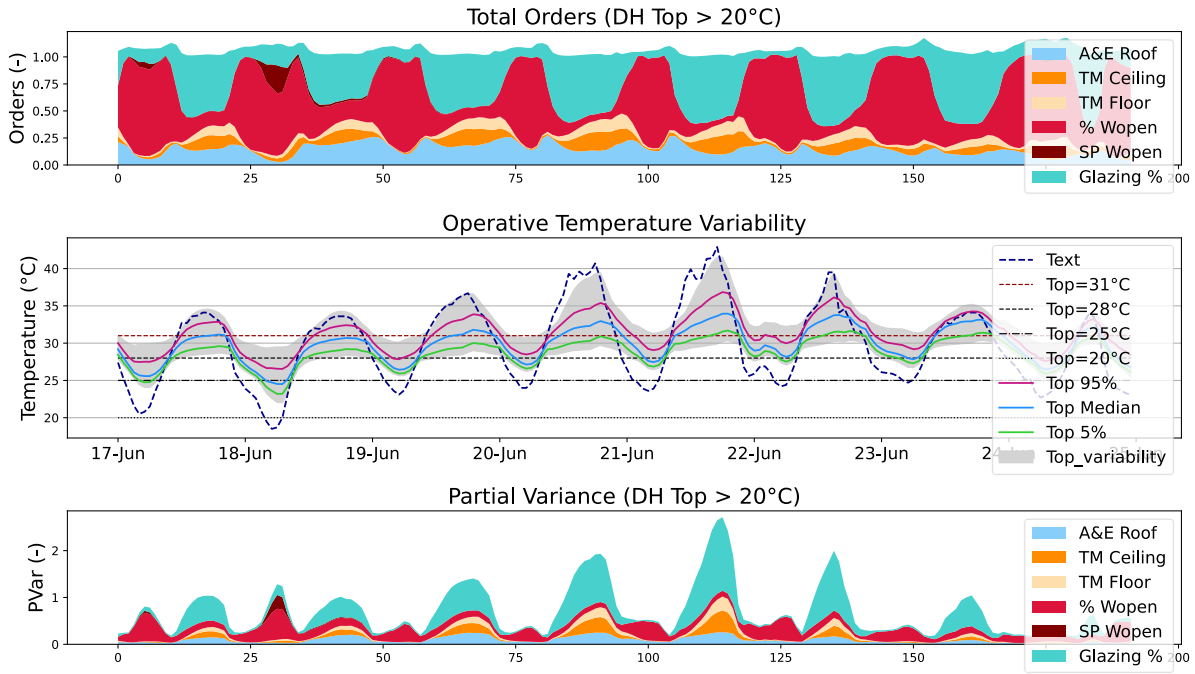

Figure 102 - Temporal analysis during the future heatwave climate in Roissy – 8 warmest days of the summer. Top: ST Sobol index, Middle: Operative temperature, Bottom: Partial variance of each design variable

We can also observe that the parameters related to the optical properties of the exterior coating of the roof has more influence during the heatwave sequence, which means that with a reduced natural ventilation potential, this is needed to reduce the incoming solar heat gains by the roof. The thermal mass has also more influence as the climate gets warmer, as it helps to store the cooled air during the night to release during the day, and to dampen the solar heat

gains. Analyzing the partial variances (bottom of Figure 100 to Figure 103), we observe that during the present climate, the temperature variation is greater during the night, as the operative temperature conditioning the windows opening is the driving parameter. During the warmest days the glazing percentage influences the partial variance. During the future climate sequences, the glazing percentage is the driving parameters as the variation is higher during the day. Results for the future heatwave in Roissy can be compared with those during the future heatwave in Carpentras (Figure 103). Results are similar but the optical properties of the exterior coating have more influence in Carpentras. This can be explained because the solar radiation received by the roof is 10 % higher in Carpentras than in Roissy. This parameter also has an influence during the night, at this moment only the coating emissivity influences how the heat gains can be released towards the sky by longwave radiation. In Carpentras the glazing percentage has an influence during the night, which can be because as temperatures are warmer, even more airflow is needed to cool the space. From Figure 100 to Figure 103, we can conclude that all parameters influence the indoor operative temperature at different times. As expected, the thermal mass influences during the day, while ventilation related parameters have an influence during the night. It is interesting to note that as temperatures are warmer, a high glazing percentage is needed during the night to increase the airflow whereas the opposite is required during the day to reduce the incoming solar heat gains. Furthermore, optical properties of the roof become more important as the space overheats. Regarding the operative temperatures, in the warmest days the 28 °C threshold is reached for all simulations (Figure 103). We added in Figure 100 to Figure 103 a fixed threshold at 31 °C that we consider a limit for health effects, especially for vulnerable people. We can observe that during the future heatwave it is reached for half of the designs during the day. It is necessary to emphasize that the investigated future heatwaves are not rare events, they will occur every five years according to the model projections (Figure 78).

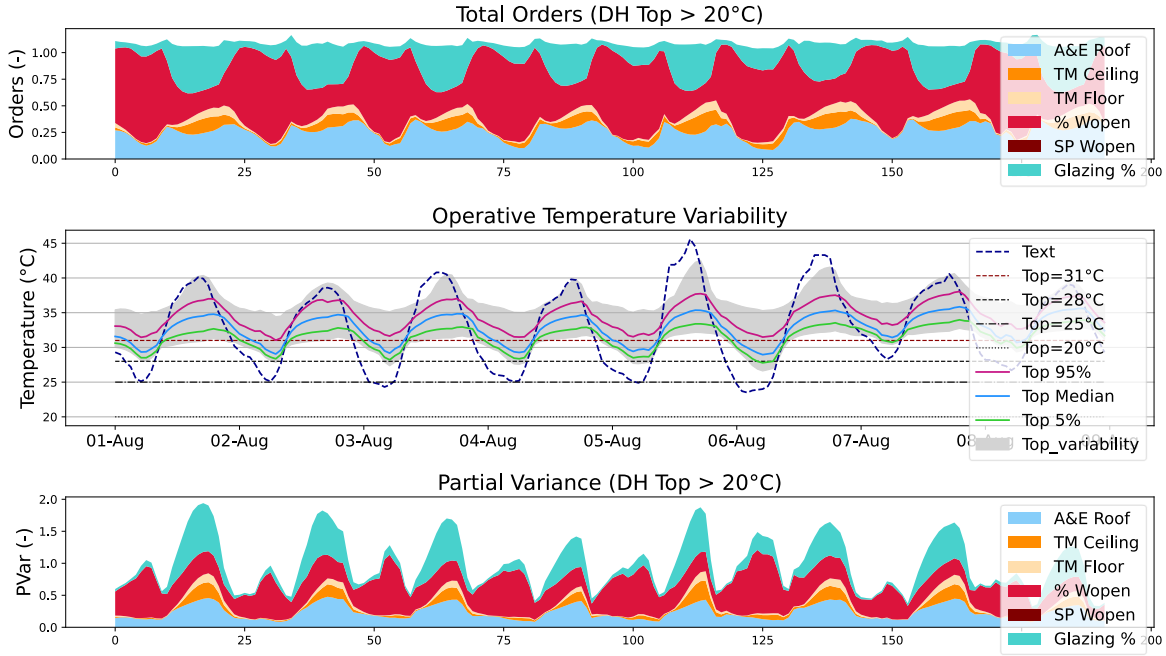

Figure 103 - Temporal analysis during the future heatwave climate in Carpentras – 8 warmest days of the summer. Top: ST Sobol index, Middle: Operative temperature, Bottom: Partial variance of each design variable

Designing robust designs for these extreme heat sequences with a short return period is therefore crucial. The selected heatwaves were matching the criteria of the health warning system, which is confirmed by the number of operative temperatures above the 31 °C health risk threshold.

4.3.4 Building robustness to outdoor heat and effect of solar protections

For the previous simulations, no shades nor overhang are used. Results are presented in this section for SA conducted during the future typical and future heatwave sequences in Roissy with solar protections (these parameters are fixed). The solar protections are interior shades on half of the windows of the North façade when the incoming solar radiation on each window is above 100 W/m², which occurs on most days from 8 am to 4 pm (note that the North façade is equipped with a 0.5 m overhang that is there for the glazed cavity maintenance). Additionally, an overhang of 1 m is also used on the South façade on top of the exterior windows of the veranda (Figure 104). According to Figure 90, the number of shades used on the veranda exterior windows have slightly more influence than the overhang length, however these are varied from 0 to 6, and using shades on all windows will considerably reduce the daylight entering the living space. For this reason, we choose to model an overhang, instead of shades.

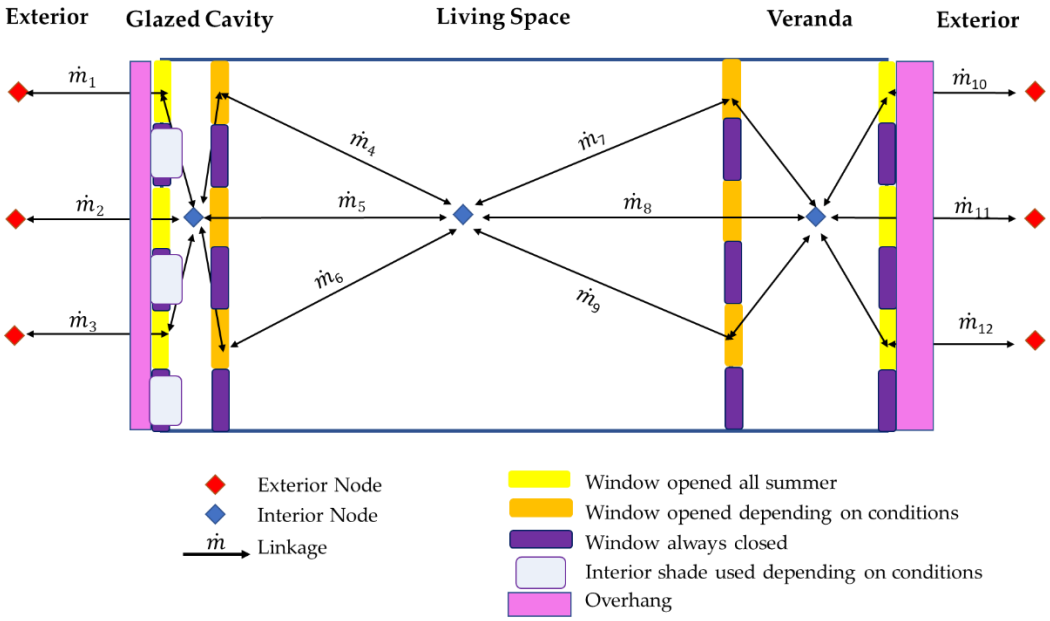

Figure 104 - Configuration with solar protections

In Figure 105, the operative temperature variation for the three climate sequences in Roissy are compared, for the configurations without solar protections. A fixed threshold at 28 °C is a simple representation of summer thermal discomfort. During the present climate, this threshold is almost never reached, even for the worst designs, except on the three warmest days. However, it is reached for half of the simulations during the future typical climate and for 95 % of the simulations during the future heatwave in Roissy. Compared to the variance of the operative temperature above the summer thermal discomfort threshold, it is much more

elevated for the future heatwave in comparison to the other climate sequences (Figure 102 bottom). The use of solar protections allows to reduce this variance, especially for the future typical climate the variance is closer to 0. However, during the future heatwave, even with solar protections the variance above the threshold is still elevated. This indicates that climate change effects decrease the building robustness to outdoor climate variations.

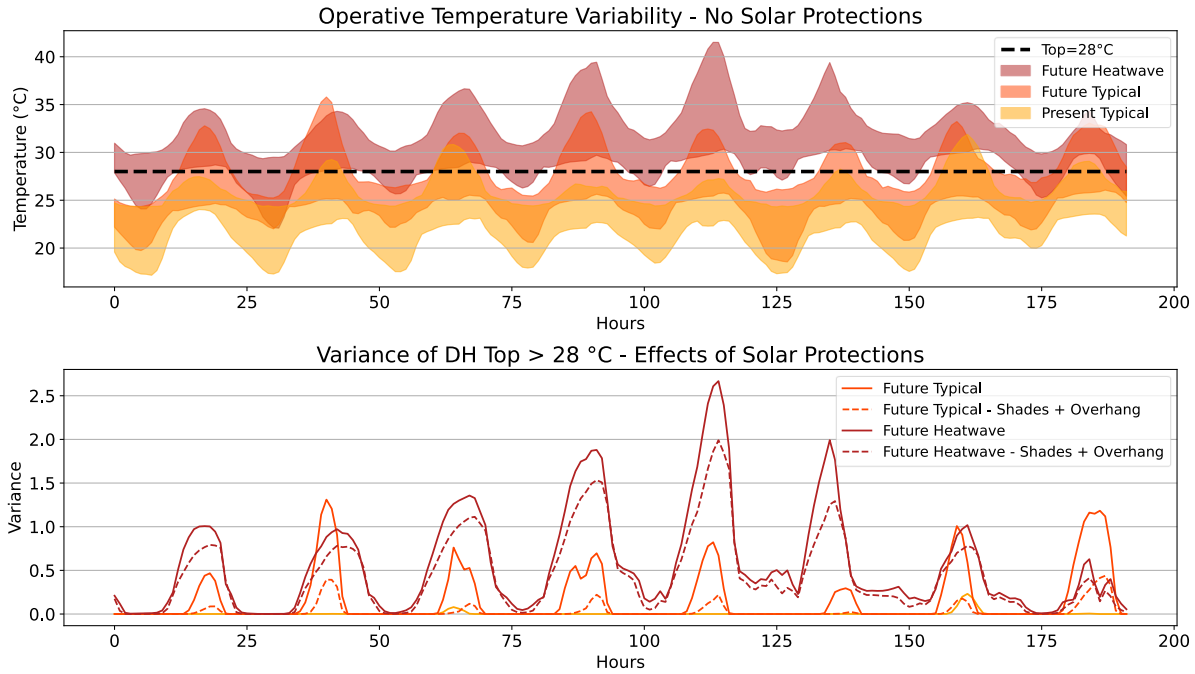

Figure 105 – Top: Operative temperature without solar protections, Bottom: Variance of summer thermal discomfort during the three climate sequences in Roissy with and without solar protections

4.4 Discussion on the sensitive design variables impacting summer thermal comfort

We analyzed the impact of different design variables on the summer thermal discomfort successively with two methods. The Morris method allowed us to distinguish important and less important design variables for the considered case-study. In all studied locations, for the future typical summer period, the parameters having the most influence are the ones related to the building envelope, namely the optical properties of the roof coating and the glazing percentage. In the warmest climate Carpentras, the optical properties of the roof coating are the most important parameters, whereas the most important in La Rochelle and in Roissy is the glazing ratio. This can be explained by the fact that in Carpentras the amount of solar radiation received by the roof is higher than in La Rochelle and in Roissy.

In the three cities, the parameters controlling the ventilation airflow for the different ventilative cooling strategies (i.e the number of windows opened, the Delta FC of the free cooling and the EAHX airflow rate) are also in the most important parameters clusters. This means that these ventilative cooling strategies largely contribute to decreasing the summer thermal discomfort. For the simulations with natural ventilation, the living space ceiling and floor thermal mass have a strong influence on the summer discomfort, in the three cities, even though in Carpentras their importance is less than the glazing percentage and optical properties of the roof, due to the reduced NV potential. For the simulations with mechanical free-cooling, thermal mass is an important parameter in Roissy and in La Rochelle, but in Carpentras it is not, which might indicate that the free-cooling potential is too low to reduce summer thermal discomfort in Carpentras. For the simulations with the EAHX, thermal mass of the ceiling and of the floor are parameters of second influence in La Rochelle and in Roissy, but of very little influence in Carpentras, both in the present and in the future.

Parameters related to reducing the solar gains entering the veranda and the glazed cavity (number of shades on exterior windows, shades set-point, and overhang length on the South façade) are constantly in the cluster of second importance, except the number of shades on the glazed cavity in Carpentras which becomes a more important parameter since it impacts the most the solar gains entering the living space. This is noticed for the three configurations (NV, FC, EAHX). The stronger influence in Carpentras can be explained because summer thermal discomfort is higher, due to a reduced cooling potential by ventilation and higher solar gains, so reducing incoming solar gains becomes more critical. The solar shades parameters are of second influence on the indoor conditions of the living space, but of first influence on the indoor conditions of the glazed cavity and of the veranda, which are not-conditioned. This means that the buffer spaces are efficient to reduce the incoming solar gains inside the living space since they absorb a part of the incoming radiation. With this architecture, the living space benefits from reduced solar gains as the direct incoming solar radiation falls on and is absorbed by the veranda floor or reflected uniformly. Common to all simulations, the optical properties of the exterior wall, the thermal mass of the interior wall and of the exterior wall are of less importance.

It is important to note that these results are very specific to the case-study. Indeed, the fact that the studied apartment is located on the top floor impacts the solar gains received by and redistributed inside the apartment. Furthermore, the building is oriented North-South and a different orientation (i.e East-West) might lead to different results. The fact that the living space is located in between two buffer spaces also greatly impacts the results as the buffer spaces allow to dampen the heat and reduce the incoming solar gains in the living space. Due to modelling limitations, no direct radiation reaches the interior of the living space. The fact that the apartment has a high floor-to-wall ratio impacts the distribution of solar gains, so the results might be different for a smaller apartment with a reduced surface area. As the wall surface area is inferior to the ceiling and floor, this explains that the thermal mass has less importance on these surfaces. Even if the thermal delay of the exterior wall is longer than of the floor (Table 24), the surface plays a larger influence to store thermal mass. Finally, the fact that the architectural configuration favors cross-ventilation creates elevated airflows, higher than in a single sided configuration. The results are also influenced by the range of variation in the design variables. An extended range was chosen for the optical properties of the exterior coating and for the glazing ratio, and these resulted in being the most important parameters. Changing the variation range might change the results.

The analysis was then refined with the variance-based indexes calculated with the Sobol method. The results with the Sobol method gave the same tendency as the results found with the Morris method. However, the range of variables and the method itself can influence the outcome. For instance, when comparing Figure 85 left and Figure 98 right, the parameter related to window opening is the most impactful in both cases, but with the Morris simulations this parameter was varied from not opened to fully opened, while in the simulations with Sobol it is varied from 10 % to 100 % opened. This impacts the interpretation of the results, as with Figure 85 left there is a possibility for the space to overheat greatly with no windows opened, therefore the other important parameters that can reduce summer thermal discomfort are the roof coating optical properties, the glazing percentage and the shadings, while in Figure 98 right and Figure 85 right, as natural ventilation potential is always possible, thermal mass has a great impact on the results. Nevertheless, the tendencies with both methods are similar in the different climates.

Using the Sobol method allowed us to calculate second order parameters which provided insights on interactions between the parameters related to natural ventilation, glazing percentage influencing the airflow rate, and thermal mass. The second order parameters convergence is hard to obtain, as even with 3000 samples the indexes did not seem stable, and the values found are very low, however it provides insights. The fact that the calculated second orders are very low is due to the calculation of the second orders itself, indeed with the Sobol method it is hardly likely to find elevated second orders. A few authors use this method to calculate second order indexes for building thermal simulations, and they were also found to be quite low (close to or inferior to 0.15). (Gagnon et al., 2018) ran 10,000 simulations to reach stabilization of the second order indexes for more than 15 design variables. (Menberg et al., 2016) ran 6,500 simulations for six design variables with 500 samples. In comparison, we ran 42,000 simulations for 6 design variables with 3000 samples. In order to reach a better convergence of the second order indexes, we could re-run the simulations with a smaller number of design variables to reduce the calculation of the second order indexes. For instance, combining the two parameters related to thermal mass and

removing the parameters related to the set-point temperature for windows opening for the warmer climate sequences during which it has no impact would result in four input parameters and only 7 second-order indexes instead of 15. Finally, EnergyPlus is a rather complex model for using this method, so the interpretation of results is difficult. Analyzing different outputs rather than the operative temperature, such as different thermal fluxes, might give more precisions regarding the parameter interactions.

We conducted the sensitivity analysis to analyze summer thermal discomfort with different thresholds as to quantify this summer thermal discomfort for both Morris and Sobol methods. A low threshold of 20 °C or 25 °C allows us to analyze night hours and therefore to see the impact of the parameters related to natural ventilation. A higher threshold, such as 28 °C or the limits from the adaptive comfort standard EN15251, allows to assess daytime summer thermal discomfort. From both methods we could observe that the threshold greatly impacts the interpretation of the results.

The temporal analysis confirmed the trends found when comparing the indicators, that the parameters related to natural ventilation have an impact on the night thermal comfort while the thermal mass has an impact during the day. Interestingly, the glazing percentage sensitivity indexes behavior is modified along the climate sequences: While during the present climate in Roissy it has an impact only during the day to reduce the incoming solar gains, during the future heatwaves, especially in Carpentras it also has an impact during the night, as the ventilation potential is reduced due to higher temperatures, the window sizes have an impact as well to increase the airflow. The evolution of the impactful parameters amongst the climate sequences emphasize the need to adapt the buildings to future summers, as the results show that with reduced natural ventilation potential the building behavior greatly differs.

The analysis of partial variances and of the variance confirmed that the variation in operative temperatures above the fixed threshold of 28 °C for summer thermal discomfort is much higher during the future heatwave while it is close to 0 during the present climate. Using solar protections reduces the variance, especially during the future typical climate, however it remains high for future heatwave sequences.

Chapter 5
Building design at the convergence of mitigation and adaptation to climate change

In this chapter, we illustrate the last part of the methodology that is to optimize buildings for both mitigation and adaptation to climate change. We present the results for the building case study. In the first section, we analyze the heating needs and cooling needs of the building with an imaginary cooling system, to understand if more care should be given to passive winter or summer design. We present the results of the optimization of the apartment case-study for different building configurations: with and without buffer zones (glazed cavity and veranda), with an active cooling system or with alternative ventilative cooling strategies (natural ventilation, mechanical free-cooling and earth-to-air heat exchanger). The optimized building designs are investigated in all these cases, in the three cities. In the second part of the chapter, the summer thermal discomfort and potential health-heat-related risk is assessed, analyzing the increase between the present typical summer, future typical summer and future typical heatwave. This chapter will aim to answer the following questions:

Are heating needs or cooling needs predominant for the building case study under present and future typical climate?

Which design solutions should be prioritized? That this depends on the climate change impact between future and present period, or on the climate location?

What is the indoor environment of the building during the summer, especially under future typical heatwaves period, without an active cooling system?

Summary

5.1 Optimization of energy needs and summer thermal comfort

5.1.1 Optimized design variables

From the sensitivity analysis, a reduced number of key input variables is selected for the optimization. The variables and their variation range are presented in Table 30.

Table 30 - Design parameters and variation range for the optimization

	Design Parameter	Variation range	Unit
	Envelope thermal mass	650 - 2300	kg/m^3
	Roof Absorptivity & Emissivity	0.1 - 0.9	-
	Glazing % on North & South facades	35 - 95	%
	Overhang length	0 - 1	m
Ventilative cooling strategy parameter	Percentage of window opening	10 - 100	%
	DT Free-cooling	1 - 6	°C
	Airflow rate of EAHX	0.6 - 3	ACH

First, the thermal mass (ρ, Cp, λ) is modified following Equations (68), (69) and (70). Through the sensitivity analysis we noticed that for our building case-study, the ceiling and floor thermal mass had the most impact, due to their large surface area in comparison to the walls (ten times higher). However, for the optimization, we choose to modify the thermal mass of all envelope components for uniformity (ceiling, floor, and walls).

The glazing and roof optical properties were found to be the most important parameters in the three cities. More restricted ranges of variations are selected for this parameter for more realistic values: The roof absorptivity varies from 0.1 to 0.9 and the emissivity accordingly opposite but from 0.5 to 0.9 this time (Equation (78)). When the absorptivity equals 0.1, the emissivity equals 0.9 and when the absorptivity equals 0.9, the emissivity is about 0.5.

$$\varepsilon_{roof} = -0{,}5.\,\alpha_{SW_{roof}} + 0.95 \quad (78)$$

The minimum glazing percentage, on the North and South façade, is 35 %, which corresponds to 1/4 of the floor surface (120 m²). The minimum imposed from the French regulation is 1/6 of the floor surface, but this corresponds only to 16 % of the window to wall ratio, so we used 35 % as a minimum value instead (Table 31).

Table 31 - Windows size and glazing to floor and to wall ratios

Glazing percentage on North/South façade	Window length & height (6 windows per façade)	Total window surface	Window to floor ratio	Window to wall ratio
%	m	m²	%	%
25	1.32	20	1/6	16
35	1.57	30	1/4	24
95	2.58	80	2/3	63

The overhang length on the veranda (south façade) varies between 0 and 1 m. No other solar protections are assumed to be used, to investigate the effect of the overhang only.

Regarding the three different ventilative cooling strategies investigated, they are similar to the SA parameters related to natural ventilation, mechanical free-cooling, and earth-to-air heat exchanger. For the three ventilative cooling strategies, the temperature set-point allowing cool air to enter the living space is set to 20 °C, to maximize the cooling potential. This low set-point might lead to overcooling at times, but we do not investigate cool thermal discomfort.

For the natural ventilation strategy, one window on each opposed façade (North and South) can be opened, as three windows opened as in the sensitivity analysis lead to very elevated airflow. The two opened windows have their opening coefficient varying together, from 0.1 to 1 so there is always a minimum airflow for natural ventilation.

Regarding the free-cooling, the delta FC varies between 1 °C and 6 °C, this way the minimum airflow is used when the indoor air temperature is between 20 and 21 °C and the airflow is increased to reach its maximum at 26 °C. The minimum airflow is about 0.6 ACH and the maximum 3 ACH.

Regarding the earth-to-air heat exchanger, the airflow rate varies between 0.6 and 3 ACH. The earth-to-air heat exchanger consists of one single pipe buried at a 2 m depth and has a fixed length of 40 m for a diameter of 0.25 m.

The investigated variables (Table 30) are usually fixed at different moments of the design stage. For instance, the glazing ratio and the presence of an overhang or not, are early architectural choices and are often chosen during the design sketch. The selection of building materials and coatings is usually done during the basic preliminary design and refined during the detailed preliminary design. The design airflow of passive ventilative cooling strategies (ie. natural ventilation, mechanical free-cooling and EAHX) is usually calculated during the detailed preliminary design. Using an optimization algorithm would occur during the detailed preliminary design, while simple building simulations can be done during the sketch phase. Nevertheless, we investigate these different variables using the optimization algorithm.

5.1.2 **NSGA-II algorithm parameters settings**

The algorithm parameters are subject to debate. The number of individuals, of generations, the crossover, and mutation coefficients are the main NSGA-II parameters that need to be input by the user. There is no general rule in the literature, and some authors choose a high number of generations with a small number of individuals, or the opposite. However, a minimal number of runs is necessary to obtain convergence, as shown by (Hamdy 2016) who demonstrated that around 1400-1800 evaluations were needed to reach stabilized non-dominated solutions. Values for these four parameters are reported from the literature in Table 32.

Table 32 – NSGA-II algorithm parameters settings from literature

Number of objectives	**2 (energy, cost)**	**2 (energy, summer comfort)**	**2 (energy, summer comfort)**	**2 (cost, life cycle analysis)**	**3 (energy, summer comfort, cost)**	**2 (annual heating demand, peak heating load)**
Source	(Chardon et al., 2015)	(Lapisa et al., 2018)	(Ascione et al., 2017)	(Recht, et al.)	(Chantrelle et al., 2011)	(Forde et al., 2020)
Number of variables	8	8	6	11	9	14
Number of individuals	12	200	25	400	48-96	200
Number of generations	300	10	30	20	70-150	100
Number of model iterations	3600	2000	750	8000	6720-7200	20000
Crossover coefficient	0.5	0.9	0.6	0.8	0.3, 0.7, 0.9	0.7
Mutation coefficient	0.5	0.04	0.1	0.15	0.02, 0.1, 0.5	0.5

We ran the simulations for one configuration (energy needs in Roissy future typical climate with the model IPSL) with different NSGA-II algorithm parameters. The crossover and mutation coefficient were respectively set to 0.9 and 0.2, and we compared the results for a population of 96 individuals and 20 generations, 48 individuals and 40 generations, and 24 individuals and 80 generations which were equivalent to 1920 runs for all configurations. From Figure 106, we can observe that increasing the number of generations while decreasing the number of individuals allow reaching convergence faster.

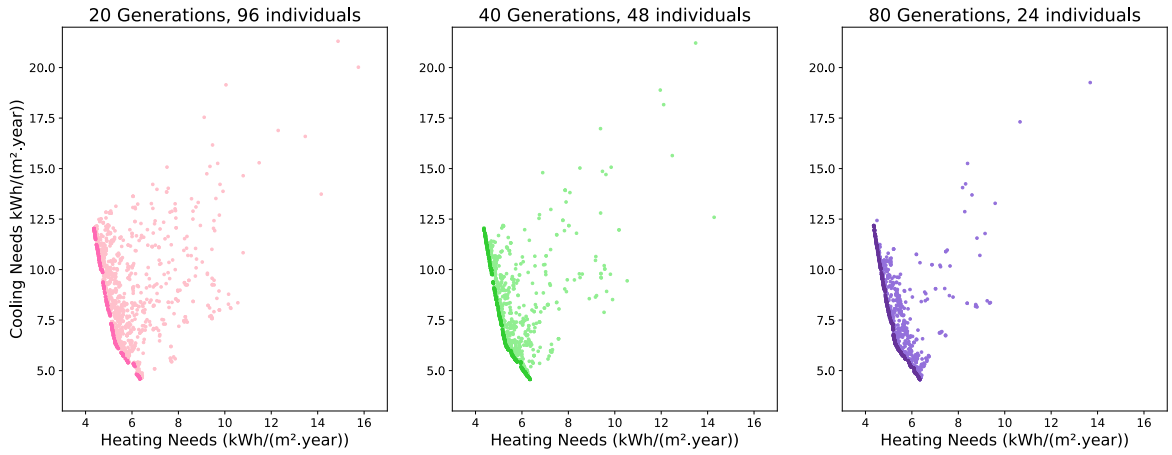

Figure 106 - Comparison of solutions for different NSGA-II algorithm parameters

The three Pareto fronts are very similar, both in the distribution in solutions, minima and maxima. Regarding the simulation time, it was about 1h25, 1h50, and 1h40 respectively with the 1920 simulations parallelized on 15 processors. Considering the number of configurations under study, and that simulations with the Airflow Network are three times more consuming, we chose to select the algorithm parameters with the shortest computational time, as choosing this option did not decrease the Pareto front accuracy. Different values were also tested for crossover (0.5, 0.7 and 0.9) and mutation coefficients (0.1, 0.2, 0.5), but these did not impact the different Pareto fronts either. We fixed the mutation coefficient to 0.2, as (Deb et al., 2002) recommends a value of 1/p, with p being the number of input parameters (4 or 5 in our case-study, depending on the configuration) and the crossover coefficient to 0.9.

5.1.3 **Optimization results: energy needs**

In this section we analyze the energy needs of the case-study with building, with heating and cooling possible. The windows of the living space are always closed, but the ones exterior to the glazed cavity and of the veranda are opened all summer to prevent these two zones from overheating and allow people to spend time in the veranda (Figure 107). During winter, the exterior windows of the glazed cavity are always closed, but the windows of the veranda are opened if the veranda operative temperature reaches above 26 °C, otherwise the veranda tends to overheat on sunny days. Shutters are used on the exterior windows of the north façade during winter nights.

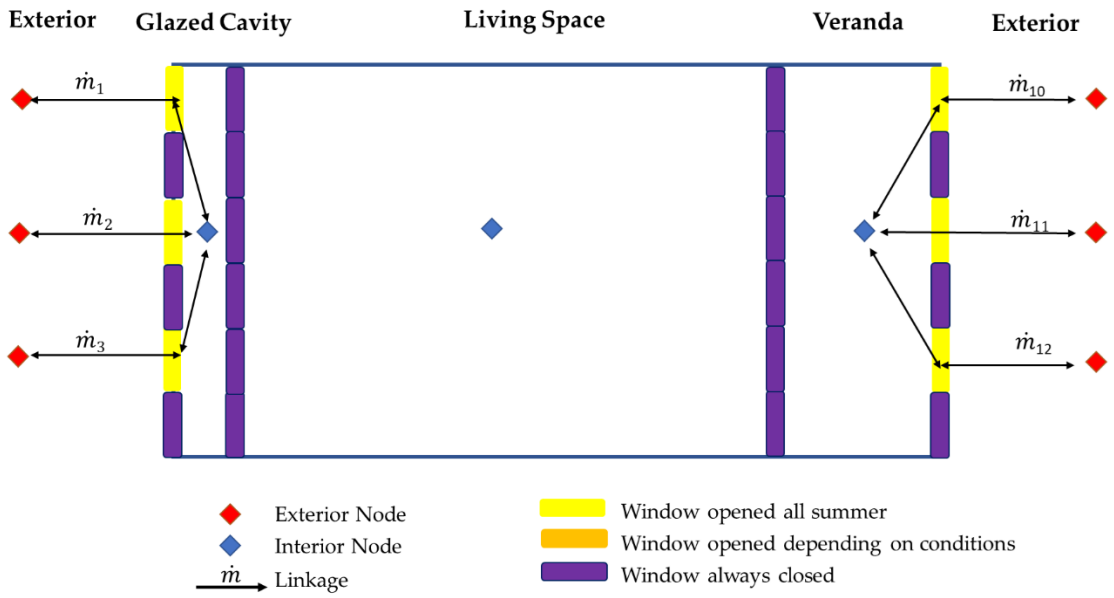

Figure 107 - Schematics of airflows when the living space windows are closed (configuration with air-conditioning)

The actions to prevent the buffer zones to overheat are summarized in Table 33. The extended winter period, in La Rochelle and Roissy, is from the 1st of November until the 15th of May. During this period, heating is allowed with a set-point temperature of 20 °C. In these cities the extended summer period is from the 16th of May until the 31st of October, during which cooling is allowed for a set-point indoor temperature of 26 °C. In Carpentras, the extended winter period is reduced from one month in spring, from the 1st November until the 30th of March, and the extended summer period longer, from the 1st of April until the 31st October. These were defined after parametric studies to best control the veranda and the glazed cavity to reduce both heating and cooling needs in the three cities.

Table 33 - Solar control and ventilation control of the buffer zones to reduce heating needs or overheating

	Action	**Control**
Extended Winter Period (11-01 to 05-15 in Roissy and La Rochelle, 11-01 to 03-31 in Carpentras)	Shutters on the exterior windows of the glazed cavity during the night	10 pm to 7 am
	Ventilation of the veranda during winter	When $T_{air\_veranda}$ > 26 °C
Extended Summer Period (05-16 to 10-31 in Roissy and La Rochelle, 04-01 to 10-30 in Carpentras)	Ventilation of the glazed cavity and of the veranda	On during the extended summer period

5.1.3.1 Energy needs

The results for the cities of La Rochelle, Roissy and Carpentras are presented in Figure 108. On the left, both x and y axes purposely have similar maxima for a quick visual assessment of the predominant cooling needs in contrast with the heating needs, especially in Carpentras. On the right part of the Figure we can observe more in detail the variation in heating needs.

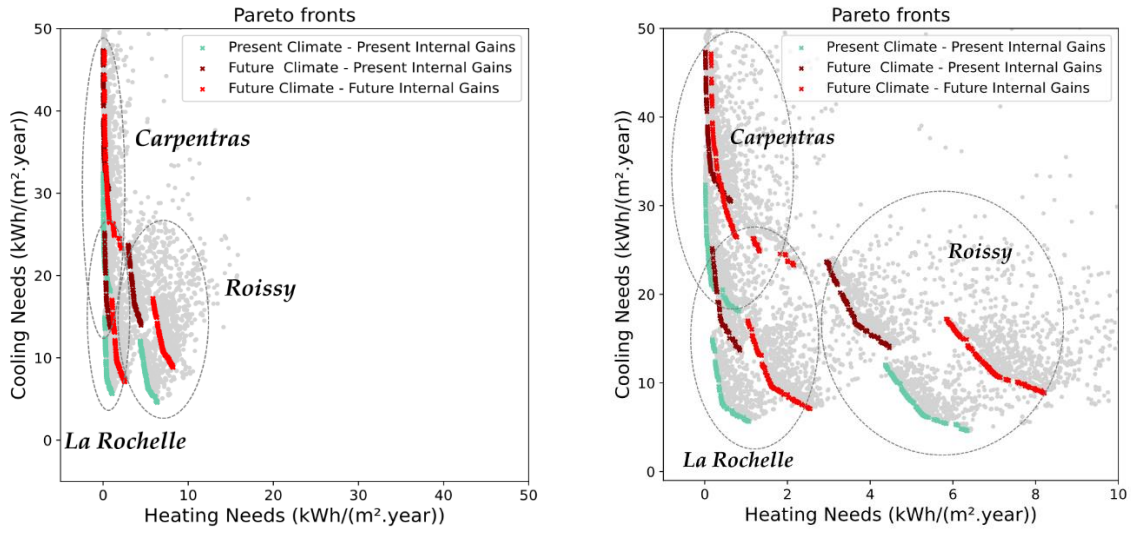

Figure 108 - Pareto fronts for La Rochelle, Roissy and Carpentras - Present & Future energy needs (left-Pareto fronts normed, right-zoom)

The Pareto fronts for the simulations during the present typical year are in green, while those for the future are in red. Between the green and the dark red Pareto fronts, only the climate file was changed, from present typical to future typical. Between the green and the red Pareto fronts, the climate file was changed, and as well the internal gains in the future period by about a third (53 kWh/m².year to 37 kWh/m².year) assuming future energy-efficient specific equipment (see section 2.4.1).

We can observe that in all cities, during both present and future periods, the cooling needs are predominant in comparison to the heating needs. This can be explained by the fact that the building envelope is optimized and well insulated, no infiltrations on the building envelope were modelled, the mechanical ventilation functions during the winter with heat-recovery at 70 % efficiency, and the presence of the buffer zones and windows-oriented South largely contribute to reducing the heating needs.

The daily mean air temperatures of the three zones are illustrated in Figure 109, for the contemporary climate in La Rochelle. During the winter, the exterior windows of the buffer zones are closed (at some specific moments the exterior windows of the veranda are opened in the winter when the air temperature exceeds 26 °C, not shown here). During the winter, the air temperatures inside the buffer zones are much more elevated than the outdoor air temperature. During the summer, as the exterior windows of the buffer zones are opened, the air temperatures of the buffer zones are almost equal to the outdoor air temperature. It is necessary to open these in the summer, otherwise the buffer spaces greatly overheat. By comparing the delta between the living space air temperature, the adjacent buffer zones and the delta between the living space air temperature and the outdoor air temperature, it is clear that the buffer zones greatly dampen the outdoor variations which highly contribute to the low heating needs. Indeed, the mean delta during the winter period between the daily air temperature of the living space and the outdoor air temperature is 11.7 °C, while it is 4.9 °C with the glazed cavity air temperature, and 3.8 °C with the veranda air temperature.

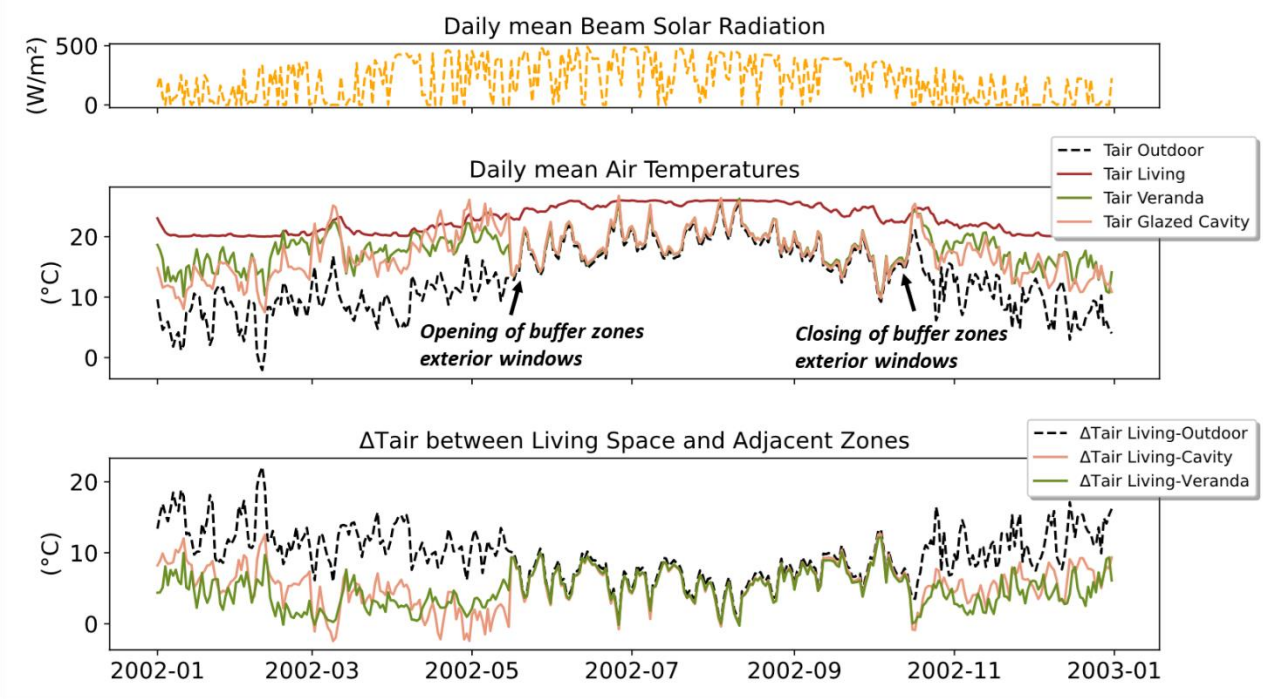

Figure 109 - Daily mean indoor air temperatures in the three zones and temperature difference between the living space and buffer zones or exterior – La Rochelle, historical, model IPSL, for optimized building design with the highest heating needs

From Figure 108, in each city, and for all non-dominated (optimized) solutions, the cooling needs increase in the future, no matter the internal gains assumption. With the same assumption in present internal gains (dark red Pareto fronts versus green Pareto fronts), the cooling needs are more than doubled in the future in La Rochelle and in Roissy and are increased by a third in Carpentras, due to the increase in outdoor temperatures. With the same assumption in present internal gains (dark red), the heating needs decrease is more pronounced in Roissy where they are the highest. In La Rochelle and in Carpentras the heating needs decrease is observed for the Pareto front solutions with the highest heating needs, for other solutions the heating needs are very low (< 1 kWh/m².year) so the decrease is less obvious. While in Roissy the cooling needs increase somewhat counterbalance the heating needs decrease, in Carpentras and in La Rochelle the cooling needs increase is much larger compared to the heating needs decrease, resulting in much higher total energy needs.

With the projected reduction in internal gains related to new energy-efficient specific equipment (red Pareto fronts versus green Pareto fronts), the increase in cooling needs is less pronounced, and the heating needs actually increase in each of the three cities. The decrease in internal gains for the same future climate (dark red Pareto fronts versus red Pareto fronts) therefore produces two expected contrasted effects: A high reduction in cooling needs (in La Rochelle, they are divided by two, in Carpentras the lowest cooling needs are reduced by 5 kWh/m².year and in Roissy they are decreased by a third) and an increase in heating needs especially in Roissy where they are doubled.

Comparing the energy needs calculated with the assumption in internal gains reduction that we will carry along this chapter (green Pareto fronts and red Pareto fronts), the increase in cooling needs is the highest in Carpentras (around +10 kWh/m².year depending on

the Pareto front solution), then in Roissy (around +5 kWh/m².year depending on the Pareto front solution), then in La Rochelle (around +3 kWh/m².year depending on the Pareto front solution). The increase in heating needs is low in Carpentras and in La Rochelle, and the highest in Roissy (around +2 kWh/m².year). In Roissy, the difference in heating and cooling needs is less pronounced than in the other cities, and future lowest optimized heating needs are about 8.5 kWh/m².year, slightly lowest than the future lowest optimized cooling needs which are around 10 kWh/m².year.

The energy needs of the case study apartment are highly sensitive to the assumption in internal gains. This is especially true in La Rochelle where the decrease in cooling needs is higher between the high and low internal gains (dark red Pareto front and red Pareto front) than between the changing climate (green Pareto front and red Pareto front). In Roissy, the increase in cooling needs is somewhat similar, while in Carpentras it affects only the solution with the lowest cooling needs. As the buffer zones dampen the outdoor variations, the energy needs are less sensitive to outdoor variations and more sensitive to indoor variations (i.e internal gains related to specific equipment for instance). For a building without buffer spaces, the energy needs sensitivity to internal gains would be lower.

This comparison between present and future heating and cooling needs (green Pareto fronts and red Pareto fronts) provides some insight on the thermal building design prioritization between the winter and summer periods. In Carpentras, a Mediterranean city already known for its warm summers, the elevated increase in cooling needs contrasted by the very low heating needs is an indication that if design strategies are opposed between the winter and summer period, it might be more judicious to prioritize the summer period. The same is observed in La Rochelle, even though the cooling needs are lower than in Carpentras, the heating needs are almost null. In this city, air-conditioning is not a common practice and it might be surprising that the present cooling needs are more elevated than the heating needs, but this is explained by the presence of the buffer zones which allow to almost offset the heating needs. Finally, in Roissy, for the Pareto front solution with the lowest cooling needs (bottom right of the Pareto front), the optimized cooling needs are almost equal to the heating needs, while for the other solutions on the Pareto fronts the cooling needs are higher than heating needs, but resulting in higher total energy needs. Therefore, in Roissy, equal care should be given to winter and summer design.

5.1.3.2 Energy needs sensitivity to the presence of buffer zones

As demonstrated in the previous section and from Figure 109, we could observe that the presence of the buffer spaces is highly beneficial to reduce the winter heating needs. However, how does their presence influence the cooling needs and to which extend? To explore the influence of the buffer zones, the optimization is conducted this time for the same apartment but without the buffer zones. The Pareto fronts are compared in Figure 110 for Roissy and La Rochelle. The green and red Pareto fronts are the same ones as those represented in Figure 108, while the blue and yellow are the ones simulated without the buffer zones.

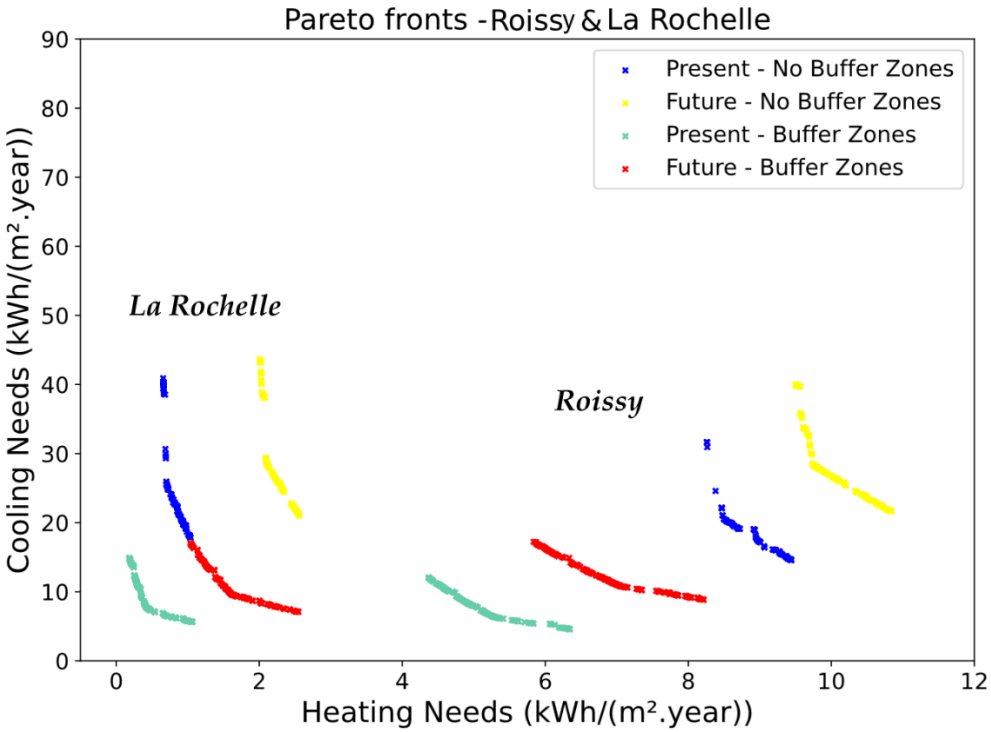

Figure 110 - Pareto fronts for configurations with and without buffer zones in La Rochelle & Roissy, Present & Future typical years

We can observe that in La Rochelle and in Roissy, the presence of the buffer zones is largely beneficial to reduce both heating and cooling needs, as for all configurations without buffer zones, the energy needs are always higher in both present (blue and green Pareto fronts) and future (yellow and red Pareto fronts) typical years. In both La Rochelle and Roissy, and for both present and future typical years, the presence of the buffer spaces leads to a reduction in cooling needs (by three for a medium configuration on the Pareto front) much higher than the reduction in heating needs (by a third for a medium configuration on the Pareto front). The buffer spaces benefit the indoor environment of the living space in the summer period as well, as they allow to reduce the solar heat gains received on the facades. In the veranda, the solar gains received are mostly absorbed by the floor (see interior solar distribution Figure 53), or reemitted towards the living space. Furthermore, due to the modelling of interior windows in EnergyPlus, all solar gains entering the living space are treated as diffuse which probably contributes as well to reduce the cooling needs.

The same results are presented for Carpentras in Figure 111. The presence of the buffer zones allows to reduce the cooling needs by around two both for the highest and lower cooling needs. Considering the very high cooling needs, this strategy is very beneficial for this city, as without the buffer zones the lowest optimized cooling needs are 45 kWh/m².year in the future, versus less than 20 kWh/m².year with the buffer zones. For the optimized building designs with the lowest cooling needs, with the buffer zones, the heating needs in present and future typical winters are actually increased (bottom right of green and red Pareto Fronts) compared to the simulations without the buffer zones (bottom right of blue and yellow Pareto Fronts). This can be explained because the optimized building design to reduce the cooling needs include a 1 m overhang (this is shown from Figure 112 to Figure 114). With the 1 m overhang and the veranda that is 3 m long, the solar heat gains are greatly reduced in the winter, which results in an increase in heating needs. This occurs in Carpentras and not in La Rochelle neither

in Roissy because winter days are much sunnier in the Mediterranean city. For the optimized building designs with the lowest heating needs (top left of the Pareto fronts), the optimized heating needs with the buffer spaces are lower than those without, because without the overhang the living space receives solar gains. However, the drastic reduction in cooling needs versus heating needs in absolute values between the different Pareto front solutions balances more the focus towards summer passive design. It is worth mentioning that the exterior windows of the buffer zones must be left open during the entire summer period, otherwise the veranda and the glazed cavity highly overheat. Due to security concerns (the veranda is 50 m² so occupants might leave personal belongings in it) this might not always be possible.

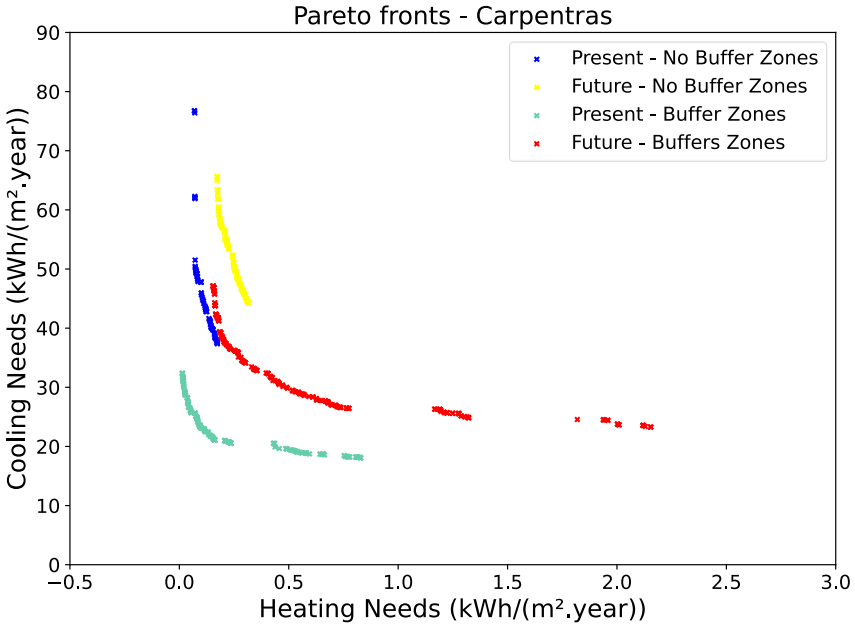

Figure 111 - Pareto fronts for configurations with and without buffer zones in Carpentras, present & future typical years

5.1.3.3 Analysis of optimized building design variables

In Figure 112 to Figure 114, Pareto fronts and their respective design variables for each optimized building design in La Rochelle, Roissy and Carpentras respectively, with and without buffer zones, are represented. In each Figure, on the middle graph are the Pareto fronts for two separate optimizations with the two typical weather files, present (green with buffer zones and blue without) and future (red with buffer zones and yellow without). The top and bottom graphs in each Figure represent the normed input parameters (maximum value of each design variable corresponds to 1 and minimum value to 0) for the solutions of the Pareto fronts. The top graph represents the design variables of the Pareto front for the present typical climate and the bottom graph is for the future typical climate. By vertical visualization, one can understand the corresponding four design variables for each of the Pareto front optimized solutions.

In all three cities, the behavior of the design variables is similar, and it is also similar during the present and the future periods, except the glazing percentage in Carpentras. However, the presence or not of the buffer zones influences the optimized design variables.

The design variable that is similar in all cases is the thermal mass, it is always optimized at the highest value, in all cities, during both present and future typical years, meaning that it is beneficial to reduce both heating and cooling needs. This can be explained because the building envelope is well insulated by the exterior, so the exterior outdoor temperatures (and solar radiation in summer) are blocked by the exterior insulation, while the heated or cooled air blown into the apartment is stored in the building thermal mass in direct contact with the interior.

The three other design variables (roof albedo/emissivity, glazing percentage on North and South facades, and overhang length) are optimized differently to reduce the heating or cooling needs. Indeed, a high albedo/emissivity is beneficial to reduce cooling needs while it will increase the heating needs during the winter, the same is true for a low glazing percentage, and for a long overhang.

Regarding the glazing percentage, it is always optimized at the lowest value, except in the optimized building designs in Carpentras with the lowest heating needs, as they allow to maximize the solar heat gains. However, this is at the cost of the cooling needs, which are much higher with the increase in window sizes (as there is no overhang on the south façade in this configuration). In Roissy and in La Rochelle, the window sizes are always optimized at the lowest, during both present and future typical years, for configurations with and without buffer spaces. This can be explained by the fact that during the winter, the heating losses through the windows are higher than the solar heat gains, which can be explained because the North façade is glazed, even with the glazed cavity which reduces the temperature variations between outdoor and indoor for the configuration with the buffer zones. Analyzing the windows sizes variations on different orientations, or optimizing the size on the different facades independently might lead to different results. In the summer, minimizing the windows sizes lead to reduced cooling needs which is expected since it reduces the incoming solar heat gains through windows.

Regarding the roof albedo/emissivity and the overhang on the South facade length design variables, they are optimized differently depending on the presence of the buffer zones or not, and their behavior is similar in all three cities, during present and future climate. For the configuration with buffer zones, a change in albedo value from small to high (high albedo corresponding to a small absorptivity and a high emissivity) lead to a large reduction in cooling needs for a small increase in heating needs: in La Rochelle future, reduction of 9 kWh/m².yr cooling versus an increase of 0.5 kWh/m².yr heating; in Roissy future, reduction of 6 kWh/m².yr cooling needs for an increase of 2 kWh/m².yr in heating needs; and in Carpentras future, reduction of 21 kWh/m².yr cooling needs versus 0.6 kWh.m².yr heating needs increase. To reduce further the cooling needs, the overhang length linearly increases with the increase in heating needs. The fact that the roof albedo/emissivity has a stronger impact to decrease the cooling needs in the configuration with the buffer zones can be explained by the fact that most solar heat gains are received by the roof since the ones received on the South façade are mostly blocked by the presence of the veranda. Indeed, the opposite is observed for the configuration without buffer zones: Increasing the overhang length allows to quickly decrease the cooling needs, without compromising too much the heating needs (in La Rochelle future, a decrease of 15 kWh/m².yr in cooling needs versus an increase of 0.2 kWh/m².yr heating needs, and in Roissy future, a decrease of 12 kWh/m².yr in cooling needs for an increase of 0.2 kWh/m².yr

heating needs). Without the veranda, the solar heat gains on the South façade have more impact than those received by the roof, as they enter the living space through the windows as beam radiation. In Carpentras, in the future, without the veranda, an overhang length of 1 m is always optimized, and a small increase in glazing ratio allows to decrease further the already low heating needs. The albedo value increase then allows to linearly reduce the cooling needs at the cost of the heating needs, but as cooling needs are higher a high albedo value is preferred to reduce total energy needs.

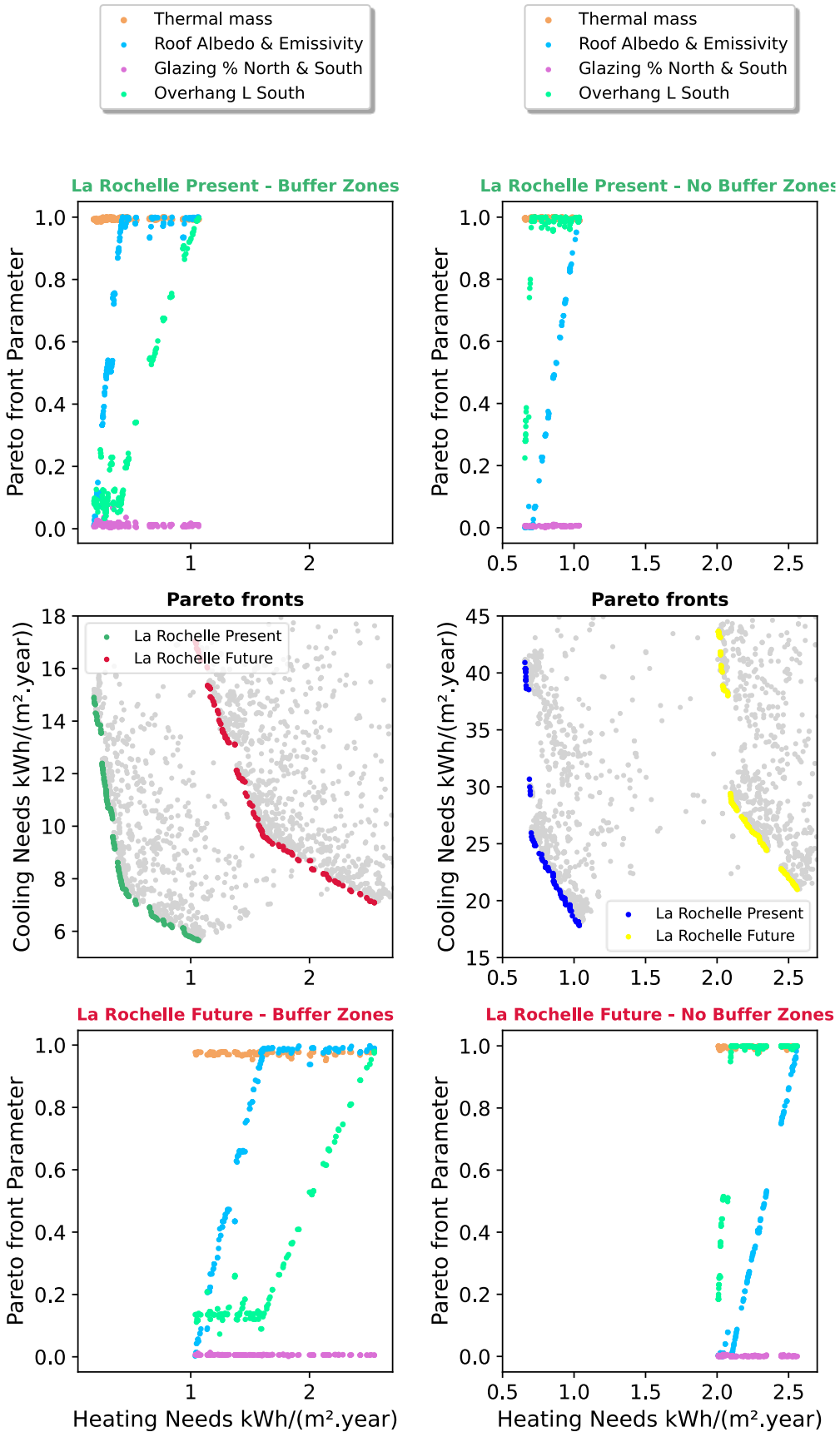

Figure 112 - Design variables for non-dominated solutions - La Rochelle present (top) and future (bottom) with buffer zones (left) and without (right)

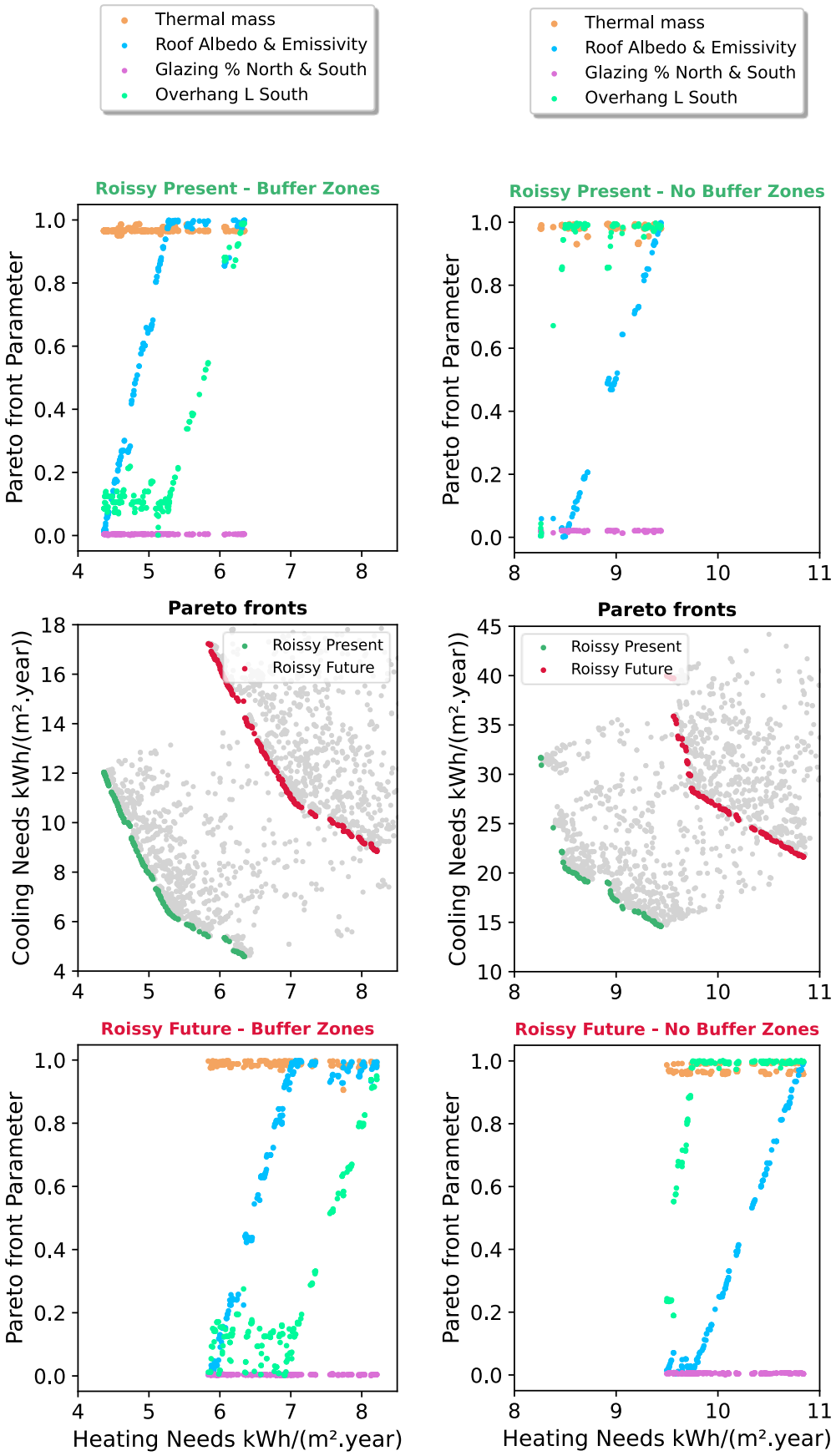

Figure 113 - Design variables for non-dominated solutions - Roissy present (top) and future (bottom) with buffer zones (left) and without (right)

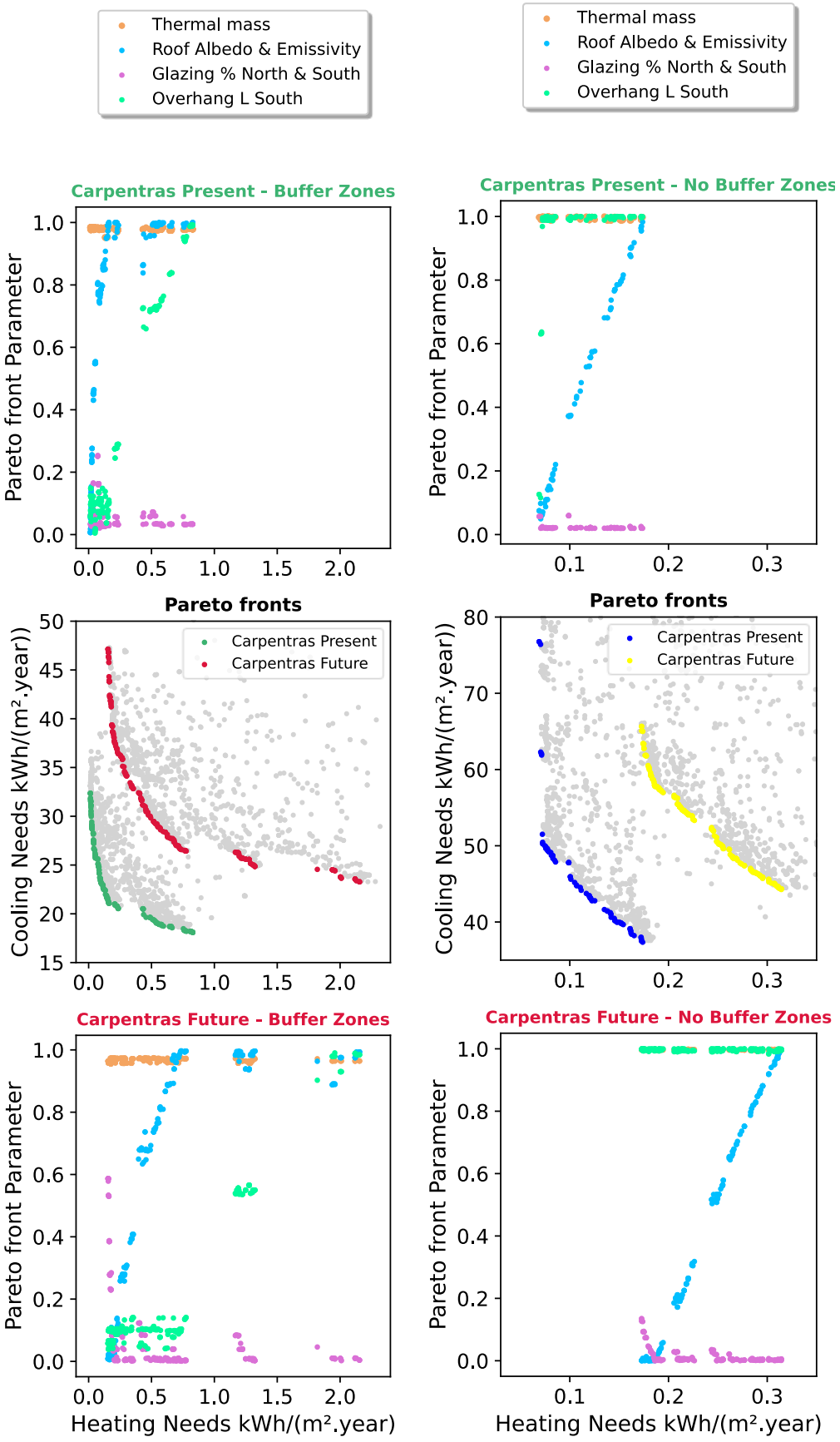

Figure 114 - Design variables for non-dominated solutions - Carpentras present (top) and future (bottom) with buffer zones (left) and without (right)

5.1.3.4 Energy needs sensitivity to climate projections uncertainty

All the results presented above were calculated using the future typical years selected in section 3.2.1. In this section, we evaluate the influence of the different typical years reassembled from several climate models on future energy needs. In other terms, we evaluate the energy needs sensitivity to climate projections uncertainty (related uniquely to the climate model, for the same RCP scenario 8.5). From Figure 63, we could observe a high variation in weather variables and especially the dry-bulb temperature amongst the different climate models during the future. We evaluate the energy needs for two building design solutions.

The choice of which non-dominated solutions to analyze is debatable. In this chapter we will analyze the two extreme building designs of the Pareto fronts (A and B) and an intermediate building design (AB) , defined by the one having the lowest distance to the ideal point. The ideal point is an imaginary point, the one with the lowest summer thermal discomfort and the lowest heating needs. Building design A is the solution with the summer thermal discomfort the highest heating needs. Building design B is the solution with the highest summer thermal discomfort and the lowest heating needs. The compromise building design AB is the one with the lowest distance *dist* to the ideal point (Figure 115). To find building design AB, we calculated for each Pareto front solution x the distance to the ideal point (Equation (79)) and kept the point with the lowest distance *dist*.

$$dist = \sqrt{\left(\frac{HNx - HNmin}{HNmax - HNmin}\right)^2 + \left(\frac{DHx - DHmin}{DHmax - DHmin}\right)^2} \quad (79)$$

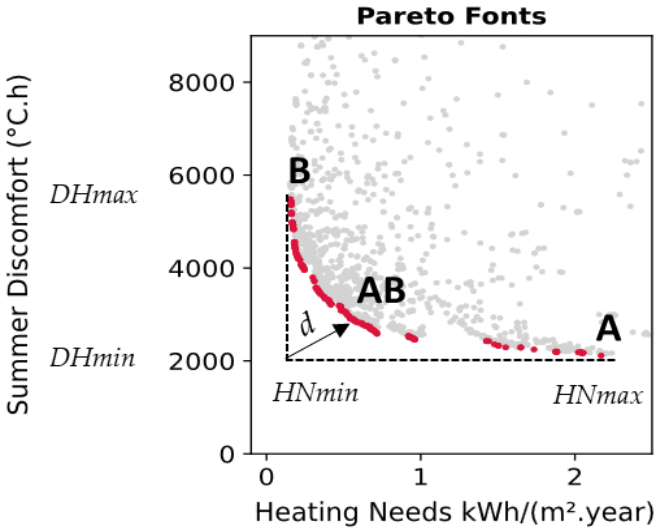

Figure 115 – Solutions A, AB and B on the Pareto front

The energy needs are evaluated for solution A and B. In Figure 116, the energy needs calculated with the four typical years reassembled from the four climate models in La Rochelle for the two extreme optimized building designs on the Pareto front are presented.

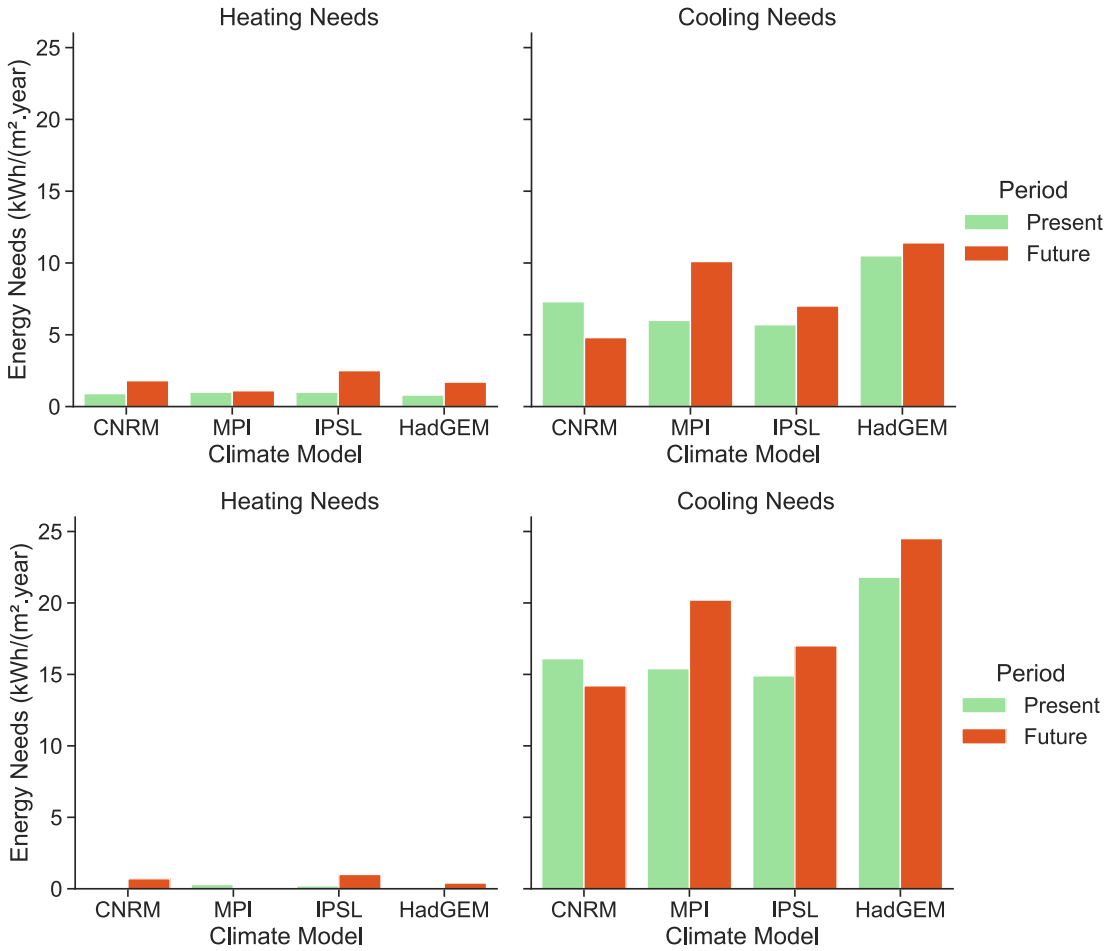

Figure 116 – Energy needs sensitivity to climate model – La Rochelle - (Top: optimized design solution A, with lowest cooling needs on the Pareto front, bottom: front optimized design solution B, with highest cooling needs on the Pareto)

As observed on the Pareto Fronts (Figure 112), the heating needs are lower than the cooling needs during both present and future periods, and for all the optimized solutions (since we analyze the two extremes). We can observe that building design A leads to the least energy needs as the cooling needs are reduced. In the future, the heating needs consistently increase for all models which are due to the reduction in internal gains, however, these remain very low (< 2.5 kWh/m².year). Regarding the cooling needs, they increase for the three climate models MPI, IPSL and HadGEM, but decrease for the model CNRM, because the increase in outdoor temperatures is much lower than the other models, so the reduction in internal gains lead to a decrease of cooling needs. The model MPI lead to the highest increase in cooling needs, while the model HadGEM lead to the highest cooling needs absolute values. In outdoor dry-bulb temperatures, the model HadGEM generally showcases warmer summer temperatures, but the model MPI showcases higher maxima. We used the future typical year reassembled from the model ISPL in La Rochelle. In absolute values the future cooling needs vary between 14 and 24 kWh/m².year depending on the model, however there is a general trend of increase in cooling needs amongst the climate models.

In Figure 117 the energy needs sensitivity to the climate models is presented for Roissy.

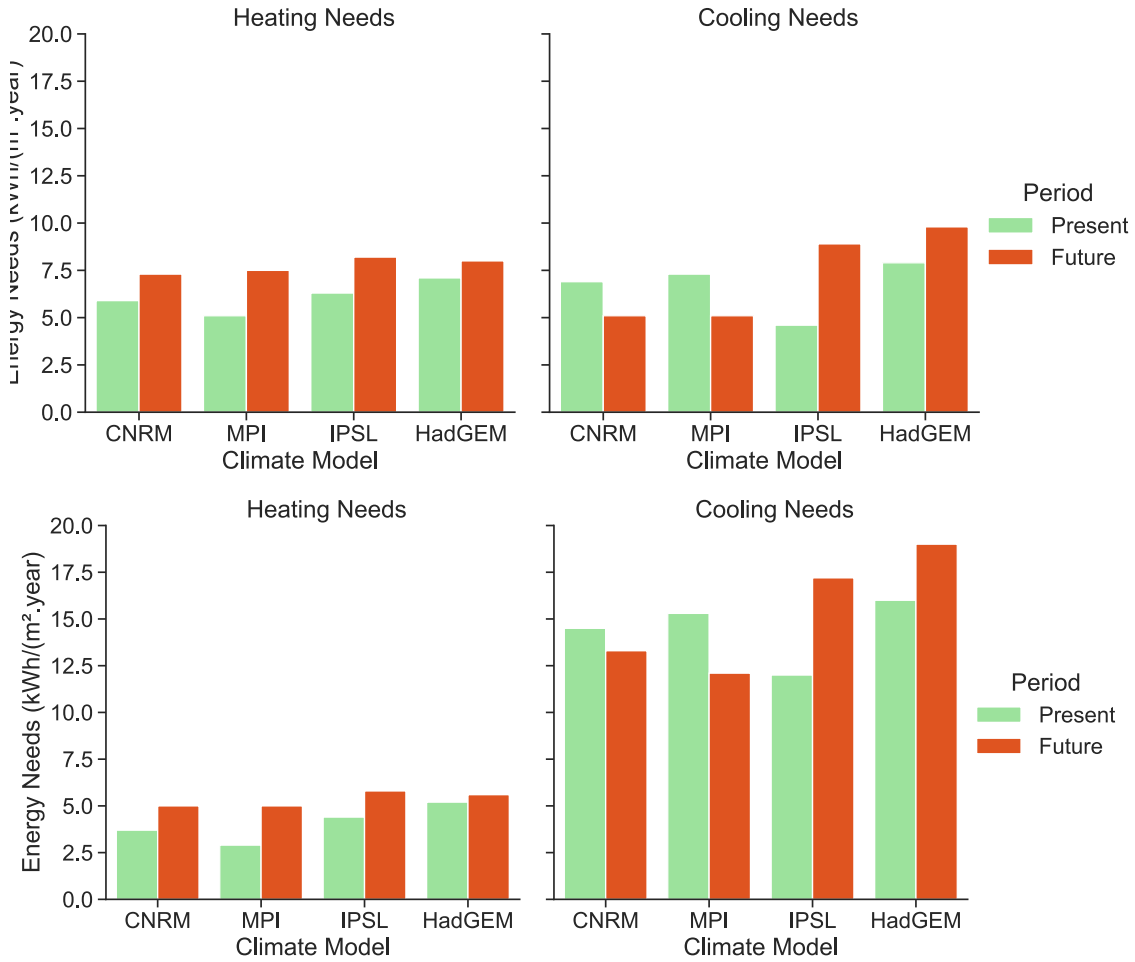

Figure 117 - Energy needs sensitivity to climate model – Roissy - (Top: optimized building design A, with lowest cooling needs on the Pareto front, bottom: front optimized building design B, with highest cooling needs on the Pareto)

The results are quite different as this time the heating needs are more elevated than in La Rochelle, and somewhat equivalent to the cooling needs for building design A. The optimized design solution A consistently leads to lower total energy needs for each climate model and during both present and future periods. For building design A, the heating needs all increase in the future, as observed in La Rochelle, due to the reduction in internal gains. The cooling needs trends are similar for the models CNRM and MPI (equivalent decrease) and for the models IPSL and HadGEM (equivalent increase). The cooling needs follow the trend of the outdoor air temperatures of these models, for which the increase is much more pronounced for the models IPSL and HadGEM (Figure 63). In the future period, the heating and cooling needs are somewhat equivalent.

In Figure 118 the energy needs sensitivity is calculated for Carpentras. Again, building design A leads to lower total energy needs than building design B. The heating needs are almost inexistent while the increase in cooling needs is consistent amongst the climate models. The highest future cooling needs are calculated with the typical year recomposed from the model HadGEM which is the one we used. In outdoor temperatures, it is the model IPSL that has the highest outdoor temperatures, meaning that the increase in cooling needs is related to the outdoor solar radiation or relative humidity.

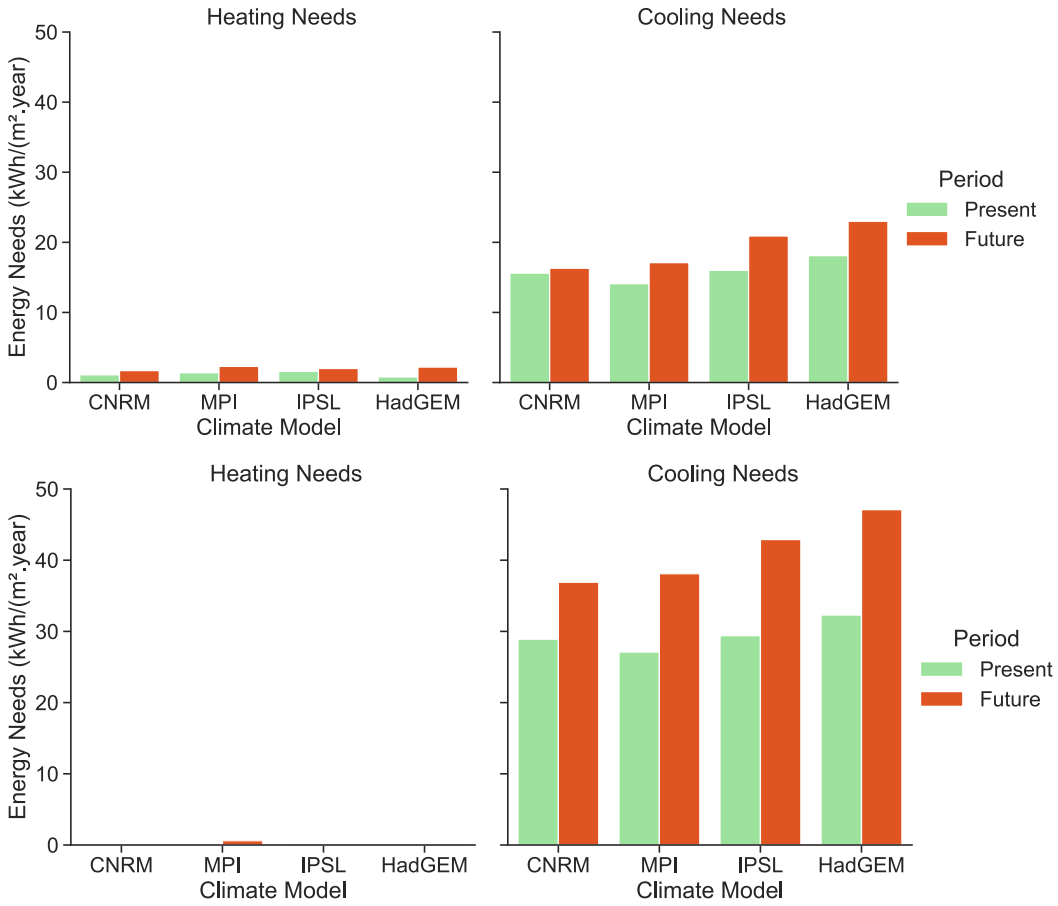

Figure 118 - Energy needs sensitivity to climate model – Carpentras - (Top: optimized building design A, with lowest cooling needs on the Pareto front, bottom: front optimized building design B, with highest cooling needs on the Pareto)

In La Rochelle, the typical year used is recomposed from the model IPSL, leading to the third present and future higher cooling needs. In Roissy, the typical year used is recomposed from the model IPSL as well, which leads to the second highest cooling needs in the future, but the lowest cooling needs in the present. In Carpentras, the typical year is recomposed from the model HadGEM, which leads to the highest cooling needs in both present and future typical summers. Even though the heating and cooling needs calculated with the different typical years differ in absolute values, the trend in increase and decrease in energy needs for each city is similar for the warmest models. For these warmer models, the optimization results will most likely give similar trends even if using a typical year recomposed from climate data from another model (such as in section 4.2.2.2).

5.1.4 Optimization results: ventilative cooling strategies

5.1.4.1 Heating needs and summer thermal comfort

In this section, we present the optimization results of the initial case with the buffer zones for the five design variables presented in Table 30. Similar to in the sensitivity analysis, the three ventilative cooling strategies (natural ventilation, mechanical free-cooling, and earth-to-air heat exchanger) are analyzed independently. No active cooling system is present, cool air is provided by one of the three ventilative cooling strategies.

The two minimized objectives are:

- The heating needs;
- The summer thermal comfort.

We evaluated the summer thermal discomfort with the Standard Effective Temperature (SET), based on the comfort model proposed by Gagge (Gagge et al., 1986). This indicator was chosen because it allows distinguishing different thermal sensation categories, especially in regard to heat. The different categories were introduced in Table 1.

With the aim of building adaptation to heat and reducing health effects during extreme heat events, we needed to select a threshold that is applicable for vulnerable people, such as the elderly. We chose the threshold of 25.6 °C to quantify summer thermal discomfort. While conditions between 25.6 and 30 °C might not be severe for young and healthy people, they might be for older people which are more vulnerable. Indeed, it was demonstrated that older people are physically warmer than younger people at the same conditions above an ambient temperature of 25 °C (Itani et al., 2020), while their thermal sensation is to feel cooler than younger people (Vellei et al., 2017). Other factors, such as reduced mobility, might prevent them to act with adaptation measures (move to open windows, adjust clothing, turn on fans, use solar shading, etc).

The choices of this indicator, and of this threshold are arguable, but using a different indicator such as the degree hours where the indoor operative temperature is above a threshold would lead to similar results in terms of Pareto fronts and optimized design variables. Indeed, the SET accounts for the radiant temperature and dry-bulb air temperature, relative humidity and indoor air velocity. However, in the simulations, the chosen conduction algorithm does not calculate humidity transfers through the building envelope.

During the optimization algorithm, the outputs of each building simulation contain the heating needs, and the parameters needed to calculate the SET. The building thermal simulation timestep is of 10 min, but the output variables are provided hourly to reduce the computational time during the optimization process. The SET was calculated on an hourly time-step, using as input the hourly indoor air temperature, radiant temperature, and indoor relative humidity. It is calculated with a conventional fixed indoor air velocity of 0.1 m/s, a standard met of 1, and standard clothing of 0.5. The indoor air velocity is fixed for the solutions to be comparable. We used the Python module *pythermalcomfort* (Tartarini & Schiavon, 2020) to calculate the SET.

The summer thermal discomfort is calculated at the hourly time-step according to Equation (80). Similar to the SA, the summer thermal discomfort °C.h (DH) are calculated with Equation (81).

$$std_{OPT}(t) = (\mathrm{SET}_t - 25.6)_{\mathrm{SET}_t > 25.6} \tag{80}$$

$$DH_{OPT} = \sum_{t=0}^{n\Delta t} std_{OPT}(t).\Delta t \tag{81}$$

The Pareto fronts, comparing the three ventilative cooling strategies in the three case-study cities (Roissy, La Rochelle and Carpentras) were calculated for the present typical year (Figure 119) and the future typical year (Figure 120) weather files.

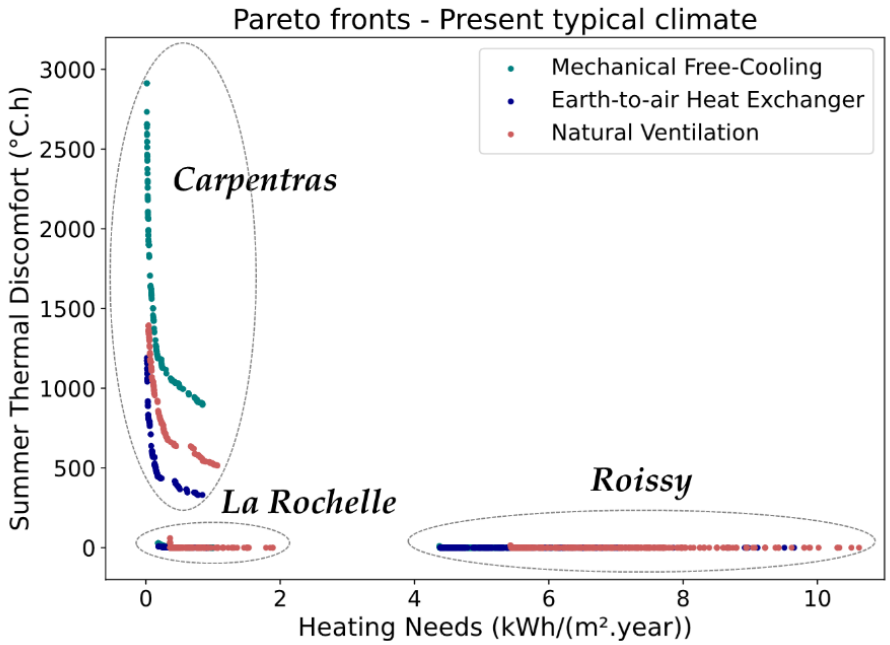

Figure 119 – Pareto fronts during the present typical climate in La Rochelle, Roissy and Carpentras for the three ventilative cooling strategies with natural ventilation, mechanical free-cooling and earth-to-air heat exchanger

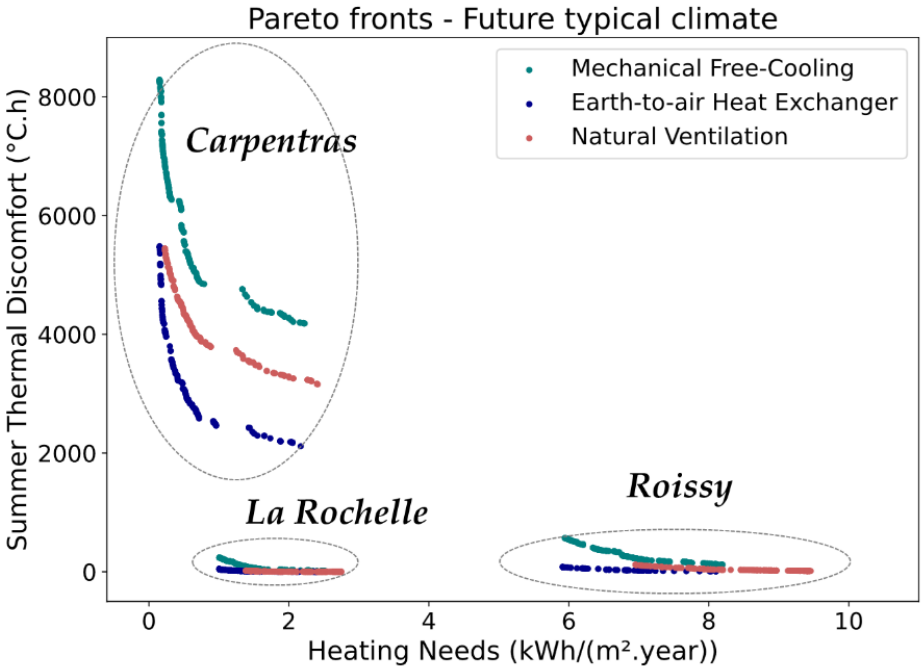

Figure 120 - Pareto fronts during the future typical climate in La Rochelle, Roissy and Carpentras for the three ventilative cooling strategies with natural ventilation, mechanical free-cooling and earth-to-air heat exchanger

We can observe that the summer thermal discomfort degree hours in both present and future and periods are much lower in La Rochelle and Roissy than in Carpentras, similar to the cooling needs, which is expected due to local climate variations. In all three cities, configurations with mechanical free-cooling lead to the higher summer thermal discomfort, while the configurations with earth-to-air heat exchanger lead to the lowest. The fact that the natural ventilation leads to lower summer thermal discomfort than the free-cooling is due to the higher airflow rates entering through the windows. Furthermore, as windows are displayed in a cross-ventilation configuration, the airflow is further enhanced. During the present typical climate in La Rochelle and in Roissy, it seems that the summer thermal discomfort is null or close to zero. During the future typical climate, in La Rochelle and in Roissy, the natural ventilation and earth-to-air heat exchanger strategies lead to low levels of summer thermal discomfort, while the building designs with the free-cooling strategy display quite elevated values, especially in Roissy. In Carpentras, during the present typical climate, discomfort is high but there is a strong increase in the future typical climate. Indeed, in the future, even in the best configuration with the earth-to-air heat exchanger, the summer thermal discomfort is still very elevated, with more than 2000 °C.h above the threshold. The discomfort values are presented more in detail in the next section.

5.1.4.2 Analysis of optimized building designs

From Figure 121 to Figure 125, the values of the Pareto fronts are analyzed more in detail for each city and each case-study, with their associated optimized design variables. For each Pareto fronts, all corresponding design variables are shown on the top (present climate) and bottom (future climate) and can be associated with a Pareto front point by vertical visualization. Additionally, the design variables for some specific building designs are given for each city in Appendix C in Table 38, Table 39 and Table 40. The summer thermal discomfort for these specific building designs will be investigated in section 5.2.

We can first observe that in some cases, the design variables parameters have a large variation:

- Roissy present mechanical free-cooling (Figure 121-left);
- Roissy present earth-tube (Figure 121-right);
- Roissy present natural ventilation (Figure 122-left);
- La Rochelle present natural ventilation (Figure 122-right).

In these cases, the summer thermal discomfort (sum of degree hours of SET > 25.6 °C, Equation (81)) is equal to 0 for building designs A and AB, and very low for building design B, and the Pareto fronts are horizontal or almost horizontal, the variation only or mostly occurs for the heating needs. The fact that this is the case in Roissy for all configurations, in La Rochelle for only one configuration and does not occur in Carpentras is related to the summer outdoor temperatures, which are lower in Roissy, then in La Rochelle, then in Carpentras during the contemporary climate (Figure 63).

For the other configurations, and in all cases during the future period, a high thermal mass is always optimized. This means that when summer thermal discomfort occurs, a high thermal mass is necessary to minimize the summer thermal discomfort. This can be explained because the thermal mass both dampen and time shifts the indoor temperatures. With the high

thermal mass and exterior insulation, the indoor temperature peak is at moments 10 °C lower than the outdoor temperature. With a lower thermal mass, nighttime temperatures are more elevated, however daytime indoor air temperatures are elevated to dangerous levels.

Also, for all other configurations, the parameter related to the control of each ventilative cooling strategy is always optimized to maximize the cooling potential (highest window opening percentage for natural ventilation, lower delta for the free-cooling to reach the highest airflow rate, or highest airflow rate of the earth-to-air heat exchanger). The ventilative cooling strategies are operated only during the summer and do not concur with the winter period (i.e with the heating needs).

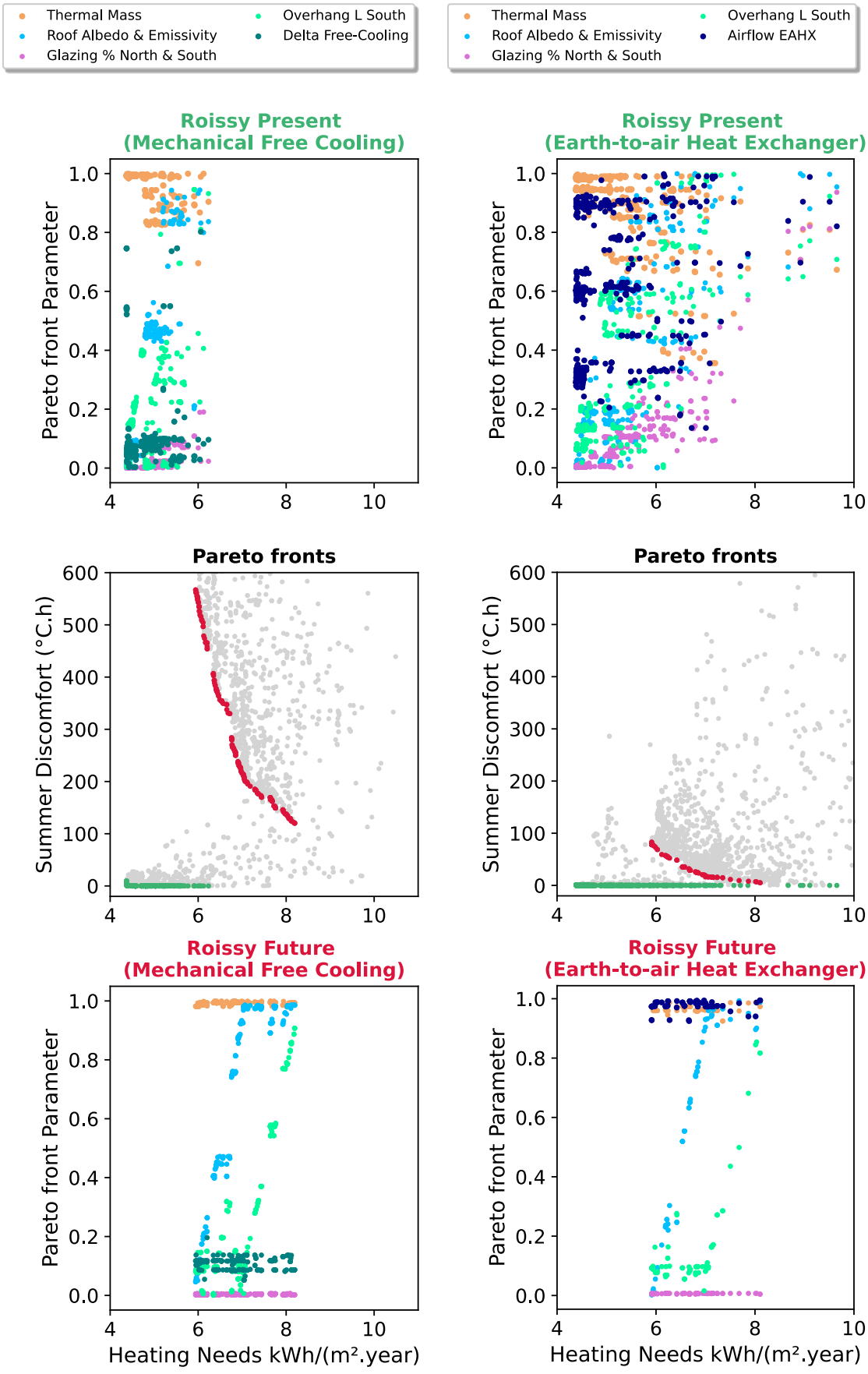

Figure 121 - Pareto fronts and associated optimized design variable values (normed) in Roissy

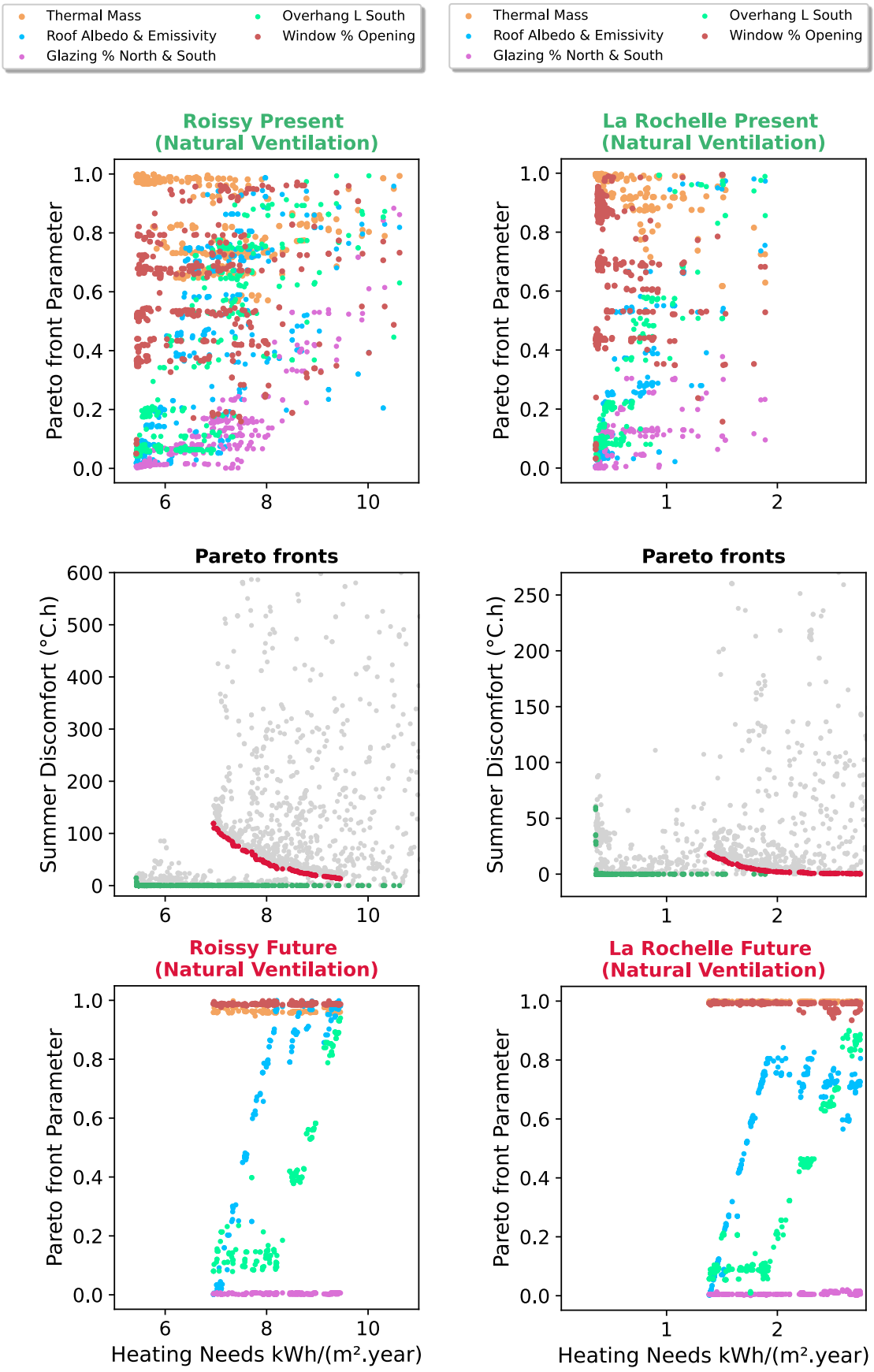

Figure 122 - Pareto fronts and associated optimized design variable values (normed) in Roissy (left) and in La Rochelle (right)

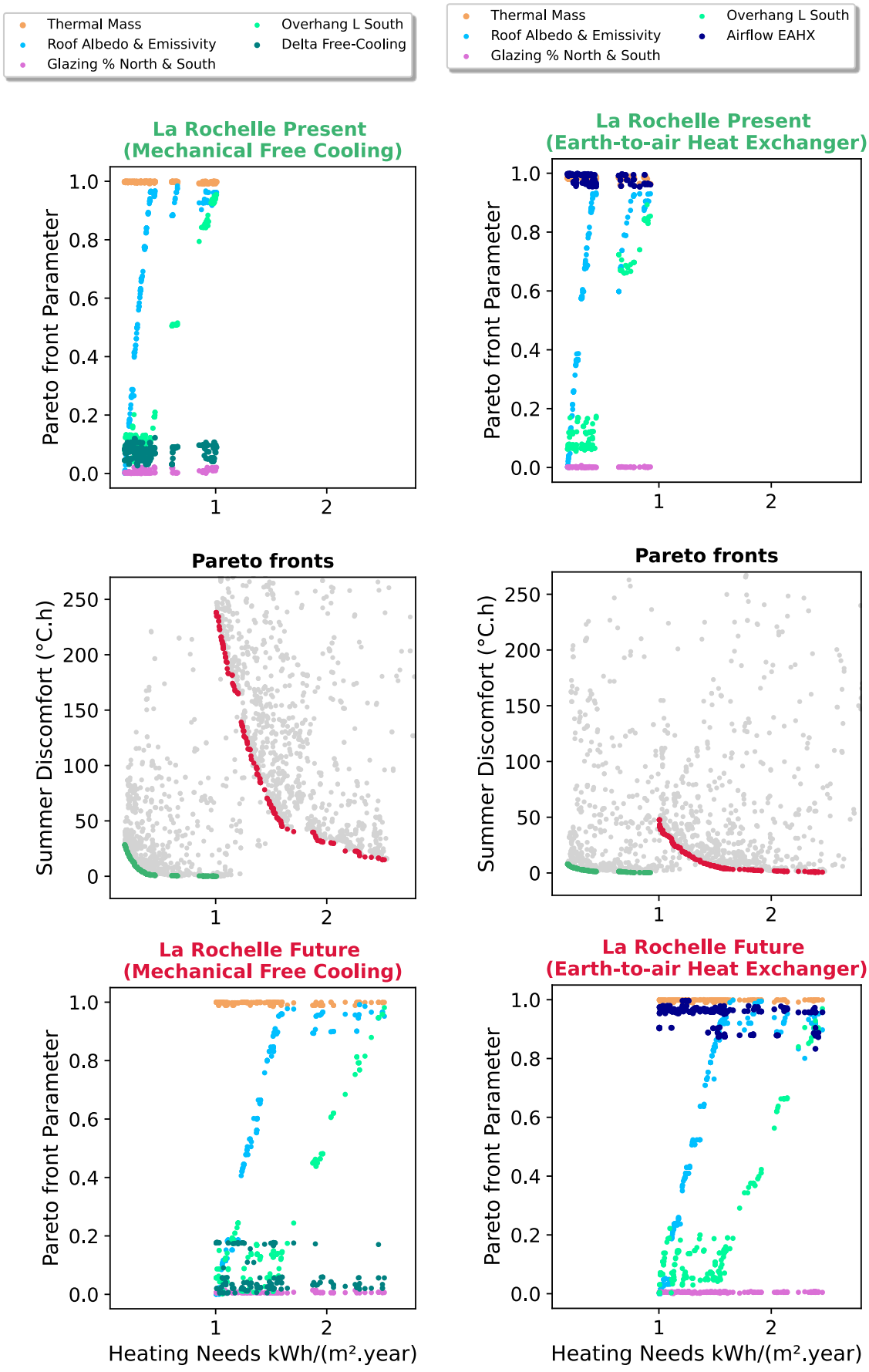

Figure 123 - Pareto fronts and associated optimized design variable values (normed) in La Rochelle

Regarding the four configurations mentioned above: In Roissy, for all ventilative cooling strategies during the present period, and for all Pareto front solutions, the parameter related to the ventilative strategy control is not maximized, meaning that zero summer thermal discomfort is reached without needing to use the full cooling potential. This is also the case in La Rochelle for designs AB and B with natural ventilation. In that case, building design A is not an improvement of building design AB, as it represents the solution with highest heating needs and lowest summer discomfort, but 0 is already reached with building design AB, which represents the ideal solution. The difference in design variables is that building design A has a medium thermal mass and an overhang of 0.5 m, which both contribute to an increase the heating needs. In Roissy, an improvement of only 0.1 kWh/m².year is made between building design AB and building design A to the cost of little summer thermal discomfort. The same as in La Rochelle is observed, an increase in thermal mass and in overhang length leads to higher heating needs (in that case they are twice higher). If we analyze the variation in glazing percentage of these four configurations, it is optimized at the lowest, such as in simulations for the energy needs.

During the future typical summer, in La Rochelle and in Roissy (bottom of Figure 121 to Figure 123), the summer thermal discomfort is higher than during the present period, however in the best case (building design A) it is low (maximum value of 120 °C.h for the free-cooling system in Roissy) or even reaches 0 for the building design with natural ventilation in La Rochelle. The worst summer thermal discomfort is reached in Roissy, it is about 600 °C.h for the configuration with the mechanical free-cooling, while the other two systems lead to around 100 °C.h of discomfort in the worst optimized case (building design B). In La Rochelle during the future typical climate, the worst summer thermal discomfort is also reached with the mechanical free-cooling, but it is lower than in Roissy, maximum of around 250 °C.h, and less than 50 °C.h for the two other ventilative cooling strategies. We can also note that in the worst case (building design B), the summer thermal discomfort is higher in Roissy than in La Rochelle during the future period, but it is the opposite in the present period. This is due to a larger increase in outdoor summer temperatures in Roissy (Figure 63).

Regarding the effectiveness of the building envelope and of the ventilative cooling strategies to reduce the summer thermal discomfort during the future typical summers in contrast with the heating needs penalty during the winter, in Roissy it can be minimized at the cost of 2 kwh/m².year in heating needs, or around 30 % of the heating needs. In La Rochelle, it can be minimized at the cost of 1.5 kWh/m².year in heating needs, or around 50 % of the heating needs, but these are already very low

In the future, in La Rochelle and in Roissy (bottom of Figure 121 to Figure 123), all configurations are optimized similar to the ones with the cooling system with the buffer space investigated in section 5.1.3.2. There are similarities in optimized variables of the building envelope between building designs A, AB, and B, which are similar for the three ventilative cooling strategies. All three optimized building designs in the future have high thermal mass, low glazing percentage and maximized airflow for the ventilative cooling strategies. The only variables that differ among the three designs are the value of the roof albedo and emissivity and the overhang length. Building design A (lowest summer thermal discomfort) consistently

has a high albedo of 0.9 and overhang value close to 1 m, which are the maximum values. Building design AB consistently has an intermediate albedo value (0.6, or 0.7 in Roissy, 0.6 or 0.8 in La Rochelle, with the highest value of 0.7 or 0.8 only for the free-cooling configuration always leading to the highest summer thermal discomfort in com Roissy on with the other two ventilative cooling strategies) and no overhang or very low (between 0 and 0.1 m). Building design B consistently has the lowest albedo value (0.1) and no overhang or very low (between 0 and 0.1 m). These values can be visualized on the Figures, but they are also given on the tables in Appendix C. We can observe that the optimization of a higher albedo (building design AB) is much more efficient to reduce the summer thermal discomfort than the optimization of the overhang length (building design B), as a change of albedo value from 0 to 1 lead to the greatest reduction by far in summer thermal discomfort. From section 5.1.3.2, we could observe that this is because of the presence of the buffer zones, indeed the trend is inversed without the buffer space: a long overhang is more efficient to reduce the summer thermal discomfort than a high albedo.

We can conclude that to reach the minimum summer thermal discomfort (building design A), the highest albedo value and the longest overhang are needed in La Rochelle and in Roissy during the future period, which was not the case during the present period. As an example, in Roissy with the natural ventilation strategy, during the present solution A has an albedo value of 0.3 and an overhang length of 0.9 m, while in the future it has an albedo value of 0.9 and the same overhang length. For the free-cooling configuration, in the present solution A has an albedo value of 0.8 and an overhang length of 0.2, while in the future it has an albedo value of 0.9 and overhang length of 0.9. Similar to the thermal mass and the ventilative cooling potential, to reach the lowest summer thermal discomfort in the future (building design A), the albedo value and overhang length need to be the highest. The same is observed in La Rochelle.

The results for Carpentras are presented in Figure 124 and Figure 125. The heating needs are very low due to the elevated solar gains, they vary between 0 and 1 kWh/².year during the present and up to 2.5 kWh/².year during the future (due to the decrease in internal gains related to specific equipment). The summer thermal discomfort is very elevated, especially during the future period, and varies greatly between the two extreme building designs. The optimization of the building envelope (building design A to B) reduces the summer thermal discomfort more than between the mechanical free-cooling (worst) and earth-to-air heat exchanger (best) for instance.

The optimized design variables during both present and future typical climates display similar values as in the other cities in the future. In Carpentras, as the summers are already warm today, no modification in the building envelope is needed in the future. Furthermore, already in the present a high thermal mass is optimized, and the ventilative cooling strategies potential is always fully used. The only difference with the other two cities, as already observed in section 5.1.3.2, is the medium glazing percentage to reduce the heating needs, at the cost of the summer thermal discomfort (building design B). For the natural ventilation strategy, larger windows produce a contrast effect in the summer as they lead to cooler interior air temperatures during the night but warmer interior air temperatures during the day. However, the decrease in airflow is not linear to the window size.

As observed already in La Rochelle and Roissy for the future typical climate, an increase in albedo value reduces highly the summer thermal discomfort. In Carpentras, in both present and future climate, the albedo of solution AB (intermediate) is of 0.8 or 0.9, whereas it was of 0.6 to 0.8 in La Rochelle and in Roissy for the future climate, of 0.1 or 0.2 in Roissy for the present climate and of 0.1 to 0.7 in La Rochelle during the present climate. Since the summer thermal discomfort is much higher, and also the roof receives 10 % solar radiation more than in Roissy and in La Rochelle, a high albedo value is even more important. In contrast, during the present climate with the lowest albedo value of 0.1 (building design B), heating needs are equal to 0, and in the future, they are equal to 0.2 even with the reduction in internal heat gains. However, considering the trade-off in summer thermal discomfort, this solution is probably not very realistic to gain 2 kWh/m².year.

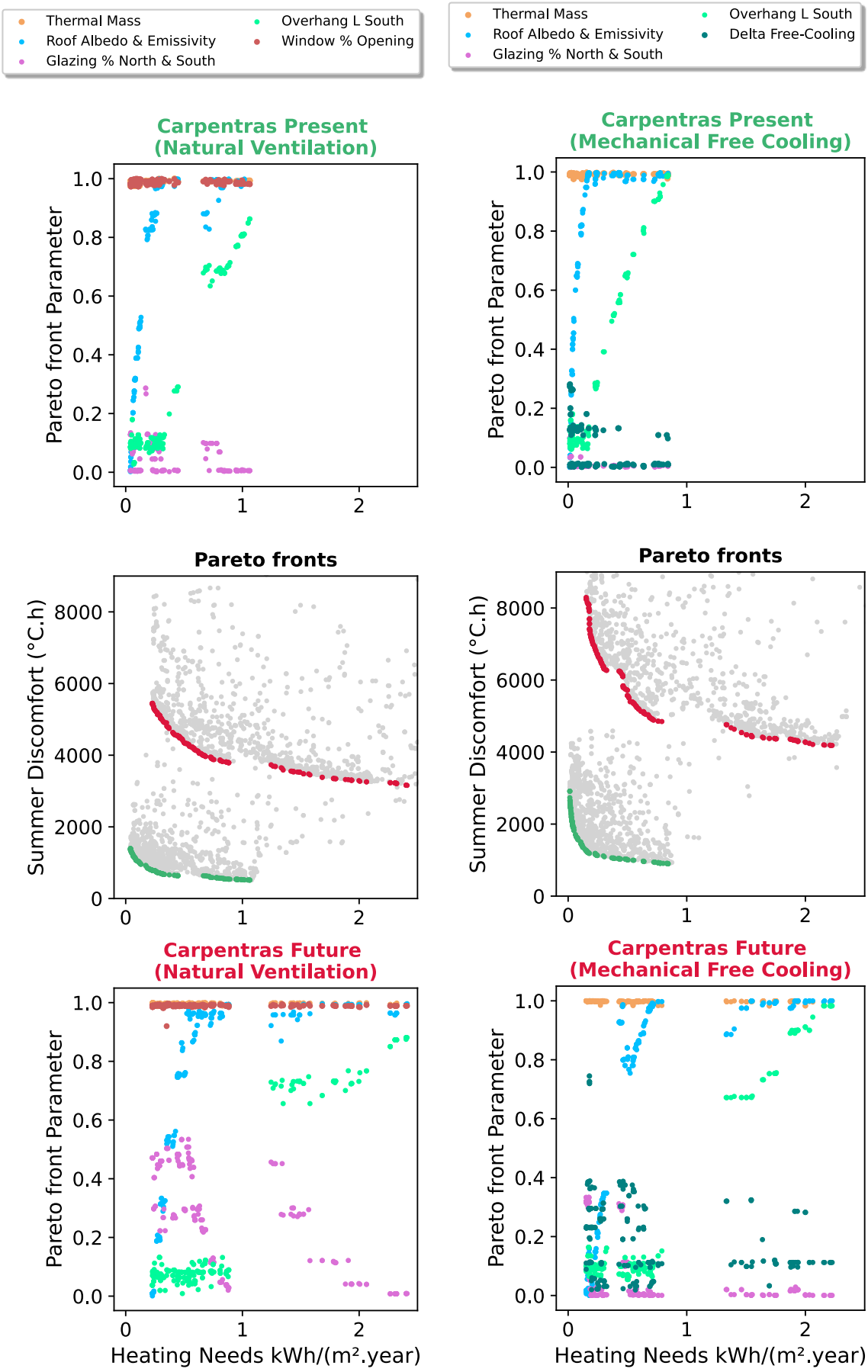

Figure 124 - Pareto fronts and associated optimized design variable values (normed) in Carpentras

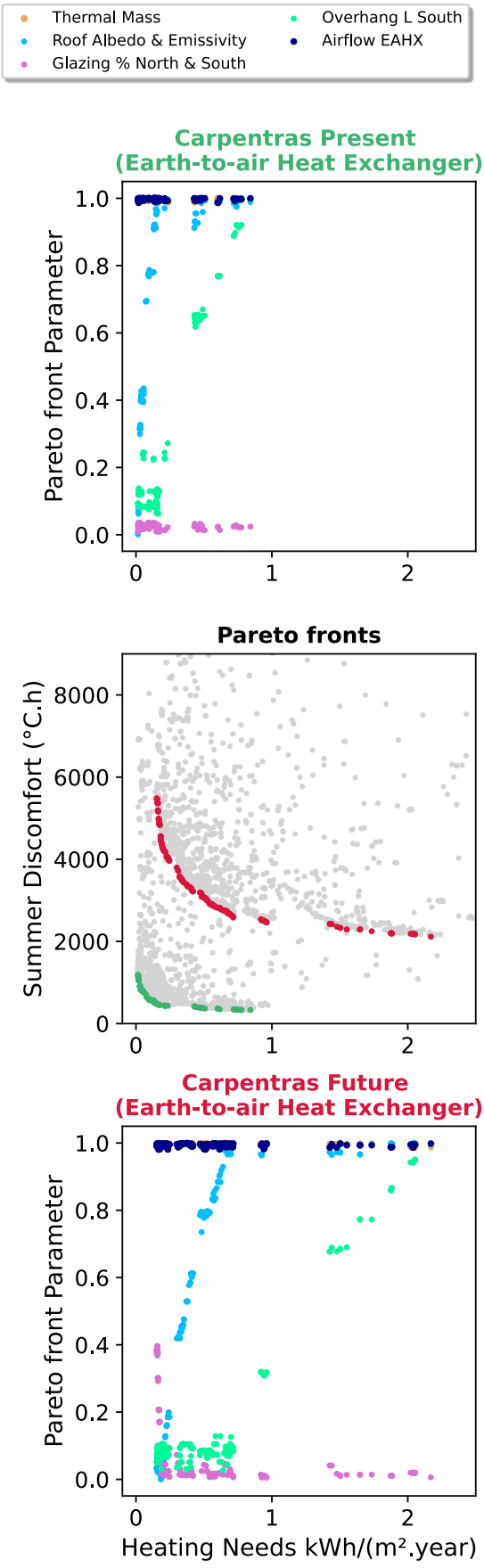

Figure 125 - Pareto fronts and associated optimized design variable values (normed) in Carpentras

5.1.5 **Conclusive remarks on optimized building designs**

Section 5.1.3 focused on optimizing the building case study design to minimize two objectives: the heating needs and the cooling needs for the simulations with an active cooling system, and section 5.1.4 focused on minimizing the heating needs and summer thermal discomfort for the simulations with the ventilative cooling strategies.

For this specific building case study, the optimized designs have lower heating needs than cooling needs in both present and future climate, in La Rochelle and in Carpentras. In La Rochelle, the cooling needs in the future are four times higher than the heating needs with the model IPSL, while without the buffer zones they would be around fifteen times higher. In Carpentras, the heating needs are very low (< 1 kWh/m².year) and the cooling needs are increased by a third in the future with the buffer zones, up to 24 kWh/m².year for the climate model considered (HadGEM, leading to the highest cooling needs in that case) for the most optimized design. In Roissy, the heating and cooling needs are somewhat equivalent depending on the climate model used for the calculation (Figure 117). The presence of the buffer zones, especially the veranda, is even more beneficial during the summer period, given that the exterior windows remain open. Without the buffer zones, the future cooling needs would be three times higher than the heating needs in Roissy (for the model considered, IPSL). Even though these results are specific to the building case study, the modelling assumptions, and the climate data used, there is a general trend that cooling needs will be higher than heating needs in the future for a new energy efficient building, well insulated by the exterior and with low internal gains related to energy efficient specific equipment. Furthermore, building design A (the one with the optimized building design leading to the minimum cooling needs) always leads to lower total energy needs than building design B (the one with the optimized building design leading to the minimum heating needs), even in Roissy. These results are a confirmation that a change of paradigm is needed to design buildings in France: designing to reduce cooling needs might be considered as much as designing to reduce heating needs, if not more. Indeed, the cooling needs of optimized designs are multiplied by around two in the future in comparison with the present in Roissy (models IPSL and HadGEM) and in La Rochelle (models MPI, IPSL, HadGEM). In Carpentras, the cooling needs are already quite elevated in the present climate: For the optimized building design with the lowest cooling needs, in the configuration with the buffer zones, they are around 10 kWh/m².year today, with a projected increase between 16 and 24 kWh/m².year depending on the climate model for the mid-century.

In section 5.1.4 the building design was optimized to reduce the heating needs and potential summer thermal discomfort with three independent ventilative cooling strategies: natural ventilation through windows displayed in an advantageous cross-configuration, mechanical free cooling and earth-to-air heat exchanger through the ventilation system. During the present typical summer, in Roissy and in La Rochelle, each of the three building designs could maintain a comfortable indoor environment according to our criterion (degree hours of SET superior to 25.6 °C), as it reached zero for several optimized building designs. In the future typical summer, in Roissy and in La Rochelle, the combination of the optimized building envelope and one of the three ventilative cooling strategies allows reaching almost zero summer thermal discomfort for some building designs, at the cost of the heating needs.

In Carpentras, summer thermal discomfort during the future typical summer is much more elevated than during the present typical summer, and it is very elevated even with the most optimized solution to reduce summer thermal discomfort, this is investigated further in the next section 5.2.

Regarding the design solutions, it was observed that the presence of the buffer spaces is beneficial to reduce both winter heating needs (reducing the temperature delta between the living space and its boundary conditions) and summer thermal discomfort (reducing solar heat gains on the south façade by the presence of the veranda), in both present and future periods, and in all climates (Figure 110 and Figure 111).

In La Rochelle and in Roissy, it was demonstrated that building design will need to evolve: During present climate, summer thermal comfort can be achieved without the "maximization" of the design parameters with an emphasis on the summer design: different combinations of medium thermal mass, medium glazing percentage, medium or low overhang length and medium or low albedo value can lead to no thermal discomfort. Furthermore, the full potential of the ventilative cooling strategies is not necessarily used either to reach zero discomfort, depending on the design solutions. The presence of the buffer spaces probably largely contributes to enhancing the thermal comfort experience (Figure 110). In the future, in Roissy and La Rochelle, to reach zero summer thermal discomfort, the parameters are optimized fully for the summer design, and a high thermal mass is needed, combined to the maximum albedo value in Roissy and a medium-high in La Rochelle, a long overhang, a low glazing percentage, and the full ventilation potential. A high roof albedo/emissivity value is a more efficient strategy to reduce the summer thermal discomfort than the overhang length, but this is the case for the configuration with the veranda only, as without the buffer zones the opposite was observed (Figure 112 to Figure 114). The summer thermal discomfort is slightly more elevated in the future in Roissy than in La Rochelle, but it is not clear if this is due to the climate model uncertainty projections or to the local climatic conditions themselves. While in La Rochelle optimizing for "summer design" will lead to minimal heating needs (for the specific building case-study), in Roissy this is at the cost of the heating needs and compromised design solutions between winter and summer design should be found.

In Carpentras, the building design does not evolve in the future, as the heating needs are already minimal during the winter and summer thermal discomfort elevated during the present climate. A high roof albedo/emissivity is even more beneficial in this climate than in La Rochelle and in Roissy, as already observed in Chapter 3 since the roof receives more solar radiation. However, this strategy is only applicable to the top-floor apartment of a collective building and the apartments under will not benefit from this strategy. For reducing the summer thermal discomfort, the windows were systematically minimized in all climates with a long overhang on the South façade, however additional solar shading was not used. The use of integrated shading devices on windows might be an interesting option to allow large windows (Chapter 1), but this needs to be accepted by the building occupants. With larger windows, even with the veranda and an overhang of 1 m, the summer thermal discomfort reaches very elevated levels as observed in Carpentras. Finally, the building with high thermal mass with exterior insulation was systematically optimized during present and future typical climates, as thermal mass was largely beneficial to reduce daytime temperature peaks. It

would be interesting to investigate the building response after a very long heatwave, as a building with high thermal mass will have a return period to acceptable indoor levels longer than with lower thermal mass. From a health point of view, very elevated daytime peak temperatures might lead to excessive morbidity, but in that sense, people could evacuate the building and seek refuge in air-conditioned spaces. Prolonged periods of hot temperatures during long but less intense heatwaves maintained indoor by the building high thermal mass will lead to a different health crisis management.

5.2 Analysis of the indoor overheating for optimized designs

In the first section, we analyzed the optimized Pareto solutions in each case-study city and for each ventilative cooling strategy. In this section, we assess more in detail the summer thermal discomfort, indoor overheating and potential health-heat-related-risk for the three optimized designs A, AB and B.

The summer indoor overheating is assessed under the three distinct climate periods:

- the present typical summer;
- the future typical summer;
- the future typical heatwave.

The three weather files used for the assessment were presented in Chapter 3. The solutions for the present-typical and future-typical summers are taken from the Pareto fronts presented in section 5.1.4.2. For the future heatwave period, building thermal simulations are conducted using the optimized solutions from the future-typical period, with the future heatwave weather files. Each solution A, AB and B represent a different optimized building design, a different combination of envelope parameters (thermal mass, glazing percentage, albedo and overhang length) and of the parameter related to ventilation. However, for a city and a ventilative cooling strategy, the design parameters of the optimized solutions A, AB and B during the present TMY are not necessarily the same as explained previously in Roissy and La Rochelle. During the future period in Roissy and in La Rochelle, and during present in future and Carpentras, building designs A, AB and B consistently have similar characteristics summarized in Table 34, so the designs are comparable amongst the ventilative cooling strategies. The building designs between future TMY and future HW are the same since the optimized solutions during the future TMY were used to conduct the heatwave building thermal simulations.

Table 34 – Summary of optimized building designs A, AB and B in future typical climates in the three cities (building configuration with buffer zones)

	Thermal mass	**Glazing Percentage**	**Roof albedo/emissivity**	**Overhang 1 m**	**Ventilative cooling parameter**
A	High	Low	High	Yes	Max airflow
AB	High	Low	Medium in Roissy and La Rochelle, High in Carpentras	No	Max airflow
B	High	Low in Roissy and LR, Medium in Carpentras	Low	No	Max airflow

5.2.1 Comparison of indoor overheating between present and future summers

The assessment of indoor overheating of the different designs is made using three indicators. The first is the maximum standard effective temperature, the second is the summer thermal discomfort as a sum of degree hours above a threshold (Equation (81)), and the third is the number of consecutive days of exposure to indoor overheating for which we consider there is potential heat-related health risk.

5.2.1.1 Maximum standard effective temperature

First, we compare for each ventilative cooling strategy the maximum standard effective temperatures SET of building designs A, AB and B during the three climate periods. This is done for the three cities (Figure 126 for la Rochelle, Figure 127 for Roissy and Figure 129 for Carpentras). "Present TMY" refers to the present typical summer, "Future TMY" refers to the future typical summer, and "Future HW" refers to the future typical heatwave. From the hourly calculated SET during the summer period, we found the maximum SET and the associated nighttime SET on that same day, considered as the hottest day.

The SET categories 25.6-30 °C, 30-34.5 °C and 34.5-37.5 °C are indicated on Figure 126, Figure 127 and Figure 129 as references. A SET between 25.6 and 30 °C, according to Table 1, indicates a thermal sensation "slightly warm" and "slightly unacceptable", and a physiological state of "slight sweating", and "vasodilation". A SET above 30 °C and under 34.5 °C, according to Table 1, indicates a thermal sensation "warm", "uncomfortable", and "unacceptable", while the equivalent physiological state is "sweating". A SET above 34.5 °C is considered as "hot" and "very unacceptable" and a physiological condition of "profuse sweating". For vulnerable people with reduced physiological adaptations (and lower thermal sensations), these physiological states and thermal sensations can be worse. In La Rochelle (Figure 126) and in Roissy (Figure 127), for each ventilative cooling strategy, we can observe a linear increase in both maximum daytime and nighttime temperatures from solution A to B and from the present typical summer to the future heatwave summer.

As observed in section 5.1.4.1, during the present and future typical years, building designs A and AB usually allow to maintain acceptable maximum SET, especially with the natural ventilation and earth-to-air heat exchanger solutions. For most simulations, the SET are higher with the free-cooling strategy than for the two other ventilative cooling strategies. During the nighttime, on the hottest day SET are always under the 25.6 °C threshold, except during the future heatwave period. During the present TMY with natural ventilation, we disregard solution B, because solution AB is the ideal solution (see green Pareto front in Figure 122-right-middle): from solution AB to solution B, there is no decrease in heating needs, as according to Appendix C, they have the same design variables, but only the windows opening percentage that varies from 50 to 10 %.

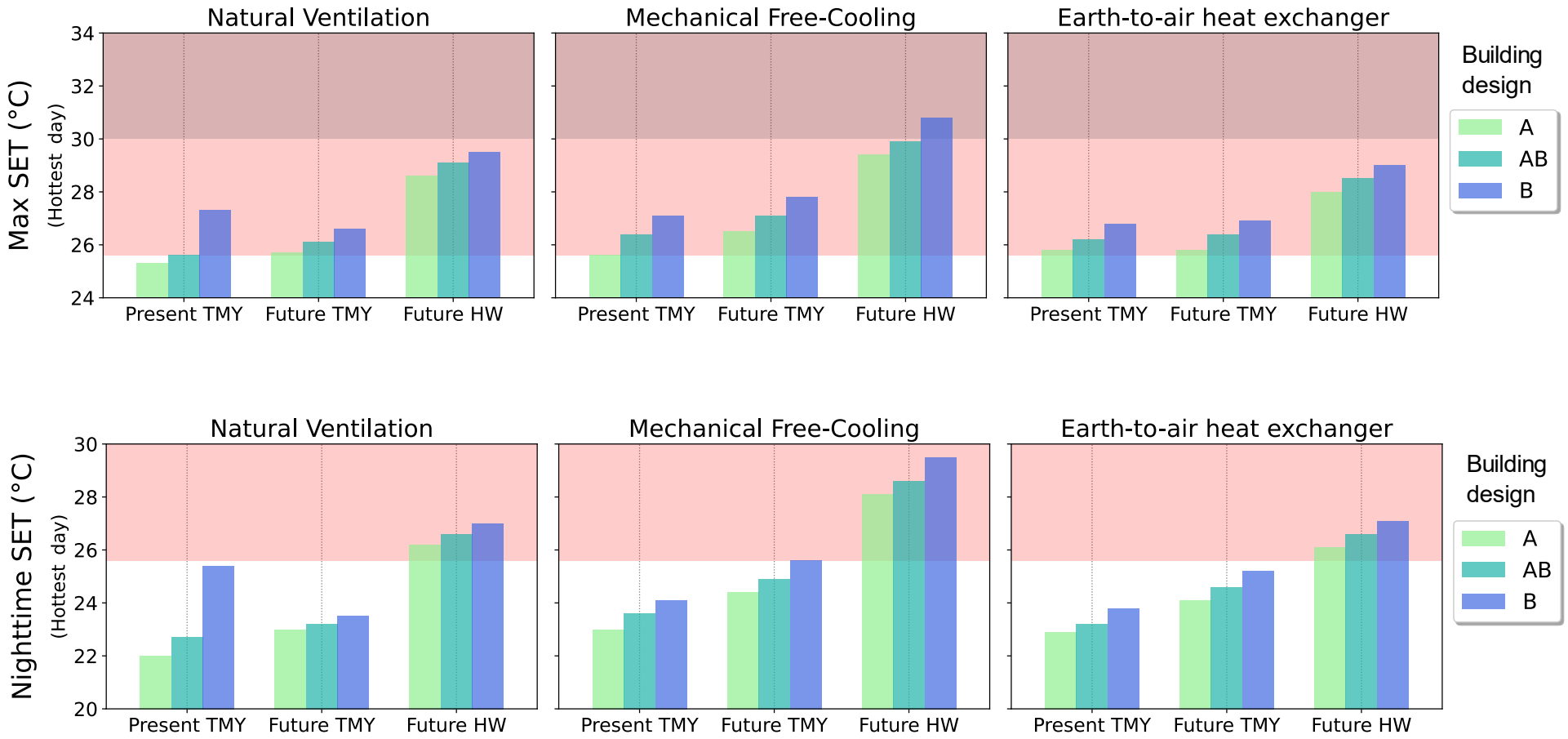

Figure 126 - Maximum daytime standard effective temperatures (top) and associated nighttime temperatures on the hottest day (bottom) in La Rochelle (indoor air velocity v = 0.1 m/s)

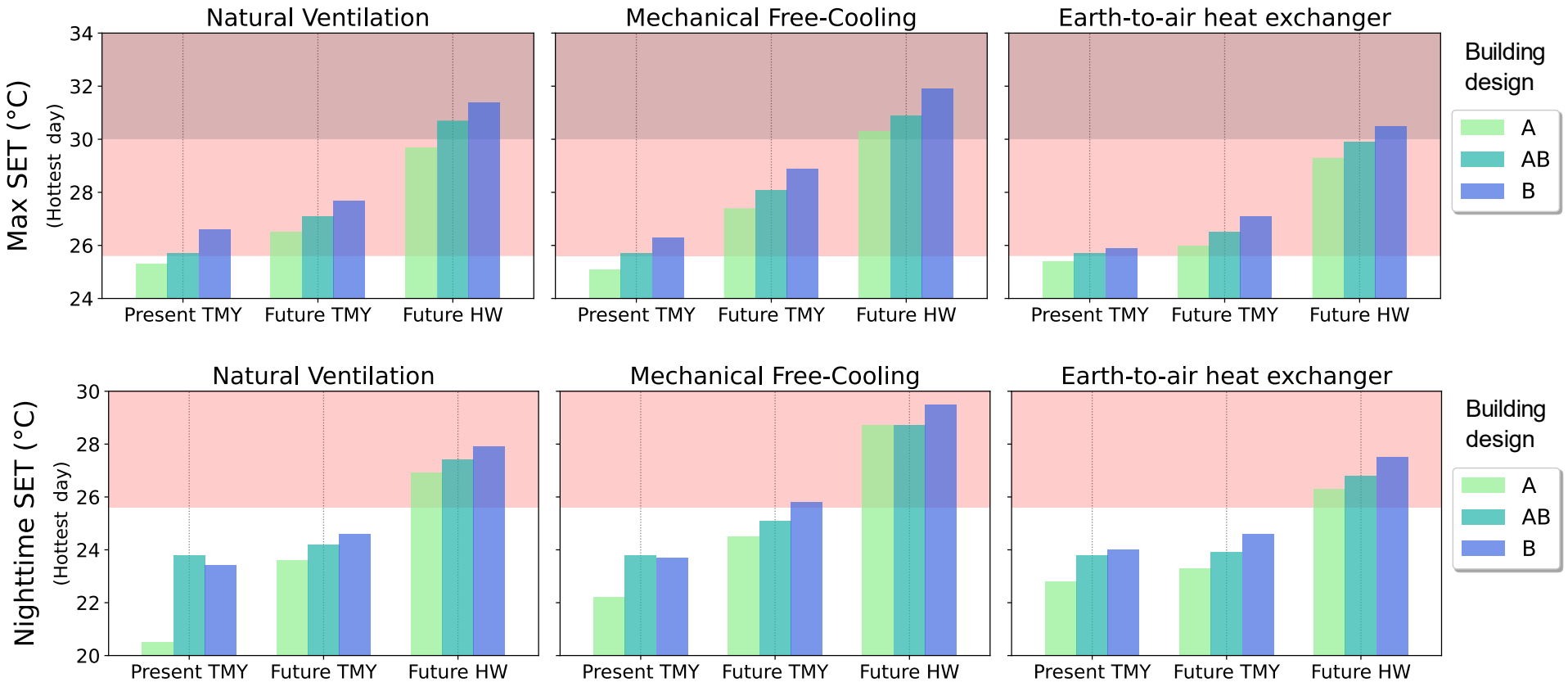

Figure 127 - Maximum daytime standard effective temperatures (top) and associated nighttime temperatures on the hottest day (bottom) in Roissy (indoor air velocity v = 0.1 m/s)

In Roissy, the increase in SET maximum temperatures is more pronounced between future TMY and present TMY than in La Rochelle, but it is unclear if this is due to local climate variations or due to the climate model used (Figure 116 and Figure 117). During the daytime, the increase is of around +1.2 °C for natural ventilation, +2.5 °C for free-cooling and +0.9 °C for earth-to-air heat exchanger in Roissy, while in La Rochelle it is of +0.5 °C, +0.8 °C and +0.1 °C on average between solutions A, AB, and B. In both cities, the increase in maximum SET is more pronounced between the future typical heatwave and the future TMY than between the future TMY and the present TMY. During the future heatwave, it is of +4.2 °C for natural ventilation, +5.4 °C for free-cooling and +4.2 for earth-to-air heat exchanger in Roissy, and +3.5, +3.7, and +2.2 in La Rochelle respectively. We can notice that the increase is the highest for the free-cooling and the lowest for the earth-to-air heat exchanger. This difference in maximum daytime temperatures between the future typical summer and future typical heatwave emphasizes the need to analyze future indoor conditions during future typical heatwaves, which might or might not be included in future typical years (Figure 74 to Figure 76).

During the nighttime, the SET increase between the future TMY and the present TMY are about +1 °C for natural ventilation, +1.8 °C for free-cooling and +0.5 °C for earth-to-air heat exchanger in Roissy, and about +1 °C, +1.5 °C and +1.4 °C in La Rochelle. While the increase in daytime SET is higher in Roissy than in La Rochelle, the increase in nighttime temperatures on the hottest day it is quite similar. The increase between the future typical heatwave and present TMY during nighttime is about +4 °C for natural ventilation, +5 °C for free-cooling and +3.3 °C for earth-to-air heat exchanger in Roissy, while it is of 4 °C, +5 °c and +3.5 °C in La Rochelle so this equivalent increase in nighttime SET is also consistent during the future heatwave.

In terms of absolute temperatures, during the future typical heatwaves, the daytime SET are well above 25.6 °C and above to 30 °C in some cases (solution B in La Rochelle free-cooling, solution AB, B in Roissy natural ventilation, A, AB, B in Roissy free-cooling, B in Roissy earth-to-air heat exchanger). Also, the nighttime SET temperatures are also above 25.6 °C for almost all optimized solutions. During the present and future TMY, the maximum SET (both daytime and nighttime) for the earth-to-air heat exchanger is not lower than for the natural ventilation strategy but is still better than the mechanical free-cooling. During the future heatwave however, the earth-to-air heat exchanger is the best ventilative cooling strategy. The poor efficiency of the earth-to-air heat exchanger can be explained because, at maximum airflow, its efficiency is only of 37 %. Indeed, the exchanger is buried at a 2 m depth with a length of 40 m. Even though the outlet air temperature exiting the tube is 10 °C lower than the outdoor air temperatures, at times, especially during daytime temperature peaks, it is actually higher than the indoor air temperature. However, it will be difficult to improve the EAHX efficiency considering the space constraints on site. This is investigated in section 5.2.4.

The air temperatures provided for the optimized envelope solution AB and for each of the three ventilative cooling strategies during the future typical heatwave in Roissy is presented in Figure 128. During the heatwave, the daytime indoor air temperatures with the earth-to-air heat exchanger are consistently lower than the two other solutions, of about 2.5 °C less than with the free-cooling solution and 1.5 °C less than the natural ventilation solution. As mentioned previously, the earth-to-air efficiency is quite low and if improved the air

temperatures would be lower. The natural ventilation strategy, due to high airflow rates, is efficient to reduce the air temperature, especially during the nighttime.

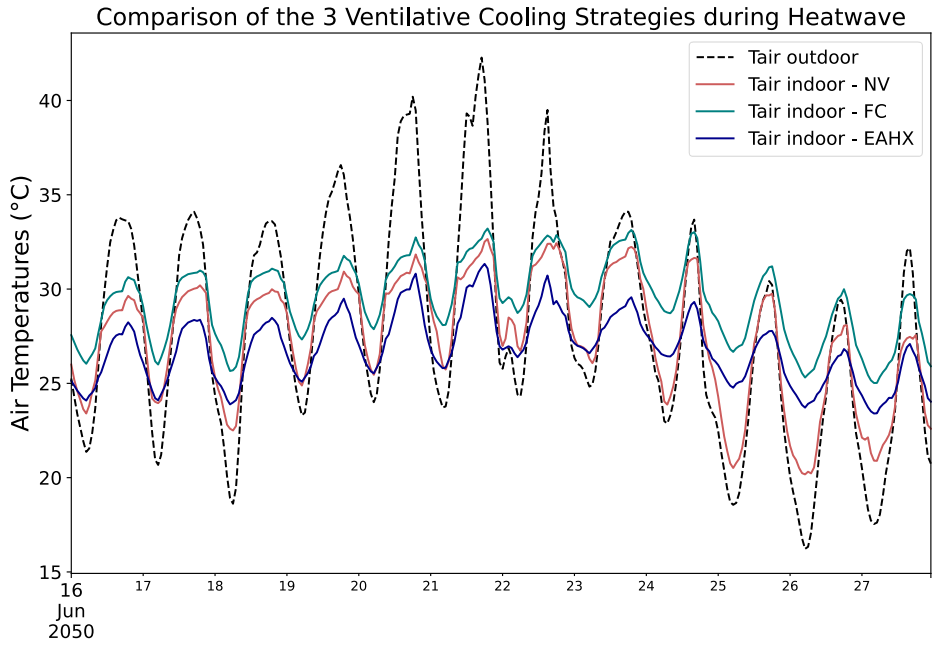

Figure 128 - Indoor air temperatures for the optimized building envelope design solution AB with the three ventilative cooling strategies during (06-16 to 06-22) and after (06-23 to 06-27) the future typical heatwave in Roissy

We can observe that after the heatwave the nighttime indoor air temperatures are much lower with the natural ventilation than with the two other ventilative cooling strategies. Due to the higher airflow rates, in comparison with the free-cooling, natural ventilation has a very high potential. As the airflows are maximized to lower the summer thermal discomfort during the entire period, this could result in cool discomfort. The optimization of the hourly or daily control of the ventilative cooling strategy would be ideal and is one of the perspectives of this work. However, we examine in particular the warm summer thermal discomfort, and no ventilative cooling strategy allows to maintain the indoor air temperature under 25 °C on the warmest nights. The nighttime temperatures are reduced by 2 °C for the same airflow rate between the earth-to-air heat exchanger and the free-cooling.

In Figure 129 the daytime and nighttime SET on the hottest day are presented for Carpentras. During the present TMY, for solutions A and AB each ventilative cooling strategy allows the daytime SET to remain under or close to the 30 °C threshold, and the nighttime SET close to the 25.6 °C on the hottest day of each period. Contrary as to the results in La Rochelle and in Roissy, there is a high distinction in SET temperatures between the optimized investigated solutions. Indeed, solution B consistently leads to a much higher maximum temperature than the other two, and during the future typical heatwave the daytime SET is above the 34.5 °C threshold (category of “hot” and “very unacceptable” indoor environment) for the three ventilative cooling strategies. This strong thermal discomfort of design solution B was already observed in Figure 124 and Figure 125 (top left of the Pareto Fronts). According to Table 34, solution B is optimized with medium sizes windows, no overhang, and a roof with low albedo and emissivity, it has no protection against solar heat gains. For the hot climate of Carpentras, this solution might not be realistic, especially during the future climate, unless additional solar shading is used on windows. This option is examined later in section 5.2.3.

Comparing the three ventilative strategies, the earth-to-air heat exchanger always leads to the lower SET, especially during the daytime. For each solution, the increase in daytime maximum SET is of around +2.5 °C between the future TMY and the present TMY, and +4 °C between the future heatwave and the present TMY. In this city, the increase is more pronounced between present and future, which can be explained because the future typical year already contains a heatwave, as heatwaves are projected to occur every year in the mid-century in Carpentras (Figure 76). The increase in nighttime temperature is +2.5-3 °C for both future heatwave and TMY compared to the present.

The effect on an increased indoor air velocity due to the use of fans for instance, on the SET calculation is shown in Figure 130 for Carpentras. We can observe a reduction in the maximum SET of around 2 °C for each solution. In the future TMY, the solutions A and AB are under the 30 °C threshold, while during the future typical heatwave the maximum solutions are about 32 °C instead of 34 °C. The nighttime temperatures SET are also decreased to a maximum of 27 °C.

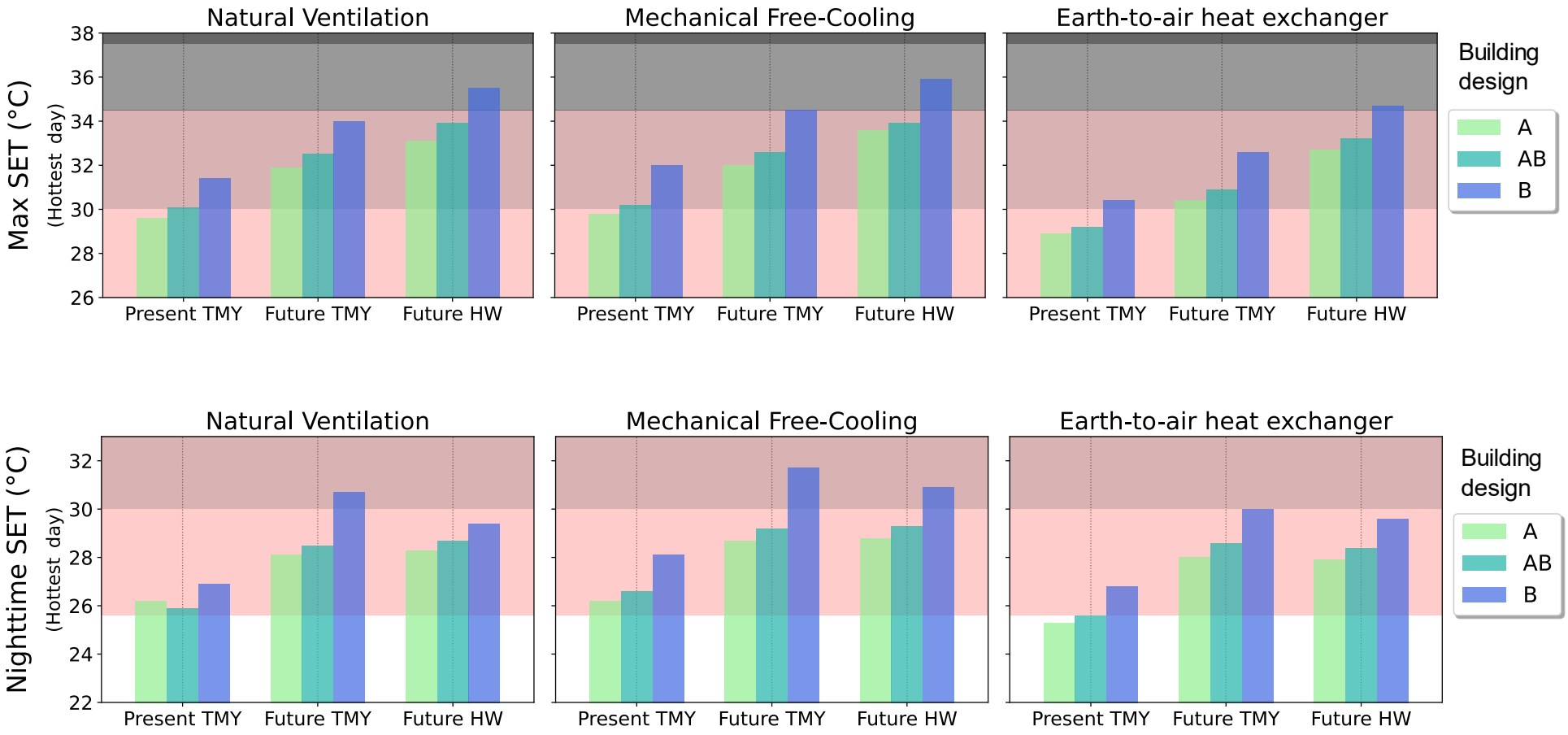

Figure 129 - Maximum daytime standard effective temperatures (top) and associated nighttime temperatures on the hottest day (bottom) in Carpentras **(indoor air velocity v = 0.1 m/s)**

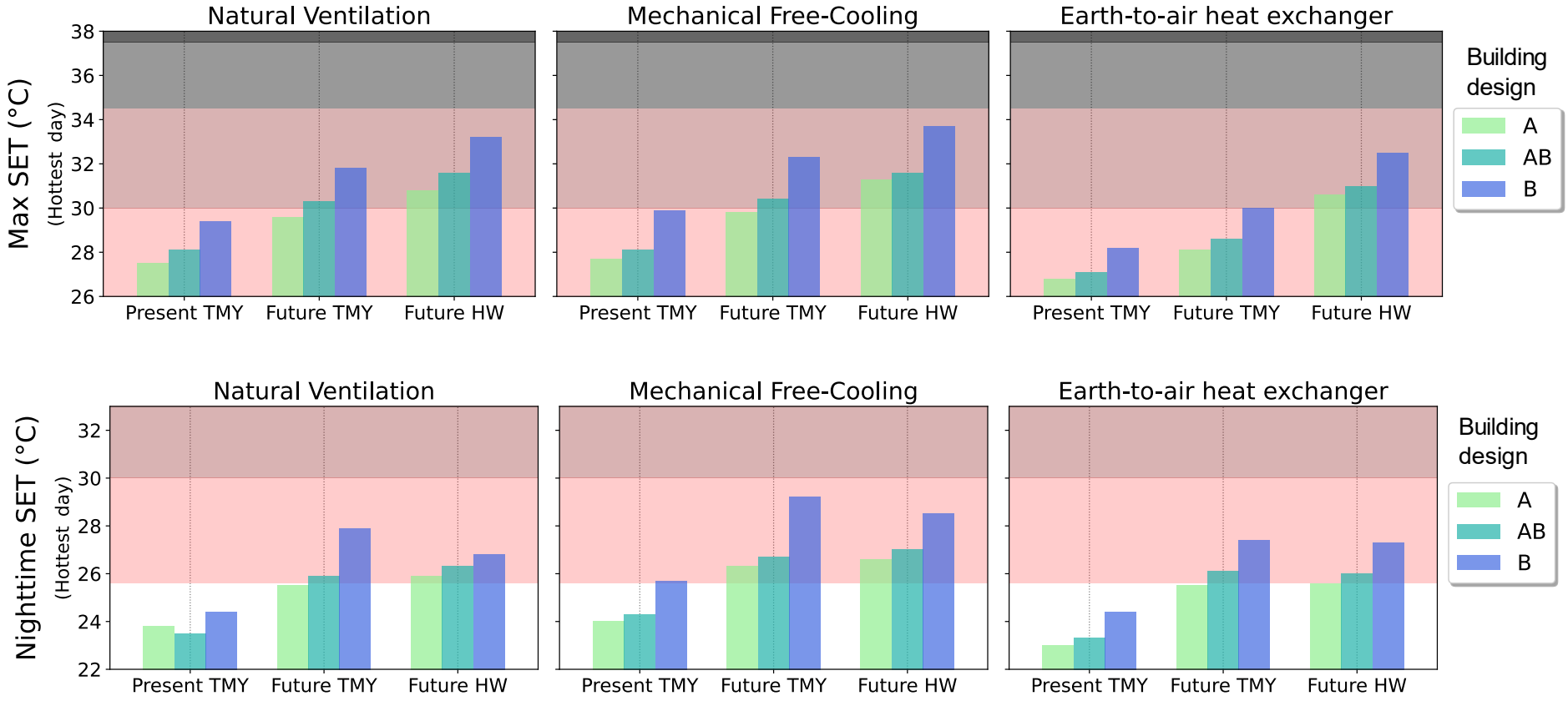

Figure 130 - Maximum daytime standard effective temperatures (top) and associated nighttime temperatures on the hottest day (bottom) in Carpentras **(indoor air velocity v = 0.4 m/s)**

5.2.1.2 Summer thermal discomfort hours (DH)

This is the indicator used in the optimization in section 5.1.4. The summer thermal discomfort hours is presented for La Rochelle in Figure 131 , for Roissy in Figure 132 and for Carpentras in Figure 133.

In La Rochelle, as noticed previously, we can observe that the summer thermal discomfort is low during present and future TMY for all ventilative cooling strategies, except the free-cooling for which it is around 200 °C.h. However, for all three air passive cooling systems, summer thermal discomfort occurs under the future typical heatwave, and it is more elevated with the free-cooling system (1254 °C.h), especially for building design B. For this configuration, there are 7 °C.h above the SET threshold at 30 °C which is a high threshold for vulnerable people corresponding to an operative temperature of 31.6 °C on the hottest day (Table 44 in Appendix D). On the opposite, the lowest summer thermal discomfort is reached with solution A with the earth-to-air heat exchanger, it is seven times less (173 °C.h) than the one with the free-cooling and building design B and the maximum operative temperature is reduced to 29.2 °C. Therefore, in La Rochelle, even under the future typical heatwave, it is possible to reach an "acceptable" indoor environment with the envelope optimized for the summer (building design A) and the earth-to-air heat exchanger. Another alternative is to promote the use of indoor fans, as an increased indoor velocity of 0.4 m/s will result in much lower indoor overheating under the future typical heatwave (227 °C.h for the worst building design FC-B, so divided by more than five, and 5°C hours for the best building design EAHX-A).

In Roissy, the results are quite similar as in La Rochelle, with slightly higher summer thermal discomfort during future climate sequences but the trend amongst the solutions is similar such as for the maximum SET. The highest severity is of 1856 °C.h for the worst solution (FC-B), which can be reduced by two with the same building design (B) but increased airflow rate by natural ventilation, or by three for the same building design (B) with cooler air provided by the earth-to-air heat exchanger. With the increased air velocity (0.4 m/s), the severity remains below 200 °C.h under the future typical heatwave for all solutions except for the free-cooling solutions AB and B.

In Carpentras, as observed previously, in this city the summer thermal discomfort is very elevated. The difference with the two other cities is that during the future typical summer, the aggregated summer thermal discomfort is higher than during the future typical heatwave summer. This is explained because the typical summer contains multiples heatwaves, while the year containing the most intense heatwave contains only one shorter heatwave. This demonstrates the variety of different climatic conditions that can be found while reassembling typical years. We can clearly observe the limits of the three ventilative cooling strategies during the future periods: The summer thermal discomfort °C.hours are between four to six times higher between the future and present typical summers for all ventilative cooling strategies (simulations with the default air velocity of 0.1 m/s). With the increase in indoor air velocity (Figure 134), the summer thermal discomfort is reduced by around three for the solutions with natural ventilation and free-cooling, and by five for the solutions with earth-to-air heat exchanged, because the delivered air to the living space is cooler so this result in a larger decrease.

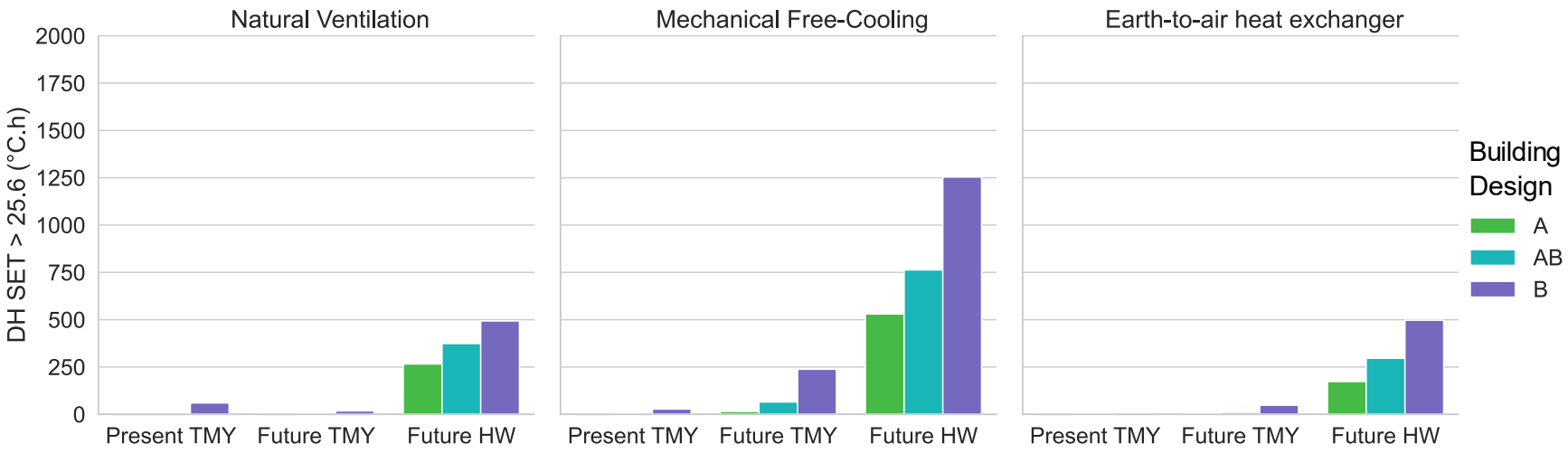

Figure 131 – Summer thermal discomfort: SET > 25.6 (°C.h) in La Rochelle, indoor air velocity = 0.1 m/s

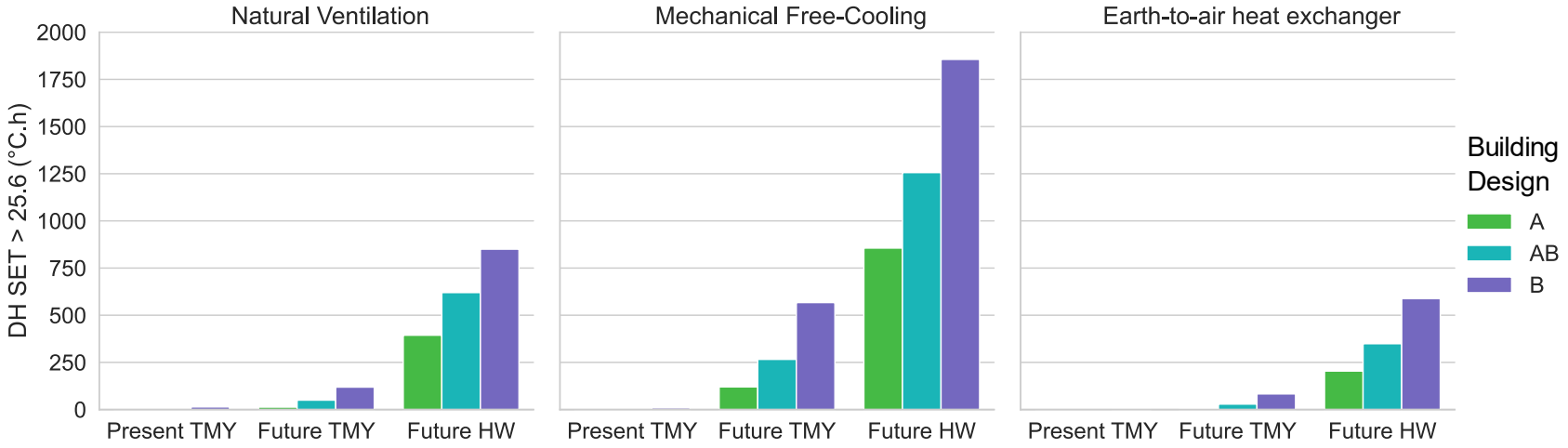

Figure 132 - Summer thermal discomfort: SET > 25.6 (°C.h) in Roissy, indoor air velocity = 0.1 m/s

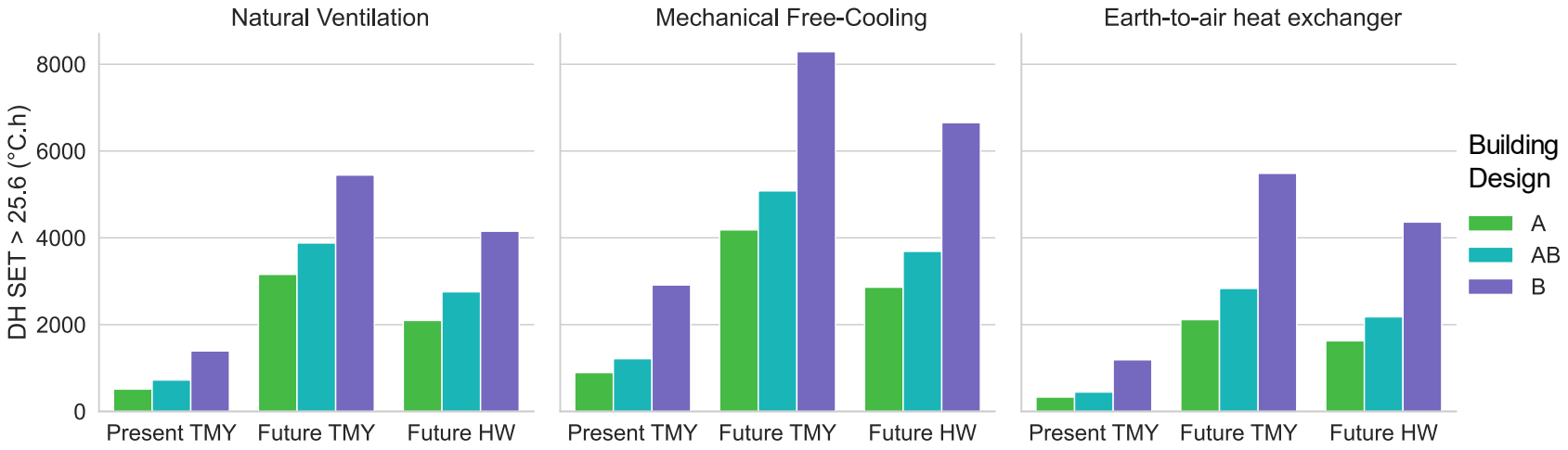

Figure 133 - Summer thermal discomfort: SET > 25.6 (°C.h) in Carpentras, **indoor air velocity = 0.1 m/s**

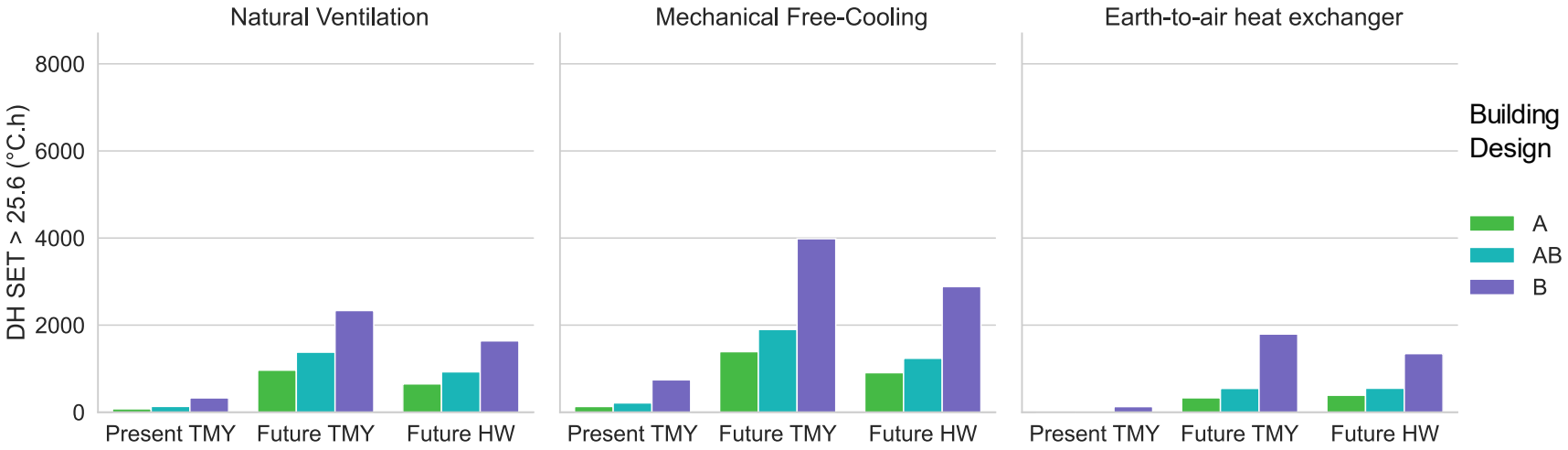

Figure 134 - Summer thermal discomfort: SET > 25.6 (°C.h) in Carpentras, **indoor air velocity = 0.4 m/s**

5.2.2 Evaluation of potential heat-health-related risk during future typical heatwaves

In this section, we evaluate the duration and severity of consecutive days of indoor overheating during future typical heatwaves. We defined two indicators that correlate indoor overheating with potential health-heat-related risk. The indicators are based on both daytime and nighttime thresholds, similar as the definition of outdoor IBM heatwave events (Equation (31)). The first indicator is the indoor overheating duration ($IOH\_Duration_{HW}$) related to potential health-related-heat risk during consecutive days (N) of heat exposure when both daytime and nighttime SET are above the 25.6 °C threshold, Equation (82). The second represents the severity of the indoor overheating during the consecutive days, it is calculated with Equation (83) and (84).

$$IOH\_Duration_{HW} = \sum_{N} (\mathrm{SET}_{\mathrm{daytime}}\ AND\ \mathrm{SET}_{\mathrm{nighttime}}) > 25.6 \tag{82}$$

$$IOH_{HW}(t) = (\mathrm{SET}_t - 25.6)_{\mathrm{SET}_t > 25.6} \tag{83}$$

$$IOH\_Severity_{HW} = \sum_{t}^{n\Delta t} IOH_{HW}(t_{daytime}).\Delta t_{daytime} + IOH_{HW}(t_{nighttime}).\Delta t_{nighttime} \tag{84}$$

The indoor overheating correlated to potential heath-heat-related risk was evaluated during the future typical years in Roissy and in La Rochelle, but it never occurs. However, during the future typical heatwaves, it occurs for all optimized designs and in each of the three cities. An example of indoor warm consecutive days with potential heat-health-related risk during the heatwave in Carpentras is presented in Figure 136.

The top part of the graph showcases the indoor and outdoor relative humidity. As no humidity sources are modelled indoors, the difference is calculated from the air temperature difference. The part below are the outdoor air and indoor operative temperatures. Below, the indoor conditions: The hourly SET is represented, with the indoor operative temperature as an indication. The indoor overheating severity, during the heatwave period is highlighted in orange. The two lower graphs represent the indoor daytime (in red) and nighttime (in blue) overheating separately, counted above the 25.6 °C threshold.

The heatwave period, according to its definition, is from the 27th of July until the 12th of August 2051. We can observe that the indoor overheating period starts on the 26th of July and ends of the 21st of August, nine days after the end of the outdoor heatwave, which is the time the building fabric needs to cool down. This signifies that the outdoor IBM heatwaves (defined in section 2.3.1.6) are well-chosen as they lead to indoor periods of consecutive warm days. The highest health-heat related risk (SET > 30 °C, highlighted in dark orange and dark red) occurs around the outdoor temperature peak. This elevated temperature represents a high risk especially for vulnerable people and the elderly.

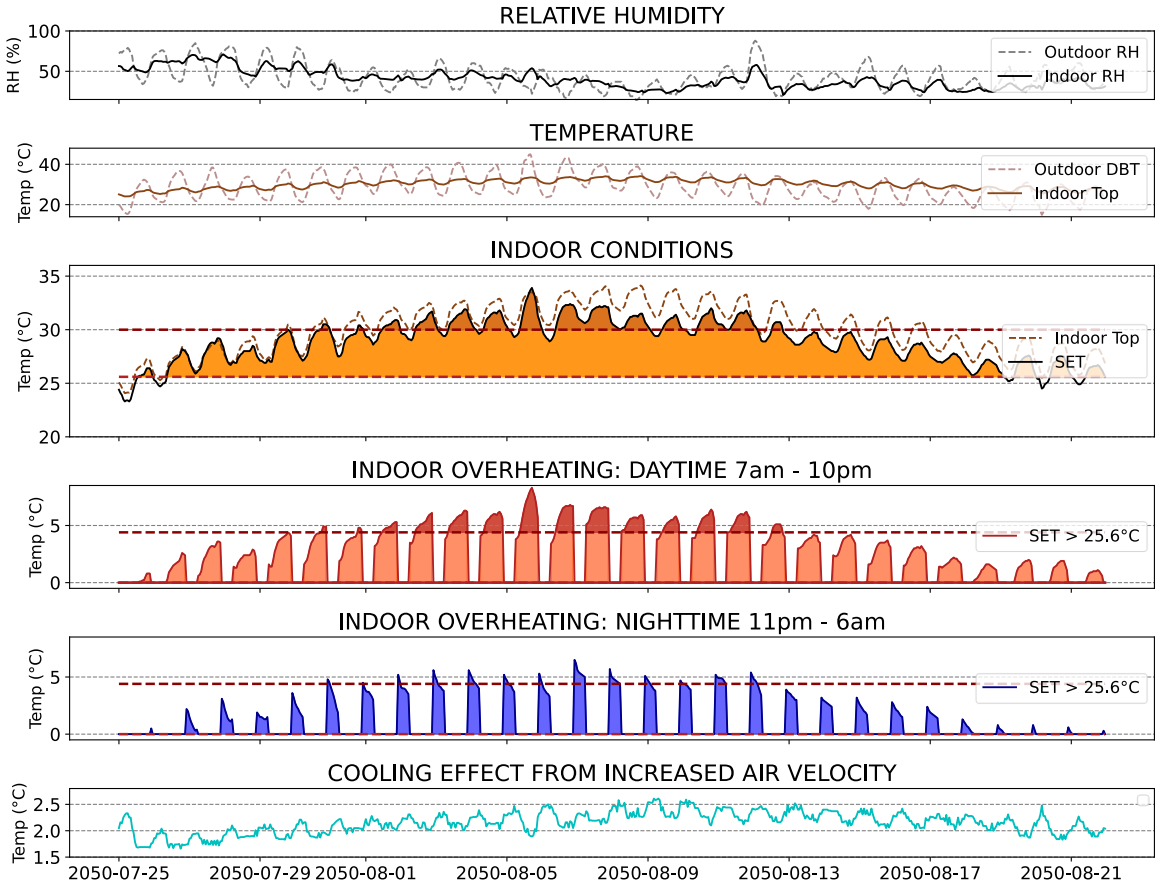

Figure 135 – Consecutive days of potential health-heat-related risk during (27th July – 12th August) and after (13th-22th of August) the future typical heatwave in Carpentras for building design AB with the free-cooling system, default air velocity = 0.1 m/s. The indoor overheating severity is highlighted in colors.

We can observe that after the hottest day of the heatwave (6h of August), the SET decreases due to a decrease in outdoor relative humidity, but the indoor operative temperature keeps increasing and starts lowering 3 days after the outdoor peak. A building with a lighter thermal mass will cool down faster, however the heat stress during the hottest days would probably be much worst. Mechanical free-cooling ventilation is not enough to lower the indoor temperatures quickly.

The number of consecutive days of indoor overheating above the SET threshold of 25.6 °C during both daytime and nighttime was calculated for each city and for each solution, they are shown in Figure 136. The severities during these consecutive days were also calculated, they are in Figure 137. We can observe for instance that for the building design AB presented in Figure 135 in Carpentras, the indoor overheating period is reduced of 5 days (28 to 23) with nocturnal ventilation through windows (higher airflow rates).

In all cities, consecutive exposure to heat indoor is present during at least a week, and can be correlated to a health-heat-related risk, according to our definition. The earth-to-air heat exchanger leads, in all cases, to the lowest severity and the lowest number of consecutive days with heath-heat-related risk. In La Rochelle, during the heatwave, the outdoor maximum air temperatures are elevated for a shorter period than in the two other cities (Figure 79). This can explain why even with the building design B that does not protect from heat the natural

ventilation is efficient to evacuate the heat gains within a week. The number of days is similar for the earth-to-air heat exchanger, but the severity is lower for this latter, which is explained by the fact that with natural ventilation the nighttime temperatures cool down faster, but with the earth-to-air heat exchanger the daytime temperatures cool down faster. In the two other cities, as maximum temperatures are more elevated, the interest in using the earth-to-air heat exchanger instead of nocturnal ventilation is more obvious. In Carpentras, all design solutions lead to a calculated health-heat-related risk of minimum three weeks. For the worst building design (B), the number of consecutive days is over two months (not shown in Figure 138 but in Appendix D), because it merges with another heatwave occurring earlier that same year. The nighttime temperatures in the case of the earth-to-air heat exchanger and free-cooling remain above SET 25.6 °C during the two indoor overheating periods. The same analysis is conducted with an indoor air velocity of 0.4 m/s (Figure 138 and Figure 139). We can observe that the decrease of indoor overheating exposure and related health-heat-related risk is quite impressive, as in Roissy and La Rochelle the severity is very low or even null for the best building design (A) with the earth-to-air heat exchanger. In Carpentras the severity is reduced by more than half and the duration by around a third.

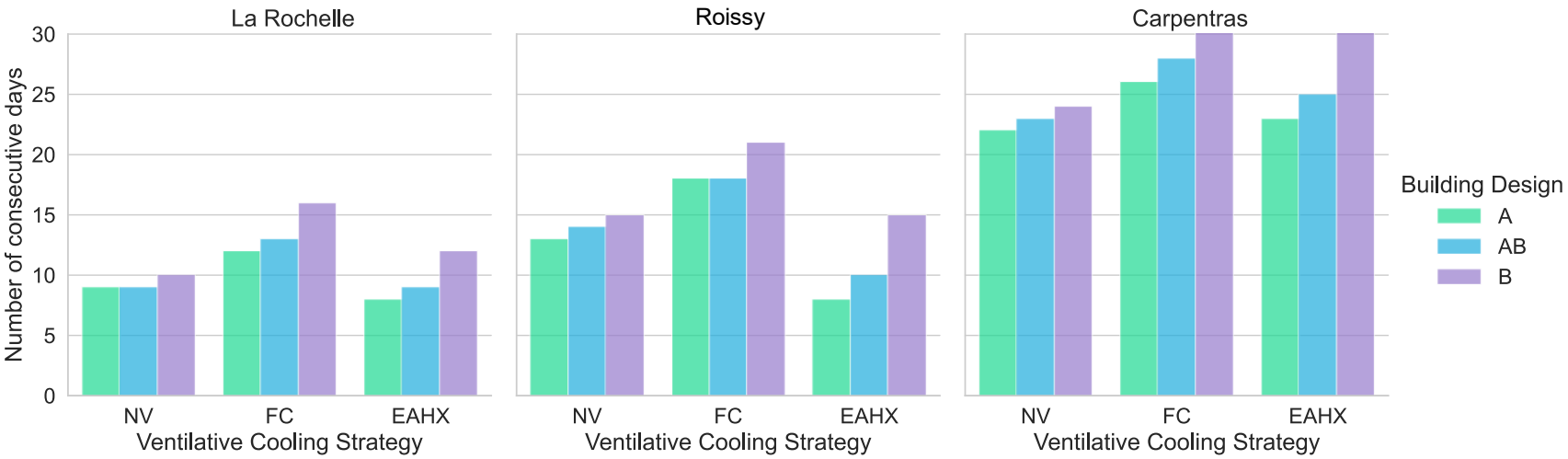

Figure 136 - Number of consecutive days of potential health-heat-related risk during future typical heatwave (indoor air velocity = 0.1 m/s)

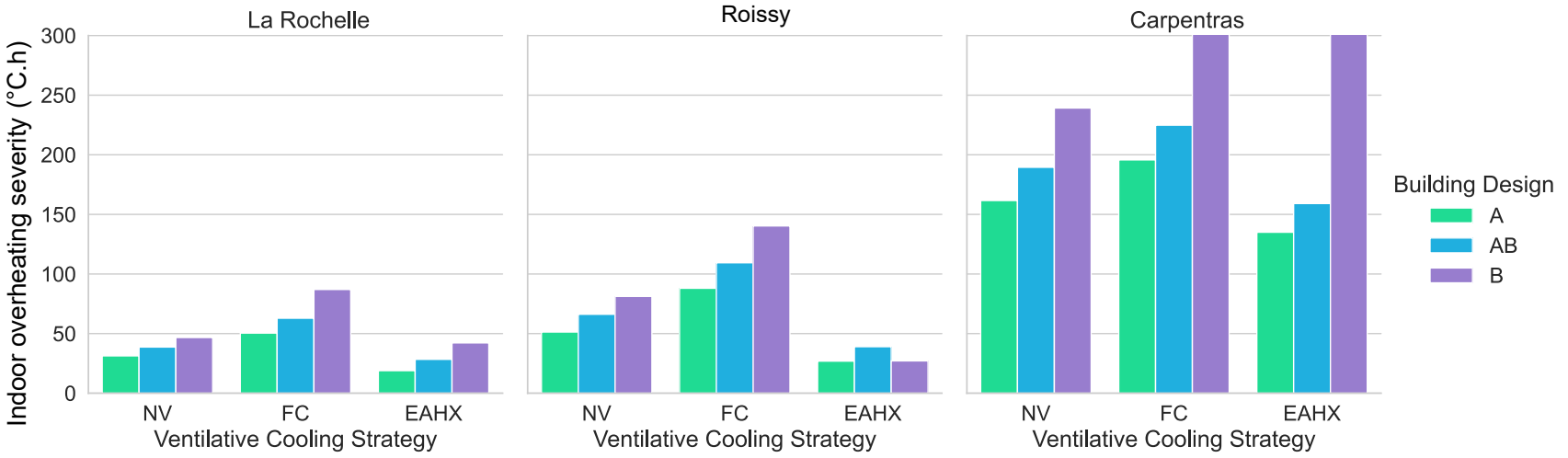

Figure 137 – Indoor overheating severity during future typical heatwave (indoor air velocity = 0.1 m/s)

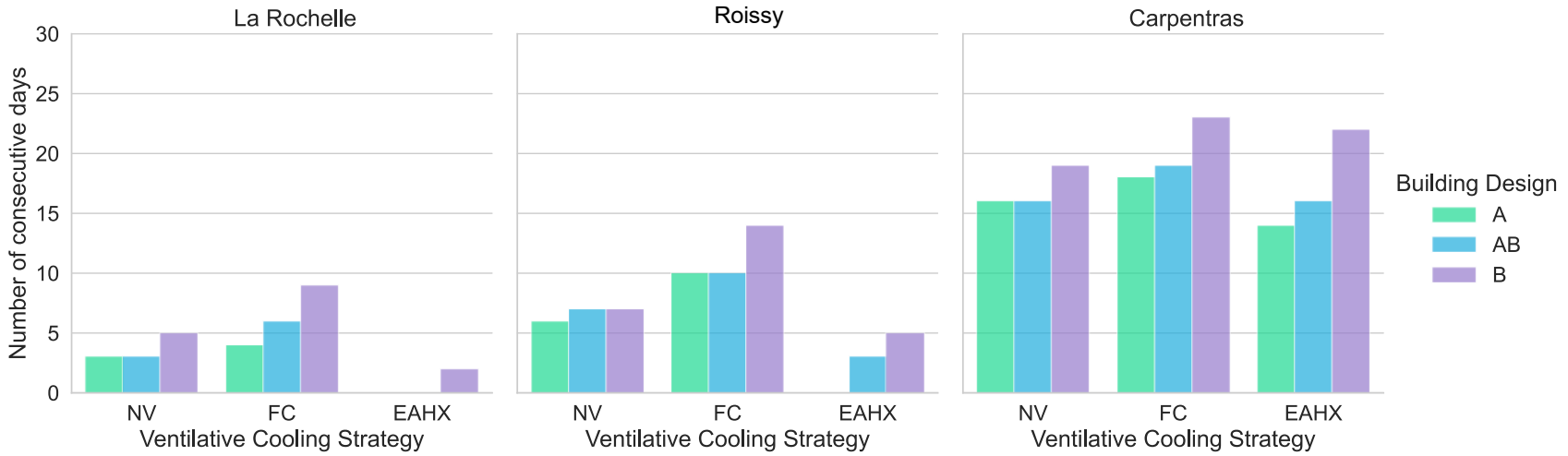

Figure 138 - Number of consecutive days of potential health-heat-related risk during future typical heatwave **(indoor air velocity = 0.4 m/s)**

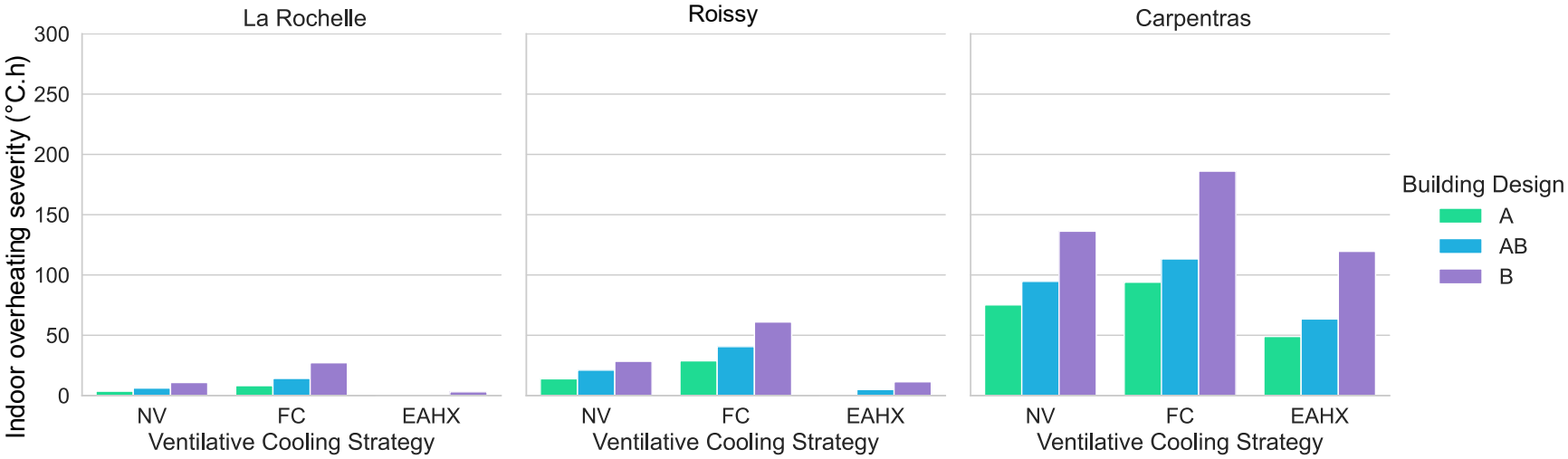

Figure 139 – Indoor overheating severity during future typical heatwave **(indoor air velocity = 0.4 m/s)**

5.2.3 Impact of solar shading: a balance between illuminance and indoor overheating

In this section, we evaluate the influence of additional solar shading on windows. This is about internal or external shades, independent of the overhang. This strategy is complex because it totally depends on the building occupants' habits and adaptive opportunities, or acceptability if the shades are operated. It is even more complex as solar shading reduces indoor daylight and visual comfort, which occupants usually appreciate. However, in Mediterranean climates the population is used to prevent from heat and to maintain shutters closed during the daytime. We investigate different types of shades (interior shades, exterior rollers, exterior shutters) and their impact on the indoor overheating.

As an illustration we assess the potential reduction of indoor overheating during the future typical summer in Carpentras with the ventilative cooling strategy leading to the highest indoor overheating, the mechanical free-cooling. For each shading system, the overheating severity is calculated, as well as the illuminance inside the living space. The illuminance was calculated using the SplitFlux algorithm presented in section 2.4.2.2. The living space floor plan was divided into a grid with 9 luminance points equally spaced. Here is presented only the luminance point that is in the middle of the living space (Figure 140). It receives more natural light that the points located closer to the walls without windows, but it receives less light than the points located closer to the walls with windows.

Figure 140 - Floor plan partitioned and illuminance point of interest (Splitflux calculation), top view

The analysis is conducted on the 1st of August which is in the middle of the summer period for building designs A, AB, and B (Figure 141). According to Table 34, the building design A has small windows with an overhang of 1 m, building design AB has small windows with an overhang of 0.1 m, and building design B has medium sizes windows with an overhang of 0.1 m. This distinction will greatly impact the indoor illuminance, especially because the presence of the veranda already greatly reduces the illuminance in the living space. The building design B has a roof albedo of 0.1 so it receives much more solar gains from the roof than the two other solutions with albedo of 0.8 and 0.9. All building designs have high thermal mass.

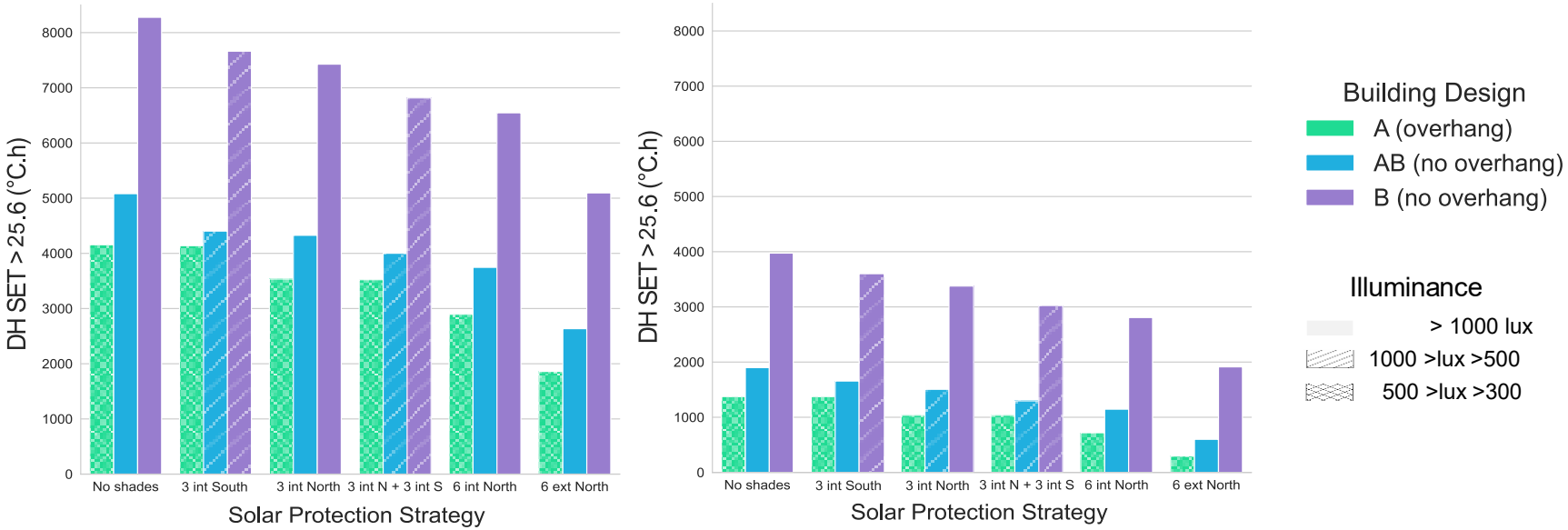

Figure 141 - Indoor overheating severity in future typical summer in Carpentras with free-cooling as ventilative cooling strategy: Effect of solar protection and increased indoor air velocity (left air velocity = 0.1 m/s, right air velocity = 0.4 m/s)

In Figure 141 the indoor overheating severity (°C.h of SET > 25.6) during the future typical summer of Carpentras is presented for an indoor air velocity of 0.1 m/s and 0.4 m/s for the different shading configurations. For each solution the illuminance of the point in the center of the living space is presented in hatches. The severity of solution B is much more elevated than the two others due to the low roof albedo.

In comparison with the configuration with no shades, we first investigated the use of three interior shades on the South façade. They are used when the incoming solar radiation on the façade is superior to 300 W/m². Using these three shades contributes to reduce the indoor overheating severity of around 1000 °C.h for both building designs AB and B (low indoor air velocity), and of about 400 °C.h for the calculation with elevated indoor air velocity. For design A with the overhang, it does not reduce the indoor severity, since the overhang already blocks all incoming radiation at the time the shades are on. The illuminance at the center of the living space around 650 lux at noon for building designs AB and B (without overhang), and of around 350 lux for building design A. The difference is from the incoming illuminance from the three unshaded windows on the South façade with and without the overhang presence. We then investigated the use of three interior shades on the North façade instead of on the South façade. These are used when the incoming solar radiation on the North façade is > 100 lux (the North façade has a 0.6 m overhang). For building designs AB and B it leads to similar indoor overheating severity than with the shades on the South facade, however for the building design A it is reduced. Similar illuminance is noted for the building design A, a higher illuminance is noted for building designs AB and B of about 1200 lux. The third configuration is the combination of the three interior shades on the North and South façade, which is a further reduction in indoor overheating severity for building designs AB and B (no overhang), with reduced indoor illuminance to 630 lux, as expected the indoor overheating severity is the same for building design A (overhang). Then, we investigated six shades on the North façade and no shades on the South façade (to allow some illuminance), which is a greater improvement for building design A, with still more than 300 lux in the middle of the room. For building designs AB and B the illuminance is over 1000 lux as it comes from the six South windows. Finally, we analyzed using exterior shutters instead of interior shades on the North façade, which further reduces the indoor overheating. The effectiveness of the shades on the North façade in comparison with the South façade is increased by two factors: Due to the interior solar distribution of EnergyPlus, the living space does not receive direct solar radiation from the South façade but only diffuse radiation. The presence of the veranda also reduces the amount of beam radiation received by the living space windows (which enters as diffuse).

We can conclude that the use of solar shading during warm periods with an acceptable level of indoor illuminance (300 lux, acceptable according to (European Standard, 2007)) can greatly reduce the indoor overheating severity. It is divided by around two for all building designs (best shades option to reduce indoor overheating). On the right part of Figure 141 we can see the combined effect of solar shading and increased air velocity. For the two building designs A and AB, the resulting indoor overheating severity is of 297 °C.h and 600 °C.h respectively. This is a reduction by factors thirteen and eight respectively in comparison with no shades and no increased indoor air velocity. The low reduction of indoor severity with the overhang (difference between solution A and AB) is specific to the building case-study, as we understood from section 5.1.3.2 that the effectiveness of the overhang is reduced by the veranda presence. Without the overhang, the indoor overheating severity of building design

AB would be closer to the one of solution B and it would be greatly reduced by building design A.

5.2.4 **Improving the earth-to-air heat exchanger efficiency**

We could observe previously that the earth-to-air heat exchanger efficiency is only about 38 % which is not usual, as their efficiency can be up to 90 %. Due to its low efficiency, and the energy efficient optimized building envelope, for very high outdoor temperatures, the outlet air temperature of the EAHX can be slightly (not more than 1 °C) superior to the indoor air temperature. For instance, when the outdoor air temperature is equal to 40 °C, the inlet air temperature is reduced of 10 °C by the earth-to-air heat exchanger, but as the optimized building design has high thermal mass, the indoor air temperature is already of 29 °C. In these cases, ideally the earth-to-air heat exchanger would be by-passed. However, as in the EnergyPlus model the tube has no inertia between two timesteps, when the EAHX is bypassed the outlet air temperature is directly equal to the ground temperature, leading to a lower temperature than the indoor air temperature. At the next timestep, the EAHX is reactivated which results in a ping-pong on and off of the EAHX airflow. Increasing the delta temperature between the outlet EAHX air temperature and the indoor air temperature does lead to lowered maximum indoor air daytime temperatures, however it highly reduces the cooling potential at other moments so it is not beneficial.

Ideally, the earth-to-air heat exchanger efficiency must be improved. Usually, several tubes are displayed in parallel instead of one single tube, with lower airflows in each tube to reach the same outlet aggregated airflow. For instance, to reach 0.27 m^3/s of cooled air (972 m^3/h, corresponding to 3 ACH of the living space) needed to refresh one apartment (the airflow rate of the EAHX was maximized in the optimization as it renews higher indoor air volumes), three tubes could be placed in parallel with each an airflow of 0.09 m^3/s, resulting in much better efficiency. However, the apartment case-study is part of a collective building in an urban context. The building is made of eight floors with approximately three apartments of the same size on each floor (equivalent to more apartments of lower sizes), resulting in 24 apartments that need to be delivered 3 ACH of cooled air each at maximum capacity. The building footprint is of length 48 m and width 11.5 m (assuming a 0.5 m overhang on the North façade and 1 m overhang on the South façade). Different spacing between pipes is reported in the literature, varying from 1.1 m to 2 m. We assume a spacing of 1.1 m as in (Grosso & Chiesa, 2015) and pipes length of 40 m. With the given building footprint, even with two rows of pipes on top of each other, that is a total of 20 pipes, there is not even enough space for one pipe per apartment (Figure 142).

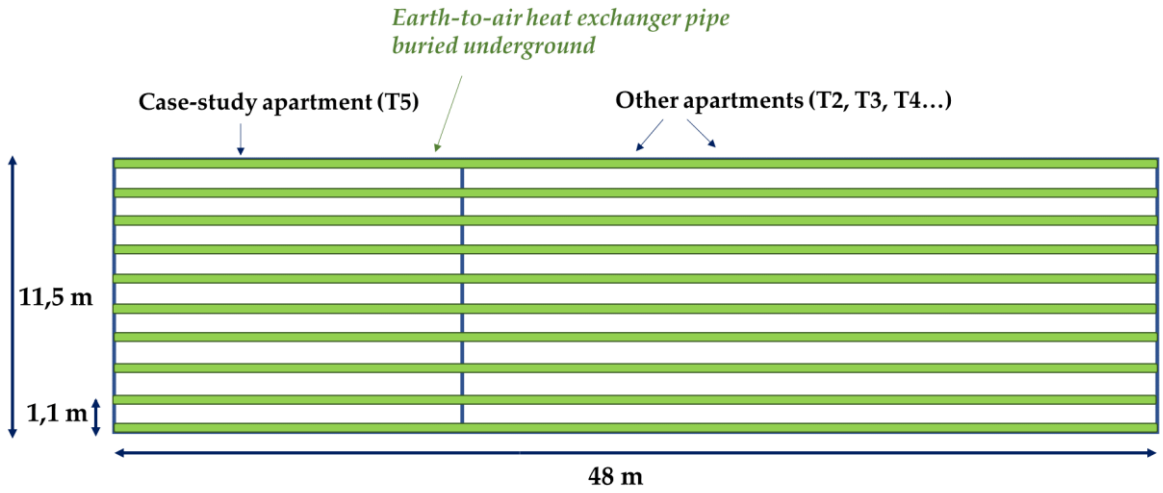

Figure 142 - Representation of earth-to-air heat exchanger pipes disposition under the building

For a collective building we can imagine that pipes are buried under the parking, so at a 4 m and 5 m depth. We conducted the simulation for one single tube, burring the pipe from 2 m to 4 m leads to a reduction of an indoor air temperature of 1 °C only. Furthermore, the ground thermal diffusivity was assumed for a wet clay which is more advantageous than a drier soil with lower thermal diffusivity for heat transfer. With climate change, the ground could be drier. In an urban context, there are space limitations for the implementation of an earth-to-air heat exchanger. Imagining for instance an underground pipes system implemented during the construction phase of an entire eco-district with a garden footprint, many more pipes could be buried resulting in better efficiency and lower indoor air temperatures.

5.2.5 Discussion on summer thermal comfort, discomfort, and heat-heath-related risk

In this section, we analyzed the indoor overheating and associated summer thermal discomfort and health-heat-related risk of the optimized building designs with the three ventilative cooling strategies. The analysis was conducted with three indicators: one analyzing daytime and nighttime temperatures on the hottest day of the summer, one analyzing the aggregated summer thermal discomfort during the summer or heatwave period, and one analyzing the duration of indoor overheating, correlated to health-heat-related risk during the future heatwaves. The three indicators are complementary in the sense that they bring different information. Indeed, the heat stress is different if people are subject to hot or very hot temperatures, during a short or prolonged period of time, recurrently or during consecutive days. These indicators, with this methodology analyzing the conditions during future typical heatwaves, give potential for more detailed studies to analyze heat stress, using more developed comfort models such as the one developed in the CSTB (El Kadri et al., 2020).

We could observe that while the summer thermal discomfort is low for some optimized building designs under future typical summers in La Rochelle and in Roissy, during future

heatwaves the maximum temperatures were around 3 °C higher than during the future typical summers. Similarly, while the summer thermal discomfort with the threshold at 25.6 °C was almost null, we could observe consequent indoor overheating during consecutive days for some building designs under the future typical heatwaves. The analysis during the heatwaves periods showed that at least one week and up to three of consecutive exposure to indoor heat, which could result in a health-heat-related risk according to the selected thresholds. The threshold of 25.6 °C during daytime and nighttime temperatures is subject to debate, however we assume that the building can be occupied by the most vulnerable elderly, which have reduced adaptation capacities and lower thermal sensations. In that sense, they might not feel hot and therefore not take appropriate action to reduce the heat stress they are under, unaware. In all cases, increasing the indoor air velocity resulted in lower standard effective temperatures. However, people with reduced adaptive opportunities might not use indoor fans if these are not automatized, and during very hot periods elevated air velocities might also increase dehydration.

This analysis does point out that using only future typical years to assess potential summer thermal discomfort can lead to misleading beliefs that there is no health-heat-related risk. As future typical years might or might not contain future heatwave periods, using a single future typical heatwave period as well for the assessment is a complementary, necessary approach to ensure safe buildings are designed in regard to heat related risk. Furthermore, only future typical heatwaves were analyzed here, but more intense and severe heatwaves will occur, and this work opens the door to assess the building resilience under future extreme heatwaves.

In Carpentras, the analysis showed that all building designs led to high maximum values, severity and projected health-heat-related risk duration. However, using additional shutters to the overhang, allowing acceptable levels of indoor daylighting led to a reduction by two of the indoor overheating severity, and in the best case, with increased indoor air velocity, to acceptable indoor levels of overheating severity. Again, this is complex as environmental adaptations from building occupants (use of fans, or solar shading) considerably lower the indoor overheating, however the occupants most vulnerable to indoor overheating are the ones with reduced adaptation capability.

It is not one strategy, but the combination of several strategies, that will allow reducing the expected indoor overheating increase in the next thirty years. It will be necessary to optimize the building design envelope, but also to educate building occupants to appropriately adapt to heat, by opening windows only during nighttime, and using shades during the day, or to automatize some of these adaptive strategies. In the warmest climate of Carpentras, one emergency "cool room" might be needed in the building, for people to seek refuge under very hot days such as studied in Australia (Palmer et al., 2014).

5.3 Conclusive remarks

In this chapter, different passive cooling solutions were evaluated, based on the results from the sensitivity analysis. Due to the modelling assumptions made, and the building case-study chosen (highly insulated, RT-2012 compliant), the cooling needs, even during the present period, are higher than the heating needs. This difference is more pronounced during the future period. It is difficult to assess precisely the future cooling needs, or the indoor overheating increase, as the climate model, and the socio-economic RCP scenario chosen impacts greatly the results. Indeed, some future typical years contain heatwaves, and some others don't, due to the way typical months are selected. A different weighting of the weather variables might lead to a better uniformity. Using more climate models, and several scenarios, would allow a more complete analysis. Beyond the future climate uncertainty, the weather file choice for the future indoor overheating assessment is subject to debate. While using future typical weather files are needed to assess projected future energy needs, using a heatwave weather file is needed, from the design stage, to adapt the building design to maintain comfortable indoor conditions during recurring heatwave periods. We found that heatwaves with higher intensities than in 2003 would occur at least every five years during the future period under investigation (2040-2069), so this reinforces the need to use heatwaves weather files. All heatwaves led to indoor periods of overheating, and the analysis for the optimized building design solutions demonstrated that indoor overheating was much higher during future heatwave periods than future typical years.

For the specific building case-study, the architectural configuration using buffer zones is very beneficial to reduce both heating and cooling needs. Especially the presence of the veranda reduces considerably the solar heat gains received by the living space. In the three case-study cities, all optimized designs were with high thermal mass, low or medium glazing percentage, and the absorptivity and emissivity values, as well as the overhang length, were varying linearly along with the heating and cooling needs. A high thermal mass is beneficial for both winter and summer periods, such as low glazed windows (analysis only conducted for North and South facades). Without the buffer zones, the overhang on the South facade has the highest effect to reduce cooling needs or summer thermal discomfort, but with the presence of the veranda its influence is reduced and it is the roof albedo that has the highest effect. While in Roissy the optimized heating and cooling needs are almost equivalent, optimizing in favor of reducing cooling needs results in lower total energy needs. Optimizing without an active cooling system would require adequate care to be given to the winter period. In La Rochelle and in Carpentras, heating needs are lower during both present and future periods. In La Rochelle this is due to warmer outdoor air temperatures, in Carpentras to a sunnier climate in winter. In these two cities this study has shown that more care should be given to summer design than winter design, at least for the studied apartment.

The evaluated three ventilative cooling strategies (natural ventilation, mechanical free-cooling, earth-to-air heat exchanger) proved to be efficient to refresh the building during warm periods, especially in La Rochelle and Roissy. As the optimization was conducted yearly, these systems airflows were maximized during the entire period, which might not be realistic. Daily optimization of the airflow control would be more realistic but would lead to similar results as it would be maximized during warm sequences. The earth-to-air heat exchanger allowed to

reduce the exposure period and severity under future heatwaves to a greater extent than the other ventilative cooling strategies, since the ground is a better heat sink than the air during hot periods. Given that the building site provides enough space for its implementation, its design could be optimized with tubes in parallel to increase the efficiency and result in much lower outlet air temperatures. Furthermore, considering the low calculated heating needs, the earth-to-air heat exchanger could also have the potential to be used during winter and totally offset these, which was not studied here.

The natural ventilation solution was found to be more efficient than the mechanical free-cooling, due to a larger air section and therefore higher air volumes. The cross-ventilation disposition was highly beneficial for this. However, in an urban context, noise and safety concerns might be an issue for natural ventilation use. In Carpentras, the exposure was still elevated for all three ventilative cooling strategies, even though it was greatly reduced by the use of solar shades. Strategies related to the building envelope (thermal mass, glazing percentage, overhang or not), on the other hand, need to be taken at an early stage in the building design and cannot be changed later on. Some other passive cooling strategies require heavy control from the occupants (close shutters during the day, open windows at night) if they are not automatized, while others require less participation (free-cooling and earth-to-air heat exchanger). In all cases, increasing the indoor air velocity allows to reduce the thermal sensation by about 2 °C, so the use of fans is highly beneficial. While the indoor overheating was evaluated using the SET indicator, some hygroscopic materials could also improve indoor thermal comfort. Finally, the SET chosen thresholds to correlate indoor overheating to health-heat-related risk are debatable, but these were purposely chosen low to account for the most vulnerable.

Conclusion

With climate change, the dangerous increase of heatwaves events is predicted to drastically escalate heat-related health concerns. On one hand, climatologists work on climate projections and the occurrence of these future heatwave events while on the other hand, epidemiologists quantify the excessive morbidity associated with these extreme outdoor climate projections. As most heatwave deaths take place inside buildings, there is a pressing need to correlate heat stress to indoor environments. In the literature of the civil engineering field, there is a lack of an overall methodology to identify these future extreme heat events, account for future projections uncertainty, propose resilient building designs to heat that also mitigate climate change, and quantify future indoor overheating risk.

Our proposed building design innovative methodology consists of:

- Characterizing the future extreme heat exposure at regional or city scale, in terms of occurrence frequency, intensity, and severity;
- Accounting for future climate uncertainty and how to consider it in the building design process;
- Defining indicators to correlate outdoor exposure to indoor heat stress, and quantifying the projected indoor overheating and correlated health-heat-related risk on building occupants;
- Identifying passive cooling strategies that both mitigate and adapt to climate change;
- Conducting many building thermal simulations with the use of sensitivity analysis and optimization methods to compare different building designs and understanding which strategies have the most impact to minimize indoor overheating;
- Finding the appropriate compromise between passive winter and summer design that might be in concurrence for certain strategies;
- Proposing general guidelines for long-term mitigation and adaptation measures at the building scale, ensuring the proposed designs are resilient to extreme heat.

In the state-of-the-art chapter, we identified that future weather files typically used in building thermal simulations do not incorporate future extreme heat events, they are not bias-adjusted, and that researchers do not systematically account for climate projections uncertainty. For this reason, we reassembled our own future typical and future heatwave weather files from regional climate models' multiyear bias-adjusted projections. While the four typical years allowed to account for the uncertainty related to the climate models chosen, the heatwaves detected from several climate models lead to quantify their frequency of occurrence. Even though our heatwaves detection method is based only on exterior dry-bulb temperature and direct normal solar radiation, the thresholds defined by climatologists and epidemiologists together with our defined indicators proved to be efficient to detect indoor overheating during consecutive days and health-heat-related risk associated with these outdoor heatwaves. The method developed to reproduce future heatwaves weather files ready to use for building thermal simulations offers tremendous potential for various types of studies related to adaptation and resilience assessments to indoor overheating. Indeed, as

climate data were bias-adjusted, it is possible to quantify the indoor overheating and associated potential related heat stress risk, given that many climate models and scenarios are accounted for to quantify uncertainties. It is clear that using these weather files in early building design stages will be of great interest for building practitioners to understand if their building design is resilient to extreme heat. Furthermore, these weather files will enable researchers in civil and energy engineering to test the resilience of different passive cooling solutions under future extreme heat conditions.

We tested our proposed methodology with one case study apartment located on the top floor of a collective residential building in three French cities. Since all passive cooling strategies rely on local climatic conditions by definition, we could assess the limit of their potential in both present and future climates. In Paris and in La Rochelle, we showed that under present climate, the building design does not need to be fully oriented towards passive cooling to reach comfortable indoor conditions, whereas under future typical climate, and even more during future recurring heatwaves, all design parameters need to be optimized for summer design to reduce the potential health-heat-related risk. This is a crucial result because it means that a change in paradigm must arise during the building design. In Carpentras, passive summer design is already predominant over passive winter design during present climate, with much higher emphasis during future climate. In La Rochelle and in Carpentras, heating needs were calculated low during the present and future periods, so emphasis can easily be put on summer design. In Paris, the task is more complex as optimized heating needs are almost equivalent to optimized cooling needs in both present and future climate, and the right balance between passive bioclimatic winter and summer design must be found. In all cities, we found out that the cooling needs will increase by at least a factor of two between present and future typical summers, and these will be much higher during recurring heatwave periods.

Some bioclimatic design strategies are beneficial to both winter and summer passive design and have a strong potential to reduce indoor overheating, these are the use of buffer spaces around the conditioned space and a high thermal mass for a building well insulated with exterior insulation. However, we could observe that the potential of thermal mass coupled to ventilative cooling strategies based on the outdoor temperature daily range (natural ventilation through windows, free-cooling) was reduced in periods of extreme heat in all three cities, and even more in Carpentras for the lowest airflows (free-cooling through the mechanical ventilation system). Furthermore, the veranda oriented south considerably contributes to reducing the incoming solar gains on the conditioned living space, assuming it is adequately operated (exterior windows opened during the entire summer period), otherwise the opposite effect would be observed.

Some other strategies greatly impacting the summer indoor overheating are in contradiction with winter passive design, these are the windows sizes, the roof albedo, and the presence of an overhang on the South façade. For the building configuration without the veranda (oriented South), we identified that the overhang on the South façade was more important than the roof albedo to reduce indoor overheating, while with the veranda the roof albedo was more important than the overhang. The issue of the window sizes is complex: smaller windows contribute to reducing both heating and cooling needs (in the studied configuration, with windows facing North and South), however the occupants' desire is to

maximize them for visual comfort and connection to the outdoors. During summer, we found out that using additional solar shading to the overhang while allowing comfortable illuminance levels could reduce indoor overheating by a factor of two. The solar protections would have a higher impact without the veranda presence.

We could observe the limits of the three assessed ventilative cooling strategies. While in present climate the airflow rate for all these three strategies did not need to be maximized to reach summer thermal comfort in La Rochelle and in Paris, during future these were systematically maximized. Nocturnal ventilation through windows in cross-configuration consistently led to greater temperature reduction than through the mechanical system, due to higher airflow rates. This emphasizes the need to adequately design windows to create higher airflow rates inside buildings if passive cooling by air is a considered strategy. For instance, the temporal sensitivity analysis revealed that the size of the windows had a great effect in Carpentras during the night to enhance natural ventilation. Nocturnal ventilation was especially efficient to reduce nighttime temperatures, while the ground cooling via the earth-to-air heat exchanger was more efficient to reduce maximum daytime temperatures. Ideally, these two should be used in combination but it was not possible to model this with EnergyPlus. Indeed, during the nighttime the outlet air temperature of the earth-to-air heat exchanger is only slightly lower than the outdoor temperature especially at the end of the summer, whereas ventilation rates are higher through windows. The earth-to-air heat exchanger system offers great potential to considerably lower outside daytime air temperatures, however it is limited by space constraints in the urban context.

We can conclude that it is not one, but the combination of all the above-mentioned strategies that are needed to reduce health-heat-related risk inside buildings under future recurring heatwaves. Categorically, we found out that even for the most optimized building envelope designs for the summer period, consecutive days of exposure to elevated daytime and nighttime indoor temperatures would occur during future typical heatwaves, while it is never the case during the present summers in each of the three cities. This result was already sensed when comparing the indoor overheating variance above 28 °C increase between present summer and future heatwave. We found an increase in maximum indoor daytime temperatures up to +5 °C between present summer and future typical heatwaves. Under future typical summers, in Paris and La Rochelle, no health-heat-related risk was found. However, under future typical heatwaves, we could quantify a risk for at least a week, even for the most optimized building designs. This demonstrates and stresses the crucial need to use future typical heatwave weather files for building thermal simulations. Nevertheless, with the appropriate use of solar shading and increased indoor air velocities, the health-heat-related risk could be highly reduced and almost disappears, up to a factor of ten in Carpentras. The increase of indoor air velocity from 0.1 m/s to 0.4 m/s consistently led to a reduction of 2 °C in standard effective temperature, with an even more pronounced effect for the hottest temperatures.

These results confirm the key stakes of this research work. It is the adequate use of both the building envelope (presence of buffer spaces, windows orientation, and sizes, thermal mass) and behavioral adaptation strategies (use of solar shadings, window openings, increasing indoor air velocities) that will enable the possibility to ensure low energy and adapted buildings to projected extreme heat in France during the mid-century.

Decisions related to the building envelope need to be taken in the early stage of design and will remain fixed under the entire lifetime of the building. Architectural choices are constrained by many objectives, and the ones analyzed in this Ph.D. (reduced energy needs, summer thermal comfort, reduced health-heat-related risk at the convergence of mitigation and adaptation) add a level of complexity to the design process. This methodological approach aims to be a contribution to give to the contracting firm (MOA) hints on the influence of their decisions in early stage design on our three performance objectives. The ultimate design decisions are taken by the contracting firm (MOA), which will balance out the design risk with the other project compromises. This research work has shown that if decisions are not taken at this particular stage of design, important health-heat-related risk could result in buildings. It is most important that this new perspective is included at the design stage, to design resilient buildings to extreme heat and able to protect the occupants independently to their use of the building.

It has been shown in many works of literature, observed in many real case study buildings, and demonstrated once enough in this Ph.D. that occupant's behavior (use of solar shadings, window openings, increasing indoor air velocities) highly influences the indoor environment conditions and thermal perception. While in present typical summers the building envelope satisfies comfortable indoor conditions (with observed hottest temperatures during recent heatwaves), the occupant's perception of heat has only started to shift. In this Ph.D. we demonstrated that to maintain acceptable indoor conditions under future recurring heatwaves, the operation of solar protections and ventilative cooling strategies will have a tremendous impact to reduce the potential health-heat-related risk. The advantage of these strategies is that contrary to some building envelope strategies, these are not in opposition with passive winter design. They are also more flexible than the building envelope as they can evolve over time, for instance they do not necessarily need to be used every future summer, but only during recurring heatwave periods. However, appropriate occupant behavior to reduce indoor overheating is limited by a number of factors (heat perception, mobility, acceptability of automatisms) and is not certain science. In France, people are not used to extreme heat and therefore might not be aware of good practices, especially for adequate building operation. While some of these strategies could be automatized, experience has shown that people in buildings like to have control, and a fine balance between occupant's behavior education and automatizations must be found. For the most vulnerable with reduced adaptative opportunities, or in warmest cities, a room in the collective building could be equipped with air-conditioning, similarly as in elderly healthcare houses. However, this opens the door to other questions (use, acceptability, indoor air quality, etc.)

The results of this work need to be nuanced by the climate data used, the building case study, the modelling assumptions in thermal simulations, and the thresholds used to detect health-heat-related risk. First, we only used four different climate models and one socio-economic scenario, and using more models and several scenarios will be needed for a more holistic assessment. However, the models used already represent a large variation in result outputs. Furthermore, the detection of recurring heatwaves was based on three climate models with similar heatwaves occurrence. The method used to classify heatwaves occurrence based on their intensity is up to debate and could probably be improved, however we were able to position the 2003 heatwave in regards to future projected heatwaves and conclude that it will

reoccur very frequently during the mid-century. We did not assess the building resilience to future extreme heatwaves, but the proposed weather files allow us to conduct this work in future studies. Our methodology to reassemble the weather files also gave us the option to include urban heat island effects, however these also need to be added as boundary conditions in building thermal simulations, and this was not done in this work. Regarding the modelling assumptions, the airflow of ventilative cooling strategies was always maximized, which might not always be evident to implement, especially for natural ventilation (windows opening), which potential would also be reduced in an urban context.

Finally, the methodology was only tested on one case study building and testing it with other types of buildings will add value and knowledge to this analysis. A perspective work would be to test the methodology in a real building during future typical summer conditions and future heatwaves as well. Measuring the building's indoor thermal conditions, people's perceptions and adaptations to heat, people's thermal sensations, and people's acceptance of proposed measures would add considerable knowledge to this conceptual modelling analysis.

Current research work on other passive cooling measures offers great potential, as these are under current development and might be commercialized and ready to be implemented in buildings before the mid-century, for instance research in hygroscopic materials, or in evaporative and radiative cooling. Testing the methodology with these innovative materials and systems is also promising. This research work has shown that these systems will be interesting to be implemented in France, where a cooling demand was not present before.

This research has also pointed out that both daytime and nighttime indoor thresholds are needed to quantify health-heat-related risk under future heatwaves, and more research on the definition of these thresholds, especially for the elderly increasing population is needed.

All in all, this developed methodology demonstrates that the time is ripe for a paradigm change in the design of French buildings: the frequency of occurrence of future heatwaves with higher intensity than that of 2003 during the mid-century must guide our design choices today to minimize the health burden on society. Long-term adaptation measures that also mitigate climate change are more than ever needed to reduce human impact on climate and climates impact on human kind.

References

Aburas, M., Soebarto, V., Williamson, T., Liang, R., Ebendorff-Heidepriem, H., & Wu, Y. (2019). Thermochromic smart window technologies for building application: A review. *Applied Energy*, *255*(June), 113522. https://doi.org/10.1016/j.apenergy.2019.113522

Agrawal, K. K., Misra, R., Agrawal, G. Das, Bhardwaj, M., & Jamuwa, D. K. (2019). The state of art on the applications, technology integration, and latest research trends of earth-air-heat exchanger system. *Geothermics*, *82*(January), 34–50. https://doi.org/10.1016/j.geothermics.2019.05.011

Akeiber, H., Nejat, P., Majid, M. Z. A., Wahid, M. A., Jomehzadeh, F., Zeynali Famileh, I., Calautit, J. K., Hughes, B. R., & Zaki, S. A. (2016). A review on phase change material (PCM) for sustainable passive cooling in building envelopes. *Renewable and Sustainable Energy Reviews*, *60*, 1470–1497. https://doi.org/10.1016/j.rser.2016.03.036

Al Horr, Y., Tashtoush, B., Chilengwe, N., & Musthafa, M. (2020). Operational mode optimization of indirect evaporative cooling in hot climates. *Case Studies in Thermal Engineering*, *18*(December 2019), 100574. https://doi.org/10.1016/j.csite.2019.100574

Alawadhi, E. M. (2018). Double solar screens for window to control sunlight in Kuwait. *Building and Environment*, *144*(August), 392–401. https://doi.org/10.1016/j.buildenv.2018.08.058

Alessandrini, J. M., Ribéron, J., & Da Silva, D. (2019). Will naturally ventilated dwellings remain safe during heatwaves? *Energy and Buildings*, *183*(april 2014), 408–417. https://doi.org/10.1016/j.enbuild.2018.10.033

Allard, F. (1998). *Natural Ventilation in Buildings - A Design Handbook*. James & James.

Allard, F., Dorer, V. B., Feustel, H. E., Rodriguez Garcia, E., Grosso, M., Herrlin, M. K., Mingsheng, L., Phaff, H. C., Utsumi, Y., & Yoshino, H. (1990). Technical Note AIVC 29 - Fundamentals of the Multizone Air Flow Model - COMIS. In *Journal of Chemical Information and Modeling* (Vol. 53, Issue 9).

Arima, Y., Ooka, R., Kikumoto, H., & Yamanaka, T. (2016). Effect of climate change on building cooling loads in Tokyo in the summers of the 2030s using dynamically downscaled GCM data. *Energy and Buildings*, *114*, 123–129. https://doi.org/10.1016/j.enbuild.2015.08.019

Armstrong, B. G., Chalabi, Z., Fenn, B., Hajat, S., Kovats, S., Milojevic, A., & Wilkinson, P. (2011). Association of mortality with high temperatures in a temperate climate: England and Wales. *Journal of Epidemiology and Community Health*, *65*(4), 340–345. https://doi.org/10.1136/jech.2009.093161

Ascione, F., Bianco, N., de' Rossi, F., Turni, G., & Vanoli, G. P. (2013). Green roofs in European climates. Are effective solutions for the energy savings in air-conditioning? *Applied Energy*, *104*, 845–859. https://doi.org/10.1016/j.apenergy.2012.11.068

Ascione, F., Bianco, N., De Masi, R. F., Mauro, G. M., & Vanoli, G. P. (2017). Resilience of robust cost-optimal energy retrofit of buildings to global warming: A multi-stage, multi-objective approach. *Energy and Buildings*, *153*, 150–167. https://doi.org/10.1016/j.enbuild.2017.08.004

ASHRAE. (2001). *ASHRAE Fundamentals Handbook* (A. S. of H. R. and A.-C. Engineers (ed.)).

Badiei, A., Akhlaghi, Y. G., Zhao, X., Li, J., Yi, F., & Wang, Z. (2020). Can whole building energy models outperform numerical models, when forecasting performance of indirect evaporative cooling systems? *Energy Conversion and Management*, *213*(April). https://doi.org/10.1016/j.enconman.2020.112886

Bamdad, K., Cholette, M. E., Omrani, S., & Bell, J. (2021). Future energy-optimised buildings — Addressing the impact of climate change on buildings. *Energy and Buildings*, *231*, 110610. https://doi.org/10.1016/j.enbuild.2020.110610

Belcher, S., Hacker, J., & Powell, D. (2005). Constructing design weather data for future climates. *Building Services Engineering Research and Technology*, *26*(1), 49–61. https://doi.org/10.1191/0143624405bt112oa

Berardi, U., & Jafarpur, P. (2020). Assessing the impact of climate change on building heating and cooling energy demand in Canada. *Renewable and Sustainable Energy Reviews*, *121*(December 2019), 109681. https://doi.org/10.1016/j.rser.2019.109681

Berdahl, P., Chen, S. S., Destaillats, H., Kirchstetter, T. W., Levinson, R. M., & Zalich, M. A. (2016). Fluorescent cooling of objects exposed to sunlight - The ruby example. *Solar Energy Materials and Solar Cells*, *157*, 312–317. https://doi.org/10.1016/j.solmat.2016.05.058

Besancenot, J.-P. (2002). Vagues de chaleur et mortalité dans les grandes agglomérations urbaines. *Environnement, Risques & Santé*, *1*(4), 229–240.

Bordoloi, N., Sharma, A., Nautiyal, H., & Goel, V. (2018). An intense review on the latest advancements of Earth Air Heat Exchangers. *Renewable and Sustainable Energy Reviews*, *89*(March), 261–280. https://doi.org/10.1016/j.rser.2018.03.056

Boukhanouf, R., Alharbi, A., Ibrahim, H. G., Amer, O., & Worall, M. (2017). Computer modelling and experimental investigation of building integrated sub-wet bulb temperature evaporative cooling system. *Applied Thermal Engineering*, *115*, 201–211. https://doi.org/10.1016/j.applthermaleng.2016.12.119

Bozonnet, E., Doya, M., & Inard, C. (2019). *Propriétés radiatives des bâtiments pour le rafraîchissement passif*.

Bozonnet, E., Musy, M., Calmet, I., & Rodriguez, F. (2015). Modeling methods to assess urban fluxes and heat island mitigation measures from street to city scale. *International Journal of Low-Carbon Technologies*, *10*(1), 62–77. https://doi.org/10.1093/ijlct/ctt049

Breesch, H., & Janssens, A. (2010). Performance evaluation of passive cooling in office buildings based on uncertainty and sensitivity analysis. *Solar Energy*, *84*(8), 1453–1467. https://doi.org/10.1016/j.solener.2010.05.008

Bueno, B., Pigeon, G., Norford, L. K., Zibouche, K., & Marchadier, C. (2012). Development and evaluation of a building energy model integrated in the TEB scheme. *Geoscientific Model Development*, *5*(2), 433–448. https://doi.org/10.5194/gmd-5-433-2012

Bueno, Bruno. (2012). *Study and prediction of the energy interactions between buildings and the urban climate*. Massachusetts Institute of Technology.

Bueno, Bruno, Norford, L., Hidalgo, J., & Pigeon, G. (2013). The urban weather generator. *Journal of Building Performance Simulation*, *6*(4), 269–281. https://doi.org/10.1080/19401493.2012.718797

Bueno, Bruno, Roth, M., Norford, L., & Li, R. (2014). Computationally efficient prediction of canopy level urban air temperature at the neighbourhood scale. *Urban Climate*, *9*, 35–53. https://doi.org/10.1016/j.uclim.2014.05.005

Cabeza, L. F., & Chàfer, M. (2020). Technological options and strategies towards zero energy buildings contributing to climate change mitigation: A systematic review. *Energy and Buildings*, *219*. https://doi.org/10.1016/j.enbuild.2020.110009

Cannon, A. J. (2018). Multivariate quantile mapping bias correction: an N-dimensional probability density function transform for climate model simulations of multiple variables. *Climate Dynamics*, *50*(1–2), 31–49. https://doi.org/10.1007/s00382-017-3580-6

Cannon, A. J., Sobie, S. R., & Murdock, T. Q. (2015). Bias correction of GCM precipitation by quantile mapping: How well do methods preserve changes in quantiles and extremes? *Journal of Climate*, *28*(17), 6938–6959. https://doi.org/10.1175/JCLI-D-14-00754.1

Chantrelle, F. P., Lahmidi, H., Keilholz, W., Mankibi, M. El, & Michel, P. (2011). Development of a multicriteria tool for optimizing the renovation of buildings. *Applied Energy*, *88*(4), 1386–1394. https://doi.org/10.1016/j.apenergy.2010.10.002

Chardon, S., Brangeon, B., Bozonnet, E., Inard, C., & Montecot, R. (2015). A multi objective design tool for the French detached house market: Cost and energy performance optimization. *14th International Conference of IBPSA - Building Simulation 2015, BS 2015, Conference Proceedings*, *December*, 2073–2079.

Chen, Y., Tong, Z., & Malkawi, A. (2017). Investigating natural ventilation potentials across the globe: Regional and climatic variations. *Building and Environment*, *122*, 386–396. https://doi.org/10.1016/j.buildenv.2017.06.026

Chiesa, G. (2017). Climate-potential of earth-To-Air heat exchangers. *Energy Procedia*, *122*, 517–522. https://doi.org/10.1016/j.egypro.2017.07.300

Chiesa, G. (2018). EAHX – Earth-to-air heat exchanger: Simplified method and KPI for early building design phases. *Building and Environment*, *144*(August), 142–158. https://doi.org/10.1016/j.buildenv.2018.08.014

Chiesa, G., Simonetti, M., & Grosso, M. (2014). A 3-field earth-heat-exchange system for a school building in Imola, Italy: Monitoring results. *Renewable Energy*, *62*, 563–570. https://doi.org/10.1016/j.renene.2013.08.020

Ciancio, V., Falasca, S., Golasi, I., de Wilde, P., Coppi, M., de Santoli, L., & Salata, F. (2019). Resilience of a building to future climate conditions in three European cities. *Energies*, *12*(23), 1–13. https://doi.org/10.3390/en12234506

Corso, M., Pascal, M., & Wagner, V. (2017). *Impact of Heat and Cold on Total Mortality in France Between 2000 and 2010*. 634–640. http://invs.santepubliquefrance.fr/beh/2017/31/pdf/2017_31_1.pdf

Costanzo, V., Evola, G., Gagliano, A., Marletta, L., & Nocera, F. (2013). Study on the application of cool paintings for the passive cooling of existing buildings in mediterranean climates. *Advances in Mechanical Engineering*, *2013*. https://doi.org/10.1155/2013/413675

De Antonellis, S., Cignatta, L., Facchini, C., & Liberati, P. (2020). Effect of heat exchanger plates geometry on performance of an indirect evaporative cooling system. *Applied Thermal Engineering*, *173*(March), 115200. https://doi.org/10.1016/j.applthermaleng.2020.115200

De Munck, C., Pigeon, G., Masson, V., Meunier, F., Bousquet, P., Tréméac, B., Merchat, M., Poeuf, P., & Marchadier, C. (2013). How much can air conditioning increase air temperatures for a city like Paris, France? *International Journal of Climatology*, *33*(1), 210–227. https://doi.org/10.1002/joc.3415

de Wilde, P., & Tian, W. (2009). Identification of key factors for uncertainty in the prediction of the thermal performance of an office building under climate change. *Building Simulation*, *2*(3), 157–

174. https://doi.org/10.1007/s12273-009-9116-1

Deb, K., Pratap, A., Agarwal, S., & Meyarivan, T. (2002). A fast and elitist multiobjective genetic algorithm: NSGA-II. *IEEE Transactions on Evolutionary Computation*, *6*(2), 182–197. https://doi.org/10.1109/4235.996017

Djedjig, R., Bozonnet, E., & Belarbi, R. (2013). INTEGRATION OF A GREEN ENVELOPE MODEL IN A TRANSIENT BUILDING SIMULATION PROGRAM AND EXPERIMENTAL COMPARISON. *Proceedings of BS2013 - 13th Conference of International Building Performance Simulation Association*, 47–53.

Doya, M., Bozonnet, E., & Allard, F. (2012). Experimental measurement of cool facades' performance in a dense urban environment. *Energy and Buildings*, *55*, 42–50. https://doi.org/10.1016/j.enbuild.2011.11.001

Du, H., Underwood, C. P., & Edge, J. S. (2012). Generating design reference years from the UKCP09 projections and their application to future air-conditioning loads. *Building Services Engineering Research and Technology*, *33*(1), 63–79. https://doi.org/10.1177/0143624411431775

Duan, Z., Zhan, C., Zhang, X., Mustafa, M., Zhao, X., Alimohammadisagvand, B., & Hasan, A. (2012). Indirect evaporative cooling: Past, present and future potentials. *Renewable and Sustainable Energy Reviews*, *16*(9), 6823–6850. https://doi.org/10.1016/j.rser.2012.07.007

El Kadri, M., De Oliveira, F., Inard, C., & Demouge, F. (2020). New neurophysiological human thermal model based on thermoreceptor responses. *International Journal of Biometeorology*, *64*(12), 2007–2017. https://doi.org/10.1007/s00484-020-01990-1

EnergyPlus. (2015). ENERGYPLUS Version 8.8.0 Documentation - Auxiliary Programs. *Bigladder Software*, 0–201.

EnergyPlus. (2017). *EnergyPlus Version 8.8.0 Documentation - Application Guide for EMS*.

Engerer, N. A. (2015). Minute resolution estimates of the diffuse fraction of global irradiance for southeastern Australia. *Solar Energy*, *116*, 215–237. https://doi.org/10.1016/j.solener.2015.04.012

ESGF. (2019). *Welcome to the ESGF Node @ IPSL*. https://esgf-node.ipsl.upmc.fr/projects/esgf-ipsl/

EUROCORDEX. (2019a). *CORDEX_variables_requirement_table*. =

EUROCORDEX. (2019b). *Cordex Archive Specifications*.

European Standard. (2007). *EN 15193 Energy performance of buildings - Energy requirements for lighting*.

Fabiani, C., Pisello, A. L., Bou-Zeid, E., Yang, J., & Cotana, F. (2019). Adaptive measures for mitigating urban heat islands: The potential of thermochromic materials to control roofing energy balance. *Applied Energy*, *247*(August 2018), 155–170. https://doi.org/10.1016/j.apenergy.2019.04.020

Fanger, P. O. (1972). *Thermal Comfort - Analysis and Applications in Environmental Engineering*. McGraw Hill Book Company.

Feng, C., Meng, Q., & Zhang, Y. (2010). Theoretical and experimental analysis of the energy balance of extensive green roofs. *Energy and Buildings*, *42*(6), 959–965. https://doi.org/10.1016/j.enbuild.2009.12.014

Fischer, E. M., & Schär, C. (2010). Consistent geographical patterns of changes in high-impact European heatwaves. *Nature Geoscience*, *3*(6), 398–403. https://doi.org/10.1038/ngeo866

Folland, C. K., Karl, T. R., Christy, J. R., Clarke, R. A., Gruza, G. V., Jouzel, J., Mann, M. E., Oerlemans, J., Salinger, M. J., & Wang, S.-W. (2001). 2001: Observed Climate Variability and Change. In:

Climate Change 2001: The Scientific Basis. Contribution of Working Group I to the Third Assessment Report of the Intergovernmental Panel on Climate Change [Hougton, J.T., Y. Ding, D.J. Griggs, M.Noguer, P. *Cambridge University Press*, 881. https://doi.org/10.1256/004316502320517344

Forde, J., Hopfe, C. J., McLeod, R. S., & Evins, R. (2020). Temporal optimization for affordable and resilient Passivhaus dwellings in the social housing sector. *Applied Energy*, *261*(January), 114383. https://doi.org/10.1016/j.apenergy.2019.114383

Fosas, D., Coley, D. A., Natarajan, S., Herrera, M., Fosas de Pando, M., & Ramallo-Gonzalez, A. (2018). Mitigation versus adaptation: Does insulating dwellings increase overheating risk? *Building and Environment*, *143*(May), 740–759. https://doi.org/10.1016/j.buildenv.2018.07.033

Gagge, A. P., Fobelets, A. P., & Berglund, L. G. (1986). A standard predictive Index of human reponse to thermal enviroment. *American Society of Heating, Refrigerating and Air-Conditioning Engineers*, *92(2B)*, 709–731. https://www.aivc.org/sites/default/files/airbase_2522.pdf%0Ahttp://oceanrep.geomar.de/42985/

Gagge, A. P., Nishi, Y., & Gonzales, R. . (1972). Standard Effective Temperature - A single index temperature index of temperature sensation and thermal discomfort. *CIB Commssion W45 - Symposium Thermal Comfort and Moderate Heat Stress*.

Gagnon, R., Gosselin, L., & Decker, S. (2018). Sensitivity analysis of energy performance and thermal comfort throughout building design process. *Energy and Buildings*, *164*, 278–294. https://doi.org/10.1016/j.enbuild.2017.12.066

Garcia Sanchez, D., Lacarrière, B., Musy, M., & Bourges, B. (2014). Application of sensitivity analysis in building energy simulations: Combining first- and second-order elementary effects methods. *Energy and Buildings*, *68*(PART C), 741–750. https://doi.org/10.1016/j.enbuild.2012.08.048

Garshasbi, S., & Santamouris, M. (2019). Using advanced thermochromic technologies in the built environment: Recent development and potential to decrease the energy consumption and fight urban overheating. *Solar Energy Materials and Solar Cells*, *191*(November 2018), 21–32. https://doi.org/10.1016/j.solmat.2018.10.023

Gasparrini, A., Guo, Y., Hashizume, M., Lavigne, E., Zanobetti, A., Schwartz, J., Tobias, A., Tong, S., Rocklov, J., Forsberg, B., Leone, M., De Sario, M., L Bell, M., Guo, Y.-L. L., Wu, C.-F., Kan, H., Yi, S.-M., Coelho, M. de S. Z. S., Saldiva, P. H. N., … Armstrong, B. (2015). Mortalité attribuable au froid et à la chaleur : Analyse multi-pays. *Environnement, Risques et Sante*, *14*(6), 464–465. https://doi.org/10.1016/S0140-6736(14)62114-0

Giorgi, F. (2006). Regional climate modeling: Status and perspectives. *Journal De Physique. IV : JP*, *139*, 101–118. https://doi.org/10.1051/jp4:2006139008

Giorgi, F. (2019). Thirty Years of Regional Climate Modeling: Where Are We and Where Are We Going next? *Journal of Geophysical Research: Atmospheres*, *124*(11), 5696–5723. https://doi.org/10.1029/2018JD030094

Giorgi, Filippo. (2005). Climate change prediction. In *Climatic Change* (Vol. 73, Issue 3, pp. 239–265). https://doi.org/10.1007/s10584-005-6857-4

Givoni, B. (1992). Comfort, climate analysis and building design guidelines. *Energy and Buildings*, *18*(1), 11–23. https://doi.org/10.1016/0378-7788(92)90047-K

Givoni, B. (1994). *Passive and low energy cooling of buildings*. John Wiley & Sons, Inc.

Givoni, B. (1998). *Climate considerations in building and urban design*. John Wiley & Sons, Inc.

Goffart, J., Mara, T., & Wurtz, E. (2017). Generation of stochastic weather data for uncertainty and sensitivity analysis of a low-energy building. *Journal of Building Physics*, *41*(1), 41–57. https://doi.org/10.1177/1744259116668598

Goldstein, E. A., Raman, A. P., & Fan, S. (2017). Sub-ambient non-evaporative fluid cooling with the sky. *Nature Energy*, *2*(September), 1–7. https://doi.org/10.1038/nenergy.2017.143

Gondian, L. (2019). *Application de l ' analyse de sensibilité temporelle pour la description de la réponse thermique d 'un bâtiment aux actions des habitants .*

Gondian, L., Goffart, J., Woloszyn, M., Buhé, C., Maréchal, P., & Blanc, M. (2019). Towards Assessing Houses Resistance and Resilience Indicators At Inhabitants ' Actions Using Temporal Sensitivity Analysis Indicators development. *IBPSA 2019 - International Building Performance Simulation Association 2019*.

Gros, A., Bozonnet, E., & Inard, C. (2014). Cool materials impact at district scale - Coupling building energy and microclimate models. *Sustainable Cities and Society*, *13*, 254–266. https://doi.org/10.1016/j.scs.2014.02.002

Grosso, M., & Chiesa, G. (2015). Horizontal earth-to-air heat exchanger in Imola, Italy. A 30-month-long monitoring campaign. *Energy Procedia*, *78*, 73–78. https://doi.org/10.1016/j.egypro.2015.11.117

Gu, L. (2007). Airflow network modeling in energyplus. In Florida Solar Energy Ce (Ed.), *10th International Building Performance Simulation Association Conference and Exhibition* (pp. 964–971).

Gueymard, C. A., & Ruiz-Arias, J. A. (2016). Extensive worldwide validation and climate sensitivity analysis of direct irradiance predictions from 1-min global irradiance. *Solar Energy*, *128*, 1–30. https://doi.org/10.1016/j.solener.2015.10.010

Habets, F., Boé, J., Déqué, M., Ducharne, A., Gascoin, S., Hachour, A., Martin, E., Pagé, C., Sauquet, E., Terray, L., Thiéry, D., Oudin, L., & Viennot, P. (2013). Impact of climate change on the hydrogeology of two basins in northern France. *Climatic Change*, *121*(4), 771–785. https://doi.org/10.1007/s10584-013-0934-x

Hajat, S., Vardoulakis, S., Heaviside, C., & Eggen, B. (2014). Climate change effects on human health: Projections of temperature-related mortality for the UK during the 2020s, 2050s and 2080s. *Journal of Epidemiology and Community Health*, *68*(7), 641–648. https://doi.org/10.1136/jech-2013-202449

Hallegatte, S., Viguié, V., Masson, V., Lemonsu, A., Pigeon, G., Beaulant, A.-L., Bueno, B., Marchadier, C., & Salagnac, J.-L. (2013). *VURCA PROJECT Cities vulnerability to future heat waves & adaptation strategies*. 1–57.

Hamdi, R., & Masson, V. (2008). Inclusion of a drag approach in the Town Energy Balance (TEB) scheme: Offline 1D evaluation in a street canyon. *Journal of Applied Meteorology and Climatology*, *47*(10), 2627–2644. https://doi.org/10.1175/2008JAMC1865.1

Hamdy, M., Nguyen, A. T., & Hensen, J. L. M. (2016). A performance comparison of multi-objective optimization algorithms for solving nearly-zero-energy-building design problems. *Energy and Buildings*, *121*, 57–71. https://doi.org/10.1016/j.enbuild.2016.03.035

Hanna, E. G., & Tait, P. W. (2015). Limitations to thermoregulation and acclimatization challenge human adaptation to global warming. *International Journal of Environmental Research and Public Health*, *12*(7), 8034–8074. https://doi.org/10.3390/ijerph120708034

Hansen, A., Bi, P., Nitschke, M., Pisaniello, D., Newbury, J., & Kitson, A. (2011). Perceptions of heat-

susceptibility in older persons: Barriers to adaptation. *International Journal of Environmental Research and Public Health*, *8*(12), 4714–4728. https://doi.org/10.3390/ijerph8124714

Hawkins, E., & Sutton, R. (2009). The potential to narrow uncertainty in regional climate predictions. *Bulletin of the American Meteorological Society*. https://doi.org/10.1175/2009BAMS2607.1

Hawkins, E., & Sutton, R. (2011). The potential to narrow uncertainty in projections of regional precipitation change. *Climate Dynamics*, *37*(1), 407–418. https://doi.org/10.1007/s00382-010-0810-6

Heiselberg, P., Brohus, H., Hesselholt, A., Rasmussen, H., Seinre, E., & Thomas, S. (2009). Application of sensitivity analysis in design of sustainable buildings. *Renewable Energy*, *34*(9), 2030–2036. https://doi.org/10.1016/j.renene.2009.02.016

Herman, J., & Usher, W. (2018). *SALib : Sensitivity Analysis Library in Python (Numpy). Contains Sobol , SALib : An open-source Python library for Sensitivity Analysis*. *41*(April), 2015–2017. https://doi.org/10.1016/S0010-1

Herrera, M., Natarajan, S., Coley, D. A., Kershaw, T., Ramallo-González, A. P., Eames, M., Fosas, D., & Wood, M. (2017). A review of current and future weather data for building simulation. In *Building Services Engineering Research and Technology* (Vol. 38, Issue 5, pp. 602–627). https://doi.org/10.1177/0143624417705937

Humphreys, M. A. (1976). Field studies of thermal comfort compared and applied. *Building Services Engineering Research and Technology*, *44*(1), 5–23.

INSEE. (2021). *Population projections to 2070*. https://www.insee.fr/en/statistiques/2581288

Institut du monde arabe – Rambaud. (2018). *Institut du monde arabe : moucharabiehs mécaniques*. https://www.filiere-3e.fr/2018/01/05/institut-du-monde-arabe/

International Energy Agency. (2018). *The Future of Cooling Opportunities for energy- efficient air conditioning*.

Invidiata, A., & Ghisi, E. (2016). Impact of climate change on heating and cooling energy demand in houses in Brazil. *Energy and Buildings*, *130*, 20–32. https://doi.org/10.1016/j.enbuild.2016.07.067

Iooss, B., & Lemaître, P. (2015). A review on global sensitivity analysis methods. *Operations Research/ Computer Science Interfaces Series*, *59*, 101–122. https://doi.org/10.1007/978-1-4899-7547-8_5

IPCC. (2007). Climate Change 2007: impacts, adaptation and vulnerability: contribution of Working Group II to the fourth assessment report of the Intergovernmental Panel. In *Genebra, Suíça*. https://doi.org/10.1256/004316502320517344

IPCC. (2014). Summary for policymakers. In *Climate Change 2014: Mitigation of Climate Change. Contribution of Working Group III to the Fifth Assessment Report of the Intergovernmental Panel on Climate Change*. https://doi.org/10.1016/j.renene.2009.11.012

ISO. (2004). *NF_EN_ISO_15927-1: Performance hygrothermique des bâtiments. Calcul et présentation des données climatiques. Partie 1 : Moyennes mensuelles et annuelles des éléments météorologiques simples*.

ISO. (2005). *ISO 7730 - Ergonomie des ambiances thermiques — Détermination analytique et interprétation du confort thermique par le calcul des indices PMV et PPD et par des critères de confort thermique local*.

ISO. (2006). *15927-4: Performance hygrothermique des bâtiments. Calcul et présentation des données climatiques. Partie 4 : Données horaires pour l'évaluation du besoin énergétique annuel de chauffage et de refroidissement*.

ISO. (2009). *NF_EN_ISO_15927-2: Performance hygrothermique des bâtiments. Calcul et présentation des*

données climatiques - Partie 2 Donnees horaires pour le dimensionnement de la charge de refroidissement.

Itani, M., Ghaddar, N., Ghali, K., & Laouadi, A. (2020). Development of heat stress charts for older people under indoor environmental conditions. *Energy and Buildings*, *224*, 110274. https://doi.org/10.1016/j.enbuild.2020.110274

Jacob, D., Petersen, J., Eggert, B., Alias, A., Christensen, O. B., Bouwer, L. M., Braun, A., Colette, A., Déqué, M., Georgievski, G., Georgopoulou, E., Gobiet, A., Menut, L., Nikulin, G., Haensler, A., Hempelmann, N., Jones, C., Keuler, K., Kovats, S., … Yiou, P. (2014). EURO-CORDEX: New high-resolution climate change projections for European impact research. *Regional Environmental Change*, *14*(2), 563–578. https://doi.org/10.1007/s10113-013-0499-2

Jaffal, I., Ouldboukhitine, S. E., & Belarbi, R. (2012). A comprehensive study of the impact of green roofs on building energy performance. *Renewable Energy*, *43*, 157–164. https://doi.org/10.1016/j.renene.2011.12.004

Jentsch, M. F. (2012). *Technical reference manual for the CCWeatherGen and CCWorldWeatherGen tools Version 1.2* (Issue November).

Jentsch, M. F., Eames, M. E., & Levermore, G. J. (2015). Generating near-extreme Summer Reference Years for building performance simulation. *Building Services Engineering Research and Technology*, *36*(6), 701–721. https://doi.org/10.1177/0143624415587476

Jentsch, M. F., James, P. A. B., Bourikas, L., & Bahaj, A. B. S. (2013). Transforming existing weather data for worldwide locations to enable energy and building performance simulation under future climates. *Renewable Energy*, *55*, 514–524. https://doi.org/10.1016/j.renene.2012.12.049

Jones, P., Harpham, C., Kilsby, C., Glenis, V., & Burton, A. (2010). *UK Climate Projections science report: Projections of future daily climate for the UK from the Weather Generator* (Issue November). http://ukclimateprojections.defra.gov.uk

Kashyap, S., Sarkar, J., & Kumar, A. (2020). Comparative performance analysis of different novel regenerative evaporative cooling device topologies. *Applied Thermal Engineering*, *176*(August 2019), 115474. https://doi.org/10.1016/j.applthermaleng.2020.115474

Katić, K., Li, R., & Zeiler, W. (2016). Thermophysiological models and their applications: A review. *Building and Environment*, *106*, 286–300. https://doi.org/10.1016/j.buildenv.2016.06.031

Kershaw, T., Eames, M., & Coley, D. (2011). Assessing the risk of climate change for buildings: A comparison between multi-year and probabilistic reference year simulations. *Building and Environment*, *46*(6), 1303–1308. https://doi.org/10.1016/j.buildenv.2010.12.018

Kim, H., & Clayton, M. J. (2020). A multi-objective optimization approach for climate-adaptive building envelope design using parametric behavior maps. *Building and Environment*, *185*(2020), 107292. https://doi.org/10.1016/j.buildenv.2020.107292

Kolokotsa, D., Diakaki, C., Papantoniou, S., & Vlissidis, A. (2012). Numerical and experimental analysis of cool roofs application on a laboratory building in Iraklion, Crete, Greece. *Energy and Buildings*, *55*, 85–93. https://doi.org/10.1016/j.enbuild.2011.09.011

Koppe, C., Kovats, S., Jendritzky, G., & Menne, B. (2004). Heat-waves: risks and responses. In *Health and Global Environmental Health Series: Vol. No.2* (Issue 2). https://doi.org/10.1007/s00484-009-0283-7

Kotlarski, S., Keuler, K., Christensen, O. B., Colette, A., Déqué, M., Gobiet, A., Goergen, K., Jacob, D., Lüthi, D., Van Meijgaard, E., Nikulin, G., Schär, C., Teichmann, C., Vautard, R., Warrach-Sagi, K., & Wulfmeyer, V. (2014). Regional climate modeling on European scales: A joint standard

evaluation of the EURO-CORDEX RCM ensemble. *Geoscientific Model Development*, *7*(4), 1297–1333. https://doi.org/10.5194/gmd-7-1297-2014

Laaidi, K., Ung, A., Wagner, V., Beaudeau, P., & Pascal, M. (2013). *The French Heat and Health Watch Warning System : principles , fundamentals and assessment*.

Laaidi, K., Zeghnoun, A., Dousset, B., Bretin, P., Vandentorren, S., Giraudet, E., & Beaudeau, P. (2012). The impact of heat islands on mortality in Paris during the August 2003 heat wave. *Environmental Health Perspectives*, *120*(2), 254–259. https://doi.org/10.1289/ehp.1103532

Laouadi, A., Bartko, M., & Lacasse, M. A. (2020). A new methodology of evaluation of overheating in buildings. *Energy and Buildings*, *226*, 110360. https://doi.org/10.1016/j.enbuild.2020.110360

Lapisa, R. (2016). *Etude du rafraichissement passif de batiments commerciaux ou industriels*. La Rochelle University.

Lapisa, R., Bozonnet, E., Salagnac, P., & Abadie, M. O. (2018). Optimized design of low-rise commercial buildings under various climates – Energy performance and passive cooling strategies. *Building and Environment*, *132*(January), 83–95. https://doi.org/10.1016/j.buildenv.2018.01.029

Lavell, A., Oppenheimer, M., Diop, C., Jeremy, H., Lemper, R., Muir-Wood, R., & Myeong, S. (2012). Climate Change : Vulnerability , and Resilience Coordinating Lead Authors : Review Editors : Contributing Authors : In *Managing the Risks of Extreme Events and Disasters to Advance Climate Change Adaptation [Field, C.B., V. Barros, T.F. Stocker, D. Qin, D.J. Dokken, K.L. Ebi, M.D. Mastrandrea, K.J. Mach, G.-K. Plattner, S.K. Allen, M. Tignor, and P.M. Midgley (eds.)]. A S* (pp. 25–64). Cambridge University Press. http://www.ipcc.ch/pdf/special-reports/srex/SREX-Chap1_FINAL.pdf

Lazzarin, R. M., Castellotti, F., & Busato, F. (2005). Experimental measurements and numerical modelling of a green roof. *Energy and Buildings*, *37*(12), 1260–1267. https://doi.org/10.1016/j.enbuild.2005.02.001

Le Roy, B., Lemonsu, A., & Schoetter, R. (2021). A statistical–dynamical downscaling methodology for the urban heat island applied to the EURO-CORDEX ensemble. *Climate Dynamics*, *0123456789*. https://doi.org/10.1007/s00382-020-05600-z

Lee, K. H., & Strand, R. K. (2006). Implementation of an Earth Tube System Into EnergyPlus Program. *Simbuild 2006*, *March*, 58–66. http://www.ibpsa.org/proceedings/SB2006/SB2006_papers.zip%5Cnhttps://www.scribd.com/doc/193820500/Eart-Earth-Tube-Design%5Cnhttp://eetd.lbl.gov/node/52040%5Cnhttps://www.researchgate.net/publication/240638104_IMPLEMENTATION_OF_AN_EARTH_TUBE_SYSTEM_INTO_EN

Lee, W., Kim, Y., Sera, F., Gasparrini, A., Park, R., Michelle Choi, H., Prifti, K., Bell, M. L., Abrutzky, R., Guo, Y., Tong, S., de Sousa Zanotti Stagliorio Coelho, M., Nascimento Saldiva, P. H., Lavigne, E., Orru, H., Indermitte, E., Jaakkola, J. J. K., Ryti, N. R. I., Pascal, M., … Kim, H. (2020). Projections of excess mortality related to diurnal temperature range under climate change scenarios: a multi-country modelling study. *The Lancet Planetary Health*, *4*(11), e512–e521. https://doi.org/10.1016/S2542-5196(20)30222-9

Lemonsu, A., Viguié, V., Daniel, M., & Masson, V. (2015). Vulnerability to heat waves: Impact of urban expansion scenarios on urban heat island and heat stress in Paris (France). *Urban Climate*, *14*, 586–605. https://doi.org/10.1016/j.uclim.2015.10.007

Lemonsu, Aude, Beaulant, A. L., Somot, S., & Masson, V. (2014). Evolution of heat wave occurrence

over the Paris basin (France) in the 21st century. *Climate Research*, *61*(1), 75–91. https://doi.org/10.3354/cr01235

Leroux, G., Le Pierrès, N., Stephan, L., Wurtz, E., Anger, J., & Mora, L. (2019). Pilot-scale experimental study of an innovative low-energy and low-cost cooling system for buildings. *Applied Thermal Engineering*, *157*(October 2018), 113665. https://doi.org/10.1016/j.applthermaleng.2019.04.075

Levinson, R., Berdahl, P., Akbari, H., Miller, W., Joedicke, I., Reilly, J., Suzuki, Y., & Vondran, M. (2007). Methods of creating solar-reflective nonwhite surfaces and their application to residential roofing materials. *Solar Energy Materials and Solar Cells*, *91*(4), 304–314. https://doi.org/10.1016/j.solmat.2006.06.062

Lewis, S. C., & King, A. D. (2017). Evolution of mean, variance and extremes in 21st century temperatures. *Weather and Climate Extremes*, *15*(November 2016), 1–10. https://doi.org/10.1016/j.wace.2016.11.002

Lhotka, O., Kyseley, J., & Plavcova, E. (2017). Evaluation of major heat waves' mechanisms in EURO-CORDEX RCMs over Central Europe. *Climate Dynamics*.

Liu, C., Kershaw, T., Fosas, D., Ramallo Gonzalez, A. P., Natarajan, S., & Coley, D. A. (2017). High resolution mapping of overheating and mortality risk. *Building and Environment*, *122*, 1–14. https://doi.org/10.1016/j.buildenv.2017.05.028

Liu, Chunde, Chung, W.-J., & Coley, D. (2019). Creation Of Future Hot Event Years For Assessing Building Resilience Against Future Deadly Heatwaves Chunde Liu , Woong-June Chung , David Coley Centre for Energy and the Design of Environments , University of Bath , BA2 7AY , UK Abstract. *IBPSA 2019 - International Building Performance Simulation Association 2019*.

Lomas, K. J., & Porritt, S. M. (2017). Overheating in buildings: lessons from research. *Building Research and Information*, *45*(1–2), 1–18. https://doi.org/10.1080/09613218.2017.1256136

Long, L., & Ye, H. (2014). How to be smart and energy efficient: A general discussion on thermochromic windows. *Scientific Reports*, *4*, 1–10. https://doi.org/10.1038/srep06427

Lu, X., Xu, P., Wang, H., Yang, T., & Hou, J. (2016). Cooling potential and applications prospects of passive radiative cooling in buildings: The current state-of-the-art. *Renewable and Sustainable Energy Reviews*, *65*(4800), 1079–1097. https://doi.org/10.1016/j.rser.2016.07.058

Machard, A., Inard, C., Alessandrini, J. M., Pelé, C., & Ribéron, J. (2020b). A Methodology for Assembling FutureWeather Files including Heatwaves for Building Thermal Simulations from the European Coordinated Regional Downscaling Experiment (EURO-CORDEX) Climate Data. *Energies*, *13*(13), 1–36. https://doi.org/10.3390/en13133424

Machard, A., Martinez, S., Bozonnet, E., Lacedra, E., & Inard, C. (2020b). How to assess ecodistrict resilience to urban heat stress under future heatwaves? A case study for the city of Paris. *ICRBE Procedia*, *1*(1), 11–24. https://doi.org/10.32438/icrbe.202044

Mairie de Paris. (2017). *Stratégie de Résilience de Paris*. https://cdn.paris.fr/paris/2019/07/24/ebc807dec56112639d506469b3b67421.pdf

Masson, V. (2000). A PHYSICALLY-BASED SCHEME FOR THE URBAN ENERGY BUDGET IN ATMOSPHERICMODELS. *Boundary-Layer Meteorology*, *94*(September 1999), 357–397.

McGregor, G. R. (2015). *Heatwaves and Health: Guidance on Warning-System Development* (Issue 1142). http://www.who.int/globalchange/publications/WMO_WHO_Heat_Health_Guidance_2015.pdf

McLeod, R. S., Hopfe, C. J., & Kwan, A. (2013). An investigation into future performance and overheating risks in Passivhaus dwellings. *Building and Environment*, *70*, 189–209.

https://doi.org/10.1016/j.buildenv.2013.08.024

Meinshausen, M., Smith, S. J., Calvin, K., Daniel, J. S., Kainuma, M. L. T., Lamarque, J., Matsumoto, K., Montzka, S. A., Raper, S. C. B., Riahi, K., Thomson, A., Velders, G. J. M., & van Vuuren, D. P. P. (2011). The RCP greenhouse gas concentrations and their extensions from 1765 to 2300. *Climatic Change*, *109*(1), 213–241. https://doi.org/10.1007/s10584-011-0156-z

Menberg, K., Heo, Y., & Choudhary, R. (2016). Sensitivity analysis methods for building energy models: Comparing computational costs and extractable information. *Energy and Buildings*, *133*, 433–445. https://doi.org/10.1016/j.enbuild.2016.10.005

Meteonorm. (2017). *Handbook part II: Theory, Version 7.2. Global Meteorological Database Version 7, Software and Data for Engineers, Planers and Education. The Meteorological Reference for Solar Energy Applications, Building Design, Heating & Cooling Systems, Education Rene* (Issue March).

Miller, W., Machard, A., Bozonnet, E., Yoon, N., Qi, D., Zhang, C., Liu, A., Sengupta, A., Akander, J., Hayati, A., Cehlin, M., Kazanci, O. B., & Levinson, R. (2020). How can we define and measure "resilient cooling"? - A review and evaluation of resilience frameworks and criteria. *Submitted to Applied Energy*.

Ministère de l'Ecologie, du D. durable et de l'Energie. (2013). *Découvrir les nouveaux scénarios RCP et SSP utilisés par le GIEC*.

Ministère de la Transition Ecologique et Solidaire. (n.d.). *Drias Les futurs du climat, projections climatiques pour l'adaptation de nos sociétés*. http://www.drias-climat.fr/

Ministère de la Transition écologique et Solidaire. (2011). *Plan National d'Adaptation au Changement Climatique*. http://dx.doi.org/10.1016/j.cirp.2016.06.001%0Ahttp://dx.doi.org/10.1016/j.powtec.2016.12.055%0Ahttps://doi.org/10.1016/j.ijfatigue.2019.02.006%0Ahttps://doi.org/10.1016/j.matlet.2019.04.024%0Ahttps://doi.org/10.1016/j.matlet.2019.127252%0Ahttp://dx.doi.o

Mirianhosseinabadi, S., Cho, S., Kang, E. C., & Lee, E. J. (2014). Simulation modeling of Earth-To-Air Heat Exchanger (buried pipe) for the performance analysis of a School Building In Mid-Atlantic region. *2014 ASHRAE/IBPSA-USA Building Simulation Conference*, 378–385.

Moazami, A., Carlucci, S., & Geving, S. (2017). Critical Analysis of Software Tools Aimed at Generating Future Weather Files with a view to their use in Building Performance Simulation. *Energy Procedia*, *132*, 640–645. https://doi.org/10.1016/j.egypro.2017.09.701

Moazami, A., Carlucci, S., Nik, V. M., & Geving, S. (2019). Towards climate robust buildings: An innovative method for designing buildings with robust energy performance under climate change. *Energy and Buildings*, *202*, 109378. https://doi.org/10.1016/j.enbuild.2019.109378

Moazami, A., Nik, V. M., Carlucci, S., & Geving, S. (2019). Impacts of future weather data typology on building energy performance – Investigating long-term patterns of climate change and extreme weather conditions. *Applied Energy*, *238*, 696–720. https://doi.org/10.1016/j.apenergy.2019.01.085

Morris, M. D. (1991). Factorial Sampling Plans for Preliminary Computational Experiments. *Technometrics*, *33*(2), 161–174.

Moshari, S., Heidarinejad, G., & Fathipour, A. (2016). Numerical investigation of wet-bulb effectiveness and water consumption in one-and two-stage indirect evaporative coolers. *Energy Conversion and Management*, *108*, 309–321. https://doi.org/10.1016/j.enconman.2015.11.022

Moss, R. H., Edmonds, J. A., Hibbard, K. A., Manning, M. R., Rose, S. K., Vuuren, D. P. Van, Carter, T. R., Emori, S., Kainuma, M., Kram, T., Meehl, G. A., Mitchell, J. F. B., Nakicenovic, N., Riahi, K.,

Smith, S. J., Stouffer, R. J., Thomson, A. M., Weyant, J. P., & Wilbanks, T. J. (2010). The next generation of scenarios for climate change research and assessment. *Nature*, *463*(7282), 747–756. https://doi.org/10.1038/nature08823

Nairn, J., & Fawcett, R. (2013). Defining heatwaves: heatwave defined as a heat-impact event servicing all communiy and business sectors in Australia. In *CAWCR technical report* (Issue 60). https://doi.org/551.5250994

Nairn, J. R., & Fawcett, R. J. B. (2014). The excess heat factor: A metric for heatwave intensity and its use in classifying heatwave severity. *International Journal of Environmental Research and Public Health*, *12*(1), 227–253. https://doi.org/10.3390/ijerph120100227

National Weather Service. (2020). *The Atmospheric Window*. https://www.weather.gov/jetstream/absorb

Nguyen, A. T., Rockwood, D., Doan, M. K., & Dung Le, T. K. (2021). Performance assessment of contemporary energy-optimized office buildings under the impact of climate change. *Journal of Building Engineering*, *35*(December 2020), 102089. https://doi.org/10.1016/j.jobe.2020.102089

Niachou, A., Papakonstantinou, K., Santamouris, M., Tsangrassoulis, A., & Mihalakakou, G. (2001). Analysis of the green roof thermal properties and investigation of its energy performance. *Energy and Buildings*, *33*(7), 719–729. https://doi.org/10.1016/S0378-7788(01)00062-7

Nicol, F., Bahadur Rijal, H., Imagawa, H., & Thapa, R. (2020). The range and shape of thermal comfort and resilience. *Energy and Buildings*, *224*, 110277. https://doi.org/10.1016/j.enbuild.2020.110277

Nik, V. M. (2010). *Climate Simulation of an Attic Using Future Weather Data Sets - Statistical Methods for Data Processing and Analysis* [Chalmers University of Technology]. http://www.chalmers.se

Nik, V. M. (2016). Making energy simulation easier for future climate - Synthesizing typical and extreme weather data sets out of regional climate models (RCMs). *Applied Energy*, *177*, 204–226. https://doi.org/10.1016/j.apenergy.2016.05.107

Nik, V. M., Sasic Kalagasidis, A., & Kjellström, E. (2012). Statistical methods for assessing and analysing the building performance in respect to the future climate. *Building and Environment*, *53*, 107–118. https://doi.org/10.1016/j.buildenv.2012.01.015

Nishi, Y., & Gagge, A. P. (1977). Effective temperature scale useful for hypo and hyperbaric environments. In *Aviation Space and Environmental Medicine* (Vol. 48, Issue 2, pp. 97–107). https://doi.org/10.1097/00006534-197801000-00129

O'Neill, B. C., Kriegler, E., Riahi, K., Ebi, K. L., Hallegatte, S., Carter, T. R., Mathur, R., & van Vuuren, D. P. (2014). A new scenario framework for climate change research: The concept of shared socioeconomic pathways. *Climatic Change*, *122*(3), 387–400. https://doi.org/10.1007/s10584-013-0905-2

O'Sullivan, Paul.; O'Donovan, A. (2018). *Ventilative Cooling Case Studies* (Issue May). International Energy Agency (IEA) - Energy in Buildings and Communities Programme (EBC). http://www.iea-ebc.org/Data/publications/EBC_Annex_62_Design_Guide.pdf

Okeke, F. O., Okekeogbu C. J., & A., A. F. (2019). Biomimicry and sustainable architecture : A review of existing literature. *Journal of Environmental Management and Safety*, *8*(February), 11–24.

Olgay, V. (1963). *Design with Climate - Bioclimatic approach to architectural regionalism* (2015 Editi). Princeton University Press.

Ouzeau, G., Déqué, M., Jouini, M., Planton, S., Vautard, R., & Jouzel, J. (2014). *Le Climat de la France au XXIème siècle Volume 4. Scénarios régionalisés : édition 2014 pour la métropole et les régions d'outre-mer*.

Ouzeau, G., Soubeyroux, J. M., Schneider, M., Vautard, R., & Planton, S. (2016). Heat waves analysis over France in present and future climate: Application of a new method on the EURO-CORDEX ensemble. *Climate Services*, *4*, 1–12. https://doi.org/10.1016/j.cliser.2016.09.002

Palmer, J., Bennetts, H., Pullen, S., Zuo, J., Ma, T., & Chileshe, N. (2014). Adaptation of Australian houses and households to future heat waves. *7th Australasian Housing Researchers' Conference, AHRC 2013: Refereed Proceedings*, *February*.

Pang, Z., O'Neill, Z., Li, Y., & Niu, F. (2020). The role of sensitivity analysis in the building performance analysis: A critical review. *Energy and Buildings*, *209*, 109659. https://doi.org/10.1016/j.enbuild.2019.109659

Pascal, M., Laaidi, K., Ledrans, M., Baffert, E., Caserio-Schönemann, C., Le Tertre, A., Manach, J., Medina, S., Rudant, J., & Empereur-Bissonnet, P. (2006). France's heat health watch warning system. *International Journal of Biometeorology*, *50*(3), 144–153. https://doi.org/10.1007/s00484-005-0003-x

Pascal, M., Lagarrigue, R., Tabai, A., Bonmarin, I., Camail, S., Laaidi, K., Le Tertre, A., & Denys, S. (2021). Evolving heat waves characteristics challenge heat warning systems and prevention plans. *International Journal of Biometeorology*. https://doi.org/10.1007/s00484-021-02123-y

Pascal, M., Wagner, V., Corso, M., Laaidi, K., Ung, A., & Beaudeau, P. (2018). Heat and cold related-mortality in 18 French cities. *Environment International*, *121*(September), 189–198. https://doi.org/10.1016/j.envint.2018.08.049

Pascal, M., Wagner, V., Le Tertre, A., Laaidi, K., Honoré, C., Bénichou, F., & Beaudeau, P. (2013). Definition of temperature thresholds: The example of the French heat wave warning system. *International Journal of Biometeorology*, *57*(1), 21–29. https://doi.org/10.1007/s00484-012-0530-1

Peretti, C., Zarrella, A., De Carli, M., & Zecchin, R. (2013). The design and environmental evaluation of earth-to-air heat exchangers (EAHE). A literature review. *Renewable and Sustainable Energy Reviews*, *28*, 107–116. https://doi.org/10.1016/j.rser.2013.07.057

Perez, R., Ineichen, P., Moore, K., Kmiecik, M., Chain, C., George, R., & Vignola, F. (2002). A new operational model for satellite-derived irradiances: Description and validation. *Solar Energy*, *73*(5), 307–317. https://doi.org/10.1016/S0038-092X(02)00122-6

Perkins, S. E., & Alexander, L. V. (2013). On the measurement of heat waves. *Journal of Climate*, *26*(13), 4500–4517. https://doi.org/10.1175/JCLI-D-12-00383.1

Petersen, S., Kristensen, M. H., & Knudsen, M. D. (2019). Prerequisites for reliable sensitivity analysis of a high fidelity building energy model. *Energy and Buildings*, *183*, 1–16. https://doi.org/10.1016/j.enbuild.2018.10.035

Pigeon, G., Legain, D., Durand, P., & Masson, V. (2008). Anthropogenic heat release in an old European agglomeration (Toulouse, France). *International Journal of Climatology*, *27*(March 2008), 1969–1981. https://doi.org/10.1002/joc

Pigeon, G., Zibouche, K., Bueno, B., Le Bras, J., & Masson, V. (2014). Improving the capabilities of the Town Energy Balance model with up-to-date building energy simulation algorithms: An application to a set of representative buildings in Paris. *Energy and Buildings*, *76*, 1–14. https://doi.org/10.1016/j.enbuild.2013.10.038

Pyrgou, A., Castaldo, V. L., Pisello, A. L., Cotana, F., & Santamouris, M. (2017). On the effect of summer heatwaves and urban overheating on building thermal-energy performance in central Italy. *Sustainable Cities and Society*, *28*, 187–200. https://doi.org/10.1016/j.scs.2016.09.012

Pyrgou, A., & Santamouris, M. (2020). Article probability risk of heat-and cold-related mortality to temperature, gender, and age using GAM regression analysis. *Climate*, *8*(3). https://doi.org/10.3390/cli8030040

Raji, B., Tenpierik, M. J., & Van Den Dobbelsteen, A. (2015). The impact of greening systems on building energy performance: A literature review. *Renewable and Sustainable Energy Reviews*, *45*, 610–623. https://doi.org/10.1016/j.rser.2015.02.011

Raman, A. P., Anoma, M. A., Zhu, L., Rephaeli, E., & Fan, S. (2014). Passive radiative cooling below ambient air temperature under direct sunlight. *Nature*, *515*(7528), 540–544. https://doi.org/10.1038/nature13883

Ramon, D., Allacker, K., van Lipzig, N. P. M., De Troyer, F., & Wouters, H. (2018). Future Weather Data for Dynamic Building Energy Simulations: Overview of Available Data and Presentation of Newly Derived Data for Belgium. In *Energy Sustainability in Built and Urban Environments* (pp. 111–138).

Recht, T., Schalbart, P., & Peuportier, B. (n.d.). ECODESIGN OF A ' PLUS-ENERGY ' HOUSE USING STOCHASTIC OCCUPANCY MODEL , LIFE-CYCLE ASSESSMENT AND MULTI-OBJECTIVE OPTIMISATION. *Building Simulation and Optimization Conference*.

Ren, Z., Chen, Z., & Wang, X. (2011). Climate change adaptation pathways for Australian residential buildings. *Building and Environment*, *46*(11), 2398–2412. https://doi.org/10.1016/j.buildenv.2011.05.022

Ribéron, J., Vandentorren, S., Bretin, P., Zeghnoun, A., Salines, G., Cochet, C., Thibault, C., Hénin, M., & Ledrans, M. (2006). Building and Urban Factors in Heat Related Deaths during the 2003 Heat Wave in France. *Healthy Buildings Conference*.

Robinson, P. J. (2001). On the definition of a heat wave. *Journal of Applied Meteorology*, *40*(4), 762–775. https://doi.org/10.1175/1520-0450(2001)040<0762:OTDOAH>2.0.CO;2

Roelofsen, P. (2017). Healthy ageing: differences between elderly and non-elderly in temperature sensation and dissatisfied. *Intelligent Buildings International*, *9*(3). https://doi.org/10.1080/17508975.2015.1063474

Rossi, F., Morini, E., Castellani, B., Nicolini, A., Bonamente, E., Anderini, E., & Cotana, F. (2015). Beneficial effects of retroreflective materials in urban canyons: Results from seasonal monitoring campaign. *Journal of Physics: Conference Series*, *655*(1). https://doi.org/10.1088/1742-6596/655/1/012012

RTE. (2017). *Bilan prévisionnel de l'équilibre offre-demande d'électricité en France*. https://www.rte-france.com/sites/default/files/bp2017_complet_vf.pdf

Russo, S., Dosio, A., Graversen, R. G., Sillmann, J., Carrao, H., Dunbar, M. B., Singleton, A., Montagna, P., Barbola, P., & Vogt, J. V. (2014). Magnitude of extreme heat waves in present climate and their projection in a warming world. *Journal of Geophysical Research Atmospheres*, *119*(22), 12500–12512. https://doi.org/10.1002/2014JD022098

Safari, A., Saidur, R., Sulaiman, F. A., Xu, Y., & Dong, J. (2017). A review on supercooling of Phase Change Materials in thermal energy storage systems. *Renewable and Sustainable Energy Reviews*, *70*(November 2015), 905–919. https://doi.org/10.1016/j.rser.2016.11.272

Salagnac, J.-L. (2015). *Adaptation du cadre bâti aux conditions climatiques actuelles et futures : le cas des canicules*.

Salmeron, J. M., Alvarez, S., Sanchez, J., Ford, B., & Gillott, M. (2012). Analysis of a PHDC (Passive and

Hybrid Downdraft Cooling) Experimental Facility in Seville and its Applicability to the Madrid Climate. *International Journal of Ventilation*, *10*(4), 391–404. 10.1080/14733315.2012.11683964%0A

Salomon, T., Mikolazek, R., Peuportier, B., Thiers, S., Jautard, Y., & Trombe, A. (2003). *Dimensionnement du « puits climatique » Analyse, modélisation, validation d'un modèle de simulation dynamique pour les puits « canadiens » ou « provençaux »*.

Saltelli, A., Tarantola, S., Campolongo, F., & Ratto, M. (2004). Sensitivity Analysis in Practice - A Guide to Assessing Scientific Models. In I. John Wiley & Sons (Ed.), *Sensitivity Analysis in Practice*. https://doi.org/10.1002/0470870958.ch6

Salvati, A., Palme, M., Chiesa, G., & Kolokotroni, M. (2020). Built form, urban climate and building energy modelling: case-studies in Rome and Antofagasta. *Journal of Building Performance Simulation*, *13*(2), 209–225. https://doi.org/10.1080/19401493.2019.1707876

Santamouris, M., Fergus, N., Susan, R., Hashem, A., Voss, K., E. Kuhn, T., Nitz, P., Herkel, S., Wall, M., Hellström, B., Kolokotroni, M., Santamouris, M., Pfafferott, J., Walker-Hertkorn, S., Sanner, B., & Ereel, E. (2007). *Advances in passive cooling* (Mat. Santamouris (ed.)). Earthscan.

Santamouris, Mat. (2016). Cooling the buildings – past, present and future. *Energy and Buildings*, *128*, 617–638. https://doi.org/10.1016/j.enbuild.2016.07.034

Santamouris, Mattheos, & Feng, J. (2018). Recent progress in daytime radiative cooling: Is it the air conditioner of the future? *Buildings*, *8*(12). https://doi.org/10.3390/buildings8120168

Santamouris, Mattheos, & Kolokotsa, D. (2015). On the impact of urban overheating and extreme climatic conditions on housing, energy, comfort and environmental quality of vulnerable population in Europe. *Energy and Buildings*, *98*, 125–133. https://doi.org/10.1016/j.enbuild.2014.08.050

Sarrazin, F., Pianosi, F., & Wagener, T. (2016). Environmental Modelling & Software Global Sensitivity Analysis of environmental models : Convergence and validation. *Environmental Modelling and Software*, *79*, 135–152. https://doi.org/10.1016/j.envsoft.2016.02.005

Savima. (2020). *Pourquoi Choisir des Fenêtres Jalousies ?* https://www.savima.fr/pourquoi-choisir-fenetres-jalousies/

Sharifi, A., & Yamagata, Y. (2015). Roof ponds as passive heating and cooling systems: A systematic review. *Applied Energy*, *160*, 336–357. https://doi.org/10.1016/j.apenergy.2015.09.061

Shivanna, K. R. (2020). The Sixth Mass Extinction Crisis and its Impact on Biodiversity and Human Welfare. *Resonance*, *25*(1), 93–109. https://doi.org/10.1007/s12045-019-0924-z

Sobol, I. M. (2001). Global sensitivity indices for nonlinear mathematical models and their Monte Carlo estimates. *Mathematics and Computers in Simulation*. https://doi.org/10.1016/S0378-4754(00)00270-6

Solomon, S. D. Qin, M. Manning, R.B. Alley, T. Berntsen, N.L. Bindoff, Z. Chen, A. Chidthaisong, J.M. Gregory, G. C. H., M. Heimann, B. Hewitson, B.J. Hoskins, F. Joos, J. Jouzel, V. Kattsov, U. Lohmann, T. Matsuno, M. Molina, N. Nicholls, J., & Overpeck, G. Raga, V. Ramaswamy, J. Ren, M. Rusticucci, R. Somerville, T.F. Stocker, P. Whetton, R. A. W. and D. W. (2007). Climate Change 2007: The Physical Science Basis. Contribution of Working Group I to the Fourth Assessment Report of the Intergovernmental Panel on Climate Change. In *Cambridge University Press*.

Soubeyroux, J.-M., Ouzeau, G., Schneider, M., Cabanes, O., & Kounkou-Arnaud, R. (2016). Les vagues de chaleur en France : analyse de l'été 2015 et évolutions attendues en climat futur. *La*

Météorologie, *8*(94), 45. https://doi.org/10.4267/2042/60704

Sutton, M. A., Billen, G., Bleeker, A., Erisman, J. W., Grennfelt, P., van Grinsven, H., Grizzetti, B., Howard, C. M., & Leip, A. (2011). Technical summary. *The European Nitrogen Assessment*, xxxv–lii. https://doi.org/10.1017/cbo9780511976988.003

Swami, M. V., & Chandra, S. (1988). Correlations for pressure distribution on buildings and calculation of natural-ventilation airflow. *ASHRAE Transactions*, 243–266.

Synnefa, A., Garshasbi, S., Haddad, S., Paolini, R., & Santamouris, M. (2018). Impact of the mitigation of the local climate on building energy needs in Australian cities. *Engaging Architectural Science: Meeting the Challenges of Higher Density: 52nd International Conference of the Architectural Science Association 2018*, 277–284.

Taesler, R., & Andersson, C. (1984). A method for solar radiation computations using routine meteorological observations. *Energy and Buildings*, *7*(4), 341–352. https://doi.org/10.1016/0378-7788(84)90080-X

Tartarini, F., & Schiavon, S. (2020). pythermalcomfort: A Python package for thermal comfort research. *SoftwareX*, *12*, 100578. https://doi.org/10.1016/j.softx.2020.100578

Taurines, K. (2019). Energy and thermal analysis of an innovative earth-to-air heat exchanger: Experimental investigations. *Energy and Buildings*, *187*, 1–15. https://doi.org/10.1016/j.enbuild.2019.01.037

Tavares, P. F., Gaspar, A. R., Martins, A. G., & Frontini, F. (2014). Evaluation of electrochromic windows impact in the energy performance of buildings in mediterranean climates. *Energy Policy*, *67*, 68–81. https://doi.org/10.1016/j.enpol.2013.07.038

Taylor, J., Wilkinson, P., Picetti, R., Symonds, P., Heaviside, C., Macintyre, H. L., Davies, M., Mavrogianni, A., & Hutchinson, E. (2018). Comparison of built environment adaptations to heat exposure and mortality during hot weather, West Midlands region, UK. *Environment International*, *111*(November 2017), 287–294. https://doi.org/10.1016/j.envint.2017.11.005

Thevenart, & Humphries. (2005). The Calculation of Climatic Design Conditions in the 2005 ASHRAE Handbook of Fundamentals. *ASHRAE Transactions*, *111*, 457–466.

Thiers, S., & Peuportier, B. (2008). Thermal and environmental assessment of a passive building equipped with an earth-to-air heat exchanger in France. *Solar Energy*, *82*(9), 820–831. https://doi.org/10.1016/j.solener.2008.02.014

Tian, W., & De Wilde, P. (2011). Uncertainty and sensitivity analysis of building performance using probabilistic climate projections: A UK case study. *Automation in Construction*, *20*(8), 1096–1109. https://doi.org/10.1016/j.autcon.2011.04.011

Triana, M. A., Lamberts, R., & Sassi, P. (2018). Should we consider climate change for Brazilian social housing? Assessment of energy efficiency adaptation measures. *Energy and Buildings*, *158*, 1379–1392. https://doi.org/10.1016/j.enbuild.2017.11.003

Troup, L., Eckelman, M. J., & Fannon, D. (2019). Simulating future energy consumption in office buildings using an ensemble of morphed climate data. *Applied Energy*, *255*(February). https://doi.org/10.1016/j.apenergy.2019.113821

Troup, L., & Fannon, D. (2016). Morphing Climate Data to Simulate Building Energy Consumption. *ASHRAE and IBPSA-USA SimBuild 2016 Building Performance Modeling Conference*, 439–446. https://www.ashrae.org/File Library/docLib/Events/Simbuild2016/.../C058.pdf

Ulpiani, G., Ranzi, G., Feng, J., & Santamouris, M. (2021). Expanding the applicability of daytime

radiative cooling: Technological developments and limitations. *Energy and Buildings*, *243*, 110990. https://doi.org/10.1016/j.enbuild.2021.110990

Vall, S., & Castell, A. (2017). Radiative cooling as low-grade energy source: A literature review. *Renewable and Sustainable Energy Reviews*, *77*(May), 803–820. https://doi.org/10.1016/j.rser.2017.04.010

Vall, S., Johannes, K., David, D., & Castell, A. (2020). A new flat-plate radiative cooling and solar collector numerical model: Evaluation and metamodeling. *Energy*, *202*. https://doi.org/10.1016/j.energy.2020.117750

van Vuuren, D. P., Kriegler, E., O'Neill, B. C., Ebi, K. L., Riahi, K., Carter, T. R., Edmonds, J., Hallegatte, S., Kram, T., Mathur, R., & Winkler, H. (2014). A new scenario framework for Climate Change Research: Scenario matrix architecture. *Climatic Change*, *122*(3), 373–386. https://doi.org/10.1007/s10584-013-0906-1

Vandentorren, S., Bretin, P., Zeghnoun, A., Mandereau-Bruno, L., Croisier, A., Cochet, C., Ribéron, J., Siberan, I., Declercq, B., & Ledrans, M. (2006). August 2003 heat wave in France: Risk factors for death of elderly people living at home. *European Journal of Public Health*, *16*(6), 583–591. https://doi.org/10.1093/eurpub/ckl063

Vautard, R., Gobiet, A., Jacob, D., Belda, M., Colette, A., Déqué, M., Fernández, J., García-Díez, M., Goergen, K., Güttler, I., Halenka, T., Karacostas, T., Katragkou, E., Keuler, K., Kotlarski, S., Mayer, S., van Meijgaard, E., Nikulin, G., Patarčić, M., … Yiou, P. (2013). The simulation of European heat waves from an ensemble of regional climate models within the EURO-CORDEX project. *Climate Dynamics*, *41*(9–10), 2555–2575. https://doi.org/10.1007/s00382-013-1714-z

Vellei, M., Ramallo-González, A. P., Coley, D., Lee, J., Gabe-Thomas, E., Lovett, T., & Natarajan, S. (2017). Overheating in vulnerable and non-vulnerable households. *Building Research and Information*, *45*(1–2), 102–118. https://doi.org/10.1080/09613218.2016.1222190

Walton, G. N. (1983). *The Thermal Analysis Research Program Reference Manual Program (TARP)* (N. B. of S. (now N. I. of S. and Technology) (ed.)).

Wang, L., Mathew, P., & Pang, X. (2012). Uncertainties in energy consumption introduced by building operations and weather for a medium-size office building. *Energy and Buildings*, *53*, 152–158. https://doi.org/10.1016/j.enbuild.2012.06.017

Wang, W., Fernandez, N., Katipamula, S., & Alvine, K. (2018). Performance assessment of a photonic radiative cooling system for office buildings. *Renewable Energy*, *118*, 265–277. https://doi.org/10.1016/j.renene.2017.10.062

Wang, Y., Tahmasebi, F., Cooper, E., Stamp, S., Burman, E., & Mumovic, D. (2020). Capturing the diversity of household window operation behaviour : Lessons from a monitoring campaign in London. *Building Simulation and Optimization Conference*.

Waqas, A., & Ud Din, Z. (2013). Phase change material (PCM) storage for free cooling of buildings - A review. *Renewable and Sustainable Energy Reviews*, *18*, 607–625. https://doi.org/10.1016/j.rser.2012.10.034

Wei, T. (2013). A review of sensitivity analysis methods in building energy analysis. In *Renewable and Sustainable Energy Reviews*. https://doi.org/10.1016/j.rser.2012.12.014

Winkelmann, F., & Selkowitz, S. (1984). *DAYLIGHTING SIMULATION IN THE DOE-2 BUILDING ENERGY ANALYSIS PROGRAM*.

WRCP. (2019). *Coordinated Downscaling Experiment - European Domain*. https://www.euro-cordex.net/

Xie, X., & Jiang, Y. (2015). Comparison of Two Kinds of Indirect Evaporative Cooling System: To Produce Cold Water and to Produce Cooling Air. *Procedia Engineering*, *121*(February 2017), 881–890. https://doi.org/10.1016/j.proeng.2015.09.044

Xuan, Y. M., Xiao, F., Niu, X. F., Huang, X., & Wang, S. W. (2012). Research and application of evaporative cooling in China: A review (I) - Research. *Renewable and Sustainable Energy Reviews*, *16*(5), 3535–3546. https://doi.org/10.1016/j.rser.2012.01.052

Yang, W., Adréasson, J., Graham, L. P., Olsson, J., Rosberg, J., & Wetterhal, F. (2010). Distribution-based scaling to improve usability of regional climate model projections for hydrological climate change impact studies. *Hydrology Research*, *41*(3–4), 211–229. https://doi.org/10.2166/nh.2010.004

Yang, Y., Cui, G., & Lan, C. Q. (2019). Developments in evaporative cooling and enhanced evaporative cooling - A review. *Renewable and Sustainable Energy Reviews*, *113*(June 2016), 109230. https://doi.org/10.1016/j.rser.2019.06.037

Yao, J. (2020). The uncertainty of manual shade control on west-facing facades and its influence on energy performance. *Applied Thermal Engineering*, *165*(March 2019), 114611. https://doi.org/10.1016/j.applthermaleng.2019.114611

Young, A. T. (1994). Air mass and refraction. *Applied Optics*. https://doi.org/10.1364/ao.33.001108

Zeinelabdein, R., Omer, S., & Gan, G. (2018). Critical review of latent heat storage systems for free cooling in buildings. *Renewable and Sustainable Energy Reviews*, *82*(October 2017), 2843–2868. https://doi.org/10.1016/j.rser.2017.10.046

Zhai, Z. J., & Helman, J. M. (2019). Climate change: Projections and implications to building energy use. *Building Simulation*, *12*(4), 585–596. https://doi.org/10.1007/s12273-019-0509-5

Zinzi, M., & Agnoli, S. (2012). Cool and green roofs. An energy and comfort comparison between passive cooling and mitigation urban heat island techniques for residential buildings in the Mediterranean region. *Energy and Buildings*, *55*, 66–76. https://doi.org/10.1016/j.enbuild.2011.09.024

Appendix A – EAHX Pressure Losses Calculation

D_{pipe} (m) Tube diameter
v_{pipe} (m/s) Air velocity inside the EAHX pipe
fr (-) friction coefficient
VK_{air} (m²/s) Air kinematic viscosity
PL (Pa/m) Linear pressure losses
P (Pa) Pressure losses
$Qvol_{pipe}$ (ACH) Volumetric flow rate
Qv_{pipe} (m^3/h) Volumetric flow rate
S_{pipe} (m^2) Air cross section
Re (-) Reynolds number
VL (m^3) Living space volume

VL = 324 (m^3)
k_{tube} (PVC) = 0.17 W/(m.k)
ρ_{air} = 1.2 (kg/m^3)
VK_{air} = $1.51.10^{-5}$ (m^2/s)

Proposition of variation range for diameter D and airflow rate $Qvol_{pipe}$:
D (150-500) mm
$Qvol_{pipe}$ (0.6-5) ACH

The relationship between the airflow rate Qv_{pipe} inside the EAHX pipe and the pipe diameter D_{pipe} is given by Equations (85), (86) and (87):

$$S_{pipe} = \frac{\pi.\left(D_{pipe}{}^{2}\right)}{4} \quad (85)$$

$$Qv_{pipe} = Qvol_{pipe} * VL \quad (86)$$

$$v_{pipe} = \frac{\frac{Qv_{pipe}}{3600}}{S_{pipe}} \quad (87)$$

The linear pressure losses (PL) are calculated with Equation (88):

$$PL = \frac{fr * \rho_{air} * {v_{pipe}}^2}{2 * D_{pipe}} \quad (88)$$

f is calculated from the Reynolds number Re and the tube roughness $\frac{k_{tube}}{D_{tube}}$ by Equation (89):

$$Re = \frac{v_{pipe} * D_{pipe}}{\mathrm{VK}_{air}} \quad (89)$$

We use the formula given by the EnergyPlus Engineering Reference to calculate fr (Equation (90)):

$$fr = (1.58 * \ln(Re) - 3.28)^{-2} \quad (90)$$

The pressure losses will be maximal for the following:

- Minimal D_{pipe}
- Maximal $Qvol_{pipe}$
- High v_{pipe}
- Long pipe

PL are calculated for the maximal pipe length at 40 m.

<u>Case 1</u>: D_{pipe} = 150 mm

$Qvol_{pipe}$ is calculated from D_{pipe} and v_{pipe}:

$$Qvol_{pipe} = \frac{3600 * v_{pipe} * \pi * {D_{pipe}}^2}{\mathrm{VL} * 4} = 8.72. v_{pipe}. {D_{pipe}}^2 = 0.20. v_{pipe}$$

Table 35 – Pressure losses calculation for D_{tube} = 150 mm

	$Qvol_{pipe}$ (ACH)	Re	f	PL (Pa/m)	P (Pa)
$v_{pipe} = 1$	0.20	9,868	0.0079	0.03	1.3
$v_{pipe} = 3$	0.60 (min)	29,605	0.0059	0.21	8.5
$v_{pipe} = 5$	1.20	49,342	0.0053	0.53	21
$v_{pipe} = 10$	2.00	98,684	0.0045	1.80	72
$v_{pipe} = 15$	3.00	148,026	0.0041	3.69	148
$v_{pipe} = 25$	5.00(max)	246,711	0.0037	9.25	370

<u>Note</u>: To reach the maximal airflow rate (5 ACH) an air velocity of 25m/s is necessary, and linear pressure losses are of 33 Pa/m. These values are too high. We raise the minimal value for D_{pipe} to achieve lower pressure losses and airflow rates.

Case 2: $D_{pipe} = 200\ mm$

$Qvol_{pipe}$ is calculated from D_{pipe} and v_{pipe}:

$Qvol_{pipe} = 8.72.v_{pipe}.D_{pipe}{}^2 = 0.35.v_{pipe}$

Table 36 - Pressure losses calculation for D_{tube} = 200 mm

	$Qvol_{pipe}$ (ACH)	Re	f	PL (Pa/m)	P (Pa)
$v_{pipe} = 1$	0.35	13,158	0.0073	0.02	0.9
$v_{pipe} = 1.7$	0.60 (min)	22,368	0.0064	0.06	2.2
$v_{pipe} = 5$	1.75	65,789	0.0049	0.37	14.7
$v_{pipe} = 10$	3.50	131,579	0.0042	1.26	50.4
$v_{pipe} = 14.3$	5.00 (max)	188,158	0.0040	2.45	98.2

Note: To reach the maximal airflow rate (5 ACH) an air velocity of 14 m/s is necessary, for which pressure losses are about 98 Pa for a pipe length of 40 m. These values are still elevated.

Case 3: $D_{tube} = 250\ mm$

$Qvol_{pipe}$ is calculated from D_{pipe} and v_{pipe}:

$Qvol_{pipe} = 8.72.v_{pipe}.D_{pipe}{}^2 = 0.55.v_{pipe}$

Table 37 - Pressure losses calculation for D_{tube} = 250 mm

	$Qvol_{pipe}$ (ACH)	Re	f	PL (Pa/m)	P (Pa)
$v_{pipe} = 1.1$	0.60 (min)	18,092	0.0067	0.02	0.8
$v_{pipe} = 3$	1.65	49,342	0.0053	0.11	4.6
$v_{pipe} = 5.5$	3.0	90,461	0.0046	0.33	13.4
$v_{pipe} = 10$	5.0 (max)	164,474	0.0041	0.98	39.4

Note: To reach the maximal airflow rate (5 ACH) an air velocity of 10 m/s is necessary, for which pressure losses are about 40 Pa for a pipe length of 40 m. For a maximal airflow rate of 3 ACH, the pressure losses are acceptable (13.4 Pa) for the higher pipe length (40 m) and the air speed in the tube (5.5 m/s) is also acceptable. A higher air velocity is not recommended for noise constraints.

Conclusions

With the initial smaller diameter (150 mm) and maximal airflow rate (5 ACH), pressure losses and air velocity inside the tube are too high. With a diameter of 200 mm and maximal airflow rate of 5 ACH, the values are still elevated. For a higher diameter of 250 mm and maximum airflow rate of 5 ACH, pressure losses air velocities are still elevated. For a lower maximum airflow rate (3 ACH), for the higher diameter air velocity (around 5 m/s) and pressure losses (13.4 Pa for 40 m) are acceptable. Therefore, we choose to fix the diameter to 250 mm for the sensitivity analysis, and the maximum air flow rate at 3 ACH, which is also the same as for the mechanical free-cooling system.

Appendix B – Additional Morris simulation results

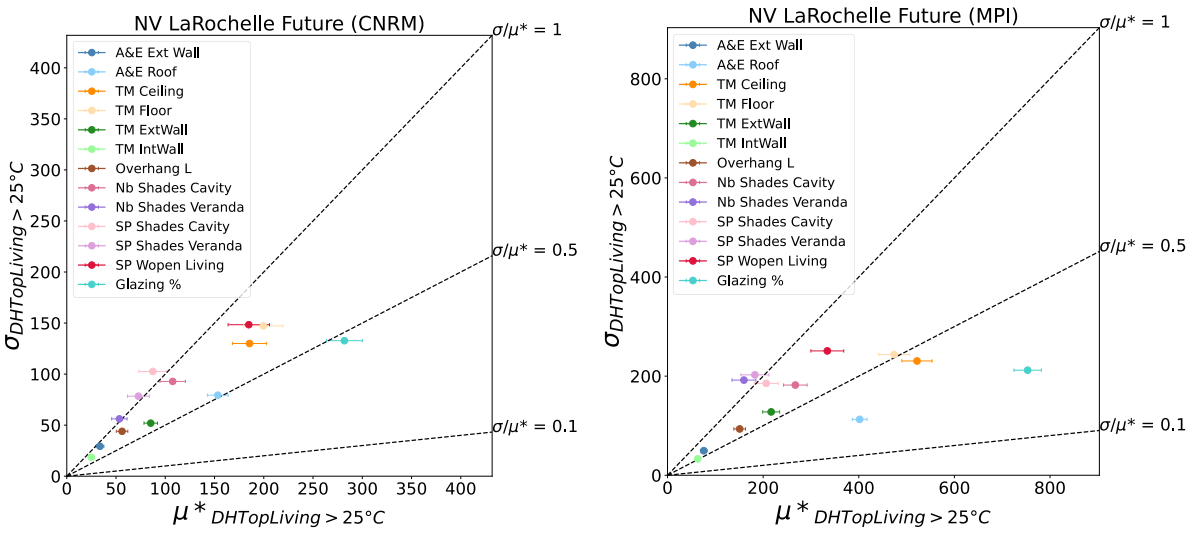

Figure 143 - SA results with Morris for the models with the lowest (CNRM) and highest (MPI) outdoor temperatures and indoor overheating in La Rochelle during the future typical summer – Natural Ventilation

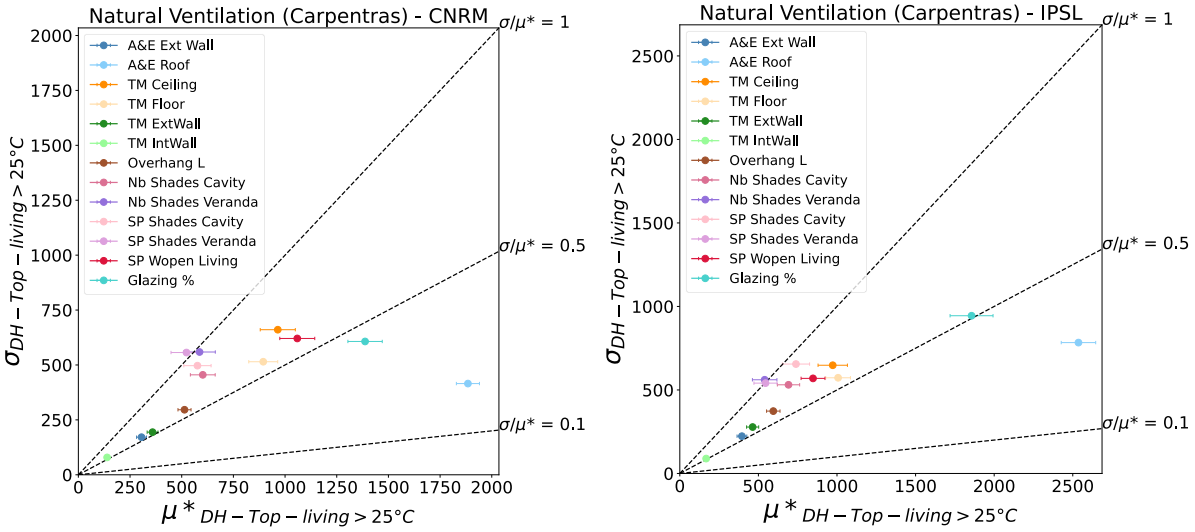

Figure 144 - SA results with Morris for the models with the lowest (CNRM) and highest (IPSL) outdoor temperatures and indoor overheating in Carpentras during the future typical summer – Natural Ventilation

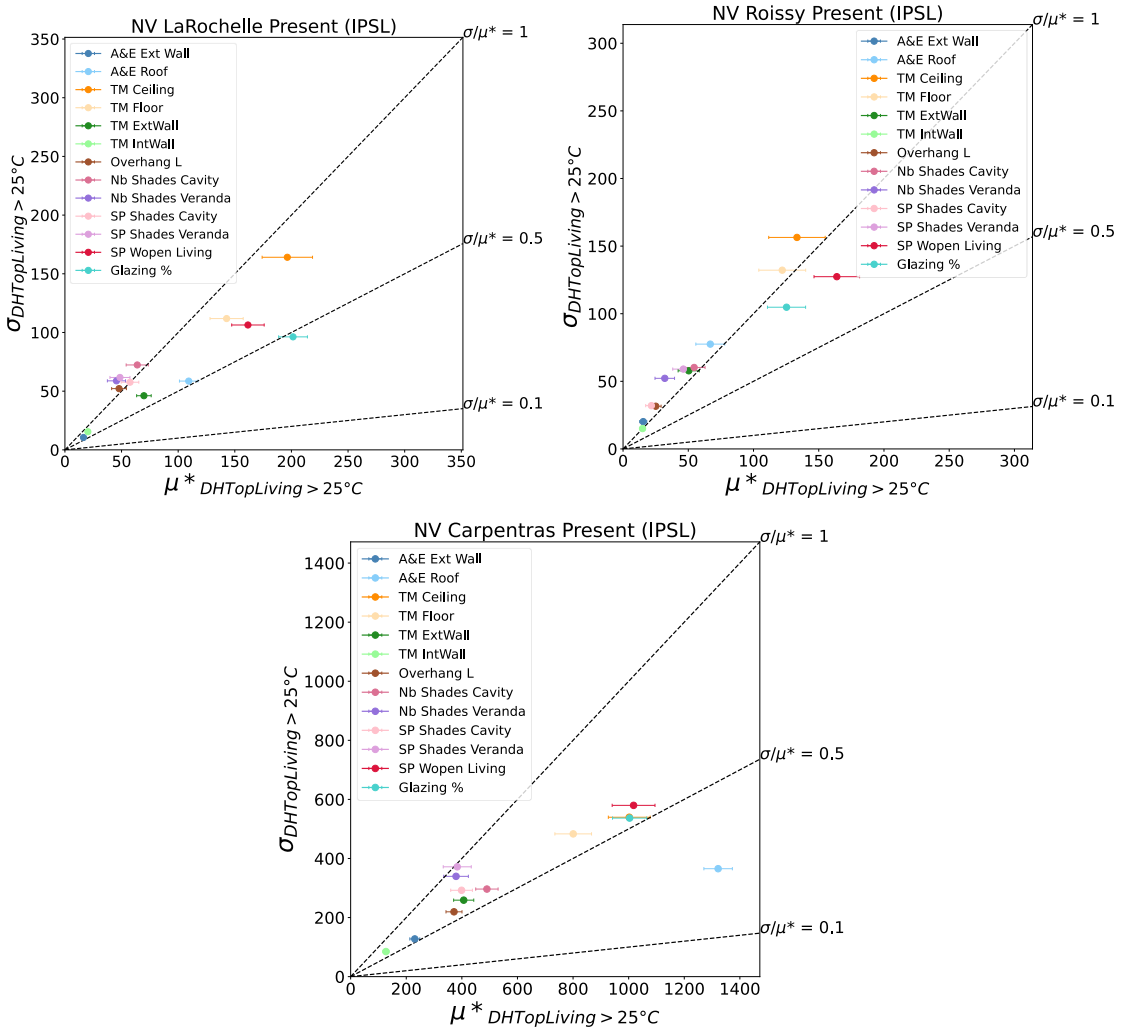

Figure 145 - SA results with Morris for the three cities during the present typical summer –Natural Ventilation

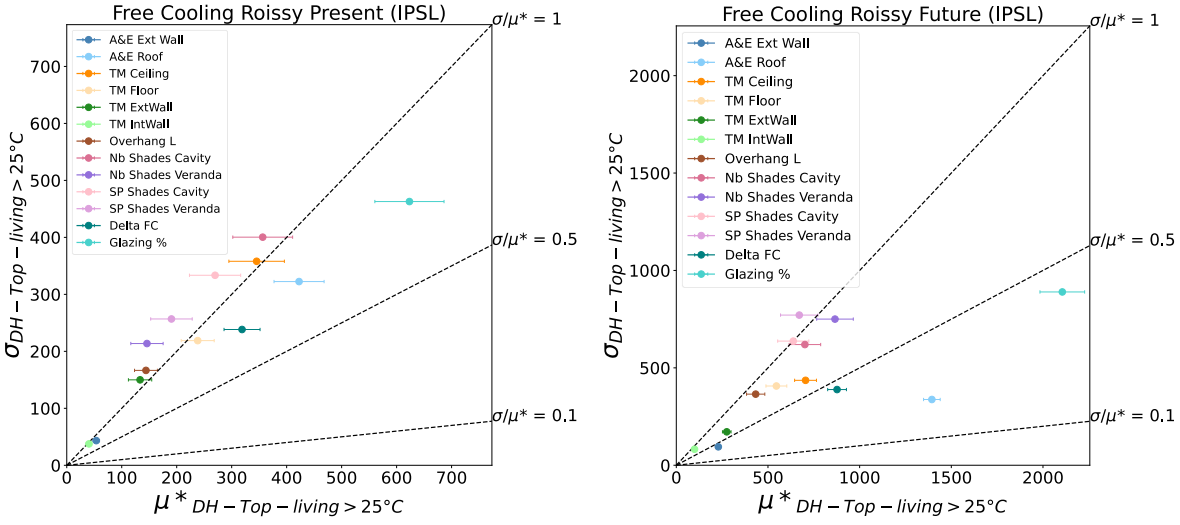

Figure 146 - SA results with Morris for Roissy during the typical summer – present & future - Free Cooling

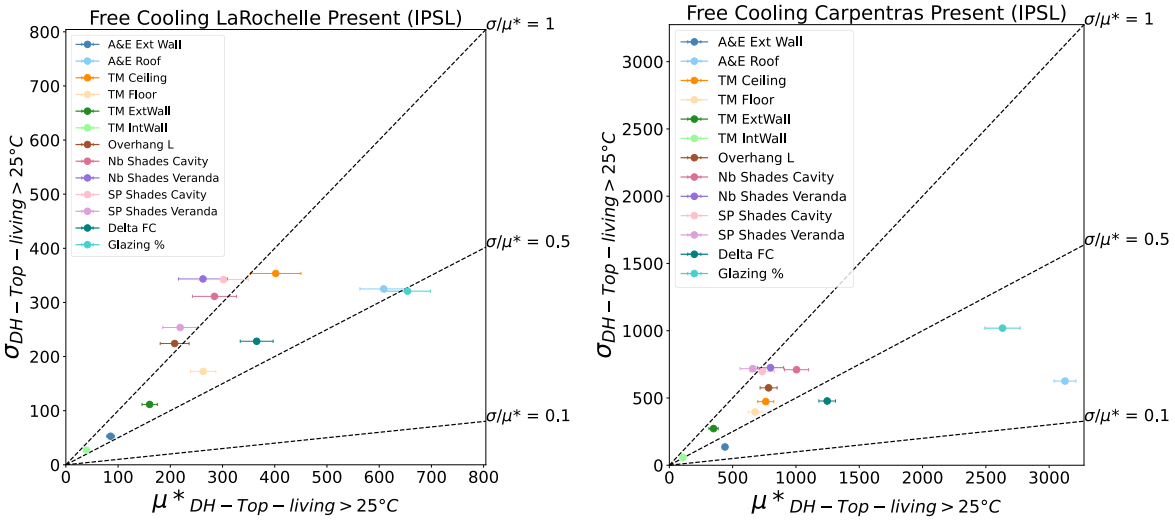

Figure 147 - SA results with Morris during the typical present summer in La Rochelle & Carpentras - Free Cooling

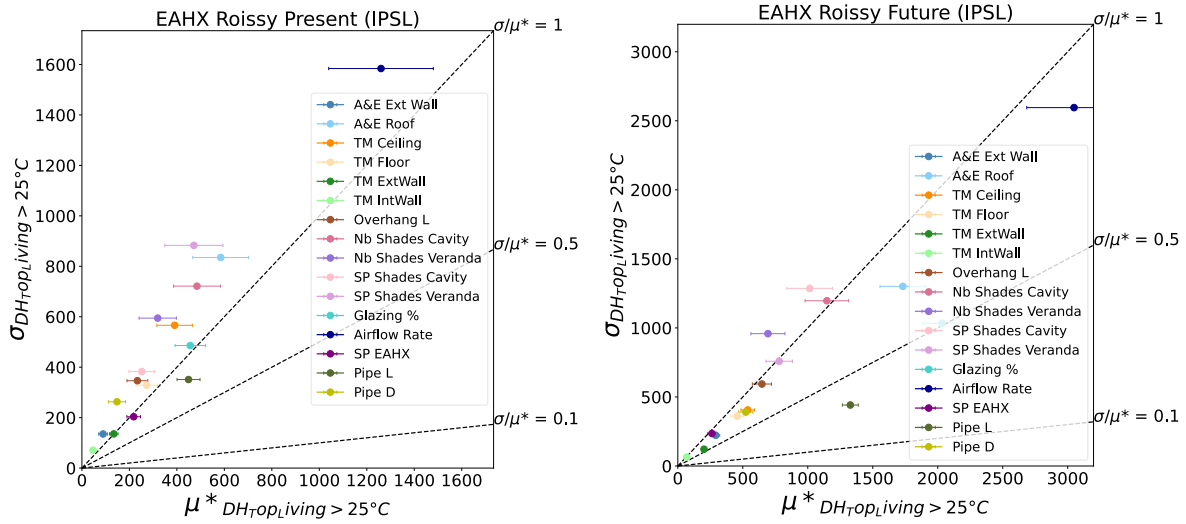

Figure 148 - SA results with Morris for Roissy during the typical summer – present & future – EAHX

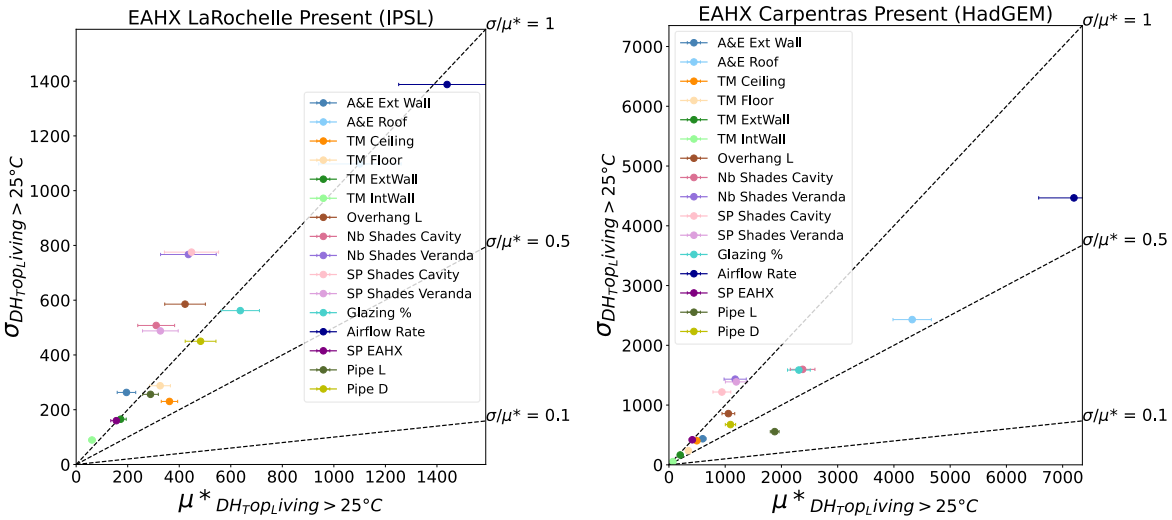

Figure 149 - SA results with Morris during the typical present summer in La Rochelle & Carpentras - EAHX

Appendix C – Optimized building design configurations

Table 38 – Design Variables for A, AB & B solutions in La Rochelle

	Objective Functions		**Design Variables**					
	Heating Needs *(Obj 1)*	DH SET > 25.6 °C *(Obj 2)*	Roof Albédo /Emissivity	Thermal Mass (density)	Glazing Percentage on North & South facades	Overhang length	Ventilative Cooling Parameter	
	kWh/m².yr	°C.h	-	Kg/m³	%	m		
NATURAL VENTILATION								
Present typical year								
A	1.5	0	0.9	1668	41	0.50	100	%
AB	0.4	0	0.1	2294	35	0.07	50	%
B	0.4	60	0.1	2294	35	0.06	10	%
Future typical year								
A	2.8	0	0.7	2298	35	0.83	99	%
AB	1.8	5	0.6	2298	35	0.09	99	%
B	1.4	18	0.1	2299	35	0.06	99	%
MECHANICAL FREE-COOLING								
Present typical year								
A	1	0	0.9	2297	36	0.95	1.5	°C
AB	0.3	4	0.6	2297	35	0.12	1.4	°C
B	0.2	28	0.1	2297	35	0.08	1.2	°C
Future typical year								
A	2.5	15	0.8	2298	35	0.98	1.2	°C
AB	1.5	65	0.8	2300	35	0.06	1.2	°C
B	1.0	238	0.1	2299	35	0.06	1.9	°C
EARTH-TO AIR HEAT EXCHANGER								
Present typical year								
A	0.9	0	0.8	2240	35	0.84	0.26	*m³/s*
AB	0.4	2	0.7	2269	35	0.12	0.27	*m³/s*
B	0.2	8	0.1	2273	35	0.06	0.27	*m³/s*
Future typical year								
A	2.4	1	0.8	2299	35	0.91	0.26	*m³/s*
AB	1.4	10	0.6	2300	35	0.04	0.26	*m³/s*
B	1.0	48	0.1	2298	35	0.00	0.25	*m³/s*

Table 39 – Design Variables for A, AB & B solutions in Roissy

	Objective Functions		Design Variables					
	Heating Needs *(Obj 1)*	DH SET > 25.6 °C *(Obj 2)*	Roof Albédo /Emissivity	Thermal Mass (density)	Glazing Percentage on North & South facades	Overhang length	Ventilative Cooling Parameter	
	kWh/m².yr	°C.h	-	Kg/m³	%	m		
NATURAL VENTILATION								
Present typical year								
A	11.5	0	0.3	1986	66	0.86	76	%
AB	5.5	0	0.1	2290	35	0.07	43	%
B	5.4	14	0.1	2290	35	0.04	15	%
Future typical year								
A	9.5	13	0.9	2234	35	0.94	99	%
AB	7.8	50	0.6	2270	35	0.11	99	%
B	7	119	0.1	2232	35	0.08	99	%
MECHANICAL FREE-COOLING								
Present typical year								
A	5.6	0	0.8	2083	40	0.22	1.2	°C
AB	4.5	0	0.1	2293	35	0.15	1.4	°C
B	4.4	9	0.1	2288	35	0.01	4.7	°C
Future typical year								
A	8.2	120	0.9	2290	35	0.91	1.4	°C
AB	6.8	266	0.7	2298	35	0.08	1.6	°C
B	5.9	567	0.1	2270	35	0.08	1.6	°C
EARTH-TO AIR HEAT EXCHANGER								
Present typical year								
A	7.0	0	0.6	1501	49	0.80	0.15	m^3/s
AB	4.5	0	0.2	2209	35	0.06	0.11	m^3/s
B	4.4	0.5	0.1	2207	35	0.06	0.12	m^3/s
Future typical year								
A	8.1	5	0.9	2257	35	0.82	0.27	m^3/s
AB	6.7	29	0.6	2256	35	0.09	0.27	m^3/s
B	5.9	83	0.1	2258	35	0.09	0.26	m^3/s

Table 40 – Design Variables for A, AB & B solutions in Carpentras

	Objective Functions		Design Variables					
	Heating Needs *(Obj 1)*	DH SET > 25.6 °C *(Obj 2)*	Roof Albédo /Emissivity	Thermal Mass (density)	Glazing Percentage on North & South facades	Overhang length	Ventilative Cooling Parameter	
	kWh/m².yr	°C.h	-	Kg/m³	%	m		
NATURAL VENTILATION								
Present typical year								
A	1.1	515	0.9	2289	35	0.86	98	%
AB	0.3	724	0.9	2288	40	0.08	100	%
B	0.0	1393	0.1	2260	43	0.09	98	%
Future typical year								
A	2.4	3158	0.9	2289	36	0.88	99	%
AB	0.7	3881	0.9	2298	43	0.10	99	%
B	0.2	5446	0.1	2299	63	0.04	99	%
MECHANICAL FREE-COOLING								
Present typical year								
A	0.8	895	0.9	2292	35	0.99	1.05	°C
AB	0.2	1215	0.9	2292	35	0.08	1.05	°C
B	0.0	2913	0.1	2284	41	0.08	1.64	°C
Future typical year								
A	2.2	4183	0.9	2300	35	0.98	1.56	°C
AB	0.6	5081	0.8	2297	35	0.09	2.13	°C
B	0.2	8289	0.1	2300	55	0.08	1.55	°C
EARTH-TO AIR HEAT EXCHANGER								
Present typical year								
A	0.8	331	0.9	2292	36	0.91	0.27	m^3/s
AB	0.2	446	0.9	2298	36	0.13	0.27	m^3/s
B	0.0	1190	0.1	2297	37	0.09	0.27	m^3/s
Future typical year								
A	2.2	2115	0.9	2279	36	1.00	0.27	m^3/s
AB	0.6	2834	0.8	2298	36	0.13	0.27	m^3/s
B	0.2	5485	0.1	2299	58	0.05	0.27	m^3/s

Appendix D – Indoor overheating assessment of optimized building designs

Table 41- Assessment of summer indoor overheating for A, AB & B solutions in La Rochelle

	Heating Needs *(Obj 1)*	***DH*** **SET > 25.6 °C** ***(Obj 2)***		***DH*** **SET > 30 °C**		**SET Max Daytime (hottest day)**		**SET Min Nighttime (hottest day)**		**Top Max**	**Top Min**
		v = 0.1 m/s	v = 0.4 m/s	v = 0.1 m/s	v = 0.4 m/s	v = 0.1 m/s	v = 0.4 m/s	v = 0.1 m/s	v = 0.4 m/s		
	kWh/m².yr	°C.h	°C.h	°C.h	°C.h	°C	°C	°C	°C	°C	°C
NATURAL VENTILATION											
Present typical year											
A	1.5	0	0	0	0	25.3	23.6	22.0	20.2	26.4	22.8
AB	0.4	0	0	0	0	25.6	23.8	22.7	20.9	26.4	23.4
B	0.4	60	0	0	0	27.3	25.2	25.4	23.6	27.5	25.5
Future typical year											
A	2.8	0	0	0	0	25.7	23.6	23.0	20.6	26.0	23.4
AB	1.8	5	0	0	0	26.1	24.0	23.2	20.8	26.4	23.6
B	1.4	18	0	0	0	26.6	24.4	23.5	21.1	26.4	23.9
Future typical heatwave summer											
A	-	266	23	0	0	28.6	26.6	26.2	23.4	29.4	25.9
AB	-	374	44	0	0	29.1	27.1	26.6	23.7	29.9	26.2
B	-	493	71	0	0	29.5	27.4	27.0	24.0	30.1	26.5
MECHANICAL FREE-COOLING											
Present typical year											
A	1	0	0	0	0	25.6	23.7	23.0	20.8	26.3	23.9
AB	0.3	4	0	0	0	26.4	24.4	23.6	21.4	27.0	24.4
B	0.2	28	0	0	0	27.1	25.1	24.1	21.9	27.7	25.0
Future typical year											
A	2.5	15	0	0	0	26.5	24.3	24.4	22.2	26.7	24.8
AB	1.5	65	0	0	0	27.1	24.9	24.9	22.6	27.2	25.2
B	1.0	238	0	0	0	27.8	25.6	25.6	23.2	27.9	25.8
Future typical heatwave summer											
A	-	530	52	0	0	29.4	27.3	28.1	25.4	30.0	27.7
AB	-	763	106	0	0	29.9	27.8	28.6	26.0	30.6	28.3
B	-	1254	227	7	0	30.8	28.6	29.5	26.9	31.6	29.2
EARTH-TO AIR HEAT EXCHANGER											
Present typical year											
A	0.9	0	0	0	0	25.8	23.9	22.9	20.6	26.5	23.8
AB	0.4	2	0	0	0	26.2	24.3	23.2	20.9	26.9	24.0
B	0.2	8	0	0	0	26.8	24.9	23.8	21.5	27.4	24.6
Future typical year											
A	2.4	1	0	0	0	25.8	24.1	24.1	22.0	27.1	25.0
AB	1.4	10	0	0	0	26.4	24.7	24.6	22.5	27.7	25.5
B	1.0	48	0	0	0	26.9	25.1	25.2	23.2	28.2	26.1
Future typical heatwave summer											
A	-	173	2	0	0	28.0	26.2	26.1	23.7	29.2	26.3
AB	-	296	11	0	0	28.5	26.7	26.6	24.2	29.8	26.8
B	-	497	28	0	0	29.0	27.1	27.1	24.8	30.4	27.4

Table 42 - Assessment of summer thermal comfort for A, AB & B solutions in Roissy

	Heating Needs *(Obj 1)*	***DH*** **SET > 25.6 °C *(Obj 2)***		***DH*** **SET > 30 °C**		**SET Max Daytime (hottest day)**		**SET Min Nighttime (hottest day)**		**Top Max**	**Top Min**
		v = 0.1 m/s	v = 0.4 m/s	v = 0.1 m/s	v = 0.4 m/s	v = 0.1 m/s	v = 0.4 m/s	v = 0.1 m/s	v = 0.4 m/s		
	kWh/m².yr	°C.h	°C.h	°C.h	°C.h	°C	°C	°C	°C	°C	°C
NATURAL VENTILATION											
Present typical year											
A	11.5	0	0	0	0	25.3	23.5	20.5	17.8	26.2	21.2
AB	5.5	0	0	0	0	25.7	23.9	23.8	21.7	26.7	24.8
B	5.4	14	0	0	0	26.6	24.8	23.4	21.4	27.7	24.6
Future typical year											
A	9.5	13	0	0	0	26.5	24.6	23.6	21.3	27.2	24.1
AB	7.8	50	0	0	0	27.1	25.1	24.2	21.8	27.8	24.5
B	7	119	0	0	0	27.7	25.7	24.6	22.1	28.4	24.9
Future typical heatwave summer											
A	-	394	74	0	0	29.7	27.7	26.9	24.7	31.0	27.8
AB	-	620	129	1	0	30.7	28.7	27.4	25.1	31.8	28.3
B	-	850	201	7	0	31.4	29.3	27.9	25.5	32.5	28.8
MECHANICAL FREE-COOLING											
Present typical year											
A	5.6	0	0	0	0	25.1	23.4	22.2	19.8	26.1	23.1
AB	4.5	0	0	0	0	25.7	23.9	23.8	21.8	26.7	24.9
B	4.4	9	0	0	0	26.3	24.5	23.7	21.5	27.3	24.7
Future typical year											
A	8.2	120	0	0	0	27.4	25.4	24.5	22.2	27.9	25.0
AB	6.8	266	4	0	0	28.1	26.0	25.1	22.7	28.5	25.5
B	5.9	567	30	0	0	28.9	26.8	25.8	23.4	29.3	26.1
Future typical heatwave summer											
A	-	856	194	1	0	30.3	28.3	28.7	26.3	31.8	29.4
AB	-	1256	311	17	0	30.9	28.9	28.7	26.5	32.4	29.9
B	-	1856	526	61	0	31.9	29.8	29.5	27.2	33.5	30.8
EARTH-TO AIR HEAT EXCHANGER											
Present typical year											
A	7.0	0	0	0	0	25.4	23.5	22.8	20.5	26.3	23.7
AB	4.5	0	0	0	0	25.7	23.9	23.8	21.7	26.7	24.8
B	4.4	0.5	0	0	0	25.9	24.1	24.0	22.0	26.9	25.0
Future typical year											
A	8.1	5	0	0	0	26.0	24.1	23.3	21.1	26.7	24.0
AB	6.7	29	0	0	0	26.5	24.5	23.9	21.6	27.2	24.4
B	5.9	83	0	0	0	27.1	25.1	24.6	22.3	27.7	25.1
Future typical heatwave summer											
A	-	204	12	0	0	29.3	27.2	26.3	24.1	29.8	27.2
AB	-	349	32	0	0	29.9	27.7	26.8	24.6	30.4	27.7
B	-	588	69	0	0	30.5	28.3	27.5	25.2	31.0	28.4

Table 43 - Assessment of summer thermal comfort for A, AB & B solutions in Carpentras

	Heating Needs *(Obj 1)*	***DH*** **SET > 25.6 °C** ***(Obj 2)***		***DH*** **SET > 30 °C**		**SET Max Daytime (hottest day)**		**SET Min Nighttime (hottest day)**		**Top Max**	**Top Min**
		v = 0.1 m/s	v = 0.4 m/s	v = 0.1 m/s	v = 0.4 m/s	v = 0.1 m/s	v = 0.4 m/s	v = 0.1 m/s	v = 0.4 m/s		
	kWh/m².yr	°C.h	°C.h	°C.h	°C.h	°C	°C	°C	°C	°C	°C
NATURAL VENTILATION											
Present typical year											
A	1.1	515	77	0	0	29.6	27.5	26.2	23.8	30.1	26.8
AB	0.3	724	133	0	0	30.1	28.1	25.9	23.5	30.7	26.4
B	0.0	1393	328	28	0	31.4	29.4	26.9	24.4	32.3	27.3
Future typical year											
A	2.4	3158	965	88	0	31.9	29.6	28.1	25.5	31.7	28.4
AB	0.7	3881	1378	222	1	32.5	30.3	28.5	25.9	32.6	28.7
B	0.2	5446	2335	695	68	34.0	31.8	30.7	27.9	34.5	30.3
Future typical heatwave summer											
A	-	2096	650	79	2	33.1	30.8	28.3	25.9	32.4	29.1
AB	-	2756	927	166	7	33.9	31.6	28.7	26.3	33.3	29.5
B	-	4152	1638	433	62	35.5	33.2	29.4	26.8	35.1	30.2
MECHANICAL FREE-COOLING											
Present typical year											
A	0.8	895	131	0	0	29.8	27.7	26.2	24.0	30.4	26.8
AB	0.2	1215	213	1	0	30.2	28.1	26.6	24.3	30.9	27.2
B	0.0	2913	743	71	0	32.0	29.9	28.1	25.7	33.0	28.8
Future typical year											
A	2.2	4183	1390	152	0	32.0	29.8	28.7	26.3	32.0	29.2
AB	0.6	5081	1899	326	1	32.6	30.4	29.2	26.7	32.7	29.8
B	0.2	8289	3984	1406	192	34.5	32.3	31.7	29.2	35.1	31.7
Future typical heatwave summer											
A	-	2862	907	132	5	33.6	31.3	28.8	26.6	32.7	29.9
AB	-	3688	1238	232	10	33.9	31.6	29.3	27.0	33.5	30.4
B	-	6653	2884	855	145	35.9	33.7	30.9	28.5	36.1	32.3
EARTH-TO AIR HEAT EXCHANGER											
Present typical year											
A	0.8	331	14	0	0	28.9	26.8	25.3	23.0	29.3	25.9
AB	0.2	446	25	0	0	29.2	27.1	25.6	23.3	29.6	26.2
B	0.0	1190	128	1	0	30.4	28.2	26.8	24.4	30.9	27.3
Future typical year											
A	2.2	2115	330	2	0	30.4	28.1	28.0	25.5	31.0	28.3
AB	0.6	2834	546	18	0	30.9	28.6	28.6	26.1	31.6	28.9
B	0.2	5485	1794	310	0	32.6	30.0	30.0	27.4	33.4	30.4
Future typical heatwave summer											
A	-	1627	389	20	1	32.7	30.6	27.9	25.6	32.2	28.7
AB	-	2180	550	45	2	33.2	31.0	28.4	26.0	32.8	29.2
B	-	4363	1345	265	14	34.7	32.5	29.6	27.3	34.7	30.7

Table 44 – Assessment of indoor overheating during the ***future typical heatwave*** for A, AB & B solutions in La Rochelle

	$IOH\_Duration_{HW}$		$IOH\_Severity_{HW}$					
	Number of consecutive days when SET,*daytime AND* SET,*nighttime* > 25.6 °C		DH SET,*daytime* > 25.6 °C		DH SET,*nighttime* > 25.6 °C		DH SET,*total* > 25.6°C	
	v = 0.1	v = 0.4	v = 0.1	v = 0.4	v = 0.1	v = 0.4	v = 0.1	v = 0.4
	days	days	°C.h	°C.h	°C.h	°C.h	°C.h	°C.h
NATURAL VENTILATION								
A	9	3	17.9	2.7	13.4	0.9	31.3	3.6
AB	9	3	22.0	4.2	16.7	2.0	38.7	6.2
B	10	5	26.6	7.5	20.1	3.3	46.7	10.8
MECHANICAL FREE-COOLING								
A	12	4	27.4	5.3	23.0	2.9	50.4	8.2
AB	13	6	34.0	8.8	28.9	5.4	62.9	14.2
B	16	9	46.9	16.3	40.1	10.9	87.0	27.2
EARTH-TO AIR HEAT EXCHANGER								
A	8	0	11.7	0	7.2	0	18.9	0
AB	9	0	16.7	0	11.7	0	28.4	0
B	12	2	23.9	2.4	18.3	0.7	42.2	3.1

Table 45 – Assessment of indoor overheating during the ***future typical heatwave*** for A, AB & B solutions in Roissy

	$IOH\_Duration_{HW}$		$IOH\_Severity_{HW}$					
	Number of consecutive days when SET,*daytime AND* SET,*nighttime* > 25.6 °C		DH SET,*daytime* > 25.6 °C		DH SET,*nighttime* > 25.6 °C		DH SET,*total* > 25.6°C	
	v = 0.1	v = 0.4	v = 0.1	v = 0.4	v = 0.1	v = 0.4	v = 0.1	v = 0.4
	days	days	°C.h	°C.h	°C.h	°C.h	°C.h	°C.h
NATURAL VENTILATION								
A	13	6	29.0	9.3	22.3	4.6	51.3	13.9
AB	14	7	37.7	13.8	28.5	7.3	66.2	21.1
B	15	7	45.9	17.8	35.3	10.6	81.2	28.4
MECHANICAL FREE-COOLING								
A	18	10	48.0	17.2	40.0	11.6	88.0	28.8
AB	18	10	59.1	23.3	50.3	17.3	109.4	40.6
B	21	14	76.4	35.4	63.9	25.6	140.3	61.0
EARTH-TO-AIR HEAT EXCHANGER								
A	8	0	16.6	0	10.3	0	26.9	0
AB	10	3	23.3	4.6	15.7	0.4	39.0	5
B	15	5	33.5	8.8	23.6	2.6	27.1	11.4

Table 46 - Assessment of indoor overheating during the ***future typical heatwave*** for A, AB & B solutions in Carpentras

	$IOH\_Duration_{HW}$		$IOH\_Severity_{HW}$					
	Number of consecutive days when SET,*daytime AND* SET,*nighttime* > 25.6 °C		DH SET,*daytime* > 25.6 °C		DH SET,*nighttime* > 25.6 °C		DH SET,*total* > 25.6°C	
	v = 0.1	v = 0.4	v = 0.1	v = 0.4	v = 0.1	v = 0.4	v = 0.1	v = 0.4
	days	days	°C.h	°C.h	°C.h	°C.h	°C.h	°C.h
NATURAL VENTILATION								
A	22	16	88.7	44.9	72.9	30.3	161.6	75.2
AB	23	16	105.5	56.5	84.0	38.2	189.5	94.7
B	24	19	134.6	82.9	104.6	53.4	239.2	136.3
MECHANICAL FREE-COOLING								
A	26	18	107.3	55.1	88.4	38.9	195.7	94.0
AB	28	19	123.1	65.9	101.7	47.4	224.8	113.3
B	87	23	393.5	106.7	305.2	79.4	698.7	186.1
EARTH-TO AIR HEAT EXCHANGER								
A	23	14	76.7	23.8	58.3	16.2	135.0	49.0
AB	25	16	89.4	40.9	69.7	22.6	159.1	63.5
B	66	22	223.4	71.6	171.6	48.0	395.0	119.6

Contribution à la conception des bâtiments : Convergence des solutions d'atténuation et d'adaptation au changement climatique

Résumé:

Compte tenu de l'augmentation de la fréquence des canicules, il est nécessaire de s'assurer que les bâtiments conçus et construits aujourd'hui seront adaptés aux futures températures plus élevées. Le périmètre de cette thèse consiste à proposer une méthodologie de contribution à la conception des bâtiments considérant à la fois les enjeux d'atténuation (réduction des besoins énergétiques) et d'adaptation (confort thermique estival, réduction du risque sanitaire en période de canicule) au changement climatique. La méthodologie a pour vocation d'être adaptable à différents types de bâtiments et de climats. Dans ce but, nous avons développé des fichiers météorologiques contenant des séquences typiques, ainsi que des vagues de chaleur futures. Par la suite, des méthodes d'analyse de sensibilité et d'optimisation couplées à des simulations thermiques dynamiques du bâtiment ont permis d'évaluer le potentiel de différentes techniques de rafraîchissement passif utilisées pour diminuer la surchauffe d'été en climats futurs. Les résultats de ces travaux de recherche mettent en évidence que les stratégies évaluées sont efficaces pour maintenir un confort thermique estival lors des étés futurs types à Paris et à La Rochelle. Cependant, à Carpentras, pour un été type futur, et pour ces trois villes en périodes de canicules futures récurrentes, les limites de ces solutions sont mises en exergue. En effet, les résultats de l'étude montrent que les occupants sont exposés à la chaleur lors de plusieurs jours consécutifs au-dessus de seuils à la fois diurnes et nocturnes ce qui résulte en un risque sanitaire pour les personnes vulnérables. Ces séquences ne sont pas détectées en utilisant des fichiers futurs types uniquement, ce qui démontre la pertinence de ces travaux. La combinaison d'enveloppes de bâtiments optimisées, de stratégies de rafraîchissement et d'adaptation des occupants se révèle être nécessaire afin d'atténuer le risque sanitaire récurrent auguré pour le milieu du siècle en France.

Mots clés : changement climatique, vagues de chaleur, atténuation, adaptation, conception du bâtiment, confort d'été, surchauffe, risque sanitaire, analyse de sensibilité, optimisation

Towards mitigation and adaptation to climate change: Contribution to Building Design

Summary:

Due to climate change projecting increased heatwaves occurrence, ensuring that buildings designed and built today will be adapted to future warmer temperatures is essential. The scope of this Ph.D. is to propose a methodological contribution to the design of buildings that both mitigate (minimize yearly energy needs) and adapt (minimize summer indoor overheating, limit health-heat-related risk) to climate change. The methodology can be applied to any building case study in any climate. For this purpose, bias-adjusted weather files containing both present, future typical conditions and future heatwave periods were developed. The potential of different passive cooling mitigation and adaptation strategies to reduce summer indoor overheating is evaluated using these weather files through dynamic thermal simulations, sensitivity analysis and optimization methods. The results of this research work highlight that for the building case study, the evaluated strategies (buffer spaces, thermal mass, roof optical properties, glazing ratio, ventilative cooling) have a strong capacity to enable summer thermal comfort in future typical summers in Paris and in La Rochelle. However, in Carpentras, and under recurring heatwaves in all three cities, the limits of these mitigation and adaptation measures are recognized. In fact, the future heatwaves consistently lead to consecutive days of indoor overheating exposure during both daytime and nighttime for building occupants, leading to a health-heat-related risk especially for the most vulnerable. These sequences are not detected when using only future typical years, which stresses the relevance of this work. Only the combination of optimized building envelopes, ventilative cooling strategies and adaptive opportunities from building occupants (solar control, increased indoor air velocities) have the potential to offset the projected recurring health-heat-related risk, particularly elevated in the South of France.

Keywords: climate change, heatwaves, mitigation, adaptation, building design, summer thermal comfort, overheating, health-heat-related risk, sensitivity analysis, optimization

LaSIE (Laboratoire des Sciences de l'Ingénieur pour l'Environnement)

Faculté des Sciences et Technologie

Avenue Michel Crépeau

17042 LA ROCHELLE CEDEX 1 - France